NASA TECHNICAL TRANSLATION NASA TT F-15,881

LUNAR SOIL FROM THE SEA OF FERTILITY

A. P. Vinogradov, Editor

Translation of Lunnyy grunt iz Morya Izobiliya, "Nauka" Press, Moscow, 1974,

pp 1-22, 29-63, 106-110, 122-162, 209-214, 225-238, 262-277, 283-289, 294-298, 319-374, 377-385, 405-426, 430-437, 444-447, 455-460, 496-608

(NASA-TT-F-15881) LUNAR SOIL FROM THE SEA OF FERTILITY (Kanner (Leo) Associates) 642 p HC $15.25 CSCL 03B

N75-11814 THRU N75-11877 Unclas G3/91 53147

ORIGINAL CONTAINS BORDER ILLUSTRATIONS

NATIONAL AERONAUTICS AND SPACE ADMINISTRATION
WASHINGTON, D.C. 20546 OCTOBER 1974

STANDARD TITLE PAGE

1. Report No.	2. Government Accession No.	3. Recipient's Catalog No.
NASA TT F-15,881		

4. Title and Subtitle	5. Report Date
LUNAR SOIL FROM THE SEA OF FERTILITY	October 1974
	6. Performing Organization Code

7. Author(s)	8. Performing Organization Report No.
A. P. Vinogradov, Editor	
	10. Work Unit No.

9. Performing Organization Name and Address	11. Contract or Grant No.
Leo Kanner Associates Redwood City, California 94063	NASw-2481
	13. Type of Report and Period Covered
	Translation
12. Sponsoring Agency Name and Address	14. Sponsoring Agency Code
National Aeronautics and Space Administration, Washington, D.C. 20546	

15. Supplementary Notes

Translation of Lunnyy grunt iz Morya Izobiliya, "Nauka" Press, Moscow, 1974, (selected pages)
pp 1-22, 29-63, 106-110. 122-162,209-214, 225-238, 262-277, 283-289, 294-298, 319-374, 377-386, 405-426, 430-437, 444-447, 455-470, 496-608

16. Abstract

The collection contains articles by Soviet and foreign authors on the investigation of lunar surface material returned by the Soviet Luna 16 automatic station. Physical and mechanical properties of the lunar surface material are examined; many studies deal with mineralogical investigation and analysis of the chemical composition and distribution of rare elements in the regolith, and individual rock and mineral fragments. Constituents incorporated in the regolith are represented by both primary magmatic lunar rock as well as by formations emerging at the lunar surface during the long history of the Moon. Of great importance are studies determining, by geochronological methods, the age of regolith and individual particles of magmatic rocks demonstrating their great age and that their age is comparable with the age of the Earth and its most ancient geological formations.

17. Key Words (Selected by Author(s))	18. Distribution Statement
	Unclassified - Unlimited

19. Security Classif. (of this report)	20. Security Classif. (of this page)	21. No. of Pages	22. Price
Unclassified	Unclassified	644	

NASA HQ

PRECEDING PAGE BLANK NOT FILMED

LUNAR SOIL FROM THE SEA OF FERTILITY

Editor: A. P. Vinogradov

ANNOTATION /4

The collection contains articles by Soviet and foreign authors on the investigation of lunar surface material returned by the Soviet Luna 16 automatic station. Physical and mechanical properties of the lunar surface material are examined; many studies deal with mineralogical investigation and analysis of the chemical composition and distribution of rare elements in the regolith, and individual rock and mineral fragments. The object of the investigation -- lunar surface material -- is complex. Constituents that are included in it are represented both by primary magmatic lunar rock as well as by formations emerging at the lunar surface during its long history. X-ray structural and x-ray spectral methods, mass spectrometry, Mossbauer and x-ray electronic spectroscopy, EPR /electron paramagnetic resonance/, activation analysis, and many other of the latest methods made it possible to characterize the samples of surface material from the most diverse aspects. Geochemical characteristics are given in comparison with geochemical features of samples returned by the American Apollo missions. Of great importance are the studies determining, by geochronological methods, the age of regolith and individual particles of magmatic rocks demonstrating their great age and that their age is comparable with the age of the Earth and its most ancient geological formations.

Editor-In-Chief: Academician A. P. Vinogradov

FOREWORD /5

The book Lunnyy grunt iz Morya Izobiliya /Lunar Soil from the Sea of Fertility/ collects more than 90 studies on inequigranular rock -- regolith returned by the Soviet Luna 16 automatic space station. Most studies appear here for the first time in the Russian language. Sampling of the soil and its return to Earth by the automatic station was achieved in September, 1970. The automatic station landed in the northeastern part of the Sea of Fertility. At the present time it has become well known that a layer of friable surface inequigranular material lies on the surface of the Moon, regolith, whose character changes from one province of the Moon to another. Regoliths from the regions of the lunar maria and the mountainous terrae regions of the Moon differ especially widely in their properties and composition. Luna 16 regolith is a typical rock of the mare regions of the Moon. It consists of particles of different sizes -- -- magmatic rocks of the basalt type and particles subjected to appreciable transformations on the lunar surface -- melting, sintering, formation of spheroids, and so on. Each regolith particle preserves the history of events on the lunar surface. That is why, as the reader will find out for himself, that scientists of various countries -- Soviet Union, the United States, France, and Hungary -- have presented with extraordinary care their complex investigations of lunar regolith in this book. It appears that all the modern physicochemical methods have been used to investigate the lunar regolith.

Studies of Luna 16 regolith naturally were compared with analogous data for regolith from the Sea of Tranquillity and the Ocean of Storms returned by Apollo 11 and Apollo 12 astronauts, in particular, with data obtained in the laboratories of the USSR. Owing to the large volume of investigations, at the present time we already know quite a great deal about the mare regions of the Moon, about their surface, rock formations -- morphology, mineralogical and petrographic composition, the possible mode of their formation, the geochemistry of this process, and the absolute

and radiation age of regolith, and much else besides. Of exceptional significance are data on galactic and solar radiation and their action on lunar material. Reactions arising under their effect left behind in lunar material isotopic and other traces, which are a record of the cosmic history of the Moon. This cosmochemical direction, which naturally will acquire in the immediate future even greater significance in the study of geochemical processes in space, is also represented in this collection.

All that we have learned about lunar rocks of ancient age enables us for the first time to approach more closely the history of the Earth in its initial stages of life -- approximately the first billion years of its existence. It is highly probable that much of what we see preserved in the landscape of the Moon disappeared on Earth under intense precipitation. Thus, it appears possible to expand the study of the geological history of the Earth not only in our day, but also in the inception of the planet. Studies included in our collection in addition serve to unify the efforts of scientists devoting their energies to comparative cosmochemistry.

We wish to dwell further on the specific features of this collection. Naturally, the terminology used at present for lunar rocks, including for the regolith proper, is based on ideas of Earth objects. However, the application of several terms cannot be regarded as successful. First of all, we must note the names of these surface lunar rock so widely employed in foreign literature -- "lunar soil" or simply "soil" (soil - English). As applied to Earth conditions of soil, this refers to a product of a complex of phenomena and processes, and above all the active influence of the biosphere, of the climate. It is widely known that with the same bedrock in different climatic-landscape zones /6 soils of different types are formed. Since on the Moon there are no biologic-climatic factors or water, the application of the term "soil" to lunar surface rock is incorrect. Therefore we employ the perhaps more general, more technical term "surface material," or "lunar surface material." Here naturally we mean that the other term "regolith" is its synonym. The latter was introduced into the literature by Merill in 1897 to refer to the set of all friable surface formations -- soils, alluvial, eluvial, glacial, colluvial, and other deposits -- regardless of their mode of formation. It did not become accepted for the Earth, but for the Moon especially given the conditions of its thus far limited study, this generalizing term must be regarded as very successful, and we use it widely on a par with "lunar surface material."

Another term used widely in American literature is fines -- -- the regolith fraction smaller than 1 cm, as was determined in a report on the preliminary results of investigating Apollo 11

regolith and samples. As applied to drill cores of surface material returned by Soviet automatic stations, it can be stated that the entire volume of their material is classified as fines, so that thus in this case it makes it a full synonym of "lunar surface material" and "regolith". Moreover, this word that is new to the English language is impossible to simply translate into Russian, and in each specific case it must be replaced by definitions, which better convey the characteristics of the object -- the fine fraction of regolith, fine surface material, and so on.

The application to lunar formations of the sinter type of the names agglutinate and microagglutinate, the first of which was used to describe terrestrial sintered slag and pumice rocks with glassy cementing, bonding material, must be regarded as very successful.

American investigators introduced the acronym KREEP to refer to specific basalt rocks rich in potassium (K), rare earths (REE), and phosphorus (P); this acronym was first applied to glasses and their rock-equivalents in normative composition, and later to specifically basalt rocks of this type. The acronym successfully conveys the primary geochemical specifics of the objects, and since this group of rocks is extremely important to lunar petrology, the continual use of the abbreviation KREEP in the Russian text produces large inconveniences. Therefore in translation it is everywhere replaced with the words "krip", "krip constituent," "krip basalt." An analogy can be drawn with terms such as sial, sima, simatic, sialic, mafic, and so on. We assume that this term will easily gain currency, all the more so in that evidently considerable attention will be given to rocks of the krip type also among Earth formations.

To avoid confusion between the English, Latin, and Russian names, as a rule we used the Russian and most common names for the seas, craters, mountains, and so on, objects on the lunar surface. For example, we chose the name More Izobiliya /Sea of Fertility/, and not More Plodorodiye.

The Luna 16 drill core was divided by us into layers A, B, V, G, and D. Samples for our foreign colleagues were given from the zones A, B, V, G, so that in the English and French transcriptions they are expressed in different ways, either as A, B, C, D, or as A, B, C, G. Again, however to avoid confusion in translation, all sample numbers were referred to our nomenclature A, B, V, G. At the same time, the numbers with indexes SAO.(for example, section SAO-303, and so on) were kept for the numbers of the Luna 16 sections prepared, for example, in the Smithsonian Astrophysical Observatory.

Since no letter subdivisions of the cores are employed for subsequent returned samples, beginning with Luna 20, all the layers have either an Arabic or Latin numbering.

The translations of the articles were made based on preprints and from the journal Earth and Planetary Science Letters, Vol. 13, No. 2, 1972. The article by K. Allegre et al. was translated from C. R. Acad. Sci. Paris, ser. D., Vol. 273, p. 779 (1971). We wish to note the preliminary nature of a number of the articles by both Soviet and foreign investigators and that many studies were translated from preprints. Where it was possible, corrections were made in these translations based on the versions of the studies published in journals. Unfortunately, this was not possible in each instance or in full extent.

The publication of this collection does not write finis to the investigation of Luna 16 samples. It is continuing along with the study of other samples in both our own and foreign laboratories, and at this stage of detailed examination a great deal more of interest can be found.

A. P. Vinogradov

TABLE OF CONTENTS

	Page
Annotation	iii
Foreword	iv
Preliminary Data on Lunar Surface Material Returned by Luna 16 Automatic Station A. P. Vinogradov	1
Geologo-Morphological Characteristics of the Landing Site of Luna 16 Automatic Station K. P. Florenskiy, A. T. Bazilevskiy, and A. A. Pronin	19
The Geologic Setting of the Luna 16 Landing Site J. F. McCauley and D. H. Scott (Earth and Planetary Science Letters 13 (1972), North-Holland Publishing Company [hereinafter cited as EPSL], pp. 225-232)	
Reception and Study of Lunar Surface Material in Inert Gas Medium Yu. A. Surkov, Ye. M. Rudnitskiy, and V. A. Glotov	27
Box for Working with Lunar Samples in Nitrogen Atmosphere Yu. I. Stakheyev, L. S. Tarasov, K. K. Krestinina, and A. V. Ivanov	34
Morphology and Types of Particles of Regolith Sample from the Sea of Fertility K. P. Florenskiy, A. V. Ivanov, L. S. Tarasov, Yu. I. Stakheyev, and O. D. Rode	40
Granulometric Characteristics of Lunar Surface Material from the Sea of Fertility Yu. I. Stakheyev, Ye. K. Vulfson, A. V. Ivanov, and K. P. Florenskiy	51

Morphometric Characteristics of Particles of Regolith Returned by Luna 16 Automatic Station
P. V. Florenskiy, V. Ya. Belenkiy, N. M. Karachenzeva, and L. F. Pankratova 61

Measurement of Density and Porosity of Lunar Rocks Based on Samples of Luna 16 Automatic Lunar Station
V. F. Volynets, K. P. Florenskiy, and A. V. Ivanov 69

Petrology of Lunar Rocks from the Sea of Fertility
A. S. Pavlenko, L. S. Tarasov, I. D. Shevaleyskiy, and A. V. Ivanov 74

Petrology of a Portion of the Mare Fecunditatis Regolith
P. Jakes, J. Warner, W. I. Ridley, A. M. Reid, R. S. Harmon, R. Brett, and R. W. Brown /EPSL, pp. 257-271/

Luna 16: Relative Proportions and Petrologic Significance of Particles in the Soil from Mare Fecunditatis
J. B. Reid, Jr., G. J. Taylor, U. B. Marvin, and J. A. Wood /EPSL, pp. 286-299/

Petrology of Basaltic and Monomineralic Soil Fragments from the Sea of Fertility, A. E. Bence, W. Holzwarth, and J. J. Papike /EPSL, pp 299-311/

Preliminary Report on Mineralogical and Petrographic Study of the Luna 16 Lunar Surface Material Sample
M. Christophe-Michel-Levy, C. Levy, and R. Pierrot 86

Shock Metamorphic Effects in the Luna 16 Soil Sample from Mare Fecunditatis
B. M. French /EPSL, pp. 316-322/

Feldspathic Basalts in Lunar Soils and the Nature of the Lunar Highlands
A. M. Reid, W. I. Ridley, R. S. Harmon, J. Warner, R. Brett, P. Jakes, and R. W. Brown /source not given/

Petrographic-Mineralogical Investigation of Magmatic Rocks from the Sea of Fertility
L. S. Tarasov, I. D. Shevaleyevskiy, and M. A. Nazarov 94

X-ray Diffraction Identification of Minerals in Lunar Regolith Returned by Luna 16 Automatic Station
Ye. S. Makarov et al. 121

Mineralogy, Petrology, and Chemistry of a Luna 16 Basaltic Fragment, Sample B-1
A. L. Albee, A. A. Chodos, A. J. Gancarz, E. L. Haines, D. A. Papanastassiou, L. Ray, F. Tera, G. J. Wasserburg, and T. Wen /EPSL, pp. 353-367/

Luna 16 Sample G 36: Another Crystalline Product of an Extremely Mafic Magma
L. S. Hollister and C. G. Kulick /EPSL, pp. 312-315/

Luna 16: An Opaque Mineral Study and a Systematic Examination of Compositional Variations of Spinels from Mare Fecunditatis
S. E. Haggerty /EPSL, pp. 328-352/

Mineral and Bulk Compositions of Three Fragments from Luna 16
J. M. Steele and J. V. Smith /EPSL, pp. 323-327/

X-ray Spectral Microanalysis of Composition of Individual Lunar Regolith Particles
N. P. Il'in, L. Ye. Loseva, and V. G. Senin 145

Microprobe Studies of Three Luna 16 Basalt Fragments
R. A. F. Grieve, G. A. McKay, and D. F. Weill /EPSL, pp. 233-242/

Scanning Electron Microscopy of Lunar Regolith from the Sea of Fertility
M. K. Antoshin, N. P. Il'in, and G. V. Spivak 155

Silicate Spherules in Sample of Regolith Returned by Luna 16 Automatic Station
A. V. Ivanov, O. D. Rode, Yu. I. Stakheyev, and K. P. Florenskiy 166

Investigation of a Luna 16 Glass Bead
B. P. Glass /source not given/

Silicate Melt Inclusions and Glasses in Lunar Soil Fragments from the Luna 16 Core Sample
E. Roedder and P. W. Weiblen /EPSL, pp. 272-285/

Lithic Fragments, Glasses and Chondrules from Luna 16 Fines
K. Keil, G. Kurat, M. Prinz, and J. A. Green /EPSL, pp. 243-256/

X-ray Structural Study of Chrome-Aluminum Spinel from the Sea of Fertility
Yu. Z. Nozik and A. B. Tovbis 174

Chemical Composition of Luna 16 Lunar Regolith
A. P. Vinogradov, M. S. Chupakhin et al. 179

Determination of 29 Elements in Luna 16 Soil by Nondestructive Activation Analysis
D. Y. Jerome et al. /EPSL, pp. 436-440/

Neutron Activation Study of the Composition of Lunar Surface Material from the Sea of Fertility
Yu. A. Surkov et al. 202

Nondestructive Activation Analysis of Sample of Lunar Surface Material Returned by Luna 16 Automatic Station
M. Chayka and E. Sabo 209

Meteoritic and Nonmeteoritic Trace Elements in Luna 16 Samples
J. C. Laul, R. Ganapathy, J. W. Morgan, and E. Anders /EPSL, pp. 450-454/

Determination of Rare-earth Elements in Luna 16 Regolith Sample by Chemical-Spectral Method
N. S. Strogonova, V. A. Ryabukhin, N. V. Laktionova et al. 214

Rock-forming and Trace Elements in Lunar Surface Material from the Sea of Tranquillity and the Ocean of Storms
I. D. Shevaleyevskiy and M. S. Chupakhin 220

Bulk and Rare Earth Abundances in the Luna 16 Soil Levels A and D
D. E. Gillum, W. D. Ehmann, H. Wakita, and R. A. Schmitt /EPSL, pp. 444-449/

Rare Earths and Other Trace Elements in Luna 16 Soil
P. A. Helmke and L. A. Haskin /EPSL, pp. 441-443/

Chemical Features of the Luna 16 Regolith Sample
N. J. Hubbard, L. E. Nyquist, J. M. Rhodes, B. M. Bansal, H. Wiesmann, and S. E. Church /EPSL, pp. 423-428/

Luna 16: Some Li, K, Rb, Sr, Ba, Rare-earth, Zr, and Hf Concentrations
J. A. Philpotts, C. C. Schnetzler, M. L. Bottino, S. Schumann, and H. H. Thomas /EPSL, pp. 429-435/

X-ray Electron Study of Lunar Regolith from the Seas of Fertility and Tranquillity
A. P. Vinogradov, V. I. Nefedov et al. 224

Electron Paramagnetic Resonance of Several Lunar Rock Samples
I. N. Marov, Yu. N. Dubrov, and A. N. Yermakov 232

Mossbauer Spectroscopic Study of Luna 16 Lunar Regolith
T. V. Malysheva 238

Mossbauer Analysis of Luna 16 Lunar Surface Material
D. L. Nady, L. Cher, and K. Kulecar 250

Abundance of Mercury in Regolith of the Sea of Fertility, Sea of Tranquillity, and Ocean of Storms
Yu. I. Belyayev and T. A. Koveshnikova 253

Determination of Copper, Scandium, Molybdenum, Tin, Lead, and Iron Group Elements in Lunar Surface Material
L. I. Pavlenko, L. V. Simonova, and A. V. Karyakin 260

Determination of Volatile Anions -- Phosphorus, Sulfur, Fluorine, and Also Boron and Beryllium in Lunar Regolith by Emission Spectral Analysis
Ye. N. Savinova, A. V. Karyakin, and T. P. Andreyeva 269

Genesis of Lunar Regolith
A. P. Vinogradov 277

Results of Investigating Gases from Inclusions in Lunar Glasses
Yu. A. Dolgov and N. A. Schugurova 293

Isotopic Composition of Lithium, Potassium, Rubidium, and Strontium in Lunar Surface Material
V. G. Zaslavskiy, L. K. Levskiy, and A. N. Murin 306

Study of Isotopic Composition of Helium in the Fine Fraction of Luna 16 Lunar Surface Material
B. S. Boltenkov, V. N. Gartmanov et al. 311

Content of Lithium, Beryllium, Boron, and Titanium, and the Isotopic Composition of Lithium, Boron, and Magnesium in Luna 16 Regolith Sample
O. Eugster 320

Oxygen Isotopic Composition of the Luna 16 Soil
R. N. Clayton /EPSL, pp. 455-456/

Neutron Activation Determination of the Oxygen Content in the Luna 16 Lunar Surface Material
D. L. Nady et al. 330

Inert Gases in Sea of Fertility Regolith
A. P. Vinogradov and I. K. Zadorozhniy 334

Inert Gases in Twelve Particles and One "Dust" Sample from Luna 16
D. Heymann, A. Yaniv, and S. Lakatos /EPSL, pp. 400-406/

Rare Gas Studies in Luna 16 Fines by Stepwise Heating Techniques
W. A. Kaiser /EPSL, pp. 387-399/

Problem of Nature of Inert Gases in Lunar Surface Material
L. K. Levskiy 348

Cosmogenic Al^{26} and Na^{22} in Luna 16 Lunar Regolith
A. P. Vinogradov, A. K. Lavrukhina et al. 358

Gamma-spectrometric Analysis of Luna 16 Sample of Lunar Surface Material
Yu. A. Surkov et al. 370

Some Results of Track Method of Investigating Luna 16 Lunar Material
L. L. Kashkarov et al. 379

Neutron Capture on Gd and Sm in the Luna 16 Soil
G. P. Russ /EPSL, pp. 384-386/

Radiation Damage and Structure Recorded at High Resolution in Grains from Fine Fractions of Luna 16 Surface Material
L. Durrieu, C. Jouret et al. 388

Study of Sample of Sea of Fertility Lunar Surface Material by the Track Method
G. Poupeau et al. 400

Fossil Track and Thermoluminescence Studies of Luna 16 Material
R. Walker and D. Zimmerman /EPSL, pp. 419-422/

The Particle Track Record of the Sea of Plenty
G. M. Comstock, R. L. Fleischer, and H. R. Hart, Jr. /EPSL, pp. 407-409/

Study of Radiation Damage and Structure of Luna 16 Sample Particles Using High-Resolution Electron Microscopes
J. Borg, L. Durrieu et al. 404

Extreme Radiation Damage in Soil from Mare Fecunditatis
P. P. Phakey and P. B. Price /EPSL, pp. 410-418/

Absolute Age of Lunar Regolith Material from the Sea of Fertility
A. P. Vinogradov and Yu. M. Artemov 410

Rb-Sr Age and Content of Potassium, Rubidium, Strontium, Barium, and Rare-earths in the Surface Material from the Sea of Fertility
J. Allegre et al. 436

Rb-Sr Age of a Luna 16 Basalt and the Model Age of Lunar Soils
D. A. Papanastassiou and G. J. Wasserburg /EPSL, pp. 368-374/

U-Th-Pb Analyses of Soil from the Sea of Fertility
F. Tera and G. J. Wasserburg /EPSL, pp. 457-466/

Gas Retention and Cosmic-Ray Exposure Ages of a Basalt Fragment from Mare Fecunditatis
J. C. Huneke, F. A. Podosek, and G. J. Wasserburg /EPSL, pp. 375-383/

Optical Characteristics of Regolith from the Sea of Fertility, Sea of Tranquillity, and Ocean of Storms
I. I. Antipova-Karatayeva et al. 441

Light Scattering Indicatrices of Lunar Surface Material Returned by Luna 16 Automatic Station
N. P. Barabashov /dec./ and L. A. Akimov 449

Infrared Spectroscopy of Lunar Mare Regolith
M. V. Akhmanova et al. 453

Photometric and Polarimetric Analysis of Samples of Lunar Surface Material Returned by Luna 16 Automatic Station
A. Dollfus and E. Bowell 468

Photo-Polarization Study of Lunar Sample -- Negative Branch
A. Dollfus and E. Bowell 477

Infrared Transmission Spectra of Sea of Fertility Regolith
M. V. Akhmanova et al. 486

Cathodoluminescence of Regolith Returned by Luna 16 Automatic Station
G. V. Spivak et al. 496

Magnetic Properties of Lunar Samples Returned by Luna 16 Automatic Station
Ye. S. Gorshkov et al. 502

Metallcgraphic Study of Metallic Fragment of Lunar Surface Material
R. I. Mints et al. 512

Exoelectronic Emission of Particles of Lunar Surface Material
R. I. Mints et al. 521

Temperature Emission Spectrum of Exoelectrons of Lunar Regolith
R. I. Mints et al. 528

Heat-Physical Properties of Lunar Surface Material Returned to Earth by the Luna 16 Automatic Station
V. S. Avduyevskiy et al. 538

Results of Investigating Thermal and Electrical Properties of Lunar Surface Material and Its Analogs
A. R. Golovkin et al. 549

Results of Investigating the Physicomechanical Properties of a Sample of Lunar Surface Material in a Research Chamber in Nitrogen
A. K. Leonovich et al. 556

Investigation of Mechanical Properties of Lunar Surface Material and Its Analogs in Different Atmospheric Conditions and in Vacuum on the TOR-1 Unit
A. I. Vedenin 570

Study of Friction Properties of Lunar Surface Material and Its Analogs
Ye. A. Dukhovskoy et al. 590

Microbiological and Experimental Histological Investigation of Lunar Samples Returned by the Luna 16 Automatic Station
D. R. Kaulen et al. 597

Investigation of Biological Activity of Fine Fraction of Lunar Surface Material Returned to Earth by the Luna 16 Automatic Station
V. V. Kustov et al. 606

Investigation of Biological Action of Lunar Surface Material Returned to Earth by Luna 16 Automatic Station
V. V. Antipov 613

REPRODUCIBILITY OF THE ORIGINAL PAGE IS POOR

N75 11815

ORIGINAL SCRIPTS
COLOR ILLUSTRATIONS

PRELIMINARY DATA ON LUNAR SURFACE MATERIAL RETURNED BY LUNA 16 AUTOMATIC STATION

/7

A. P. Vinogradov

Abstract

Results of preliminary investigations of a sample of lunar surface material returned by Luna 16 automatic station are reported. Information on the granulometric characteristics of regolith, its optical properties, types of its constituent rocks, and its mineral composition is given. The chemical composition of major and trace elements for different sections of the core and for the lunar basalt was determined. Isotopic composition of inert gases and of several elements was studied. The Rb/Sr age was determined at 4.85-4.25 billion years.

As already known, the Luna 16 automatic station returned a sample of lunar surface material taken in the Sea of Fertility, in its northeastern part, at the point with coordinates 0°41' S. Lat and 56°18' E. Long, approximately 100 km west of Webb Crater (Fig. 1).

The Sea of Fertility bears traces of a relatively quiet descent; its shores do not have a circular mountainous rimming and has broken contours. The mare is a plain with ramified-type shallow (100-300 m) ridges running through it. There are no ray systems of large craters in this section. The lunar surface material of the Sea of Fertility characterizes the new region of the "mare" surface of the Moon. Thus, the three broad maria on the visible side located along the lunar equator: Sea of Tranquillity (Apollo 11 samples), Ocean of Storms (Apollo 12 samples), and Sea of Fertility (Luna 16 samples) -- make it possible to quite fully represent the character of the surface rocks of the Moon.

The friable surface material of the Sea of Fertility -- -- regolith -- was taken with a drill, which was driven 35 cm

into the rock. Below this it touched solid rock or individual large fragments of rock. The regolith core filled the drill. In the helium chamber the core of friable surface material -- regolith -- was transferred into a receiving tray and had no visible stratification, appearing to be homogeneous (Fig. 2). Only a small part of the surface material at the face, at a depth of 35 cm, was made up of coarse-grained material. The total weight of the regolith returned by Luna 16 was 101 g. The regolith as a whole consisted of inequigranular dark-gray (blackish) powder, which was easily shaped or agglomerated into separate loose clods. The grains were either fused, rounded, or angular. The grain size of the regolith increased with depth: average grain dimensions of about 0.1 mm predominated. The numerical distribution of the grains corresponded closely to the exponential law which the distribution of particles obeys in multiple crushing. The median size of the grains increases downward from the surface into the regolith in the range 70-120 μm. On this basis and from the nature of the regolith core, it can be divided into several zones: A, B, V, G, and D. The regolith in each core underwent study. The zones A and B, fine-grained material with small content of coarse fraction, occupied 0 to 15 cm of the core length. Zones V, and G, inequigranular material with inclusions of rock fragments and other particles greater than 3 mm in size occupied 15-33 cm of the core length. The zone D -- coarse-grained material -- occupied 33-35 cm of the length (Fig. 3).

Thus, the thickness of the regolith in the Sea of Fertility, at the sampling point, is small, about 35 cm and, possibly, extends to 0.5-1 m or somewhat more than 1 m, similar to the thickness of the regolith in the Ocean of Storms, which is assumed to be about 1-3 m, while it is assumed to be 6 m for the Sea of Tranquillity. It is probable that thus far we do not know the true mean thickness of the regolith.

Study of physical properties shows that the regolith has a specific weight in situ of about 1.17 (1.20) g/cm^3.

By mechanical compaction, its density can be brought to 2.3 /8 g/cm^3. The specific heat capacity is 0.17 kcal/kg·deg, thermal conductivity $1.9 \cdot 10^{-3}$ kcal/m·hr·deg, specific electrical resistance $3.42 \cdot 10^6$ ohms·m, and so on. This refers to the regolith not in situ, but under the condition that the ambient pressure is 10^{-5} torr and the load on the regolith is 160 kg/m^2.

Optical properties were determined. For the Sea of Fertility, the albedo averages 0.069, and in the immediate proximity to the Luna 16 landing site -- 0.105. The direct determination of regolith with the sample gave 0.107. The normal albedo is somewhat increased

in red light: 0.086 in the ultraviolet region, 0.126 in the near infrared, and 0.107 in the visible spectral region. Based on the indicatrices of reflection, a specular component is clearly noticeable, and the angle of maximum reflection of light is somewhat greater than the angle of incidence. This regularity becomes stronger with increase in the wavelength of light and with decrease in the angle of illumination.

Friable surface material of the lunar maria, regolith, under microscopic examination is highly contrasty compared with the friable surface material of the Earth. The regolith is also not similar to the pumice of terrestrial volcanoes. Two main particle modifications can be singled out: particles of primary magmatic surface rocks of the basalt type, which we indicated also based on the data of gamma spectra of the lunar surface obtained by the Luna 10 automatic station in 1966, and particles subjected to appreciable transformations on the lunar surface. Whereas characteristic of the first is the surprisingly fresh appearance, observed on Earth only for freshly crushed samples of unchanged rocks, they show practically no roundedness, and have angular forms, the latter kind of particles have clear traces of fusion -- -- sintered particles of complex configuration, vitrified from the surface, considerable numbers of spherical fused formations -- -- like cooled droplets, of glassy and metallic appearance, resembling "cosmic spherules" on Earth. This indicates that they were formed from liquid and cooled rapidly. Under the microscope, regolith particles are shown in the color Plate II, 2, and in the color Plate III various particles are collected into groups: gabbro, basalts, anorthosites, breccias, slags, sinters, glasses, and single grains, spherules, and various particles (see also Fig. 4). With the scanning electron microscope it can be seen (Fig. 5 and 6) how the large silicate particles are agglomerated with a small fraction of other particles. The content of various particles up to the + 0.45 mm regolith fraction is shown in Table 1.

Particles of basalt rocks are of at least two types characterizing the conditions of the cooling of the basalt melt -- fine-grained basalts (containing glass) and coarse-grained basalts of the gabbroid type (corresponding to color plates VII, 1, 2, and VIII, 1, 2). They are of ophitic texture and constitute about one-fourth of the entire coarse-grained fraction (above 0.45 mm). The primary minerals of these rocks are plagioclases, pyroxenes, ilmenite, and less often olivine. Their relative content varies appreciable in different particles; thus, we can already state that on the Moon there had been a volcanic process with the outflow of basalts and obviously the formation of the lunar crust, whose thickness is not yet exactly known.

In our view, this universal process of outflow of fusible material from the lunar interior (with outgassing) follow the

TABLE 1. DISTRIBUTION OF PARTICLES OF DIFFERENT ROCKS IN THE + 0.45 mm FRACTION FOR THE ZONES A, B, V, AND G (IN PERCENT)

Rocks	A	B	V	G
Gabbro	13,1	17,5	8,1	15,2
Basalt	7,3	9,0	4,9	7,9
Anorthosite	1,1	3,7	2,5	4,5
Breccias	33,9	41,4	35,5	8,3
Slags and sinters	40,0	17,5	41,8	53,5
Glasses and single grains	2,3	4,0	6,2	6,1
Spherules	1,2	1,3	1,2	1,6
Various particles	1,2	5,7	—	2,6
Total no. of particles	838	297	2351	755
Weight of fraction, g.	0,230	0,100	0,560	0,260

mechanism of zone melting. Feldspar rocks (anorthosites) and white crystalline grains are also encountered. Their content is low. Their origin on Earth as well is not very clear.

Breccias are cemented, lithified rocks formed through the compaction of finely crushed regolith material and containing in different proportions all the constituents, including particles of primary magmatic rocks, iron-nickel melt, and so on. A rounded particle shape is noted for some breccias, while sometimes also slight compaction, which leads to their easy disintegration. Breccias are magnetic; they comprise up to 40 percent of the total number of particles.

Slags and sinters are fine sintered particles forming aggregates of highly complex irregular dendritic shape. Their composition includes all constituents of the regolith. /10

Glasses and vitrified and slagged particles are widely distributed; at least half of all regolith particles are fused or slagged on one or several sides. Depending on the composition (content of Fe and Ti, and so on), they are different in color -- -- dark-brown to black. Vesicular slagged melting is also encountered, as well as smooth glazed vitrifying. This is the typical lunar melting occurring in the instantaneous heating of a particle that is cold as a whole.

The cooled droplets are spherules and similar formations. Spherules of different shape -- pear-shaped, dumbbell-shaped --

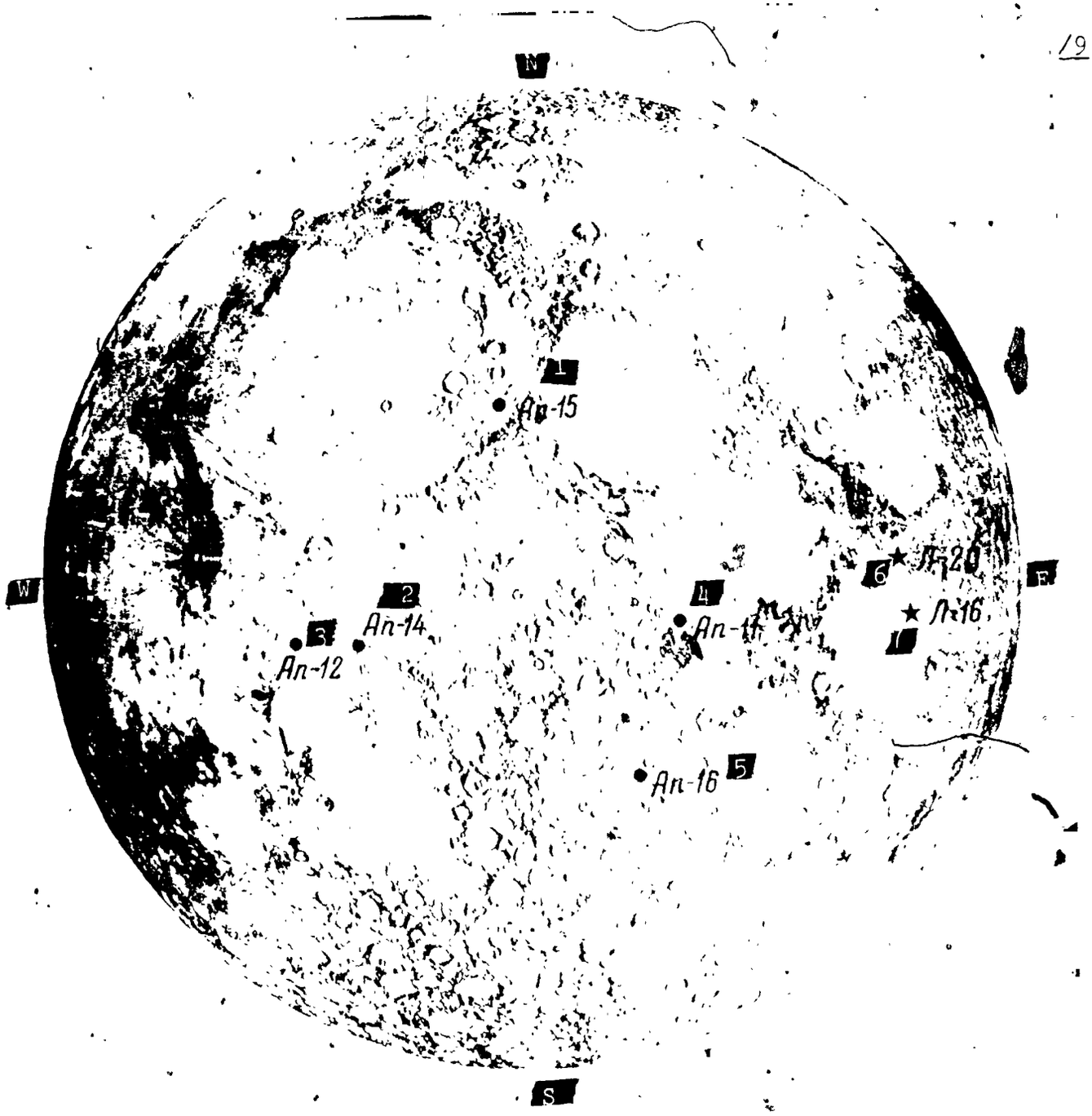

Fig. 1. Map of Moon

/Key on following page/

/Key to Fig. 1 on preceding page./

KEY: 1. Apollo 15
2. Apollo 14
3. Apollo 12
4. Apollo 11
5. Apollo 16
6. Luna 20
7. Luna 16

are in color clear, cloudy white, greenish, yellow-brown, opaque, and often hollow. Their lustre ranges from glassy to metallic. Their number increases in the fine fractions. They are formed at temperatures considerably exceeding the melting point of the rocks when they were splashed in the molten state.

Finally, grains of individual minerals are encountered: plagioclase, olivine, anorthite, pyroxene, spinels, ilmenite, and iron particles. We will turn to the iron-nickel particles in regolith later. An idea of the content of various minerals in regolith is given by Table 2. From the table it follows that the content, for example, of olivine generally is quite appreciable and resembles its content in the regolith of Apollo 12 samples, while the content of olivine in Apollo 11 samples is considerably less. But the content, for example, of ilmenite is close to its content in the Apollo 12 samples, while it is much more evident in the Apollo 11 samples than in the Luna 16 and Apollo 12 samples. Olivine is present in regolith only in the form of individual monocrystalline fragments of irregular shape (acute-angled pieces), of different coloring, and also included in gabbro particles. X-ray diffraction patterns indicate the absence of lattice deformation and twinning effects, that is, the absence of lattice stress. This is the ordinary alpha-modification of olivine and is characterized by the disordered distribution of magnesium and iron atoms in the structure. As we can see from the data of micro-x-ray spectral analysis of a section of a similar silicate particle, /11 it has the following composition (in weight percent):

SiO_2	36,0	Al_2O_3	0,05
MgO	27,5	TiO_2	<0,01
FeO	33,8	CoO	0,03
CaO	0,38	NiO	<0,01
MnO	0,29		
Cr_2O_3	0,15		Σ 98,2

This is a homogeneous olivine crystal, whose iron content is 40 mole percent Fe_2SiO_4; the composition corresponds to the following molecular formula: $/Mg_{1.14}Fe_{0.79}$ (Ca, Mg, Cr)$_{0.02}/SiO_4$.

The most widely distributed regolith mineral is anorthite, followed by augite and ilmenite. Anorthite is encountered as fine-grained aggregates in samples of basalt and gabbro, spherules, and in the fine regolith fraction. No isolated monocrystals were

Fig. 2. Photograph of lunar surface material on tray in receiving chamber. The coarser-grained material is visible in the deep section of the core, on the tray.

found. Plagioclase is also found as a monocrystal of triclinic symmetry. Pyroxenes of the augite-pigeonite type are encountered in rock fragments where in several cases they play the main role in gabbro basalts. X-ray spectral analysis was used to study the distribution of elements in basalt sections, which assisted in identifying the minerals (Fig. 7).

Ilmenite was found in the gross regolith sample, sometimes in intergrowths with augite. Chromian spinel was found in the form of dark monocrystals. As for magnetic material, we can present the micro-x-ray spectral analysis of sample 3-4 b. Analysis from the surface (without preparation of the section) revealed uneven distribution of Fe, Ni, Cr, Ti, Si, Al, Mg, and Ca. Zones with rock-forming elements and zones with increased concentrations of Fe and Ni were distinguished -- Fe ~ 6 percent and Ni ~ 1 percent (Fig. 8). Several points iron content up to 66 percent, and nickel content up to 6 percent was observed. However, Mossbauer spectroscopy did not disclose Ni /12 in magnetic particles. X-ray analysis of iron particles revealed alpha-iron, that is, kamacite. No taenite was found. The volume of iron particles did not reach 1 percent in the regolith. It is at present difficult to say anything definite about the origin of these particles. As we will see further, the amount of nickel in regolith compared with its content in monolithic rock (basalts) increases in the case of Luna 16 material and also Apollo 11 and Apollo 12 material, by an average of five times, but cobalt increases only by a maximum of 1.5 times. Still, we see a very low content of platinoids in regolith, while in iron meteorites they are many hundreds of times more evident than in rocks. Chemical analysis was performed in parallel with x-ray spectral (principally of the primary elements), mass-spectral (all elements), and spectral and activation methods, by sampling for individual elements (Table 3).

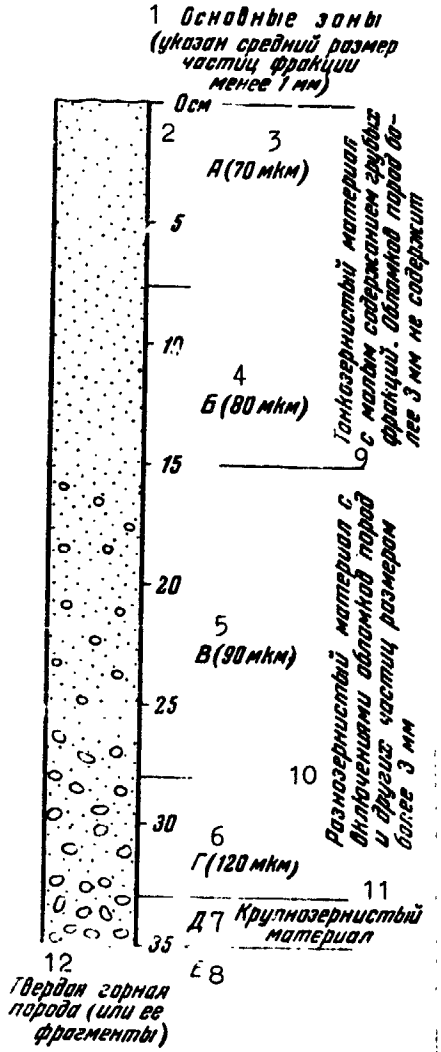

Fig. 3. Schematic core of lunar surface material

KEY:
1. Main zones (the mean particle size of the fraction smaller than 1 mm is indicated)
2. 0, cm
3. 70 μm
4. B (80 μm)
5. V (90 μm)
6. G (120 μm)
7. D
8. Ye
9. Fine-grained material with low content of coarse fractions. No rock fragments larger than 3 mm are present.
10. Inequigranular material with inclusions of rock fragments and other particles greater than 3 mm in size
11. Coarse-grained material
12. Solid rock (or its fragments)

As we see, fluctuations in the principal composition of regolith at the four levels are slight. Much more appreciable is the difference in compositions between regolith and basalt rock. If we compare the composition of Luna 16 rocks with the lunar rock samples of Apollo 11 and Apollo 12, the differences as a whole are also small, with the exception of the content of Ti, Zr, and several other chemical elements present in small amounts in lunar rocks (trace elements; Table 4). /13

The high content of F, S, Cl, and other volatiles, which dissipate from the Moon, bears noting. However, vacuoles possibly containing the common gases are observed in regolith particles; they are under investigation.

A comparison of the chemical composition of regolith and monolithic rocks from the three maria indicates that the material everywhere has the same character with compositional variation in both regolith and monolithic rocks. The most decided difference in the composition of Luna 16 rocks consists of the low Ti content. It is virtually identical with Ocean of Storms rocks (Apollo 12), or nearly half the value for rocks from the Sea of Tranquillity. The variations in Mg and Fe content are small (Table 5). /15

TABLE 2. RESULTS OF MEASUREMENTS OF MOSSBAUER SPECTRA OF LUNAR MATERIAL /10

Minerals	Fraction of total area of Mossbauer spectrum of iron-containing mineral, %: Our measurements			US (Apollo 11)	
	A-3	A-3	G-8, +0.20—0.45	84-14	45-24
Ilmenite	7.7	8.7	9.2	19.7	26.9
Pyroxene	69.0	71.5	65.1	67.6	60.8
Olivine	18.8	16.7	25.5	4.4	6.1
Iron	4.5	3.1	Not calc.	5.8	2.1
Troilite	⩽1	⩽1	⩽1	⩽1	⩽2
Magnesite	⩽2	⩽2	⩽2	1.4	2.1

The largest amount of Zr was noted in the crystalline rocks of the Sea of Fertility, where there is much Ti, Y, and Sc. The content of most major elements, as well as Ni and many trace elements are virtually identical in the three maria. Surprisingly identical is the content of Ni in the regolith of the three maria. Of greatest interest are the compositional differences of regolith and the parent rock of the same sea. These differences are repeated for the three maria. For example, the content of Fe, Ti, and Zr is always higher in the parent rock than in the regolith. But the content of Ni is always higher in the regolith than in the crystalline rock. Correspondences in Ti content in crystalline rocks and in the regolith indicated that the regolith was formed in situ and was not brought in from somewhere distant (like volcanic pumices). The amount of Ca as well as Al_2O_3 increases in the regolith. Thus, the regolith is rich in plagioclase and poor in pyroxene, olivine, and ilmenite (and in spinel); that is, crystalline rocks are more mafic than regolith. Rare lithophilic elements are present mostly in the crystalline rocks of the Sea of Tranquillity -- Y, TR, Zr, and Sc. This is also true of Th and U (Table 6). /15

We have already discussed the low content of platinoids and gold in regolith. Data are not yet very numerous in this direction, but we can see the following distribution of platinoids and gold in lunar rocks (Table 7).

The determination of all rare earth is not yet complete. Isotopic analysis of Li^7/Li^6 for regolith gives 12.28; K^{39}/K^{41} -- 14.00 $\pm$ 0.18; and for Rb^{85}/Rb^{87} (mean sample) -- 2.57 $\pm$ 0.04, that is, the isotopic composition corresponds to the isotopic composition of these elements on Earth. At the same time, a disturbance of isotopic composition in meteorites is observed, for example, for lithium.

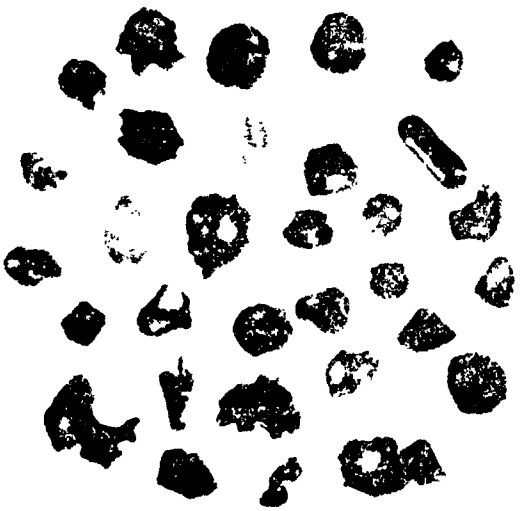

Fig. 4. Various types of particles: spherules and spherical formations, glasses, sinters

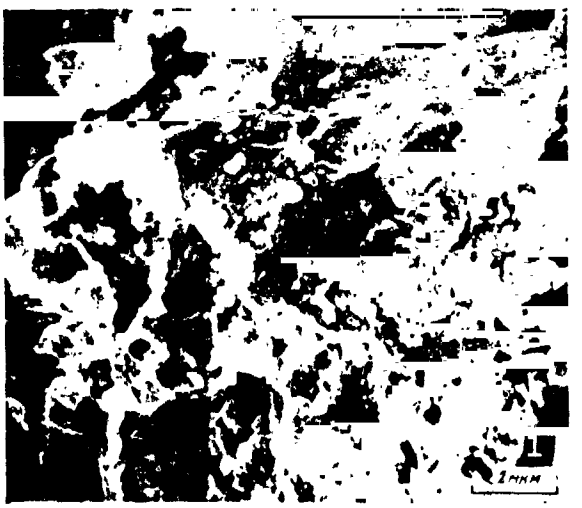

Fig. 5. Photograph of particles of fine regolith fraction obtained with scanning electron microscope using secondary electrons. Finer silicate particles adhere to the large silicate ones

KEY: 1. 2 μm

As we know, under the effect of solar wind spallation products appear. They were found in the regolith -- Na^{22}, Al^{26}, and so on. For example, Al^{26} yields 173 ± 113 disintegration/min·kg. This study is continuing, and we would wish to have data both for the zone A fraction, as well as for the zone G fraction of the deeper part of the regolith core. This would make it possible to explain a great deal.

Not without interest in this respect is the fact that the IR /infrared/ structure of regolith showed the presence of a broad featureless absorption band in the region of vibration of silicon-oxygen bonds. Calcining of a regolith sample in argon to 1000° C led to the appearance in the IR spectrum of a well-defined structure -- individual bands associated with the absorption of isolated and connected SiO_4 groups, phyllosilicate, and so on. Therefore, it can be hypothesized that regolithic material was once irradiated and that the possible changes resulting from this are removed by calcining.

Solar wind acts on the rock, causing it to become metamict and to form spallation products at a shallow depth -- 3-5 cm. Therefore we decided to measure the induced activity both in the upper layers of the regolith as well as at its base. The results may explain the history of regolith accumulation.

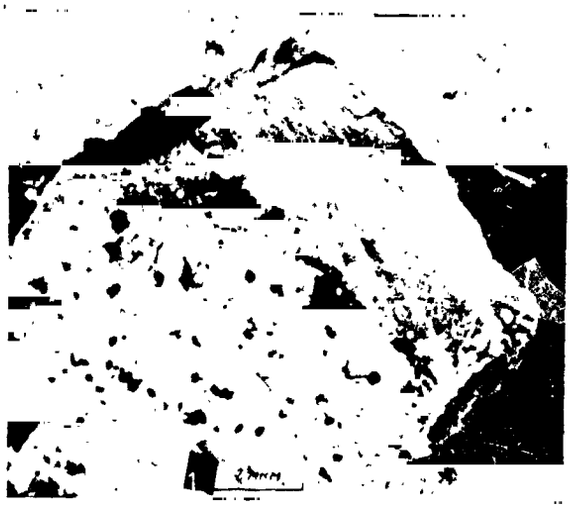

Fig. 6. Photograph of particles of fine regolith fraction obtained with a scanning electron microscope using secondary electrons. The large silicate particles with near-hexagonal cross section and traces of growth on surfaces are sprinkled with very fine material. KEY: 1. 2 μm

The regolith contained inert gases of unusual composition, whose content does not depend on the regolith depth (the regolith sample pertains to zone G; Table 8).

The dominant gas constituent is represented by solar wind gases. Their composition differs widely from the composition of terrestrial gases and meteoritic gases. The concentration of the gases is very high, several orders higher than in Earth materials and in meteorites. The content of He and [illegible] coincides with their content in several neutral gas-rich meteorites. The isotopic composition of Ar differs particularly, for example, $Ar^{40}/Ar^{36} \sim 1$, $Ar^{36}/Ar^{38} \sim 5.25$ -- corresponding to the terrestrial value. The amount of Ar^{40} is 4-5 times greater than its amount that could be formed in rocks due to the decay of K^{40}. The isotopic composition of Xe also differs from the terrestrial value and is studied further. In content of inert gases, material from the Sea of Fertility is closer to their content in the regolith of the Sea of Tranquillity. The first determinations of the age of the Moon were obtained by the Rb/Sr method, and firstly for the fine regolith fraction, which yielded $4.85 \cdot 10^9$ to $4.25 \cdot 10^9 \pm 0.75 \cdot 10^9$ years. The isochron mean is 4.45 and $4.65 \cdot 10^9 \pm 0.5 \cdot 10^9$ years. Thus, samples of three maria are very similar in absolute age, that is, the age of the Moon corresponds to the age of Earth. The same values were obtained for Pb^{206}/Pb^{207}. The age based on the K/Ar method is difficult to compute. Of particular interest is the exposure age of the regolith.

Thus, lunar rocks from the three maria are of the same general type -- basaltic, and their compositional variations depend on the conditions of melting out, while the variations in the composition of the regolith depends on its somewhat different history thereafter.

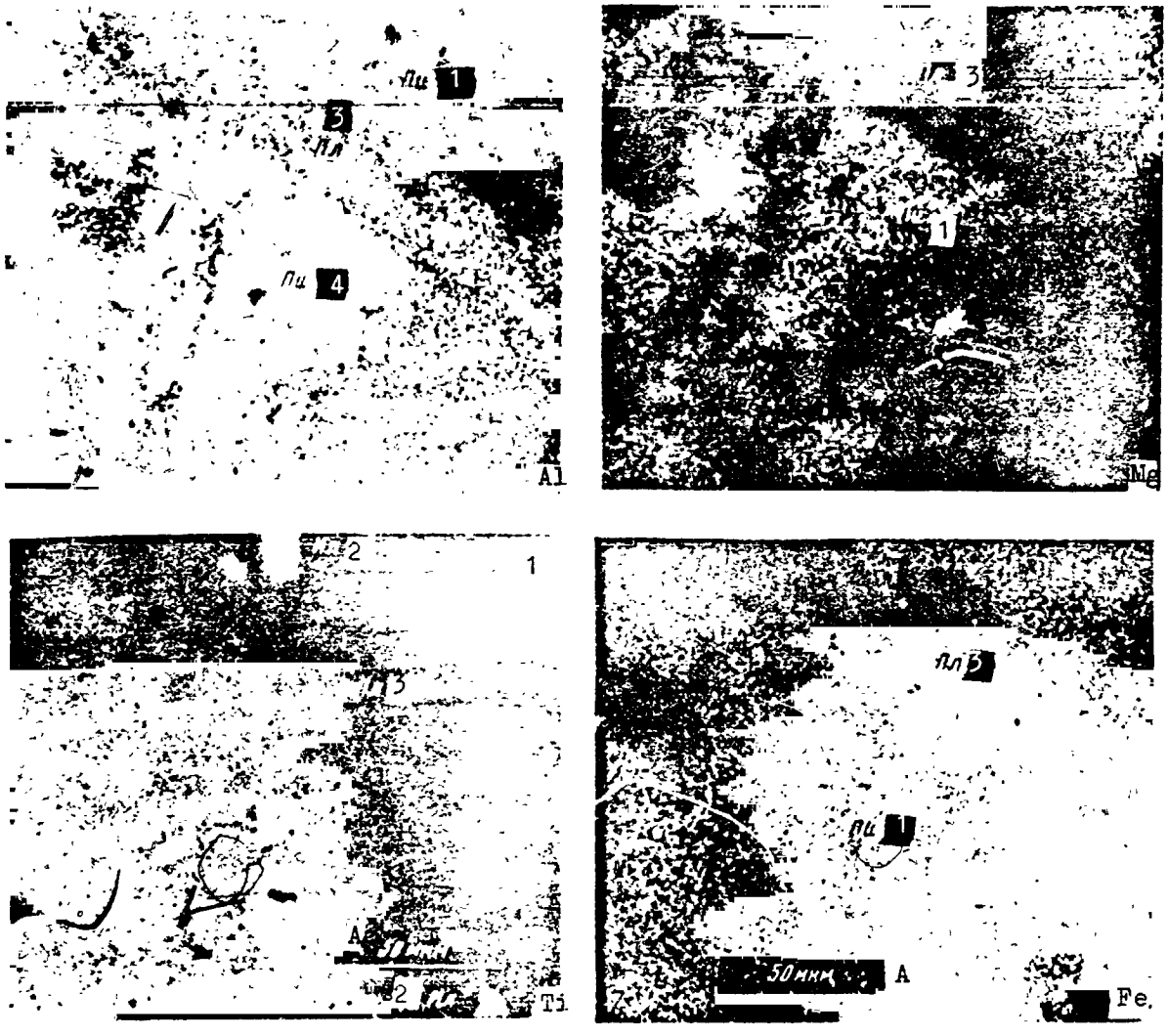

/12

Fig. 7. Photographs of area of section of coarse-grained basalt (gabbro) obtained on an x-ray microanalyzer Minerals: 1. Pyroxene; 2. Ilmenite; 3. Plagioclase; patterns of distribution of alumirum, magnesium, titanium, and iron

KEY: A. 50 μm

The rocks of the Sea of Fertility, as we have seen, are closer to the composition of the Ocean of Storms rocks. However, in content of neutral gases in the regolith they are closer to the Sea of Tranquillity regolith. /17

Let us turn to several preliminary considerations. It is as yet premature to state a final concept on the nature of processes on the lunar surface. We will adhere to data obtained from a study of the Luna 16 rock samples from the Sea of Fertility and, naturally,

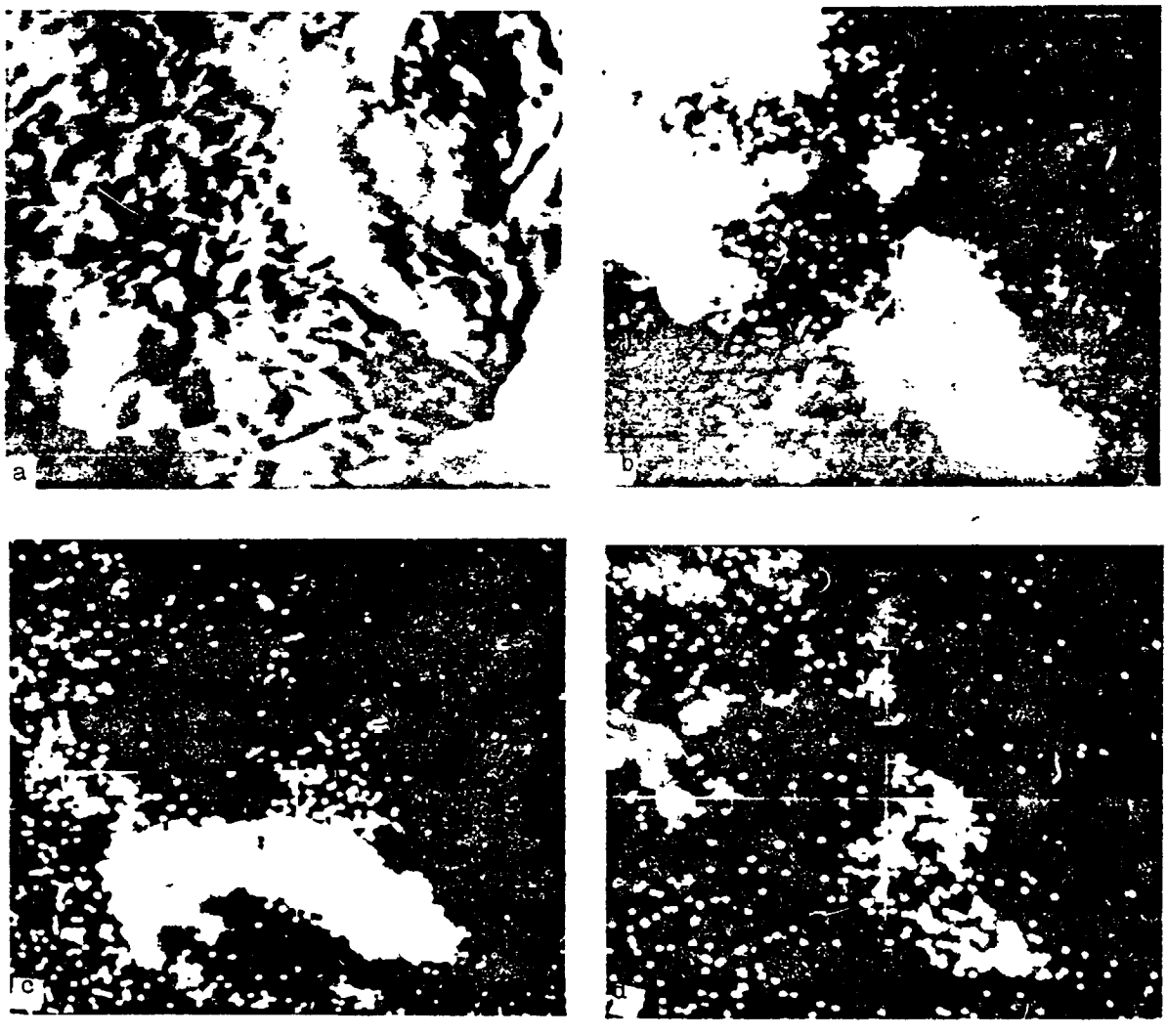

Fig. 8. Scanning photographs of magnetic particle recorded on an x-ray microanalyzer
a. Image in absorbed electrons; b. Pattern of iron distribution; c. silicon; d. nickel

we will compare these data with the data obtained from the flights of Apollo 11 and Apollo 12. The material of all three maria -- -- Sea of Tranquillity, Ocean of Storms, and Sea of Fertility -- is amazingly close in its petrological, mineralogical, and chemical compositions, although the details do differ. The enormous lunar maria lying along the lunar equator are depressions that were once filled with primary lava. In ancient times, in the era of intensive vulcanism on the Moon, a vast mass of basaltic rocks accompanied by the dissipation of gases poured over the surface. Depending on the conditions of outflow, depth, and temperature, a certain diversity

TABLE 3. CONTENT OF MACROELEMENTS IN THE REGOLITH FRACTION OF ZONES A, B, V, AND G (IN WEIGHT PERCENT)

Component	Regolith				Basalt
	A	B	V	G	
SiO_2	41,7	41,2	42,5	41,3	43,8
Al_2O_3	15,32	15,40	15,45	15,15	13,65
FeO	16,80	16,55	16,30	16,90	19,35
CaO	12,20	12,80	12,42	12,55	10,40
MgO	8,73	8,82	8,96	8,60	7,05
TiO_2	3,39	3,46	3,30	3,42	4,90
ZrO_2	0,015	—	0,013	—	0,04
Cr_2O_3	0,31	0,25	0,30	0,26	0,28
MnO	0,21	0,20	0,20	0,22	0,20
Na_2O	0,37	0,36	0,36	0,28	0,33
K_2O	0,10	0,12	0,10	0,10	0,15
S	0,19	0,20	0,18	0,25	0,17

of a single basaltic type of surface lunar rocks was produced in terms of the content of Fe, Ti, Zr, Ba, and other elements. The ferruginicity of the magma was very important in this endogenic process. It is possible that derivatives of basalts (anorthosites, rhyolites, and so on) will be encountered on the Moon. We do not know exactly the thickness of the basaltic crust of the Moon.

The absolute age of the surface rocks of the Moon, more exactly, the age of the Moon, compares virtually exactly with the age of the Earth. The lunar maria are covered with a layer of regolith. Its thickness evidently has changed considerably and it is no more than 0.5 m in the Sea of Fertility, at the Luna 16 sampling site. The limits of the fluctuation probably amount to several meters. The regolith, as we have already seen, is a nonhomogeneous mixture of grains of rock, minerals of different sizes, shape, and coloration, of both fused and angular particles. With increasing depth, the ratio between different grains changes, although no stratification of the material can be noted. This material is the result of the grinding of rock in conditions of exposure to high temperature, causing the formation not only of fused regolith particles, but also the formation of spheroids. The regolith is not similar to volcanic sand of terrestrial volcanoes. The composition of the regolith, as we have seen, differs somewhat from the composition of crystalline lunar rocks. It contains a reduced amount of mafic elements and therefore must be more fusible than the primary basaltic rock. Before we deal with the problem of the formation of the regolith, let us recall the main factors of lunar "weathering." These involve, first of all, temperature fluctuations in the surface rocks of the Moon

TABLE 4. CONTENT OF TRACE ELEMENTS IN LUNA 16 ROCKS (MASS SPECTRAL AND SPECTRAL DETERMINATIONS: IN PPM) /14

Element	Regolith A	Regolith B	Regolith V	Regolith G	Basalt
Li*	—	10	—	10	—
Be*	—	2,8	2	2,7	—
F	265	292	246	277	181
B	4,5	3,9	6	4,6	5
P	—	254	—	200	511
Sc	27	33	23,3	25	20
Cl	66	74	36	72	—
V	64	73,5	55,3	55	42,5
Co	68	56	44	61	29
Ni	190	137	250	178	147
Cu	36	39,8	35	36	13
Zn	10	20	33	21,5	26
Rb	3	6,3	5,5	—	—
Sr	90	156	—	182	445
Cs	0,05	0,26	—	0,08	0,75
Zr	350	334	354	346	—
Hf	1,1	3,6	1,2	1	0,3
Mo	7	12	3,6	5	1,2

Element	Regolith A	Regolith B	Regolith V	Regolith G	Basalt
Ga	11	—	4,9	—	1,2
Ge	1,3	1,2	1,2	1,5	2,5
As	0,4	0,36	0,6	0,3	2,9
Se	0,45	0,5	—	0,4	0,7
Br	0,26	0,27	0,24	0,33	1,3
Ru	0,03	0,044	0,01	—	6
Rh	—	0,0037	—	—	—
Pd	0,0096	0,012	—	0,01	0,027
Ag*	0,05	0,059	0,02	0,07	0,2
Cd	1	0,75	1	1,3	—
In	0,06	0,025	0,086	0,08	—
Ba	42	259	37	48	206
Sn	1,6	1,4	—	2	4
Sb	0,4	0,3	0,7	0,35	0,5
Te	0,2	—	0,15	0,2	—
W	—	4,7	5,3	3,5	9
Au	0,0033	0,0013	0,003	—	—
Tl	0,3	0,2	—	0,5	—

Element	Regolith A	Regolith B	Regolith V	Regolith G	Basalt
Pb	6,4	6,6	7	6	7,7
I	0,15	—	0,26	0,14	—
Y	5	49	50	56	58
La	27,3	8	7,4	7,2	7,7
Ce	1	26	24	23	24,6
Pr	4,5	4,7	4,6	4,5	4,8
Nd	20	28	21	23	25
Sm	5,6	6,8	6,2	6,8	7,1
Eu	1,6	1,2	1,3	1,4	1,2
Gd	6,0	4,7	4,6	5,8	4,8
Tb	0,75	1,0	0,9	0,9	0,9
Dy	5,0	5,3	5,0	5,0	5,2
Ho	2,0	2,2	1,9	1,8	2,0
Er	5,0	5,0	5,0	4,7	5,0
Tm	0,4	0,4	0,4	0,4	0,4
Yb	3,5	3,6	3,5	3,5	3,6
Lu	0,28	0,3	0,3	0,3	0,3
—	—	—	—	—	—

* Spectral determination

over billions of years from lunar day to lunar night -- in a temperature range of about ± 100° C. Then follows the irradiation of the surface lunar rocks by solar wind and galactic cosmic rays. Next comes the vacuum in which lunar rocks exist, and, finally, possible meteoric impacts. It is probable that the temperature fluctuations in surface lunar rocks in some way affect their strength, but we cannot estimate this at present. A considerably greater effect is caused by solar wind and galactic radiation. First of all, based on our observations it would follow that the entire regolith to a depth of 35 cm bears signs of having been affected by solar wind. In the sample from zone G the regolith contains a large amount of neutral solar gases. On the other hand, based on the infrared spectrum of the regolith signs of its irradiation were observed. Finally, we must await determinations of radioactive spallation products from the deeper regolith layers. This all preliminarily indicates either the mixing of regolith in situ or that the history of its formation is written in the regolith layerwise.

Irradiation does not penetrate deeply; it covers only the first several centimeters of the surface material. Based on observations and the study of the so-called metamicticity in minerals containing radioactive elements, it follows that they lose strength, that their crystal lattices undergo deformation,

TABLE 5. COMPARISON OF COMPOSITION OF REGOLITH AND CRYSTALLINE ROCKS FROM THREE MARIA (MACROELEMENTS, IN PERCENT, TRACE ELEMENTS IN PPM)

Components	Crystalline Rocks			Regolith		
	Sea of Tranq. Apollo 11 collection	Ocean of Storms Apollo 12 coll.	Sea of Fertility Luna 16 coll.	Sea of Tranq. Apollo 11 collection (mean)	Ocean of Storms Apollo 12 coll.	Sea of Fertility Luna 16 (mean)
SiO_2	41	45	43,8	43	42	41,7
Al_2O_3	12	11,2	13,65	13	14	15,33
TiO_2	10	3,7	4,9	7	3,1	3,39
FeO	19	21,3	19,35	16	17	16,64
MgO	8	11,7	7,05	8	12	8,78
CaO	10	10,7	10,4	12	10	12,49
Na_2O	0,5	0,95	0,38	0,54	0,4	0,34
K_2O	0,12	0,065	0,15	0,12	0,18	0,10
MnO	0,4	0,26	0,20	0,23	0,25	0,21
Cr_2O_3	0,6	0,55	0,28	0,37	0,41	0,28
ZrO_2	0,1	0,023	0,04	0,05	0,09	0,013
NiO	(0,007)	—	0,04	0,03	0,025	—
Rb	2,5	0,64	—	2,2	3,2	5,9
Ba	90	72	206	68	420	114
Sr	110	145	445	99	170	169
Yb	2,5	—	3,5	2,5	—	3,5
Y	250	51	54,0	130	130	58,0
Zr	700	170	300	400	670	347
V	45	88	42,5	42	64	61
Sc	110	50	20	55	47	27
Ni	55	54	147	250	200	190
Co	9	40	29	18	42	54
Cu	5	—	13	—	—	37
Li	15	5,5	—	15	11	10*
Ga	6	—	11	—	—	4,9

*Spectrally, all the rest -- mass spectrally.

and so on. However, this usually does not lead to the total disintegration of minerals. We attempted to find metamicticity in regolith particles. Still, irradiation begins its work primarily when the material has already been disintegrated. Therefore solar wind has no direct participation in the disintegration of the material in regolith formation (its fusion), but does affect the strength of the material. Usually the formation of the lunar maria and, therefore, above all the regolith which fills them is associated with the action of impacting meteorites, with their impacts. It is curious to represent the process of the falling of a meteor shower on the side of the Moon facing the Earth in the region of present-day lunar maria located along the equator. Why did they fall in showers only on the visible surface of the Moon that is most convex toward the Earth? This is difficult to explain. The most reliable proof of the "work" of meteorites would be their discovery on the surface of the Moon. /18

TABLE 6. CONTENT OF Th AND U (IN PPM) AND Th/U RATIO

Elements	Regolith			Crystalline rocks		
	Apollo 11	Apollo 12	Luna 16	Apollo 11	Apollo 12	Luna 16
Th	2,24±0,06	6,0±0,6	0,474±0,05	2,9±0,4	0,88±0,09	1,14±0,1
U	0,59±0,02	1,5±0,2	0,1±0,01	0,7±0,1	0,24±0,035	0,2±0,02
Th/U	3,8	4,0	4,7	4,0	3,7	5,7

TABLE 7. DISTRIBUTION OF PLATINOIDS AND GOLD IN LUNAR ROCKS (IN PPM)

Rocks	Pt	Pd	Ir	Ru	Rh	Au
Terrestrial basalts	0,02	0,02	—	—	—	0,004
Lunar crystalline rocks						
Apollo 11 collection	—	0,006*	0,0001—0,01	—	—	—
Apollo 12 collection	—	0,1[2*]	—	—	—	0,0016[4*]
Luna 16 collection	—	—	0,0013[3*]	—	—	0,0011[3*]
In the regolith	—	0,027	—	6,3	—	—
Apollo 11 collection	—	0,04[3*]	—	—	—	0,0021[4*]
Apollo 12 collection	—	0,01	—	0,027	0,0037	0,002
Luna 16 collection	12,0	3,7	2,8	—	—	1,0

*Baedecker, Wasson, Sci. 167(3918), (1970)
2* Morrison et al, Sci. 167(3918), (1970)
3* Laul, Keays, Ganapathy, Anders, Earth a. Planetary Sci. Letters 9(2), (1970)
4* Wanke et al., Sci. 167(3918), (1970)

However, meteorites and micrometeorites fly toward the Moon at cosmic velocities. Experiment and calculation shows that 1 g of meteoric material is capable under these conditions of exploding 2-3 times as much material of lunar rock, crushing them, and so on. During this process the rock particles fly off at enormous velocities, with a wide velocity spectrum. Some of them can leave the Moon, escaping from its gravity field and land on Earth (for example, eucrites). We must always remember this situation of the material balance of the Moon when we attempt to explain the formation of the regolith. However, some portion, even though very small, of the meteoritic material remains on the lunar surface. Above we presented preliminary data on the finding

TABLE 8. CONTENT AND ISOTOPIC COMPOSITION OF INERT GASES IN DUST SAMPLES (IN 10^{-8} cm^3)

Isotope	Sea of Fertility, sample G-7	Apollo 11		
		Schaffer, Zaringer	Reynolds	Hintenberger
He^4	18 000 000	11 000 000–19 000 000	20 000 000	9 000 000
He^4/He^3	2 670	2 540	2 130	2 770
Ne^{20}	340 000	313 000	530 000	125 000
Ne^{20}/Ne^{22}	12,80	12,4	12,85	12,6
Ne^{21}/Ne^{22}	0,00332	0,0340	0,00332	0,0352
Ar^{40}	53 000	38 500	57 000	56 000
Ar^{40}/Ar^{36}	0,98	1,1	1,126	3,04
Ar^{36}/Ar^{38}	5,26	5,20	5,19	5,08
Kr^{84}	22	21	37	8,5
Xe^{132}	8,5	10	4,6	2,2

of meteoritic material in the regolith. Doubtless it has been found. But this is as yet far from adequate to explain the formation of the entire lunar regolith.

I wish to direct attention to another factor. The most unusual part of the endogenic process of the outflow of basaltic rocks on the Moon is their instantaneous contact with the high vacuum of space. The lunar magma approaches the top of the stratum and breaks through it. Molten magma and its gases burst out into the vacuum. Splashing of the molten magma and the loss at the same time of its gases and other volatiles at enormous velocities must have occurred. In parallel with other motivations, we would wish to follow this endogenic approach of explaining the origin of the regolith by setting up appropriate experiments. All the more so in that the fundamental problem of the lunar material balance is not without interest for an understanding of geochemical processes on the Earth, especially during the first billion years of its evolution.

REPRODUCIBILITY OF THE ORIGINAL PAGE IS POOR.

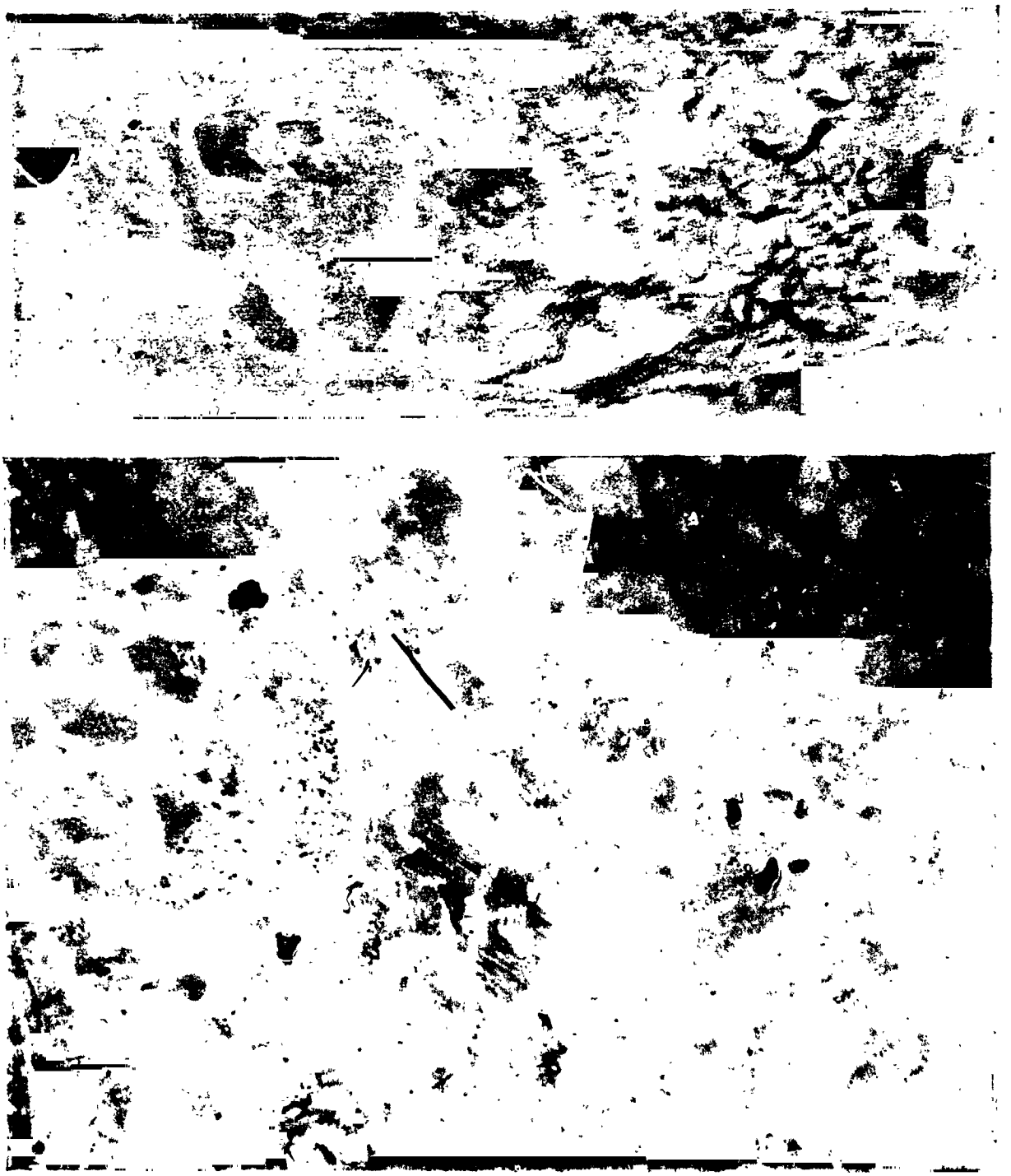

PLATE I.
1. Lunar surface material on trap in receiving chamber (part of tray)
2. Section of surface material on tray from deep portion of core containing coarser-grained material, X 15

REPRODUCIBILITY OF THE ORIGINAL PAGE IS POOR.

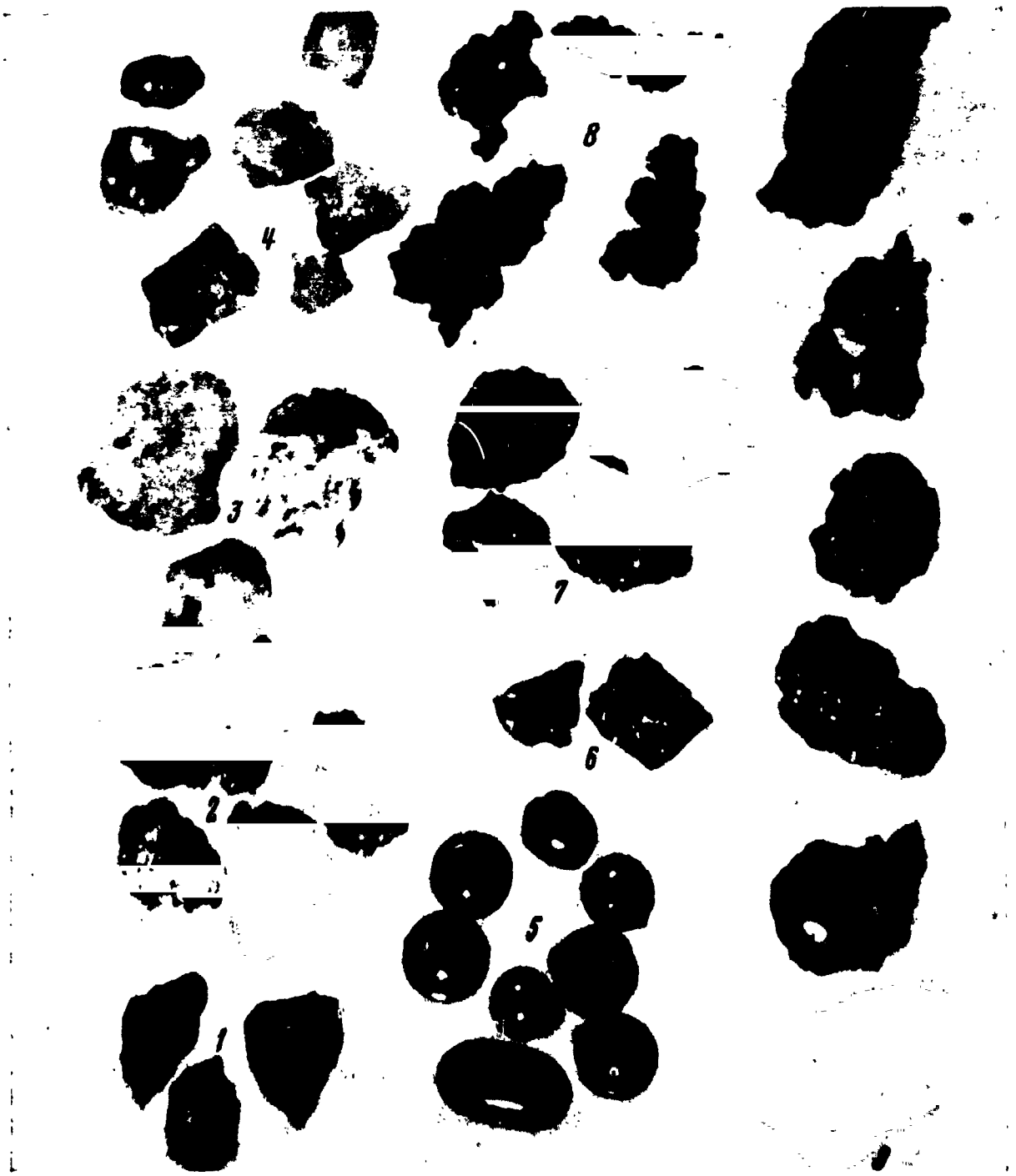

PLATE III

Groups of most representative particles of lunar surface material from the +0.45 mm fraction, X 30.
1. Basalt; 2. Coarse-grained basalt (gabbro); 3. Anorthosites; 4. Homogeneous glasses and grains of minerals; 5. Spherules and spherical formations: 6. Brown glasses; 7. Breccia; 8. Sintered particles (sinters); 9. Slags and fused particles

REPRODUCIBILITY OF TH ORIGINAL PAGE IS POOR.

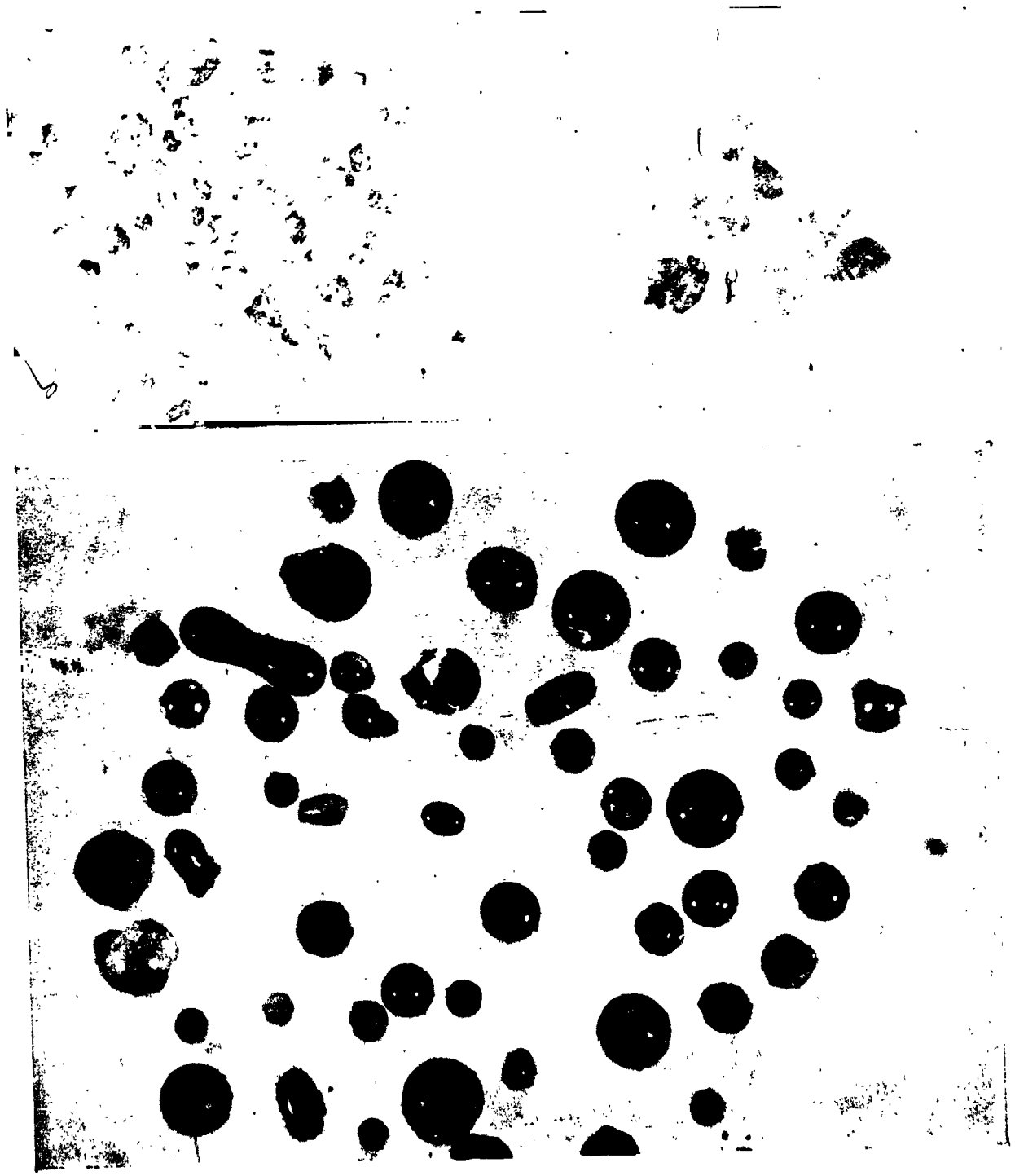

PLATE V

1. Single grains of olivine, X 30
2. Feldspar particles, X 20
3. Spherical particles, X 60

REPRODUCIBILITY OF THE ORIGINAL PAGE IS POOR

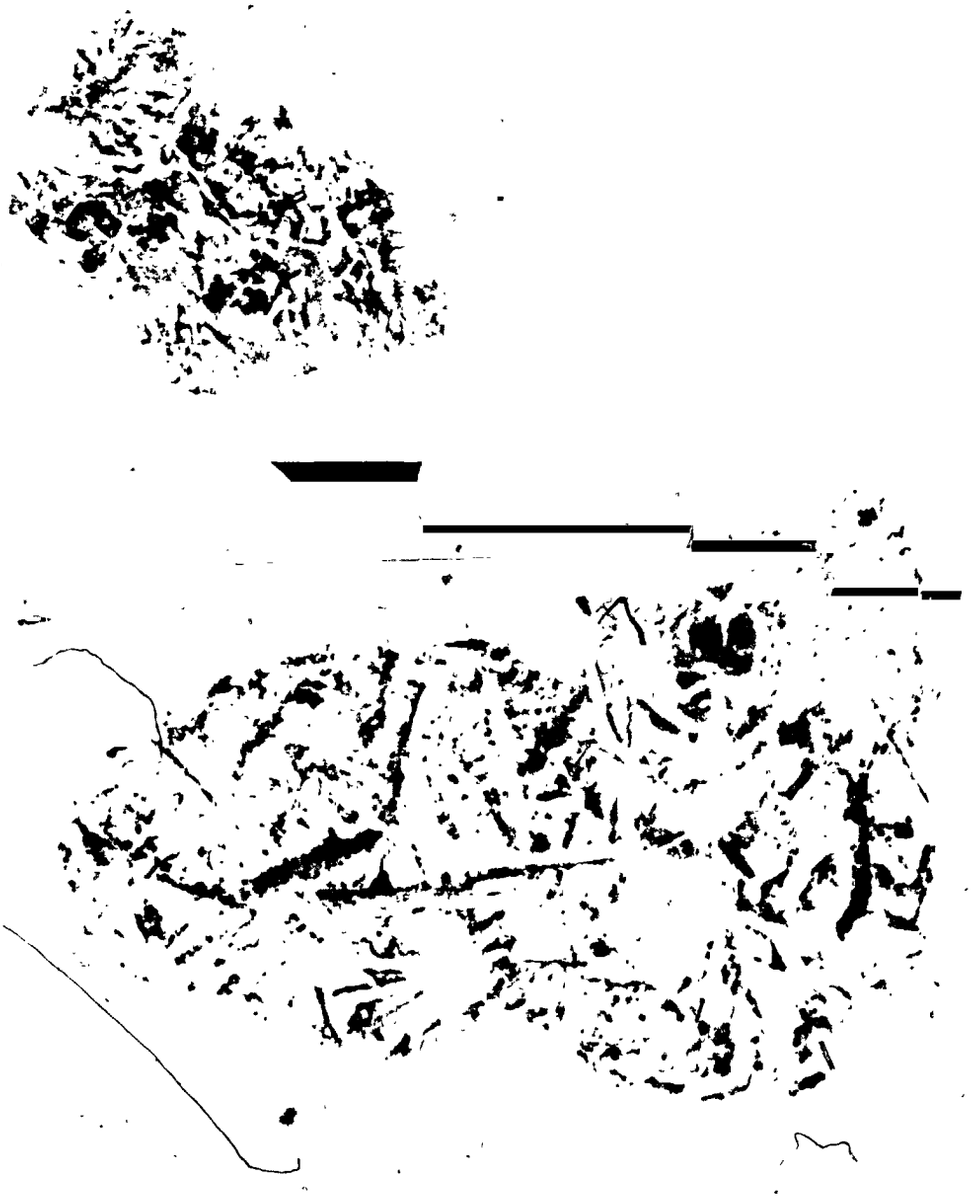

PLATE VII

1. Section of basalt with hypidiomorphic texture, crossed Nicol prisms, X 30
2. Section of basalt with ophitic texture, crossed Nicol prisms, X 50

N75 11816

GEOLOGO-MORPHOLOGICAL CHARACTERISTICS OF THE LANDING SITE OF LUNA 16 AUTOMATIC STATION

/19

K. P. Florenskiy, A. T. Bazilevskiy, and A. A. Pronin

Abstract

The article presents a brief geological outline of the landing site of Luna 16 automatic lunar station, including data on the structural features, estimate of thickness, and stratigraphic position of the lava infilling of the Sea of Fertility. Determinations are made of the relative duration of surface formation near the landing site based on data of the statistical counts of crater distribution. Descriptions and several morphometric characteristics of noncrater forms of relief complicating the surface of the Sea of Fertility are given. Possible sources of the regolith material returned by Luna 16 ALS /automatic lunar station/ are examined.

The Luna 16 automatic station returned to Earth a sample of lunar surface material from the northeastern part of the Sea of Fertility[1]. The landing site of the station was at the point with coordinates 0°41' S. Lat, 56°18' E. Long. It is 280 km southwest of Langrenue Crater and 360 km southeast of Taruntius Crater. 100-120 km north of the landing site begins the highland region separating the Sea of Fertility and the Sea of Crises. 120 km east of the landing site is a region with mountainous and hilly relief, which gives way farther toward the east to lowland regions with mare type surface, and then a region with developed highland type relief surrounding the Foaming Sea.

[1] The following abbreviations are used: ALS = automatic lunar station; MSC = manned spacecraft; and SC = spacecraft.

The landing site structurally is a typical representative of mare type areas. Judging from the results of the analysis of materials returned by the Luna 16 ALS [1], and on analogy with other regions of lunar maria [2-6] investigated, the depression of the Sea of Fertility is filled with a complex of lava flows of basaltoid composition. M. S. Markov et al [7] classifies these formations with the Procellarum complex [8].

The total thickness of Procellarum rocks in the littoral zone of the Sea of Fertility (region of Webb P crater) can be estimated by a technique of A. L. Sukhanov and L. M. Shkerin [9] as being of the order of 0.5 km. Directly in the landing site the thickness of these rocks evidently somewhat exceeds this value.

The northeast part of the Sea of Fertility juts in a semi-circular bay into the highland region (Fig. 2). The impression is gained that this bay is part of an ancient crater-like basin about 150 km in diameter inundated by lava flows, whose margins are marked by the craters Webb, Webb R, Webb P, and Webb U. Some of the mountainous rim of this basin is quite well preserved between craters Webb and Webb R. The southwest part of this rim of the basin evidently is covered with the procellarum complex. It is interesting to note that the supposed origin of this part of the mountainous rimming is apparently transected by systems of mare ridges.

The landing site is beyond the limits of this assumed basin and is a relatively level region of the mare surface containing no craters larger than 1 km in diameter, surrounded by mare ridges.

At a distance from the landing site sometimes on the surface of the Sea of Fertility there can be observed, in addition to the craters of various sizes and the mare ridges, flat-topped, ridge-like, and dome-like elevations, and infrequently -- rilles.

The craters in the landing site were studied with 1:170,000 photographs obtained during the flight of Apollo 15, and from 1:500,000 photographs obtained by Lunar Orbiter 1. These materials were used to investigate the features of the morphology and the distribution of craters with diameters greater than 200 m. Craters of smaller size were not always reliably distinguished in these /20 photographs, and the estimates of their distribution density are evidently understated.

In the immediate proximity to the landing site craters with diameters from 200 m to 1 km are distributed quite uniformly area-wise. The density distribution in this diameter range is illustrated by Fig. 1 and can be approximated by the function

$N = 10^{12.9} D^{-3}$, where N is the cumulative number of craters with diameter greater than D (m) over an area of 10^6 km^2. The point at which the graph of this function intersects the graph of the function of the equilibrium distribution /10/ is at a diameter of about 100 m, that is, in this respect the Luna 16 landing site is similar to the region studied by Lunokhod 1 /2, 3/. These data afford grounds for assuming that the mean thickness of the regolith in the Luna 16 landing site exceeds 2-3 m.

Among the craters having diameters less than 100-200 m, there is a predominance of the bowl-shaped forms. Larger craters are often flat-bottomed. This fact evidently indicates that some interface exists at the depth of 20-40 m. No anomalies were observed in the distribution of craters with respect to the degree of morphological definition that differentiate the Luna 16 landing site from other earlier-studied mare regions /11/.

Craters greater than 1 km in diameter are unevenly distributed in the area of investigation, forming clusters of irregular shape and linearly elongated systems. The area of these accumulations can amount to tens and several hundreds of square kilometers, and the number of craters of this size an accumulation is 10-20. The length of the linear systems is usually 10-15 km, and less often -- -- up to 50 km; the number of craters in the systems varies from 5 to 10. As a rule, they are oriented in the north-south and northwest-southeast directions and disclose a spatial relationship with the Langrenus Crater (secondary craters?).

In morphology, craters with diameters greater than 1 km are highly variegated. Most of them are bowl-shaped and less often flat-bottomed and cone-like craters are encountered. The largest of the craters in the area of the mare surface studied has a diameter of about 10 km (Webb I.). Among craters having diameters greater than 1 km there is a predominance of craters sharply defined in relief, which can be compared with the craters of morphological classes A, AB, and B /11/. Strongly worn craters belonging to class BC are very infrequently encountered. Virtually no craters with signs of morphological class C could be distinguished.

Some craters in this size range have a plan-view asymmetric, elongated (usually in the northwest direction) form and seemingly consist of two to three craters merging into one. Evidently these are also secondary craters.

Mare ridges in the landing site are ridge-like elevations from 5-10 to 30-40 km in length, with widths from hundreds of meters to several kilometers. Their height over the surrounding locale usually is not more than 100-200 m, seldom attaining 300-400 m. The grade of the ridge slopes usually does not

exceed 10-15°, only seldom attaining 20-25°. Sometimes one of the slopes is markedly steeper than the other, and the ridge resembles a cuesta in shape. In planform, there is a predominance of sinuous and arc-like ridges and they follow one another echelon-like. They form two systems. One of them runs from the area of Webb S Crater through the vicinity of the landing site in the meridional direction to the highland cape with crater Webb U. The other system of ridges intersects the first in a region 40 km southwest of Webb S Crater and extends in the latitudinal direction toward Webb Crater. The northern terminus of the meridional system and the eastern part of the latitudinal system of ridges runs over the assumed site of the inundated ridge of the above-mentioned basin, about 150 km in diameter.

In profile, the ridges have a box-like shape with a flat summit or a rounded shape without an abrupt inflection between the slope and the summit surface. The planform arc-like curved flat-topped ridge, about 2-4 km in width, is 20 km east of the Luna 16 landing site.

Flat-topped elevations are observed 45 and 60 km southwest of Webb U Crater (80 and 60 km northwest of the landing site, respectively). Their shape in the planform is near-polygonal. The dimensions of one of them is 4 x 6 km, and the other 2 x 3 km. The slopes have a grade of 15-20°. The flat summit surfaces of the elevations differ practically not at all from their surrounding mare surface.

A ridge-like elevation lies 80 km northeast of the landing site. Its length is about 25 km, and its width -- 1-3 km. Its height is about 300 m. It extends northwesterly. This elevation reached its maximum width in the southeastern part. The slope of the curves of this relief form lies in the range 10-20°.

Dome-like elevations are highly representative of several regions of the northwest part of the Sea of Fertility. They are /22 encountered in the form of isolated elevations or segregated groups of elevations on the mare surface between craters Webb and Webb P, but they are most numerous in the zones that are intermediate between the mare surface and the highland region and the area northwest of Webb Crater, and southwest of Webb U Crater, where the hilly character of the relief is practically entirely determined by the presence of these forms. Dome-like elevations are 1 to 5 km in diameter with a height from tens to several hundreds of meters. The grade of the slopes of these elevations usually increases toward the middle of the slope and can reach 20-25°. The regions of extensive development of this terrain form, the density of the distribution of craters less than 1 km in diameter is markedly less than in the adjoining sections of the mare surface. Craters larger than 1 km are

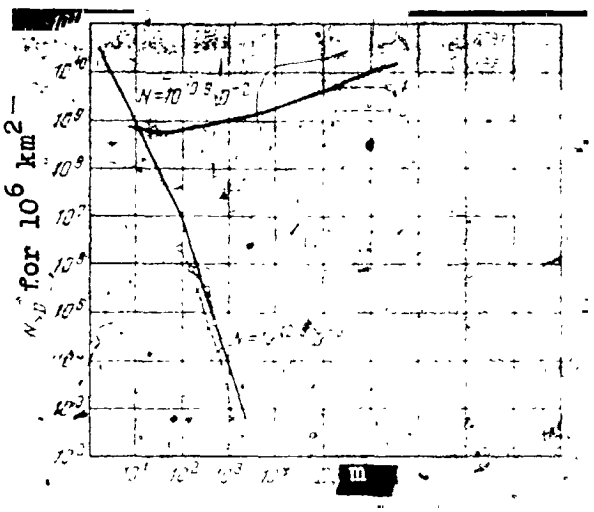

Fig. 1. Cumulative area of craters in the Luna 16 landing site
1. Apollo 15
2. Lunar Orbiter 1
KEY: A. N_D for 10^6 km^2

distributed in the areas of developed dome-like elevations approximately in the same manner as on the mare surface. Considering the probable situation of the dome-like elevations on rocks of the Procellarum complex, their confinement to the zones of coupling of mare plains with the mountainous regions of the highlands and the deep-slope character of these elevations, it can be assumed that these relief forms result from the manifestations of post-Procellarum vulcanism of the nonbasaltoid type. The andesite-basaltic composition of the rocks comprising the domes is highly probable. Asymmetric craters of supposedly secondary (ejecta from Langrenus Crater?) origin are observed seldom on the dome-shaped elevations. This is grounds for assuming that the age of these forms is more ancient than the age of Langrenus Crater. /21

Rilles in the region described are encountered only in direct proximity to Webb Crater. Here two rilles are observed, one of which is about 20 km in length and trends in the northeasterly direction, and the other has a length of about 40 km and trends in the northwesterly direction. These rilles are weakly sinuous valleylike depressions with trough-shaped transverse profile. The width of the rilles is about 2 km. The grade of the slopes evidently is 10-15°. The bottom of the rilles is virtually no different in the nature of the surface from the surrounding regions of the mare. One of the rilles is intersected by submeridional chainlets of craters of supposedly secondary genesis. This affords grounds for assuming that the rilles were formed before Langrenus Crater was formed.

Analysis of the geologo-morphological situation in the landing site leads to the conclusion that material from four different sources must be present in the regolith, a sample of which was returned to Earth by Luna 16. The main source of the regolith material is the basalt rocks of the Procellarum complex filling the depression of the Sea of Fertility. Another source can be the rocks of the pre-Procellarum complexes that must have been

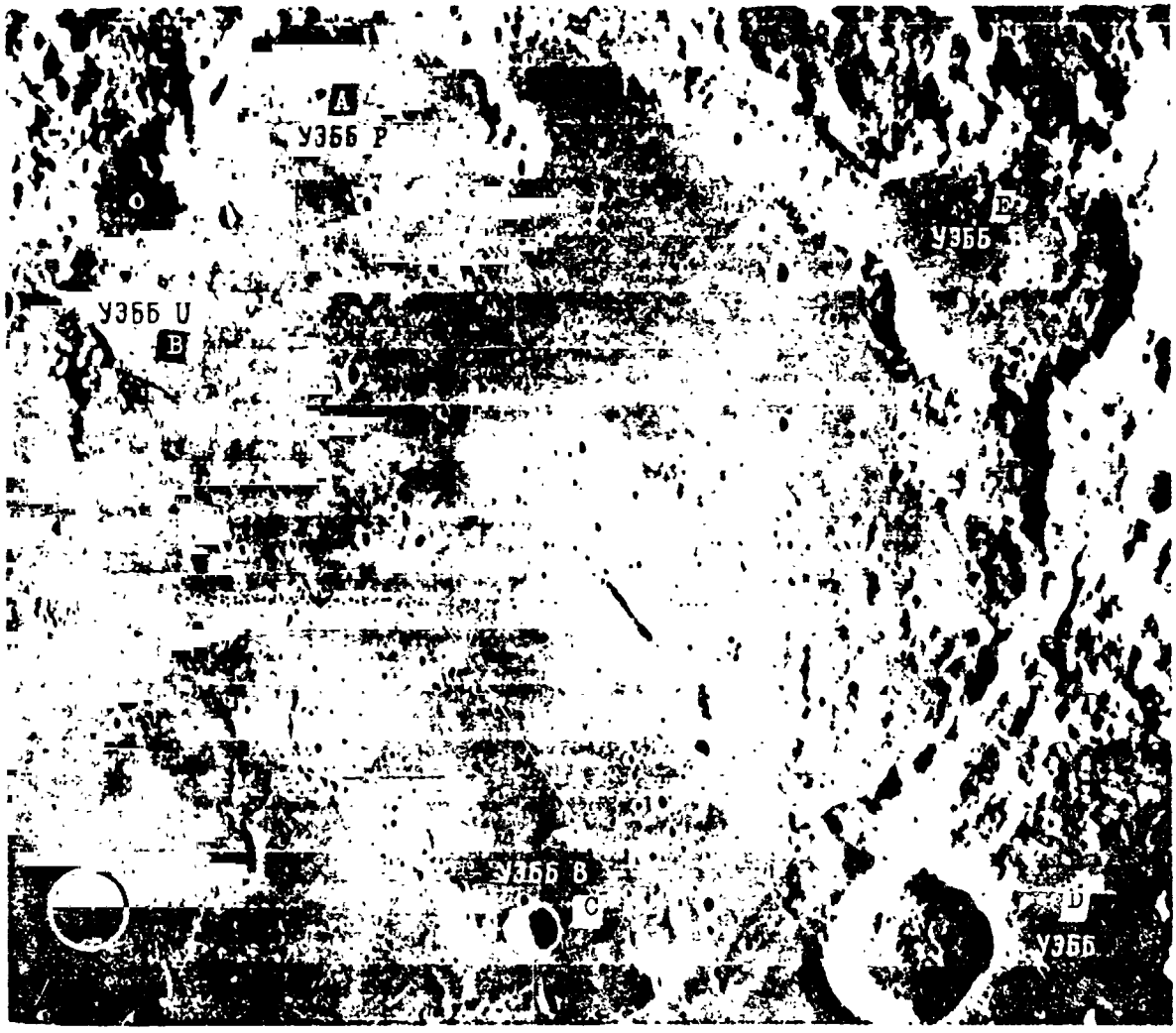

Fig. 2. Northeastern part of the Sea of Fertility. Photograph KA of Orbiter 1, No. 34-M. The extent of the area is 150 x 150 km, north is at the top. The circle in the left lower corner of the photograph indicates the Luna 16 landing site.

KEY: A. Webb P
B. Webb U
C. Webb B
D. Webb
E. Webb R

broken through by the largest of the craters disturbing the surface of the Sea of Fertility. The third source of the material is to be found in the regions of developed dome-like elevations

in the zones of coupling of mare plains with the highlands. A fourth source is represented by the rocks comprising the highland regions surrounding the Sea of Fertility. The principal mechanism of the shifting of material in these cases evidently was of various explosive processes.

REFERENCES

1. Vinogradov, A. P., "Preliminary Data on Lunar Surface Material Returned by Luna 16 Automatic Station," Geokhimiya (3), 261-274 (1971).

2. Peredvizhnaya laboratoriya na Lune -- "Lunokhod-1" /Roving Laboratory on the Moon: Lunokhod 1/, "Nauka", 1971.

3. Florensky, K. P., Basilevsky, A. T., Gurshtein, A. A., Zasetsky, V. V., Pronin, A. A., Zezin, K. V., and Popova, Z. V., "Geomorphological Analysis of the Area of Mare Imbrium Explored by Automatic Roving Vehicle Lunokhod-I" Report presented at the 14-th COSPAR session, Seattle, 1971.

4. Surveyor Project Final Report, Part II, Science Results /sic/, TR 32-1265, JPL, Pasadena, 1968.

5. Apollo 11 Preliminary Science Report, NASA SP-214, 1969.

6. Apollo 12 Preliminary Science Report, Pt. A, NASA Sp-272, 1971.

7. Markov, M. S., Sukhanov, A. L., Trifonov, V. G., Florenskiy, P. V., and Shkerin, L. M., "Geological Mapping of the Moon," in the collection: Sovremennyye predstavleniya o Lune /Modern Concepts of the Moon/, "Nauka", 1971.

8. Sukhanov, A. L., and Trifanov, V. G., "Method of Compiling and Legend of 1:1,000,000 Geologo-morphological Maps of the Moon," in: Problemy geologii Luny /Problems of Lunar Geology/, Trudy GIN /Transactions of the Institute of Geology, USSR Academy of Sciences/ (204), (1969).

9. Sukhanov, A. L., and Shkerin, L. M., "Thickness of Rock in the Procellarum Complex," in the book: Problemy geologii Luny [Problems of Lunar Geology], Trudy GIN, No. 204, 1969.

10. Trask, N., Size and Spatial Distribution of Craters Estimated from the Ranger Photographs, Ranger VIII and IX, Pt. II, NASA TR 32-800, JPL, Pasadena, 1966.

11. Florenskiy, K. P., et al., "Problem of the Structure of the Surface of Lunar Mare," in: Sovremennyye predstavleniya o Lune, "Nauka", 1971.

Institute of Space Research, USSR Academy of Sciences, Moscow.

N75 11817

RECEPTION AND STUDY OF LUNAR SURFACE MATERIAL IN INERT GAS MEDIUM

/29

Yu. A. Surkov, Ye. M. Rudnitskiy, and V. A. Glotov

Abstract

The reception and study of lunar material returned by the Luna 16 space station is described in the article. The layout of a vacuum receiving chamber for working with material in a helium atmosphere is examined along with the main operations involved in extracting the material from the ampule and drill.

On 24 September 1970, the Luna 16 automatic interplanetary station brought to Earth lunar surface material from the Sea of Fertility. The reception and initial study of the material was carried out in a facility specially designed for this purpose. The work was carried out in a chamber filled with ultrapure helium (the helium was selected as a gas least reacting with material).

The main elements of the device include: working chamber, air-lock, glove units, vacuum evacuation system, and control panel. The general view of the apparatus is shown in Fig. 1, and its layout -- in Fig. 2.

The working chamber is cylindrical in form. It is made, as most of the parts of the installation, of stainless steel. The diameter of the chamber is 1200 mm and its length is 1600 mm. The chamber houses accessories and instruments for opening containers and working with the material, bagging containers, scales, transducers, and instruments.

For a detailed examination of the material, the working chamber is provided with a stage together with a stainless steel tray, which by means of a rotation mechanism can be brought right up against the observation window where the material can be studied by means of optical devices.

In the chamber is mounted a device for securing and immobilizing the container in a position that is most suitable for opening it and removing from it the drill containing the material. Containers and drill rigs of various configurations can be secured in this device by means of replaceable prisms.

To monitor the hermeticity of the containers brought to Earth with the extraterrestrial material and not provided with their own manometer transducers, the facility is equipped with a drilling unit that can be placed either in the chamber or in the air lock. The device includes a case, polished drill with rotation leads, and a drive. The drill is secured in a chuck fitting tightly on the shaft. The shaft is given longitudinal displacement by the amount of the feed by means of a drive, simultaneously as it is being rotated. The vacuum seal of the shaft is achieved with two bushings made of teflon, on the thin-walled ends of which are fitted rubber rings pressing the bushings against the polished surface of the shaft. The hermeticity of the containers is estimated from the change in pressure recorded with the manometer transducers installed in the chamber and in the air lock.

At different places in the working chamber are located observation windows with illuminators for examining the material, and for still and motion picture photography. For access into the working chamber in order to carry out cleaning and installing of large accessories and instruments, at one of the chamber ends is installed a cover hinged on loops with a 500 mm diameter flange welded to it. The provision is made for installing on this flange an instrument for studying the physicomechanical characteristics of the material.

An air lock and two magnetic-discharging pumps are installed on the opposite end of the chamber.

The power supply to the instruments and the transducers within the chamber as well as the output of information from them is achieved via vacuum plugs mounted on one of the flanges of the working chamber.

The facility is equipped with standby flanges, that can be used for the installation of research apparatus. /30

Work is carried out in the chamber by the operator using three glove units that are provided along the cylindrical part of the chamber.

To remove the material from the chamber and to transfer it into specialized laboratories without disrupting the purity of the helium medium surrounding the lunar surface material, the facility is equipped with an air lock device.

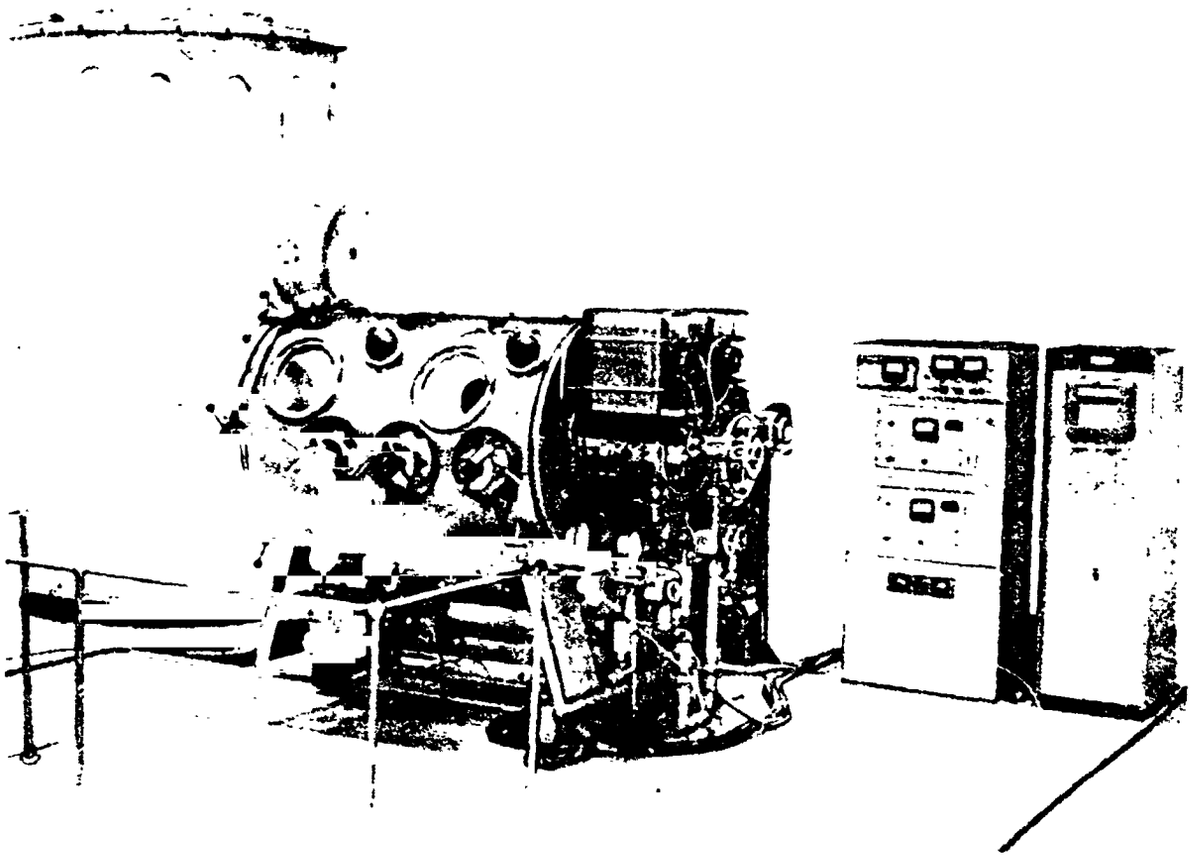

Fig. 1. General view of installation

The air-lock device consists of an air-lock chamber in two vacuum locks. The element /sic/ inserted into the chamber is placed in the air-lock chamber via a lock. Then the lock is made hermetic, and the air-lock chamber is evacuated. Next, the air-lock is filled with helium, and after this the lock connecting the air-lock chamber with the working chamber is opened. By using gloves, the operator inserts the element being transferred into the working chamber.

The glove units include rubber gloves, vacuum locks, and hoods. Working with gloves is possible only when the chamber is filled with gas to atmospheric pressure. In this case, the vacuum seals

of the locks and the hoods are dehermeticized, and the operator gains access to the gloves. During extended storage, the gloves are insulated from the volume of the working chamber with vacuum locks, and from the atmosphere -- by the hoods. The design of the glove units enables vacuum degassing of the gloves to be carried out, for which a provision is made for simultaneous evacuation of the volumes of the hoods and locks. /31

System of vacuum evacuation. Vacuum evacuation is needed to evacuate the atmospheric air from the working and air-lock chambers before admitting helium. The preliminary evacuation of the facility is carried out with a vacuum device consisting of mechanical and two-rotor pumps.

A thermal sterilizer is placed in the forevacuum line, so that the device is designed with a provision for receiving toxic material.

Two turbomolecular pumps (one of which is a standby) are used for high-vacuum evacuation with the facility. The turbomolecular pumps (the rate of evacuation of each pump is 200 liters/sec) are connected to the device via vacuum locks and are used to evacuate the working and air-lock chambers. The maximum rarefaction achieved in the facility by means of these pumps is $2 \cdot 10^{-5}$ torr.

For vacuum conditioning of the working chamber, use is made of diode-type magnetic discharge pumps with cooled anodes. The evacuation rate of each of them is 250 liters/sec. Owing to the cooling of the anodes, these pumps have high productivity in the high pressure range. The maximum rarefaction achieved in the chamber using these pumps is $2 \cdot 10^{-6}$ torr. /32

Helium is admitted into the working and air-lock chambers via a cylinder filled with high-purity helium.

The pressure in the facility is measured by means of membrane, thermocouple, and ionization manometer transducers.

To monitor the composition of the residual gases in the chamber, the device is provided with mass spectrometers -- a chronotron and an omegatron. A mass spectrogram of the residual gases taken with the chronotron when the magnetic pumps are in operation is shown in Fig. 3.

The control panel of the facility consists of two cabinets which house the equipment for controlling the pumps, the vacuum valves of the evacuation system, and the instruments for monitoring the vacuum in the facility. Light signals on the panel of one of the cabinets are combined with a mnemonic scheme of evacuation and make it possible to estimate the status of any facility element. The facility is also provided with a system for emergency, sound, and light signalling.

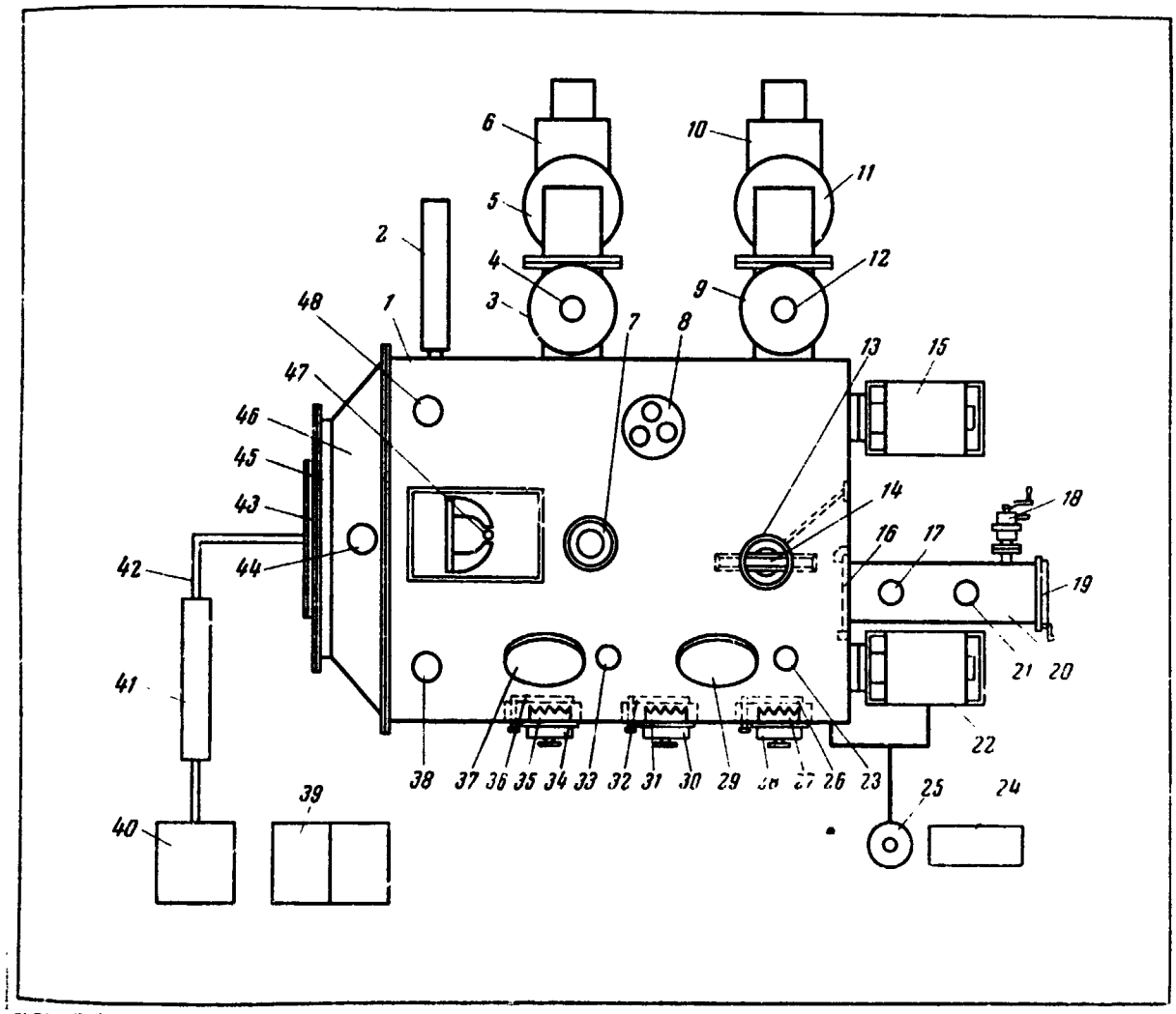

Fig. 2. Layout of installation

1. Working chamber
2. Chronotron transducer
3,7,9,38,44,48. Flanges
4,12,17,21. Manometer transducers
5,11,16,19. Vacuum locks
6,10. Turbomolecular pumps
8. Flange with current leads
13,29,37,43. Observation windows
14. Stage
15,22. Magnet-discharging pumps
18. Drilling mechanism
20. Air-lock chamber
23,33. Illuminators
24. Welding mechanism
25. Helium tank
26,32,36. Vacuum locks
27,31,35. Gloves
28,30,34. Hoods
39. Control panel
40. Vacuum unit
41. Thermal trap
42. Forevacuum line
45. 500 mm diameter flange
46. Cover
47. Omegatron transducer

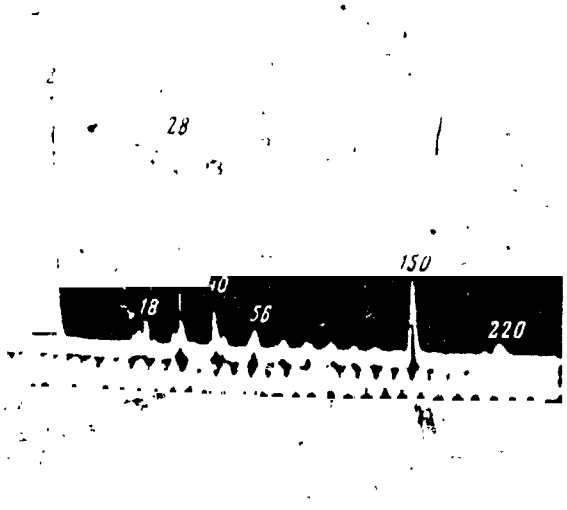

Fig. 3. Mass-spectrogram of residual gases taken on chronotron when the chamber was evacuated with magnetic-discharge pumps

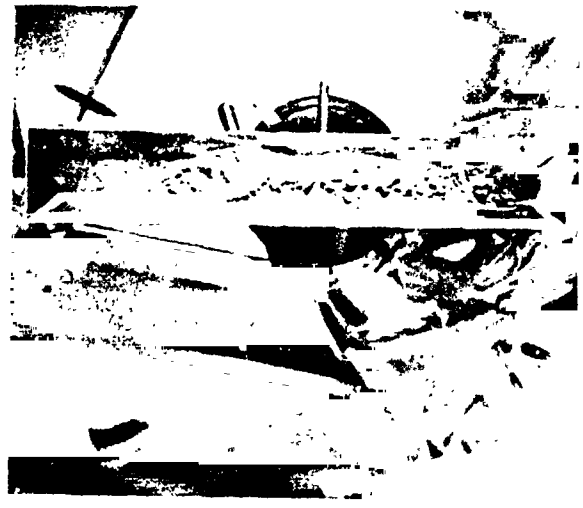

Fig. 4. Lunar surface material on tray in working chamber

Reception and initial study of lunar surface material. The returned lunar surface material was in a drill enclosed in a hermetic container. Before reception of the material, the working chamber, instruments, and accessories for opening the container and working with lunar surface material were carefully washed and subjected to extended vacuum conditioning. In order to prevent the helium from being contaminated with organic compounds contained in the heat-insulating covering of the container (the container was one of the units of the equipment being returned), the heat-insulating layer was enclosed in a hermetic sleeve made of stainless steel. Then the container with the sleeve were secured in the clamp of the working chamber. Next, hermetization and evacuation of the facility was carried out. Before beginning the steps in opening the container, by sublimating hydrogen peroxide into the chamber, the facility was sterilized. The purpose of the sterilization was to prevent contact of terrestrial microorganisms with the lunar material, which is necessary in conducting medical-biological studies.

After sterilization and evacuation of the working chamber was carried out to a pressure of $2 \cdot 10^{-5}$ torr, high-purity helium was admitted into the chamber. When the helium in the working chamber with the glove units had reached atmospheric pressure, the gloves were removed, the locks were opened, and the operation in opening the container was carried out.

Using special accessories, from the container the drill containing the lunar surface material was extracted. Then the lunar surface material was weighed and placed on the tray (Fig. 4). The weight of the lunar surface material was somewhat more than 100 g. Next, an investigation was made of the material; the nature of the variation of the sample core depthwise was studied; initial study was carried out of the morphology of the sample of lunar surface material and several optical and physico-mechanical properties were determined. In particular, it was found that the loose surface material changes color depending on the angle of view and the position of the light source; the lunar surface material is easily molded and aggregated in individual clods and well withstands large angles of natural repose. These and other interesting properties of the regolith are discussed in detail in special studies. /33

Then sampling of the regolith was carried out for special investigations. These samples, after being weighed, were placed in specially developed hermetic containers made of stainless steel and were transferred through the air-lock into the laboratory for further and comprehensive investigations.

In developing the facility, measures were taken to reduce the content in the residual gases of water vapor and hydrocarbons. In particular, the use in the evacuation system of magnetic discharge and turbomolecular pumps, magnetic rotation leads made of teflon without using lubricant, which was mentioned in the description of the drill unit, considerably reduced the content in the residual gases of these components.

The experience in the reception of the lunar surface material returned by the Luna 16 automatic interplanetary station shows that the facility and the technology of receiving the material meets the requirements imposed on it.

Order of Lenin Institute of Geochemistry and Analytical Chemistry imeni V. I. Vernadskiy, USSR Academy of Sciences, Moscow

N75 11818

BOX FOR WORKING WITH LUNAR SAMPLES IN NITROGEN ATMOSPHERE

/34

Yu. I. Stakhyev, L. S. Tarasov,
K. K. Krestinina, and A. V. Ivanov

Abstract

The design and equipment of a box specially built for working with lunar surface material is described.

The box is intended for preliminary investigations, packing of samples, and carrying out a large number of operations necessary for this stage in the study of samples.

To prevent contact of lunar samples investigated with air oxygen, water vapor, and atmospheric aerosols, a special box was designed and built. The box is intended for preliminary physicochemical investigations, studies of mechanical and several physical properties of samples, preparation of polished sections and transparent sections of samples, and also the packaging and hermetic packing of samples in appropriate weighing bottles, ampules, cuvettes, and substrates for investigation in specialized laboratories. To minimize contamination, in the construction of the box plexiglas and the stainless steel 1X18H9T were used as the construction materials.

The box is a rotating drum of plexiglas, 1600 mm in diameter and 500 mm in height, installed on a central support leg. At the top of the drum is located a plexiglas box-air lock for introducing and withdrawing from the box containers containing samples and necessary equipment without disturbing the inert atmosphere of the working chambers of the box.

The entire internal volume of the box is divided into two hermetically isolated halves, and communication between each and the outer space takes place via an air lock located on the cover

of the box (Fig. 1). One of the halves of the box is divided into three bays: 1) bay of gravimetric equipment, 2) packing-research bay, and 3) bay of vibratory ball mill. The other half has two bays: 4) bay for cutting section blanks and 5) a grinding-polishing bay. The bays in each of the halves connect with each other via windows covered by plexiglas louviers (Fig. 2).

The box is equipped with a gas system to fill the inner cavity with nitrogen and to maintain excess pressure. Operations within the box are carried out by means of ten gloves, simultaneously by two or three investigators. The box is placed on a slab secured to the floor of the laboratory and in order to be installed in a place convenient for operation the position can be rotated about the vertical axis by 355°. Rotation by more than one revolution is restricted by a stop, which also serves to secure the box in the selected position.

The inner cavity of the box and the air lock is filled with nitrogen rated "extra pure" from tanks. The pressure within the box is maintained at 20 mm H_2O using an automatic regulator providing for gas feed. When the operator makes movements within the box, the pressure within the box rises above the desired value; at this instant a preventive release valve is triggered and the excess gas is discharged through a Petryanov filter into the atmosphere.

The automatic regulator is triggered when the pressure within the box falls, relative to the atmosphere, down to 15 mm H_2O, and the relief valve is triggered when the pressure rises to 25 mm H_2O. Thus, within the box a pressure of 20 $\pm$ 5 mm H_2O above the atmospheric is maintained.

The gravimetric equipment bay houses beam pan scales with a limit load of 200 g, and VT-500 torsion scales. The compartment has two gloves for operation.

In the packing-investigation bay (Fig. 3) is placed the required tools for packaging the samples (spatulas, small spoons, and tongs), as well as a series of tared weighing bottles with ground caps for accommodating the samples of lunar surface material. /36 The investigation equipment is introduced into the bay before the operations begin. To connect the transducers of the instruments with the measuring devices, two hermetic multipin plugs are used. The compartment is equipped with two gloves for operations and with a MBS-2 binocular microscope.

The bay of the vibratory ball mill includes an eccentric vibratory mechanism driven by a 100 W dc electric motor. The

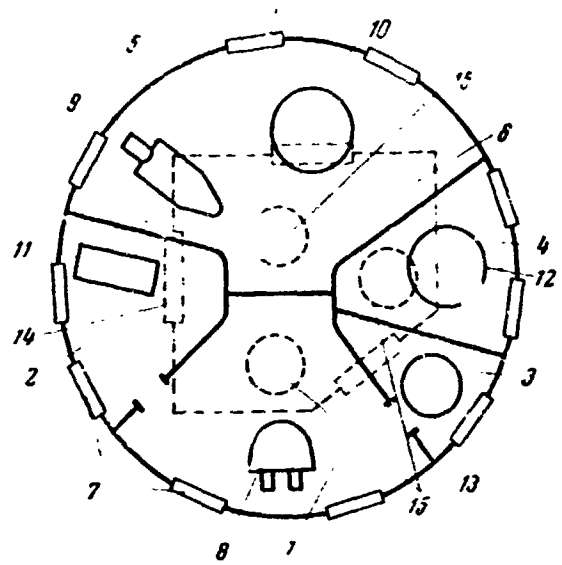

Fig. 1. Layout of equipment in box (top view)

1. Packaging-investigation bay
2. Bay of gravimetric equipment
3. Bay of vibromill and vibrosieve
4. Diamond saw bay
5. Bay for sectioning
6. Air-lock (shown by dashed line)
7. Gloves
8. MBS-2 binocular microscope
9. MIN-8 microscope
10. Polishing disk
11. Balances
12. Diamond saw
13. Vibromill
14. Outer hatch
15. Inner hatches of air-lock

electric motor is installed outside the box; and within the compartment is introduced only the end of the shaft on which the mechanism is inserted, via a rubber cuff. The mechanism brings into vibration, with a 6 mm amplitude, two steel hermetic beakers containing ground samples. A steel ball is used as the grinding body. The frequency of vibrations is regulated by varying the voltage fed to the motor, within the limits 5-100 Hz. To grind a weighed sample of 100-200 mg rock of moderate strength, with grain size 100 μm to 10 μm requires 2-3 minutes (Fig. 4). /135

This same mechanism is used to drive a set of teflon sieves with capron meshes. The meshes of the sieves have square openings and the following sizes: 900, 450, 200, 125, and 83 μm. The set is used to separate the samples of lunar surface material into fractions by grain size. The procedure of sieving on the sieves proved to be also highly effective from the standpoint of cleaning the surfaces of the large particles from adhering dust material. Sieving 2-5 g of a weighed sample usually takes no more than 2-3 minutes. The compartment has one glove for operations.

In the sieve for cutting section blanks is installed a diamond saw with horizontally positioned cutting disk, with inner cutting edge of the AVRK ON-037-89-65 type, reinforced with ASV-15 diamond dust. The disk is mounted on the shaft of a dc electric motor (n = 7000 rpm). As in the preceding case, the electric motor is installed outside the box, and its shaft is introduced into the compartment through a rubber cuff. In order for displacements and feeding of the sample into the cutting zone, use is made of a cross-shaped support with a precision along both coordinates of 0.01 mm. Ethanol is used during cutting as the coolant (Fig. 5).

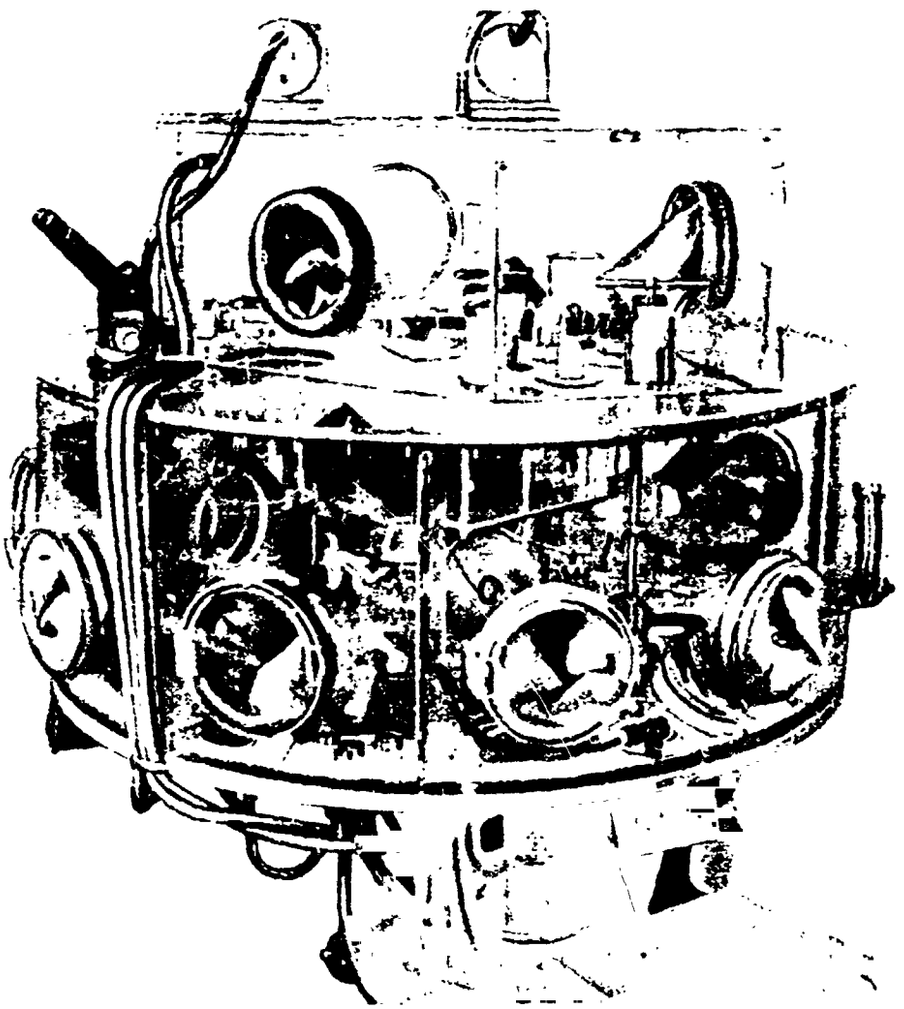

Fig. 2. General view of box

The saw makes it possible to obtain wafers 0.2-0.25 mm thick for a cutting width of 0.25 mm. The compartment has one glove.

The grinding-polishing bay contains a set of grinding and polishing disks 160 mm in diameter, a small electric motor, a set of diamond pastes for grinding and polishing, and also all accessories required for preparing sections. To monitor the quality of section preparation, use is made of a MIN-8 microscope, whose eyepiece is elongated, hermeticized, and brought out to the cover of the box via an elastic seal. /37

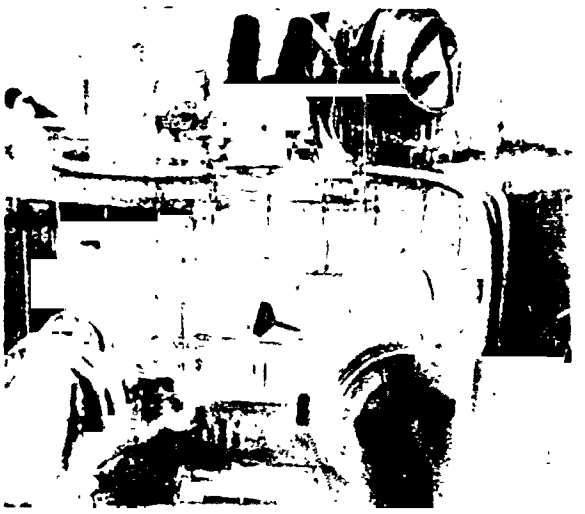

Fig. 3. Packing-investigation bay

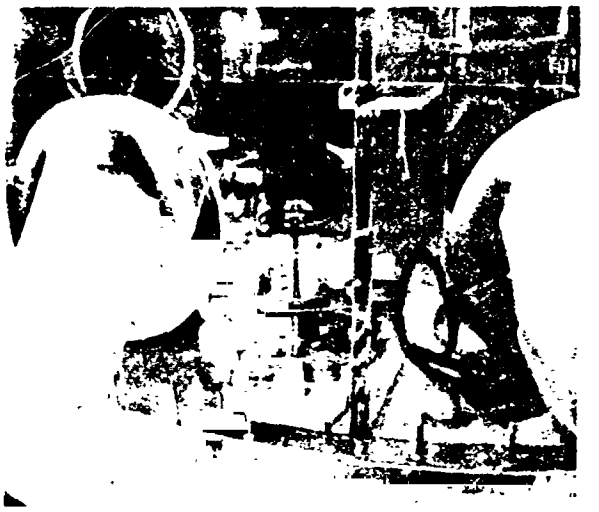

Fig. 4. Bay of vibromill and vibrosieve

Fig. 5. Bay of diamond saw

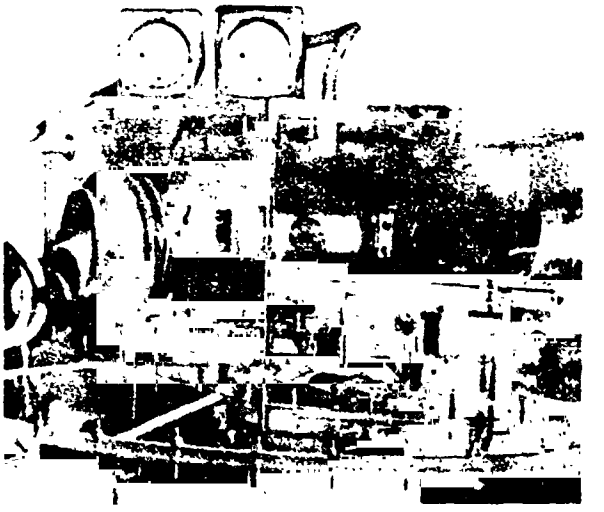

Fig. 6. Air-lock

Lunar surface material collected by the automatic station on the Moon is delivered into the receiving laboratory. The ampule is breached in the helium chamber, and the returned surface material is placed on a tray. In accordance with the developed program, surface material samples intended for investigation are sampled from the tray in the helium atmosphere of the receiving chamber and placed in hermetic containers made of stainless steel. This container together with the surface material sample is transferred

into the air lock (Fig. 6) of the investigation box. After the latter has been purged with nitrogen in order to remove the atmospheric air admitted during the introduction of the container, the container is transferred via the appropriate hatch into the packing-investigation bay of the box (Fig. 3). Here after the container has been breached the sample in it is examined under the binocular microscope and transferred to the sieve for screening. After screening, the sieve together with the sample are returned into the packing-investigation bay, where the resulting fractions are inspected under the binocular microscope, transferred into glass weighing bottles, and then weighed on the balances installed in the gravimetric bay.

This ends the stage of the preliminary preparation of the samples and their preliminary description.

In the first study of the sample of lunar surface material, a sampling is carried out for preliminary investigations of the chemical composition from fractions finer than 0.083 mm (or from unfractionated regolith material before sieving). In order to prepare the sections, samples are selected from the + 0.45 mm fraction or the + 0.9 mm fraction, and from portions of the + 0.2 mm, + 0.127 mm, and + 0.083 mm fractions weighing 1-2 mg each. In the latter case, several tens or hundreds of fine particles are recorded in the plane of the section, and subsequently the particles are studied under the microscope and with an electron microprobe.

After study of the isolated fractions under the binocular microscope, sampling is carried out from the various fractions in accordance with the program for future investigations. The fractions and their divisions allocated for detailed study are placed in small glass weighing bottles or ampules and are transferred for analysis or are moved to other special boxes with nitrogen atmosphere where they are stored and where their separation is carried out by particle types and for morphological study. The operations are conducted in air with some portions of the fractions.

Since there were not many particles 4-6 mm in size in the Luna 16 sample, they usually were kept intact as characteristic rock samples. Therefore, for this sample the diamond saw bay and the bay for preparation of sections of the investigation box went practically unused. Preliminary study of the physicomechanical properties of lunar surface material and then their study under specialized program were carried out in the packing-investigation bay of the box.

N75 11819

MORPHOLOGY AND TYPES OF PARTICLES OF REGOLITH SAMPLE FROM THE SEA OF FERTILITY

/38

K. P. Florenskiy, A. V. Ivanov, L. S. Tarasov, Yu. I. Stakhyev, and O. D. Rode

Abstract

Morphological characteristics of the sample as a whole as well as its individual components are presented. The mean specific weight of the surface material sample is determined to be about 1.2 g/cm^3, which corresponds to a mean porosity of the surface material of about 60 percent at a depth of 35 cm. The high adhesiveness of the surface material and its ability to be electrified was noted. Two main genetic groups of regolith particles are differentiated: primary, represented mainly by fragments of magmatic rocks of the basalt and gabbro types, as well as mineralized grains of their constituent minerals, and secondary, particles subjected to appreciable exogenic transformation on the surface of the Moon. The second group, representing more than 70 percent of the material in coarse fractions, includes particles of breccias, sintered aggregates of complex dendritic form, and glass and vitrified particles of varied composition. The amount of glass increases with decrease in particle size and is more than 80-90 percent of the weight of the material in fractions finer than 5 μm. The formation of the regolith occurs under the effect of two main factors -- comminution of magmatic bedrock during intense meteoritic bombardment of the surface, and change and agglomeration of the rock fragments formed during crushing. Associated with the impactive explosions is also the transport of particles of lunar material over larger distances, which leads to the averaging of the composition of the regolith over considerable areas.

A brief description of the morphology of lunar surface material returned by Luna 16 automatic lunar station has been given in the first composite studies dealing with its investigation. This

article gives a more detailed morphological characterization of the sample of lunar surface material both as a whole as well as of its individual constituents.

The column of regolith upon sampling entirely filled the drill tube, and when transporting no appreciable mixing of the material in the tube occurred. The surface material transferred in a helium atmosphere to the receiving tray had no visible stratification and appeared to be homogeneous over its entire depth. The total weight of the regolith sample was somewhat more than 100 g.

The regolith as a whole consists of friable inequigranular dark-gray (blackish) material. Externally it appears to be finely grained powder on the surface of which coarser grains exhibiting an intense specular effect are noticeable. The powder is easily molded and adheres together into individual loose clods. On its surface are clearly imprinted traces of external actions -- impressions of instruments. The soil easily maintains a vertical wall, but when poured freely it has an angle of repose of about 45° (Fig. 1).

It should be noted that in spite of the appreciable adhesiveness, the surface material exhibits instability to vibratory actions. It easily sieved, traces of the disintegration of the structure of the surface material show up in the helium chamber after several days, and the sample of surface material poured in dry nitrogen into a little pile with a repose angle of about 30° and placed in a zone of a very weak, but constant vibratory action spread out completely in several months onto the substrate, with an angle of repose of not more than 5°.

An interesting property of the lunar surface material is its high electrification, which shows up in the adhesion of particles to surfaces of glass and plastic and to the preparatory instruments.

When the sample of lunar surface material was stored in ordinary laboratory conditions, in several months the increased adhesiveness and the ability of the material to become electrified ersisted.

The mean specific weight of the surface material in situ to the depth at which the drill was inserted when it was being filled was determined to be about 1.2 g/cm^3. This nearly corresponded to the heap weight of the surface material when freely poured into a small dish, which varied from 1.1 to 1.2 g/cm^3. Considering that the regolith is easily compacted when jostled to a specific weight /39 of about 1.8-1.9 g/cm^3, and that the strength of the lunar surface material rises markedly with depth, established by Surveyor and Apollo craft and confirmed by all the work done by Lunokhod 1,

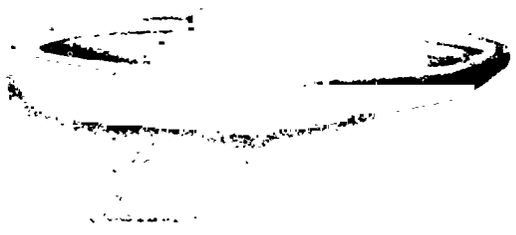

Fig. 1. Pile of lunar surface material in free heaping

it can be assumed that the density of the uppermost layer of the surface material from the Sea of Fertility approximates the density of the surface layer from the Ocean of Storms, which was determined to be 0.8 g/cm^3 by Luna 13.

Thus, with the mean specific weight of surface material particles at about 3 g/cm^3, the mean porosity of the lunar surface material in the Sea of Fertility is estimated to be about 60 percent at a depth of 35 cm, with a probable variation from 70 to 40 percent with increasing depth.

For further study, the sample on the tray was divided into zones, from which sampling was conducted. The samples were taken from depths of 1-8, 8-15, 15-28, and 28-33 cm, correspondingly, from zones A, B, V, and G.

Microscopic examination of the returned sample made it possible to differentiate two main groups of particles of lunar surface material: primary and secondary (Fig. 2). The group of primary particles is represented by fragments of magmatic rock of the basalt type filling the macro depressions of the Moon at the early stages of its geological history and the individual mineral grains comprising these rocks. The group of secondary particles includes material subjected to noticeable exogenic transformation on the surface of the Moon: they are secondarily lithified, densified grains consisting of fine fragments of regolith, and grains fused and melted at the surface to differing degrees.

Among the primary particles of lunar regolith can be singled out two groups reflecting the different conditions of the cooling of the basaltic magma -- fine-grained basalts and coarser-grained rocks of the gabbro type.

Fine-grained basalts are very fresh dense fragments of dark-gray rocks with pointwise inclusions of light minerals. These particles are characterized by angular shape and usually do not bear visible signs of roundedness. In several particles of these rocks pores and voids of various shapes are observed. Sometimes the particle surfaces can be seen to be sprinkled with fine crescents placed like glass, as a rule of rounded shape, which evidently can be attributed to impactive origin. The main rock-forming minerals of the fine-grained basalts are plagioclases, pyroxenes, ilmenite, and olivine. Glass is present at times in appreciable amount.

Particles of coarse-grained basalts, like those described above, are characterized by fresh fracture surfaces and in general by acute-angled form and do not disclose signs of weathering and roundedness (Fig. 3). Rock-forming minerals of these rocks are the same as those of finer-grained varieties, whose characteristic grain size is 0.3-0.5 mm. Quantitative ratios of the minerals vary appreciably in different fragments, which in particular is reflected in the coloring of the particles. In general, yellowish-pink tones are characteristic of the particles of these rocks. Among the particles of rocks of the microgabbro type varieties were observed containing voids, whose walls were lined with crystals of silicate minerals, markedly exceeding the size of the crystals in the ground mass.

The primary material of the lunar soil must be regarded as also including monomineralic aggregates, consisting nearly entirely of fine-grained plagioclase of the principal composition and representing formations of pure white or grayish color, of irregular shapes. Sometimes these particles contain inclusions of ilmenite crystals and grains of metallic iron. A considerable proportion of the primary material of the lunar surface material, especially in the finer fractions, is represented by monomineralic grains: olivine, pyroxene, and plagioclase.

Olivine is present in the lunar regolith in the form of well-preserved grains of irregular shape. The color of the grains varies from light-yellow to brownish-yellow. Very fresh particles of saturated yellow color with clean surfaces, sharp edges, and /40 fresh fractures are encountered, along with fused particles characterized as a rule by darker, brownish-yellow tones. Some proportion of the olivine grains are marked by a good state of preservation on the one hand, and by being fused on the other. Sometimes the olivine grains contain inclusions of dark minerals. Interestingly, in the samples examined quite often large single-grain olivine reaching 0.5-0.7 mm diagonally are encountered, which markedly exceeds the size of the olivine crystals in the fragments of magmatic rock examined.

Pyroxenes in the samples studied are present in the form of quite fine grains of yellowish-pink and reddish-pink color, of irregular shape. It bears noting that single-grain pyroxene is practically absent in the coarse fractions. An abrupt increase of these pyroxene grains was noted in fractions finer than 0.127 mm, and especially in fractions finer than 0.083 mm.

Single-grain plagioclase was found in the form of clear or matte laminae with sharp or slightly fused edges. Often the plagioclase grains showed a twinning effect. Like the single-grain pyroxene, the amount of single-grain plagioclase increases in the fine fractions. In fractions coarser than 0.127 mm as a rule plagioclase is encountered in the form of the above described aggregates.

Fig. 2. Particles of coarse regolith fraction

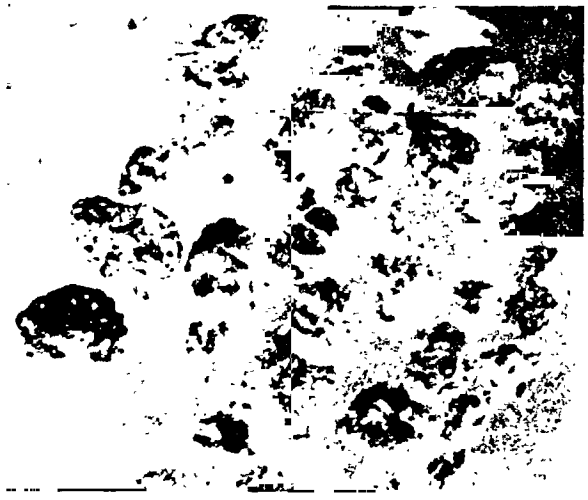

Fig. 3. Particles of igneous rock of the microgabbro type

Fig. 4. Particles of breccias with characteristic traces of melting

Fig. 5. Sintered particles of complex irregular shape

Secondary particles are a genetically important constituent of lunar regolith. Obviously, their investigation can shed light on the nature of the exogenic processes occurring on the surface of the Moon and on the possible pathways of regolith formation.

One of the main components of lunar surface material is the breccias (Fig. 4). Breccias are lithified rocks formed through the compaction of finely crushed regolith material. They are

gray or dark-gray in color and often contain light plagioclase inclusions. For the most part, the breccias are characterized by smoothed, rounded shaped, although particles with acutely-angled contours are encountered. The rounded form as a rule is intrinsic to those breccia particles that are marked by looser formation and weak compaction. These particles easily undergo disintegration when subjected to quite slight mechanical actions. Study of the breccias showed that they represent a conglomerate of mineral grains and fragments of rocks of various sizes. A considerable portion of the grains included in the breccia composition is fused.

A fairly large quantity of the breccia particles as such are subjected to fusion. Very dark, glassy crusts usually cover part of the particle, while the rest of it maintains a fresh appearance. The surface of the breccias, especially the large breccias, often prove to be layered with numerous craterlets lined with glass /41
particles giving the primary particle a cellular nature. The thickness of these crusts depends on the size of the primary particle and the degree to which the fusion process is manifested.

A no less interesting and important constituent of regolith is the secondarily consolidated formations -- sinters, very dark, nearly black aggregates of complex dendritic form consisting of sintered grains of lunar regolith (Fig. 5). In most cases, the sinters do not have acutely-angled shapes; the peripheral portions of these dendritoid aggregates usually are strongly fused and are characterized by rounded contours. Sometimes one-sided fusion of the sinters is observed. These particles exhibit different mechanical strength values, which is evidently associated with the temperature conditions in which the sintering process occurred and with the nature of the sintered particles. However, as a whole it can be noted that large sintered particles are usually stronger than small. In contrast to breccias, the morphology of these particles indicates their near-autochthonic formation directly at the surface.

It is probable that the complex shape of the sinters affects the mechanical properties of the lunar surface material and, in particular, is to some extent responsible for its low density and its considerable compaction upon vibration.

A characteristic secondary formation of the regolith is the secondary glass. Several forms of glass are differentiated, characterized by the intensity of the melting process: 1) glass films coating particles and lining the negative micromolds on their surfaces, 2) fragments of glass comprising fragments of wholly remelted rocks, and 3) diverse spherical formations.

Some of the particles are coated on one side with a thin surface film of glass glaze several microns or tens of microns thick. The color of the stone depends on the composition of the particles subjected to this fusion -- dark-brown and dark tones are common for breccias, black tones for sinters, while gabbroid rocks have films of brown, yellowish, and greenish colors. This local glazing of particles, while the fresh appearance of the rest of the grain is preserved, is possible only given the condition of a very energetic, but brief one-sided heating of the particle.

Usually the particles are fused, slagged to a considerable thickness, with a dark color and containing pores and voids in considerable numbers.

The wholly remelted particles, consisting of fragments of glasses of different forms, often with conchordal fracture, are characterized by a broad color spectrum, which reflects the composition of the fused grains. Vesicular varieties are not uncommon among the glasses. In this respect, of interest is one type of brown coarse-vesicular, thoroughly fused glasses which can be formed by crushing relatively large amounts of fused rock and externally resemble terrestrial glasses of volcanic origin.

An extreme type of glass particles is represented by the numerous spherical formations of various colors and shapes. Both particles with smooth surface exhibiting intense specular lustre /42 as well as particles with fine grains of surface material adhered to their surfaces are encountered. Not infrequently they contain bubbles, whose sizes can range up to half the diameter of the spherule.

It is probable that precisely the glass and vitrified particles with smooth surfaces on a dark base present in the surface material in considerable quantity that are responsible for the specular effect of the sample that was detected.

Among other types of particles, pieces of metallic iron observed both in the form of the regular fragments as well as in the form of spherules are encountered in small numbers. Often the pieces of the metal are included in breccias.

It is probable that meteoric origin can be attributed to these iron particles.

Obviously, the presence in particles of lunar surface material of metallic iron is responsible for their magnetism. Breccias, sinters, and slagged particles strongly adhering to a magnetized steel needle exhibit the greatest magnetism. Magnetism is also

TABLE 1. DISTRIBUTION OF TYPES OF PARTICLES IN LARGE FRACTIONS BY CORE ZONES (IN PERCENT)

Type of particle	A + B			V + G		
	+0.9 mm	+0.45–0.9 mm	$+\frac{0.127}{0.200}$ mm	+0.9 mm	+0.45–0.9 mm	$+\frac{0.127}{0.200}$ mm
Gabbro	13	14	19	18	12.5	13
Basalts	8	7.5	—	9.5	7	—
Anorthite, polycrystalline	0	2	0.5	1	3.5	1.5
Breccias	50	35	20	39	32	21
Sinters and slags	20.5	34	55.5	26	34	41.5
Glasses and monomineralic grains	5	2.5	13	2.5	5.5	21
Spherules	0	1	1	1	1.5	1
Others	3	3	—	2.5	3	—

TABLE 2. CONTENT OF GLASS IN FINE FRACTIONS OF REGOLITH (IN PERCENT OF TOTAL NUMBER OF PARTICLES)

Zone	Fraction size, microns			
	80—70	50—40	20—10	4—2
A	24	27	63	88
B	17	26	51	94
V	32	29	52	92
G	14	29	43	92

TABLE 3. MEAN WEIGHT OF PARTICLES (IN mg) BY CORE ZONES AND BY SIZE CLASSES

Class of grain size	A	B	V	G
+0.9 mm	2.00	1.87	3.12	3.22
−0.9+0.45 mm	0.274	0.294	0.302	0.344

shown by many glass spherical formations and by glass fragments (usually dark-colored), some aggregates of plagioclase, and some olivine grains. The fragments of crystalline rocks are nonmagnetic.

The nature of the distribution of the main types of particles of different sizes along core zones is extremely interesting. The data obtained for fractions greater than 0.127 mm in size are shown in Table 1. Here in the first column are grouped the monomineralic grains and glass fragments, since morphologically these particles are highly similar to each other. In the + 0.127 to 0.200 mm fractions are not included the number of fragments of finely crystalline basalts in view of the unreliability of identifying them from most of the particles.

Analysis of the table shows that secondary particles owing their origin to exogenic actions sharply predominate in the regolith composition. The content of breccias is very appreciable in the coarse fractions, while with decrease in particle size the relative content of sinters and slag materials somewhat increases. One should also note the decrease in the content of sintered aggregates of complex configuration from the surface downward along the length of the core, against a background of the total number of slags and sinters (combined in a single column in the table).

The amount of glass rises smoothly with decrease in particle size and in the finest fractions (4 μm and finer) represents their bulk (Table 2).

In determining the mean weight of particles of coarse fractions along the core length (Table 3), a well-defined /43
increase in the mean weight of particle with depth is observed not only for the +0.9 mm fraction (which could be associated with the increase in the size of the coarsest particles in the deeper zones), but also for the + 0.45 to 0.9 mm fractions. We correlate this with a decrease in the content along the core length of particles of irregularly shaped sinters. The + 0.9 mm fraction is well defined for its trend toward grouping of the two deep and two surface samples, which correlates with granulometric data.

Special underscoring must be made of the fact that the surface of numerous particles of various types bear traces of intense exogenic erosion. Here we can distinguish fine craterlets with traces of fusing of the material upon impact, as well as spalling of irregular shape, especially well defined on particles of glass and spherules. The density of these surface defects differs widely for different particles and for different surfaces of the same particle.

It is interesting to note that in several cases fine metallic films are observed on the surfaces of glass particles -- on spherules, fragments of glass of irregular shape, and slagged grains. The nature of these films can differ: in general they are uniform and translucent for spherules and glasses, while on slags the films are somewhat thicker and include irregular dabs.

As a result of the overall morphological study of the regolith sample from the Sea of Fertility, several genetic conclusions can be made.

The formation of lunar regolith occurred under the effect of two main factors -- crushing of the magmatic bedrock during vigorous meteoritic bombardment of the lunar surface (formation of groups of primary particles) and the agglomeration of the fine fragments of rocks formed during crushing into coarser secondary particles. The latter process was accompanied by intense, but short-lived thermal actions causing sintering and fusing of the regolith particles. As a whole, the regolith is a set of products of both exogenic and endogenic origins.

Active meteoritic bombardment of the lunar surface at supersonic velocities led to the fairly effective mixing of the regolith layer. This is indicated, in particular, by the absence of a rigorously defined correlation in the variation of particle content by core zones. However, as a whole the strong predominance in the regolith composition of secondary-origin particles and the increased content of the latter in the upper part of the core can be noted, indicating the intensity of the exogenic factors.

Also pointing to the vigor of the exogenic processes is the one-sided fusing of particles, the microcraters on their surfaces, the great diversity of particles, and the nature of their sintering into aggregates.

The one-sided fusing of particle surfaces and the sintering of many grains indicates an intense, but very short-lived heating of the particles not observed in processes of volcanic exposures, but typical of supersonic impacts. The diversity of the spherical silicate particles (spherules) also betokens their origin more likely due to the pointwise fusion of individual mineral grains and sections of rocks than due to the splashing of rock molten as a whole.

Traces of possible vulcanism can include no more than a percent of the well-fused glasses forming upon cooling of considerably large amounts of melt, whose origin however is possible also upon the impact of larger meteoritic bodies.

The simultaneous presence of fragments of primary magmatic rock formed in different conditions of crystallization and compositionally differing indicates the appreciable admixture of material brought in from great distances, averaging out the composition of the regolith over large areas. The transport of lunar-regolith particles also is evidently associated with impactive explosions, whose primary source was a meteoritic shower.

The general nature of the regolith sample from the Sea of Fertility is similar to the samples brought back earlier from the Sea of Tranquillity and the Ocean of Storms.

Institute of Space Research, USSR Academy of Sciences

Order of Lenin Institute of Geochemistry and Analytical Chemistry imeni V. I. Vernadskiy, USSR Academy of Sciences, Moscow

N75 11820

GRANULOMETRIC CHARACTERISTICS OF LUNAR SURFACE MATERIAL FROM THE SEA OF FERTILITY

/44

Yu. I. Stakheyev, Ye. K. Vul'fson,
A. V. Ivanov, and K. P. Florenskiy

Abstract

The particle size distributions in the 1-1000 μm range along the length of the core of lunar surface material returned by the Luna 16 AIS /automatic interplanetary station/ were recorded by electrical impulse as well as sieve methods. The measurements are represented in the form of cumulative functions of the logarithm of size versus the logarithm of particle number, and also as the logarithm of size versus particle mass on a probability scale. The former functions at all depths consist of the superpositioning of two straight lines with slopes from 2.10 to 4.05. The second functions are near-linear, which together with the closeness of the calculated asymmetries of the distribution to zero and the nearness of the calculated excess of the distributions to unity indicate the closeness of the recorded distributions to the logarithmically-normal law. This agrees with the assumption that regolith particles were formed in a process of intensive mechanical grinding. The mean particle size increases with depth from 62 to 114 μm, and the standard deviation of particle size rises from 1.80 to 2.42 (in logarithmic units). The hypothesis is advanced that the growth of the standard deviation of particle size with depth is due to processes of particle transport that are selective with respect to particle sizes.

The sample of regolith from the Sea of Fertility returned by the Luna 16 automatic interplanetary station is inequigranular disintegrated material /I_7. The granulometric composition is one of the most important primary characteristics of this kind of material. Knowing these characteristics is essential both

for understanding the process (or processes) of its formation, as well as for a proper interpretation of the results of investigating a long series of other physical characteristics of the material.

The method of transferring the lunar sample onto the receiving tray from the drill casing affords grounds to assume that during this operation the general stratigraphic sequence of the primary arrangement of material was not disturbed (or was disturbed only negligibly). It should be noted that no stratification on the tray was observed.

The sample on the tray was divided into zones /1/, from which sampling was carried out. The samples were taken from depths of 1-8, 8-15, 15-28, and 28-33 cm, respectively, from the zones A, B, V, and G. The weight of the samples varied from 2 to 5 g.

The granulometric investigation of the samples took place in two stages. The samples that were sampled from the receiving tray were divided into fractions by particle size with a sieve. To prevent contamination of the material with metals, sieves with capron meshes and teflon body were used. The use of these sieves also made it possible to appreciably reduce the effect of disintegration of the weak grains, compared with metal mesh sieves ordinarily used for this purpose. The meshes used in making the sieves had square openings with the following dimensions: 900, 450, 200, 127, and 83 μm. The coefficient of variation characterizing the scatter of the mesh openings of each sieve varied from 4.1 percent for the large sieves to 9.8 percent for the fine sieves.

For separation into fractions, the set of sieves was placed on a vibratory mechanism of a ball vibratory mill /2/ located in a box filled with ultrapure nitrogen. The mechanism provided an amplitude of vibrations in the horizontal plane of 6 mm. The frequency of the vibrations during sieving varied from 20 to 40 Hz.

Granulometric characteristics of the regolith fractions from the zones A, B, V, and G with particle size smaller than 83 μm were measured by an electrical impulse method /3/ making it possible to record the distribution of particle sizes from 0.2 to 200 μm. The particle sizes were entered in diameters of equivalent spheres. The range of sizes 0.2-83 μm was subdivided into 16 intervals for the regolith samples studied. The precision of the determination of the sizes of individual particles exceeded 1 percent. Weighed samples of about 25 mg were used in the analysis. /45

TABLE 1. NUMERICAL VALUES OF THE PARAMETERS OF THE PARTICLE SIZE-NUMBER DISTRIBUTIONS ON A BASIS OF 1 g SAMPLE BY ZONES

Parameter	A	B	V	G
Graphically determined statistical size of "coarsest" particle in sample (point of intersection with ordinate corresponding to one piece), mm	1.5	1.7	2.9	2.9
Particle size corresponding to point of interception of straight lines, μm	80	--	30	20
Number of particles with sizes greater than corresponding point of intersection of straight lines	$1.35 \cdot 10^5$	--	$2.5 \cdot 10^6$	$6.0 \cdot 10^6$
Number of particles larger than 4 μm	$1.0 \cdot 10^8$	--	$1.9 \cdot 10^8$	$1.8 \cdot 10^8$
Slope in the region of large particles	4.05	3.7	3.15	3.15
Slope in region of small particles	2.25	2.0	2.25	2.10

0.1 N HCl solution was used as the electrolyte in the measurements. The apertures of the measuring openings in the ruby washers were 270 and 140 μm. To eliminate the effects of addition of the impulses, the counting rate was lowered to 2000 impulses/sec by diluting the suspension. Repeat measurements of suspensions, taken with an interval of 24 hours, showed the absence of any appreciable effect of particle dissolution in the electrolyte used.

The dimensions of regolith particles from the Sea of Fertility varied as a whole from fractions of a 1 μm to several millimeters, which corresponds to the fine-grained portion of the regolith. The representation of the granulometric data in the following coordinates is highly revealing: logarithm of particle size versus logarithm of particle count in 1 g of material with size greater than the given value (Fig. 1). In these coordinates, the granulometric characteristics of the regolith are a superpositioning of two straight lines with different slopes, where the slope in the region of the fine particles is less than in the region of the large.

Fig. 1 shows only two such characteristics: for zones A and G, since the characteristics of zones A and B, on the one hand, and of V and G, on the other are close to each other.

From these graphs and from Table 1 it is clear that: 1) the slope (tangent of the angle of inclination) of the granulometric characteristics in the region of large dimensions decreases with increasing distance from the surface downward, from 4.05 to 3.15; 2) the slope in the region of small dimensions is larger than in the region of large, and is about 2.2 for all zones; 3) the size of the "largest particles" increases monotonely with depth from 1.5 to 2.9 mm; 4) the size of particles corresponding to the point of intersection of the lines decreases with depth from 80 to 20 μm; 5) the surface zones are depleted compared with the deep zones both in the coarsest as well as in the finest particles, which is compensated by an excess of particles of the mean sizes (50-150 μm); and 6) particles with sizes finer than 2-3 μm are in a deficit both in the deep as well as in the surface zones. The last fact is confirmed by electron microscopic examination with resolution better than 10 AU.

Morphological analysis of the sample of lunar surface material from the Luna 16 ALS /automatic lunar station/ landing site shows that the sample consists of particles of primary (fragments of magmatic rocks) and secondary (breccias, sinters, and slags) origin. This indicates that in the formation of the lunar regolith two opposing processes participated: crushing of bedrock and agglomeration of the fragments formed, with the formation of coarser secondary particles.

Two main factors affect the slope of the lines, characterizing to what extent the particle number increases in neighboring granulometric classes with decreasing size: the intensity of the crushing process and the mechanical strength of the crushed material. From /46 experience in investigating powders obtained by mechanical crushing, we know that in these coordinates they are characterized by slopes in the range 2.0-3.0 /4/. When rocks are crushed when colliding bodies are traveling at supersonic velocities, higher values of these coefficients are noted /5/.

The monotonic decrease of the slopes of the lines in the range of large particle sizes from the surface down into the deeper layers of the regolith indicates that crushing of bedrock is more intense at the surface and that its intensity falls off with depth. The high value of the slope (4.05) indicates that crushing most probably results from supersonic collisions of the crushing bodies (meteorites and micrometeorites) with the crushed material (lunar rock). The surface layers shield the deeper layers from the impacts and the intensity of crushing falls off. This is confirmed also by the increase in the sizes of the "coarsest" particles with depth.

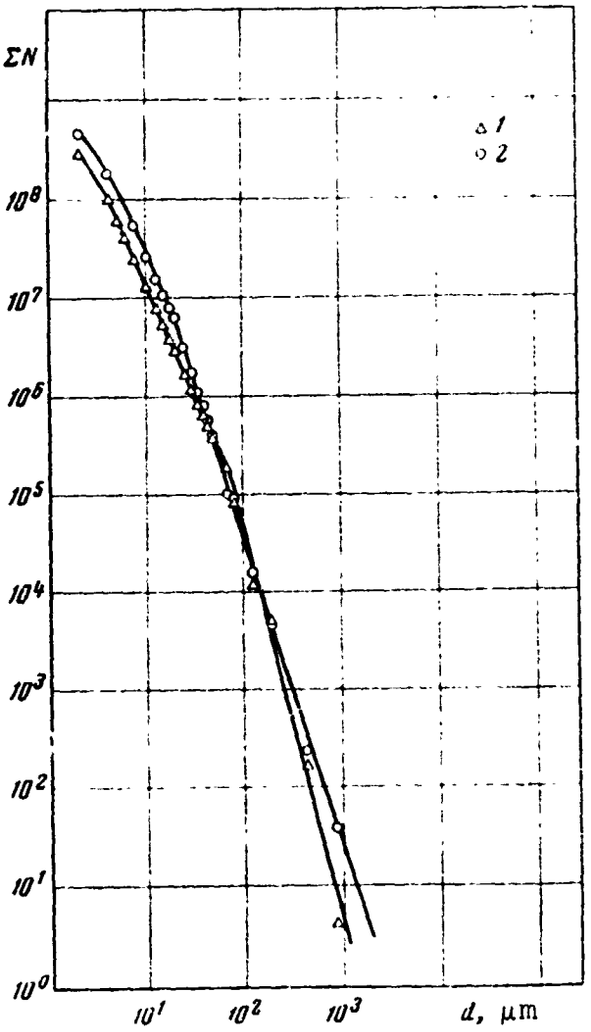

Fig. 1. Particle size distribution. Particle size is plotted along the X axis, and the overall number of particles greater than the given size, per gram of regolith, is plotted along the Y axis.
1. Zone A
2. Zone G

The approximate equality of the slopes in the region of fine classes is evidently more determined by the strength properties of the rock than by the intensity of the crushing. The mechanical strength of aggregates, pieces of rock, is always greater than for monomineralic particles, which then leads to the decrease in the slopes of the granulometric characteristics in the range of small sizes where the particles are basically single grains, and not their outgrowths, as in the range of larger sizes.

It is also highly probable that at these particle sizes in addition to crushing a marked role is played also by other processes, in particular, melting. The distribution of the sizes of the particles formed in this case will naturally obey other laws.

The larger coordinates of the points of intersection of the lines for the zones A and V (80 and 30 μm, respectively) compared with the deepest zone G (20 μm) probably reflect the corresponding contribution made by the particles of secondary origin (breccias, sinters, and slags). Actually, the counteraction of the two processes, crushing and agglomeration, for example as the result of secondary melting, caused by meteoritic bombardment occurring from the surface, must lead to a decrease in the particle sizes of primary rocks in the direction downward from the surface and simultaneously to an increase in the size of particles of secondary origin in the same direction. The crushing process will oppose the preservation of large particles of secondary origin in the surface layer.

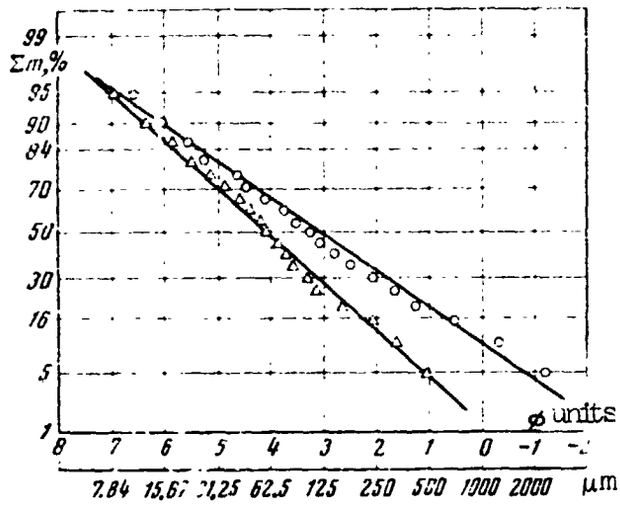

Fig. 2. Particle size distribution. Particle size -- along the X-axis, and total number of particles with size greater than the given size (in percent) -- along the Y axis

Δ. Zone A

O. Zone G

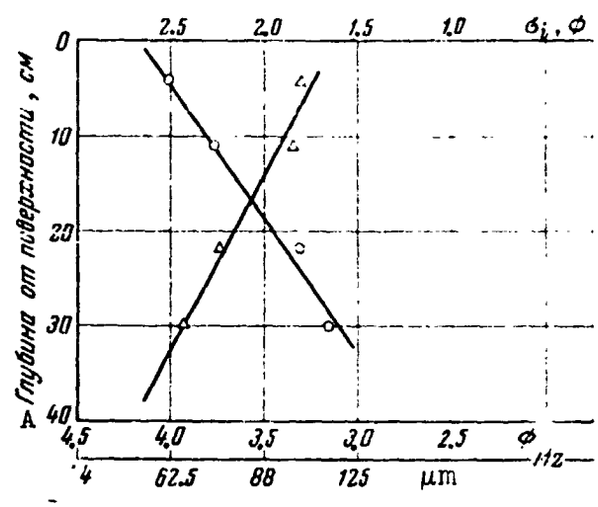

Fig. 3. Mean particle size and standard deviation of regolith particle sizes as functions of sample depth

O. Graphical mean size

Δ. Graphical standard deviation of particle size

KEY: A. Depth from surface, cm

In several cases, in particular for interpreting the data of chemical analysis of regolith fractions differing in grain size, the data must be represented on a logarithmically probable grid. This representation, moreover, is highly graphic in checking the resulting data for their closeness to the logarithmically normal law. The validity of this law for the distributions of particle sizes was demonstrated by Academician A. N. Kolmogorov for materials crushed over fairly lengthy time intervals [6].

Fig. 2 presents the data of granulometric analysis in the form of a cumulative dependence on a logarithmically probable scale. Along the X axis are particle sizes in Ø-units. They are associated with the particle sizes (in mm) by the following relation:

$$\log d = - Ø \log 2, \qquad (1)$$

where d is the diameter of the particles in mm.

Along the Y axis are laid out the total masses of particles with sizes greater than the given value, in percent.

To determine the statistical characteristics of the distributions, distribution quantiles were computed. The results of these calculations are in Table 2. Formulas proposed by Folk and Ward [7]

were employed in the calculations. The mean diameter (graphic mean) was determined from the expression:

$$M_z = \frac{\varphi 16 + \varphi 50 + \varphi 84}{3}, \quad (2)$$

where Ø 16, Ø 50, and Ø 84 are the diameters of particles in Ø-units, above which 16, 50, and 84 percent of the sample mass is contained, respectively.

The graphical standard deviation was computed by the expression:

$$\sigma_1 = \frac{\varphi 84 - \varphi 16}{4} + \frac{\varphi 95 - \varphi 5}{6.6}. \quad (3)$$

Graphical asymmetry was determined by the formula:

$$S_{K_1} = \frac{\varphi 16 + \varphi 84 - 2\varphi 50}{2(\varphi 84 - \varphi 16)}. \quad (4)$$

The graphical excess was computed by the relation

$$K_G = \frac{\varphi 95 - \varphi 5}{2.44(\varphi 75 - \varphi 25)}. \quad (5)$$

From Fig. 2 it is clear that the experimental points fit satisfactorily along a straight line and therefore the distribution of particle sizes can be approximated by the logarithmically normal law. Thus, this method of representing the granulometric analytical data also confirms the assumption that the regolith was formed in a process of intense, prolonged, mechanical crushing.

Analysis of the data in Table 2 shows that the numerical values of such distribution characteristics as graphical asymmetry and excess deviate negligibly from 0 and 1, respectively, indicating the closeness of the distributions to the logarithmically-normal. This is also indicated by the closeness of the median sizes (Ø 50) and the graphical means for each sample along the core depth. Two /48 characteristics: graphical mean and standard deviation -- disclose a systematic variation with depth. The mean particle size increases with depth, and the standard deviation of the grain sizes also rises with depth. These two functions are represented graphically in Fig. 3. Here the circles denote mean particle sizes and the triangles -- the numerical values of the standard deviations, and both are in Ø-units. The depth is plotted along the Y axis.

From experience in rock crushing we know that with increase in the crushing time or with the transition to more intense crushing processes, the mean particle size decreases, tending to some limit that is characteristic for the given crushed material and for the given crushing process (device). The standard deviation of the particle size rises in this case.

TABLE 2. QUANTILES AND STATISTICAL CHARACTERISTICS OF REGOLITH PARTICLE SIZE DISTRIBUTIONS BY CORE DEPTH

Sample	L-16A	L-16B	L-16V	L-16G
Mean depth from surface, cm	4	11	22	30
Quantiles				
5	1,029	0,761	−0,632	−1,203
16	2,184	2,000	1,000	0,644
25	3,120	2,556	2,184	1,643
50	4,058	3,662	3,473	3,251
75	5,158	5,011	4,878	4,836
84	5,795	5,644	5,442	5,506
95	6,965	6,878	6,796	6,796
Graphical mean, μm	62	73,5	101	114
As above, Ø-units	4,012	3,769	3,305	3,134
Graphical standard deviation	1,800	1,837	2,235	2,425
Graphical asymmetry	−0,029	+0,026	−0,109	−0,093
Graphical excess	1,107	0,989	1,099	1,015

The observed regularities of the variation of mean particle size of lunar regolith and the corresponding standard deviations with increasing depth of sampling from the surface cannot be accounted for only by the process of crushing originating from the surface.

In terrestrial conditions a decrease of the standard deviation of particle size (sorting) relative to the initial value is widely known in the formation of riverine and aeolian deposits, dune and beach sand, and loess. In all these cases the cause of the decrease of the standard deviation of particle size is the transport of parcels formed in the given erosional processes by water or air. These transporting media are not present on the surface of the Moon. Nonetheless it can be assumed that the decrease of the standard deviation of particle size in regolith in the direction toward the surface is caused by processes of transporting (transport) of particles that are selective with respect to particle size. The causes of this transport can be explosive phenomena occurring in the collision of meteorites with the surface of the regolith. Relatively fine particles with greater ratio of cross section to mass compared with the coarser particles will under the action of an explosion acquire greater velocities and be transported over greater distances, spending more time in flight. It is not precluded that here the finest particles can acquire velocities exceeding the second cosmic velocity for the Moon and leave it. This possibly accounts for the deficit of particles

with sizes finer than 1-2 μm in the regolith composition. Quantitative estimates of the scales of this kind of process require a knowledge of the distributions of the masses and velocities of meteorites striking the surface of the Moon and also the distributions of the masses and velocities of fragments formed in these collisions.

Summing up, we can note:

1. The law of the distribution of lunar regolith particle size to depths of about 40 cm from the lunar surface is close to logarithmically normal.

2. The mean size of lunar regolith particles increases with depth from 62 to 114 μm. /49

3. The standard deviation of particle size increases with depth from 1.80 to 2.43 in passing from the surface layers to the deeper layers.

4. Asymmetry and excess of the distributions of particle sizes differ only slightly from those characteristic of the logarithmically normal law and do not disclose regular changes with depth.

5. A deficit of particles with sizes smaller than 1-2 μm is observed in the lunar regolith.

6. These granulometric characteristics of the regolith are in agreement with the assumption that the regolith was formed in the collisions of meteorites with the lunar surface. It is suggested that these collisions are both a cause of the grinding of the primary lunar rocks as well as the selective, with respect to size, transport of particles on the lunar surface as well as the departure from the Moon of some fraction of particles with sizes smaller than 1-2 μm.

REFERENCES

1. Vinogradov, A. P., "Preliminary Data on Lunar Surface Material Returned by Luna 16 Automatic Station," Geokhimiya (3), 261-274 (1971).

2. Vul'fson, Ye. K., Ivantsov, L. M., and Stakheyev, Yu. I., "Method of Rapid Granulometric Analysis with High Resolution," Zav. labor. 32(10), 1226 (1966).

3. Kuznetsov, Yu. N., and Stakheyev, Yu. I., "Mechanization and Automation of Operations in the Spectral Analysis of Ore," Tsvetnaya metallurgiya (5) (202), 38 (1962).

4. Hartmann, W. K., "Terrestrial, Lunar, and Interplanetary Rock Fragmentation," Icarus 10(2), (1969)

5. Mukhametzhanov, A. K., "Functions of Distribution by Fragment Size in Intense Explosions," Astronom. vestnik (2), 90-96 (1968).

6. Kolmogorov, A. N., "Logarithmically Normal Law of the Distribution of Particle Size in Crushing," Dokl. AN SSSR 31(2), 99 (1948).

7. Folk, R. L., and Ward, W. C., "Brazos River Bar: A Study in the Significance of Grain Size Parameters," J. Sediment Petrol., 27, 3-26 (1957).

Order of Lenin Institute of Geochemistry and Analytical Chemistry imeni V. I. Vernadskiy, USSR Academy of Sciences

Institute of Space Research, USSR Academy of Sciences, Moscow

N75 11821

MORPHOMETRIC CHARACTERISTICS OF PARTICLES OF REGOLITH RETURNED BY LUNA 16 AUTOMATIC STATION

/50

P. V. Florenskiy, I. Ya. Belen'kiy,
N. M. Karachentseva, and L. F. Pankratova

Abstract

A study was made of the shape of regolith particles in the 0.5-1.0 mm fraction; two parameters were calculated for this fraction: 1. sphericity -- the ratio of the projection area of a particle to the area of the minimum circumscribed circle; and 2. the ratio of the perimeter of the projection of the particle to the perimeter of a circle having the same width. For comparison, this technique was used in studying geometrical figures and terrestrial formations: sands, slags of present-day volcanoes, and crushed basalt. It was established that as to shape regolith particles form the following groups: spherules; breccias and fragments; slags and sinters. Regolith differs sharply from ordinary homogeneous terrestrial formations in the diversity of particle shapes, associated with their polygenicity. Fragments of crushed basalt are less regular than fragments of basalt from regolith, which is probably associated with some processing of the regolith particles. The proposed technique can be used when working with an electronic computer and a scanning device.

Processes occurring in friable material are essentially associated with the shape of its individual particles, which depends, on the one hand, on their internal properties, and on the other -- on their history. Particle shape determines in turn numerous properties of a material, in particular, friability, abrasiveness, density, porosity, permeability, and many others. Many studies have dealt with formalized numerical morphometric characteristics, most often referring not to the spatial shape of the particle, but with its plane image. It was established that it is possible to quite exactly characterize a plane figure by comparing it with another figure adopted as a reference standard;

and in practice it is most convenient to select a circle as this reference standard. Here the features of the distribution permit an evaluation not only of the features of the composition, but also of the genesis and history of the rock, as shown for the example of terrestrial sedimentary formations [5].

Particles of lunar regolith from the 0.5-1.0 mm fraction corresponding to coarse-grained sand were studied with photographs. As we know [1], several petrographic subdivisions were made in its composition: sinters and slags (34 percent) breccias (33 percent), coarse-grained basalts not containing glasses (13 percent), fine-grained basalts containing glass base (7 percent), fragments of glasses and monocrystals (4 percent), intergrowths of plagioclases are predominantly bytownite (3 percent), and spherules (1 percent). For comparison, terrestrial sands of various degrees of roundedness, basaltic slag from the cone of a Late Quaternary volcano, and basalt crushed in a mortar were analyzed. Both samples were from Armenia [3].

Two of the numerous morphometric characteristics proposed by various investigators were selected. The first of these characterizes the sphericity of a particle [2] and is the ratio of the projection area of the particle to the area of the minimum circumscribed circle. Determining it is easy, by weighing figures of the particle and the circumscribed circle cut out of paper. This ratio varies from unity for a circle to zero for a thin line with infinitely distant ends; actually, it exceeds 0.20 and usually varies in the range 0.40-0.80.

The second parameter characterizes the unevenness of the contour of the particle and is the ratio of the perimeter of the circle as wide as the particle to the perimeter of the particle itself. It is determined by superimposing a rectangular grid by the method of S. A. Saltykov [4], using the formula:

$$\frac{R_{\text{equivalent circle}}}{R_{\text{particle}}} = 4.513 \frac{\sqrt{F}}{P},$$

where F is the number of intersections of the gridlines with each other within the bounds of a particle, and P is the number of intersections of the gridlines with the particle contour. This ratio varies from unity for a circle to zero for extremely fanciful formations of the spiderweb type; but actually it ranges in the limits 0.60-1.00.

The precision of determining both ratios is not less than 3 percent, but usually 1-2 percent; their convergence is approximately the same for different positions of the particle. Both ratios can be easily determined on an electronic computer with a scanner [4]. In the graph (Fig. 1), where the sphericity of the

/51

MORPHOMETRIC CHARACTERISTICS OF PARTICLES OF LUNAR REGOLITH AND SEVERAL TERRESTRIAL FORMATIONS /51

Constituents of regolith and terrestrial formations	Number of particles in regolith	Number of measured particles	Ratio of particle area to area of inscribed circle (sphericity)		Ratio of circle perimeter equal to particle diam. to particle perimeter	
			mean	Standard deviation	mean	Standard deviation
Regolith (Luna 16)						
Sinters		10	0.43	0.09	0.71	0.09
Glasslike crusts (slags)	34	6	0.51	0.13	0.76	0.09
Breccia	33	16	0.65	0.06	0.91	0.05
Coarse-grained basalt without glass	13	9	0.64	0.07	0.86	0.07
Fine-grained basalt with glass	7	7	0.56	0.06	0.91	0.02
Fragments of glass and monocrystals	4	16	0.65	0.07	0.93	0.03
Intergrowths of plagioclases	3	7	0.64	0.06	0.91	0.04
Spherules	1	17	0.80	0.07	0.98	0.02
Total: regolith as a whole	95	81	0.59	0.20	0.84	0.13
Terrestrial formations						
Sand, well-rounded	—	—	0.73	0.05	0.98	0.02
Sand, poorly rounded	—	—	0.53	0.08	0.92	0.03
Slag from rim of volcanic crater	—	—	0.58	0.13	0.86	0.06
Crushed basalt	—	—	0.53	0.15	0.89	0.06

grains is plotted along the vertical and the degree of the non-uniformity of their contour -- along the horizontal, are presented all the regolith particles analyzed. Shown in the same graph is a line along which the circle is advanced with increasing transition to an ellipse with increasing degree of compression, and along which a square is advanced with increasing transition to an elongated rectangle, and an equilateral triangle -- with increasing transition to an acute wedge. Some figures are drawn on the graph. Thus, in the upper right-hand corner of the graph is placed a circle, and in the lower left-hand portion -- figures of the type of snowflakes or needlelike formations. Most of the actual particles lie to the right and to the bottom of the diagonal near the line of the evolution of ellipses.

The mean and standard deviations were calculated for all the petrographic groups of regolith particles (see Table). The probable deviations of the mean do not exceed 1-3 percent, that is, they correspond to the precision of the determination. By analyzing the graph (Fig. 1) and the table, one can make several observations.

1. Regolith particles lie in three nearly nonoverlapping fields: I. spherules; II. breccias and fragments of minerals and rocks; and III. slags and sinters.

2. The shape of nearly all particles is intermediate from rectangular to ellipse, and to a lesser extent -- from triangle to rectangle; only the slags and sinters have more complex surface and are located to the left.

3. Fine-grained basalts are most elongated and closest to ellipses; in contrast coarse-grained basalts have the most acicular contour; it is probable that in the 0.5-1 mm fraction their shape depends strongly on their internal polycrystalline structure. Fragments of glasses, monocrystals, and outgrowths of plagioclases are more isometric than basalts, and their facets are simple.

4. Grains from different terrestrial sands tend to ellipses by the nature of their surface and do not have analogs in the regolith (excluding spherules).

5. Fragments of terrestrial basalts crushed in a mortar are very similar to the fragments of fine-grained basalt from the regolith by the regularity of the facets, but are more diverse in shape and differ from the regolith by the presence of highly elongated and acute-angled fragments. It is not precluded that /52
the absence of these particles in the regolith is not so much associated with the particular differences of the basalts as much as indicative of some treatment of the regolith particles resulting from multiple redeposition owing to meteoric impacts.

6. Particles of basaltic slag from the rim of the cone of a present-day volcano, not subjected to any appreciable treatment, are also more heterogeneous in shape than the breccias of regolith and tend to slags and sinters.

Considering the ratio in the regolith of particles of different petrographic types /1/, their distribution curves with respect to both ratios were plotted -- overall, by component (not shown in the graphs), and the distribution for particles of terrestrial formations (Figs. 2 and 3). Analysis of these distributions confirms the earlier-made observations and others as well.

7. By the diversity and heterogeneity of the sphericity and surfaces, the regolith as a whole differs very strongly from terrestrial formations, which as a rule are more homogeneous.

8. The specific distribution of regolith particles, having several peaks, reflects differences in shape and genesis of regolith /53
components, which are nearly totally unobserved in terrestrial formations, incomparably more homogeneous.

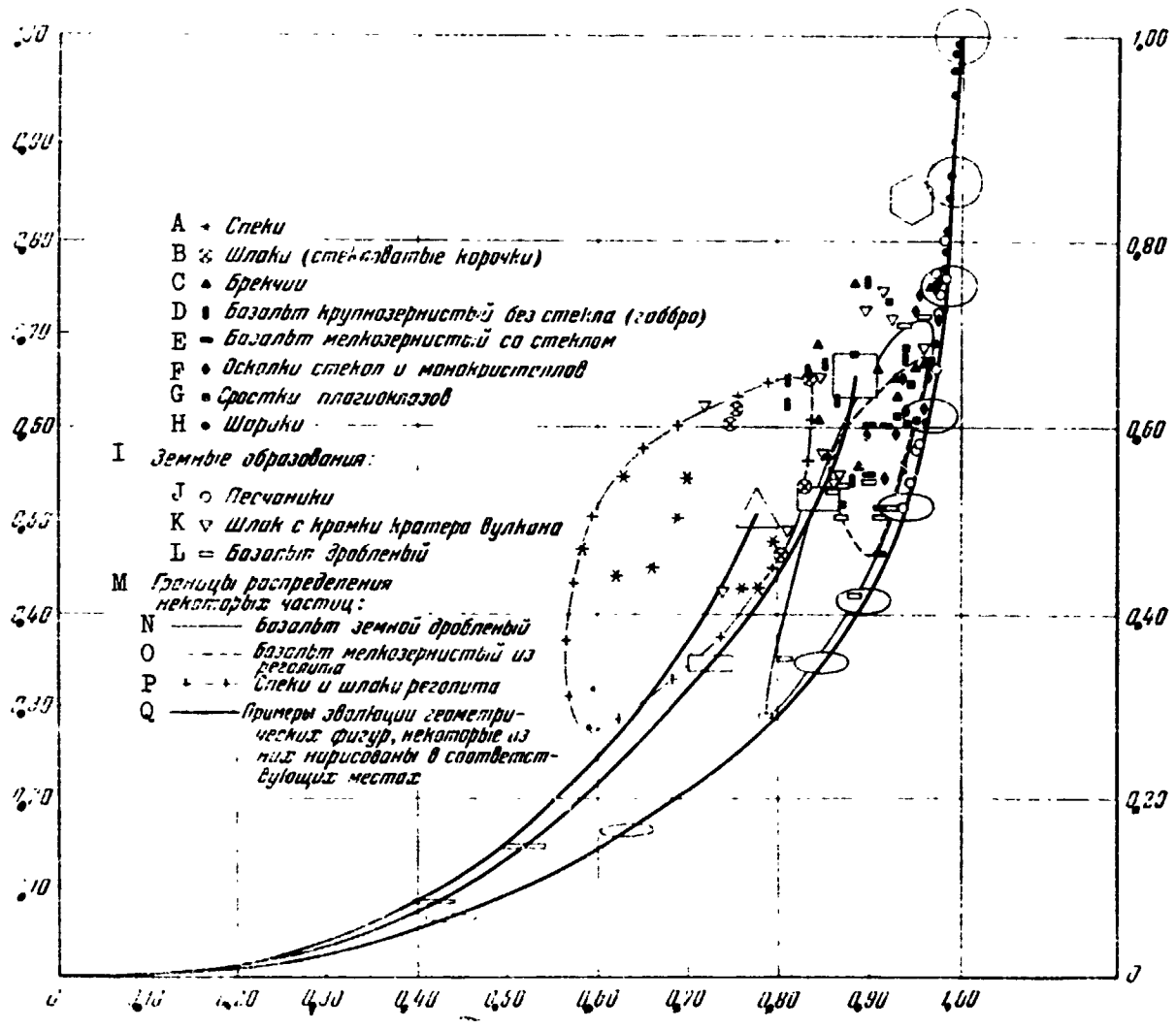

Fig. 1. Distribution of lunar regolith particles and of several terrestria. formations, by form. Plotted along the vertical is the sphericity (ratio of area cf particle to area of minimum circumscribed circle), and along the horizontal -- the nature of the surface (ratio of perimeter of circle as wide as the particle to the perimeter of the particle itself).

KEY:
A. Sinters
B. Slags (glassy crusts)
C. Breccias
D. Coarse-grained basalt containing no glass (gabbro)
E. Fine-grained basalt containing glass
F. Fragments of glasses and monocrystals
G. Growths of plagioclases
H. Spherules
I. Terrestrial formations
J. Sandstones
K. Slag from rim of volcanic crater
L. Crushed basalt
M. Limits of the distribution of several particles
N. Basalts, terrestrial, crushed
O. Fine-grained basalt of regolith
P. Sinters and slags of regolith
Q. Examples of evolution of geometric figures, several of which are inscribed at the corresponding places.

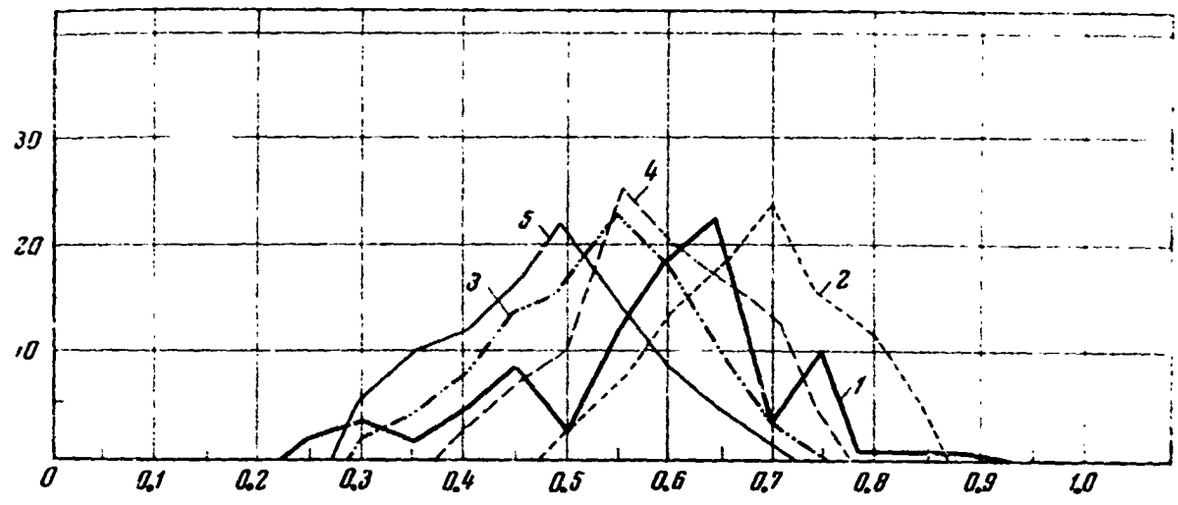

Fig. 2. Sphericity distribution of particles
1. Regolith
2. Rounded sand (after T. A. Lapinskaya [2])
3. Unrounded sand (after T. A. Lapinskaya [2])
4. Basaltic slag
5. Basalt, crushed in mortar

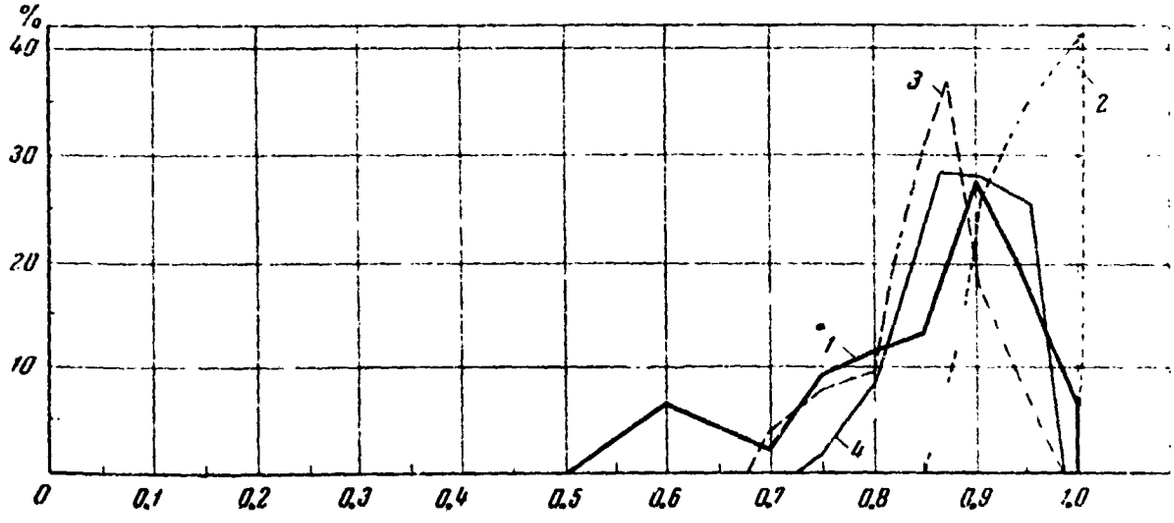

Fig. 3. Distribution of particles by nature of surface
1. regolith
2. sand
3. basaltic slag
4. basalt, crushed in mortar

9. Thus, based on morphometric analysis of regolith particles and a comparison of these particles with terrestrial and artificial formations, not only can a classification reproducible on an electronic computer be proposed, but also the assumption of the genesis of the particles and the trends in the evolution of their shape, similarity, and differences with terrestrial rocks.

In assembling the initial material and in the discussion of the results, much assistance was given by A. V. Ivanov, for which the authors are grateful.

REFERENCES

1. Vinogradov, A. P., "Preliminary Data on Lunar Surface Material Returned by the Soviet Luna 16 Station," Geokhimiya (3), 261-274 (1971).

2. Lapinskaya, T. A., "Quantitative Characterization of Shapes of Grains of Fragmental Minerals," Sov. geologiya (18), 156-163 (1947).

3. Mkrtchyan, K. A., Trifonov, V. G., and Florenskiy, P. V., " 'Picture Gallery' of the Stone Age," Prioroda (3), 78-79 (1969).

4. Saltykov, S. A., Stereometricheskaya metallografiya /Stereometric Metallography/, "Metallurgiya", 1970.

5. Florenskiy, P. V., and Lapinskaya, T. A., "Problems in the Theory of Sedimentary Formation," in the book: K voprosu o sostoyanii nauki ob osadochnykh porodakh /Problem of the Status of the Science of Sedimentary Rocks/, USSR Academy of Sciences Press, 1951.

Moscow Institute of Petrochemical and Gas Industry imeni I. M. Gubkin.

N75 11822

MEASUREMENT OF DENSITY AND POROSITY OF LUNAR ROCKS BASED ON SAMPLES OF LUNA 16 AUTOMATIC LUNAR STATION

/54

V. F. Volynets, K. P. Florenskiy,
and A.V. Ivanov

Abstract

Three fragments of holocrystalline igneous rocks of the gabbro type, weighing 30-50 mg each, were investigated. The density of the fragments was established with a mercury pycnometer and was found to be 3.05-3.12 g/cm^3, with a relative error not more than 2 percent. The porosity was found for the difference between the volumes determined with the mercury and with the gas techniques; for all three samples together it was 13 percent, and the error of determination was 70 percent owing to the small volumes. It can be anticipated that the porosity of the rock in bulk will be higher than the value obtained based on small fragments. The porosity of lunar rocks can markedly affect the isostatic distribution of rocks and must be taken into account when developing models of lunar structure.

In estimating the internal structure of the Moon, it is often stated that its mean density (3.34 g/cm^3) is close to the mean density of stony meteorites (ordinary chondrites 3.5-3.6; carbonaceous chondrites of type III 3.4-3.5 g/cm^3) and of ultrabasic rocks comprising the Earth's mantle (3.3-3.4 g/cm^3) [1-3].

These values do not agree closely enough with the high density of lunar rocks [4] and the isostatic structure of the lunar crust [5, 6], which can be partially accounted for by the inadequate allowance for the porosity of lunar rocks; this property can markedly affect the isostatic distribution of rocks. Actually, in conditions of the reduced gravity on the Moon (gravitational acceleration at its surface is 162 cm/sec^2, or 0.16 of the terrestrial acceleration), it can be anticipated that the plasticity yield of rocks corresponding to the disappearance of porosity on the Moon will correspond to a depth of 60-70 km.

DENSITY AND POROSITY OF LUNA 16 LUNAR SAMPLES

Sample number	Weight mg	Total vol. based on Hg, mm^3	Volume based on gas, mm^3	Sp. gr. g/cm^3	Density g/cm^3	Porosity %
L-1611-013	51.1	16.4	33.5	3.12	3.5	13
L-1611-007	36.2	11.6		3.12		
L-1611-009	30.5	10.0		3.05		
		38.0				

Existing definitions give the porosity of stony meteorites of the order of 10-15 percent /7/, which then must be taken into account when setting up meteoritic models of lunar structure. The porosity of rocks, plainly visible to the eye, has not been adequately studied. Data in the literature indicate that the porosity of lunar samples is close to the porosity of meteorites /4, 8/. Unfortunately, in several cases the terminology used by the authors and the physical meaning of the quantities presented remain unclear in the studies.

Our investigations unfortunately cannot be regarded as adequately representative, since we studied only small fragments of crystalline rocks of the Moon and there are grounds to suggest that the porosity of the rock in the bulk will be higher than the value [illegible] from its small fragments.

[illegible] fragments of holocrystalline igneous rocks of the gabbro type [illegible] from the fraction coarser than 1 mm of the zone G of the [illegible] regolith core were investigated (see Table). Two particles [illegible] of irregular acicular shape, and the third particle was lamellar. The maximum particle sizes were as follows: L1611-013 -- 4 x 3.2 x 3 mm, L1611-007 -- 4 x 3 x 2.5 mm, and L1611-009 -- -- 4 x 3.5 x 1.5 mm.

Sample L1611-013. The mineralogical composition is as follows: pyroxenes, plagioclase, ilmenite, and infrequent olivine crystals. /55 The predominant grain size is 0.1-0.25 mm. Pores of irregular shape are noted on the sample surface.

Sample L1611-007. In mineralogical composition and grain size, this sample is similar to the first. Here, in addition to irregularly shaped pores there are appreciably larger vacuoles of regular spherical shape, about 0.5-0.7 mm in diameter. The pores and the vacuoles sometimes are interconnected. It is important to note that the walls of the spherical vacuoles are formed of crystals of the primary minerals of the rock, which evidently indicates the formation of these vacuoles during their crystallization period.

Sample L1611-009. The general mineralogical composition of the particle is overall the same as for the preceding samples, however it has an appreciably more leucocratic appearance, determined

by the considerably greater plagioclase content. In addition, the grain sizes of this fragment are somewhat coarser than the preceding samples and as a whole vary in the range 0.2-0.4 mm. Pores of irregular shape are detected in the particles, and the crystals of minerals surrounding these pores are characterized by regularity of shape and by larger size, compared with the groundmass.

The porosity of the lunar rock fragments was determined with a mercury pycnometer fitted with a glass filter. The sample was placed under the glass filter and the pycnometer was filled with mercury through a capillary. The excess drop of mercury from the capillary was removed mechanically. Air bubbles trapped in the mercury were cleared out by vacuum evacuation. To average the degree of pycnometer filling for all random positions of the sample fragment, 20-30 parallel determinations were run. And only for the third sample was this procedure found to be inappropriate, since this piece of rock had the shape of a thin lamina and could be measured only in two positions. All the densities in the table are given for 20° C. The relative root mean square error of the method for samples weighing 30 to 50 mg does not exceed 2 percent.

The porosity was determined directly from the difference of the total volume of the sample immersed in mercury and the true volume of the solid constituent measured by the gas technique with all open pores filled. The porosity could be measured only for all three samples together. The determination was made using the gas device designed by K. P. Florenskiy [9] for nitrogen and argon at room temperature. The device can evacuate a sample to a pressure of $1 \cdot 10^{-6}$ mm Hg and measure down to $1 \cdot 10^{-5}$ cm^3 of gas. Using the calibrated volume V_1 at the pressure P_1, n moles of gas was introduced into the volume containing the sample, and the gas was used in filling the volume of the sample pores and in adsorption, as a result of which a gas pressure P_2 was established in the system. The determination of the volume in which the sample was placed was made by an independent method.

The calculations presented show that these results agree closely with the calculated results if we take $n_{ads} = cP^2$. In this case the formula for computing the volume of the sample excluding pores V_x can be represented as follows:

$$V_x^{ef} = V_x - cP^2T, \quad \text{where } V_x^{ef} = V - \frac{P_1V_1}{P_2},$$

and V is the volume of the system. Owing to the very small volumes of the measured sample, the relative error of determination of V_x in this case was $\pm$ 70 percent.

These measurements indicate high porosity of the lunar sample studied, which must be taken into account when estimating the density of the lunar crust.

REFERENCES

1. Vinogradov, A. P., "High-Temperature Protoplanetary Processes," Geokhimiya (11), (1971).

2. Zharkov, V. N., Pan'kov, V. L., Kalachnikov, A. A., and Osnach, A. I., Vvedeniye v fiziku Luny /Introduction to the Physics of the Moon/, "Nauka", 1969.

3. Mason, B., Meteoritiy /Meteorites/, "Mir", 1965.

4. Kanomori, H., et al., "Elastic Wave Velocities of Lunar Samples at High Pressures and Their Geophysical Implications," Proc. Apollo 11 Lunar Sci. Cont., 3, 2289-2293 (1970).

5. Wood, J. A., Marvin, U. B., Povell, B. N., and Dickey, J. S., Jr., "Mineralogy and Petrology of the Apollo 11 Lunar Sample," SAO SR 307, 1970.

6. Jeffries, G., Zemlya, yeye priskhozhdeniye, istoriya i stroyeniye /Earth: Its Origin, History, and Structure/, Foreign Literature Publishing House, 1960.

7. Alekseyeva, K. N., "Physical Properties of Stony Meteorites and Their Interpretation in the Light of the Hypotheses on the Origin of Meteorites," Meteoritika (15), (1958).

8. Anderson, O. L., et al., "Elastic Properties of Microbreccia, Igneous Rock, and Lunar Fines from Apollo 11 Mission," Proc. Apollo 11 Lunar Sci. Conf., 3, 1959-1973 (1970).

9. Florenskiy, K. P., "Device for Microanalysis of Inert Gases," Dokl. AN SSSR 12(3), (1957).

Order of Lenin Institute of Geochemistry and Analytical Chemistry imeni V. I. Vernadskiy, USSR Academy of Sciences

Institute of Space Research, USSR Academy of Sciences, Moscow

N75 11823

PETROLOGY OF LUNAR ROCKS FROM THE SEA OF FERTILITY

/56

A. S. Pavlenko, L. S. Tarasov,
I. D. Shevaleyevskiy, and A. V. Ivanov

Abstract

Based on a comparative analysis of the petrochemistry of an integrated sample of gabbro-basalts and a fine fraction from regolith returned by Luna 16 automatic station from the Sea of Fertility, with the mean compositions of various types of mare basalts, and anorthosites, and regolith from the Sea of Tranquillity and the Ocean of Storms, with reference to several data on rare elements, the nature of the course and fine fractions is discussed. It is shown that the integrated sample of gabbro-basalt from the coarse fraction in the lower part of the core can be represented as mixture of mare basalts of the Sea of Tranquillity and nonmare basalts of the krip type in the ratio of about 3:2. It is confirmed that the compositions of the Apollo 11 and Apollo 12 regolith are complementary with the compositions of basalts and anorthosites of the Sea of Tranquillity and the Ocean of Storms, and thus they correspond to their compositions in ratios that are close to those calculated for the "mixture model" of Hubbard and Gast. The composition of the fine fraction of the Sea of Fertility regolith is very close to the composition of the Sea of Fertility regolith and cannot be obtained by adding some actual composition to the gabbro-basaltic constituent.

The central problem in investigating the regolith returned by the Luna 16 automatic station from the Sea of Fertility is comparing its composition with rocks and samples of surface material from the Sea of Tranquillity and the Ocean of Storms. This is of paramount value for determining the differentiation of the Moon and the nature of the regolith proper.

Several constituents have been distinguished in the regolith composition in terms of mineral and chemical compositions [1-7]. The principle of these are: gabbro and basalts, hypersthenic gabbro and their glassy analogs, norite-anorthosites, and possibly unusual granitelike rocks rich in SiO_2, K_2O, ZrO_2, Li, Y, Ba, Rb, Pb, Nb, Y, Th, and U, from the sample 12013 and acidic residual glasses similar to it in the basalts of Sea of Tranquillity [8].

According to the concepts of Hubbard and Gast [7], two types of basaltic-composition rocks are represented in the regolith of the Ocean of Storms and the Sea of Fertility: "mare" and "nonmare". The latter have increased content of silica that is close to terrestrial basalts, and also several rare elements (Yb, Zn, P, Rb, U, and Th) and a deep Eu minimum. They constitute 30-70% of Apollo 12 regolith and about 10% in the Apollo 11 samples. Anorthsites amount to 20% in the Sea of Tranquillity regolith.

By comparison with terrestrial basalts, "mare" basalts of the Moon are strongly enriched in iron and poor in sodium. At the same time, the content of calcium and aluminum in these basalts are comparable. The distribution of rare earths (the Eu minimum is absent in the earth, and the content of light and intermediate to heavy rare-earth elements fluctuates widely) differs fundamentally in lunar and terrestrial basalts.

Among the mare lunar basalts basalt are singled out three groups (Table 1).

1. Those with high Fe content, moderate Ti, and low K, Ba, La, and U (Apollo 12, analysis 1 and some in their opinion, the Luna 16 sample).

2. Those with a high content of Fe, high Ti, and low K, Ba, La, and U (Apollo 11, analysis 4).

3. Those with a high content of Fe, high Ti, and high K, Ba, La, and U (Apollo 11, analysis 3).

To this it should be added that the basalts of the Sea of Storms compared with the Sea of Tranquillity are somewhat more silicic and less calcic (Figs. 1-3).

While the mare basalts are encountered both as a regolith fraction as well as in the form of large rocks and clods, hypothetical "nonmare" glasses and breccias were detected only in the regolith composition. The yellow-brown glasses and crystalline breccias containing hypersthene -- pigeonite -- included therein are similar compositionally to terrestrial basalts [7]. They differ from the latter only by a low Na_2O content, and from mare lunar basalts -- by higher Al_2O_3 content compared with CaO, and lower TiO_2 and F

[57]

content. According to McKey et al [4], Hubbard and Gast [7], these breccias include 40% plagioclase, 13% clinopyroxene, 13% orthopyroxene and 17% glass; Wood et al. [5] also noted olivine. And thus, these formations differ from mare basalts by the abundance of low-calcic pyroxene varying from hypersthene to ferrohypersthene, and by the predominance of plagioclase over the mafic minerals. Some investigators called them KREEP (krip) [7] from their high content of K, TR, and P, or norite [5]. Hubbard and Gast believed that the dark fractions of the rock 12013 and Lunar Rock 1 are also close to krip. Judging from the chemical composition, the yellow-brown glasses are contaminated with mare basalts. Interestingly, their composition is very close to eucrites differing from the latter only by the higher Mg/Fe ratio (see Table 1 and Fig. 2).

TABLE 1. CHEMICAL COMPOSITION OF LUNAR ROCKS AND METEORITES

No.	SiO_2		TiO_2		Al_2O_3		FeO		MgO		CaO		Na_2O		K_2O		P_2O_5
	Wt.%	Mol.%	Wt.%	Mol.%	Wt.%	Mol.%	Wt.%	Mol.%	Wt.%	Mol.%	Wt.%	Mol.%	Wt.%	Mol.%	Wt.%	Mol.%	Wt.%
1	45.03	45.7	3.36	2.6	9.17	5.5	21.60	18.3	10.89	16.5	9.81	10.7	0.29	0.2	0.58	0.5	0.10
2	46.4	50.2	3.0	2.5	14.1	9.0	10.6	9.6	10.3	16.6	10.0	11.6	0.40	0.3	0.20	0.2	0.21
3	40.30	43.0	11.49	9.2	8.72	5.4	19.55	17.4	7.64	12.2	10.45	12.0	0.52	0.5	0.30	0.3	0.13
4	40.58	43.5	10.23	8.2	10.19	6.5	19.03	17.0	6.92	11.0	11.55	13.3	0.41	0.4	0.08	0.1	0.09
5	42.3	44.5	8.0	6.3	14.0	8.6	15.5	13.6	8.0	12.5	12.2	13.7	0.62	0.6	0.19	0.2	0.15
6	43.8	46.8	4.9	3.9	13.65	8.5	19.35	17.3	7.05	11.2	10.40	11.9	0.33	0.3	0.15	0.1	0.20
7	41.6	44.3	3.4	2.8	15.3	9.6	16.4	14.6	8.8	14.0	12.6	14.3	0.34	0.3	0.11	0.1	0.13
8	49.0	52.2	2.0	1.6	15.0	9.4	11.5	10.2	8.0	12.6	11.0	12.5	0.8	0.7	0.8	0.7	0.6
9	48.0	51.9	1.6	1.3	19.0	12.1	9.0	8.1	8.0	12.8	10.5	12.1	1.0	0.9	0.9	0.8	0.8
10	48.41	52.3	1.66	1.4	20.13	12.8	8.14	7.3	7.41	11.9	11.03	12.7	0.89	0.9	0.88	0.7	1.2
11	45.65	50.0	0.18	0.2	31.1	20.0	3.65	3.3	4.03	6.6	15.53	19.3	0.48	0.5	0.1	0.1	—
12	73.5	82.5	0.5	0.4	12.2	8.1	0.9	0.4	0.4	0.7	1.2	1.4	1.4	1.2	6.9	5.3	—
13	70.8	80.5	0.6	0.5	12.7	8.2	6.3	2.5	0.4	0.7	1.0	1.2	1.1	0.8	7.4	5.6	—
14	60.7	70.2	0.3	0.3	20.5	13.9	0.2	0.1	0.2	0.3	3.5	4.3	1.1	0.9	13.1	10.0	—
15	48.06	52.3	0.5	0.5	13.90	9.0	17.03	12.8	7.04	11.5	10.99	12.9	0.70	0.9	0.21	0.2	0.12
16	49.64	54.2	0.27	0.3	9.26	6.0	16.81	8.5	12.69	20.8	7.57	8.9	0.89	1.1	0.30	0.2	0.07
17	38.04	36.3	0.11	0.1	2.50	1.4	25.07	25.5*	23.84	33.7	1.96	2.0	0.98	0.9	0.17	0.1	0.1

* Atomic %.

Analyses:

1. Mean for mare basalts of the Ocean of Storms.
2. Mean for the regolith of the Ocean of Storms (computed by the authors).
3. Mean for high-rubidium mare basalts of the Sea of Tranquillity.
4. Mean for high-rubidium mare basalts of the Sea of Tranquillity.
5. Mean for the regolith of the Sea of Tranquillity (computed by the authors).
6. Integrated sample of gabbro-basalts from the lower part of the core of the Sea of Fertility regolith.

7. Fine fraction of Sea of Fertility regolith, mean of five analyses.
8. Mean for yellow-brown glasses of the Ocean of Storms.
9. Mean for hypersthene-containing nonvaried basalts of the Ocean of Storms type.
10. Mean of eight analyses of Ocean of Storms anorthosites.
11. Salic constituent of tests made in sample 12013 -- mean of nine analyses.
12. Mean of six Sea of Tranquillity anorthosites.
13. Potassic rhyolite, fragment in regolith of Ocean of Storms (102-5).
14. Potassic residual glass in norite-anorthosites of Ocean of Storms.
15. Mean for 12 eucrites.
16. Mean of 11 howardites.
17. Mean composition of chondrites (data of Hubbard and Gast [7], Wood et al. [5], and Mason [9] were used).

The group of norite-anorthosites and anorthosites approaches "nonmare" basalts in a number of features. They are also found exclusively in the form of fragments and breccias in the regolith, contain low-potassic hypersthene or pigeonite, and have reduced ilmenite contents. Wood et al. [5] differentiates two types among the Ocean of Storms norite-anorthosites: A -- recrystallized breccias and B -- less abundant -- uncrystallized breccias. The latter /58
are present to a greater extent than plagioclase (in fragments) and are closer to anorthosites in gross composition. On the other hand, in type A pyroxene is ferruginous, and plagioclase is sodic. Among the anorthosite particles of the Sea of Tranquillity is also a predominance of recrystallized breccias of type A, although in a relatively lesser amount. In contrast to Apollo 12 material, Apollo 11 anorthosites contain much more plagioclase and with a single exception are very poor in ilmenite; they are devoid of witlokite, zircon, and are rich in residual-glass potassium typical of Ocean of Storms norite-anorthosites. Correspondingly, the Apollo 11 anorthosites have a low content of K_2O and TiO_2 (see Table 1, analyses 10 and 11), but a higher content of normative olivine. However, in the view of these authors, the differences do not preclude interconversions and a genetic relationship between Apollo 11 /59
and Apollo 12 anorthosites. As for the potassic granite-rhyolites, as far as we know only one particle with this composition (102-5) was found thus far in the regolith (Wood, Marvin et al. [5], see Table 1, analysis 13). However, as suggested by Drake et al. [4], the textural features of sample 12013 containing voids and lead-vein-like precipitates of potassic granites (see Table 1, analysis 12) show that these rocks should have been formed during the recrystallization of rhyolitic ignimbrites. In this case, the possibility of their appearance in regolith is increased.

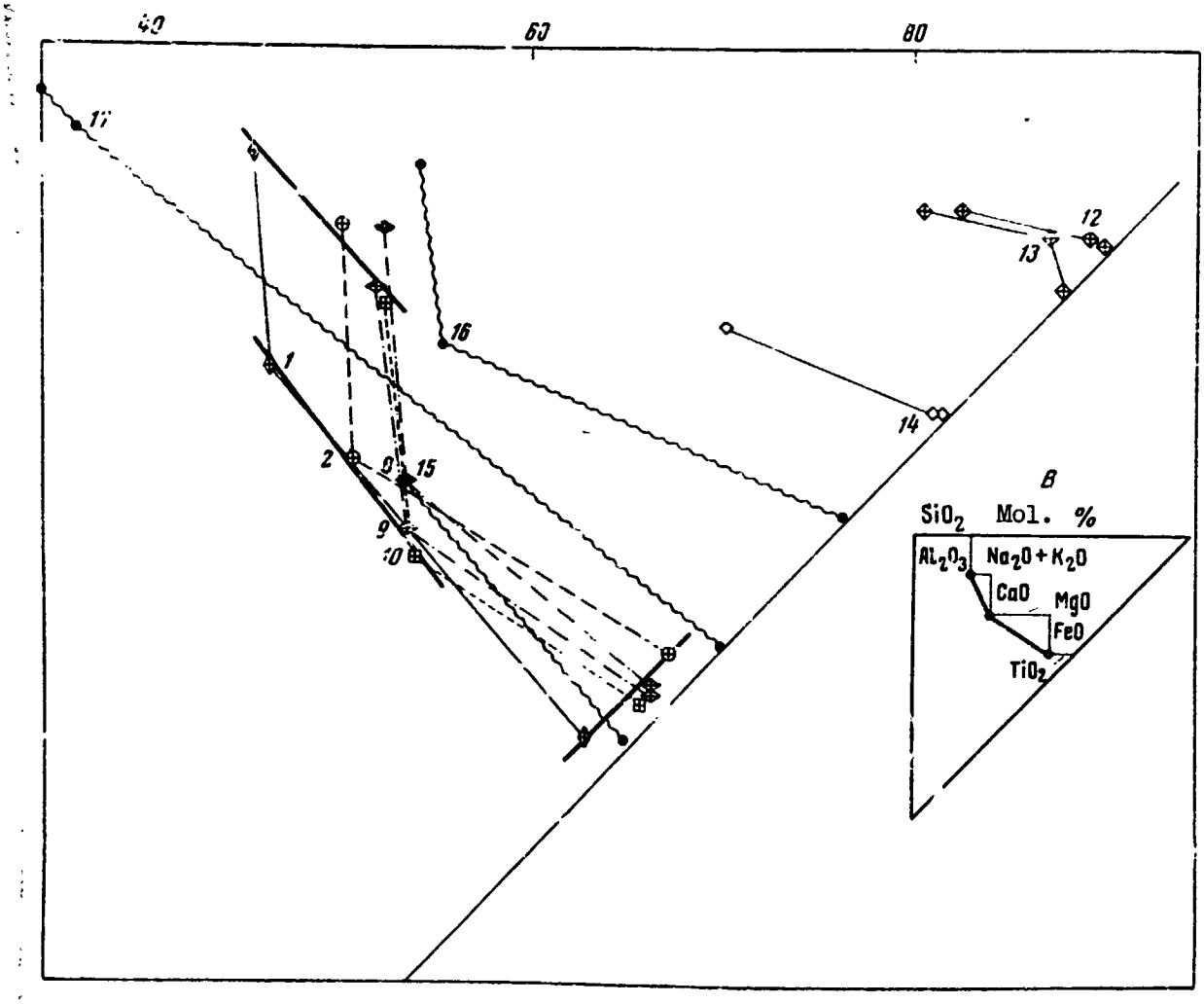

Fig. 1. Seven-constituent composition diagram of rocks and regolith of the Ocean of Storms. The method of constructing the diagrams in Figs. 1-3 is shown in the lower right hand corner.

1. mare basalts
2. regolith
8. yellow-brown glasses
9. nonmare basalts (krip)
10. anorthosites
15. eucrites
16. howardites
17. chondrites

12-14. "granitic", K-enriched compositions. The numbers 1-17 in Figs. 1-3 correspond to the analysis numbers in Table 1. The bold-faced numbers in Figs. 1-3 are the lines of complementarity.

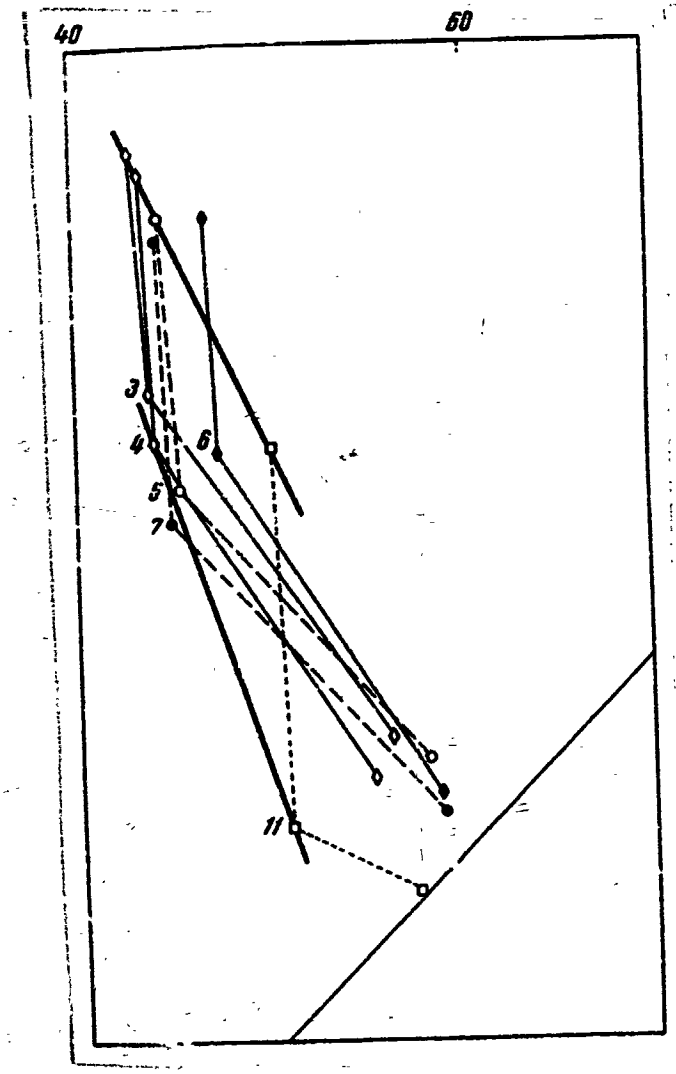

Fig. 2. Composition diagram of and regolith of the Sea of Tranquillity and Sea of Fertility
3. high-rubidium basalt
4. low-rubidium basalt
5, 7. regolitn
6. basalt
11. anorthosite

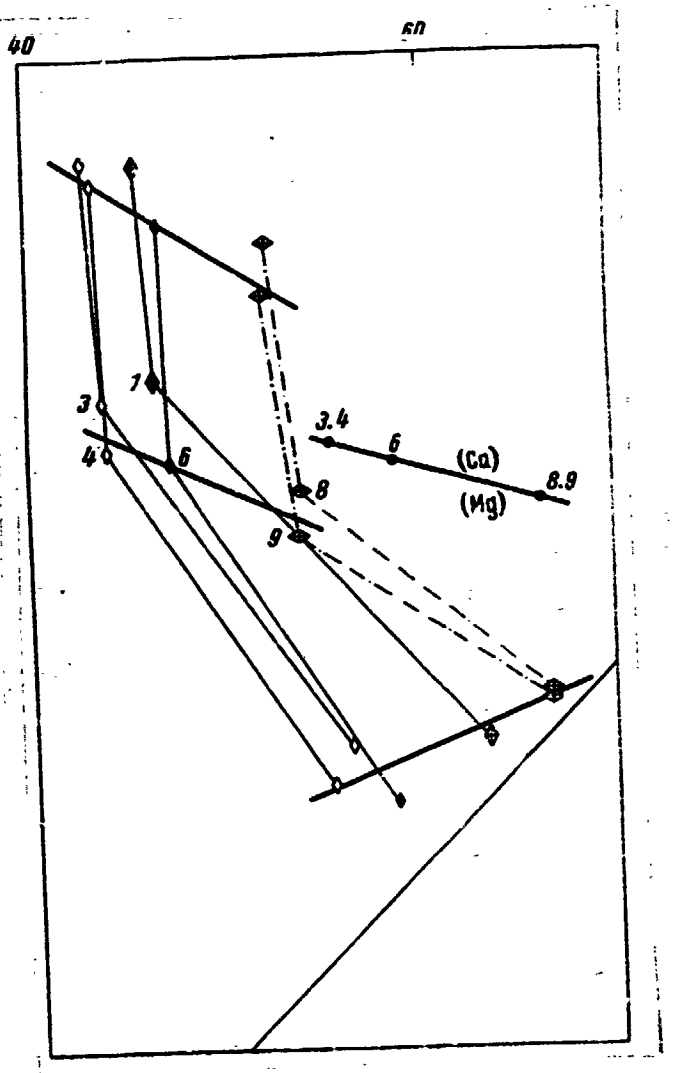

Fig. 3. Composition diagram of basaltic rocks of the Moon. The Arabic numbers indicate the same as in Fig. 1. Clearly seen is the complementarity of the mare basalts of the Sea of Tranquillity, the gabbro-basalts of the integrated sample of the Sea of Fertility, and the nonmare hypersthene-containing basalts of the type of Ocean of Storms krip.

Based on the chemical and isotopic "mixture" model developed by Hubbard and Gast, the Apollo 12 regolith contains 70-30% mare basalts, 30-70% nonmare krip rocks, and about 1% silicaceous rocks. Apollo 11 regolith developed with considerably more intense working and hybridization. This was reflected in the appearance of two types of basalts with low and

high Rb content of different ages and probably from different sources. The "mixture" model gives the following composition for it: 70% low-rhbidium basalt, 20% anorthosite, and 10% krip.

Let us examine the petrochemical characteristics of samples of Sea of Fertility lunar rocks compared with the same for the Sea of Tranquillity and the Ocean of Storms. As already reported [6], basalts and gabbro from regolith returned by Luna 16 are characterized by an integrated sample weighing 100 mg composed of fragments of the primary representatives of these rocks taken approximately in proportion to their distribution in the regolith. The most widely distributed varieties in the sample are characterized by the photographs in Figs. 4-8. The composition of plagioclases, the ferruginicity of olivines, and the especially high calcicity of the clinopyroxene indicates their origin in mare type basalts. As shown by Table 1 and the diagram in Fig. 3, the composition of the integrated sample of Luna 16 gabbro-basalts differs appreciably from the mare and nonmare basalts of the Sea of Tranquillity and the Ocean of Storms. By content of alkalies, CaO, MgO, and FeO, it is compositionally similar to the low-rubidium basalts of the Sea of Tranquillity, differing from them by the considerably higher silica content, and is comparable in SiO_2 and TiO_2 content with the mare basalts of the Ocean of Storms. The alumina content is higher than in any of the groups of the mare basalts. /60

As we can see from the construction on the diagram (see Fig. 3), in terms of the content of all constituents except FeO and TiO_2, which is associated with some deficit of ilmenite, the composition of the sample is complementary with the compositions of Apollo 11 mare basalt and Apollo 12 nonmare basalts (krip rocks) and occupies an intermediate position with respect to them. Thus, judging from the content of the rock-forming constituents, the composition of the integrated sample of gabbro-basalts from the Sea of Fertility can be interpreted as a mixture of Sea of Tranquillity mare basalts and nonmare krip rocks in approximately the ratio of 3:2. A confirmation of the existence in the Sea of Fertility regolith of fragments of rocks of the krip type is found in the discovery of pyroxene grains with augite-pigeonite composition in the ratio 1:2 (augite and pigenite are closely intergrown, forming a disintegration structure) [10]. In favor of this assumption, indirect support is given also by the increased content of K. Ba (206 g/ton), Sr (445 g/ton), and P (Table 2) compared with the Sea of Fertility basalts. True, the content of the rare earth is only slightly increased, but this too can indicate the presence of krip rocks (Table 3). /61

Proceeding to consider the petrochemistry of the regolith (see Table 1, analyses 2, 5, and 7; and Figs. 1 and 2), we know first of all that the mean compositions of soils computed by the data [1-3] for the Sea of Tranquillity and the Ocean of Storms differ widely from each other and are clearly associated with the

Fig. 4. Basalt. In composition: olivine, brown clinopyroxene, plagioclase, ilmenite, and some dark glass. The idiomorphism of the plagioclase with respect to the dark-colored constituent is clearly evident (section 8)
a. photograph 30/7, without analyzer
b. photograph 30/6, crossed Nicol prisms, X 40.

Fig. 5. Olivine-augite melanocratic fine-medium granular gabbro (section 12)
a. photograph 21/11, without analyzer
b. photograph 21/10, crossed Nicol prisms, X 40.

compositions of the rocks of the given region. There is a strict complementarity between low-rubidium basalt, regolith, and anorthosite for the Sea of Tranquillity where the extreme values of these constituents (see construction in Fig. 1) are mixed in the regolith in a ratio 1:5 - 1:6, which is very close to the above-presented data of the working mixture model of Hubbard and Gast. /62

Fig. 6. Melanocratic olivine-augite fine-grain gabbro with hypidiomorphogranular texture (section 15, photograph 23/1, crossed Nicol prisms, X 30)

Fig. 7. Ophitic olivine-pyroxene gabbro (section 29, photograph 23/10, crossed Nicol prisms, X 30)

Fig. 8. Coarse-grain olivine-augite gabbro (section 14, photograph 22/9, crossed Nicol prisms, X 30)

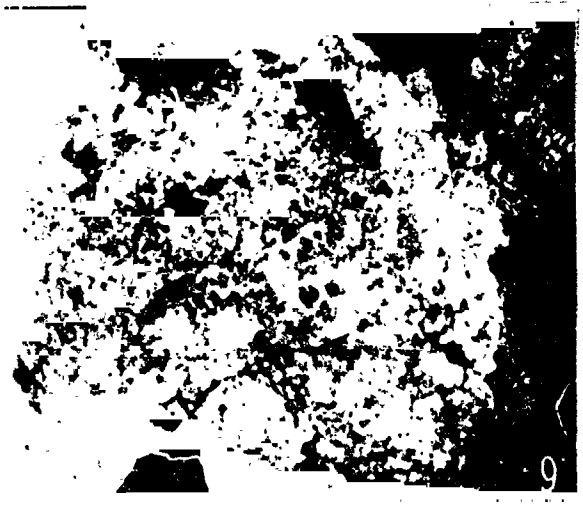

Fig. 9. Anorthosite with "metamictized" texture (section 16, photograph 28/5, crossed Nicol prisms, X 30)

Similarly, in the "mean" regolith of the Ocean of Storms, mare basalts and anorthosites are mixed in approximately equal amounts (see Fig. 2); they nearly entirely coincide in composition with the nonmare krips. This is also in accord with the mixture model. It

is appropriate to note the Mg/(Mg + Fe) ratio that is the inverse of terrestrial evolution, in rocks that can be considered as successive differentiates. It increases in the series mare basalt -- nonmare basalts -- anorthosite -- potassic granitoid residue. The magnesiality of the regolith is distinctly shifted toward the side of the later differentiates (Table 4), which also indicates its hybrid nature.

TABLE 2. CONTENT OF ALKALIES AND ALKALINE TURFS IN BASALTS OF THE SEA OF TRANQUILLITY, OCEAN OF STORMS, AND SEA OF FERTILITY (in g/ton), ACCORDING TO HUBBARD AND GAST [7] AND VINOGRADOV [6]

Rock type	Na	K	Sr	Ba
Low-rubidium basalts, Apollo 11	3100	665	110	90
Mare basalts, Apollo 12 (mean of 8)	1820	520	112	60
Gabbro-basalts of integrated regolith sample	2440	1250	445	206
Soils and breccias, Apollo 12 (mean of 5)	4400	3009	178	587
Nonmare basalts, Apollo 12 (krip type, mean of 6)	7000	5196	198	1050

TABLE 3. CONTENT OF RARE EARTH IN APOLLO 12 MARE BASALTS, AND IN LUNA 16 GABBRO-BASALTS AND REGOLITH, ACCORDING TO HUBBARD AND GAST [7] AND VINOGRADOV [6]

La	Ce	Pr	Nd	Sm	Eu	Gd	Tb	Dy	Ho	Er	Tu	Yb	Lu	
6,02	17,6	—	13,5	4,73	0,995	6,29	—	7,36	—	4,45	—	4,40	0,58	Mare basalts, Apollo 12, mean of 6
7,7	23,6	4,8	25	7,1	1,2	4,8	0,9	5,2	2,0	5,0	0,4	3,6	0,3	Gabbro basalts, Luna 16
7,5	23,5	4,6	23	6,3	1,4	5,3	0,9	5,1	2,0	4,9	0,4	3,5	0,3	Fine fraction, Luna 16 regolith

TABLE 4. MAGNESIALITY (Mg/(Mg + Fe), MOLE FRACTION) OF LUNAR ROCKS

Landing site	Mare basalts		Nonmare basalts		Potassic granitic residue		
	low-rubidium	high-rubidium	Brown glass	krip	Anorthite		Regolith
Apollo 11	0,393	0,411	—	—	0,667	0,833	0,478
Apollo 12	0,475		0,554	0,614	0,619	0,625	0,634
Luna 16		0,394			—	—	0,490

An entirely different pattern is characteristic of the Sea of Fertility regolith. Its composition coincides nearly entirely with the mean composition of Sea of Tranquillity regolith, with only a slightly higher Al_2O_3 content and reduced TiO_2 content. This is also confirmed by the data of fraction analysis [11]. None of the conceivable compositions, including meteoritic (see Figs. 1 and 2), can upon being mixed with "integrated" basalt (Table 1, analysis 6) yield the composition of Luna 16 regolith. The latter can be regarded as representative: the mean of four X-ray spectral and one chemical analysis from various core zones. Therefore, the only explanation of the unusual compositional ratio of Luna 16 gabbro-basalt and regolith is the enrichment of the coarse fraction with krip type material concentrating in the lower part of the core from which the integrated sample was taken. The fine fraction of regolith containing a constant composition virtually identical with the mean (see Table 1, analysis 7) [6] was found to contain no material of the krip type in appreciable amounts. From the similarity of the chemical and mineral compositions, it can be regarded as ilmenite-poor, an analog of Sea of Fertility regolith. [63]

REFERENCES

1. Science 167, 3918 (1970).

2. Proc. Apollo 11 Lunar Science Conference, Vol. 1, 1970.

3. Science 167, 1325 (1970).

4. Drake, M. J., McCallum, J. S., McKey, G. A., and Weill, D. F., "Mineralogy and Petrology of Apollo 12 Sample, No. 12013" (a progress report).

5. Wood, J. A., Marvin, U., Reid, I. B., Teilor, G. I., Bower, J. E., Powell B. N., and Dickey, I. C., "Relative Proportion of Rock Types and Nature of the Light Colored Lithic Fragments in Apollo 12 Soil Sample," Proc. Second Lunar Sci. Conf., 1971.

6. Vinogradov, A. P., "Preliminary Data on Lunar Surface Material Returned by Luna 16 Advanced Station," Geokhimiya (3), 261-274 (1971).

7. Hubbard, N. I., and Gast, P. W., "Chemical Composition and Origin of Nonmare Lunar Basalts," NASA Manned Spacecraft Center, Houston, Texas, 1971.

8. Roedder, E., and Weiblen, P. W., "Lunar Petrology of Silicate Melt Inclusions, Apollo 11 Rocks," Proc. Apollo 11 Lunar Sci. Conf., Vol. 1, 801-837 (1970).

9. Mason, Ye., Meteority /Meteorites/, "Mir", 1965.

10. Makarov, Ye. S., et al., "Mineralogy and Crystal Chemistry of Lunar Surface Material Returned by Luna 16 Station," Report Presented at a Session of COSPAR, 1971.

11. Florenskiy, K. P., Ivanov, A. V., Stakheyev, Yu. I., and Tarasov, L. S., "Morphology, Particle Types, and Granulometry of Regolith From the Sea of Fertility," paper presented at a session of COSPAR, 1971.

Order of Lenin Institute of Geochemistry and Analytical Chemistry imeni V. I. Vernadskiy, USSR Academy of Sciences

Institute of Space Research, USSR Academy of Sciences, Moscow

N75 11824

PRELIMINARY REPORT ON MINERALOGICAL AND PETROGRAPHIC STUDY OF THE LUNA 16 LUNAR SURFACE MATERIAL SAMPLE

/106

M. Christophe-Michel-Levi, C. Levi,
and P. Pierreault

We had made available to us 33.6 mg of unsorted powder and 13.4 mg of grains larger than 0.5 mm from the portion 118-111 with a total weight of 59 mg from the sample L-16-19-118. The largest particles were cleaned with ultrasound in triply distilled alcohol, then dried in a drying oven. They consisted of eight basaltic fragments, four fragments of breccias, of which one was quite light, one white grain (which proved to be maskelynite), one chondrule, and slagged dark, partially glassy chunks.

The single fragment of basalt, the two breccias, the one white grain, and the one chondrule were mounted in a clear-polished section. Preliminarily, the morphology of the chondrule was studied. 33.6 mg of the powder was sieved into two fractions with grain size smaller than and larger than 100 μm. A clear-polished section was prepared also from a batch of grains taken at random from the fraction finer than 100 μm (section No. 21395).

Electron-microscopic study of particles. Many grains were investigated by electron microscopy after gold deposition in vacuum.

Fig. 1 shows the typical appearance of the dark slags. The strongly vesicular glass enclosed crystals (evidently, the feldspar barely broke through to the surface) and trapped dust particles which adhered to its surface.

We also studied the surface of the "chondrule", which we thus named in contradistinction to the spherules of clear glass and on analogy with the meteoritic chondrules (Figs. 2-5).

Chondrules and rounded particles. This spherule 1.3 mm in diameter had a rough surface to which dust particles adhered. The "hollows" showed a glassy fracturing, where no texture could be

differentiated (Fig. 3). One typical impact microcrater with fragments of spherules lies in this hemisphere (Fig. 4), while the brittle growth of the minute prism embedded in the phenocryst of the feldspar projecting at the surface of the chondrule (Fig. 5) was preserved. This chondrule was cut across its diameter, part being preserved and a thin lamella being forced into the other (Fig. 6). It made it possible to see the phenocrysts of anorthite with straight contours, and pyroxene with rounded contours, about which very thin fibers of pyroxene and feldspar developed in glass similar to the structure of honeycomb. The nature of the fibers was checked with an x-ray diffraction pattern.

The coarse anorthite crystal contains numerous cavities in the form of bubbles, a single drop of troilite, and fine inclusions of oxides concentrated in the crack. The phenocrysts here are not crystals randomly embedded in the glass, rather they were formed in it.

Another chondrule was in section 21,395. This is a minute spherule of devitrified glass, 50 μm in diameter, not containing phenocrysts (Fig. 7). Several infrequent spherules of devitrified glass were noted in the Apollo 11 and Apollo 12 regolith. They also contain no phenocrysts. Several chondrules were noted in the breccia of Apollo 14 (especially, in sample 14,318). /108

Here we can also include the more or less rounded grain in whose glass olivine is developed in the form of parallel laths. This structure is similar to the lathlike structure of meteoric chondrules, however in the chondrule we studied the olivines were more dendritic (skeletal crystals; Fig. 8). Three grains of pyroxene which partially fused, preserving a thin film of glass on their surfaces, were also classed in this group of particles.

Each spherule consists of a single crystal (Fig. 9). The mineralogical composition of all these rounded particles led us to the assumption that they are all of lunar origin, but their presence in the regolith gives valuable information that can assist us in understanding the method by which the chondrulic meteorites were formed. The existence of several grains of pyroxene coated with a thin glassy film, so precisely that it gives the impression of having been formed by fusion without visible distortion of the margins of the crystalline grain, also merits attention.

Study of minerals. This study has not been completed. We have not attempted to classify all the fragments of minerals of our preparations, but we wish to revise the properties of some of them. /109

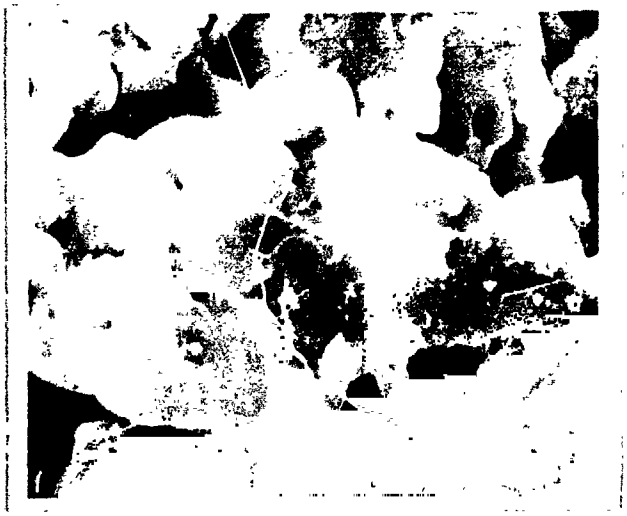

Fig. 1. Brown slag embedding crystals and cementing dust, X 1600. View in scanning electron microscope (also the same for Figs. 2-5)

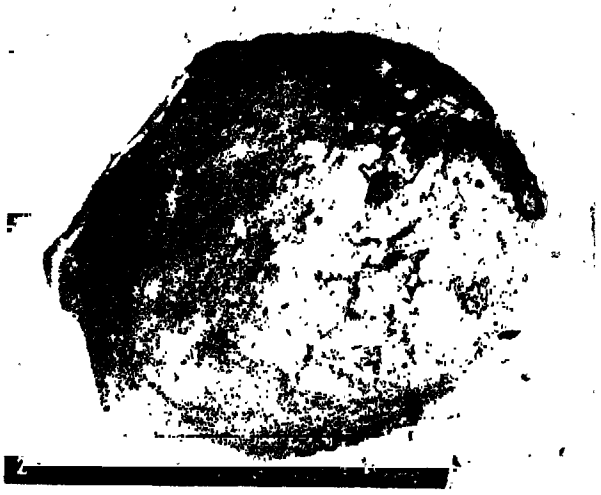

Fig. 2. Lunar "chondrule", general view, X 50.

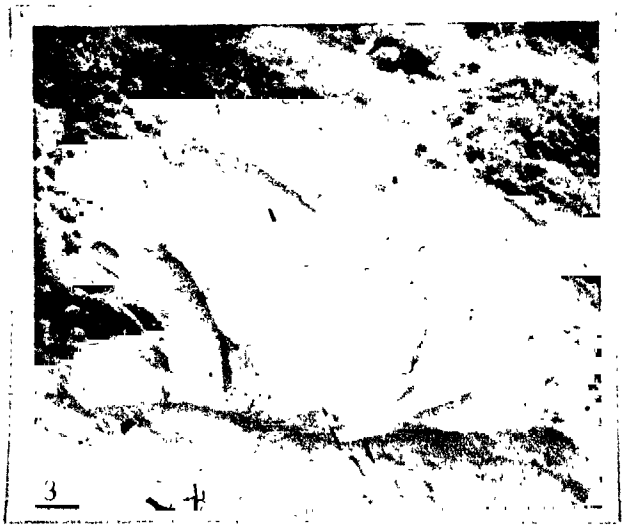

Fig. 3. Glassy fracture on surface of chondrule, X 2000

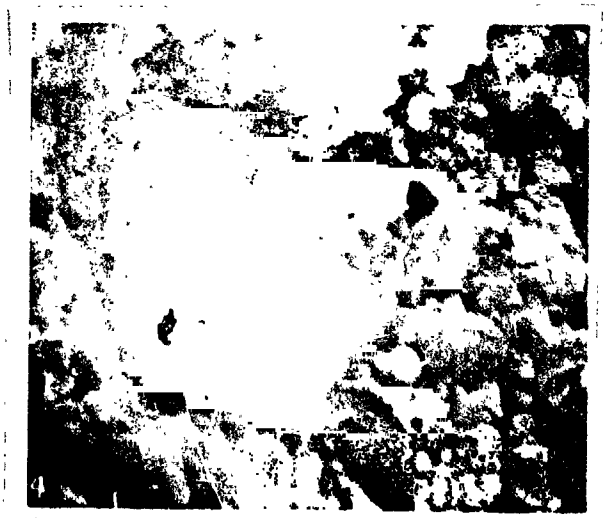

Fig. 4. Opening from impact with splashed droplets, X 8000

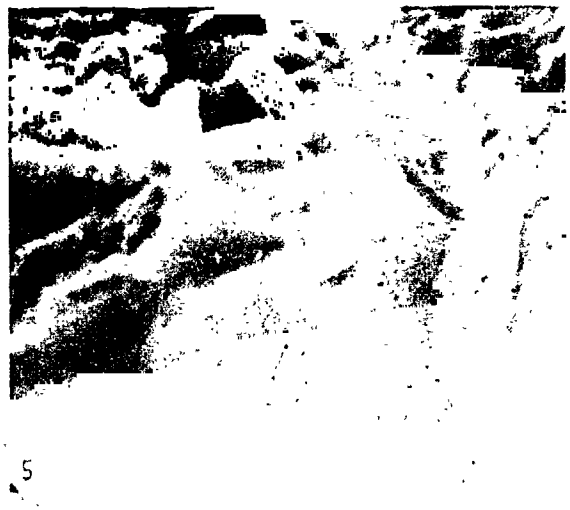

Fig. 5. Phenocryst of feldspar emerges at the surface of the chondrule; on it is a minute prism projecting beyond the margin of the crystal, X 8000

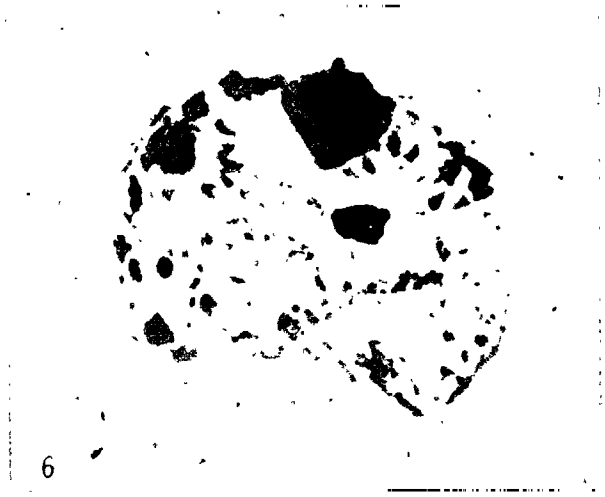

Fig. 6. Thin lamella set into chondrules; polarized light, crossed Nicol prisms, phenocrysts and fibers of devitrified glass, X 35.

Fig. 7. Spherule of devitrified glass, without analyzer, X 1400.

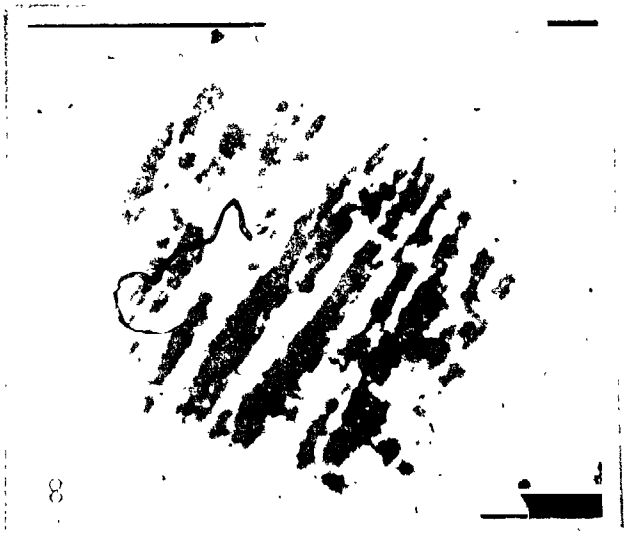

Fig. 8. Skeletal olivine in sills, crossed Nicol prisms, X 1650.

Fig. 9. Crystal of pyroxene, rounded and covered with glassy film, transmitted light, X 1120.

Fig. 10. Beams of nickelous iron (white) and gaps of triolite (gray) in reflected light, X 1160.

Fig. 11. Grain of fayalite, probably with spheroid inclusions, transmitted light, X 1500

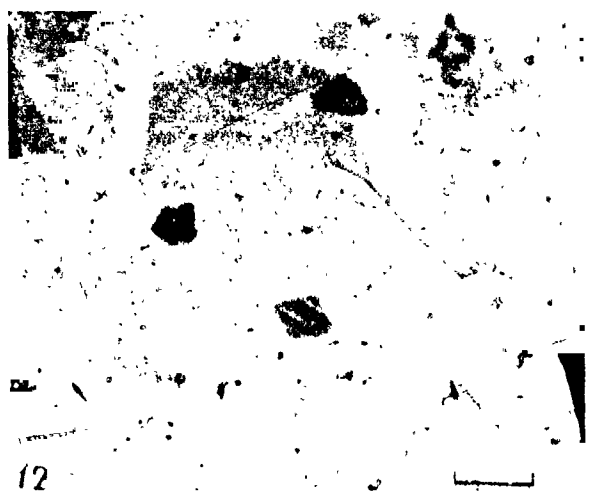

Fig. 12. Idiomorphic crystals of oxide in pyroxene grain, reflected light, X 500.

Fig. 13. Microdolerite, poor in ilmenite, transmitted light, X 960

Fig. 14. Fragment of rock with parallel lamella of ilmenite reflected light, X 960.

Metallic particles. A grain of nickelous iron was found in association with troilite (Fig. 10), similar to the "mini-luna" [1] in the Apollo 11 sample.

Ilmenite. Reflectivity curves as a function of the wavelength of light were obtained for the ilmenite grain imbedded in basalt.

Fayalite. An interesting grain of fayalite was encountered in the mounted section. The grain exhibited a high index of refraction and a poikilitic appearance: it included numerous, evidently glassy spherules (Fig. 11). This determination is preliminary.

Other minerals. 1. Many pyroxene grains contain octahedra or cubes of oxides with 10 microns on the side, which are still being studied (Fig. 12). 2. A clear lamella, yellow, isotropic with an index close to 2.05, not more than 20 microns in size, is siliceaceous chromite with the following composition (in weight percent):

/110

FeO	22,1	Al_2O_3	18,41
MgO	5,84	Cr_2O_3	51,03
TiO_2	0,61	V_2O_3	0,92
		Total	98,91

Rocks. Basalts. All our basaltic fragments have doleritic texture; the ratios of pyroxene, feldspar, and ilmenite vary widely from types rich simultaneously in both pyroxene and ilmenite (as in the Apollo 11 samples),to types rich in feldspar and poor in ilmenite (Fig. 13). Of course, only the fine-grained rocks are represented in our selection of samples differently than the individual crystals. Some fragments, such as those shown in Fig. 14 which contain fine parallel lamellae of ilmenite, do not correspond to the well-defined type of rock and can be interstitial mineral of the end of the crystallization of coarse-grained rocks, such as are found in several Apollo samples, for example, in basalt 14,310.

Anorthosites. Light anorthositic or noritic grains are much less common than basalts.

Very intense traces of shock action appeared in feldspar, all the way to the melting of maskelynite, which was observed in the form of two grains in two thin sections.

Breccias. Our large lamella of breccia -- the largest -- apparently represents in general ratios of diverse fragments of rocks, minerals, glasses in fragments and bubbles present in the surface material. This fragment, the largest dimension being 2 mm, contains no less than six detected basaltic fragments, but no anorthosite, which can be predicted judging from the ratios of the types of particles published in the preliminary report by A. P. Vinogradov.

In conclusion we wish to state that whereas the preliminary work given here obviously cannot assist in solving the problems represented by lunar geology, their general orientation nonetheless is toward several special problems whose interest value was emphasized by A. P. Vinogradov. How can we explain the participation by (some) meteorites in the formation of the regolith and the nonobservability of meteoritic remains? To which factors (solar wind, or melting of thermal origin) can we ascribe the "erosion" of rounded regolith grains, especially when they are coated with a glassy layer; more complete and more detailed results of this investigation, which is underway at the present time, will be published later.

REFERENCE

1. Goldstein, J. I., Henderson, E. P., and Yakowitz, H., "Investigation of Lunar Metal Particles," Proc. Apollo 11 Lunar Sci. Conf. 1, 499 (1970)

Laboratory of Mineralogy and Crystallography of the Paris University, Paris.

Administration of Geology and Mining Research, Orleans, France.

N75 11825

PETROGRAPHIC-MINERALOGICAL INVESTIGATION OF MAGMATIC ROCKS FROM THE SEA OF FERTILITY

/129

L. S. Tarasov, I. D. Shevaleyevskiy,
and M. A. Nazarov

Abstract

Petrographic and mineralogical features of fragments of magmatic rock of regolith from the Sea of Fertility are examined. The textures and mineral composition vary in relation to the type of rock. More than 50 x-ray spectral analyses of minerals (olivine, pyroxenes, plagioclases, and ores) were made; their chemical composition varies even within the limits of individual rock fragments.

A regolith sample from the Sea of Fertility contains numerous fine fragments of igneous rocks. In total, they can provide quite full characteristics of the magmatic manifestations of the immediate vicinity.

The landing site of Luna 16 station was in the northeastern part of the Sea of Fertility. This is a representative lunar mare region, and one of the most ancient. The nearest highland region is 70-80 km to the north. On analogy with regolith from the Sea of Fertility and the Ocean of Storms, one can anticipate the predominantly basaltic type of rocks also in the sample returned by Luna 16. The nearest highland lies 300 km to the southeast of the large Langrenus Crater, which is among the formations of Copernican age, and possibly sources for some fraction of the material of the highland /terra/ type in the Luna 16 regolith composition. The fact that sources of the material in the Luna 16, Apollo 11, and Apollo 12 regoliths were generally local has already been indicated earlier /1-3/. Subsequent investigations confirmed this.

Method of investigation. After the description of the sample on the tray in the receiving chamber, a separation was made of part of it for granulometric differentiation and then from the fraction

(+ 0.45-0.9 mm) and partially from the + 0.9 mm fraction, particles were sampled, after morphological investigation /4_7, for preparation of clear-polished sections. Each of these sections contained one rock particle. In addition to these, sections were prepared from randomly sampled groups of grains, each weighing about 2 mg, from the regolith fractions + 0.200, + 0.127, and + 0.083 mm. This present work examines data obtained mainly from the microscopic study of more than 70 sections of individual grains and only in part from the sections of the second type.

After studying the sections in the microscope in transmitted and reflected light, the entire area of the section was photographed. The resulting photographs of the section served as the basis for plotting points in the investigation of the composition of minerals with a microprobe. It was carried out on a JXA-5 microanalyzer with an x-ray exit angle of 40°. The accelerating voltage was 15 kV. The current of the absorbed electrons was $1.5 \cdot 10^{-8}$ A. The probe size was 1-5 μm. Used as reference standards were quartz (Si), corundum (Al), rutile (Ti), chromite (Cr), hematite (Fe), manganilmenite (Mn), spinel (Mg), wollastonite (Ca), albite (Na), glass (K), monazite, and apatite (P). The results were recomputed by introducing corrections after the Bence and Albee method /5, 6/. The relative of the analysis was to within less than 5 percent.

Petrographic description. The content of unchanged primary fragments of magmatic rocks in the Sea of Fertility regolith in general is not very large, since most of the sample (up to 50-70 percent) was made of breccias, slags, sinters (microagglutinates), and particles of transitional appearance. Fig. 1 shows a section of the deep profile of the Luna 16 regolith core taken on the tray in the helium chamber immediately after the sample was brought to the receiving laboratory. In this photograph one can see a number of interesting details: angular shapes of most of the particles, variations in their size, numerous glassy, fused particles. Easily /130 discernible are breccias and white fragments of feldspar rocks. Fragments of basaltic rocks of various types can be differentiated by mineral composition, crystallinity, or massive formation (see also Color Plates I, 1 and 2, and II, 1). In our calculation, we related to the class of purely magmatic /4_7 fragments with massive crystalline or aphanitic appearance and that did not bear on their surface continuous or extensive coatings of glass, glazing, and foam glass. These are particles that were not significantly affected by metamorphizing exogenic processes on the lunar surface.

As we can see from Table 1, the total content of magmatic fractions in coarse fractions (+ 0.45 mm) is 20-30 percent and decreases in the finer fractions (- 0.200 + 0.127 mm) to 11-15 percent, where in the latter no fragments of fine-grained basalts were detected under the binocular microscope. This is probably accounted for by the fact that rocks of this type are poorly

TABLE 1. RELATIVE CONTENT OF PARTICLES OF PRIMARY MAGMATIC ROCK IN VARIOUS GRANULOMETRIC FRACTIONS (IN mm) OF LUNA 16 REGOLITH

Type of rock fragments	Layers A + B			Layers V + G		
	+0,9	−0,9 +0,45	−0,200 +0,127	+,09	−0,9 +0,45	−0,200 +0,127
Content in fraction, percent						
Gabbro and coarse-grained basalts	13	14	10	18	12,5	13
Basalts, fine-grained	8	7,5	—	9,5	7	—
Feldspar rocks	0	2	0,5	1	3,5	1,5
Monomineralic grains and glasses	5	2,5	13	2,5	5,5	21
Fraction among rock fragments, percent						
Gabbro and coarse-grained basalts	62	60	95	63	55	90
Basalts, fine-grained	38	32	—	33	30	—
Feldspar rocks	—	8	5	4	15	10

fragmented into small fractions in view of their high viscosity caused by the fine-granular texture. The fraction of fine-grained basalts among magmatic fragments proper (Table 1) is no more than 20-30 percent, and 50-70 percent for the coarser-grained basalts and gabbro. The fraction of feldspar (anorthosite) rocks is 1-3 percent in the coarser fractions of the regolith, which is 5-15 percent of the total number of the primary magmatic fractions.

The number of the particles of magmatic genesis must be increased even further by means of the fraction of single-grained minerals included in the regolith composition. As a rule, this is represented by olivine, pyroxene, plagioclase, and much less often -- by ilmenite or spinel.

Among the primary magmatic rocks the following types can be singled out in Luna 16 regolith:

I. Basaltic rocks.
   1. Coarse-grained basalts and gabbro.
   2. Medium-grained basalts.

In each of these groups, leucocratic and melanocratic varieties can be differentiated.

   3. Gabbro-anorthosites.
   4. Fine-grained and aphanitic basalts, dark-gray to nearly black.

II. Feldspar (anorthosite) rocks.

Basaltic rocks vary texturally and by their relative content of rock-forming minerals. The main minerals are plagioclase, monoclinic pyroxene, olivine, and ilmenite. Most of the rocks are holocrystalline, and sections of the glass are encountered infrequently.

A characteristic feature is th coarseness of the grain in rocks. The coarsest-grained rocks rain size 0.3-0.5 to 1-2 mm) are represented by gabbro-type fragments. In these well-defined ophitic textures are evident (Color Plate IV, 1, and Color Plate VIII, 3). The medium-grained basalts externally similar to the preceding group, but the size of the mineral grains they contain varies on the average from 0.1 to 0.3 mm. Rocks with finer texture and aphanitic appearance are classified in the fourth group. For rocks of the first, second, and third groups, the primary mineral composition can be preliminarily determined by an external examination of the particles under a binocular microscope (at a magnification of 15-30 times). The mineral composition /131
of the fourth-group rocks is established only in sections under the microscope.

In the basalts of the first three groups, plagioclase has the appearance of lamellae or individual grains; it is very often pure, clear, and sometimes milky, white. The color of pyroxene represented in these rocks by the monoclinic variety is unusual: it is pinkish-brown, sometimes more pinkish, similar in color to almandine, but there are varieties that are more yellow, brown, or chestnut. Olivine varies in color from yellowish-greenish to amber tones. Ilmenite is present in the form of dark lamellae and segregations. Spinels are also black in color, usually in the form of fine idiomorphic inclusions in the olivine. In other minerals under the binocular microscope they are indistinguishable from small irregular segregations of ilmenite.

The color of rock fragments as a whole depends on the content of plagioclases and dark-colored minerals. Melanocratic varieties of rocks of the first two groups can be differentiated, when the amount of plagioclase does not exceed 20-30 percent, all the way up to fragments that approximate in composition peridotites (feldspar peridotites). These are rocks of dark-brown dark-gray, nearly black colors, but with readily discernible crystallinity. Ordinary gabbro and coarse-grained and medium-grained basalts are /132
characterized by lighter colors, and even more leucocratic varieties are characterized by the predominance of light tones (Figs. 2 and 3, and also Color Plate III, group 2 -- below are the more leucocratic varieties, and above are the more melanocratic). Variation in the ilmenite content (from 9 to 20 percent) is very strongly reflected in the color of the rocks, although the total increase in its content as a rule is accompanied also by an increase in the amount of pyroxene. Owing to the high variability of the relative

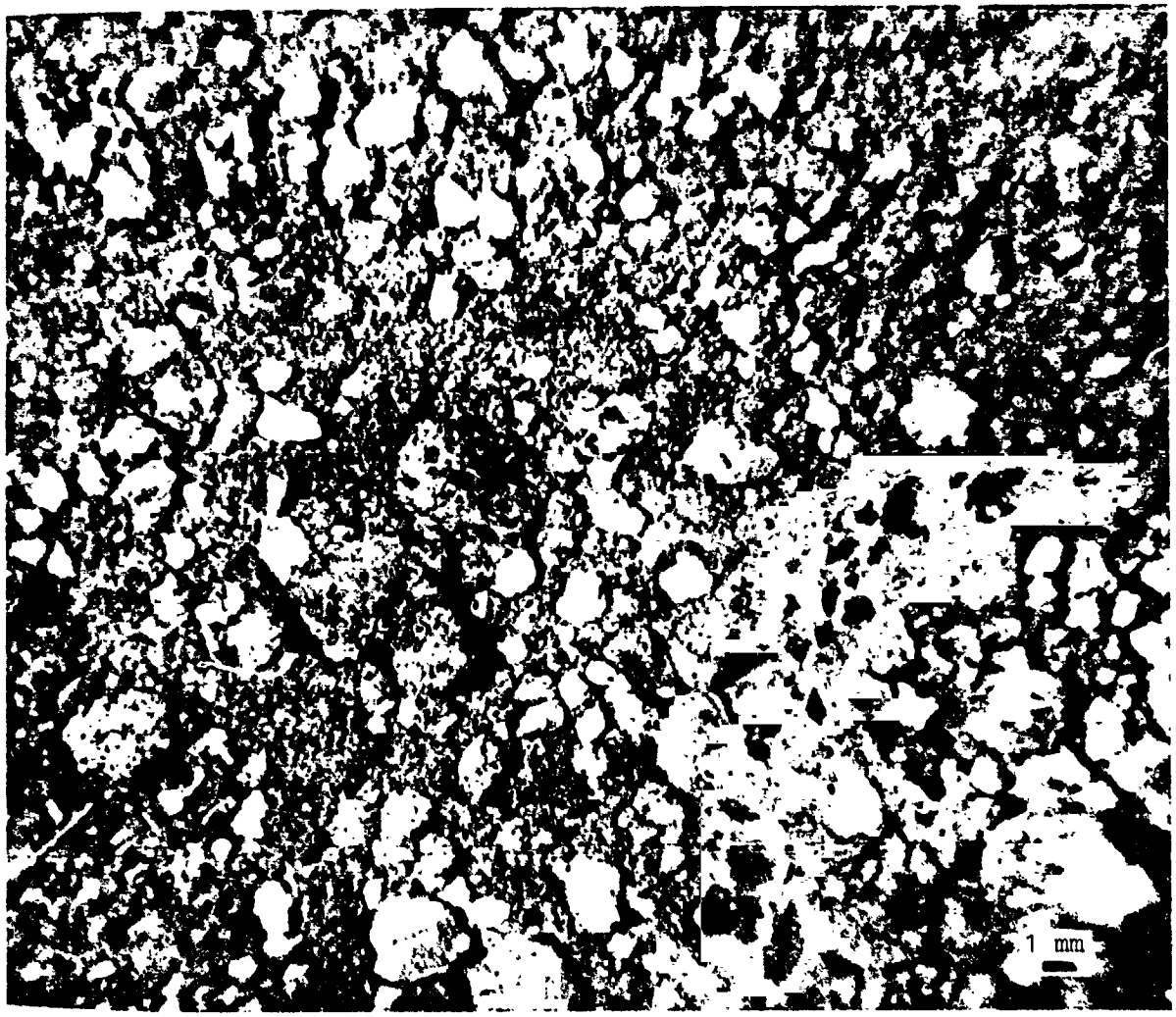

Fig. 1. General appearance of regolith from the deep section of core; numerous fragments of minerals and rocks are visible.

contents of the primary of rock-forming minerals -- plagioclase, pyroxene, olivine, and ilmenites, it is difficult to give averaged contents. However, for the most commonly encountered varieties of rocks, the mineral content fluctuates evidently within the following ranges (in volume percent): 30-60 -- for plagioclase; 20-40 -- for pyroxene; 0-10 -- for olivine; and 5-20 -- for ilmenite.

Extreme representatives of the basaltic group of rocks are the most leucocratic of its members, which we classified as gabbro-anorthosite. They are characterized by medium and coarse-grained texture, the strong predominance of plagioclase (anorthite) over

Fig. 2. Particle of melanocratic fine-grained gabbro

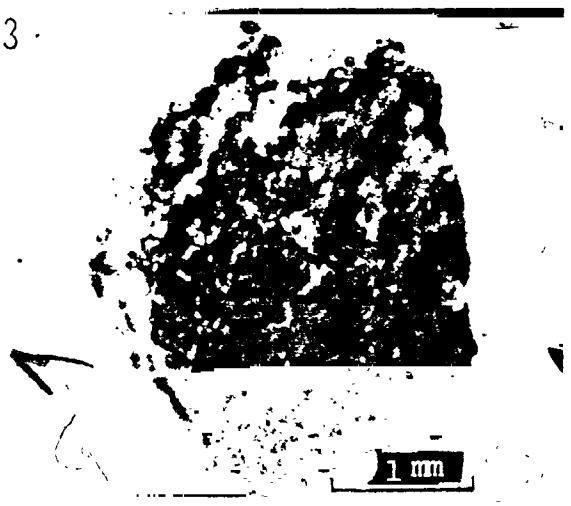

Fig. 3. Particle of leucocratic fine-grained gabbro

Fig. 4. Particle of medium- and fine-grained basalt

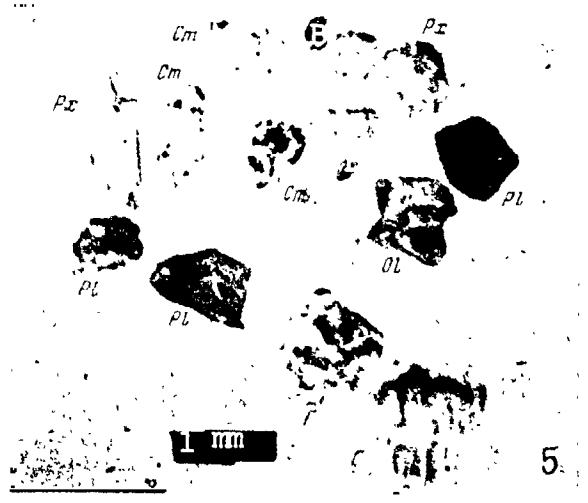

Fig. 5. Minerals and fragments of rocks from the + 0.45 mm fraction, sample L-1609
Px = pyroxene; Ol = olivine;
Pl = plagioclase; Cm = glass;
B = basalts; Г = gabbro.

all other minerals, and also by the infrequent presence of individual olivine grains, or pinkish-brown pyroxene, or ilmenite. It is precisely the presence of the last two minerals, especially characteristic of basalts from the mare regions of the Moon, that does not enable us to classify these gabbro-anorthositic rocks in the specifically anorthositic series typical of rocks of lunar highlands. /133

It should be noted that we should realistically evaluate the possiblities of investigating the fine rock fragments. Each fragment 0.5-3 mm in size we examined as a lump whose spatial-genetic origin can be established only at the end of the investigation, and then by no means always. The entire array of fragments of magmatic rock can be classified into groups, but in principle it is not precluded for the fragments of coarse-grained rocks of melanocratic and leucocratic types that they can be actually classified as of the same highland rock with taxitic or striated structure. Medium-grained and especially fine-grained fragments in this sense are more representative and it can be assumed that they characterize considerable rock volumes.

Compared with the basalts described, the last -- fourth -- group of basalts differ sharply in external appearance. These are dark-gray, often nearly black rocks, very fine-grained or aphanitic in formation (Fig. 4 and Color Plates III, 1, and IV, 2). As already stated, they are less often encountered in the lunar regolith. It can be assumed that they either represent individual flows or else marginal zones of ordinary basaltic flows. As a whole, these are melanocratic rocks, not yet adequately studied.

Of particular interest are fragments of individual minerals of igneous rocks dispersed in various regolith fractions. Their amount in the fine fractions increases, which is quite natural. Detailed x-ray structural investigations of Luna 16 minerals were carried out precisely on monomineralic grains extracted from various granulometric fractions. They are described in detail in the papers /7, 8/. Most often encountered were olivine, plagioclase, pyroxene, and less often, ilmenite, and even less often, spinels. Fig. 5 shows individual fragments of minerals and for comparison -- fragments of rocks (gabbro and fine-grained basalts). The color photographs of these grains are in Color Plate V, 1 and 2.

As a rule, the monograins in the regolith were represented by well-preserved clear fragments of minerals, partially similar in color and character of surface to the fine-glasses corresponding to them in color. They could be differentiated in a number of cases only by checking with crossed Nicol prisms. The preserved facets of the crystals are infrequent. Importantly, among the monograins of olivine in the + 0.45 mm and the + 0.9 mm fractions are to be found fragments of even coarser olivine grains (Color Plate IV, 1). No such large olivines could be encountered in the fragments of regolith rocks. Therefore it can be assumed that either they had to be extracted from even coarser-grained rocks, or else are classified as late olivines segregating in cavities in basaltic rocks. /134

The textures of the basaltic series of rocks varies, but not very broadly. As a rule, these are holocrystalline, inequigranular,

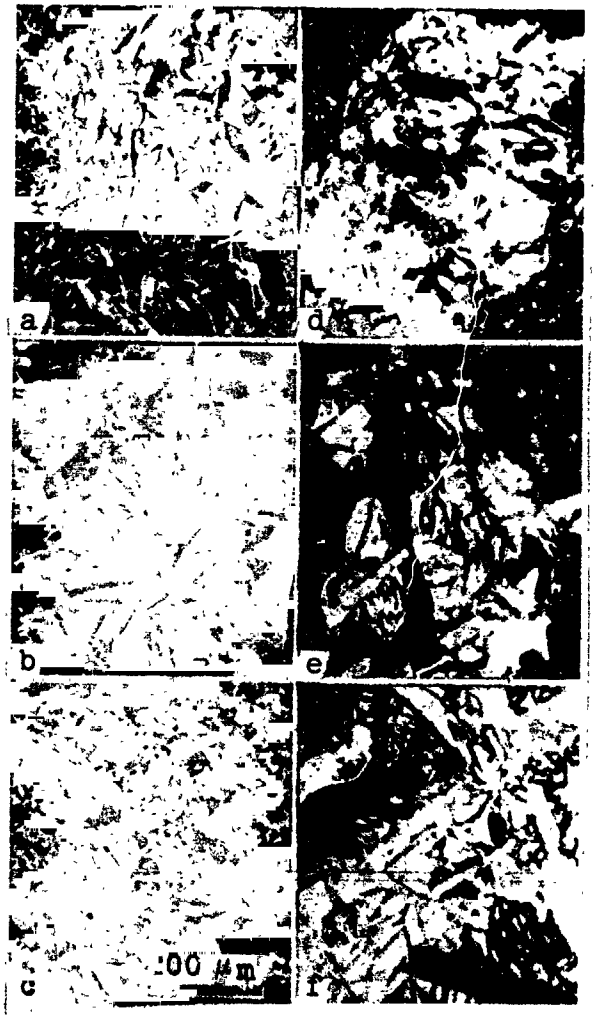

Fig. 6. Types of texture of Sea of Fertility magmatic rocks
a. fine-grained basalt, ophitic texture b. fine-medium-grained melanocratic basalt, ophitic texture, porphyroid, in places the texture arrangement resembles raying c. inequigranular (fine- and medium-grained basalt), hypidiomorphogranular texture, in places intergrading into ophitic d. medium-grained gabbro, hypidiomorphogranular texture
e. as above, intergrading to ophitic texture
f. coarse-grained gabbro, distinct ophitic texture

sometimes porphyroid textures, hypidiomorphogranular, ophitic, and diabasic (subophitic), and less often nonholocrystalline interstitial textures. The latter are encountered more often in finer-grained rocks. Infrequently present are fragments with variolitoid structure. Fragments are encountered in which the structure varies in grain size or in the nature of grains. The coarsest-grained rocks of the gabbro type are characterized, as already stated, by ophitic texture. Allotriomorphogranular textures of gabbro rocks were not encountered. Examples of the textures of basaltic-series rocks are in Fig. 6 and Color Plate VII. All these textures are characteristic of mare type lunar rocks. They indicate the magmatic nature of the rocks and the various depths of their formation. Coarse-grained gabbro rocks were crystallized in a more quiescent environment and evidently at greater depths. True, it can be assumed that these depths were not intrusive and even hypabyssal for medium-grained and fine-grained rocks. Accordingly, it is necessary to direct attention to the constant presence of voids in the rocks. The most widely found type are gas bubbles, which existed during the crystallization of the magma (see Figs. 2 and 7). As we can see, even in the medium-grained gabbro rocks these gas voids are quite numerous (see Fig. 2). They differ by their regular spheroid form and by the fact that the pyroxene or plagioclase crystals in their walls lie parallel to the surface of the void, indicating crystallization at the instant when the gas pressure existed in the void. Near the boundaries with

it there are neither changes in the rock structure or in the chilled zones. The same observations, for Apollo 11 material, were made by H. Schmitt et al. /9 7. These voids can appear in the magma only as gas bubbles, and until profuse gas release at the instant of surfacing occurred. These are bubbles coexisting in the magma. Evidently, their presence indicates the limited depth gas release and crystallization of the magma until its direct contact with tne rarefied lunar atmosphere. The location of this crystallization can be either the deep-lying zones of lava flows, or else the near-surface "funnel" facies. Evidently, pressures at these depths already could drop the gas bubbles in the magmatic melt without enabling them to surface in the viscous crystallizing magma.

The main type of rocks are the feldspar rocks. Here we do not refer to monograins of anorthite or leucocratic gabbro rocks (gabbro-anorthosites). They were discussed above. This group of rocks in the Luna 16 regolith essentially is represented by metamorphized, primarily magmatic rocks. In external appearance these are light, white, grayish to gray, medium- and fine-grained particles (Color Plave V, 2). However, among the fragments studied in the /135 sections no particles with allotriomorphogranular (anorthositic) texture were encountered, which can be associated with the specifically magmatic intrusive nature of their origin, and to some extent they are arbitrarily classified in the group of anorthositic rocks. Nonetheless, this classification must be regarded as valid, since the principal component of these rocks is plagioclase and to some extent crystallized plagioclasic glass. Moreover, similar particles, including specifically of the anorthositic type, are encountered in Apollo 11 and Apollo 12 regoliths /2 and 3/. This indicates the validity of separating the anorthositic group of fragments.

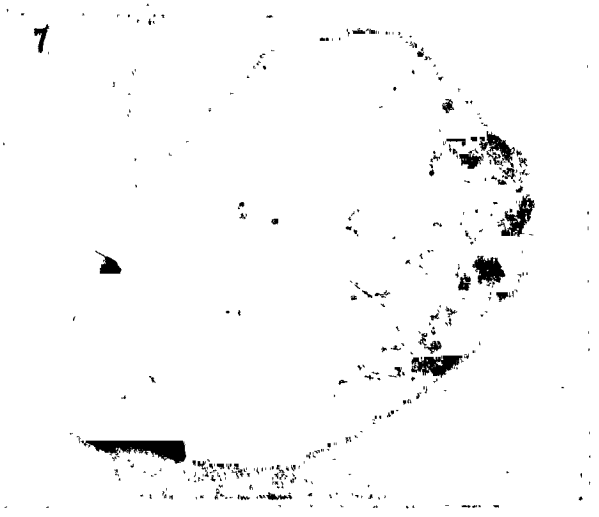

Fig. 7. Surfaces of gas bubbles in medium-grained gabbro

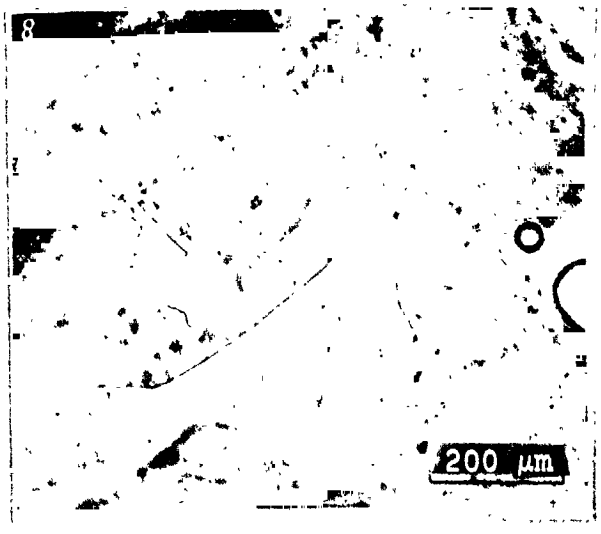

Fig. 8. Recrystallized feldspar particles -- result of shock action

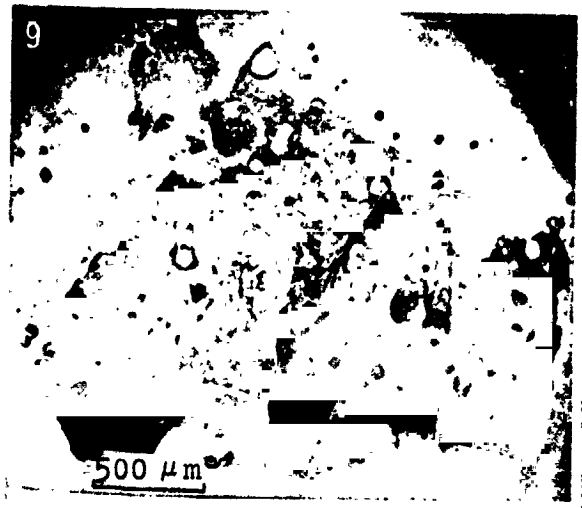

Fig. 9. Breccias with numerous fragments of feldspars and large fragment of medium-grained holocrystalline basalt

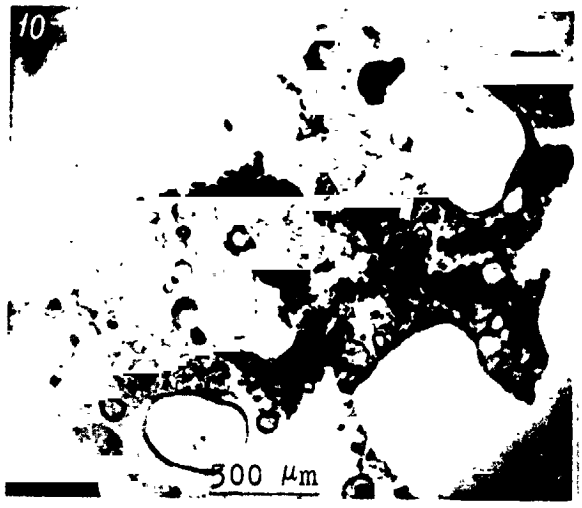

Fig. 10. Slag, incompletely fused particle with well-preserved relicts of primary magmatic rocks, but with a larger number of secondary pores arising during remelting

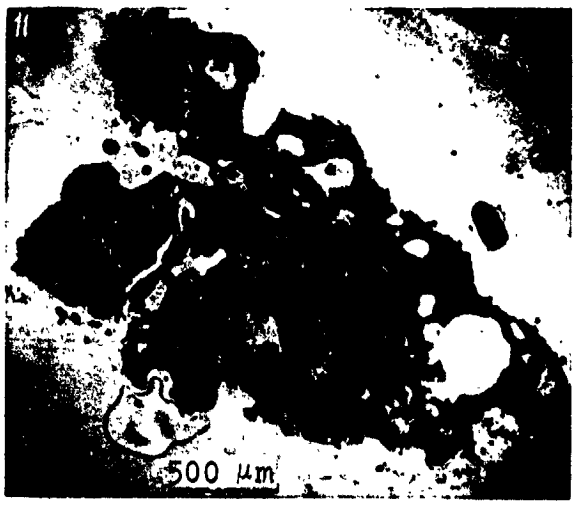

Fig. 11. Wholly remelted slag particle formed by black opaque glass.

Characteristic of these are cataclastic and nonhomogeneous catablastic structures of recrystallization, at times porphyroblastic. Frequently remelting and subsequent crystallization of anorthitic glass was noted. An example of this recrystallized glassy rock containing numerous pointwise segregations of all minerals is in Fig. 8. We will not dwell here in detail on the characteristics of these rocks, since they are of independent interest. We only note that it is precisely these rocks that evidently can be classified as nonmare, terra /highland/ formations. Obviously, they are witnesses to powerful impactive events, which then led to their metamorphosis and ejection into the mare region. Rock similar to krip nonmare basalts (norites) with orthopyroxene as the predominant dark-colored mineral /107 were not encountered in well-defined fragments, although certain petrological indications of the possibility of their existence do exist /117. /136

Under the conditions in which feldspar (anorthositic) rocks were formed, one important problem becomes studying the manifestations of shock (impact) effects and establishing the stages and features of the recrystallization of these primordially magmatic rocks.

Concluding our general characterization of the main types of magmatic rocks, we should note that their fragments are encountered in the regolith not only in independent form, but also as inclusions in the breccias (Fig. 9). An amorphous opaque glassy isotropic mass serves as the cement of the breccias; in this mass are distributed fragments of feldspar or other composition. The structure of breccias is clearly evident in the Color Plate VI. With the example of the breccias we can readily trace the successive stages from the surface partial melting (Fig. 10) to the formation of a black opaque vesicular slag glass (Fig. 11), which preserved only relicts of the fragments initially present there. Obviously, these transformations can be traced also in a number of fragments of magmatic rocks. Total melting of small fragments leads to the formation of well-melted, clear, variously colored spherules (Color Plate V, 3). Data on their chemical composition have been borrowed by us from a paper by N. P. Il'in et al. /12/ (Table 2). The very high content of calcium in all the spherules, at its content level in pure anorthite or calcic clinopyroxene, is uncommon. Evidently, spherule 58-1 arose through melting of an anorthite fragment in which there was an admixture of diopside, and spherule 58-2 formed mainly due to augite. The high chromium content indicates the presence in these spherules of accessory chromite. The remaining four spherules are compositionally similar to the mare basalts and can be the products of the melting of their fragments as a whole. It is not precluded that during melting there were losses of some and relatively high increases in the contents of other elements. This problem has not yet been studied.

Mineralogy of basaltic rocks. The geochemical specifics of magmatic processes on the Moon, in particular the virtual absence of water and volatiles, impose a certain limit on the diversity of minerals. The number of minerals thus far known does not exceed twenty to thirty. In the basaltic rocks, which will be discussed, the predominant minerals are plagioclase, clinopyroxene, ilmenite, and olivine. Several secondary accessory minerals are also known. Most of the sparsely distributed minerals were segregated in the late stages and were distributed in the interstices between the primary rock-forming minerals.

Luna 16 rocks in mineral associations differ from the basalts of the Sea of Fertility and the Ocean of Storms. Some minerals known in them were not detected in the basalts of the Sea of Fertility.

TABLE 2. X-RAY SPECTRAL ANALYSES OF GLASS SPHERULES OF VARIOUS COLORS (FRACTION -0.340 TO + 0.200 mm) FROM LUNA 16 REGOLITH ACCORDING TO /127 (IN WEIGHT PERCENT)

Component	58-1, White	58-2, Yellow	13-2, Yellow	13-4, Yellow	13-3, Brown	58-3, Violet
SiO_2	42.0	42.5	46.4	44.2	41.5	47.5
TiO_2	0.01	0.3	1.0	2.2	2.2	0.4
Al_2O_3	23.4	11.8	7.4	11.9	12.5	11.8
Cr_2O_3	1.2	1.2	0.4	0.17	0.1	0.3
FeO	3.2	15.3	17.5	15.6	15.6	16.3
MnO	0.01	0.2	0.2	0.2	0.2	0.4
MgO	9.8	6.5	9.2	7.9	7.9	6.2
CaO	21.3	19.7	16.1	17.3	20.2	19.1
Total	100.9	97.5	98.2	99.5	100.2	102.0

Let us examine the characteristics of individual minerals of lunar basalts, using microscopic data from the results of an examination of chemical composition with a JXA-5 microanalyzer. Examples of chemical composition of the minerals are given in the corresponding tables.

Olivine. Quantitatively, as a rule it is much less evident than pyroxene. Only in a handful of fragments of melanocratic fine- and medium-grained basalts and in a number of coarse-grained fragments does it represent up to 15-20 percent of the rock. But usually the olivine content in basaltic rocks and gabbro does not exceed 5-7 percent. Earlier olivine in the form of grains 100-400 μm diagonally may have segregated in rocks, expecially coarse-grained rocks. Olivine is often present in medium-grained and fine-grained rocks as porphyroid phenocrysts. In the sections, olivine is colorless, and infrequently faintly greenish and yellowish. Usually it contains, especially in early olivine, fine, isometric, sometimes distinctly cubic segregations of chromite. Olivines lie in the series 30-35 percent Fa in terms /138 of magnesiality-ferruginicity, only infrequently departing from it (Table 3). In it ΣA -- Σ Mg, Fe, Mn, Ca; ΣB -- Σ Si, Ti, P. It should be noted that there is no clear zonality like that discovered in Apollo 11 olivines, in Luna 16 olivines. However, in the coarser grains of this mineral, for example, in section 202 where the diagonal reaches 200-300 μm, greater ferruginicity of the peripheral portions of the grain was noted. Thus, in section 202 36 and 43 percent Fa was established in the center of the grains (analyses 202-24 and 202-27), and 54 percent Fa in the periphery (analysis 202-25). Present in nearly all olivines (see Table 3) is chromium (up to 0.19 percent), titanium (up to 0.06 percent), and calcium in considerable amounts (0.32-0.53 percent). The latter finding evidently can be representative of lunar olivines. Unusual is the composition of olivine 17-53, in which Al_2O_3 is present to the extent of 0.99 percent, K_2O -- 0.17 percent, and P_2O_5 -- 0.14 percent. The least ferruginous olivine -- 29.2 percent Fe -- is from its coarse monograin. This probably is the olivine that

TABLE 3. X-RAY SPECTRAL ANALYSES OF OLIVINES FROM LUNA 16 BASALTIC ROCKS (IN WEIGHT PERCENT) /137

Component	17-53	72-2	55-23	55-21	202-24	202-27	202-25
SiO_2	36,0	37,8	36,3	36,3	36,9	35,3	34,6
TiO_2	0,05	0,00	0,03	0,06	0,00	0,04	0,06
Al_2O_3	0,99	0,02	0,04	0,01	0,05	0,00	0,01
Cr_2O_3	0,15	0,14	0,19	0,08	0,07	0,02	0,06
FeO	32,1	26,1	31,2	33,6	31,5	36,4	43,4
MnO	0,42	0,35	0,33	0,33	0,44	0,63	0,56
MgO	28,6	35,1	31,3	29,3	30,7	26,6	20,6
CaO	0,53	0,32	0,36	0,35	0,48	0,32	0,32
Na_2O	0,00	0,03	0,00	0,15	0,09	0,04	0,04
K_2O	0,17	0,00	0,03	0,02	0,01	0,01	0,02
P_2O_5	0,14	0,00	0,00	0,00	0,00	0,00	0,00
Total	99,1	99,9	99,8	100,2	100,2	99,4	99,7
Coefficients for 4 [O]							
Si	0,994	1,004	0,992	0,999	1,004	0,996	1,008
Ti	0,001	0,000	0,001	0,001	0,000	0,001	0,001
Al	0,032	0,001	0,001	0,000	0,002	0,000	0,000
Cr	0,003	0,003	0,004	0,002	0,001	0,000	0,001
Fe	0,741	0,580	0,713	0,773	0,717	0,859	1,058
Mn	0,010	0,008	0,007	0,008	0,010	0,015	0,014
Mg	1,179	1,389	1,275	1,201	1,244	1,119	0,895
Ca	0,015	0,009	0,010	0,010	0,014	0,010	0,010
Na	0,000	0,001	0,000	0,008	0,005	0,002	0,002
K	0,006	0,000	0,001	0,001	0,000	0,000	0,001
P	0,003	0,000	0,000	0,000	0,000	0,000	0,000
ΣB	0,997	1,004	0,992	0,999	1,004	0,996	1,008
ΣA	1,987	1,991	2,012	2,004	1,993	2,005	1,982
Fa	38,6	29,5	35,9	39,2	36,6	43,4	54,2
Fo	61,4	70,5	64,1	60,8	63,4	56,6	45,8

TABLE 4. X-RAY SPECTRAL ANALYSES OF OLIVINES FROM INDIVIDUAL MONOGRAMS IN REGOLITH ACCORDING TO /137 (IN WEIGHT PERCENT)

Component	52-2	52-4	52-1	52-5	52-3	M-4
SiO_2	36,9	37,7	37,2	37,1	35,2	36,0
TiO_2	0,03	0,06	0,05	0,06	0,06	0,01
Cr_2O_3	0,22	0,17	0,21	0,22	0,2	0,15
FeO	27,4	27,3	29,6	30,6	41,5	33,8
MnO	0,26	0,22	0,29	0,29	0,3	0,3
MgO	35,5	33,0	32,0	31,8	22,6	27,5
CaO	0,48	0,57	0,49	0,52	0,5	0,38
Total	100,8	99,0	99,8	100,6	99,9	98,1

Component	52-2	52-4	52-1	52-5	52-3	M-4
Coefficients for 4 [O]						
Si	0,980	1,015	1,000	1,000	1,001	1,013
Ti	0,001	0,001	0,001	0,001	0,001	0,000
Cr	0,005	0,003	0,004	0,005	0,004	0,003
Fe	0,608	0,615	0,669	0,690	0,987	0,796
Mn	0,006	0,005	0,007	0,007	0,007	0,007
Mg	1,405	1,325	1,289	1,278	0,958	1,154
Ca	0,014	0,016	0,014	0,015	0,015	0,011
ΣB	0,980	1,015	1,006	1,000	1,001	1,013
ΣA	2,039	1,965	1,984	1,998	1,972	1,971
Fa	30,2	31,7	34,2	35,1	50,7	40,8
Fo	69,8	68,3	65,8	64,9	43,9	59,2

TABLE 5. X-RAY SPECTRAL ANALYSES OF PYROXENES FROM LUNA 16 BASALTIC ROCKS (IN WEIGHT PERCENT)

Component	155-3	155-2	155-1	55-17	55-16	55-22	202-19	202-20	202-23	202-21	202-22
SiO_2	47,8	48,5	47,0	48,9	52,2	53,4	49,0	49,9	50,3	49,1	49,2
TiO_2	2,17	1,65	1,05	1,07	0,92	1,22	2,37	1,48	1,35	1,18	1,06
Al_2O_3	2,96	2,35	1,37	1,08	0,88	1,72	3,05	2,31	1,89	1,47	1,56
Cr_2O_3	0,50	0,38	0,20	0,20	0,18	0,23	0,42	0,31	0,26	0,07	0,10
FeO	15,2	16,4	32,1	28,9	21,9	20,3	14,1	19,1	19,8	26,8	28,9
MnO	0,38	0,34	0,66	0,60	0,35	0,33	0,40	0,42	0,47	0,62	0,44
MgO	15,1	14,3	3,52	9,34	18,0	16,7	13,7	13,5	13,2	11,1	4,88
CaO	16,1	16,9	14,6	9,08	6,43	6,04	16,5	12,6	12,9	9,69	13,6
Na_2O	0,00	0,00	0,00	0,18	0,08	0,13	0,05	0,02	0,05	0,03	0,06
K_2O	0,01	0,02	0,03	0,03	0,05	0,02	0,02	0,02	0,00	0,00	0,02
P_2O_5	0,00	0,00	0,00	0,00	0,00	0,00	0,00	0,00	0,00	0,00	0,00
Total	100,2	100,8	100,5	99,4	101,0	100,1	99,9	99,7	100,2	100,1	99,8
Coefficients for 6 [O]											
Si	1,821	1,848	1,924	1,955	1,957	1,994	1,861	1,914	1,928	1,930	1,964
Ti	0,062	0,047	0,032	0,032	0,026	0,034	0,068	0,043	0,039	0,035	0,051
Al	0,133	0,105	0,066	0,051	0,039	0,076	0,136	0,104	0,085	0,068	0,073
Cr	0,015	0,011	0,006	0,006	0,005	0,007	0,012	0,009	0,008	0,002	0,003
Fe	0,484	0,522	1,039	0,966	0,687	0,634	0,457	0,612	0,634	0,881	0,965
Mn	0,012	0,011	0,023	0,020	0,011	0,010	0,013	0,014	0,015	0,021	0,015
Mg	0,857	0,812	0,215	0,556	1,006	0,929	0,775	0,772	0,753	0,650	0,290
Ca	0,657	0,690	0,640	0,389	0,258	0,242	0,671	0,518	0,529	0,408	0,582
Na	0,003	0,000	0,000	0,014	0,006	0,009	0,004	0,001	0,004	0,007	0,005
K	0,000	0,001	0,001	0,001	0,002	0,001	0,001	0,001	0,000	0,000	0,001
P	0,000	0,000	0,000	0,000	0,000	0,000	0,000	0,000	0,000	0,000	0,000
ΣB	2,000	2,000	2,000	2,000	2,000	2,000	,000	2,000	2,000	2,000	2,000
ΣA	2,041	2,047	2,006	1,990	1,997	1,936	1,998	1,988	1,993	2,002	1,949
Fs	24,2	25,8	56,2	50,5	35,2	35,1	24,0	32,2	33,1	45,4	52,5
En	42,9	40,1	11,0	29,1	51,6	51,5	40,7	40,6	39,3	33,5	15,8
Wo	32,9	34,1	32,8	20,4	13,2	13,4	35,3	27,2	27,6	21,1	31,7
$\frac{Mg}{Mg+Fe+Mn}$	0,634	0,605	0,161	0,859	0,590	0,590	0,622	0,552	0,536	0,418	0,228

was earliest in its formation. But the similar pattern was noted for monograins of olivine from 170 to 350 μm in size /7/ (Table 4). These grains were dispersed in the regolith and subsequently were segregated as independent fragments while still on the Moon in the course of the gradual fragmentation of the rocks and the regolith. Evidently they originated from the coarser olivine grains from the coarser-grained gabbro rocks. X-ray structural data for these olivines are in the reports /7, 8/. The ferruginicity (see Table 4) of the minerals analyzed lies in the already-indicated interval of 30-45 percent Fa and only one sample (M-4) proved to be more ferruginous -- 50.7 percent Fa. Possibly, this olivine can be classified as a late mineral segregating already in geodes. /139

TABLE 6. X-RAY SPECTRAL ANALYSES OF PLAGIOCLASES FROM LUNA 16 BASALTIC ROCKS (IN WEIGHT PERCENT)

Component	155-9	55-12	55-13	55-18	202-18	202-13	202-17	202-16
SiO_2	48,7	45,3	45,2	49,4	46,4	47,0	48,0	50,5
TiO_2	0,00	0,00	0,01	0,00	0,00	0,01	0,03	0,00
Al_2O_3	32,6	35,3	35,3	32,7	33,9	33,1	32,8	31,1
Cr_2O_3	0,00	0,00	0,00	0,00	0,00	0,00	0,00	0,00
FeO	0,54	0,10	0,15	0,52	0,16	0,20	0,36	0,72
MnO	0,00	0,00	0,00	0,00	0,00	0,00	0,00	0,00
MgO	0,23	0,22	0,27	0,19	0,20	0,17	0,32	0,14
CaO	16,1	18,1	17,8	15,5	17,6	17,5	16,9	15,1
Na_2O	2,51	0,98	1,27	2,37	1,16	1,54	1,63	2,47
K_2O	0,15	0,08	0,08	0,28	0,03	0,07	0,11	0,36
P_2O_5	0,00	0,00	0,00	0,00	0,00	0,00	0,00	0,00
Total	100,8	100,1	100,1	101,0	99,5	99,6	100,1	100,4
Coefficients for 8 [O]								
Si	2,218	2,085	2,082	2,240	2,143	2,171	2,200	2,301
Ti	0,000	0,000	0,000	0,000	0,000	0,000	0,000	0,000
Al	1,751	1,915	1,916	1,748	1,846	1,802	1,772	1,670
Cr	0,000	0,000	0,000	0,000	0,000	0,000	0,000	0,000
Fe	0,020	0,004	0,006	0,020	0,006	0,008	0,014	0,027
Mn	0,000	0,000	0,000	0,000	0,000	0,000	0,000	0,000
Mg	0,015	0,015	0,018	0,013	0,013	0,012	0,022	0,009
Ca	0,786	0,892	0,878	0,753	0,871	0,866	0,830	0,737
Na	0,222	0,087	0,113	0,208	0,104	0,138	0,145	0,218
K	0,009	0,005	0,005	0,016	0,005	0,004	0,006	0,021
P	0,000	0,000	0,000	0,000	0,000	0,000	0,000	0,000
ΣB	3,969	4,000	3,998	3,988	3,989	3,973	3,973	3,971
ΣA	1,052	1,003	1,020	1,010	0,999	1,028	1,017	1,012
An	77,4	90,8	89	76,5	89,7	86,1	84,7	75,5
Ab	21,6	9,2	11,1	21,4	10,3	13,9	14,3	22,4
Or	1,0	—	—	2,0	—	—	1,0	2,0

Earlier [13, 14] it was shown that the content of fayalite molecule in these olivines reaches 50 and even 70-90 percent for Apollo 11 rocks. Present in all olivines (see Tables 3 and 4) is manganese (MnO 0.22-0.63 percent), that is, the tephroite constituent is always present in lunar olivines.

Pyroxenes. Monoclinic pyroxenes are the most widely distributed dark-colored materials in lunar mare rocks. In sections as a rule they are colorless, or faintly brown, or brownish, xenomorphic with respect to all other rock-forming minerals, and less often idiomorphic. The time of their segregation was extended over a considerable interval, owing to which the chemical composition

even within a single rock fragment fluctuates quite widely. Examples of the chemical compositions of monoclinic pyroxenes are in Table 5 (Σ A — Σ Ca, Mg, Fe, Mn, Ti (VI), Na, K; Σ B — — Σ Si, Ti (IV), Al, P).

For typical fine-grained porphyroid mare basalts (section 55), the compositions vary in different grains from yellowish pigeonite to subcalcic augite. In the coarser-grained rocks (sections 155 and 202) -- the range is from subcalcic augite and augites to ferruginous augites. Accordingly, the content Fs varies from 24 to 56 percent, En -- from 16 to 51 percent, and Wo -- from 13 to 35 percent, and correspondingly the parameter Mg/(Mg + Fe + Mn) fluctuates in the range 0.161-0.859. The general trend toward increased ferruginicity in silicates during the crystallization of rocks was confirmed also with the example of pyroxenes. However, in the Luna 16 samples we did not record the extreme case of increase in ferruginicity -- the formation of pyroxferroite /15/ in the form of shells of clinopyroxene. These observations are very frequent in Apollo 11 samples. There was a single indication /16/ for Luna 16 of the peripheral substitution of augite by pyroxferroite, but the analysis of the latter was not conducted, so that one cannot talk about its monotypicity with its counter parts in Sea of Fertility rocks. All Luna 16 pyroxenes are rich in TiO_2 (0.92-2.37 percent), contain chromium (Cr_2O_3 0.07-0.50 percent), and are nearly devoid of calcium, sodium, and phosphorus. /141

Plagioclases. In addition to pyroxenes, plagioclases are the most essential rock-forming mineral constituent, especially for ordinary and leucocratic varieties of lunar rocks. The common feature that differentiates them from terrestrial rocks is the constant, very high content of anorthite molecule (Table 6). As a rule, plagioclases are classed as bytownite (75-90 percent An) or anorthite (>90 percent An). Labradorites are infrequently found. Variations in the composition of plagioclases within individual rock fragments are given. For example (Table 6, Σ A — — Σ Ca, Na, Fe, Mg, K; Σ B — Σ Al (IV), Si, Ti): fine-grained mare basalt An_{91}-An_{76} (section 55); and coarser-grained rocks An_{90} - An_{76} (section 202 and 155). As we can see, the range of variation in the plagioclase composition is identical for rocks of different granularity, which indicates similarity in the general crystallization orientation for the different rocks. As a whole, plagioclases contain few admixtures: they have no chromium, titanium, manganese, phosphorus, and their iron content varies from 0.1 to 0.72 percent FeO. And the richest in iron are the most acidic varieties of plagioclases -- An_{75-76} (analyses 155-9, 55-18, and 202-16, and Table 6). The calcium content is low, not more than 0.4 percent. As already noted by us, idiomorphism of

/140

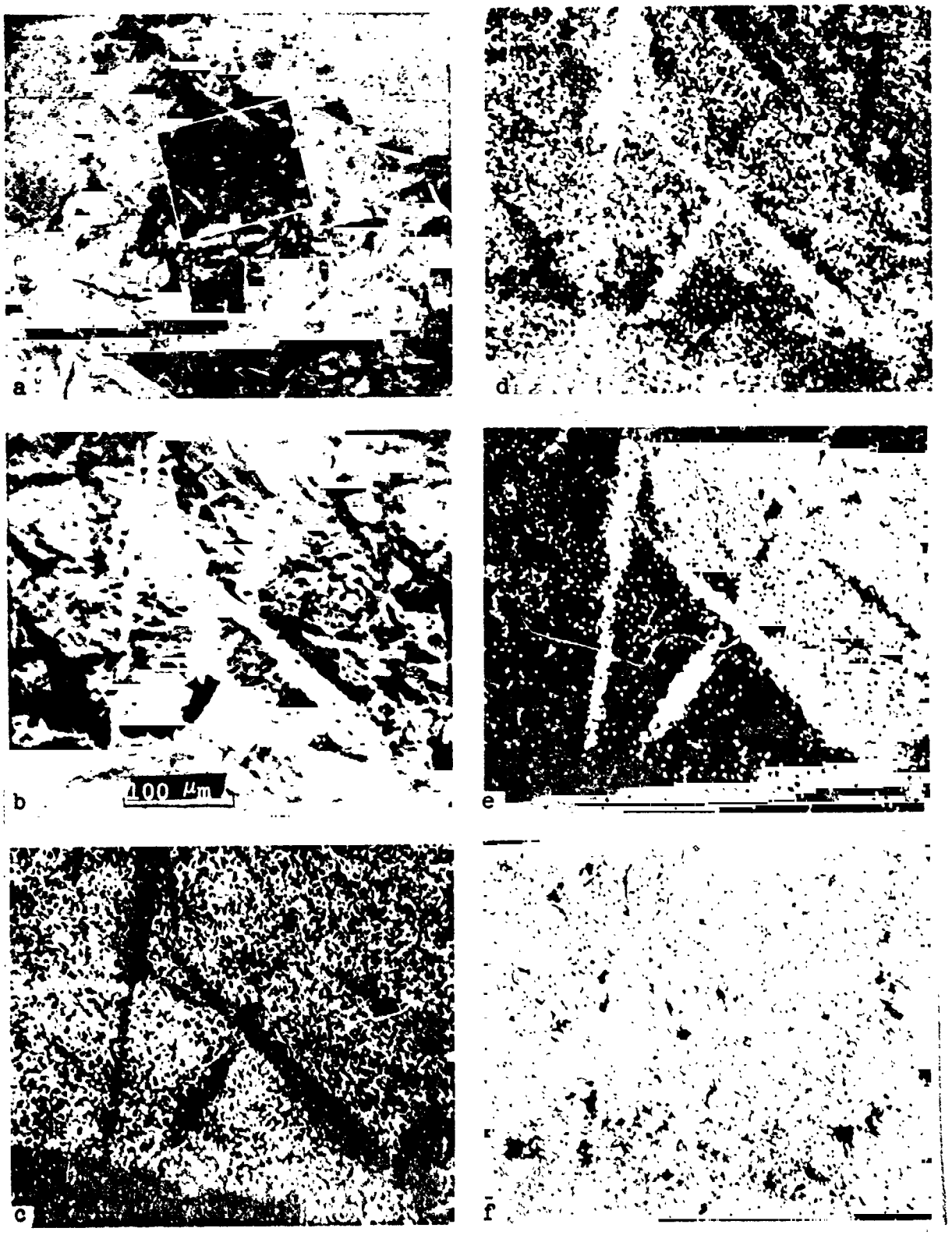

Fig. 12

/Caption on following page/

magnesium, reaching 1 percent MgO (Table 7, Σ A — Σ Fe, Mg, Mn, Ca, Na, K; Σ B — Σ Ti, Cr, Al, P). The trend toward an inverse relationship between the crystallochemical coefficients of magnesium and iron can be noted, which indicates the isomorphic miscibility and negligible presence of the geikielite molecule.

Spinels. One of the most interesting minerals in lunar rocks are the spinels (we refer not to magnesio-aluminum spinel as such /142 ($MgAl_2O_4$) but to the entire group of these oxidic minerals, including the series chromite-hercynite-ulvospinel-spinel). Several investigators described for Apollo 11 rocks solid solutions between the extreme members of ulvospinel (Fe_2TiO_4) -- chromite ($FeCr_2O_4$) -- hercynite ($FeAl_2O_4$) /177 and distinguished titanian chromite, aluminian chromite, and chromian ulvospinel.

In Luna 16 rocks these spinels studied contain a very appreciable fraction of titanian, ulvospinel constituent and essentially in most cases are varieties of ulvospinels (Table 8).

During crystallization, spinels are segregated at different stages usually in the form of fine grains (10-20-50 μm). The earliest, included in the form of idiomorphic segregations in early olivines, are the more chromian and magnesian, for example, chromo-alumino-magnesian ulvospinel in section 202 (analysis 202-11) in early olivine. Pure titanian chromites are seldom found -- analysis 12-8 (Fig. 14, a-d).

In the polished sections one can see, as gray nuclei formed by chromite clothed with the brownish-pinkish anisotropic ore mineral -- ulvospinel. Very often it is segregated also as an independent mineral, that is, without chromite nuclei, simultaneously with the minerals of the later stages. Ulvospinels of these stages are diverse (see Table 8): chromian (analysis 55-1), aluminian (55-9), and chromo-aluminian (202-9a, 202-9).

In passing from spinel ($MgAl_2O_4$) to chromite ($FeCr_2O_4$), there /143 is an isovalent substitution within the limits of the sites of octahedral coordination -- 2 Al (VI) ← 2 Cr (VI) without a change in the structural plan. But in the cases of the transition from spinel or chromite to ulvospinel ($FeFeTiO_4$), there is a heterovalent substitution 2 Al (VI) ← Ti (VI) + Fe (VI) or 2 Cr (VI) ← Ti (VI) + Fe (VI). The structure of the newly formed ulvospinel is now inversion ulvospinel -- not of the type A (IV) B_2 (VI) O_4, but B (IV) A (VI) B (VI) O_4 /187. The appearance of Ti^{4+} in the spinel structure forbids the presence of Al^{3+} or Cr^{3+} in the lattice. If the diagram is replotted in the coordinates Ti vs (Cr + Al), the

/Caption to Fig. 12 on preceding page./

Fig. 12. Distribution of elements obtained on an electron microscope; medium-grained basalt, section 12

a. Optical image of part of the section in transmitted light, the rectangle refers to the part of the section for which pictures (b-f) were obtained
b. Compositional constitution
c. Distribution of calcium
d. Distribution of iron
e. Distribution of titanium
f. Distribution of calcium

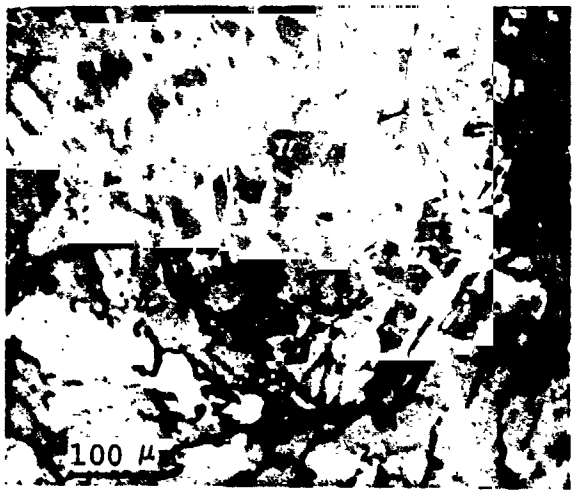

Fig. 13. Image of surface of section of medium-grained basalt in reflected light, section 55.

plagioclases varies -- from the formation of well-defined ophitic structures to hypidiomorphogranular and xenomorphic segregations of this mineral. These and the compositional variations indicate its crystallization over an extended period of rock formation.

Ilmenites. This ore mineral found most widely in lunar rocks is encountered in considerable amounts -- from 5 to 15 percent and even 20 percent. As a whole, its content is still 1.5-2 times lower than in Sea of Fertility rocks. Usually it forms elongated lamellar crystals. In coarse-grained rocks they are 1-2 mm in length. Sometimes its segregations are observed in the form of lamella of more isometric shape. In addition to the lamellar crystals, always present are either truncated tabular lamella of ilmenite, or segregations of irregular shapes. In rocks with ophitic and near-ophitic textures, ilmenite is generally found in the grains of pigeonite-augites. Thus, like silicated minerals ilmenite is segregated over a wide range of time during the crystallization of rocks. The shapes of its segregations are very satisfactorily recorded both in scanning photographs of elemental distribution (Fig. 12, a-e), and in polished sections (Fig. 13). Ogival, at times intersecting forms, are shown in Fig. 13, highly representative of the ilmenite in mare lunar basalts. Always noted for ilmenites is the presence of chromium, aluminum, calcium, and especially

TABLE 7. CHEMICAL COMPOSITION OF ILMENITES FROM LUNA 16 BASALTIC ROCKS (IN WEIGHT PERCENT)

Component	55-6	55-5	55-11	202-8	202-7	202-76
SiO_2	0,10	0,11	0,20	0,38	0,23	0,06
TiO_2	51,8	51,3	51,9	51,2	53,1	52,7
Al_2O_3	0,20	0,21	0,21	0,20	0,14	0,11
Cr_2O_3	0,00	0,31	0,45	0,33	0,58	0,40
FeO	47,3	47,0	45,5	45,4	44,9	45,6
MnO	0,40	0,52	0,55	0,57	0,41	0,59
MgO	0,08	0,54	0,84	1,00	1,08	1,10
CaO	0,15	0,20	0,31	0,26	0,11	0,07
Na_2O	0,00	0,00	0,00	0,00	0,00	0,00
K_2O	0,07	0,05	0,05	0,05	0,04	0,04
P_2O_5	0,00	0,00	0,00	0,04	0,00	0,00
Total	100,1	100,2	100,0	99,4	100,6	100,7
Coefficients for 3 [O]						
Si	0,003	0,003	0,005	0,009	0,006	0,001
Ti	0,985	0,973	0,980	0,972	0,991	0,987
Al	0,006	0,006	0,006	0,006	0,004	0,003
Cr	0,000	0,006	0,009	0,006	0,011	0,008
Fe	1,000	0,992	0,956	0,958	0,931	0,950
Mn	0,008	0,011	0,012	0,012	0,009	0,012
Mg	0,003	0,020	0,031	0,038	0,040	0,041
Ca	0,004	0,005	0,008	0,007	0,003	0,002
Na	0,000	0,000	0,000	0,000	0,000	0,000
K	0,002	0,002	0,002	0,002	0,001	0,001
P	0,000	0,000	0,000	0,001	0,000	0,000
ΣB	0,994	0,988	1,000	0,994	1,012	0,999
ΣA	1,017	1,030	1,009	1,017	0,984	1,006

TABLE 8. CHEMICAL COMPOSITION OF SPINELS FROM LUNA 16 BASALTIC ROCKS (IN WEIGHT PERCENT)

Component	55-1	55-9	202-9a	202-9	202-11	12-8	M-16
SiO_2	0,15	0,24	0,10	0,34	0,21	—	—
TiO_2	29,2	33,5	21,1	21,6	33,0	6,5	3,0
Al_2O_3	2,70	1,71	7,61	7,37	3,57	13,2	36,0
Cr_2O_3	9,28	0,03	19,6	19,1	9,28	51,3	24,9
FeO	56,6	63,4	48,4	47,8	43,5	24,2	23,4
MnO	0,40	0,42	0,59	0,51	0,44	0,39	—
MgO	1,06	0,17	2,91	3,31	9,04	2,1	10,0
CaO	0,14	0,28	0,08	0,03	0,16	—	—
Na_2O	0,00	0,00	0,00	0,07	0,00	—	—
K_2O	0,00	0,10	0,04	0,04	0,06	—	—
P_2O_5	0,00	0,00	0,00	0,00	0,00	—	—
Total	99,5	99,8	100,4	100,2	99,3	97,7	100,3
Coefficients for 32 [O]							
Si	0,040	0,072	0,024	0,036	0,056	—	—
Ti	6,424	7,472	4,448	4,541	6,744	1,328	0,536
Al	0,928	0,600	2,520	2,432	1,144	4,232	10,672
Cr	2,144	0,008	4,344	4,224	1,992	11,040	4,696
Fe	13,848	15,720	11,352	11,184	9,880	5,496	4,856
Mn	0,096	0,104	0,136	0,120	0,104	0,088	—
Mg	0,464	0,072	1,216	1,376	3,656	0,848	3,552
Ca	0,040	0,088	0,024	0,024	0,048	—	—
Na	0,000	0,000	0,000	0,040	0,000	—	—
K	0,000	0,040	0,016	0,016	0,024	—	—
P	0,000	0,000	0,000	0,000	0,000	—	—
Σ(A+B)	23,984	24,176	24,080	24,056	23,648	23,032	24,312

points of the analyses in Table 8 will lie virtually on the same straight line with the inverse function Ti = 1 - (Al + Cr)/2. In other words, one titanium atom causes the lattice to lose two atoms (2 Al, or Cr + Al, or 2 Cr), which then must follow from what has just been stated. Analysis 12-8 is characterized by an overstated amount of aluminum, therefore does not fit within this general sequence.

Evidently, the composition of spinels can serve as a good geochemical indicator of physicochemical conditions of the crystallization of melts.

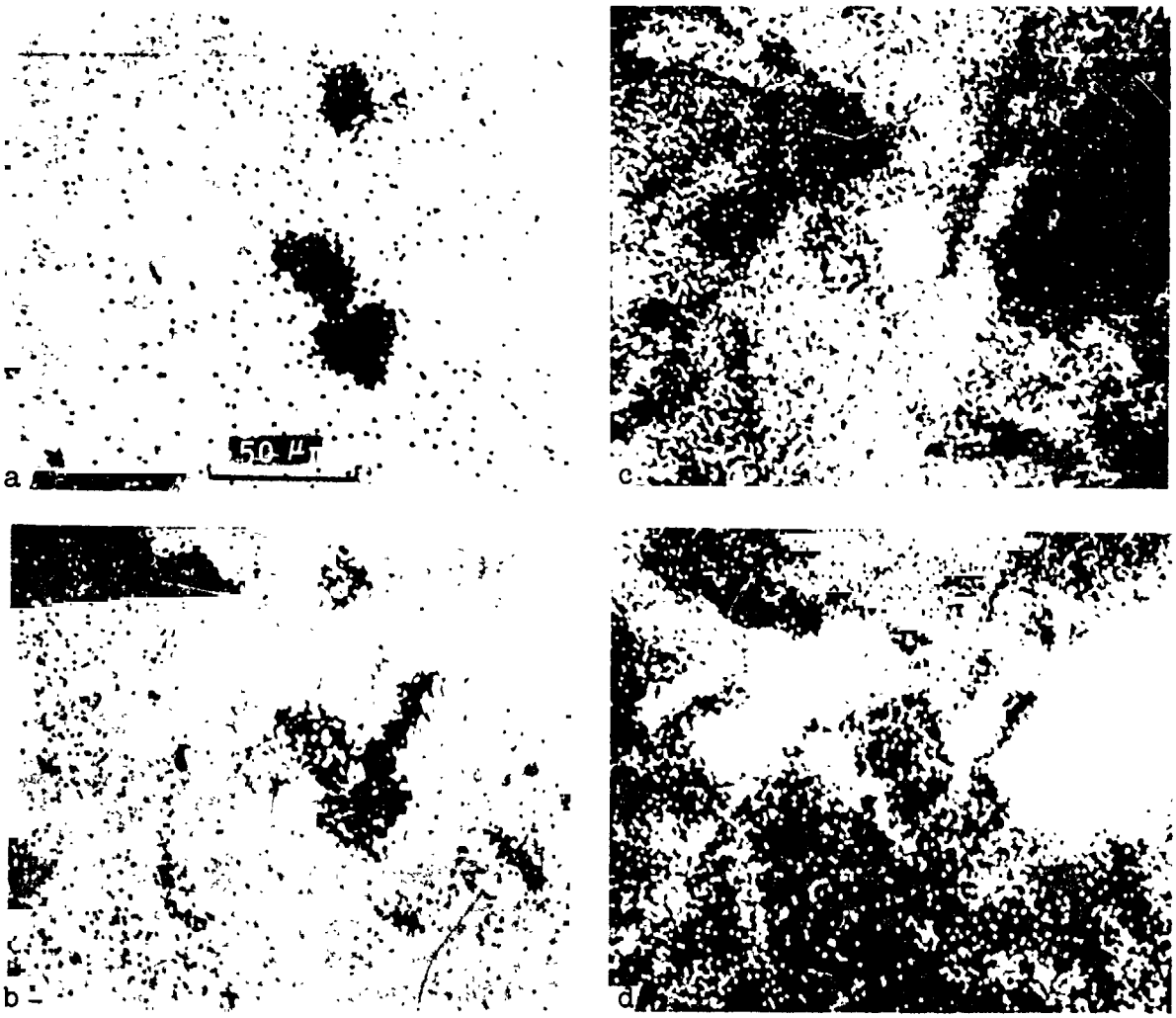

Fig. 14. Distribution of elements obtained on an electron microscope, medium-grained basalt, chromian ulvospinel in the center (three grains), and ilmenite -- above it

a. Distribution of chromium
b. Distribution of titanium
c. Distribution of iron
d. Distribution of aluminum

Troilite. Fine segregations of troilite are always present in basaltic rocks. Their size is 20-30 microns, and 100-150 microns at the maximum. They usually tend both to the interstices between the grains of the rock-forming minerals as well as to their facets. The composition of troilite is in Table 9. For the case of the higher quality analysis (analysis 202-1; analysis 17-9, just as the chromite analysis 12-8, Table 8, belongs to an earlier series performed on low-grade reference standards), the ratios of Fe and S are very close to stoichiometric. /144

Metallic iron. This is encountered in the form of very fine individual segregations in basalt (1-5 microns) and in individual fragments in various regolith fractions. The lava can belong to meteoritic iron. The data from the analysis of two such fragments (Table 9) does not contradict this.

Potassium-rich glasses. When the scanning photographs of the distribution of elements in the basalt sections was obtained, the uneven distribution of potassium was very often established. Potassium in general is present in lunar rocks and minerals in very small amounts [1, 13, 14]. Still, it was unexpected to see small local concentrations of potassium confined to the facets of grains and interstices. For example, Fig. 12 f shows that it is distributed predominantly along the facets of ilmenites with other minerals and in the interstices, reaching a size of 5-10 microns diagonally. These segregations are not identified as individual potassium minerals.

In the two cases it was possible to detect concentrations of potassium confined to the coarser segregations, 50-60 μm in size. Thus, in the section of coarse-grained gabbro whose fragment was found to contain a large ilmenite lamella, plagioclase, and two pyroxene particles, and more ferruginous and more calcic augite, a rounded segregation of glass about 50 μm in diameter was very clearly visible. It was distinguished on scanning photographs of the elemental distribution (Fig. 15) and is very strongly enriched in potassium (Fig. 15 f). A microprobe analysis of this inclusion (Table 10) showed the following: SiO_2 content 71.8-78.3 percent; Al_2O_3, 10.6-12.3 percent; FeO, 0.77-3.23 percent; and K_2O, 7.39-8.93 percent.

The glass contained 45-55 percent normative orthoclase and 28-44 percent normative quartz. An analogous glass was established in section 202 (Table 10, analysis 202-2a). These glasses, manifested in medium-grained and coarse-grained rocks, are the products of the crystallization of residual melts of very ophitic composition, indicating the considerable role of crystallization differentiation during the evolution of magmatic lunar melts and the formation of magmatic rocks. It can be assumed that these processes are typical also for finer-grained rocks similar to those shown in Fig. 12, but the very small dimensions of these segregations does not permit high quality analyses. [146]

Phosphates. These accessory materials are encountered in very fine (5-10 μm) segregations in plagioclase or in interstices. They are readily observed in sections, but it was not possible thus far to obtain their qualitative analysis owing to the small size of the segregations and their poor displaying tendency in section preparation. Judging from preliminary data, the composition of the grains studied more closely corresponds to apatite.

TABLE 9. CHEMICAL ANALYSES OF TROILITE IN METALLIC IRON FROM BASALTS IN LUNA 16 REGOLITH

Component	Troilite 202-1 Weight percent	Troilite 202-1 Coefficient	Troilite 17-9 Weight percent	Troilite 17-9 Coefficient	Metallic iron /13/ 34-1 Weight percent	Metallic iron /13/ 34-2 Weight percent
Si	0,07	0,002	—	—	—	—
Ti	0,02	0,000	0,23	0,004	—	—
Al	0,03	0,001	—	—	—	—
Cr	0,00	0,000	—	—	—	—
Fe	63,1	0,996	58,5	0,915	94,0	86
Mn	0,13	0,002	0,15	0,002	—	—
Co	0,02	0,000	—	—	0,48	0,16
Ni	0,03	0,000	—	—	5,0	13,6
Mg	0,01	0,000	—	—	—	—
Ca	0,16	0,003	—	—	—	—
S	35,8	0,985	39,5	1,078	—	—
P	0,30	0,008	—	—	—	—
Total	99,7	2,000	98,4	1,999	99,5	99,8

The unusual isotropic silicate phase is encountered in one of the sections of the melanocratic basalt. The largest segregation (200 x 100 μm) resembles an elongated hexagonal tablet. The mineral is copper-yellow and clear. No increased content of zirconium or rare earths was noted. In addition to the large segregation, fine segregations were also present, confined to the interstices between other minerals. The section was rich in ilmenite, and there were other ore minerals present as well (Color Plate VIII, 2). To solve the problem of the nature of this phase, its more detailed investigation is now underway. It is not precluded that it can prove to be glassy.

In contrast to Apollo 11 and Apollo 12 samples where crystobalite was widely distributed and tridymite was encountered, these minerals were not detected in Luna 16 rocks. There is only the indication /8/ that crystobalite was present in a fine fraction of Luna 16 regolith. Also not found in our investigations of Luna 16 rocks were armolkolite and tranquillitite. Pyroxferroite was discussed above. Thus, basaltic and gabbro rocks from the Sea of Fertility differ from the rocks of the Sea of Tranquillity and the Ocean of Storms. Besides the above-noted mineralogic distinctions, we can also mention the lower content in the former of ilmenite, and also the lower diversity in the former of structures, in particular the low distribution of interstitial and especially vitrophytic textures. In general, the zonality of plagioclases, pyroxenes, and olivines was also more poorly evident in the Sea

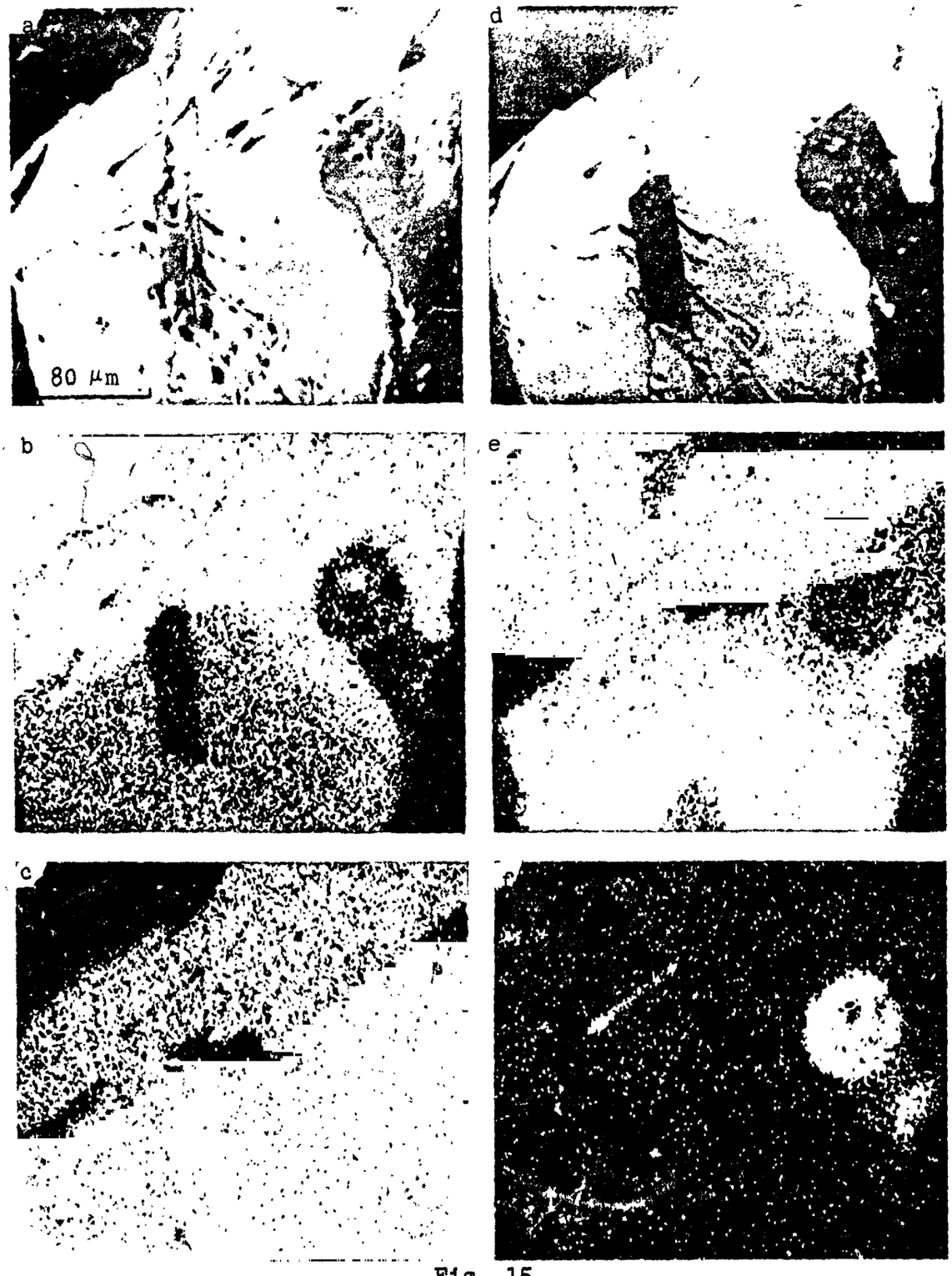

/145

Fig. 15

/Caption on following page./

/Caption to Fig. 15 on preceding page./

Fig. 15. Distribution of elements obtained with an electron microprobe in the gabbro section; upper -- ilmenite; in the lower half of the field, to the left -- low-iro pyroxene, to the right -- -- high-iron pyroxene; in the field of the last circular segregation -- a potassium-rich segregation of a glassy phase and a small section formed of plagioclase; a plagioclase lamella is also visible in the center of the field

a. View in scattered electrons
b. Distribution of iron
c. Distribution of titanium
d. Compositional constitution
e. Distribution of calcium
f. Distribution of potassium

TABLE 10. X-RAY SPECTRAL ANALYSES AND NORMATIVE COMPOSITIONS OF RESIDUAL GLASSES FROM LUNA 16 BASALTIC ROCKS (IN WEIGHT PERCENT)

Component	155-7	155-10	155-11	202-2a	Normative Composition	155-7	155-10	155-11	202-2a
SiO_2	71,8	77,8	78,3	79,3	*Q*	28	41	44	44
TiO_2	0,46	0,16	0,34	0,11	*Or*	55	47	45	49
Al_2O_3	12,3	10,6	11,7	11,0	*Ab*	5,2	6,1	4,2	2,5
Cr_2O_3	0,00	0,00	0,00	0,00	*An*	4,8	3,1	3,4	3,0
FeO	3,23	0,77	1,66	0,46	*Il*	0,7	0,2	0,6	0,2
MnO	0,00	0,15	0,00	0,00	*Hr*	—	0,4	3,0	0,9
MgO	0,10	0,31	0,02	0,06	*Sp*	—	—	—	0,2
CaO	1,38	0,87	0,66	0,74	*Wo*	1,6	—	—	—
Na_2O	0,56	0,65	0,45	0,27	*Fs*	4,5	0,7	0,2	—
K_2O	8,93	7,57	7,39	7,94	*En*	0,3	0,9	0,1	0,1
P_2O_5	0,03	0,23	0,01	0,00	*Wt*	0,1	0,5	—	—
Total	98,8	99,1	100,5	99,9					

of Fertility rocks. Although mesostasis rich in potassium and silicic acid culminated the crystallization of rocks, its amount was negligible, and it was encountered in far from all fragments.

All these features indicate a somewhat lesser role of crystallization differentiation in the formation of gabbro and basaltic rocks in the Sea of Fertility than in the two other lunar maria. The predominant distribution of gabbro and medium-grained rocks compared with fine-grained and aphanitic and the limited development of magmatic glassy phases also betokens the greater depth of crystallization in the relatively quiescent conditions of its occurrence. The absence of metastable phases of the crystobalite type confirm these considerations.

REFERENCES

/147

1. Vinogradov, A. P., "Preliminary Data on Lunar Surface Material Returned by Luna 16 Automatic Station," Geokhimiya (3), 261-274 (1971).

2. Wood, J. A., Marvin, U. B., Powell, B. N., and Dickey, J. S., Jr., "Mineralogy and Petrology of the Apollo 11 Lunar Sample," Spec. Rept. Smithsonian Astrophys. Obs., (307), (1970).

3. Wood, J. A., Marvin, U. B., Reid, J. B., Jr., Teilor, G. J., Bower, J. F., Powell, B. N., and Dickey, J. S., Jr., "Mineralogy and Petrology of the Apollo 12 Lunar Sample," Spec. Rept. Smithsonian Astrophys. Obs., (333), (1971).

4. Florensiriy, K. P., Ivanov, A. V., Tarasov, L. S., Suakheyev, Yu. I., and Rode, O. D., "Morphology and Types of Particles of Regolith Sample from the Sea of Fertility," present collection, page 38.

5. Bence, A. F., and Albee, A. L., "Empirical Correction Factors for the Electron Microanalysis of Silicates and Oxides," J. Geol., 76, 382 (1968).

6. Albee, A. L., and Ray, L., "Correction Factors for Electron Probe Microanalysis of Silicate, Oxides, Carbonates, Phosphates, and Sulfates," Anal. Chem., 42(12), 1408 (1970).

7. Makarov, E. S., Ilyin, N. P., and Ivanov, V. I., "The Composition and Crystalline Structure of the Minerals of Regolith from the Sea of Fertility," Space Research XII, 155 (1972).

8. Makarov, Ye. S., Ivanov, V. I., Mokeyeva, V. I., et al., "X-ray Diffraction Identification of Minerals in Lunar Regolith Returned by Luna 16 Automatic Station," present collection, p. 148.

9. Schmitt, H. H., Lofgren, G., Swann, G. A., and Simmons, G., "The Apollo 11 Sample: Introduction," Proc. Apollo 11 Lunar Sci. Conf., 1(1), (1971).

10. Gast, P. W., and Hubbard, N. F., "Chemistry of Lunar Basalts and Their Origin Constraints on the Composition of the Lunar Interior," Proc. Second Lunar Sci. Conf., 2, (1972).

11. Pavlenko, A. S., Tarasov, L. S., Shevaleyevskiy, I. D., and Ivanov, A. V., "Petrology of Lunar Rocks from the Sea of Fertility," present collection, p. 56.

12. Il'in, N. P., Loseva, L. Ye., and Fenin, V. G., "X-ray Spectral Microanalysis of Composition of Individual Particles of Lunar Regolith," present collection, p. 209.

13. Keil, K. T. E., Buch, T. E., and Prinz, M., "Mineralogy and Composition of Apollo 11 Lunar Samples," Proc. Apollo 11 Lunar Sci. Conf., 1, 561 (1971).

14. Dens, M. R., Douglas, J. A., Plant, A. G., and Trail, R. J., "Petrology, Mineralogy, and Deformation of Apollo 11 Samples," Proc. Apollo 11 Lunar Sci. Conf., 1, 315 (1971).

15. Chao, E. C. T., Minkin, J. A., and Frondel, C. et al., "Pyroxferroite, a New Calcium-bearing Iron Silicate from Tranquillity Base," Proc. Apollo 11 Lunar Sci. Conf., 1, 65 (1971).

16. Jakes, P., Warner, J., Readley, W. I., et al., "Petrology of a Portion of the Mare Fecunditatis Regolith," present collection, p. 64.

17. Agrell, S. O., Pecket, A., and Boyd, F. R. et al., "Titan Chromite, Aluminian Chromite and Ulvospinel from Apollo 11 Rocks," Proc. Apollo 11 Lunar Sci. Conf., 1, 81 (1971).

18. Shtrunts, H., Mineralogicheskiye Tablitsy /Mineralogical Tables/, Gosgortekhizdat, 1962.

Order of Lenin Institute of Geochemistry and Analytical Chemistry imeni V. I. Vernadskiy, USSR Academy of Sciences, Moscow.

N75 11826

X-RAY DIFFRACTION IDENTIFICATION OF MINERALS IN LUNAR REGOLITH RETURNED BY LUNA 16 AUTOMATIC STATION

/148

Ye. S. Makarov, V. I. Ivanov, V. I. Mokeyeva, K. I. Tobelko, V. I. Bukin, A. Ya. Volkova, G. A. Kuznetsova, and L. M. Kuznetsov

Abstract

The methods of powder and monocrystal x-ray diffraction served in identifying the mineral composition of gross samples of regolith from different levels of the drill core and about 80 individual regolith particles returned by the Luna 16 station. It was established that the Sea of Fertility regolith includes pyroxenes of the augite-pigeonite series, anorthites, ilmenite, olivines, spinels, α-cristobalite, iron particles, glass, and several as yet unidentified particles. Crystallographic and roentgenometric data are given for all the lunar minerals found.

Introduction. Powder and monocrystal methods of x-ray diffraction analysis were used by us in studying about 80 particles of Sea of Fertility lunar regolith. The size of individual particles was in the range 0.1-0.5 mm. In addition, we also investigated and determined the mineral composition of several powder samples of the gross sample, whose particle size was finer than 80 μm, from different levels of the drill core.

In this article we give a detailed report of the results of the x-ray phase identification of these samples of lunar regolith, listed in Table 1. We also deemed it necessary to present here factual material on the roentgenometric characteristics d (Å)/I and to give tables of interplanar spacings (d), and the line intensities (I) of powder diffraction patterns for individual lunar materials and gross samples of regolith which we adopted as reference standards. In the absence of similar data in the American literature on Apollo 11 and Apollo 12 and reliable handbook data on the analogous terrestrial materials, the original

TABLL 1. LIST OF LUNAR SAMPLES STUDIED AND THEIR MINERAL COMPOSITION BASED ON DATA OF X-RAY PHASE ANALYSIS

Sample Nr.	Particle size, mm	External appearance of particle	Mineral composition from x-ray phase analysis data	Crystallographic data
M-1a M-1b	0.5 0.5	Dark polycrystalline grains	Gabbro: anorthite + augite/pigeonite + olivine + ilmenite	Polycrystals
M-2 M-3	0.5 0.5	Light polycrystalline grains	Anorthite	"
M-4	0.3	Yellowish clear particle	Olivine	Monocrystal-fragment a = 4.780±0.005 AU b = 10.290±0.010 AU c = 6.016±0.004 AU
M-5a M-5 b	0.3 0.3	Dark polycrystalline grains	Basalt: anorthite + augite/pigeonite + olivine	Polycrystal
M-6	0.4	Red-brown glass	Glass	Glass
M-7	0.3	Dark-brown glass	"	"
M-8	0.4	Yellow-brown glass	"	"
M-9	0.3	Green glass	"	"
M-10	0.3	Light matte particle	Anorthite	Polycrystal
M-11	0.3	Light particle	"	"
M-12	0.5	Iron particle	α-Fe	" a = 2.870±0.005 AU
M-13 Powder sample 3-2ye	<80 μm	Powder of gross regolith sample	Mixture: anorthite + augite/pigeonite + olivine + ilmenite + spinel + cristobalite + α-Fe + glass	Powder with large amount of glass
M-14	0.5	Spherule, opaque, light-gray	Anorthite (rich) + augite/pigeonite (poor)	Coarse-grained polycrystal
M-15	0.15	White clear lamella	Glass	Glass
M-16	0.3	Black lamellar particle	Spinel	Monocrystal a = 8.270±0.002 AU
M-17	0.15	Dark particle	Pyroxene: augite/pigeonite	Coarse-grained aggregate
M-18	0.3	Greenish particle	Glass	Glass
M-19	0.4	Clear yellowish particle	Olivine	Monocrystal-fragment a = 4.780±0.005 AU b = 10.290±0.005 AU c = 6.021±0.005 AU
M-20	0.2	Red-brown particle	Pyroxene: augite/pigeonite + glass	Fine-grained polycrystal
M-21	0.3	Brown glass	Glass	Glass
M-22	0.3	Gray particle	Anorthite	Coarse-crystalline intergrowth

TABLE 1. LIST OF LUNAR SAMPLES STUDIED AND THEIR MINERAL COMPOSITION BASED ON DATA OF X-RAY PHASE ANALYSIS /CONTINUATION/

Sample Nr.	Particle size, mm	External appearance of particle	Mineral composition from x-ray phase analysis data	Crystallographic data
M-23	0.2	Dark-brownish intergrowth and black lamina	Augite/pigeonite + ilmenite	Intergrowth of crystals
M-24	0.2	Gray grain	Anorthite	Polycrystal
M-25	0.4	Greenish grain	Glass	Glass
M-26	0.3	Brownish grain of regular shape	Olivine	Monocrystal a = 4.78±0.01 AU b = 10.290±0.002 AU c = 6.024±0.004 AU
M-27	0.4	Brownish grain	"	Intergrowth of two monocrystals a = 4.80±0.01 AU b = 10.06±0.01 AU c = 6.00±0.01 AU
M-28	0.3	Reddish grain	Glass	Glass
M-29	0.3	Clear colorless lamella	"	"
M-30	0.04	Yellowish-green grain	Glass	Glass
M-31	0.4	Bluish particle	"	"
M-32	0.4	White clear particle of regular shape	Plagioclase	Monocrystal of triclinic syngony a = 8.17±0.01 AU b = 12.90±0.01 AU c = 7.05±0.01 AU α = 92°; β = 116° γ = 88°
M-33	0.5	Fragment of chondroid	α-cristobalite + olivine	Weakly crystallized glass
M-34	0.5	Chondroid	α-cristobalite + olivine	Polycrystal
M-35	0.3	Green	Anorthite	Polysynthetic twin
M-36	0.6	Iron particle	α-Fe in general + pyroxene (poor)	Polycrystal of iron with selvages of pyroxenes
M-37	0.3	" "	α-Fe in general + anorthite (poor)	Polycrystal of iron a = 2.867±0.005 AU with selvages of anorthite
M-38	0.3	" "	α-Fe in general + + anorthite + pyroxenes + olivine	Spongy iron a = 2.868±0.005 AU with selvages of anorthite, pyroxenes, and olivine
M-39		" "		

/150

TABLE 1. LIST OF LUNAR SAMPLES STUDIED AND THEIR MINERAL COMPOSITION BASED ON DATA OF X-RAY PHASE ANALYSIS /CONTINUATION/

Sample Nr.	Particle size, mm	External appearance of particle	Mineral composition from x-ray phase analysis data	Crystallographic data
M-40		Iron particle	/Same as description for M-39 on preceding page/	/Same as description for M-39 on preceding page/
M-41	0.3	Fragment of gabbro	Anorthite + pyroxene:augite/ /pigeonite	Coarse-crystalline intergrowth
M-42	0.4	Light-yellow elongated particle	Olivine	Monocrystal
M-43	0.3	White particle	Anorthite	Laminated texturized polycrystal
M-44	0.3	Light-yellow particle	Olivine	Monocrystal a = 4.77±0.01 AU b = 10.290±0.003 AU c = 6.018±0.004 AU
M-45	0.4	Dark-red particle	"	Intergrowth of two monocrystals a = 4.77±0.01 AU b = 10.30±0.01 AU c = 6.025±0.005 AU
M-46	0.3	Gray particle	Anorthite	Polycrystal
M-47	0.3	Red-brown particle	Glass	Glass
M-48	0.3	Dark-gray particle	Anorthite + olivine (poor)	Intergrowth of monocrystals
M-49	0.3	Dark-gray particle	Anorthite + olivine + α-cristobalite	Polycrystal
M-50	0.25	" "	Glass (rich) + olivine	Weakly crystallized glass
M-51	0.4	Dark particle	Glass	Glass
M-52	0.3	Dark-green particle	"	"
M-53	0.5	Reddish particle	Olivine (rich) + anorthite (poor)	Polycrystal
M-54	0.3	Dark particle	Olivine	Monocrystal a = 4.76±0.01 AU b = 10.15±0.01 AU c = 6.018±0.005 AU
M-55	0.15	Red planar particle	Glass	Glass
M-56	0.3	Olivine particle	Olivine	Monocrystal
M-57	0.2			
M-58	0.2	Dark particle	Glass	Glass
M-59 sample	<80 μm	Powder of gross regolith sample	Anorthite + augite/ pigeonite + olivine + ilmenite + spinel + α-cristobalite + α-Fe + glass	Powder with large amount of glass

/151

TABLE 1. LIST OF LUNAR SAMPLES STUDIED AND THEIR MINERAL COMPOSITION BASED ON DATA OF X-RAY PHASE ANALYSIS /CONTINUATION/

Sample Nr.	Particle size, mm	External appearance of particle	Mineral composition from x-ray phase analysis data	Crystallographic data
M-60a	0.2	Dark particle	Pyroxene: augite/ pigeonite	Intergrowth of several crystals
M-60b	0.2	" "	As above	Intergrowth of crystals
M-61a	0.1	" "	" "	Intergrowth of crystals
M-61b	0.2	" "	" "	Intergrowth of crystals
M-62a	0.30	" "	" "	Intergrowth of crystals
M-62b	0.35	" "	" "	Intergrowth of crystals
M-65	0.3	Green crystal	" "	Coherent intergrowth in (001) of augite and pigeonite a = 9.69±0.01 AU b = 8.90±0.02 AU c = 5.26±0.01 AU β = 106°00'±2' Pigeonite a = 9.71±0.01 AU b = 8.90±0.02 AU c = 5.22±0.01 AU β = 108°39'±2'
M-66	0.15	" "	Glass	Glass
M-70	0.3	Black particle	Ilmenite	Monocrystal
M-71a	0.10	Green particle	Glass	Glass
M-71b	0.15	" "	Pyroxene: augite/ pigeonite	Monocrystal Same as for M-65
M-72	0.25	Black particle	Spinel II	Monocrystal a = 8.457±0.005 AU
M-73	0.4	Iron spherule	α-Fe	Polycrystal a = 2.868±0.005 AU
M-74	0.25	" "	α-Fe	As above
M-75	0.30	Light gray particle	Anorthosite	Polycrystal
M-76	0.30	Black particle	Ilmenite	Monocrystal a = 5.085±0.002 AU c = 14.084±0.005 AU
M-77	0.2	Dark particle	Spinel I + Spinel II	Coherent intergrowth of two crystals Spinel I: a = 8.304±0.005 AU Spinel II: a = 8.457±0.005 AU

TABLE 1. LIST OF LUNAR SAMPLES STUDIED AND THEIR MINERAL COMPOSITION BASED ON DATA OF X-RAY PHASE ANALYSIS /CONCLUSION/

Sample Nr.	Particle size, mm	External appearance of particle	Mineral composition from x-ray phase analysis data	Crystallographic data
M-78	0.15	Dark particle	Spinel I (rich) + pyroxene (poor)	Intergrowth of crystals of spinel with pyroxene
M-79	0.3	Black particle	Ilmenite	Monocrystal

TABLE 2. INTERPLANAR SPACINGS d (IN AU) AND LINE INTENSITIES I FOR SAMPLES OF LUNAR REGOLITH AND ITS CONSTITUENT MINERALS

Regolith						Mineral					
sam. (7+8)-1d RKU-114 Fe anode	sam. (7+8)-1d RKD-57 Co anode	sam. (7+8)-1d Guinier camera Fe anode	sam. 3-2i RKD-57 Co anode	sam. 3-2ye RKD-57 Fe anode	anorthite from /7/	augite-pigeonite, lunar, sam. M-23	ilmenite, from /8/	olivine, lunar sam. M-27	α-cristobalite, from /8/	spinel, lunar sam. M-16
d, Å I	d, Å I	d, Å I	d, Å I	d, Å I	d, Å I	d, Å I	d, Å I	d, Å I	d, Å I	d, Å I
—	6,90 1	—	—	—	6,81 8	—	—	—	—	—
—	6,39 0,5	—	—	—	6,42 4	—	—	—	—	—
—	5,82 0,5	—	—	—	—	—	—	—	—	—
—	5,15 0,5	—	5,16 2	—	5,12 3	—	—	5,10 1	—	—
—	4,68 1	—	4,71 2	4,66 2	4,69 14	—	—	—	—	—
—	4,38 1	—	—	—	—	—	—	—	—	—
—	4,17 0,5	—	—	—	4,24 2	—	—	—	—	4,15 3
4,05 2	4,02 3	4,04 7	4,05 4	4,01 2	4,04 48	—	—	—	4,03 10	—
3,94 1	3,93 0,5	3,92 8	—	—	3,92 11	—	—	3,91 6	—	—
3,76 2	3,75 4	3,76 5	3,75 3	—	3,78 28 3,76 19	—	—	3,74 1	—	—
—	—	—	—	3,70 2	—	—	3,70 4	—	—	—
—	3,61 1	3,63 5	—	3,60 1	3,62 3,60 33	—	—	—	—	—
—	3,51 0,5	3,52 3	3,50 0,5	—	3,51 4	—	—	3,51 6	—	—
—	—	3,46 2	—	—	3,47 3,46 14	—	—	—	—	—
—	—	3,42 0,5	—	—	3,40 7	—	—	—	—	—
	3,35 4 sp	3,36 7	3,35 0,5	3,32 2	3,36 25	3,36 3	—	—	—	—
3,24 1	—	3,26 3	—	—	3,26 52	—	—	—	—	—
—	—	3,21 10	3,20 10 sp	—	3,21 63	3,21 9	—	—	—	—
3,20 10	3,19 10 sp	3,20 10	—	—	3,19 100	—	—	—	—	—
—	—	3,18 4	—	3,18 10	3,18 91	—	—	—	—	—
3,15 1	—	—	—	—	3,12 39	—	—	—	3,13 6	—
3,02 5	3,03 7	3,03 2	3,02 8	—	3,04 18	—	—	—	—	—
—	—	3,01 8	—	3,00 7	—	3,01 10	—	3,01 4 sp	—	—
2,95 3	—	2,95 5	—	—	2,95 27	—	—	—	—	—
2,92 2	2,93 6	2,92 2	2,91 6	2,89 6	2,93 19	2,91 9 sp	—	2,91 0,5	—	2,91 8
—	—	2,84 1	—	—	2,83 20	—	—	—	2,83 7	—
2,80 1	2,81 3	2,80 2	2,78 4	2,80 3	2,80 9	—	—	2,79 9	—	—
2,75 3	2,75 3	2,75 9	—	2,73 3	—	—	2,74 10	—	—	—
--	2,65 1	2,66 1	2,65 1	—	2,65 14	—	—	—	—	—
2,60 2	—	—	—	—	—	—	—	2,61 1	—	—
—	2,59 2	2,58 6	—	—	—	2,57 7	—	—	—	—
—	—	2,55 3	2,56 4	—	2,56 6	—	—	—	—	—
—	—	—	—	—	2,53 20	—	—	—	—	—
2,53 3	2,53 9 sp	2,52 6	2,52 9 sp	2,52 8	2,51 2,50 28	2,52 7	2,53 9	2,53 8	—	—
2,48 3	2,47 0,5	2,48 7	—	2,47 3	— —	— —	—	2,47 10	2,48 8 2,46 4	2,49 10
—	2,38 0,5	2,38 1	—	—	2,38 4	—	—	2,37 2 sp	—	-
2,29 4	—	2,29 3	—	—	2,27 2,26 7	—	—	—	—	—
—	2,28 4	2,28 1	2,28 2	2,28 0,5	2,24 2,23 4	2,28 2	—	2,28 6	—	—
2,24 2	2,23 1	2,24 4	2,22 2	2,23 0,5		—	2,23 3	—	—	—
—	—	2,16 1	—	—		—	—	2,17 3	—	—
2,15 3	2,15 7	2,14 6	2,15 5	2,13 5	2,14 17	2,14 8	—	—	—	—

/sp = spherule/

TABLE 2. INTERPLANAR SPACINGS d (IN AU) AND LINE INTENSITIES I FOR SAMPLES OF LUNAR REGOLITH AND ITS CONSTITUENT MINERALS /CONCLUSION/ /153

Regolith						Mineral					
sam.(7+8)-1d RKU-114 Fe-anode	sam.(7+8)-1d RKD-57 Co-anode	sam.(7+8)-1d Guinier camera Fe anode	sam.3-2i RKD-57 Co anode	sam. 3-2ye RKD-57 Fe anode	anorthite from /7/	augite-pigeonite, lunar sam. M-23	ilmenite, from /8/	olivine, lunar sam. M-27	α-cristobalite, from /8/	spinel, lunar sam. M-16
d, Å I	d, Å I	d, Å I	d, Å I	d, Å I	d, Å I	d, Å I	d, Å I	d, Å I	d, Å I	d, Å I
—	—	2,12 2	—	—	2,13 3	—	—	—	2,11 5	—
—	2,03 0,5	2,08 3	—	—	2,09 10	2,10 1	—	2,10 3	—	2,07 7
2,03 5	2,04 6	2,04 2	2,03 5	—	—	2,04 5	—	2,03 0,5	—	—
—	—	2,02 3	—	2,02 5	2,02 5	2,01 3	2,02 10	2,01 0,5	2,01 5	—
—	1,970 1	—	—	—	—	—	—	—	—	—
—	—	—	1,958 1	—	—	—	—	1,960 0,5	—	—
—	1,932 1	1,930 1	—	—	1,932 9	—	—	—	—	—
—	—	—	1,922 1	—	—	—	—	—	1,924 6	—
—	1,890 1	—	—	—	—	—	—	1,892 1	—	—
—	—	—	1,879 1	—	1,878 7	—	—	—	—	—
—	1,867 2	1,865 1	—	1,863 1	—	—	1,865 6	—	1,867 6	—
1,842 1	—	1,841 1	—	—	1,837 16	—	—	—	—	—
—	1,835 2	—	1,835 1	1,834 1	—	—	—	—	—	—
1,805 2	1,803 0,5	—	—	—	—	—	—	—	—	—
—	—	1,800 2	—	—	—	—	—	—	—	—
—	—	—	1,733 1	1,795 1	—	—	—	—	—	—
—	1,790 0,5	—	—	—	—	—	—	—	—	—
1,767 4	—	1,770 4	—	—	1,768 17	—	—	—	—	—
—	1,761 7sp	1,761 1	1,761 5	1,761 6	1,761 8	—	—	—	—	—
—	—	1,752 5	—	—	—	1,752 4	—	1,755 10	1,754 2	—
1,727 3	1,728 5	1,726 1	—	—	1,717 7	—	1,720 8	—	1,726 4	—
—	—	—	1,717 3	1,720 4	—	—	—	1,685 3	1,687 6	1,685 5
—	1,684 3	1,682 1	—	1,680 2	—	—	—	—	—	—
1,633 7	1,635 6	1,632 3	1,672 2	1,628 7	—	1,628 9	1,630 3	1,628 3	1,630 2	—
—	—	—	1,627 5	—	—	—	—	—	—	—
—	1,586 1	—	1,580 0,5	—	—	—	—	1,582 2	—	1,588 9
—	1,557 0,5 sp	—	—	—	—	—	—	—	—	—
—	1,538 2	—	1,541 2	1,539 2	—	1,546 3 sp	—	—	—	—
1,510 2	—	—	—	—	—	—	—	—	1,530 6	—
—	1,505 6	1,505 3	1,506 4	1,505 5	—	1,508 4	1,504 7	1,506 5	—	—
1,494 2	1,495 3	—	—	—	—	—	—	—	—	—
—	—	1,489 2	—	1,490 4	—	1,490 5	—	1,492 6	1,492 6	—
1,474 1	1,471 1	1,468 1	—	1,471 4	—	—	1,465 7	—	—	—
—	1,454 1	—	—	1,447 2	—	—	—	1,447 1	—	1,458 9
1,415 2	1,418 4 sp	—	1,413 3	1,413 3	—	1,419 6	—	1,407 7	1,428 5	—
1,393 2	1,390 1	—	1,391 3	1,390 3	—	1,391 6	—	—	—	—
—	1,376 1	—	—	—	—	—	1,375 2	—	—	—
1,367 1	1,360 2	1,360 1	1,356 1	—	—	—	—	1,360 6	—	—
1,346 1	1,340 3	—	—	—	—	—	—	—	—	—
—	1,326 2	—	—	—	—	—	—	1,327 7	—	—

data we report on the d/I of lunar materials can serve as reference standards for further x-ray diffraction investigations of lunar samples.

Experimental technique. The powder of the fine gross fraction of regolith was packed into a capillary made of acetylcellulose, 0.3 mm in diameter, and with it an x-ray diffraction pattern was recorded with a RKD-57.3 mm camera or in an RKD-114.6 mm camera with iron or cobalt filtered radiation. Use was also made of x-ray motion picture photography with a Guinier focussing camera built specially by us in the laboratory. One frame of the regolith in the Guinier camera was obtained on our request by L. M. Kovba in the inorganic chemistry department of the chemical faculty at Moscow State University.

All the manipulations with microparticles were carried out manually under a binocular with maximum power of 32 using thin bronze needles inserted into handles, and with observance of maximum care and cleanliness.

The x-ray diffraction investigation of individual regolith particles from 0.1 to 0.5 mm in size was carried out as follows. First, by the powder and Laue methods it was established whether the given particle was a monocrystal, polycrystal, glass, or intergrowth of two or several monocrystals.

All the particles were irregular in shape, and in the case of monocrystals and glasses -- acute-angled. In their dimensions, the particles were optimal for x-ray diffraction analysis, which proved to be the most convenient, rapid, and reliable method of their mineralogic identification.

Satisfactory powder x-ray diffraction patterns were obtained for the fine-grained polycrystalline particles in an RKD camera without their preliminary grinding into powder. If the particle did not provide any diffraction pattern at all, we identified it as glass and did not subject it to further study. If the particle proved to be monocrystal, then the principal crystallographic directions were determined for it, and the parameters of the /154
elementary cell were found in RKOP, RKV, or KFOR cameras. Refinement of the lattice spacings was made with a URS-50I diffractometer by a technique developed in the laboratory.

The Gandolfi method /5_7 proved extremely useful in obtaining an x-ray powder diagram from a single monocrystal and from intergrowths of crystals. A special attachment to the RKD-57.3 camera providing biaxial rotation of the monocrystalline sample, leading to the convolution of individual reflexes into Debye cones, was developed and built in our laboratory. A schematic diagram of this accessory to the RKD camera is in Fig. 1 and will be described in

detail in a special article. Obtaining x-ray diffraction patterns after Gandolfi considerably accelerated the identifying of monocrystalline particles from d/I values, without the need to determine the elementary cell by laborious investigations of monocrystals. It should be remembered that in addition to the wholly satisfactory quantitative information from the d values (AU), the Gandolfi x-ray diffraction patterns often give distorted values of the intensities I, which is not highly significant for identification purposes, but which does not prove suitable for determining the atomic structure of crystals.

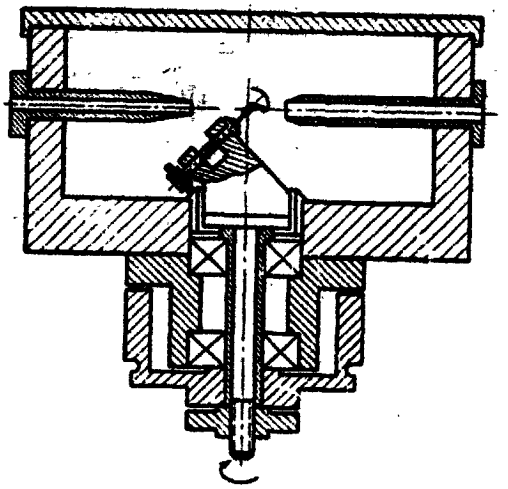

Fig. 1. Cross section of RKD-57.3 camera with biaxial rotation of sample after Gandolfi.

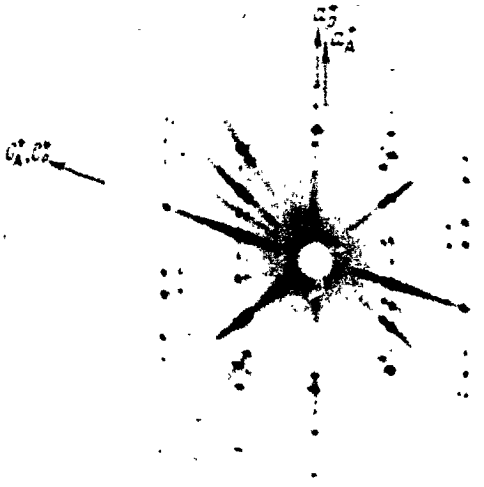

Fig. 2. KFOR diffraction pattern of a coherent intergrowth of sample M-65 of clinopyroxenes (augite-pigeonite) along the plane (001). Rotation about the b axis. Augite (in AU): a = 9.69 (1); b = 8.90 (2); c = 5.26 (1); β = 106°00'; Pigeonite: a = 9.71 (1); b = 8.90 (2); c = 5.22 (1); β = 108°39'.

Mineral composition of regolith. The x-ray powder diffraction patterns of regolith are characterized by a considerable diffuse background throughout the range of angles, indicating that a large amount of amorphous constituent is present in the regolith. This agrees qualitatively both with Soviet and American data on the presence in regolith of about 50 percent (by volume) glass particles with different composition and different sizes.

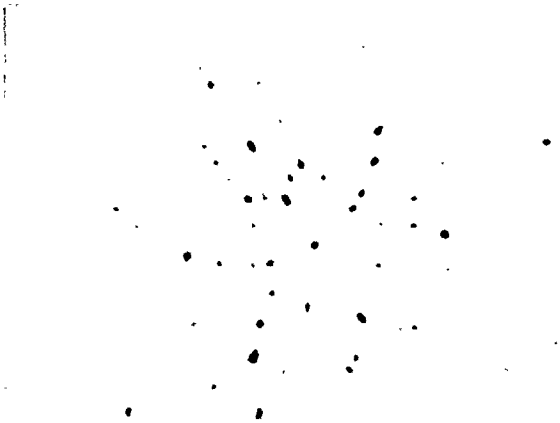

Fig. 3. Laue diffraction pattern of lunar olivine M-4

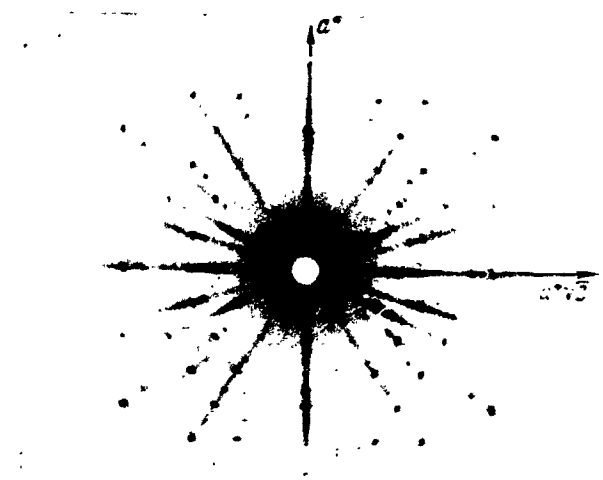

Fig. 4. KFOR diffraction pattern of intergrowth of spinels I + II of sample M-77. Rotation about the axis 2

$c_{sp\ I} = 8.304\ (5)$, AU

$a_{sp\ II} = 8.457\ (5)$, AU

Table 2 gives the values of the interplanar spacings d and line intensities I for powder x-ray diffraction patterns of three regolith samples: 1) (7 + 8)-1d; 2) 3-2ye; and 3) 3-2i, obtained in different photographic conditions: using RKD-57.3, RKU-114.6, and the Guinier cameras.

As can be seen from Table 2, the regolith composition includes the following minerals: anorthite, pyroxenes of the augite-pigeonite series, ilmenite, olivine, α-cristobalite, and spinel. Undoubtedly, also present in the regolith is metallic iron, but its lines in the x-ray diffraction pattern of regolith coincide with the lines of other minerals.

Thus, the data in Table 2 do not contradict the presence of iron in the regolith, which was proven by other independent methods.

Attempts to isolate fractions of iron particles, by magnetic separation failed, since virtually the entire bulk of the regolith is magnetic. According to electron-microscopic investigation by British colleagues [6], particles of Apollo 12 lunar rocks, especially glass, are larded with extremely minute iron spherules, whose minimum diameters amount to 50 AU. /155

Interpreting the mineral composition of the regolith in Table 2 was carried out by resorting to the following handbook or reference standard material: for anorthite and plagioclases -- according to the paper by Borg and Smith [7]; for pyroxenes, olivines, and

spinels -- from our own monocrystal data for lunar samples of the mineral indicated, presented below in this study and adopted by us as reference standards. In view of the variability of the chemical composition of pyroxenes, olivines, and spinels, the roentgenometric d/I data for these minerals can vary significantly.

Polycrystalline particles of basalts, gabbro, and anorthosites. The morphological characteristics of some varieties of lunar regolith particles are given in the paper [2]. Some particles of lunar basalts, gabbro, and anorthosites prove to be quite fine-grained and suitable for investigation by the powder techniques, without the need for grinding them. A particle was cemented en toto to a glass strip or else placed in an acetylcellulose capillary, and a powder diffraction pattern was obtained from it, in most cases wholly satisfactory for computation.

In this way, the mineral composition of relatively large (0.5-0.6 mm) dark particles of basalt (Table 3), gabbro (Table 4), and light particles of anorthosite (Table 5), was identified.

As we can see from Table 3, the basalt particles consist of pyroxenes of the augite-pigeonite series, olivine, anorthite, and judging from the considerable background in the x-ray diffraction patterns, glass. From Table 4 it follows that the gabbroid particles consist of the same materials as basalt, plus pigeonite, with a smaller amount of glass.

White and light-gray particles of anorthosite rock (sometimes in the form of powders), as is clear from Table 5, consist nearly entirely of 100 percent anorthite, or high-calcic plagioclase, for the sample M-5a.

Monocrystal of plagioclase. Among the light particles, monocrystalline and twinned particles of plagioclases are very infrequently observed. One such clear, uncolored particle of relatively regular isometric shapes, about 0.35 mm in size, was studied in detail, crystallographically. The syngony was triclinic, C1; cell dimensions: $a = 8.17 \pm 0.05$ AU; $b = 12.90 \pm 0.10$ AU; $c = 7.05 \pm 0.05$ AU; $\alpha = 92 \pm 1.0°$; $\beta = 116 \pm 1.0°$; and $\gamma = 88 \pm 1.0°$.

The powder diffraction pattern of this monocrystal obtained in the Gandolfi camera made it possible to compute the reference standard d/I values, listed in Table 6.

Pyroxenes. In complete agreement with American studies on lunar pyroxenes, especially with the data of Papike et al. [9], we found that the lunar pyroxenes we studied are clinopyroxenes of the augite-pigeonite series. A typical mineralogo-crystallographic feature of lunar clinopyroxenes is that they are encountered for the most part as combined coherent intergrowths of very thin

alternating lamellae of augite and pigeonite in the planes (001) or (100) of a monoclinic lattice, formed as a result of the spinodal disintegration of isomorphic mixtures in the system $Wo(CaSiO_3)$ -- $En(MgSiO_3)$ -- $Fs(FeSiO_3)$ /9/. /156

A very clear picture of this kind of intergrowth of augite and pigeonite is provided by the x-ray goniometric convolutions in a KFOR camera. As an example, in Fig. 2 is reproduced the KFOR diffraction pattern of the lunar pyroxene sample M-65 when it was rotated about the common axis b of the monoclinic lattice. Here we have the superimpositioning of two projections of the reciprocal lattice -- augite and pigeonite -- along the direction of the b axis (perpendicular to the plane of the photograph). It is clear that in the c_a^* axis -- augite and c_p^* axis -- pigeonite -- coincident in direction reflexes of the type (00ℓ) are resolved corresponding to several different values of the period c_a and c_p of augite and pigeonite. The rays of the reciprocal lattice directions along the axes a_a^* -- augite -- and a_p^* -- pigeonite -- diverge corresponding to the difference in the values of their monoclinic angles β_a^* and β_p^*. Here from the ratio of the reflex intensities it is clear that in this intergrowth M-65 there is considerably more pigeonite than augite, roughly in a 3:1 ratio.

The periods and angles of the monoclinic lattice of augite and pigeonite established with a diffractometer for the sample M-65, as well as their chemical composition for the primary constituents -- -- En (enstatite), Fs (ferrosilite), and Wo (wollastonite), determined from the Papike /9/ nomogram, are given below:

	a, Å	b, Å	c, Å	β	Composition
Augite	9,69 (1)	8,90 (2)	5,26 (1)	106°00'(2)	$En_{42}Wo_{43}Fs_{15}$
Pigeonite	9,71 (1)	8,90 (2)	5,22 (1)	108°39'(2)	$En_{71}Wo_{9}Fs_{20}$

Powder diffraction patterns were obtained in the Gandolfi camera for several lunar pyroxenes (M-71, M-62a, M-23, M-60a, and M-61a); roentgenometric d/I values, listed in Table 7, were calculated for them. Due to differences in composition and lattice spacings characteristic of lunar pyroxenes, the values of both d and I can differ widely for a number of pyroxenes. Indexing of the lines of the pyroxene powder diffraction patterns in Table 7 was impossible to perform uniquely at this stage of their investigation.

Olivines. Olivines are present both in basaltic as well as gabbroid particles, and also in the form of individual monocrystalline grains -- fragments of irregular shape, with fresh /157

TABLE 3. INTERPLANAR SPACINGS d AND LINE INTENSITIES I FOR LUNAR BASALT

Lunar basalt, grain, sample M-5a		Anorthite, according to [7]		Augite-pigeonite, lunar, sample M-23		Olivines, lunar, sample M-27		Lunar basalt, grain, sample M-5a		Anorthite, according to [7]		Augite-pigeonite, lunar, sample M-23		Olivines, lunar, sample M-27	
d, Å	I	d, Å	I	d, Å	I	d, Å	I	d, Å	I	d, Å	I	d, Å	I	d, Å	I
3,95	1	3,92	11	—	—	3,91	6	1,925	0,5	—	—	1,95	1	—	—
3,77	1	3,78	28	—	—	3,74	1	1,818	1	—	—	—	—	1,802	1
3,53	1	—	—	—	—	3,51	6	1,758	7	—	—	1,75	4	1,755	10
—	—	—	—	3,36	3	—	—	1,676	0,5	—	—	—	—	1,685	3
3,196	9	3,19	100	3,21	9	—	—	1,632	7	—	—	1,63	2	1,628	3
3,017	10	—	—	3,01	10	3,01	4 sp	1,539	4	—	—	1,55	3 sp	—	—
2,919	8	2,93	19	2,91	9 sp	2,91	0,5	1,503	6	—	—	1,51	4	1,508	5
2,800	4	2,83	29	—	—	2,79	9	—	—	—	—	1,49	5	1,492	6
2,550	8	2,53	20	2,57	7	2,53	8	1,410	6	—	—	1,419	6	1,407	7
2,486	10	—	—	2,52	7	2,47	10	—	—	—	—	1,391	6	—	—
2,396	0,5	—	—	—	—	2,37	2 sp	1,278	3	—	—	—	—	1,285	0,5
2,284	4	—	—	2,29	2	2,28	6	1,234	2	—	—	—	—	1,214	1
2,197	0,5	—	—	2,21	3	2,17	3	1,166	2	—	—	—	—	1,167	0,5
2,141	6	2,14	17	2,14	8	—	—	—	—	—	—	—	—	1,158	0,5
2,040	5	—	—	2,05	5	2,04	0,5	0,982	2	—	—	—	—	0,980	2
				2,01	3	2,01	0,5	0,970	2	—	—	—	—	0,975	2

fractures, 0.5 mm and smaller in size, scattered over all levels of the core in the mass of regolith dust.

Compared with the crystal grains of other minerals, monocrystal fragments of olivines of different color shadings, from yellow-amber (frequent) to reddish-brown (infrequent) are the most abundant.

Monocrystals of lunar olivines give excellent x-ray diffraction patterns with sharp reflexes, doubleted at large angles. For one of these olivine particles (sample M-4), a monocrystal Laue x-ray diffraction pattern of a lunar olivine, the first in the USSR, was obtained, reproduced in Fig. 3.

TABLE 4. INTERPLANAR SPACINGS d AND LINE INTENSITIES I FOR LUNAR GABBRO

Lunar gabbro, sample M-1b		Anorthite, according to [7]		Augite-pigeonite, lunar, sample M-23		Olivine, lunar, sample M-27		Ilmenite, according to [8]	
d, Å	I	d, Å	I	d, Å	I	d, Å	I	d, Å	I
3,74	1	3,78	25	—	—	—	—	3,70	3
3,53	1	—	—	—	—	3,51	6	—	—
3,20	10	3,19	100	3,21	9	—	—	—	—
3,02	9	3,04	19	3,01	10	3,01	4 sp	—	—
2,89	8	—	—	2,91	9 sp	2,91	0,5	—	—
2,80	7	2,83	20	—	—	2,79	9	—	—
2,75	7	—	—	—	—	—	—	2,74	10
2,54	9	—	—	2,57	7	2,53	8	2,53	9
2,50	8	2,51	28	2,52	7	2,47	10	—	—
		2,50		—	—	—	—	—	—
2,28	2	—	—	2,28	2	2,28	6	—	—
2,23	2	—	—	—	—	—	—	2,23	3
2,13	7	2,14	17	2,14	8	—	—	—	—
2,04	4	2,02	5	2,04	5	2,03	0,5	2,02	10
—	—	—	—	2,01	3	2,01	0,5	—	—
1,936	1	1,932	9	—	—	—	—	—	—
1,876	3	1,878	7	—	—	—	—	—	—
1,824	1	—	—	—	—	—	—	—	—
1,761	7	1,768	17	—	—	—	—	—	—
		1,761	8	1,752	4	1,755	10	—	—
1,721	5	1,719	7	—	—	—	—	1,720	8
		1,717		—	—	—	—	—	—
1,626	7	—	—	1,628	9	1,628	3	1,630	3
1,543	2	—	—	1,546	3 sp	—	—	—	—
1,501	6	—	—	1,506	4	1,506	5	1,504	7
1,469	3	—	—	—	—	—	—	1,465	7
1,415	5	—	—	1,419	6	1,407	7	—	—
1,392	4	—	—	1,391	6	—	—	—	—
1,365	2	—	—	—	—	1,360	6	—	—
1,338	4	—	—	—	—	1,327	6	1,347	1
1,324	2	—	—	—	—	1,327	6	—	—
1,076	3	—	—	—	—	1,073	0,5	1,069	3
1,050	3	—	—	—	—	1,045	10 sp	1,050	1
1,036	3	—	—	—	—	1,029	7	—	—

The iron content of the lunar olivines we investigated /4_7 /158 by the electron microprobe technique varies from 30 to 50 mole percent Fe_2SiO_4. In particular, the olivine of sample M-4 has the following composition (in weight percent) and iron content:

SiO_2	MgO	FeO	MnO	Cr_2O_3	TiO_2	CaO	Al_2O_3	CoO	NiO	*Fa* : *Fo*
36,0	27,5	33,8	0,3	0,15	0,01	0,38	0,05	0,03	<0,01	4,1 : 5,9

An appreciable content of calcium and chromium and traces of nickel, cobalt, aluminum, and titanium was noted in the lunar olivines.

We determined the periods of the elementary cell for a number of olivines (see Table 1); in general, these periods correlate well with those for terrestrial and meteoritic olivines. As to be expected, lunar olivines have the structure of the low-temperature α-modification of ordinary "terrestrial" olivine.

A most interesting question in the crystal chemistry of olivines, which is currently under lively discussion in the world literature, is this: why given favorable structural conditions -- -- the availability for cations of two nonequivalent positions M_1 and M_2 -- is no high-ordered distribution of magnesium and iron atoms observed in olivines with respect to these positions, while in other (Mg, Fe)-minerals -- pyroxenes and ludwigites -- this distribution is observed. Even in olivines of low-temperature genesis magnesium and iron atoms are statistically mixed with respect to the positions M_1 and M_2.

The investigation of olivines in our laboratory, carried out at a quite precise level (factor R = 5.5 percent) showed that for the olivine of sample M-19 with an iron content of 40 mole percent Fa, 53 percent of the iron atoms were in the M_1 positions, and 47 percent in the M_2 positions, that is, some tendency toward ordering was observed, with the preferential occupancy by iron atoms of position M_1. This result is in agreement with the data of an American study based on Apollo 12 material /10/.

In Table 8 we list the experimental values of d/I for the lunar olivine of sample M-19 computed from powdered diffraction patterns after Gandolfi. For the leading lines (with small angles of θ), a comparison was made with the theoretical values of d/I and the indices (*hkl*) based on /11/ were given for the composition $(Fe_{.40}Mg_{.60})_2SiO_4$. In view of the variability of the composition

of olivines complicated by the zonality of the distribution of magnesium and iron within the limits of individual monocrystal grains of the lunar olivines /6_7, typical d/I values, dependent on composition, vary. Therefore the convergence of the experimental and theoretical values is not wholly exact in Table 8. Indexing of the lines with large angles of θ for olivine was not entered in Table 8 owing to the ambiguity stemming from the coincidence of lines.

Ilmenite. Ilmenite, $FeTiO_3$, was found in gabbroid particles and also in the fine fraction of regolith, as can be seen from Tables 2 and 4. Ilmenite is often present in individual heterogeneous particles as intergrowths with olivine. We investigated several fragments of monocrystal grains 0.3 mm in size, or smaller.

X-ray structural analysis of the ilmenite monocrystal in sample M-76 showed that lunar ilmenite structurally does not differ from terrestrial ilmenite, ordinary rhombohedral, of the corundum type -- hematite, but has ordered arrangement of iron and titanium atoms, as the result of which the corundum symmetry $R\bar{3}c$ is reduced to R3, that is, the plane of symmetry c is lost.

The lattice spacings of ilmenite in sample M-76 in the hexagonal arrangement are as follows: $a = 5.085 \pm 0.002$ AU; and $c = 14.084 \pm 0.005$ AU.

Table 9 gives the d/I values for two lunar ilmenites: sample M-76 and sample M-70/51 in comparison with handbook data in /8_7.

Spinels. As shown by American and our own investigations, lunar spinels are classified as solid solutions of the system "ulvospinel (Fe_2TiO_4) -- hercynite-chromite $Fe(Al, Cr)_2O_4$" with isomorphic admixtures of magnesium and other elements. As in the case of pyroxenes, many particles of lunar spinels are coherent intergrowths of two monocrystals of different composition: one of them relates to the ulvospinel end of the system, and the other -- -- to the hercynite-chromite (otherwise known as chromopicotite) end. Spinels intergrowing in the plane (111) have markedly different periods of the cubic lattice, which shows up in the resolution of the reflexes both in powder as well as monocrystal x-ray diffraction patterns. Thus, in sample M-77, as can be seen from the interpretation of the powder diffraction pattern in Table 10, two cubic spinels were intergrown: hercynite-chromite spinel I with period $a = 8.304$ AU and ulvospinel II with period $a = 8.457$ AU; here the amount of spinel I in the intergrowth, judging from the line intensities, is much higher than for spinel II.

Fig. 4 is a KFOR diffraction pattern of the intergrowth of spinels in sample M-77, obtained by rotation around the second-order axis ($a\sqrt{2}$) with molybdenum emission. The resolution of the reflexes can be seen in it. /159

Iron particles. As can be seen from Table 1, we investigated a series of iron particles less than 0.5 mm in size, among which there were both dense magnetic spherules of steel-gray color with clean surfaces and with dull, but sometimes also very brilliant metallic lustre, as well as friable magnetic conglomerates of irregular shape with fine inclusions and blebs of silicate minerals. All iron particles are polycrystalline, and they give very sharp powder diffraction patterns, corresponding to the cubic body-centered structure of α-iron with lattice period $a = 2.867 \pm 0.002$ AU, practically the same as the corresponding value for pure α-iron (2.866 AU). Small amounts of admixtures of anorthite and pyroxene were detected in the friable conglomerates. Particles exhibiting the cubic face-centered structure of γ-iron and with very high nickel content were not found. /162

Glass particles. Most of the glass particles were concentrated in the finest (< 80 μm) regolith fraction. About 20 percent of the large particles we investigated did not give any diffraction pattern and were classified by us as glasses (see Table 1). The x-ray diffraction patterns of several glassy particles against an intense background disclosed one, two, and three very faint lines in the region of small scattering angles. They relate either to weakly crystallized α- or β-cristobalite, or else plagioclase, or olivine. In chemical composition, as shown in /4/, the glasses simulate silicate rocks and minerals encountered in the regolith.

Conclusion. The mineralogical and crystalochemical study of lunar rocks has been begun fairly recently and it is as yet too early to make any general conclusions. Our results are in good agreement with the American data for Apollo 11 and Apollo 12 /12, 13/. It evidently can be assumed that the mineral composition of the regolith of all three sections of the Moon studied in its "mare" equatorial belt -- the Sea of Tranquillity (Apollo 11), Ocean of Storms (Apollo 12), and Sea of Fertility (Luna 16) -- is basically the same.

In conclusion we are deeply grateful to Academician A. P. Vinogradov who headed the investigation of the lunar surface material in our country, for involving us in this interesting work. We are also thankful to L. S. Tarasov and A. V. Ivanov for giving us the samples they selected for x-ray diffraction analysis.

TABLE 5. INTERPLANAR SPACINGS d AND LINE INTENSITIES FOR LUNAR ANORTHOSITE

Lunar anorthosite, sample M-10		Anorthite, according to [7]		Lunar anorthosite, sample M-10		Anorthite, according to [7]		Lunar anorthosite, sample M-10		Anorthite, according to [7]		Lunar anorthosite, sample M-10		Anorthite, according to [7]	
d, Å	I	d, Å	I	d, Å	I	d, Å	I	d, Å	I	d, Å	I	d, Å	I	d, Å	I
4.85	0.5	—	—	—	—	3.19	100	2.097	2	2.095	10	—	—	—	—
4.64	0.5	4.60	14	—	—	3.18	91	2.019	2	2.019	5	1.168	1	—	—
—	—	—	—	3.03	3	3.04	18	—	—	2.016		—	—	—	—
4.45	8	—	—	2.93	3	2.95	27	—	—	—	—	—	—	—	—
4.29	1	4.24	2	—	—	2.93	19	1.928	3	1.932	9	—	—	—	—
4.00	4	4.04	48	2.82	3	2.83	20	1.878	2	1.878	7	—	—	—	—
3.89	1	3.92	11	2.64	3	2.65	14	1.843	4	1.845	12	—	—	—	—
3.76	2	3.78	28	2.51	5	2.53	20	1.799	2	1.797	9	—	—	—	—
—	—	3.76	19	—	—	2.51	28	1.768	4	1.768	17	—	—	—	—
3.61	2	3.62	33	—	—	2.50		1.716	1	1.717	7				
		3.60		2.32	0.5	2.32	8	1.623	1	1.617	4	—	—	—	—
3.46	2	3.47	14	2.27	0.5	2.27	7	1.320	1	—	—	—	—	—	—
		3.46				2.26									
3.33	2	3.36	25	2.13	3	2.14	17	1.297	1	—	—	—	—	—	—
3.19	10	3.21	63					1.274	1	—	—				

TABLE 6. INTERPLANAR SPACINGS d AND INTENSITIES FOR LUNAR PLAGIOCLASE

Plagioclase, sample M-32, d/I	An_{100}, according to [7], d/I	Plagioclase, sample M-32, d/I	An_{100}, according to [7], d/I	Plagioclase, sample M-32 d/I	An_{100}, according to [7], d/I	Plagioclase, sample M-32 d/I	An_{100}, according to [7], d/I
4.04/5	4.04/48	2.69/1	2.66/14	1.893/4	1.892/4	1.539/3	1.537/4
3.77/4	3.78/28	2.52/8	2.52/20	1.840/7	1.837/16	1.518/1	1.518/4
3.62/4	3.62/33	2.38/0.5	2.38/4	1.805/4	1.802/8	1.492/7	1.492/6
3.40/2	3.40/7	2.28/0.5	2.27/7	1.768/7	1.768/17	1.472/?	1.476/10
—	3.21/63	2.14/7	2.14/17	1.718/1	1.717/7	1.449/3	1.449/3
3.20/10	3.19/100	2.10/1	2.10/10	—	—	1.428/3	—
—	3.18/91	2.01/2	2.01/5	1.682/1	1.681/4	1.404/3	—
3.04/3	3.04/18	1.962/0.5	1.960/4	1.626/2	1.617/4	1.320/7	—
2.95/5	2.95/27	1.908/5	—	1.588/2	1.570/3	—	—
2.82/3	2.83/20			1.565/3	1.557/3		

TABLE 7. INTERPLANAR SPACINGS d AND LINE INTENSITIES I FOR LUNAR PYROXENES: AUGITE/PIGEONITE

/160

Sample M-71, d/I	Sample M-62a, d/I	Sample M-23, d/I	Sample M-60a, d/I	Sample M-61a, d/I	Sample M-65, d/I
—	—	4.44/1	—	—	4.30/4
—	—	4.06/5	4.08/3	—	4.13/4
—	—	—	3.82/1	—	—
—	3.73/2	3.74/2	—	—	—
—	—	—	3.65/1	—	—
—	3.59/1	—	—	—	—
3.266/4	3.34/1	3.36/3	—	3.33/2	3.30/4
3.174/8	3.19/10	3.21/9	3.22/10	3.22/5	3.17/5
3.003/10	3.005/8	3.01/10	3.03/8	3.01/10	2.99/9
2.895/8	2.30/6 sp	2.909/9 sp	2.94/5	2.90/10	2.89/9
—	2.812/2 sp	—	2.85/1	—	—
—	2.631/1	—	2.673/0.5	—	—
2.553/6	2.575/6	2.572/7	2.594/3	2.57/5	—
—	—	2.515/7	2.517/6	2.52/4	2.538/7
2.464/6	2.505/7	—	—	2.46/3	2.475/8
2.394/2	—	—	—	—	—
2.288/1	2.283/1	2.286/2	—	—	—
2.214/4	—	2.212/3	—	—	2.214/4
2.134/7	2.143/8	2.145/8	2.159/8	2.14/5	2.130/7
2.098/2	—	2.101/1	2.106/1	—	—
2.030/4	2.050/1	2.046/5	2.056/4	2.04/4	2.042/3
—	—	2.012/3	—	—	—
1.948/2	1.930/1	1.952/1	1.946/1	—	1.938/3
—	1.830/1	—	1.846/3	—	—
1.794/3	1.803/5	—	1.805/1	—	—
1.773/3	1.763/5	—	1.773/4	1.76/3	1.779/4
1.746/3	1.725/2	1.752/4	—	—	—
1.672/1	—	—	1.679/1	—	1.668/3
1.648/1	—	—	—	—	—
1.618/9	1.628/10	1.628/9	1.637/9	1.63/8	1.624/10
1.536/5	—	1.546/3 sp	1.544/4	—	1.538/4
1.499/2	1.494/4 sp	1.508/4	1.513/3	1.51/3	1.505/4
1.485/4	—	1.490/5	1.494/4	1.49/3	1.491/4
—	1.453/1	—	1.460/2	—	1.464/1
1.411/4	1.417/5 sp	1.419/6	1.422/6	1.42/3 sp	1.415/4
1.382/6	1.391/5	1.391/6	1.401/5	1.39/3	1.387/7
1.366/3	—	—	—	—	1.370/4
1.349/3	—	—	—	—	—
1.335/3	—	—	—	—	—
1.324/2	—	—	—	—	—
1.297/2	—	—	1.301/2	1.29/2	—
1.269/4	—	—	1.287/3	1.28/2	1.276/4
1.220/3	—	—	1.216/2	—	1.224/4
1.200/2	—	—	—	—	—
1.175/2	1.170/2	—	1.174/1	—	—
1.162/2	—	—	1.158/2	—	—
1.148/3	—	—	—	—	—
1.089/3	—	—	—	—	—
—	—	—	1.078/1	1.078/3 sp	1.079/4
1.073/6	—	—	1.069/4	—	1.071/4
1.0178/4	—	—	—	—	—
—	—	—	—	—	1.058/4
—	—	—	—	—	1.001/4
—	—	—	—	—	0.9806/4
—	—	—	—	—	0.9675/4

TABLE 8. INTERPLANAR SPACINGS d_{exp} (IN AU) AND INTENSITIES I_{exp} /161 FROM X-RAY DIFFRACTION PATTERN NO. 147 FOR LUNAR OLIVINE OF SAMPLE M-19 (MONOCRYSTALLINE PARTICLE, 0.25 mm IN SIZE), PHOTOGRAPHED AFTER GANDOLFI, FILTERED IRON RADIATION. THEORETICAL d AND I VALUES ARE TAKEN FROM /11/. I_{exp} IS ON A 10-DIVISION SCALE: I_{theor} IS ON A 100-DIVISION SCALE.

d_{exp}	I_{exp}	d_{theor}	I_{theor}	hkℓ	d_{exp}	I_{exp}
5,19	0,5	5,16	13	(020)	1,268	3
3,94	6	3,92	23	(021)	1,236	2
3,76	3	3,75	10	(101)	1,200	0,5
3,52	6	3,52	36	(111)	1,175	3
3,02	5	3,03	5	(121)	1,166	4
—	—	3,02	11	(002)	1,149	3
2,796	8	2,791	78	(130)	1,145	4
2,596	0,5	2,603	11	(022)	1,135	4
2,547	8	2,533	71	(131)	1,127	4
2,477	10	2,476	100	(112)	1,115	0,5
2,386	1	2,391	6	(200)	1,109	4
—	—	2,371	13	(041)	1,0905	2
2,286	8	2,286	26	(122)	1,0833	5
2,055	2	2,048	6	(132)	1,0732	3
1,948	1	1,960	3	(042)	1,0632	1
1,888	2	1,894	5	(150)	1,0461	9(α_1)
1,825	3	—	—	—	1,0295	6(α_1)
1,805	1	—	—	—	1,0169	2(α_1)
1,762	9	—	—	—	1,0085	3(α_1)
1,725	0,5	—	—	—	1,0025	5(α_1)
1,684	5	—	—	—	0,9934	4(α_1)
1,663	3	—	—	—	0,9877	5(α_1)
1,634	4	—	—	—	0,9794	4(α_1)
1,608	2	—	—	—	—	—
1,587	2	—	—	—	—	—
1,513	6	—	—	—	—	—
1,496	6	—	—	—	—	—
1,412	5	—	—	—	—	—
—	—	—	—	—	—	—
1,361	4	—	—	—	—	—
1,328	5	—	—	—	—	—
1,311	2	—	—	—	—	—
1,278	3	—	—	—	—	—

TABLE 9. INTERPLANAR SPACINGS d AND LINE INTENSITIES I FOR LUNAR ILMENITE SAMPLES

Sample M-76, d/I	Ilmenite, according to [8], d/I	Sample M-70/51, d/I	Sample M-76 d/I	Ilmenite, according to [8] d/I	Sample M-70/51, d/I
4.17/4	—	4.16/9	1.422/1	—	—
3.74/3	3.70/4	3.75/8	1.381/0.5	1.375/2	—
—	—	3.23/0.5	1.347/9	1.347/1	1.347/5
3.04/0.5	—	—	1.273/2	1.270/3	—
2.763/10	2.74/10	2.763/10	1.248/1	1.242/1	—
—	—	2.655/1	1.216/4	1.205/2	1.211/1
2.547/6	2.53/9	2.553/8	1.1905/9	1.185/2	1.192/4
2.494/2	—	—	1.157/4	1.147/2	1.158/3
2.242/5	2.23/3	2.252/6	1.121/7	1.111/2	1.121/4
1.910/2	—	—	1.0786/10	1.069/3	1.079/4
1.870/8	1.865/6	1.877/5	1.0688/1	—	—
1.734/10	1.720/8	1.731/8	1.0539/2	1.050/1	—
1.641/3	1.63/3	1.636/2	1.0057/4	1.000/2	—
1.509/7	1.505/7	1.511/7	—	0.980/1	0.9812/6
1.471/6	1.465/7	1.473/7			

TABLE 10. INTERPLANAR SPACINGS d (IN AU) AND LINE INTENSITIES I FOR SAMPLE M-77. INTERGROWTH OF LUNAR SPINELS I + II

Sample M-77, d/I	Spinel I, a = 8.304 AU, d	Spinel II, a = 8.457 AU, d	hkl
2.94/5	2.936	—	220
2.54/4	—	2.550	311
2.50/10	2.504	—	311
2.11/2	—	2.114	400
2.08/6	2.076	—	400
1.693/4	1.695	—	422
1.627/2	—	1.627	511,333
1.597/9	1.598	—	511,333
1.492/4	—	1.495	440
1.467/9	1.468	—	440
1.313/2	1.313	—	620
1.286/2	—	1.290	533
1.267/5	1.266	—	533
1.253/1	1.252	—	622
1.161/1	1.163	—	711,551
1.110/4	1.110	—	642
1.080/10	1.081	—	731,553
1.038/6	1.038	—	800

REFERENCES

1. Vinogradov, A. P., "Preliminary Results of Studying Lunar Surface Material," Priroda (12), 5 (1970).

2. Vinogradov, A. P., "Preliminary Data on Lunar Surface Material Returned by Luna 16 Automatic Station," Geokhimiya (3), 261-274 (1971).

3. Vinogradov, A. P., Paper Presented at Second Luna Conference, Houston, U.S., January, 1971.

4. Makarov, E. S., Ilyin, N. P., and Ivanov, V. I., "On the Composition and Crystal Structure of the Minerals of Regolith from the Sea of Fertility," Space Research XII, (1972).

5. Gandolfi, G., "Discussion upon Methods to Obtain X-ray Powder Patterns from a Single Crystal," Miner. Petrogr. Acta (Italy), 13, 67-74 (1967).

6. Champness, P. E., Dunham, A. C., Gibb, F. G. F., Giles, H. N., Mackenzie, W. S., Stumpfl, E. F., and Zussman, J., "Mineralogy and Petrology of Same Apollo 12 Lunar Samples," Preprint of paper presented at the Second Luna Conference, Houston, U.S., January, 1971.

7. Borg, I. Y., and Smith, D. K., "Calculated Powder Patterns for Five Plagioclases," Amer. Min., 53(9/10), 1709 (1968).

8. Mikheyev, V. I., Rentgenometricheskiy opredelitel' mineralov /Mineralogical Determinant/, Gosgeolizdat, 1957.

9. Papike, J. J., Bence, A. E., Brown, G. E., and Prewitt, C. T., "Apollo 12 Clinopyroxenes: Exsolution and Epitaxy," Earth Planet Sci. Letters, 10(3), 307 (1971).

10. Finger, L. W., "Fe/Mg Ordering in Olivines," Carnegie Inst. Ann. Rep. Direc. Geophys. Labor., 302 (1969-1970).

11. Jahnbagloo, J. C., "X-ray Diffraction Study of Olivine Solid Solution Series," Amer. Min., 54(1/2), 246 (1969).

12. Proceedings of the Apollo 11 Lunar Sco. Conf., Vol. 1; "Mineralogy and Petrology," Geochim. Cosmochim Acta, Suppl. 1, (1970).

13. Preprints of Papers Presented at the Second Lunar Conference, Houston, U.S., January, 1971.

Order of Lenin Institute of Geochemistry and Analytical Chemistry imeni V. I. Vernadskiy, USSR Academy of Sciences, Moscow

N75 11827

X-RAY SPECTRAL MICROANALYSIS OF COMPOSITION OF INDIVIDUAL LUNAR REGOLITH PARTICLES

N. P. Il'in, L. Ye. Loseva, and V. G. Senin

Abstract

Determinations were made of the chemical compositions of selected olivine crystals, spherical particles ranging in size from 170 to 350 μm, spinels, and magnetic particles. The livines contain 30-50 mole percent fayalite. The spherical particles of various colors are aluminosilicate glasses, significantly enriched in CaO (16.1-27.6 percent) compared with the mean composition of the regolith. The degree of coloration depends on the FeO content, varying from 2.3 to 17.7 percent, and also the admixtures TiO_2 (0.04-1.9 percent), MnO (0.01-0.4 percent), and Cr_2O_3 (0.07-1.2 percent).

Compositionally, the spinel was interpreted to be chromopicotites $(Mg_{0.44}Fe_{0.60})[Al_{1.31}Cr_{0.59}Ti_{0.08}]O_4$. Magnetic particles were shown to be complex intergrowths of nickelous iron and aluminosilicates. The composition of the metallic phase of one particle (in percent) was: Fe - 86, Ni - 13.6, and Co - 0.16 in combination with plagioclase and microinclusions of ilmenite in silicate. Kamacite was determined in another intergrowth (in percent): Fe - 94, Ni - 5, and Co - 0.5.

Lunar regolith, as characterized by A. P. Vinogradov [1], is a nonhomogeneous mixture of grains of rocks, minerals of various sizes, shapes, and colors, and fused and angular particles.

As a result of optico-mineralogical study of the regolith from the Sea of Fertility [2], the particles were classified by groups and the most representative of these were selected for further investigation. Here the problems formulated included exact quantitative diagnostics of individual minerals of grains, determining the mineralogical composition of regolith, finding characteristics

of the chemistry and structure of lunar minerals compared with terrestrial minerals, and determining the compositions of spherical particles with different colors and their relationship with the composition of the crystalline fraction of the regolith. In this investigations, determining the chemical composition of individual particles played a key role. At the present time the analysis of the composition of microobjects, whose weight is calculated in micrograms, can be done only by X-ray spectral microanalysis. Essential here is also the virtually complete state of preservation of the samples of unique value.

Experimental techniques. The chemical composition of individual particles was determined with a XMA-4B X-ray microanalyzer built by Hitachi. This device is intended for use in determining elements from Mg (Z = 12) to U (Z = 92). The usual operating conditions during the analysis of the lunar samples were as follows: accelerating voltage 18.5 kV, and probe current $3\text{-}5\cdot10^{-8}$ A. The K_α- lines of X-ray radiation of the elements determined served as the analytical lines. The end result was obtained by averaging ten measurements. Corrections for mutual influences were made by the method given in [3].

The precision of the X-ray spectral microanalysis depends on the emergence angle of the radiation in the microanalyzer, especially when Mg, Al, and Si are being determined. Therefore we designed the assembly of the objective camera as a result of which the angle of emergence was increased from 12.5 to 19.5°. With this angle of emergence the device can provide a precision of Mg, Al, and Si determinations in silicates to 2-5 relative percent when the surface of the samples and the reference standards are carefully prepared.

The reference standards used in the determination of Mg, Fe, and Mn were chemically analyzed natural forsterite Mg_2SiO_4 and knebelite $(Mn, Fe)_2SiO_4$, containing 6 percent Mn. When Al, Ca, and Si were determined, their reference standard was synthetic anorthite. The homogeneity of the reference standard samples was checked with the microanalyzer. Pure metals were used in the determination of Ti and Cr admixtures. The background was measured for forsterite in determining Fe, Ca, Al, Ti, and Cr, and for knebelite when Mg was determined. In the Si analysis the background was measured on the short-wave and long-wave side from the SiK_α line and the mean value of the intensities measured was used. /210

Owing to the unique value of the objects and their small size, a special technique of sample preparation had to be formulated. Each particle was prepared individually under a binocular microscope and secured with electroconductive cement onto a polished copper substrate in the middle of a protective metal ring also cemented onto the substrate. The ring protected the surface of the microobject from an "avalanche" during polishing. Then the

preparation was placed in a mold of a hand-operated screw press and over the preparation was poured a specially prepared electroconductive plastic. Briquetting was carried out as the mold was heated to 120-140°C. The temperature was monitored with a thermocouple. The resulting tablets 10 mm in diameter and 4 mm in height were ground and polished by hand with diamond powder on glass laps and cloth. Here the condition of the surface of the section was repeatedly monitored with the microscope. A carbon layer up to 200 AU thick was simultaneously sputtered onto the polished surface of the sample and the reference standards. To ensure the required homogeneity of the thickness of the sputtered layer, the sample holder was rotated during sputtering.

Results of the investigation. Olivines are individual monocrystalline grains or intergrowth of several microcrystals. The size of the olivines studied was 190-350 μm. The particles were irregular in shape with a fresh fracture. The color was yellow-amber in various hues. Before analysis, each preparation was studied optically.

The polished surfaces of olivines are characterized by pores and cracks. Fig. 1 is a microphotograph in polarized light of a section of one olivine particle (No. 5), an intergrowth of inequi-oriented monocrystals. Microanalysis showed that some constituents of this intergrowth are identical in composition. Fig. 2 a, b, and c are microphotographs of sections of several olivines studied. Fig. 2 d is a scanning photograph of particle No. 52-1 in absorbed electrons with the inscription of the ion distribution for line scanning. The inscription shows uniform distribution of ion in the section.

Results of quantitative X-ray spectral microanalysis of olivines are in Table 1. Analysis showed that the ion abundance of the olivines studied is 30-50 mole percent of fayalite. Calcium is present in the amount of 0.3-0.4 percent. Admixtures of Mn and Cr represent several tenths of a percent; Ti is present in hundredths of a percent; and Al -- less than 0.5 percent. The Co and Ni content was beyond the limits of sensitivity (~ 0.01 percent). /212

The very small dimensions of the specimen crystals and the presence of microcracks in them did not permit the zonality of the olivines to be detected. Observed fluctuations in spectral intensity were not ordered and were associated with structural microinhomogeneities of the surface.

The olivines we analyzed differ appreciably in their lower titanium content compared to the results obtained by American investigators working with Apollo 11 samples [4]. This finding can be regarded as predictable since even the general chemical analysis of the material returned by Luna 16 shows a lower titanium

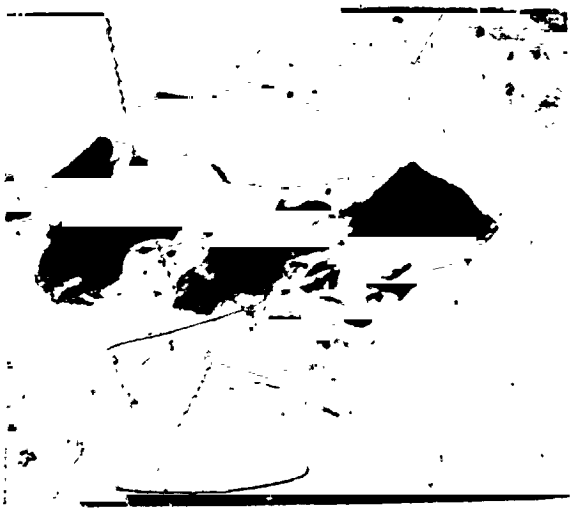

Fig. 1. Microphotograph of polished olivine section (particle No. 5) and polarized light, X 200

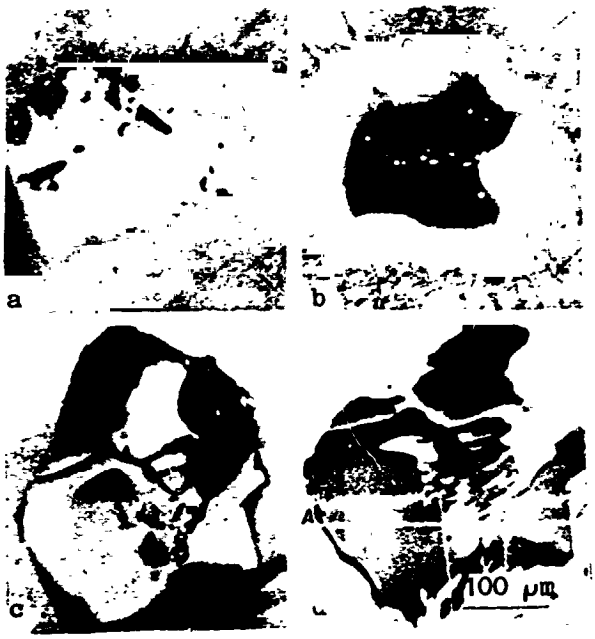

Fig. 2. Olivines
a, b, c. microphotographs of polished sections of particles 52-2, 52-3, and 52-1, respectively
d. scanning image of particle 52-1 in absorbed electrons and the distribution of ion across the section A-A

content and the analysis of the material returned by the American cosmonauts in Apollo 11. A higher level of iron content was observed than in most Apollo 11 samples.

TABLE 1. RESULTS OF X-RAY SPECTRAL MICROANALYSIS OF OLIVINES (IN PERCENT)

Constituent	52-2	52-4	52-1	52-5	5	52-3
SiO_2	36,9	37,6	37,2	37,1	36,0	35,2
MgO	35,5	33,0	32,0	31,8	27,5	22,6
FeO	27,4	27,3	29,6	30,6	33,8	41,5
MnO	0,3	0,2	0,3	0,3	0,3	0,3
Cr_2O_3	0,2	0,2	0,2	0,2	0,15	0,2
TiO_2	0,03	0,06	0,05	0,06	0,01	0,06
CaO	0,3	0,6	0,5	0,5	0,4	0,5
Al_2O_3	0,3	0,1	0,2	0,1	0,05	0,9

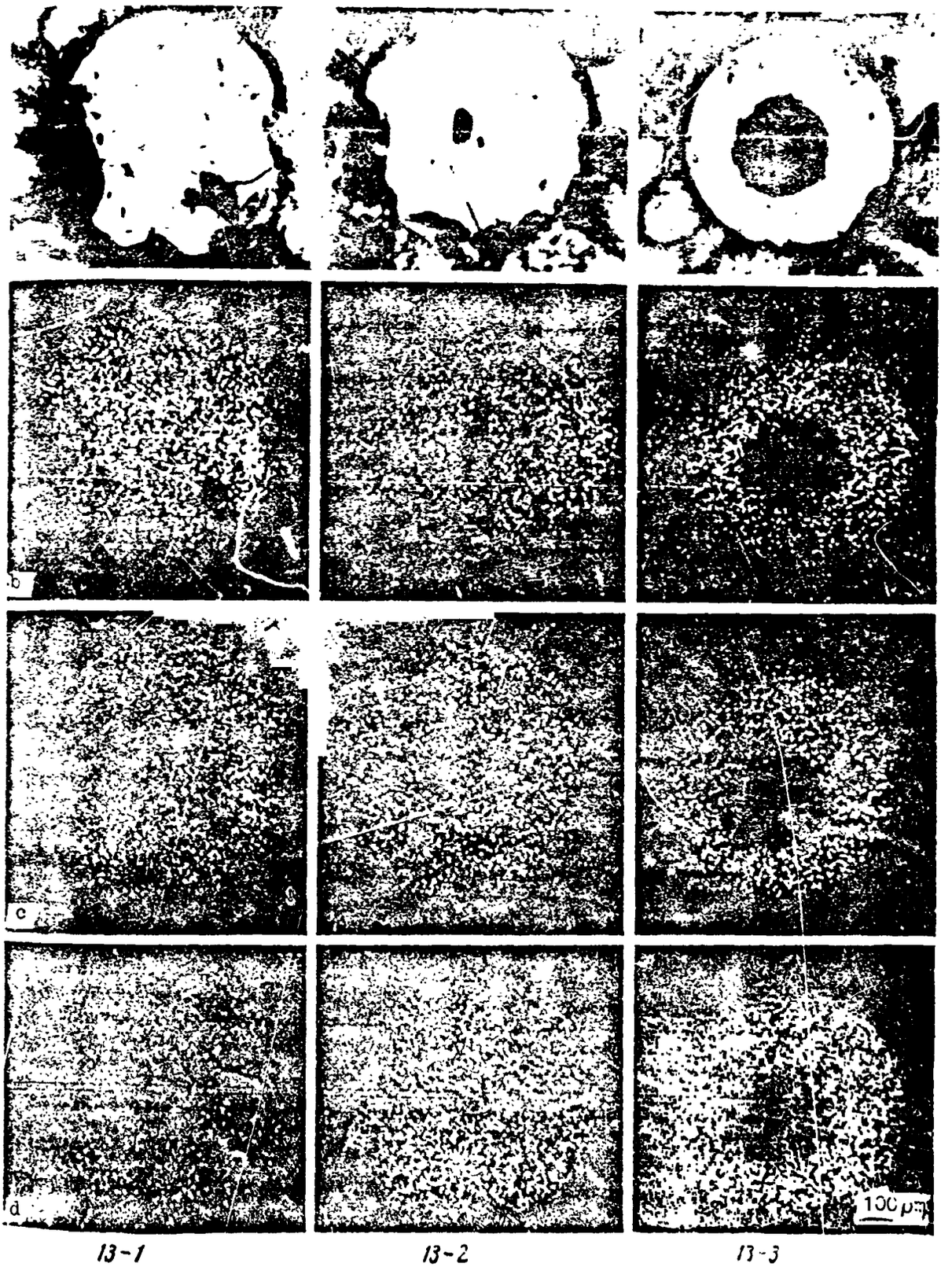

Fig. 3. Spherical particles

[Fig. 3 continued on following page]

Fig. 3 (continued from preceding page):
a. microphotographs of polished sections of spherules 13-1, 13-2, and 13-3
b, c, d. scanning images of the spheroids in the characteristic X-ray emission of Al, Ca, and Fe, respectively.

Spinel. Several individual monocrystalline and bicrystalline particles of spinels were found in the macroscopic sorting of regolith particles; they were diagnosed by X-ray phase analysis. They were black, greasy in luster, and irregular in shape. The M-16 specimen analyzed have the following composition (in percent): MgO -- 10.0; Al_2O_3 -- 38.0; FeO -- 24.4; Cr_2O_3 -- 24.9; and TiO_2 -- 3.0. The particle was diagnosed compositionally as chromopicotite: $(Mg_{0.436}, Fe_{0.604})(Al_{1.31}, Cr_{0.585}, Ti_{0.078})O_4$. The reference standards used in the Mg, Al, and Fe determinations were synthetic spinels $MgAl_2O_4$ and $MnFeO_4$. Cr and Ti were determined with respect to the pure metals.

Spherical particles. The particles investigated were quite spherical formations 170-350 μm in diameter. Some of them had smooth surfaces. In others, adhesive areas less than 1 μm in size were observed on their surface. The color of the spinels varied from white to yellow to brown and black, with violet hue.

Microscopic observation of the polished sections of the particles showed that they either were porous to some extent or contained inclusions about 1 μm in size. From the data of X-ray spectral microanalysis, the spherical particles were aluminosilicates with large variations in the content of iron and titanium. Fig. 3 presents microphotographs of the sections of three spheroids and scanning pictures of the distribution of Al, Ca, and Fe in these sections. In microphotographs of the sections can be seen voids, and spheroid No. 13-3 is a hollow sphere. The scanning pictures were taken in the same conditions and identical exposure for a given element with all samples which made it possible to compare the content of elements in the various particles.

It should be added that the presence of pores and microinclusions not determined wholly by the electron probe leads to considerable fluctuations in the spectral intensities measured at different points of the sample and to deterioration of the precision analysis. The quantitative results given in Table 2 are averaged values of measurements at ten points for each sample in the zones free of pores. In sample 58-2, a decrease of iron and an increase of aluminum, silicon, and calcium was found in the micron-sized light inclusions, qualitatively, compared with the bulk of the spheroid.

The elemental composition of these spheroids investigated is in the range (in percent): Mg 3.4-7; Al 6.2-15.1; Si 19.2-22.2; Ca 11.5-19.7, and Fe 1.8-13.7. The admixtures were present as follows (in percent): Ti 0.01-1.1, Cr 0.05-0.8, and Mn 0.01-0.3. The color of the spheroids depended mainly on their content of iron. Particles 13-1 and 58-1, whose iron concentration was 1.8 and 2.5 percent, were white. When the iron content was above 10 percent, the color of the spheroid varied from yellow to black. Various shadings of color depended on the variation in the amount of the admixtures Ti, Cr, Mn, and also evidently on the porosity /214 and quality of the sample surface. The composition of spheroids 58-1, 13-2, 13-4, and 13-5 corresponded approximately to augite content with 70-90 mole percent Ca. The spherical particles we analyzed contained increased amounts of calcium and reduced amounts of titanium compared with the data of the mean analysis of regolith returned to earth by Luna 16, Apollo 11, and Apollo 12 /17/. The composition of the spheroids indicates that they are the product of a lower-melting constituent of lunar material: regolith and even more so, rock.

The metallic particles were sampled by magnetic separation. They have various shapes, from arbitrary to nearly regular spherule. For detailed information on the structure of the metal particles and especially their surfaces, initially scanning electron and X-ray pictures were taken directly from the surfaces of the samples, without polishing them, and then from polished sections. Fig. 4 a is an optical photograph of one of the particles, approximately 300 x 700 μm in size. Fig. 4 b is a scanning picture of the ion distribution over the surface of the sample. Photographs taken by means of emission from other elements: Ni, Si, Al, and Ca showed that the particle is a complex formation, consisting of iron-nickel and silicate zones. Scanning photographs in Fig. 4 c, d, e, and f obtained with a section reveal the internal structure of the particle, which is an intergrowth of nickelous iron with silicates. Quantitative microanalysis of the content of the main elements gives the following composition of the metallic phase (in percent): Fe -- 86, Ni -- 13.6, and Co -- 0.16. In the silicate phase there is a predominance of plagioclase having the composition (in percent): SiO_2 -- to 48; Al_2O_3 -- to 36; and CaO -- to 15. Admixtures of Mg, Fe, and Ti were present. Individual microinclusions of ilmenite were also found in the silicate phase.

The composition of the metallic phase in another particle (a spherule having diameter of about 250 μm) corresponds to the kamacite composition (in percent): Fe -- 94.0; Ni -- 5; and Co -- 0.5.

Results from studying the chemical composition and features of the microscopic structure of a limited number of selected particles of several characteristic constituents of regolith naturally do not yet provide a complete enough picture of all the chemical

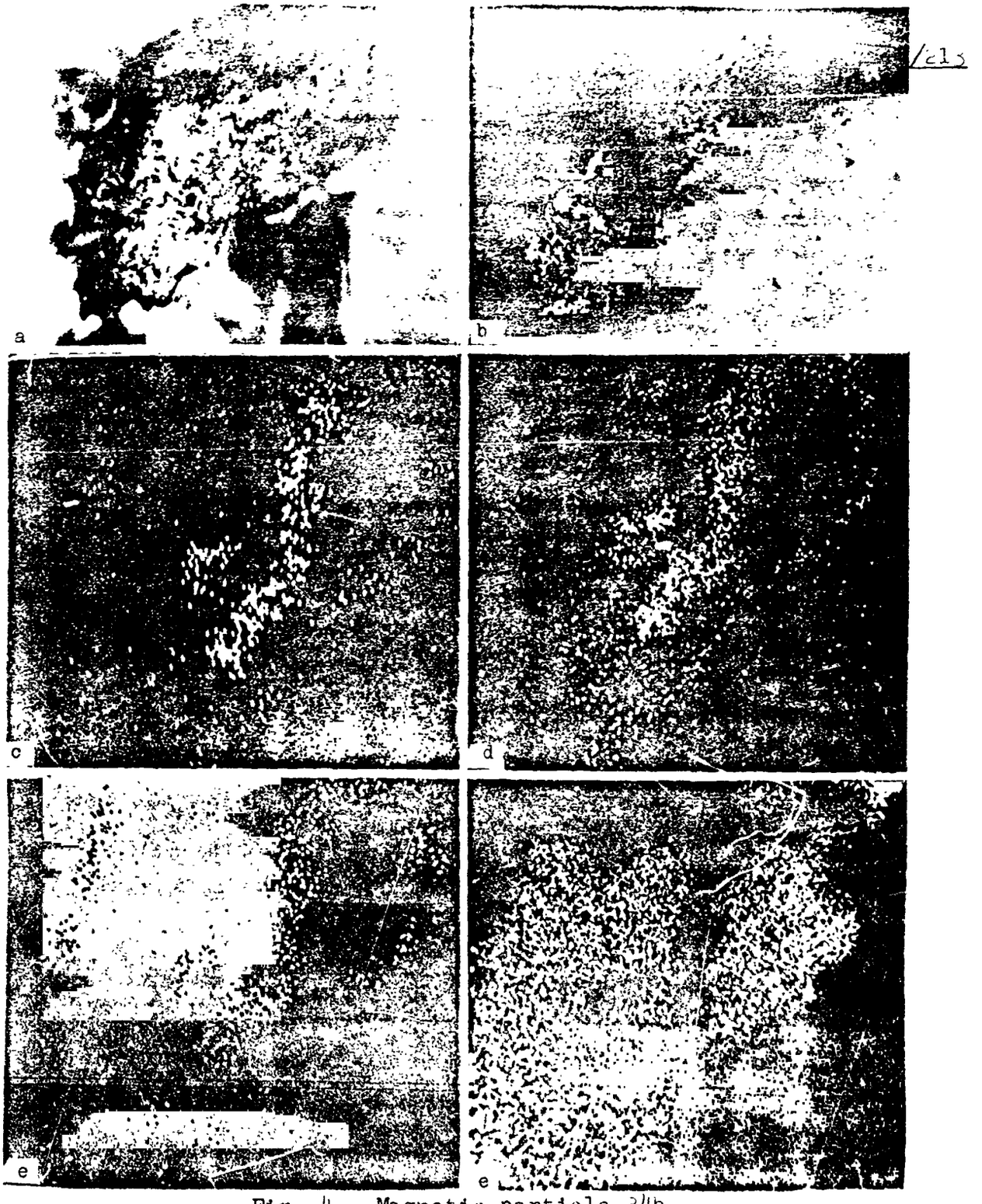

Fig. 4. Magnetic particle 34b

Fig. 4 continued on following page

Fig. 4 [continued from preceding page]:
a. optical image of surface of particle, X 120
b. scanning image of surface in FeK_{α} rays
c, d, e, f. scanning images of polished section in the characteristic X-ray emission of Al, Si, Ca, and Fe, respectively.

TABLE 2. RESULTS OF X-RAY SPECTRAL MICROANALYSIS OF SPHERICAL PARTICLES

Constituent	13-1, white	58-1, white	13-2, yellow	13-3, yellow	13-4, dark brown	13-5, brown	58-2, black	58-3, violet
MgO	5,6	9,8	11,5	7,2	8,0	6,5	6,5	6,2
Al_2O_3	28,6	23,4	7,7	15,3	14,5	11,9	11,8	11,8
SiO_2	41,0	42,0	46,4	44,2	43,0	41,5	42,5	47,5
CaO	27,6	21,3	16,1	17,3	19,8	21,8	19,7	19,1
TiO_2	0,04	0,01	0,6	1,3	1,0	1,3	0,3	0,4
Cr_2O_3	0,07	1,2	0,4	0,2	0,2	0,1	1,2	0,3
MnO	0,07	0,01	0,2	0,2	0,2	0,2	0,2	0,4
FeO	2,3	3,2	17,7	15,7	14,3	15,6	15,3	16,3

features of these objects that are uncommon for terrestrial conditions. However, it became clear that studying individual particles of all regolith constituents is most promising in solving the problems of its origin and in determining the role of secondary processes of lunar weathering.

REFERENCES

1. Vinogradov, A. P., "Preliminary Data on Lunar Surface Material Returned by Luna 16 Automatic Station," Geokhimiya (3), 261-274 (1971).

2. Florenskiy, K. P., Ivanov, A. V., Tarasov, L. S., Stakheyev, Yu. I., and Rode, O. D., "Morphology and Particle Types of Regolith Sample From the Sea of Fertility," present collection, p. 38.

3. Il'in, N. P., and Loseva, L. Ye., "Quantitative X-ray Spectral Microanalysis," Zav. labor. 33(8), 951 (1967).

4. Proc. Apollo 11 Lunar Sci. Conf. (1), (1971).

5. Ivanov, A. V., Rode, O. D., Stakheyev, Yu. I., and Florenskiy, K. P., "Silicate Spherules in Sample of Regolith Returned by Luna 16 Automatic Station," present collection, p. 232.

Order of Lenin Institute of Geochemistry and Analytical Chemistry imeni V. I. Vernadskiy, USSR Academy of Sciences, Moscow

N75 11828

SCANNING ELECTRON MICROSCOPY OF LUNAR REGOLITH FROM THE SEA OF FERTILITY

/225

M. K. Antoshin, N. P. Il'in, and G. V. Spivak

Abstract

Scanning electron microscopy was used in studying the morphology and cathodoluminescence of lunar regolith particles. At magnifications to 10,000, scanning photographs were obtained of the structural constituents of regolith: individual particles of various shapes and sizes, their conglomerates, fused particles, and breccias. By the nature of the surface and the structure, two groups of particles are differentiated:

a) crystalline with well-defined facets and spalling surfaces, which are grains of minerals and rock fragments, and

b) amorphous, fused, and partially or entirely glazed particles.

Photographs of regolith and its particles were obtained in cathodoluminescence emission at temperatures from 20 to 200°C.

local melting of particles and the round openings on their surfaces are attributed to secondary influence on the regolith of factors of lunar weathering and above all micrometeoric impacts.

Introduction. Surface material returned by the Soviet Luna 16 automatic station pertains to the surface, powdered layer of the lunar regolith. In the program of the comprehensive investigation of surface material, microscopic study of the structure of the fine-dispersed material naturally ranked first. A detailed study of the morphology of individual particles, their surfaces, individual features, and fine details of structure are of high interest in clarifying the conditions under which crystals exist on the lunar surface and the processes by which lunar regolith was formed. Material from the lunar surface bears the impression of primary processes leading to the formation of highland /terra/ rocks, and subsequent actions such as the following: "lunar weathering" and "alloying" under the action of the corpuscular component of the "solar wind," and also cosmic radiation, impacts of micrometeorites, abrupt fluctuations in surface temperature, and the vacuum of space /11/.

Microscopic investigations of the lunar surface material reveal interesting features of individual constituents of the

regolith and make it possible to differentiate two main groups of particles:

a) particles of primary rocks without noticeable erosion for the above-indicated types of secondary influence; and

b) particles bearing traces of melting, sintered, cemented, and vitrified.

However, more detailed study of the microstructure of lunar objects at higher optical magnification of the microscope is difficult owing to the restricted resolution and the low depth of focus of light optics, not yielding a detailed representation of the shape and three-dimensional characteristics of the material particles.

At the present time, in studying the macroscopic details of structure wide use is made of scanning electron microscope (SCM). In an SCM the image of a sample produced by secondary-electron emission or by the emission of fast electrons, by recombination emission in the visible or infrared spectral regions (cathodoluminescence), and by X-ray characteristic emission. This yields variegated information on the morphology of the microobject and its optical characteristics and chemical composition. The SCM can be used in studying samples without special preparation, with resolution to 150-50 AU, that is, nearly one and half orders higher than for optical microscopes. With this resolution, the SCM has a depth of field up to 0.6-0.8 mm, which is two orders higher than for optical or electron microscopes of other types.

The results of using the SCM in studying the lunar surface material returned from the Sea of Tranquillity by Apollo 11 and from the Ocean of Storms by Apollo 12 are given in the papers [3-6]. Morphological electron-scanning investigations of the particles of lunar regolith from the Sea of Fertility returned by the Luna 16 automatic station are described in [7]. This present article gives the results of a study of the morphology and several structural features of the fine fraction and some of the larger regolith particles. /226

Experimental techniques. We investigated the samples taken from the middle sections -- zone V of the drill core -- and consisting of the fine-dispersed fraction of the regolith. The maximum dimensions of individual particles did not exceed 50-60 μm, and the minimum dimension was not less than 1 μm. However, larger particles from 100 to 500 μm was selected from the lower section -- zone D -- of the surface material core.

For observation in the SCM, the samples were mounted on a standard object stage.. Small adhering crumbs of the lunar regolith rock were fixed with silver paste (mixture of colloidal silver and

Fig. 1. General view of surface of conglomerate of adhering particles of lunar regolith, with angular particles of the bedrock predominating

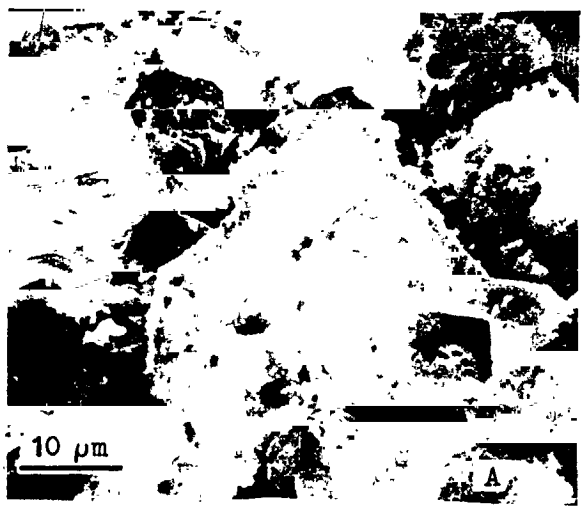

Fig. 2. Micrcphotograph of the surface of the regolith particle with circular opening

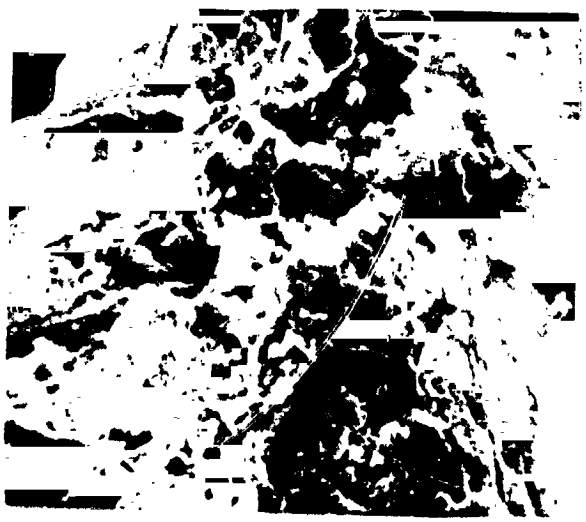

Fig. 3. General view of microbreccia with fused surface

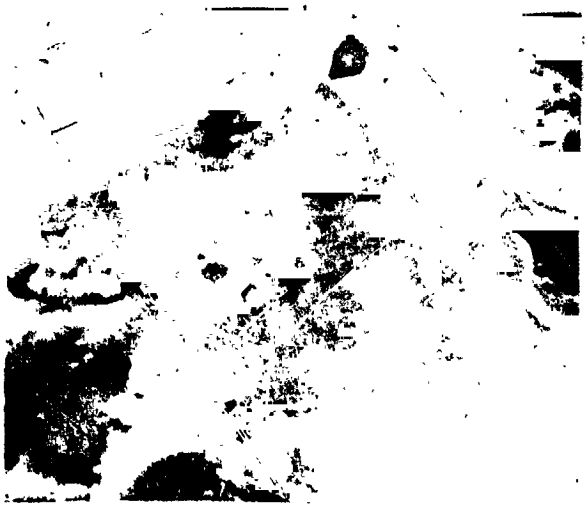

Fig. 4. Surface of partially, externally melted microbreccia

synthetic cement) to the metal of the stage. The viscosity of the silver paste was selected so that the adhesion was sufficiently strong and the cement did not envelop individual particles. In some cases, owing to the ability of the samples to adhere to the

metal and dielectric surfaces, there was no need to secure them with cement. A suspension of lunar regolith powder in ethyl alcohol was prepared, after which a drop was placed on the surface of the object stage. After the liquid evaporated, the particles proved to be quite firmly adhered to the stage surface in order not to be displaced by the air currents produced during vacuuming of the objective chamber of the device. During photography with the SCM, operating conditions were provided in which secondary-electron emission and the emission of cathodoluminescence were used for imaging, making it possible to expand the volume of resolving information on the properties of the lunar regolith. In the regime of secondary-electron emission the contrast of the image was caused by the electron-emission properties of the object, its surface geometry, and the electrical and magnetic fields of the sample. In the regime in which the cathodoluminescence emission was recorded, image contrast was affected by the ratio between the radiative and nonradiative lifetimes of the nonground-state carriers excited by electron beam, the condition of the sample surface, and the presence with emit of structurally homogeneities, dislocations, traps, and adhesion centers. Evidently, "lunar weathering" must promote the formation of large numbers of pores, structure of /227
defects, and internal inclusions, which lead to a decrease both in the lifetime as well as the diffusion paths of carriers, and this in turn makes it possible to investigate fine regolith particles in the cathodoluminescene regime with adequate resolution.

Samples of lunar rock are dielectric, therefore to photograph the charge from the electron beam scanning to produce the image, it becomes necessary to sputter a conductive film. However, this technique is inappropriate when studying local cathodoluminescence.

In the present investigation, thanks to a new technique developed at Moscow State University, we were able to photograph the charge without resorting to external sputtering of a foreign substance /8/. In this case the steady irradiation was replaced with periodic pulsed irradiation so that the charge on the sample could leak off during the time between pulses. The use of an additional gentle heating of the sample, somewhat raising the conductivity of the material, ensured complete photographing of the charge. As it turned out, it was sufficient to heat the samples to +150 to +200°C by using a temperature attachment to the microscope.

As was shown earlier /9/, upon being excited by a broad electron beam, lunar regolith begins to luminesce in the optical range of the spectrum.

We investigated cathodoluminescent emission in the optical range of the spectrum, for which a PM /photomultiplier/ was used.

The photography was carried out usually with an accelerating voltage of 20 keV in a probe current of 10^{-10} to 10^{-11} A; the vacuum in the objective chamber was of the order of 10^{-5} mm Hg.

Observational results. Scanning observation on the screen of the device and the resulting surface photographs at low magnifications showed a finely dispersed mixture of particles of diverse shape in size, and adhering conglomerates consisting of large numbers of smaller particles easily separable upon mechanical action: breccias, slags, and sinters -- formations obtained by cementing or sintering individual particles.

Let us look more closely at each of the categories of the lunar regolith particles.

1. The conglomerates of the adhering particles are formations obtained by simple mechanical compaction. The surface of this sample is shown in the microphotograph in Fig. 1. This photograph makes it possible to visually estimate the nature of the surface of lunar regolith at a power of 1200. Clearly, the constituent parts of this formation are the angular fragments of rock predominating here, and in lesser quantities -- particles with more rounded, smoothed shapes. The depth of focus of the device made it possible to see with fairly high definition nearby and distant particles. Fig. 2 shows one of the largest crystals of this fraction. In the lower part can be easily seen the opening of completely regular circular shape (arrow A) filled with minute particles. The margins of the openings, in contrast to the external edges of the crystal, are smooth, rounded, and typical of melted /228
bodies. Evidently, the opening was formed by a micrometeoric impact. For more detailed study of this surface of individual bodies of the conglomerate, the photographs were taken mainly at microscope magnifications of the order 5000-10,000.

2. Most often encountered were formations of particles in the form of sinters, partially or entirely vitrified, fused, and slagged. Breccia is the most common constituent of lunar regolith and consists of fragments of rocks and minerals cemented together with a very thin and brittle material.

In contrast to the pieces of basaltic rock, we can be most clearly seen in Fig. 1, breccias of complex and whimsical shapes are the most characteristic constituent in the fraction we investigated. Fig. 3 shows one such breccia. Visible is the strongly cemented and fused surface, characterized by granulosity and intense depth of relief. Openings can be seen on the breccia surface. This conglomerate is nearly entirely fused externally; however among the other types of lunar rock particles, many are fused or slagged to differing degrees only in one or several sides. Fig. 4 illustrates this partial surface melting of a piece of primary rock. We note that a conducting film was not deposited

Fig. 5. Image of surface formation obtained by partial surface slagging

Fig. 6. Surface of particle with hexagonal structure. The spalling lines are visible on the surface of the right facet

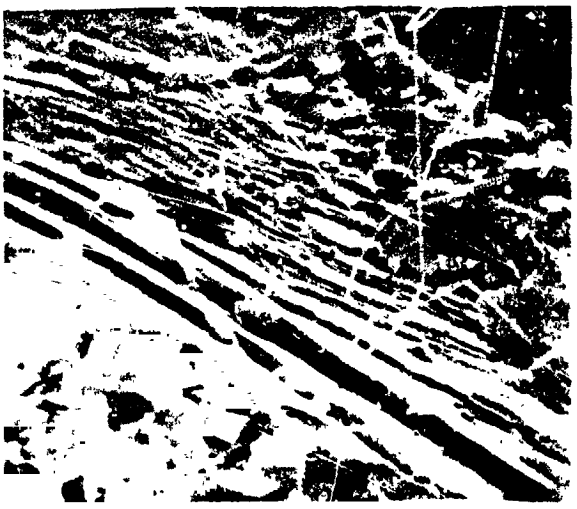

Fig. 7. General view of a chip of crystalline lamella with spalling lines on the upper facet

Fig. 8. Microphotograph of surface of lunar regolith particles with spheroid shape

on the surface of this sample. Here the entire column with the sample was heated in the vacuum chamber of the microscope to about +200°C. Periodic pulsed irradiation with an electron probe was also carried out following the technique described above. In the

upper right-hand part of the microphotograph can be seen an unslagged, rough section of the surface of the breccia sample, with fractures. It can be assumed that the breccia either was not melted on all sides, or else it was fragmented after melting. It is most likely that here local surface melting occurred. In the photograph can also be seen fine fragments of rock adhering to the particle surface. Opening from 1 to 5-6 μm in size are noticeable on the glazed surface. The nature of the coating formed indicates intense, but short-lived and local heating of a particle that was cooled overall, which strongly differentiates this vitrified particle from completely melted volcanic particles.

Another example of a formation resulting due to surface melting is the fragment that can be seen in the lower part of Fig. 5. This is a hollow glasslike crust enveloping several unchanged particles. Typical of these skeletal aggregates are the exit gas openings, which evidently can be formed in a viscous cooling liquid in vacuum conditions. In the central and upper parts of the photograph can be seen microcrystallites of primary rocks. On the surface of the fragment is a glass filament with variable thickness from 300 to 800 AU, possibly resulting from the drawing out of the thick and viscous glassy mass of a small piece as it fell under the effect of terrestrial gravity. /229

3. Some particles of regolith can be divided into two groups by the nature of the surface:

A. particles of crystals with well-defined facets, spallation surfaces, traces of growth; they are classified as crystals of primary magmatic rocks of the terrestrial basalt type emerging upon slow cooling of melted lunar magma of lunar mare /1_7. Typical of them is the angular shape and very fresh appearance. In Fig. 6 is shown one of the aluminosilicate particles with well-defined hexagonal structure. On the surface of the upper right facet can be seen the complex texture of crystal growth. On the forward facet two round depressions are noticeable (arrow A), evidently arising due to micro-impacts. On the surface can also be seen adhering microparticles of dust with sizes up to fractions of a micron.

Another crystalline lamellar particle is shown in Fig. 7. The thickness of the lamella is 5-6 μm, and the facet dimensions are 30 x 40 μm, that is, the particle is quite large for this regolith fraction. The spalling surface of this particle is representative of the spalling surface of the crystals.

B. Classified in the second group of regolith particles are those that are melted, vitrified,, or entirely remelted and forming adhering droplets: spheroid, pear-shaped, dumbbell-shaped, ellipsoidal, and threadlike. In spite of some diversity of shape, there are all characteristics of droplets cooling after the splashing of

a melt. Fig. 8 is an illustration of a group of such spheroidal particles. In the center is the "largest" spherule for the given fraction, 25 μm in diameter, with minute particles adhering to its surface. Also visible are smallest spherules and bodies of ellipsoical shape.

Glassy bodies of regular shape are encountered quite infrequently. Much more widely distributed in the lunar surface material are uneven particles, such as those shown in Fig. 9. In the lower part of the image can be seen an adhering glass rod 0.6 μm in diameter and 4.2 μm in length. Also visible there are micro-openings with round fused rims. The spalling surface of these bodies has the appearance typical of glass spalling (Fig. 10).

Scanning photographs in cathodoluminescence (CL) emission is a substantial supplement of morphological data obtained in the SCM.

Fig. 11 a is the photograph of a crystallite in secondary-electron emission, and Fig. 11 b -- in CL emission. Here it should be noted that owing to the small dimensions of the crystal, the CL emission is quenched very weakly in the object itself and no shadowing effect is produced, which is essential in photographing in secondary electron emission. Therefore the zones of varying intensity of CL are associated only with the inhomogeneity of the /230
crystal, its internal structure, lattice defects, micro-inclusions, and so on. This crystal reveals extremely high inhomogeneity with respect to CL from a very bright region 10 microns in both directions to virtually complete extinction. Evidently, this inhomogeneity of the crystal's optical properties is closely associated with the observed features of the regolith particles bearing traces of exposure in specific lunar conditions. When observations were made of the CL from the regolith as a whole, by taking the scanning photograph of powder deposited on the object stage with scanning magnification of 120, a large number of particles yielding intense CL were recorded (Fig. 12 a). With the temperature accessory it was possible to trace the variation in CL over the temperature range +20 to +200°C. The regolith constituents revealed differing temperature dependence on CL. Fig. 12 b shows the same section of the sample photographed in CL emission at +200°C. It was found that for most particles, with temperature rise, the CL is quenched or else its intensity diminishes, but some particles radiate intensely even at elevated temperatures. This difference in the
CL of regolith particles is associated not only with its complex /231
phase composition, but with the different zonal structure of the crystals.

Conclusion. 1. Scanning electron microscopy as applied to investigating lunar surface material employing various photographic techniques permits a more detailed study of the general morpholog

Fig. 9. Glass droplet with irregular, pearlike shape

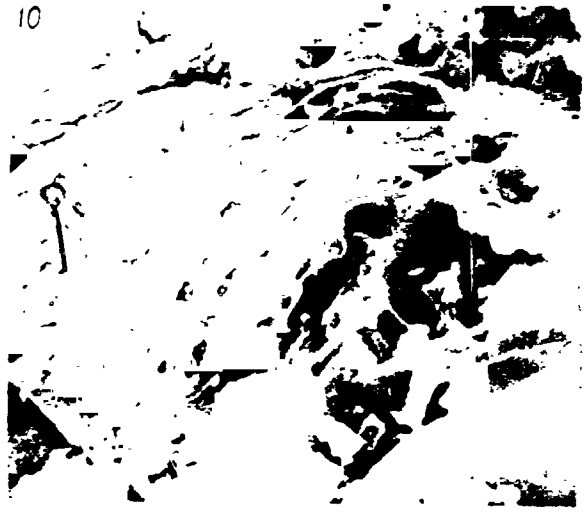

Fig. 10. Appearance of spalling lines of glass body with amorphous structure

of regolith as well as revealing the structural features of the particles of the surface material.

2. Three main classes of objects can be differentiated in the fine fraction of the regolith: a) conglomerates of minute adhesive particles; b) fused particles, sinters, and breccias; and c) individual coarser particles.

3. By the nature of the surface and structure, individual particles are divided into two groups: a) crystalline particles with distinct facets, spalling surfaces, and growth traces; they are classifed as crystals of primary minerals and rock fragments; and b) melted, and partially or entirely grazed particles. The formation of glass particles can be associated with the ejection of melt from the lunar interior into the vacuum. But partial melting evidently occurred at the surface of the moon during secondary processes of "lunar weathering" and above all through the ejection and melting of material during explosions caused by meteoritic bombardment.

The authors express their deep gratitude to Academician A. P. Vinogradov for applying the new physical method to solving fundamental cosmological problems, formulating the problem of investigating such interesting material, and continual attention to the work.

Fig. 11. Surface of crystalline particle of lunar regolith
a. secondary electron emission
b. emission of cathodoluminescence

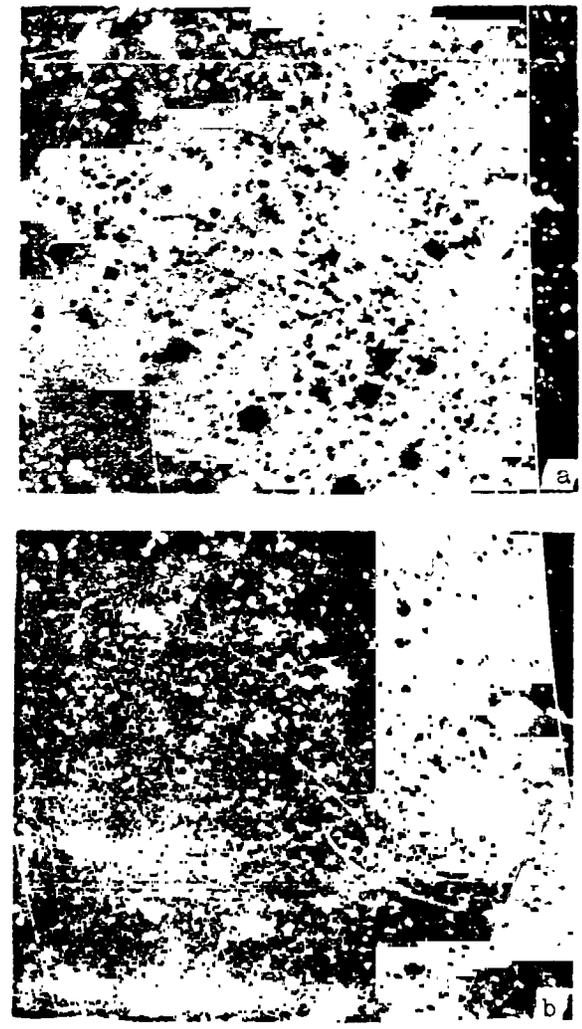

Fig. 12. Image of surface of particle detritus obtained from recording cathodoluminescence emission
a. T = +20°C
b. T = +200°C

REFERENCES

1. Vinogradov, A. P., "Preliminary Data on Lunar Surface Material Returned by Luna 16 Automatic Station," Geokhimiya (3), 261-274 (1971).

2. Spivak, G. V., Saparin, G. V., and Bykov, M. V., "Scanning Electron Microscopy," Uspekhi Fizicheskikh nauk 99(4), 635 (1969).

3. Carter, J. L., and MacGregor, I. D., "Mineralogy, Petrology, and Surface Features of Lunar Samples," Science 167, 661 (1970).

4. Agreel, S. O., Scoon, J. H., Muir, J. D., Long, J. V. P., McConnel, J. D. C., and Peckett, A., "Observation on the Chemistry, Mineralogy, and Petrology of Some Apollo 11 Lunar Samples," Geochim. Cosmochim. Acta, Suppl. 1, (1971).

5. Drew, M., McEwan, W. C., Thomas, J. E., Nagy, B., and Nagy, L. A., "The Morphological Investigations of the Fines and Rocks of Samples From Apollo 11," Proc. Third Annual SEMS, 499 (1970).

6. Phipott, D. F., and Turnbill C., "Electron Microscopy of the Lunar Sample From Apollo 11," Proc. Seventh ICEM (Grenoble) 1, 641 (1970).

7. Antoshin, M. K., Il'in, N. P., and Spivak, G. V., "Scanning Electron Microscopy of Lunar Regolith Returned by Luna 16 Automatic Station," Geokhimiya (5), (1972).

8. Spivak, G. V., Bykov, M. V., Saparin, G. V., and Andreyenko, Yu. A., "Observation of Dielectrics in Scanning Electron Microscopy," Radiotekhnika i elektronika 16, 1530 (1971).

9. Sippel, R. F., and Spencer, A. B., "Cathodoluminescence Properties of Lunar Rocks," Science 167, 677 (1970).

Moscow State University imeni M. V. Lomonosov

Order of Lenin Institute of Geochemistry and Analytical Chemistry imeni V. I. Vernadskiy, USSR Academy of Sciences, Moscow.

N75 11829

SILICATE SPHERULES IN SAMPLE OF REGOLITH RETURNED BY LUNA 16 AUTOMATIC STATION

/232

A. V. Ivanov, O. D. Roda,
Yu. I. Stakheyev, and K. P. Florenskiy

Abstract

The content of spherical fused particles in Sea of Fertility regolith increases with decrease in particle size and varies from 1-2 percent in the relatively coarse fractions to 3-4 percent in the fine fractions. Among the spherical formations was noted a wide diversity of shapes, and the most common (~ 80 percent) are particles that are similar in shape to a regular sphere, which indicates the acquisition of shape in the liquid phase under the action of surface tension. As to color, the most common are the black and dark-colored particles. No regularities of any kind were noted in the distribution of spherical particles by core zones. At the same time, spherules from zone B of the core differ markedly from those from other zones in shape and color, which can indicate regolith stratification. The distribution of spherical particles from zone A of the regolith as a function of their size in the diameter range 40-480 μm obeys a power law with an exponent which in the integral form is 2.9. In the 0.05-5 μm interval, the distribution has a mode in the region of 0.4 μm, where the left and right sides of the distribution also obey the power law with exponents of, respectively, + 0.8 and - 1.3. The presence of the distribution zone of about 0.4 μm indicates the high intensity of fusion of the silicate melt. The considerable difference of the granulometric characteristics of the spherical particles and the regolith as a whole indicates that the formation of regolith particles and the spherules included in its composition occurred as the result of different, even though possibly simultaneous, processes.

Spherical formations represent a contentwise small, but genetically important constituent of the fine-grained regolith material. They are a specific constituent of the lunar surface layer.

We investigated spherical particles selected from fractions from the entire depth of the lunar surface material core from the Sea of Fertility. The study was conducted by the optical method at magnifications up to 300.

As shown by counts of the total number of the spherical particles (Table 1), the content in fractions finer than 0.45 mm over the entire core depth of the regolith is equal to several percent of the total number of particles in fractions and varies from 1-2 percent in the relatively coarse fractions to 3-4 percent in the fine fractions. Obvious is a tendency toward increase in the total content of spherical formations with decrease in fraction size. No regularities of any kind were noted in the distribution of spherical particles by core zones. The absence of spherules in fractions coarser than 0.9 mm in the two uppermost core zones must be accounted for by the general low number here of particles of this size. Therefore, in computing the mean incidence of spherules larger than 0.9 mm, the value for the lower zones V and G was adopted as the mean for the core as a whole.

TABLE 1. INCIDENCE OF SPHERICAL PARTICLES BY CORE ZONES AND FRACTION SIZES (IN PERCENT)

Core zone	Particle size, mm					
	+0.9	−0.9 +0.45	−0.45 +0.20	−0.20 +0.127	−0.127 −0.083	−0.083 −0.040
A	—	1.2	1.4	0.9	2.3	3.3
B	—	1.2	1.4	1.5	1.5	3.1
V	1.2	1.2	1.0	1.3	2.3	3.2
G	1.3	1.7	1.1	1.2	1.5	3.0
A-G, mean	1.2	1.3	1.2	1.2	1.9	3.2

The nature of the morphology of the particles -- their shape and size distribution -- was determined for all zones for formations 0.20-0.45 mm in size. In addition, these parameters were calculated for the upper zone A of the core also for the finer particles (Tables 2 and 3). The count was made for each fraction based on /233 100-250 particles.

Among the spherical formations was noted a great diversity of shape (Fig. 1): regular spheres, ellipsoidal (flattened and elongated), dumbbell-shaped, and drop-shaped particles. The most abundant (up to 80 percent) was the shape similar to a regular sphere, with a deviation from the latter of no more than 10 percent

(see Table 2). Ellipsoidal flattened particles with a minor semiaxis-to-major semiaxis ratio up to 1:3 were quite often found, and somewhat less often observed were ellipsoidal elongated shapes with a semiaxis ratio up to 1:5. The high percentage of irregular spherules among the spherical formations indicates the acquisition of the shape under the action of surface tension, which is possible only for liquid drops with a low viscosity. The presence of dumbbell-like shapes indicates the disintegration of the coarser liquid silicate formations, which was not terminated owing to the rise in the viscosity occurring during the radiative cooling of the droplets.

Analysis of the distribution of spherical particles by shape in the various fractions of zone A indicates that as the fraction size decreases, the content of shapes differing from a regular sphere increases somewhat.

Spherical formations differed widely in color. There were blue, greenish, red, dark brown, black, and colorless varieties. As the counts show (see Table 3), most common are the opaque blackish and black particles. X-ray spectral microanalysis of several silicate spherical formations /1/ shows that the color of these particles in general is a function of their chemical composition. The more intensely colored particles are characterized by a high iron and titanium content (Fe up to 18 percent, and TiO_2 -- 1-2 percent), while the uncolored varieties contain minor amounts of these elements (up to 3.2 and 0.05 percent, respectively), but differ in higher values of CaO and Al_2O_3 (up to 24 and 28 percent, respectively).

The surfaces of spherical formations often prove to be smooth, however in most cases they are complicated by numerous impactive crater-pits. Also not infrequently observed on the surfaces are tail-shaped intergrowths, which are either adhering tiny particles of slagged surface material, or projecting inclusions of mineral grains. The void-vacuoles are characteristic of spherical particles, and they are observed most often in black and dark-colored particles. Common to the black particles are inclusions of incompletely melted mineral grains. The presence of voids and unmelted material in the black particles indicates the incompleteness of their remelting.

It is important to note that the spherical formations from zone B of the regolith core differ appreciably from those from other zones both in shape and color (see Tables 2 and 3), which can indicate some stratification of the regolith. At the same time, this zone does not differ in chemical composition from the other zones /2/.

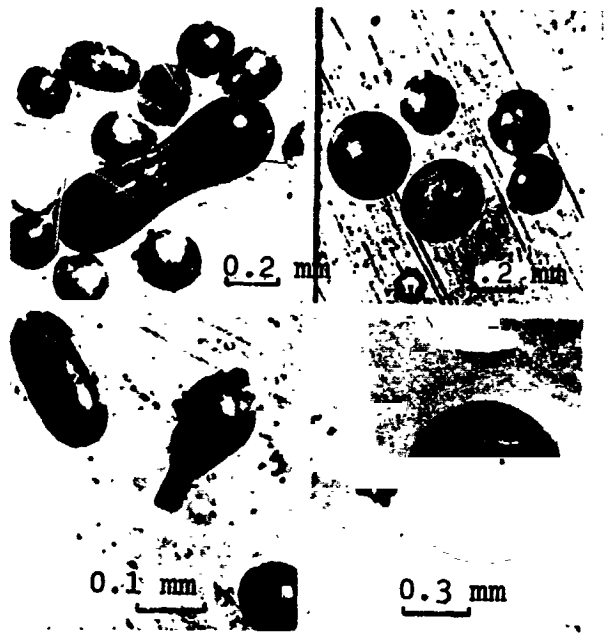

Fig. 1. Spherical silicate particles in Sea of Fertility regolith

A key characteristic of any type of dispersed material that enables one to begin to explain its disintegration is the size distribution of the particles. We found the size distribution of spherical formations in the diameter range 40-480 μm in zone A of the regolith core. Particles more than 200 μm in size were counted from a sample weighing about 5 g; aliquots of the sample (fractions) were used in counting the finer particles.

Count results are in Fig. 2 in graphical form, in the following coordinates: logarithm of particle size versus logarithm of the number of particles of given size per g of sample. The grouping interval is linear, 40 μm. As can be seen from the graph, the distribution of the number of spherical particles in relation to their size in this range of sizes is satisfactorily described by the equation $\Delta N(D) = kD^{\alpha} \cdot \Delta D$, where the exponent is close to -3.9. This evidently indicates that all the particles of this size formed in a single process, probably splashing of the melt resulting from high-velocity impact. /234

We also studied electron-microscopic photographs of the fine fraction of the zone A material. The nature of the size distribution of spherules 0.05-5 μm in diameter is in Fig. 3, in the same coordinates as in the preceding graph, but with logarithmically uniform grouping intervals. This distribution has a mode in the region of 0.4 μm. At the same time, the right and left sides of the distribution are closely described by the power equations $\Delta N(D)^{\gamma} = kD$ with $\gamma = +0.8$ and -1.3.

The graphs in Figs. 2 and 3 were constructed in different forms. When these data are reduced to the cumulative (integral) distribution form commonly used in these investigations, the exponent of the distribution in the 40-480 μm range will be -2.9, while the exponents of the distribution in the micron interval (Fig. 3) retain their value.

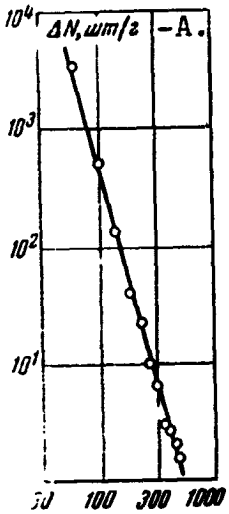

Fig. 2. Size distribution of spherical silicate formations
KEY: A. ΔN, pieces/g

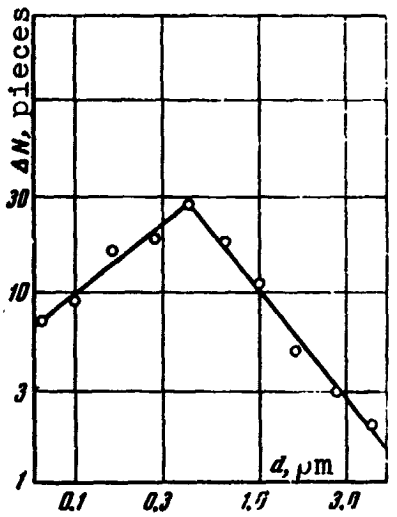

Fig. 3. Size distribution of spherical silicate formations in fine regolith fraction

The difference between the slopes of the distribution of spherules in the coarse and fine portions (-2.9 and -1.3, respectively) is appreciable and can be probably associated with the regular variation in the size of the droplets formed as the modal size is approached, though we cannot entirely preclude the effect of condensation in the range of sizes less than a micron.

A comparison of the size distribution of spherical particles from regolith zone A with diameter greater than 0.5 μm with a granulometric characteristic of this material as a whole /3/ shows the following regularities: 1) each of the distributions is characterized by two power equations, where in both cases the slopes (exponents in the integral form) are less in absolute magnitude in the range of small sizes (-1.3 for spheres and -2.25 for the regolith as a whole) than in the region of large (-2.9 and -4.05, respectively) sizes; 2) the slopes of the spherical particles in absolute value are less than the corresponding slopes for the entire material as a whole; and 3) the size of the particle corresponding to the point of inflection of the slope for the sample as a whole (80 μm) is larger than for the spherical particles from this material (lying in the 5-40 μm range). /235

The considerable difference in the granulometric characteristics indicates that the formation of particles in the regolith as a whole and its constituent spherical particles resulted from different, although possibly simultaneous, processes. In particular, the

TABLE 2. SHAPE DISTRIBUTION OF SPHERICAL FORMATIONS (IN PERCENT OF NUMBER OF PARTICLES)

Zone	Fraction, mm	Regular	Ellipsoidal		Dumb-bell-like	Droplike
			flattened	elongated		
A	0,127–0,083	72,1	10,1	11,4	3,2	3,2
A	0,20–0,127	76,9	8,4	6,3	4,2	4,2
A	0,45–0,20	80,7	9,3	6,8	1,4	1,8
B	0,45–0,20	71,4	11,2	10,2	4,1	3,1
V	0,45–0,20	74,4	14,3	4,2	0	2,1
G	0,45–0,20	78,1	11,9	7,3	2,7	0
A-G, mean	0,45–0,20	77,4	11,7	7,1	2,0	1,8

TABLE 3. COLOR DISTRIBUTION OF SPHERICAL FORMATIONS (IN PERCENT OF NUMBER OF PARTICLES)

Zone	Fraction, mm	Black	Red-dark brown	Yellow	Bluish-greenish	Colorless
A	0,127–0,083	51,3	37,9	3,4	4,0	3,4
A	0,20–0,127	54,5	30,7	6,9	3,4	4,5
A	0,45–0,20	57,2	21,7	2,2	7,1	11,8
B	0,45–0,20	22,1	56,7	1,9	14,4	4,9
V	0,45–0,20	62,8	19,2	6,0	6,0	6,0
G	0,45–0,20	59,7	12,4	7,3	8,2	12,4
A-G, mean	0,45–0,20	50	27,5	4,4	8,9	8,8

formation of spherical particles generally is not simply the result of the melting of individual regolith particles.

The distribution of spherical silicate particles observed is characterized by a very broad size spectrum, embracing more than nine orders of magnitude, which also agrees with the assumption

that the droplets formed through spraying. The presence of a diameter distribution mode in the region of 0.4 μm characterizes the high intensity of the atomization, considering the greater, compared with other liquids, viscosities of silicate melts. Thus, it can be assumed that in the balance of the transformation of impact energy, which can be subdivided into the following stages: 1) ejection and transport of regolith, 2) disintegration of the primary form of rock, 3) heating and melting, and 4) atomization of the liquid formed, that the latter stages required the highest specific outlays of energy. Therefore investigation of spherical formations can be of assistance in clarifying the energy balance of meteoritic collisions on the lunar surface.

REFERENCES

1. Il'in, N. P., Loseva, L. Ye., and Senin, V. G., "X-ray Spectral Microanalysis of Composition of Individual Particles of Lunar Regolith," present collection, p. 209.

2. Vinogradov, A. P., "Preliminary Data on Lunar Surface Material Returned by Luna 16 Automatic Station," Geokhimiya (3), 261-274 (1971).

3. Stakheyev, Yu. I., Vul'fson, Ye. K., Ivanov, A. V., and Florenskiy, K. P., "Granulometric Characteristics of Lunar Surface Material from the Sea of Fertility," present collection, p. 44.

Institute of Space Research, USSR Academy of Sciences

Order of Lenin Institute of Geochemistry and Analytical Chemistry imeni V. I. Vernadskiy, USSR Academy of Sciences, Moscow.

N75 11830

X-RAY STRUCTURAL STUDY OF CHROME-ALUMINUM LUNAR SPINEL FROM THE SEA OF FERTILITY

Yu. Z. Nozik and A. B. Tovbis

Abstract

An x-ray structural study was made of a lunar spinel sample from the Sea of Fertility. The chemical composition and distribution of cations in the structure are characterized by the formula

$$(Mg^{2+}_{0.436}Fe^{2+}_{0.604})[Cr^{3+}_{0.585}Al^{3+}_{1.310}Ti^{4+}_{0.078}]O^{2-}_{4}.$$

Interpretation of the experimental data by the least-squares method yielded the oxygen parameter u = 0.261 and the isotropic temperature factor 1.09 AU^2.

A monocrystal of spinel, described in [1] as sample M-16, was selected from the lunar regolith returned by Luna 16 automatic station. We made an x-ray investigation with the automatic DAR-UM diffractometer. The monocrystal studied was irregular in shape with a maximum size of about 0.4 mm. The intensities of the x-ray reflections with indices hkl were recorded in CuK_α-radiation, allowing for quenching for the space group $Fd3m -- O^7_h$. Equivalent reflexes were averaged in the treatment of the experimental material. The lattice parameter a = 0.270 ± 0.003 AU was determined with a DRON x-ray diffractometer.

From the data of an electron probe microanalysis [1], the chemical formula of this spinel can be written as: $Al_{1.310}Fe_{0.604}Cr_{0.585}Mg_{0.436}Ti_{0.078}O_4$ on the assumption that the valencies of the atoms are as follows: iron -- Fe^{2+}, chromium -- Cr^{3+}, magnesium -- Mg^{2+}, aluminum -- Al^{3+}, and titanium -- Ti^{4+}.

The octahedral positions in the structure were adopted for the Cr^{3+} ions. The basis for this assumption was data on the energy of the preference of chromium for octahedral coordination in spinels [2] and numerous experimental studies of spinel systems with chromium [3], in none of which chromium atoms in the tetrahedral positions were found. The possible replacements of Mg and Al in spinels [4] was not considered by us in view of the small difference in the scattering ability of magnesium and aluminum ions when diffracting x-rays. Ions of trivalent iron were not detected in the lunar samples, and we did not assume the presence of iron atoms in the octahedral positions, since the energy of preference of Fe^{2+} for the octahedral coordination is lower than for the ion Al^{3+}, and all the more so for Cr^{3+}. Since chemical analysis did not show excess Mg + Fe for the tetrahedral positions with respect to the stoichiometric composition of the spinel, and since the number of titanium atoms per formula unit is low, according to the scheme proposed in [5] for the system of solid solutions chromite ($FeCr_2O_4$) -- ulvospinel (Fe_2TiO_4), in our case we can assume the following role of the distribution of cations by positions:

tetrahedral (A) -- $(Mg, Fe)^{2+}$,

octahedral (B) -- $(Cr, Al)^{3+}$, Ti^{4+}.

The structural formula of this spinel as a whole can be written as

$$(Mg^{2+}_{0,436}Fe^{2+}_{0,504})\,[Cr^{3+}_{0,585}Al^{3+}_{1,310}Ti^{4+}_{0,078}]\,O^{2-}_4,$$

where the ions in the tetrahedral positions (A)-positions are enclosed in the parentheses, and the ions in the octahedral (B)-positions -- in the brackets.

Treatment of the experimental results was carried out on a computer by the method of least squares for the space group Fd3m. The values of the oxygen parameter (u) and the isotropic temperature factor (W) were revised. A comparison of the measured and computed x-ray diffraction intensities showed that for strong reflections a systematic excess of the calculated intensities over the measured intensities was observed. To eliminate this discrepancy, we introduced the one-parametric coefficient of secondary extinction, determined from the ratio /263

$$I_{mea} = I_{calc}\exp(-kI_{calc}).$$

TABLE 1. MODULI OF MEASURED AND COMPUTED STRUCTURE AMPLITUDES

hkl	$\|F_{mea}\|$	$\|F_{calc}\|$	hkl	$\|F_{mea}\|$	$\|F_{calc}\|$
111	4628	4839	531	3162	2840
220	2820	3252	800	5329	4991
131	314	293	733	2512	2783
222	343	416	660	1756	1614
400	4687	4839	175	145	150
422	2629	2372	555	570	551
151	471	588	662	762	836
333	1043	919	840	1415	1611
531	3162	2840	191	1304	1358
442	234	179	842	141	180
620	1946	1829	664	853	1010
335	126	145	931	200	242
622	978	913	844	3522	3564
444	2810	2532	717	2071	2010
551	1766	1838	755	1422	1538
642	1816	1726	933	1598	1452
731	531	502	862	985	979
355	276	251	864	210	126

After insertion of the correction for secondary extinction, the ratio between I_{calc} and I_{mea} significantly improved for all reflexes, except (440). Therefore this reflex was not included in the final calculations.

Table 1 presents the moduli of the measured $|F_{mea}|$ and calculated $|F_{calc}|$ structure factors for the oxygen parameter u = 0.261 and the isotropic temperature coefficient W = 1.09 AU^2, obtained by the procedure of revising the structure using the least squares technique. In the final stage of the computations, the individual temperature parameters of the oxygen atoms and the cations in the A- and B-positions were computed. The deviations from the isotropic temperature factor ΔW_o = -0.5 AU^2, ΔW_A = -0.19 AU^2, and ΔW_B = = 0.04 AU^2 are minor, which renders the variation of the atomic curves in order to revise the chemical composition useless. The final value of the structure unreliability factor R = 7.9 percent.

Table 2 gives the interatomic distances of cation (A) -- -- cation (B), and cation-oxygen in this spinel.

TABLE 2. INTERATOMIC DISTANCES IN THE STRUCTURE

Anions of oxygen -- O Cations in tetrahedra -- A Cations in octrahedra -- B	Distance, AU
B—O	1,98±0,01
A—O	1,95±0,01
B—B	2,923±0,001
A—B	3,428±0,001
A—A	3,498±0,001

The authors are grateful to Academician A. P. Vinogradov and to Professor Ye. S. Makarov for suggesting this subject for investigation, to V. I. Simonov and D. M. Kheyker for discussion of the results, and to Yu. V. Nekrasov for assistance in conducting the experiment.

REFERENCES

1. Makarov, E. S., Ilyin, N P., and Ivanov, V. I., "On the Composition and Crystal Structure of the Minerals of Regolith from the Sea of Fertility," Space Research, XIII, (1972).

2. Navrotsky, A., and Kleppa, O. I., "The Thermodynamics of Cation Distributions in Simple Spinels," J. Inorg. Nucl. Chem. 29(11), 2701 (1967).

3. Blyasse, Zh., Kristallokhimiya ferroshpineley /Crystal Chemistry of Ferrospinels/, "Metallurgiya", 1968.

4. Bacon, C. E., and Roberts, F. F., "Neutron-Diffraction Studies of Magnesium Ferrite-Aluminate Powders," Acta Cryst. 6, 57 (1953).

5. Wood, J. A., Marvin, U. B., Reid, J. B., Taylor, G. J., Bower, J. F., Powell, B. N., and Dickey, J. S., "Mineralogy and Petrology of the Apollo 12 Lunar Samples," Research in Space Science SAO, Special Report 71(333), (1971).

Order of Lenin Institute of Geochemistry and Analytical Chemistry imeni V. I. Vernadskiy, USSR Academy of Sciences

Institute of Crystallography imeni A. V. Shubinkov, USSR Academy of Sciences, Moscow.

N75 11831

CHEMICAL COMPOSITION OF LUNA 16 LUNAR REGOLITH

/264

A. P. Vinogradov, M. S. Chupakhin,
I. D. Shevalyevskiy, and Yu. I. Belyayev

Abstract

Data on the chemical composition of regolith returned by the Luna 16 automatic station and two fragments of basalts from the lower layer of the core are presented. Spark mass-spectrometric, primary x-ray spectral, emission spectral, and atomic absorption methods were used in the analysis. The regolith of mare provinces were shown to be a mixture of material of various origins. The source of the material of the mare regolith was principally basalts of the corresponding lunar lava maria. The regolith is genetically related to it. This follows from a comparison of the chemical composition, mineralogical, and petrochemical features of the basalts and the regolith from the Sea of Fertility, Sea of Tranquillity, and Ocean of Storms, respectively.

Preliminary data on the chemical composition of Luna 16 regolith were reported earlier /6_7. It appeared expedient to study further in closer detail the abundance of several chemical elements in the fine regolith fraction and the associated fragments of basalt and gabbro compared with the chemical composition of Apollo 11 and Apollo 12 regoliths. We have in mind precisely the regolith of the mare regions of the Moon. Regolith from the highland territory of the Moon, as we know from the materials of Apollo 14 and Apollo 15, and especially after a study of Luna 20 regolith, differs appreciably in petrographic, mineralogic, and chemical composition by the high content of aluminum-rich rocks -- basalt and anorthosites -- from mare regolith. We anticipate soon returning to this problem -- -- determining the composition of the regolith from the highland or mountainous regions of the Moon.

As is already known, Luna 16 regolith is an inequigranular, nearly black powder, with mean grain size 70-120 μm. The granulo-

metric and mineralogic composition of regolith for the four zones of the Luna 16 core investigated can be found in the papers presented in this collection /13, 17, 20, 21/. The nature of the particles comprising the regolith -- fragments of basalt, gabbro, microbreccias, slags, sinters, glasses, grains of various minerals, spheroids, and grains of anorthosite -- can be seen in the photographs of this collection.

Regolith particles apparently are overstrewn with an even finer powder. The following was found in the total mass of the regolith returned, on an average basis (in percent):

slag	38	glass	4.3
microbreccias	30	anorthosite	3.0
gabbro	13.5	spheroids	1.3
basalt	7.3	others	3.1

The primary minerals of regolith, as well as rock fragments, are plagioclases, pyroxenes, ilmenite, spinels, olivine, and others. Considerable numbers of grains, microbreccias, and so on, are melted or are sintered particles or glasses; spheroids are present. All this indicates the nature of the process underlying the formation of this inequigranular rock. Particle morphology, shock effects, and so on, are described in /6, 13/. Still, light, unmelted, angular fragments of basalts were found in the regolith. The content of macro- and microelements in each of the four zones A, B, V, and G of the regolith and in the basalt fragments was studied. Data on individual regolith fractions are given in the papers included in the present collection.

Analytical methods. Spark mass-spectrometry has unique analytical characteristics. Using it, in a single experiment it is possible to determine up to 60-70 elements with sensitivity up to 10^{-7} percent or better.

Still, this method has low precision due to the inequiprobable /265 ionization of the atoms of the sample in the spark discharge, nonreproducibility of the coefficients of ionization sensitivity, numerous superimpositions on the analytical lines of the sample of the lines of polyatomic ions of the matrix and admixtures, as well as oxides, nitrides, carbides, and so on. The nonreproducibility of the recorded concentrations of the elements in the sample depends mainly on the inhomogeneity of the composition of the materials being analyzed.

Our investigations made it possible to establish the multistage nature of the vacuum spark discharge, each phase of which is characterized by ions of a specific nature.

In the initial high-voltage stage of discharge, mono- and multi-charged masses are predominantly formed under the mechanism of equiprobable ionic emission; associated with the subsequent arc phase is the appearance in the mass spectrum of complex and polyatomic ions. In the concluding stage of the discharge, low-energy electrons interact with the atomized particles of the material being analyzed, which causes the inequiprobable ionization of atoms differing in potentials and ionization cross sections.

The composite ionic current includes all these constituents, usually nonreproducible from discharge to discharge, therefore the recorded mass spectra only qualitatively correspond to the composition of the sample being analyzed.

We were able to propose an original method of isolating from the entire spectrum of ions only the ions formed in the nanosecond range from the initial high-energy stage of the spark discharge.

The magnitude of the ionic current thus discriminated is about 4-7 percent of the current usually recorded when all the stages of the spark discharge are utilized.

By employing this method for an ionic spark source, a probe mass-spectrometric method of analyzing nonconductive polycomponent solids without using additions of graphite or silver was developed /26/.

The mass spectra obtained in this technique are marked by simplicity of structure and good reproducibility, since their composition now does not include the recording of polyatomic, complex, oxide, and other complex masses formed in the arc stage of the spark discharge.

For a complete analysis to high precision, about 20-25 mg of the lunar material must be consumed. A powdered material is pressed in the form of a thin layer in a high-purity aluminum crucible, and then the main constituents of the sample are determined by an x-ray spectral method; next the layer is used to establish the admixture composition with a mass sepctrometer that has an ionic spark source.

Recording reproducible mass-spectrometric results at the level of 8-12 percent was achieved during the experiment by selecting the material analyzed from the entire surface of the sample through scanning of the tablet relative to a fixed tantalum probe directly in the ionic source.

The constituents of the lunar sample were estimated based on an external standard -- diabase W-1 (NBS), whose mass spectrum was recorded on the same photographic plate as the sample under study.

Quantitative analysis of the main constituents of lunar regolith was made by the x-ray spectral method. The x-ray spectrum has a small number of lines, which simplifies identifying the elements, and the possibility of conducting the analysis from a small weighed sample (5-10 mg) even without using u$_\mu$ the material renders this method uniquely applicable in a number of cases. A major disadvantage of the primary method is its low sensitivity, in practice up to 10^{-2} percent.

The main constituents of the lunar regolith were determined with a primary JPX-3 x-ray analyzer (JEOL company, Japan). Elements with atomic number of 19 and higher were analyzed at 30 kV and 10 μA using LiF as the crystal analyzer. Lighter elements were determined with a KAP crystal at 15 kV and 20 μA. No heating of the sample in these regimes was observed. A sample in the amount of 20-25 mg was pressed into the aluminum crucible, over it carbon was vacuum-deposited, and after x-ray spectral analysis transferred for spark mass-spectrometric analysis. The diameter of the focussing spot on the sample was 6 mm, that is, the analyzed area was 25-30 mm^2. The reference standards were the familiar standards W-1, JB-1, and BCR-1, whose composition is close to the lunar samples. The background was taken into account by the usual procedure. Corrections were introduced into the measured relative intensities for absorption, fluorescence, and atomic weight after the method of Bence and Albee /287. The error of determination, when the content of the unknown element was upwards of 0.5 percent, did not exceed $\pm$ 2 percent, which was /266 confirmed by control chemical analyses.

The optical spectrum of the regolith in general is close to the spectrum of terrestrial basalts. Therefore approved methods developed in the Institute of Geochemistry and Analytical Chemistry imeni V. I. Vernadskiy, USSR, and used for many years in the systematic investigations of the abundance of elements in various types of terrestrial basalts and gabbro, were resorted to for the quantitative spectral analysis of the regolith. Optimization of the methods of the spectral analysis of regolith consisted mainly in reducing the size of the weighed sample and increasing the number of elements determined simultaneously without the loss of information on the sample composition.

Be and F were determined by the techniques of emission spectral analysis using a plasma generator to excite the spectra of the samples in powdered form /197. By using a buffer (mixture of carbon powder and KBr), the effect of the sample matrix on the results of the analysis was virtually eliminated. The sample (20 mg) was blended with the buffer (1:1). The spectrum in the visible

region was recorded on an STE-1 diffraction spectrograph with folded optics (dispersion 5 AU/mm). The analysis was based on two parallel weighed samples. The relative error for the determination of F was 15 percent, and for Be -- 10 percent, for a confidence interval[1] of 0.95. The international basalt standards BCR-1 and BM were used in the calibration.

The techniques of emission spectral analysis with a direct-current arc (15 A) and with a diffraction spectrograph (dispersion 2.75 AU/mm in the second spectral order) were used in the simultaneous determination of V, Ni, Pb, Sc, and Co. The sample was mixed (1:1) with a buffer (mixture of 90 percent graphite powder with 10 percent $BaCO_3$) /15, 18/. The analysis was performed on two duplicate 20 mg weighed samples. The correctness of the results was monitored based on the international standards. The error was 20 percent.

An ARL quantometer adapted for the analysis of geological materials was employed in the determination of Cu /4/. Silicate glass was used as the buffer. Here V and Ni were determined simultaneously. The weighed sample was 10 mg; two determinations were made. The quantometer was calibrated based on the BCR-1 and BM standards. The error was 8 percent /15/.

The determination of Li and Ga were based on the classical techniques of emission and absorption flame photometry /16/. The high-temperature flame of hydrogen-air and acetylene-air mixtures was used. The spectrometer was assembled on the basis of the ISP-51 spectrograph and the FEP-1 photoelectric accessory with the recording circuit of the Flaphokol flame photometer. The error of Li determination was 6 percent, and 25 percent -- for Ga.

In determining Ag and Cd, use was made of the atomic-absorption method with a pulsed selective atomizer of solid samples in powder form /3/. The sample (10 mg) was heated in a miniature graphite beaker to a temperature exceeding the lattice disintegration temperature. The amplitude of the pulse of atomic absorption of Ag and Cd vapors differing from the interference by shape and the instant of appearance served as the analytical signal. The pulse duration of atomic absorption was 1.5-2 sec. The nonresonant absorption was allowed for automatically based on the continuous spectrum of the auxiliary source (an Xe lamp). The sample (10 mg) was mixed with carbon powder (1:1). In optimal conditions of analysis, the effect of the gross composition of the sample on the results is virtually

---

[1] The error of all methods of spectral analysis described below corresponds to this confidence interval.

absent. Synthetic standards and the international basalt standard BCR-1 were used in the calibration. Each sample was analyzed twice. The error was 20 percent. Tl and Hg were determined by the atomic-fluorescent method with pulsed selective atomization of the solid samples /5/.

The amplitude of the pulse of atomic fluorescence from Tl and Hg served as the analytical signal. The precision was 20 percent. The international standards were used in the calibration. Preliminary mass-spectral determination of rare earths in the lunar material gave an error up to ± 20 percent for several rare-earth elements. Therefore the rare earths were determined by different techniques (indicated in the table), with the preliminary separation of the rare earths from the regolith sample[2].

Experimental data. Comprehensive determinations were made of the composition of two series of samples from all zones A, B, V, and G of the regolith returned by the Luna 16 automatic station, and of two basalt fragments from the lower zone G -- sample I and sample II. Some data for the first series of determinations were given in the preliminary report /6/. The second series differs by the numerous quantitative determinations of individual samples made by different techniques. The following tables indicate by which techniques particular results were obtained. Table 1 gives /267
the content of the major constituents in the form of oxides obtained by primary x-ray spectral analysis. From these data it is clear that the chemical compositions of individual regolith zones differ little. Good agreement was also obtained with our data for the Luna 16 regolith, noted in investigations of other authors, as is clear from Table 2. A somewhat more appreciable scatter of the data was observed for the composition of the basalt fragments (see Tables 1 and 2), which is quite understandable since the investigators studied fragments petrochemically differing --
-- from ordinary basalt to aluminum-rich basalt. In our case, /268
sample I is a composite sample (98 mg) from the + 0.9 mm fraction. Particles of coarse-grained and medium-grained gabbro of different compositions were selected. Sample II is a single particle weighing 27.7 mg. The medium-grained basalt has the approximate mineralogical composition (in percent): pyroxene -- 40, olivine --
-- 15, ilmenite -- 35, and plagioclase -- 10; the rock is melanocratic, approximating peridotite (feldspar type) in composition.

From the data for major elements, as was noted even earlier /6/, it is clear that the content in the regolith of mafic elements is somewhat lower compared to their content in the fragments of mono-

---

[2] Therefore we do not present the preliminary data on the rare earths in the table.

TABLE 1. CONTENT OF MAJOR ELEMENTS (IN OXIDE FORM) IN ZONES A, B, V, AND G OF LUNA 16 REGOLITH AND IN BASALT FRAGMENTS THEREIN (IN %)*

Component	Regolith								Basalt fragments			
	mean of series I samples (preliminary data)	A	B	V	V	V[2*]	G	mean of series II samples (A,B,V,G)	total mean	sample I	sample II	mean
SiO_2	41,7	41,7	41,2	42,50	42,4	42,53	41,3	41,93	41,90	43,8	42,1	42,95
Al_2O_3	15,33	15,32	15,40	15,45	15,30	15,42	15,15	15,33	15,33	13,65	14,10	13,88
FeO	16,64	16,80	16,55	16,30	16,20	16,90	16,90	16,65	16,66	19,35	21,00	20,17
TiO_2	3,39	3,39	3,46	3,30	3,33	3,25	3,42	3,36	3,36	4,90	6,10	5,5
MgO	8,78	8,73	8,82	8,96	8,96	8,90	8,60	8,78	8,78	7,05	5,05	6,05
CaO	12,49	12,20	12,80	12,42	12,78	12,38	12,55	12,54	12,53	10,40	11,3	10,8
Cr_2O_3	0,28	0,31	0,25	0,30	0,26	—	0,26	0,28	0,28	0,28	0,20	0,24
MnO	0,21	0,21	0,20	0,20	0,24	0,20	0,22	0,21	0,21	0,20	0,22	0,21
Na_2O	0,34	0,37	0,36	0,36	0,30	—	0,28	0,34	0,34	0,33	0,13	0,23
K_2O	0,10	0,10	0,12	0,10	0,13	—	0,10	0,10	0,10	0,15	0,17	0,16
P_2O_5	0,10	0,12	0,12	0,14	0,13	—	0,14	0,13	0,12	0,15	0,13	0,14
S	—	0,19	0,20	0,18	0,22	—	0,25	0,21	(~0,21)	0,17	0,22	0,20

* Primary x-ray spectral method, error ± 2 percent.
2* Chemical analysis

lithic rocks (for example, Fe, Ti, and Cr), but the content of Al, Ca, and alkalies in regolith is increased. This regularity is repeated when we examine the composition of regolith and of rocks of the mare regions returned by Apollo 11 and Apollo 12 from the Sea of Tranquillity and the Ocean of Storms (see Table 5). At the present time, there are numerous data on Apollo 11 and Apollo 12 rocks. Therefore in the tables we used for comparison the most extensive data of Wanke [37, 38], and also some from other authors. From all the known data on the composition of mare regolith it follows that the regolith was formed from monolithic rocks on which it lay. This follows from the correspondence of the composition of the basalt to the regolith of a given lunar mare. In other words, a relatively high content here in the regolith of Fe, Ti, and so on, corresponds to the relatively high content of Fe in the local basalt. And in increase of Al and Ca in the regolith or a decrease of Fe and Ti, and so on, that is, fractionation of trace elements, sometimes is 30 percent or higher. As we will see below, for individual trace elements in the system monolithic rock-regolith from a given lunar province it can differ by more than

TABLE 2. DATA OF OTHER INVESTIGATORS ON THE CONTENT OF MAJOR ELEMENTS IN REGOLITH AND BASALT FROM LUNA 16 MATERIAL (IN PERCENT)

Component	Regolith							Basalt		
	mean, based on our data (from series I and II)	Hubbard et al. /25/		Jerome et al. /11/	Gillum et al. /12/		mean from our data	Steel, Smith /21/		Albee et al. /2/
		G	A		A	G				
SiO_2	41.9	44 (<125 μm)	45	—	43.9	43	42.95	42.8	43.4	45.5
Al_2O_3	15.33	16	16	15.3	15.7	16.0	13.88	15.4	18.8	13.95
FeO	16.66	16.0	15.9	15.8	16.8	16.8	20.17	18.1	13.6	17.77
TiO_2	3.36	3.3	3.5	3.60	3.3	3.2	5.5	4.3	3.0	4.04
MgO	8.78	8.51	8.12	9.28	—	—	6.05	6.4	6.4	5.95
CaO	12.53	12.1	12.1	11.5	11	11	10.8	11.2	12.9	11.96
Cr_2O_3	0.28	—	—	—	0.32	0.33	0.24	0.3	0.3	—
MnO	0.21	0.23	0.23	—	0.21	0.20	0.21	0.3	0.2	0.26
Na_2O	0.34	0.42	0.42	0.34	0.3	0.37	0.23	0.7	0.7	0.63
K_2O	0.10	0.09	0.11	0.20	0.12	0.11	0.16	0.1	0.1	0.21
P_2O_5	0.12	—	—	—	—	—	0.14	—	—	0.15
S	0.21	—	—	—	—	—	0.20	—	—	—

one-half order. Apollo 11 and Apollo 12 material -- monolithic rocks and regolith -- represent extreme cases in terms of content of major elements. The rocks that are poorer in iron content are represented by Apollo 11 material. In Table 5 we give an analysis of the material of two lavas returned by Apollo 11, rocks of type A and type B (see /29/ for their detailed description). Still, these rocks are richest in titanium. Apollo 12 rocks are richest in iron (rock types I and II) and still they are poorer in titanium. Luna 16 rocks, in terms of their content of Fe, Ti, and Ca are intermediate between these extreme cases by their content of major elements. This regularity also is true of the regolith composition. An exception perhaps is represented by the content of Al in Luna 16 material that is relatively high compared with the Apollo 11 and Apollo 12 material, with a high Al/Ca ratio for the Luna 16 material; this value as a rule is attained in the Apollo 11 and Apollo 12 material only in their regolith.

Perhaps here some remarks on the form in which iron is present are in order. All other major constituents do not raise special questions, and they are distributed in the known fashion by phases of lunar rocks /33, 34/. Iron is encountered in the regolith as: 1) the oxide FeO, where the content of Fe_2O_3 or any other, more highly oxidized forms of Fe is debatable (see /34/); 2) as fragments of meteoritic iron in which kamacite and taenite phases were disclosed by x-ray analysis; 3) metallic Fe with a very low content of Ni; and 4) dispersed, passivated pure metallic Fe found on the surface of the regolith microparticles (see /8/). It was formed in vacuum at high temperatures; the absolute content of this Fe compared to total Fe in the regolith is very low.

We can compare the chemical composition of lunar basalt, on the one hand, with the compositions of tholeiitic oceanic basalts of the Earth and feldspar, potassium-rich achondrites, on the other:

	SiO_2	Al_2O_3	FeO	TiO_2	MgO	CaO	MnO	Na_2O	K_2O	P_2O_5
Tholeiitic basalts (110 determinations)	49,15	15,09	7,56 (+3,35 Fe_2O_3)	2,09	7,75	10,61	0,17	2,23	0,30	0,23
Feldspar achondrites (25 determinations)	48,65	11,71	16,31	0,50	9,87	10,39	0,47	0,83	0,17	0,10
Basalt II, Luna 16	42,95	13,88	20,17	5,5	6,05	10,80	0,20	0,23	0,16	0,14

Considerably higher content of Fe and Ti in lunar basalts was noted and, therefore, sharply reduced content of alkalies in the regolith of mare provinces, and also sharply reduced content of Al and Si compared with the composition of both basaltic and achondrites (Si), as well as especially of tholeiitic basalts (Si and Al). The Fe content, nearly 22 percent FeO in the mare basalts of the Moon, that is, more than 1.5 times higher than its mean content (as FeO) in chondrites evidently determines the nature of the eutectic of the molten lunar lavas. Ti is present chiefly as ilmenite, and Cr -- as spinels. /269

Now let us consider the content of trace elements in the regolith and basalts from mare lunar provinces. We will consider their content in basalts and regolith of the Moon also compared with their content, on the one hand, in stony meteorites -- chondrites /10/, and in terrestrial tholeiitic basalts -- on the other /7/.

Alkali elements. The contents Na, K, Rb, and Cs in general both in basalts and in the Luna 16 mare regolith is in the same order of magnitude (Tables 3-5) and differs little by individual

types of gabbro-basalts. However, it is impossible not to note that the content of Rb in the various basalts of the Moon, as is clear from Table 5, varies by half an order (for example, there is more Rb in Apollo 11 rocks of the type A than in type B). However, the content of all these alkalies in monolithic rocks and regolith differs little from their content in chondrites and does not even reach their level in the primitive basalts of the Earth -- tholeiites in which the Na_2O content is about 2 percent. There is very little K in the regolith and the lunar basalts. An exception is represented by Li, whose content in the basalts and in the mare regolith is one order higher than its ordinary content in the chondrites, and thus attains the Li content in terrestrial basalts. This is a highly interesting conclusion which thus far has not found an explanation.

The reason for the low content of alkalies in the basalts and the mare regolith of the Moon is possibly associated with the relatively higher mass of lunar material subjected to primary melting than occurred on the Earth. It is scarcely possible to speak of any considerable loss by the Moon of part of the alkalies during the primary differentiation of its material, bearing in mind the generally low content of alkalies in the chondrites.

Alkaline-earth and other lithophilic elements. All elements which will be discussed below -- Sr, Ba, TR, Y, Zr, Hf, Sc, Nb, Ta, Th, and U, and several typical lithophilic elements -- are contained in lunar mare basalts in considerably greater amounts than in average chondrites, and is higher than their order of abundance in terrestrial basalts. In other words, during the melting of basalts of the lunar mare type an enrichment (see Tables 3-5) in these elements occurred, where the content of Sr and Ba is a function of the content of Ca in the lunar rocks. It is possible that the very same relationship with Ca will be disclosed with respect to other trace elements. Further increase of Sr and Ba in the regolith of lunar mare occurred compared with their content in the basalt on which the regolith lies. We will discuss the degree of enrichment of the regolith with these elements somewhat later. Mare basalts are enriched in Zr, Hf, Nb, Ta, Sc, Y, TR, (Ti), Be, and B, and as a consequence, the regolith became enriched by them. The coefficient of enrichment basalt/regolith is difficult to calculate, since situations were encountered when evidently basaltic lavas of different types with some difference in the content of the elements indicated above evidently participated in the formation of the regolith. Most authors assume that in the case of basalts, for example, poor in Rb and rich in Rb (type A and type B) from the Apollo 11 collections, both types of basalts participated in the formation of regolith /297. However, if it is assumed, as we have done here, that during the formation of regolith further differentiation of the composition of the rock

with the same tendency toward increased content of lithophilic elements was possible /6/, material of basalt with the lowest content of lithophilic elements (type B, Apollo 11 or type II, Apollo 12 material poorer in Rb) had the principal participation in forming the regolith in this case.

In this respect, the distribution of U-Th or Nb-Ta and Zr-Hf between basalt and regolith, and also of Sc, Y, and TR is highly typical /22/. The degree of the rise in their content in the regolith fluctuates considerably. If we start from the assumption that basalt of Apollo 11 type B is the principal source of Apollo 11 regolith, then just as in the case of the Luna 16 material, enrichment of the regolith with Zr, Hf, Nb, Ta, Sc, and TR will always be very low or in general will not occur (see Table 5). For Th, for individual TR-Er, Yb, and Lu (Luna 16), and La, Ce, and Ho (Apollo 11) enrichment is noted. In other words, the distribution of TR in the Luna 16 basalt and regolith and in Apollo 11 basalt (type B) is practically the same. But if we compare the basalt-regolith of Apollo 12, we note a considerable difference in the content not only of TR, but also of many other lithophilic elements -- the values will be considerably higher in the Apollo 12 regolith. This is especially noticeable for TR (see Table 5), and also for Nb, Ta, Zr, Hf, and Th. It can be noted, therefore, that the Apollo 12 basalts richest in the mafic elements Fe, Mg, and also Cr yield, when the regolith was formed from them, regolith that is the richest in lithophilic elements.

Volatile products of F and S analogs. The content of the /273
halogenides F, Cl, Br, and I in the basalt and regolith of lunar mare provinces is at the level of their content on chondrites, that is, these elements are less abundant than in terrestrial basalts. Perhaps, the chlorine content is relatively somewhat high. There is no noticeable difference in the content of the basalts and regolith. Here there is still limited data. The content of sulfur, selenium, and tellurium is considerably lower than their gross content in the mean chondrite and corresponds to the level of their ordinary content in terrestrial basalt. It is difficult to find a difference in the content of S, Se, and Te between basalt and regolith. Data for As fluctuates significantly and requires more accumulation.

Heavy metals -- Fe, Ni, Co, V, Cu, Zn, Cr, Mn, Mo, W, and Sn. The behavior in the system lunar basalts-regolith of elements of the iron families -- Ni, Co, Mn, and V -- is most interesting. The content of total Fe in mare basalts is nearly 17 percent (Apollo 12), that is, above the mean content of bound iron (~12 percent) in chondrites. Still, the amount of ordinarily accompanying elements of the iron family -- Ni and Co -- in lunar

TABLE 3. CONTENT OF TRACE ELEMENTS IN REGOLITH AND PARTICLES OF LUNA 16 BASALT (IN PPM) /270

Element	Regolith					Basalt				
	mean of series I samples, see preliminary data /6/	A	B	V	G	mean of series II samples	total mean for series I and II samples	sample I, preliminary data /6/	sample II	mean composition of basalt from series I and II
Li	10	—	—	13**	11**	11,5	10,8	—	—	—
Be	2,5	—	2,8**	2**	2,7**	2,5	2,6	—	—	—
B	4,7	4,4	3,5	3,0	6,7	4,4	4,4	5	2,8	3,9
F	270	95,3	131	110**	127	131	200	181	64	128
Cl	62	26,4	20	31	16	23,4	42	—	29	29
Sc	27	66,5 49,0**	70 41**	45 21**	50 38**	47,5	37,2	20	43	31,5
V	61	73	54 82**	60 60** 70**	39 86**	74	67,5	42,5	45	43,8
Co	53	32,6	19 30**	35 26**	15 27**	29	41	29	14,3	21,7
Ni	190	80	220 240**	160 210**	150 250**	152	171	147	79	113
Cu	37	31,4	23 31**	35 20**	93 28**	37,3	37	13	25	19
Zn	21	26,3	72	45	40	45,7	33,4	26	21	23,5
Ga	(4,9)	4,5	4,2 2**	7,5 2**	4,5	4,1	4,5	1,2	5,2	3,2
Ge	1,3	0,64	1,0	2,45	0,7	1,19	1,25	2,5	1,1	1,8
As	0,4	—	0,15	0,62	0,4	0,42	0,41	2,9	0,25	1,5
Se	—	—	0,056	0,91	0,098	0,36	0,36	0,7	0,1	0,4
Br	0,28	—	0,8	0,83	0,62	0,75	0,5	1,3	0,3	0,8
Rb	(5,9)	1,85	1,70	2,6	1,51	1,9	1,9	—	1,3	1,3
Sr	143	285	340 290	420	350	337	220	445	420	433
Y	58	48,2	82	100	84—140	90,8	70,4	54	123	90,5
Zr	347	155	130	530	150	241	294	300	300	323
Nb	—	11,6	20,0	14	18	15,9	15,9	—	15	15
Mo	6	—	2,8 <5**	6,0	4,6	4,5	5,3	(1,2)	0,24	0,24
Ru	0,027	—	0,016	2,3	—	12	<0,10	6	—	—
Rh	0,0037	—	0,0039	0,57	—	<0,28	<0,15	—	—	—
Pd	0,01	—	0,04	1,5	—	0,76	<0,38	0,027	—	0,027
Ag	0,05	—	0,15**	1,3**	0,12	0,52	0,28	(0,2)	0,053	0,053
Cd	1	—	0,1	0,48 0,8** 0,3	—	0,52	0,52	—	0,075	0,075
In	0,06	0,002	—	0,16	0,057	0,07	0,07	—	0,012	0,012
Sn	1,6	—	2,4 <5**	7,8	3	4,4	3,0	4	0,52	2,3
Sb	0,4	—	1,0	2,2	0,6	1,3	0,85	0,5	0,2	0,35
Te	0,18	0,002	0,18	0,97	—	<0,3	—	—	—	—
I	0,2	—	0,1	0,16	—	0,13	0,14	—	—	—
Cs	<0,1	—	0,04	0,12	0,046	0,07	~0,09	0,75	<2,4	—
Ba	114	224	251	250	200	246	185	206	270	238
La	—	13 12** 15,4**	13	13	14	13,4	—	—	11	—

TABLE 3. CONTENT OF TRACE ELEMENTS IN REGOLITH AND PARTICLES OF LUNA 16 BASALT (IN PPM) /CONCLUSION/ /271

Element	Regolith					Basalt				
	mean of series I samples, see preliminary data /6/	A	B	V	G	mean of series II samples	total mean for series I and II samples	sample I, preliminary data /6/	sample II	mean composition of basalt from series I and II
Ce	—	44 35[6] 45[7]	43	31	46	40,8	—	—	45	—
Pr	—	8,8 5,5[7]	8,2	8,4	12	8,6	—	—	10	—
Nd	—	36,2 25[6] 32[7]	35	45	41	35,7	—	—	32	—
Sm	—	10,3 6[6] 12,5[7]	9,8	12	12	15	—	—	9,7	—
Eu	—	2,5 1,9[6] 2,9[7]	2,5	2,57	2,2	2,23	—	—	2,2	—
Gd	—	9,6 8—3[6]	10	7,3	15	10,0	—	—	11	—
Tb	—	1,5 1,3[6]	0,85	1,76	1,7	1,21	—	—	0,85	—
Dy	—	13,3 9,1[6] 15,3[7]	13	10,8	14	12,5	—	—	12	—
Ho	—	2,6 1,9[6]	3	2,55	3,9	2,8	—	—	2,8	—
Er	—	5,9 4,5[6] 5,6[7]	6,6	6,18	6,2	5,8	—	—	9,6	—
Tm	—	1,3 0,71[6] 0,51[7]	0,85	1,57	0,88	0,97	—	—	0,9	—
Yb	—	5,2 4,1[6] 7,4[7]	5,4	8,1	5,3	5,9	—	—	6,2	—
Lu	—	1,4 0,6[6] 1,1[7]	1,2	1,43	1,17	1,1	—	—	1,3	—
Hf	1,7	6,4 7[6]	6,5	11	7,9	7,8	—	0,3	9,0	—
W	—	(6)	—	—	(36)	(27)	—	(9)	—	—
Os	—	—	0,03	—	—	0,03	—	—	—	—
Ir	—	0,009	0,003	—	—	0,0012	—	—	—	—
Pt	—	0,05	0,05	—	—	0,05	—	—	—	—
Au	0,002	—	—	—	—	—	0,002	—	—	—
Hg	—	0,06[8]	0,22[8]	0,09[8]	—	0,12	0,14	—	—	—
Tl	(<0,2)	0,0013[8]	—	0,0036[8]	0,0031	0,0027	—	—	—	—
Pb	6	2,9	1,4 2,3[6]	1,4 3,1[6]	0,82 2,6[6]	2,7	(4)	(7,7)	0,33	—
Bi	—	0,006	—	0,45	—	0,2	—	—	—	—
Th	—	0,8[6]	—	—	—	0,8	0,8	—	—	—
U	—	0,25[6]	—	—	—	0,25	0,25	—	—	—

[Footnotes to Table 3 on following page.]

/Footnotes to Table 3 on preceding page./

* Mass-spectral data

2* Atomic-fluorescent method /5/

3* Atomic-absorption method /3/

4* gamma-Spectrometric method

5* Flame photometry

6* Spectral-emission method. TR determined after their segregation /39/. Be was determined with a direct-current arc.

7* Neutron-activation method

mare basalts is much below their content in mean regolith (even in the silicate phase). In exactly the same way, the content of Cu, Zn, Mo, and Sn in basalts is lower than their mean for chondrites. The content of Mn and V remains equal to their content in chondrites, just like the Cr content in lunar basalts is not less than its high content in chondrites, that is, considerably higher than the Cr content in terrestrial basalts by tenfold. /275

We can note a general regularity -- a decrease in the content of Fe family elements in regolith compared with basalts. This pertains not only to Fe, Cr, and Ti, but also to V and Mn. There are not enough data for Sn, W, and Mo. As for Ni, as well as elements accumulating in the iron phase of meteorites: Ga, As, Sn, Ge, Co, Sb, Cu, as well as Au and all the platinoids, we can state confidently that their relative accumulation in regolith is associated, as we now see, with the influx into the lunar regolith (but not into the monolithic rocks) of meteoritic materials from without, chiefly the iron phase of meteorites.

Platinoids and gold. The content of the platinoids Ru, Pd, Rh, Ir, Os, Pt, and Au in meteorites is of the order of $n \cdot 10^{-4}$ to $n \cdot 10^{-5}$ percent. It is well known that they are concentrated in the iron phase of meteorites. In terrestrial basalts the content of platinoids and Au is considerably less -- of the order of $n \cdot 10^{-6}$ to $n \cdot 10^{-7}$ percent. While lunar basalts do not show appreciable deviations in the content of platinoids and Au from the content in terrestrial basalts, mare regolith shows their clearly high content, approximating in order of magnitude the content of platinoids and Au in chondrites. Along with the high content of Ni in regolith, the high content of platinoids and Au is a direct indication that all these elements were brought in as meteoritic material striking the Moon /10/. In this respect, we need a more precise determination in basalts, and in turn, in the regoliths syngenetic to them, of elements typical of the iron phase of meteorites, namely: Ga, Ge, As, Sn, and Sb.

TABLE 4. CONTENT OF TRACE ELEMENTS IN LUNA 16 REGOLITH BASED ON DATA OF OTHER INVESTIGATORS (IN PPM)

Element	Regolith													Basalt			
	our data	Albee et al. [2]	Poupeau et al. [32]	Philphots et al. [23] A	Philphots et al. [23] G	Hubbard et al. [25] 125-145 μm A	Hubbard et al. [25] 125-145 μm G	Gillum et al. [12]	Helmke and Haskin [24] V	Jerome et al. [11]	Laul et al. [14] A	Laul et al. [14] G	Eigster [27]	Allegre et al. [1]	our data	Helmke and Haskin [24] A	Helmke and Haskin [24] V
Li	10,8	8,5	10	8,38	8,34												
Be	2,5																
B	4,4		2,6												3,9		
F	200														128		
Cl	42														29		
Sc	37,2							54	50	50,2					31,5	28	54
V	67,5							78		97					43,8		
Co	41							37	27	30,9	30	27			21,7	21	14
Ni	171										133	132			113		
Cu	37										12,7	10,5			19		
Zn	33,4										24	29			23,5		
Ga	4,5								7		3,5	3,5			3,2	4,3	3,6
Ge	1,25											1,3			1,8		
As	0,41														~1,5		
Se	0,38										0,34	0,37			0,4		
Br	0,5										0,72	0,15			0,8		
Rb	1,9	1,79		1,85	1,80	1,84	1,91				1,5	1,9		2,45	1,9		
Sr	220	271		244	271	279	303							284	433		
Y	70,4														90,5		
Zr	294			224	227										203		
Nb	15,9														15		
Mo	5,3									5					0,54		
Ru	<0,1																
Rh	<0,15																
Pd	0,38														0,027		
Ag	0,28										1,34	0,54			0,053		
Cd	0,52										0,2	10,9			0,075		
In	1,7										0,003	0,0019			0,012		
Sn	3,0														2,3		
Sb	0,85										0,0033	0,0042			0,36		
Te	<0,3										0,04	0,028					
I	0,14																
Cs	~0,09	0,085									0,068	0,082			<2,4		
Ba	185	168,4		169	172	166	176		203	360				266	238	203	247
La	13,4					11,2		12	12,7	10,7					11	12,0	19,4
Ce	40,8			31,2	37,5	33,8	33,5		43	37,2				46	45	10	66
Pr	8,6														10		
Nd	28,7			28,4	28,3	25,8	27,1			24,7				42,2	32		
Sm	15			7,98	8,18	7,75	8,15	8,8	9,6	7,20				10,5	9,7	8,1	16
Eu	2,2			2,16	2,22	2,15	2,34	2,3	2,87	2,15				2,4	2,2	2,04	4,04
Gd	10,0			10,5	10,5		10,4		12	10				13,5	11		17
Tb	1,2								1,9	1,44					0,85		3,1
Dy	12,5			10,1	10,4	10,5	10,8		13,5					12,7	12	8,8	17,9
Ho	2,8								3,1	2,4					2,6	2,1	3,9
Er	5,8			5,78	5,87	5,87				6,75				8,62	9,6		12
Tm	0,97									0,75					0,9		
Yb	5,9			5,65	5,44	5,74	5,26	6,3	6,2	5,23				6,2	6,2	5,2	10,9
Lu	1,1			0,82	0,84			0,93		0,78				0,92	1,3	0,89	1,51
Hf	7,8				5,88				13	6,15						0,46	1,3
W	(27)									17							
Os	0,03																
Ir	0,0012										96	93					
Pt	0,05																
Au	0,002									0,0017	0,0027	0,0026					
Hg	0,14																
Tl	0,027										0,0014	0,0019					
Pb	(~4)														0,33		
Bi	<0,2										0,0048	0,0051					
Th	0,8									1,06							
U	0,25	0,338				0,38	0,39										
Re	—	—									0,0037	0,0034					

TABLE 5. COMPARISON OF THE CONTENT OF MAJOR AND TRACE ELEMENTS IN ROCKS AND REGOLITH OF APOLLO 11 AND 12, AND LUNA 16

Component	Crystalline rocks (basalt)					Regolith		
	Apollo 11		Apollo 12					
	type A, 10057	type B, 10044	type I 12020	type II 12063	Luna 16 basalt	Apollo 11 10084	Apollo 12 12070	Luna 16
	In weight percent							
SiO_2	40.3	42.8	43.7	44.5	42.95	41.9	45.8	41.90
Al_2O_3	7.52	11.84	7.16	9.3	13.88	12.97	12.6	15.33
FeO	18.06	17.15	21.45	21.6	20.17	15.48	16.38	16.66
TiO_2	10.8	10.5	2.6	4.67	5.5	7.9	2.6	3.36
MgO	6.97	6.47	15.6	8.4	6.05	7.97	9.86	8.78
CaO	11.76	7.34	8.1	13.6	10.8	11.34	10.64	12.53
Na_2O	0.40	0.48	0.17	0.30	0.23	0.42	0.42	0.34
K_2O	0.22	0.10	0.05	0.08	0.16	0.13	0.23	0.1
P_2O_5	—	—	0.038*	0.089*	0.14	—	0.32*	0.12
	In parts per million							
Li	14	—	(4.5)	5.2	—	10.4	12	10.8
Be	—	—	1.7	1.7	—	4*	—	2.5
B	0.8	1.2	(0.9)	5.2	3.9	1.03	2.3	4.4
F	—	—	113*		128	66*	152*	200
Cl	12	(12.2)	(17.8)	17.2	29	350*	24.4	42
S	—	—	896*	—	—	—	1020*	—
Sc	87	0.2	45.2	62.9	31.5	61	37.3	37.2
V	49**	75**	148	160	43.8	63**	96*	67.5
Mn	1800	2000	2170	2200	—	1560	1500	—
Cr	2160	1300	4560	2580	—	1830	2270	—
Co	25.4	11.0	61	39.1	21.7	27.2	41.5	41
Ni	<10	—	67*	48	113	280	200	171
Cu	4.3	4.2	6.9	12.9	19	8.2	7.2	37
Zn	2.9*	—	3.5*	3.2*	23.5	22*	8.2*	33.4
Ga	5.2	5.1	(3.2)	5.3	3.2	4.9	3.3	4.5
Ge	<1	<1	(100)	100	1.8	1.4	210	1.25
As	0.04*	—	(10)	53	~1.5	0.07	22	0.41
Se	(0.4)*	—	—	—	0.4	0.2*	—	0.36
Br	0.1*	(0.2)*	0.08*	0.1*	0.8	0.2*	0.2*	0.5
Rb	5.2	5.1	1.5	1.1	1.9	3.0	8.7	1.9
Sr	100	(151)	(96)	130	433	176	140	220
Y	210*	(150)*	52*	50*	90.5	150*	135*	70.4
Zr	1200**	520**	130	115*	323	300**	480*	294
Nb	42*	47*	95*	13*	15	33*	—	15.9
Mo	0.4*	(0.4)*	0.6*	0.5*	0.24	0.7*	0.45*	5.3
Ru	—	—	—	—	—	—	—	<0.1
Rh	—	—	—	—	—	—	—	<0.15
Pd	0.01	0.2	0.003	<0.001	0.027	0.012	0.0065	<0.38
Ag	0.04*	0.07*	—	—	0.053	0.1*	—	<0.28
Cd	0.9*	(0.7)*	—	—	0.075	0.3*	—	0.52
In	0.0027	0.0032	1.9	0.0023	0.012	0.75	0.486	1.7
Sn	0.6*	(1.2)*	—	—	2.3	0.7*	—	3.0
Sb	0.005*	0.01*	—	0.04*	0.35	0.005*	0.04*	0.85

/274

TABLE 5. COMPARISON OF THE CONTENT OF MAJOR AND TRACE ELEMENTS IN ROCKS AND REGOLITH OF APOLLO 11 AND 12, AND LUNA 16 /CONCLUSION/

Component	Crystalline rocks (basalt)					Regolith		
	Apollo 11		Apollo 12					
	type A, 10057	type B, 10044	type I 12020	type II 12063	Luna 16 basalt	Apollo 11 10084	Apollo 12 12070	Luna 16
Te	—	—	—	—	—	—	—	—
I	—	—	—	—	—	—	—	0,14
Cs	0,20	(0,12)	(90)	0,08	<2,4	0,12	0,390	~0,09
Ba	208	214	(84)	140	238	176	390	185
La	25	12	4,82	6,88	11	15	33,0	13,4
Ce	79	44	(21)	19	45	47	86	40,8
Pr	9	(7,3)	(1,75)	3,1	10	5	10,6	8,6
Nd	60	50	(14,7)	—	32	47	(72)	35,7
Sm	20	17,9	3,4	6,6	9,7	12,1	14,7	15
Eu	1,8	2,69	0,82	1,62	2,2	1,67	1,8	2,23
Gd	30	24,0	(4,7)	11,0	11	18	15,7	10,0
Tb	5,0	4,5	0,91	2,65	0,85	2,8	4,0	1,21
Dy	24	(19)	5,68	10,3	12	17	20,2	12,5
Ho	5,5	(3,8)	1,07	2,46	2,8	4,[illegible]	5,2	2,8
Er	16	(13)	(4,2)	7,35	9,6	9,5	15,8	5,8
Tm	2,3*	2*	0,66*	0,53*	0,9	1,2*	1,8*	0,97
Yb	16,8	15,0	2,91	5,71	1,2	8,3	10,6	5,9
Lu	2,15	1,96	0,42	0,84	1,3	1,30	1,52	1,1
Hf	16,9	12,0	3,8	6,3	—	10,2	15,6	7,8
W	0,43	0,24	(0,15)	0,14	—	0,22	0,74	—
Os	—	—	—	—	—	—	—	0,03
Ir	—	—	0,0005	0,0013	—	—	0,0075	0,0012
Pt	—	—	—	—	—	—	—	0,05
Au	0,0016	0,0019	0,0036	0,0029	—	0,0021	0,0018	0,002
Hg	—	—	0,006*	0,002*	—	—	0,0021*	0,14
Tl	—	—	—	—	—	—	—	0,0027
Pb	3*	3*	1,7*	0,4*	0,33	6*	2,6*	(~4)
Bi	—	—	—	—	—	—	—	<0,2
Th	3,94	0,98	0,71	0,82	—	1,61	5,52	0,80
U	0,80	0,28	(0,25)	0,236	—	0,35	1,69	0,25
Ta	2,0	2,0	0,45	0,47	—	1,3	1,46	—

* Data of Morrison (see /30, 31/).

** Data of Wakita (see /35, 36/).

Easily vaporized rare metals In, Tl, Pb, Hg, and Bi. Perhaps, here the most reliable figures are those for Pb. They agree with the data for terrestrial basalts, of the order of $n \cdot 10^{-4}$ percent. As for the content of In, Tl, Bi, and Hg, we know that their content in terrestrial rocks and meteorites is of the order of $n \cdot 10^{-5}$ to $n \cdot 10^{-7}$ percent and fluctuate widely. From the data that we know

for terrestrial regolith, the order of the content of Tl, In, and Bi is $n \cdot 10^{-7}$ percent. However, sharp changes are observed in the content of these elements in the same material [30, 31, 33-35, 37, 38]. When a systematic investigation was made of the content of mercury in conditions excluding its contamination of preparations [5], it proved to be of the order of $n \cdot 10^{-6}$ percent (see Table 3).

Main findings and conclusion. The regolith of mare provinces is a mixture of material of diverse origins. Sources of the material of the mare regolith are principally the basalts of the corresponding lunar lava maria. Regolith is genetically associated with them. This follows from a comparison of the composition and the mineralogic and petrochemical features of basalts and regolith from the Sea of Fertility, Sea of Tranquillity, and Ocean of Storms, respectively. An example can be taken as the distribution therein, in the basalts-regolith system, of Fe, Ti, Al, and other major elements, and even trace elements. In composition and mode of formation, monolithic rocks and regolith in each of these three maria, in spite of the presence of a series of types, are to some extent uniform and characterize individual geological mare provinces.

A secondary source of regolith material above all is the influx into the region of the maria of highland material differing widely from the mare by the nature of the regolith and by its high content of feldspar material, in particular, anorthosite. The effect on the composition of the mare regolith of highland material is not difficult to state. However, the content of anorthosite in the mare regolith is not high, 3-5 percent. Data obtained from material returned by Luna 20 show that the highland provinces where the sample was taken by this station contain 40-60 percent anorthositic rocks, while several kilometers away along the coast of the Sea of Fertility the regolith contains only about 3 percent anorthosite. This indicates that the highland material, just like the mare, was mixed only slightly and that the transport of this material did not occur over considerable distances. We can draw a boundary line to the distribution between the mare and highland regolith.

Next in importance in the material of mare regolith is meteoritic material. Calculations show (see [6]) that this share is about 2.5 percent of the regolith material. Other investigators give approximately the same estimates [37]. Gabbro and basalts of the mare type are highly enriched, as we have seen, above all in iron and titanium, and contain chromium in amounts that are customary for chondrites, and so on. A comparison of their composition with terrestrial primitive basalts indicates their high content in mafic elements and the absence of signs of enrichment with volatile materials. H_2 was found in the vacuoles of Luna 16 lunar rocks, indicating the presence of some amounts of volatiles and H_2O, in

particular, evidently rapidly lost thereupon on the lunar surface. All this indicates that differentiation of the material of the /276
mare rocks during melting of the basalt and gabbro occurred at high temperatures, during a short time, and not deeply. The chemical composition of the regolith differs markedly from the composition of the mare basalts syngenetic to it. During the formation of the regolith a process of further differentiation of the material of the mare basalts also occurred. The content of the mafic elements -- iron, magnesium, and also titanium, chromium, and several others -- was considerably reduced, while the typically lithophilic elements of Al and Ca and many others, principally trace elements, showed a clear tendency toward increased content in the regolith. This can be seen not only from the Luna 16 material, but the same tendency was noted also in the regolith material from Apollo 11 and Apollo 12 /33, 34/.

Here we should note that the breccias and microbreccias in the materials of Apollo 11, Apollo 12, and Luna 16 are also very similar in composition to the regolith, by which they differ markedly from the composition of the monolithic rocks. When discussing the question of their origin, often it is assumed that they were formed from the regolith. However, the differentiation of the composition of the monolithic rocks forming the regolith is much more complicated. We indicated the distinction in this sense between the regolith as a whole and the monolithic rocks. But if we were to examine the chemical composition of individual portions, we would see that this differentiation, as has been shown many times, has a more profound nature. It suffices to direct attention to the composition of glasses and spheroids from the regolith to note the vast diversity of their composition. The view is held that individual particles (monominerals and so on) were subjected to melting during the time of regolith formation and that this accounts for the considerable difference in composition.

The process of lunar regolith formation is not very clear. The predominant interpretation of most authors leads them to state that the only process was collision with infalling meteoritic particles. However, it may be that there are other possible explanations /9/.

Finally, we should state that continuous galactic irradiation and the solar wind doubtless produced in the regolith particles stresses affecting their physicochemical composition and, possibly, brought in some fraction of the material, which today it is difficult to determine.

REFERENCES

1. Allegre, K., Burke, J. A., Lube, M., and Provo, A., "Rubidium and Strontium-Based Age: Content of Potassium, Rubidium, Strontium, Barium, and Rare Earths in Surface Material of the Sea of Fertility (Moon) Returned by the Luna 16 Soviet Automatic Station," present collection, p. 468.

2. Albee, A. L., Chodos, A. A., Hankarts, A. I., Heynes, Ye. I., Papanastascu, D. A., Ray, L., Tera, F., Wasserburg, G. D., and Wen, T., "Mineralogy, Petrology, and Chemistry of a Luna 16 Basaltic Fragment, Sample B-1," present collection, p. 163.

3. Belyayev, Yu. I., Zvereva, N. F., and Kostin, B. I., "Atomic-Absorption Determination of Traces of Elements in Rocks, Using Pulsed Thermal Atomization of Solid Samples, Report 1, Determination of Cadmium," Zh. anal. khimii 26(3), 492 (1971).

4. Belyayev, Yu. I., and Khitrov, L. M., "Using Quantometers in Analyzing Geological Materials," Zh. anal. khimii 1º(3), 310 (1963).

5. Belyayev, Yu. I., and Koveshnikova, T. A., "Mercury Content in the Regolith of the Sea of Fertility, Sea of Tranquillity, and Ocean of Storms," present collection, p. 335.

6. Vinogradov, A. P., "Preliminary Data on Lunar Surface Material Returned by Luna 16 Automatic Station," present collection, p. 7.

7. Vinogradov, A. P., "Mean Content of Chemical Elements in Principal Types of Igneous Rocks of the Earth's Core," Geokhimiya (7), 555 (1962).

8. Vinogradov, A. P., Nefedov, V. I., Urusov, V. S., and Zhavoronkov, N. M., "X-Ray Electron Study of Lunar Regolith from the Sea of Fertility and the Sea of Tranquillity," present collection, p. 319.

9. Vinogradov, A. P., "On the Genesis of the Regolith," present collection, p. 348.

10. Vinogradov, A. P., "High-Temperature Protoplanetary Processes," Geokhimiya (11), 1283 (1971).

11. Jerome, D. Y., Filippo, J., and Brichet, E., "Determination of 29 Elements in Luna 16 Soil by Nondestructive Activation Analysis," present collection, p. 278.

12. Gillum, D. E., Eman, W. D., Wakita, H., and Schmitt, R. A., "Bulk and Rare Earth Abundances in Luna 16 Soil Levels A and D," present collection, p. 299.

13. Il'in, N. P., Loseva, L. Ye., and Senin, V. G., "X-Ray Electron Microanalysis of Composition of Individual Particles of Lunar Regolith," present collection, p. 209.

14. Laul, J. C., Ganapathy, R., Morgan, J. W., and Anders, Ye., "Meteoritic and Nonmeteoritic Trace Elements in Luna 16 Samples," present collection, p. 290.

15. Laktionova, N. V., Ageyeva, L. V., and Simonova, L. V., "Quantometric Method of Determining Ni, Co, Cr, V, and Cu in Geological Materials," Zh. anal. khimii 26, 554 (1971).

16. Lebedev, V. I., "Enhancing the Sensitivity of Flame Determination of Elements," Zh. anal. khimii 16(2), 124 (1961).

17. Makarov, Ye. S., Ivanov, V. I., Makheyeva, V. I., Tobelko, K. I., Bukin, V. I., Volkova, A. Ya., Kuznetsova, G. A., and Kuznetsov, L. M., "X-Ray Diffraction Analysis of Minerals in Lunar Regolith Returned by Luna 16 Automatic Station," present collection, p. 148. /277

18. Pavlenko, L. I., Simonova, L. V., and Karyakin, A. V., "Determination of Cu, Sc, Mo, Sn, Pb, and Iron-Group Elements in Lunar Surface Material and in Basic and Ultrabasic Rocks of the East African Rift," present collection, p. 339.

19. Savinova, Ye. N., Karyakin, A. V., and Andreyeva, T. P., "Spectral Method of Determining Fluorine, Phosphorus, Sulfur, Boron, and Beryllium in Lunar Surface Material," present collection, p. 344.

20. Stakheyev, Yu. I., Vul'fson, Ye. K., Ivanov, A. V., and Florenskiy, K. P., "Granulometric Characteristics of Sea of Fertility Lunar Surface Material," present collection, p. 205.

21. Steele, I. M., and Smith, J. V., "Mineral and Bulk Compositions of Three Fragments from Luna 16," present collection, p. 205.

22. Surkov, Yu. A., Fedoseyev, G. A., Sobornov, O. P., Nazarkina, G. B., and Bachina, L. P., "Gamma-Spectrometric Analysis of Sample of Lunar Surface Material Returned by Luna 16 Automatic Station," present collection, p. 417.

23. Philpotts, J. A., Schnetzler, K. K., Bottino, M. L., Schumann, S., and Tomas, H. H., "Luna 16: Some Li, K, Rb, Sr, Ba, Rare-Earth, Zr, and Hf Concentrations," present collection, p. 312.

24. Helmke, P. A., and Haskin, L. A., "Rare Earths and Other Trace Elements in Luna 16 Soil," present collection, p. 304.

25. Hubbard, N. J., Nyquist, L. Ye., Rode, J. M., Banzal, B. M., and Vishmani, H., "Chemical Features of the Luna 16 Regolith Sample," present collection, p. 306.

26. Chupakhin, M. S., and Polyakov, A. L., "Method of Mass-Spectrometric Elemental Analysis of Geological Samples, Meteoritic Material, and Samples of Lunar Surface Material," Zh. anal. khimii 27(3), 523 (1972).

27. Eygster, O., "Content of Lithium, Barium, Boron, and Titanium, and the Isotopic Composition of Lithium, Boron, and Magnesium," present collection, p. 370.

28. Bence, A. E., and Albee, A. L., "Empirical Correction Factors for the Electron Microanalysis of Silicates and Oxides," J. Geol., 76, 382 (1968).

29. Gast, P. W., Hubbard, N. J., and Wiesmann, H., "Chemical Composition and Petrogenesis of Basalts from Tranquillity Base," Proc. Apollo 11 Lunar Sci. Conf., 2, 1143 (1970).

30. Morrison, G., Jesse, T., Gerard, T., et al., "Elemental Abundance of Lunar Soil and Rocks," Proc. Apollo 11 Lunar Sci. Conf., 2, 1383 (1970).

31. Morrison, G., Gerard, J., Potter, N., Gangadharam, E., Rottenberg, A., and Burdo, R., "Elemental Abundance of Lunar Soil and Rocks from Apollo 12," Proc. Second Lunar Sci. Conf., 2, 1169 (1971).

32. Poupeau, G., Berdt, G., and Pellas, P., "Lunar Regolith's Tribulations Since September 19, 1969," Third Lunar Sci. Conf., Abstracts, 1972, p. 539.

33. Proc. Second Lunar Sci. Conf., 1, 2, 3, (1971).

34. Proc. Apollo 11 Lunar Sci. Conf., 1, 2, 3, (1970).

35. Wakita, H., Schmitt, R., and Rey, P., "Elemental Abundance of Major, Minor, and Trace Elements in Apollo 11 Lunar Rocks, Soil, and Cores Sample, Proc. Apollo 11 Lunar Sci. Conf., 2, 1685 (1970).

36. Wakita, H., Rey, P., and Schmitt, R., "Abundance of the 14 Rare-Earth Elements and 12 Other Trace Elements," Proc. Second Lunar Sci. Conf., 2 1321 (1971).

37. Wanke, H., Roeder, R., Baddenhausen, Spettel, B., Teschke, F., Quijano-Rico, M., and Balacescu, A., "Major and Trace Elements in Lunar Material," Proc. Apollo 11 Lunar Sci. Conf., 2, 1719 (1970).

38. Wanke, H., Wlotzka, F., Baddenhausen, H., Belacescu, Spettel, B., Teschke, F., Jagots, E., Kruse, H., Quijano-Rico, M., and Roeder, R., "Apollo 12 Samples: Chemical Composition," Proc. Second Lunar Sci. Conf., 2, 1187 (1971).

39. Stroganova, N. S., Ryabukhin, V. A., Laktionova, N. V., et al., "Chemical-Spectral Determination of Rare-Earth Elements in the Regolith of the Luna 16 Sample," present collection, p. 294.

Order of Lenin, Institute of Geochemistry and Analytical Chemistry imeni V. I. Vernadskiy, USSR Academy of Sciences, Moscow

N75 11832

NEUTRON ACTIVATION STUDY OF THE COMPOSITION OF LUNAR SURFACE MATERIAL FROM THE SEA OF FERTILITY

/283

Yu. A. Surkov, F. F. Kirnozov, I. N. Ivanov,
G. M. Kilesov, B. N. Ryvkin, and A. P. Shpanov

Abstract

The elemental composition of samples of lunar regolith returned by Luna 16 from the Sea of Fertility was determined by a radio-activation method using generator and reactor neutrons, and also by gamma-spectrometry with scintillation and Ge(Li) detectors.

This paper presents the results of a determination of the elemental composition of samples of lunar surface material returned by Luna 16 from the Sea of Fertility. The results were obtained by the instrumental neutron activation technique of analysis, and also by chemical decomposition of the sample.

Samples for the investigation were taken from the uppermost part of the core (zone A) and represent the lunar regolith; its properties, compositions, and origin are intimately associated with the history of the lunar surface.

Irradiation of samples intended for investigation by the instrumental technique was carried out in three regimes: 1) with fast generator neutrons in a flux from 10^8 to 10^{10} neutrons/sec; with fast reactor neutrons for 0.5 hour in a flux of 10^{12} neutrons$\cdot\cdot cm^{-2}\cdot sec^{-1}$; and 3) with thermal reactor neutrons for 72 hours in a flux of $4\cdot10^{13}$ neutrons$\cdot cm^{-2}\cdot sec^{-1}$. The samples subjected to chemical decomposition were irradiated with thermal reactor neutrons for 20 hours in a flux of $1.2\cdot10^{13}$ neutrons$\cdot cm^{-2}\cdot sec^{-1}$.

Two samples weighing 61.4 mg (No. 101) and 89.8 mg (No. 102) were prepared for the determination of the main rock-forming elements. The oxygen content was determined with a specialized device incorporating a generator of 14 Mev neutrons in a sealed tube of model NGI-5, with a yield of $5 \cdot 10^8$ neutrons/sec. The silicon and aluminum were determined in a unit with evacuated generator, whose integral yield was 10^{10} neutrons/sec. The determinations were made by the relative method with comparison based on reference standards. The induced activity was measured with a scintillation gamma-spectrometer. The results are in Table 1.

To carry out the analysis of another group of elements (see Table 1), three samples each weighing about 25, 75, and 115 mg were prepared and irradiated in the reactor; here the effect of self-screening and self-absorption of the samples can be neglected. For the case of short irradiation, as well as for irradiation in the generator, the samples were sealed into polyethylene packages 15 mm in diameter. For prolonged irradiation in a flux of $4 \cdot 10^{13}$ neutrons$\cdot cm^{-2} \cdot sec^{-1}$, the samples were placed in quartz ampules, and before measurement they were repackaged in unirradiated ampules in order to eliminate their background activity. Samples of standard rocks and reference standards were similarly prepared.

Measurement of the gamma-radiation of the activated samples and reference standards was carried out with a coaxial Ge(Li)-detector with a sensitive volume of 65 cm^3, and the signals from this unit were sent to a 4096-channel analyzer. The energy calibration of the spectrometer was carried out based on the reference standard sources and for known photopeaks in the spectrum of the sample gamma-radiation.

The conditions of the analysis were selected so that it was possible to determine with highest sensitivity the content of elements forming radioactive isotopes with half-lives ranging from several hours to several days.

The isotopes were identified mainly from the gamma-radiation energy. In cases when the gamma-radiation energy of the isotopes coincided or differed by an amount that was smaller than the spectrometer resolution, data from the half-life period or the gamma-radiation of another energy of the same isotope were used.

The activity of each sample and reference standard was measured/284 several times at time intervals that were optimal for each isotope. The abundance of the elements in the samples was determined by the ratio of the photopeak area in the sample to the photopeak area in the reference standard, with allowance for the exposure time

and the duration of measurement, and also the weight of the sample and reference standard. The photopeak areas were calculated with an electronic computer.

Standard rocks with known compositions were used as reference standards for several elements. The abundances of elements for which there were no reference standards were computed by the absolute method. The curve of the relative photoefficiency was plotted from the results of measuring the activity of the standards irradiated simultaneously with the samples, and the slope of this curve was verified from measurements of the International Atomic Energy Agency calibration sources. Thus, for example, the content in the sample of europium, tungsten, ytterbium, samarium, and lutetium. The background for natural radioactivity as well as due to activation of the polyethylene package when the analysis was done by the instrumental technique was less than 0.5 percent of the measured activity of the samples. /285

TABLE 1. CONTENT OF PRIMARY ROCK-FORMING ELEMENTS IN LUNAR ROCK (IRRADIATION IN GENERATOR)

Sample number	Content, percent		
	O	Si	Al
101	41.7±0.3	21.0±2.0	5.9±0.6
102	41.1±0.2	20.6±2.0	6.5±0.6

The results of analyzing the lunar rock samples are in Table 2. /286

In order to increase the sensitivity and reliability of determining the content of rare-earth elements (r.e.e.) in lunar rocks, the chemical decomposition of the sample was used, with the total r.e.e. separated. Samples weighing 8 and 16 mg were used in the analysis. The preparation and irradiation of the samples was carried out as in the analysis by the instrumental technique, with long exposure times. Simultaneously with the lunar rocks, samples of BDR-1 basalt and a mixture of titrated solutions with a content of $(0.1\text{-}5)\cdot10^{-6}$ g of each rare-earth element were irradiated. The decomposition of the irradiated sample was conducted by fusion with sodium peroxide and leaching of the melt with hydrochloric acid. The rare-earth elements were then separated by successive precipitation in the form of hydroxides and fluorides.

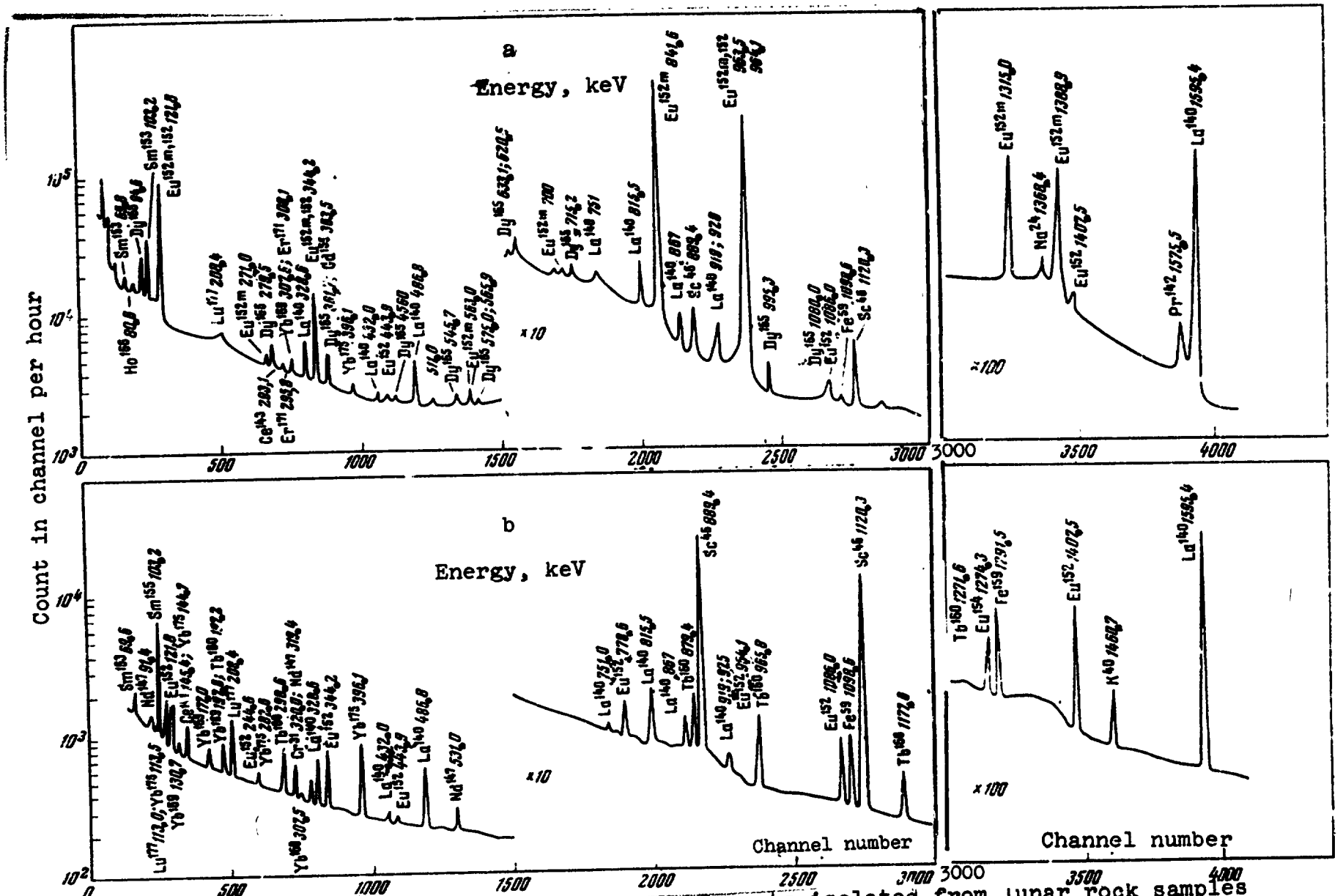

Fig. 1. Gamma-radiation spectra of rare-earth elements isolated from lunar rock samples irradiated with reactor neutrons

a. t_{ir} = 20 hours; t_{exp} = 8 hours; b. t_{exp} = 180 hours

TABLE 2. CONTENT OF SEVERAL ELEMENTS IN LUNAR ROCK DETERMINED BY INSTRUMENTAL NEUTRON ACTIVATION (IN REACTOR IRRADIATION) [1]

Element	Content, 10^{-6} g/g	Element	Content, 10^{-6} g/g
Na	0.30±0.03 (%)	La	10.7±1.2
K	0.10±0.01 (%)	Sm	5.7±0.5
Sc	49±1	Eu	2.5+0.5
Cr	2160±100	Yb	14±2
Mn	0.18±0.01 (%)	Lu	0.9±0.2
Fe	12.0±0.5	Hf	7±1
Co	34±4	W	97±5*

* The increased content is probably associated with external contamination of the sample.

TABLE 3. CONTENT OF RARE-EARTH ELEMENTS IN SAMPLES OF BCR-1 BASALT AND LUNAR ROCK (OBTAINED FROM THE CHEMICAL DECOMPOSITION OF SAMPLES AND THE SEPARATION OF THE TOTAL RARE-EARTH ELEMENTS)

Rare-earth elements	Content, 10^{-6} g/g	
	BCR-1	Luna 16 regolith
La	28±3	12±3
Ce	45±5	35±5
Pr	6.3±0.7	5.5±0.6
Nd	34±4	25±3
Sm	6.4±0.4	6.6±0.5
Eu	2.0±0.1	1.90±0.05
Gd	7.9±0.8	8.3±0.8
Tb	1.2±0.1	1.3±0.2
Dy	6.3±0.6	9.1±0.6
Ho	1.4±0.2	1.9±0.2
Er	3.7±0.5	4.5±0.3
Tm	0.57±0.15	0.71±0.1
Yb	3.1±0.1	4.1±0.3
Lu	0.56±0.05	0.63±0.1

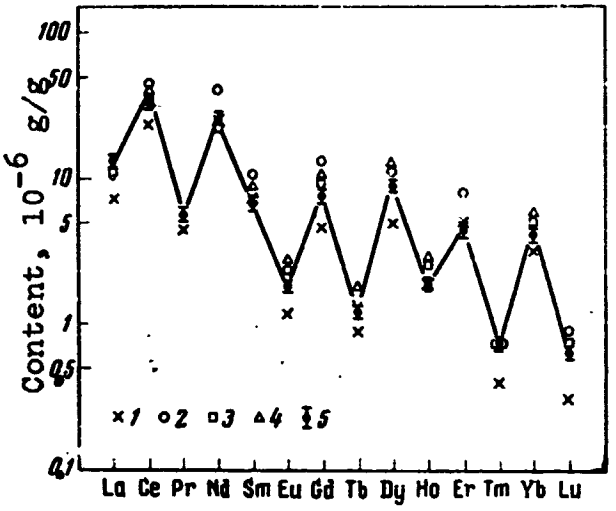

Fig. 2. Distribution of rare-earth elements in lunar rock from data of various authors:
1. [2]; 2. [3]; 3. [4]
4. [5]; 5. Present study

The intensities and spectral composition of the gamma-radiation of the separated rare-earth elements was measured also with a gamma-spectrometer incorporating a Ge(Li)-detector (see Fig. 1). The technique of interpreting the recorded gamma-spectra was the same as in the instrumental method of analysis.

These data on the rare-earth element content in the samples of lunar rock and in the international BCR-1 standard are in Table 3 and Fig. 2.

The data on the chemical composition of the samples of lunar rock returned by Luna 16 from the Sea of Fertility, given in Tables 1-3, agree with the results obtained later by other authors [2-5].

REFERENCES

1. Surkov, Yu. A., Shtan', A. S., Kirnozov, F. F., Moskaleva, L. P., and Ivanov, I. N., Paper Presented at the Fourteenth Session of COSPAR, U.S., Seattle, 1971.

2. Vinogradov, A. P., Geokhimiya (3), 261 (1971).

3. Allegre, C. J., Birck, J. L., Loubet, M., and Provost, A. C. R., Acad. Sci. Paris, 273 D, 779 (1971).

4. Jerome, D. Y., Philippot, J. C., and Brichet, E., "Earth Planet," Sci. Letters, 13(2), 436 (1972).

5. Helmke, P. A. and Haskin, L. A., "Earth Planet," Sci. Letters, 13(2), 441 (1972).

Order of Lenin Institute of Geochemistry and Analytical Chemistry imeni V. I. Vernadskiy, USSR Academy of Sciences, Moscow

N75 11833

NONDESTRUCTIVE ACTIVATION ANALYSIS OF SAMPLE OF LUNAR SURFACE MATERIAL RETURNED BY LUNA 16 AUTOMATIC STATION

/287

M. Chayko and E. Sabo

A study was made of the composition of a sample of lunar surface material returned by the Luna 16 automatic station from the Sea of Fertility, using nondestructive activation analysis. The structure of the returned surface material is inhomogeneous; the surficial material is thin, quite homogeneous, and the granularity increases with depth. Based on grain size, the sample was separated into five zones /1/. The activation analysis was conducted on a sample taken from the friable surficial layer, zone A.

The content of Al, Mn, Na, Cr, Co, Fe, and Sc was determined by nondestructive activation analysis of the sample. The sample was irradiated in an atomic reactor. Table 1 gives the nuclear reactions on the primary nuclear characteristics of the radioactive isotopes produced during the course of the reactions. The measurements were conducted differently for the two groups of elements. In determining Al, Mn, and Na, the sample was irradiated for a short time: 2 min. Al was measured immediately after irradiation, Mn -- after 1 hour, and Na -- after 10 hours. In determining Cr, Co, Fe, and Sc, the sample was irradiated for 24 hours and cooled for 10 days. The gamma-spectra of the samples were recorded with a semiconductor Ge(Li)-detector and a multichannel analyzer. The measurement data were processed with an electronic computer. To verify the precision of the method we use, simultaneously with the lunar surface material sample, we also irradiated and analyzed a reference standard of rock with known composition (a reference standard of basalt obtained from the Central Geological Institute, Berlin).

Experiments. The sample was placed in a dust-free chamber of plexiglas, where packing for activation was carried out.

Irradiation. The samples were irradiated in a TiIFI reactor of model VVRS in a neutron flux of 10^{13} neutrons·cm^{-2}·sec^{-1}. For the short (2 minutes) irradiation, the sample was packed in a bag of polyethylene foil, washed twice with distilled water. Then it was inserted into a polyethylene capsule for irradiation, which was transported into the reactor core and returned again to the laboratory by means of pneumatic transfer [rabbit]. For the more prolonged (24 hour) irradiation, the samples were placed in quartz weighing bottles. The weight of the samples subjected to short-term irradiation was 1-2 mg, while those used in measuring the isotopes with a long half life weighed 8-11 mg. /288

TABLE 1. PRINCIPAL NUCLEAR DATA OF ELEMENTS INVESTIGATED AND INTERFERING NUCLEAR REACTIONS

Element	Nuclear reaction	Half-life	E, KeV
Al	$^{27}Al(n,\gamma)^{28}Al$	2.3 mins	1.78
	$^{28}Si(n,p)^{28}Al$		
	$^{31}P(n,\alpha)^{28}Al$		
Mn	$^{55}Mn(n,\gamma)^{56}Mn$	2.56 hrs	0.84 (1.83)
	$^{56}Fe(n,p)^{56}Mn$		
	$^{59}Co(n,\alpha)^{56}Mn$		
Na	$^{23}Na(n,\gamma)^{24}Na$	15.0 hrs	1.38 (2.25 2.76)
	$^{24}Mg(n,p)^{24}Na$		
	$^{27}Al(n,\alpha)^{24}Na$		
Cr	$^{50}Cr(n,\gamma)^{51}Cr$	27.8 days	0.32
	$^{54}Fe(n,\alpha)^{51}Cr$		
Fe	$^{58}Fe(n,\gamma)^{59}Fe$	45.0 days	1.10 1.29
	$^{59}Co(n,p)^{59}Fe$		
	$^{62}Ni(n,\alpha)^{59}Fe$		
Sc	$^{45}Sc(n,\gamma)^{46}Sc$	84 days	0.89 1.12 (2.01)
	$^{46}Ti(n,p)^{46}Sc$		
	$^{59}Co(n,\gamma)^{60}Co$	5.2 yrs	1.17 1.33
	$^{60}Ni(n,p)^{60}Co$		
	$^{63}Cu(n,\alpha)^{60}Co$		

The reference standards were prepared from spectrally pure metals and salts of nitrates, analytically pure. The reference standards were irradiated together with a sample of lunar surface material and the reference basalt. For taking measurements involving short-lived isotopes, additional reference standards were also prepared, which were irradiated before and after irradiation of the samples.

To estimate the errors arising owing to the interfering nuclear reactions (Table 1), when the isotopes with short half-lives were measured, the sample and the reference standards were also irradiated when a Cd filter was in position. For a given elemental composition of the sample, no interfering effect that was noticeable under our conditions was found. In the case of isotopes with long half-lives, by calculations it was established that the effect of competing nuclear reactions does not increase the error of measurement.

Measurement of activity. For the case of isotopes with short half-lives, the sample was measured in the same sack in which it was irradiated. The purity of the foil was checked by a blank run; the activity measured during the course of this run showed virtually

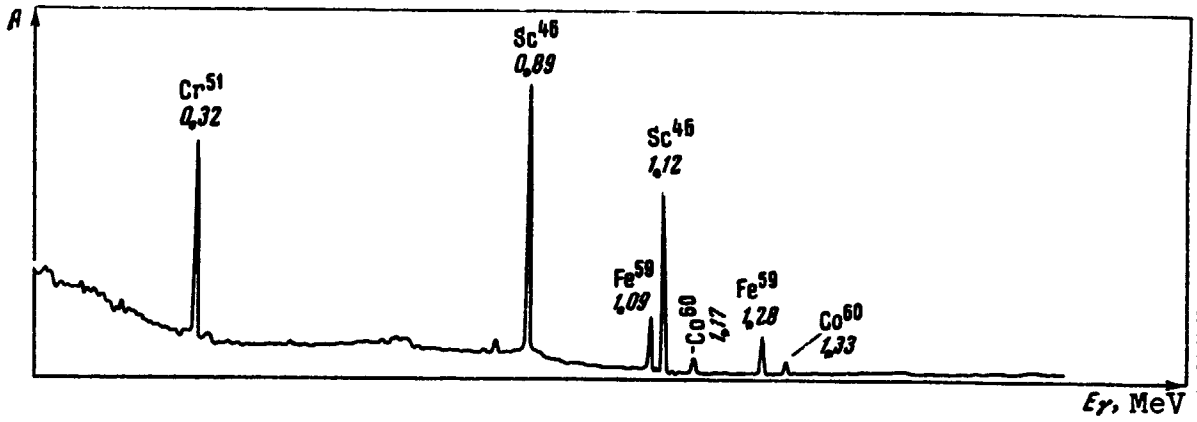

Fig. 1. Gamma-spectra after 10 days' decay of lunar surface material sample irradiated for 24 hours

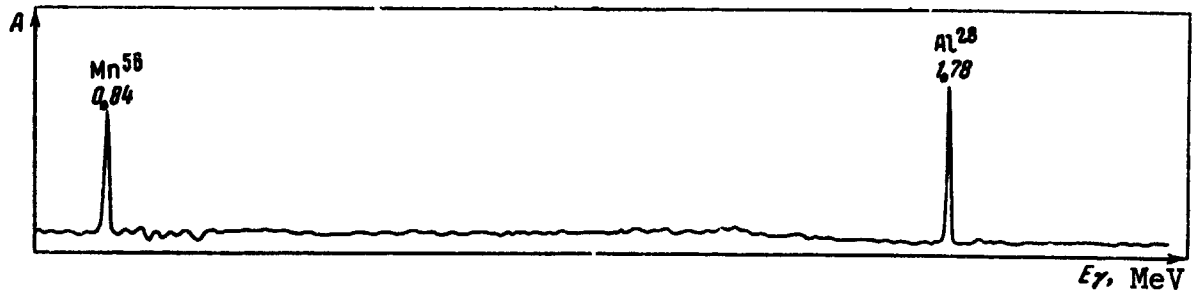

Fig. 2. Gamma-spectra after 2 minutes of cooling of sample of lunar surface material irradiated for 2 minutes

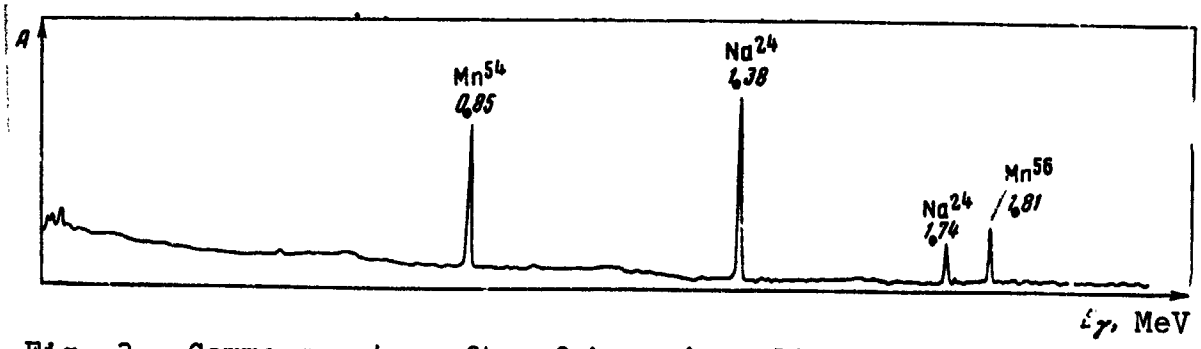

Fig. 3. Gamma-spectra after 2 hours' cooling of sample of lunar surface material irradiated for 2 minutes

no difference from the background. To measure isotopes with long /289
half-lives, the samples and the reference standards were transferred to inactive quartz weighing bottles of identical dimensions.

The gamma spectra were recorded with a semiconductor Ge(Li)-detector, with a volume of 45 cm^3 (model LGTC 5.0-3.5 built by Nuclear Diodes), and a model NTA-512-B 1024-channel analyzer. A pulsed generator was used for correction of dead time.

Figs. 1-3 give the gamma-spectra of the sample of lunar surface material.

Interpretation of data. When the gamma-spectra were interpreted, the peak areas were determined with an electronic computer; the program was developed by the Department of Computer Technology of the TiIFI /Central Institute for Physics Research/.

Results. The results of the analysis are in Table 2. The values presented there are means of three to five analyses. As the error in measuring the composition of the lunar surface material, we adopted the difference between the official and our values for the basalt reference standard. The scatter of individual measurements from the mean values for the basalt reference standard and for the lunar surface material was nearly identical: ± 15 percent; this means that no large inhomogeneity in the lunar surface material was found. The reason for further errors in the measurements can also be the fact that the isotopic composition of the lunar surface material differed from the terrestrial isotopic composition. However, we did not check this.

TABLE 2. RESULTS OF ANALYZING LUNAR SURFACE MATERIAL AND REFERENCE STANDARD (IN PERCENT)

Element	Lunar surface material	Basalt reference standards	
		our results	official values
Co	$3{,}25\cdot10^{-3}$	$3{,}6\cdot10^{-3}$	$3{,}4\cdot10^{-3}$
Cr	0,22	$1{,}07\cdot10^{-2}$	$1{,}23\cdot10^{-2}$
Fe_2O_3	20,4	9,3	9,8
Sc	$7{,}4\cdot10^{-3}$	$3{,}7\cdot10^{-3}$	$3{,}4\cdot10^{-3}$
MnO	0,22	0,15	0,15
Na_2O	0,38	4,5	4,4
AlO_2	15,3	—	—

REFERENCE

1. Vinogradov, A. P., "Preliminary Data on Lunar Surface Material Returned by Luna 16 Automatic Station," Geokhimiya (3), 261 (1971).

Central Institute for Physics Research, Academy of Sciences of the Hungarian People's Republic,
Budapest, Hungary

N75 11834

DETERMINATION OF RARE-EARTH ELEMENTS IN LUNA 16 REGOLITH SAMPLE BY CHEMICAL-SPECTRAL METHOD

/294

N. S. Stroganova, V. A. Ryabukhin, N. V. Laktinova, L. V. Ageyeva, I. P. Galkina, N. G. Gatinskaya, A. N Yermakov, and A. V. Karyakin

Abstract

An analysis was made of regolith from layer A of the Luna 16 sample for rare-earth elements, by a chemical-spectral method. Chemical and ion exchange concentration was used to determine the content of 12 elements and Y at the level 10^{-3} to 10^{-4} percent with 10-15 percent reproducibility of the emission determination. The results within the limits of reproducibility agree with the data obtained by mass spectra, activation, and X-ray fluorescent methods.

Rare-earth elements (r.e.e) in regolith of different layers of the core taken by the Luna 16 station from the surface of the Moon were determined by mass spectral [1-3], X-ray fluorescent [4], and activation [5-7] methods. This present article presents the results of an analysis of the regolith from layer A analyzed by a chemical-spectral method following a technique developed for the determination of r.e.e in basalt type rocks [8]. The method involves the chemical concentration of the r.e.e to a level of a content of the most of the r.e.e of $n \cdot 10^{-3}$ percent (the enrichment coefficient $\alpha \sim 50$) and their spectral emission determination in the concentrate.

After the chemical concentration of the r.e.e from 107 mg of a mixed regolith sample, the following operations were carried out. Alkaline cleavage of the rock and separation of silicic acid was carried out by the silicate analysis method. From the resulting hydrochloride solution, hydroxides were deposited with ammonia for the complete removal of the alkali and alkaline-earth elements. The filtered hydroxides were dissolved and washed

off the filter with a small volume of 4 N HCl, and the solution was evaporated to dryness. The residue was treated with 5 ml 0.04 N HCl; here the hydroxides of Ti and in part of Al remained as a floclike sediment, and the solution was transferred to a chromatographic column filled with KU-2 cation exchange resin in the hydrogen form. When the column was washed with 4 N HCl, 34 ml of the solution contained the basic amounts of Fe, Al, and Mg, and several other elements, and in the last 250 ml the r.e.e exited in the order from Lu to La. The solution was evaporated, and the from 0.1 N HCl the r.e.e were precipitated together with Ca (1.0 $\pm$ 0.1 mg CaO purified free of r.e.e) as oxalates. The filtered oxalates were calcined, and the concentration contained 2.8 mg with the approximate composition: 40 percent CaO, 50 percent Al_2O_3, and also Mg, Fe, Mn. The enrichment coefficient α = 38. When the samples were obtained in blank determinations, the same operations were carried out, beginning with the passage of 4 N HCl through the column.

The r.e.e losses during chemical concentration were monitored with radioisotopes. Earlier it was shown with $Eu^{152,154}$, that the losses at the stage of rock cleavage and separation of SiO_2 were about 5 percent. To monitor the losses, in all subsequent operations, before precipitation of hydroxides, to the solution was added Y^{90} (without carrier) in the amount of $2 \cdot 10^5$ pulses/min. It was found that the total yttrium yield B_Y = 87 percent. To calculate the yield of other r.e.e (B_{Ln}), the total yield was differentiated for the yield in the chromatographic process (B'_{Ln}) and the yield in subsequent operations (B''_{Ln}), so that $B_{Ln} = B'_{Ln} \cdot B''_{Ln}$. The losses in the operations before chromatography did not exceed 1 percent and were not taken into account. The yield B''_{Ln} was specific for each of the r.e.e; it was determined from a special table [8] in accordance with B''_Y = 93 percent. The yield B''_{Ln} can be considered as nonspecific, in all cases it was B''_Y = 94 percent.

In the spectral determination, the concentrate was mixed with grade B-3, extra-pure carbon powder (with the addition of 1 percent NaCl); a 20 mg sample was placed in the pouch-shaped crater of carbon electrode. Firing was conducted in a d.c., 14 A arc by the total vaporization method. The spectrum of the arcswas obtained with a Baird diffraction spectrograph with a 2.7 AU dispersion in the second order and was recorded with a 100 sec exposure on ES photographic plates with a sensitivity of 11 GOST units. On the same type of plate were recorded the spectra of concentrates of three picritobasalts from Eastern African rifts, BCR-1 basalt, blank determinations, and spectral standards. The latter were prepared on the basis of grade V-3 powder to which 5 percent CaO, 5 percent Al_2O_3, 1 percent NaCl, and r.e.e oxides in the amounts from from $3 \cdot 10^{-3}$ to $1 \cdot 10^{-4}$ percent were added. /295

The concentration of the r.e.e in the initial regolith was computed by the form

$$C = \frac{(C_{sample} - C_{blank}) \cdot 10^2}{\alpha B_{Ln}},$$

where C is the concentrations of the r.e.e obtained from the calibration graphs, for the sample and the blank determination, respectively. The correction C_{blank} is essential only for the case of Eu and it was not taken into account for other elements.

The sensitivity of the direct spectral determination was estimated by the following criterion. The minimum detectable concentration (C_{min}) was regarded as the concentration for which at the level $C_o = 2\ C_{blank}$ (percent) the probability of a false determination $P_{false} = 0.023$, and the probability of detection $P_{det} \geq 0.83$ (when solving the alternative problem: the element in the sample is at the detection limit -- the element is absent in the sample). The probability of detection was determined by the formulas $P_{det} = 1 - P_{miss}$, where the probability of a miss is

$$P_{miss} = 0.5\left[1 - \Phi\left(\frac{C_o - C_{min}}{\sigma^2_{min}}\right)\right],$$

where Φ is the Laplace function, and σ^2_{min} is the dispersion at the level C_{min}. In an analysis of natural materials for trace elements, this criterion was wholly suitable [9].

The reproducibility in the result of the coefficient of variation V was estimated from multiple (of the order of 10) determinations of the spectral standards with levels of r.e.e content 0.04 and 0.0013 percent. Two series of V values were presented in correspondence to this.

The results thus obtained are presented in the table, where the following quantities are given: the content of r.e.e in the regolith, the total sensitivity of the method, reproducibility at two levels, and also the spectral lines by which the analysis was conducted. From the table it is clear that most of the r.e.e in the regolith were determined in the range of concentration far from the detection limits; for these elements the level of random errors is 8-10 percent. For Nd, Tm, and Lu this level increased to 15-20 percent, and only for Pr -- up to 40 percent, since it was determined at the sensitivity level.

The correctness of the r.e.e concentrations in the regolith presented was confirmed by comparing the results of analyzing picritobasalts and BCR-1 with the data obtained by the X-ray spectral method with concentration of r.e.e for these objects [8]. Within the limits of random errors the both methods, the

RESULTS OF EMISSION SPECTRAL DETERMINATION OF R.E.E AND Y CONCENTRATES FROM REGOLITH OF LUNA 16 SAMPLE (ZONE A, SAMPLE NO. 3, FRACTION 0.083 mm)

Element	Wavelength, Å	Content $c \cdot 10^4$, %	Sensitivity (with enrichment) $\frac{c_{min}}{a} \cdot 10^4$, %	Reproducibility v, %*	
La	3245,13	15,4	0,26	8	10
Ce	3063,01	45	1,6	10	15
Pr	3172,31	10	13	40	45
Nd	3133,6	32	2,6	15	20
Sm	3183,9	10,9	1,8	8	15
Eu	2813,95	2,9	0,053	8	10
Gd	3100,51	15,3	0,1	10	15
Dy	3251,26	15,3	0,26	8	10
Er	2904,7	5,6	0,26	10	15
Tm	3131,26	0,51	0,09	10	15
Yb	2970,56	7,4	0,026	8	10
Lu	2911,39	1,1	0,053	15	20
Y	3045,37	12,7	2,6	10	15
Total		174			

* Reproducibility is given for r.e.e contents of 0.04 and 0.0013 percent, respectively.

results agree for most r.e.e, and no regular group deviations in the r.e.e series was noted. In the light of this comparison, some understating of the Er and Tm content in the regolith must be regarded as random.

The results of analyzing the layer A regolith for r.e.e together with the data of other authors is shown also in a figure in the form of their ratio to the ratio of the corresponding elements in chondrites. From the figure it is clear that in most cases the nature of the curves does not appreciably change: they are similar in shape and have a well pronounced europium minimum. However, in absolute content of values, differences are observed, they can be attributed not only to the systematic error of the individual methods, but also to variations in the r.e.e content in the sample selected for analysis. The entire array of data confirms the earlier-noted fact of the lower concentration of r.e.e in the Luna 16 sample prepared with samples returned on the Apollo spacecraft from other regions of the lunar surface.

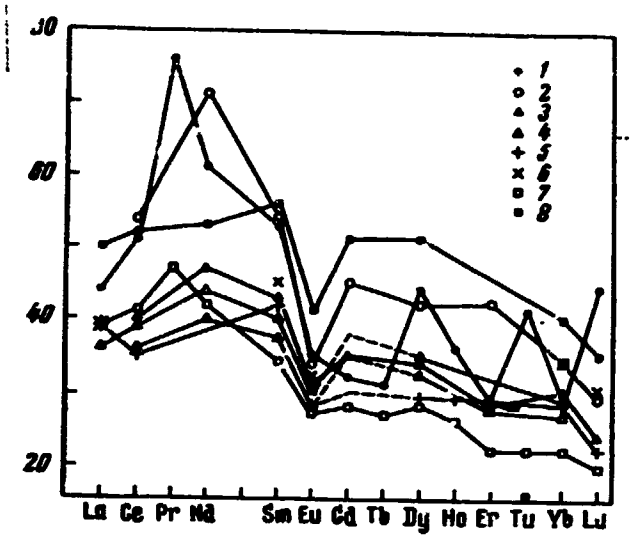

Ratios of concentrations of r.e.e in regolith to r.e.e concentrations in chondrites for samples from layer A based on the data of several authors

1. A. P. Vinogradov et al., mass-spectral method [1]
2. K. Allegre et al., mass-spectral method [2] (layer V)
3. J. A. Philpotts et al., mass-spectral method, sample A35 [3]
4. N. J. Hubbard et al., X-ray fluorescent method [4]
5. J. E. Gillum et al., activation method [5]
6. A. Helmke and L. A. Khaskin, activation method [6]
7. Yu. A. Surkov et al., activation method [7]
8. Data of present authors, chemical-spectral method

REFERENCES

1. Vinogradov, A. P., Chupakhin, M. S., Shevaleyevskiy, I. D., and Belyayev, Yu. I., "Chemical Composition of Luna 16 Lunar Regolith," present collection, p. 264.

2. Allegre, C. J., Birck, J. L., Moubet, M., and Provost, A., "Rb-Sr Age and Content of Potassium, Rubidium, Strontium, Barium, and Rare Earths in Surface Material from the Sea of Fertility," present collection, p. 468.

3. Philpotts, J. A., Schnetzler, C. C., Bottino, M. L., Schumann, S., and Thomas, H. H., "Luna 16: Some Li, K, Rb, Sr, Ba, Rare-earth, Zr, and Hf Concentrations," present collection, p. 312.

4. Hubbard, N. J., Nyquist, L. E., Rhodes, J. M., Bansal, B. M., Wiesmann, H., and Church, S. E., "Chemical Features of the Luna 16 Regolith Sample," present collection, p. 307.

5. Gillum, D. E., Ehmann, W. D., Wakita, H., and Schmitt, R. A., "Bulk and Rare Earth Abundances in the Luna 16 Soil Levels A and D," present collection, p. 299.

6. Helmke, P. A., and Haskin, L. A., "Rare Earths and Other Trace Elements in Luna 16 Soil," present collection, p. 304.

7. Surkov, Yu. A., Kirnozov, F. F., Ivanov, I. N., Kolesov, G. M., Ryvkin, B. N., and Shpanov, A. P., "Neutron Activation Study of the Composition of Lunar Surface Material from the Sea of Fertility," present collection, p. 283.

8. Ryabukhin, V. A., Stroganova, N. S., Laktionova, N. V., Galkina, I. P., Gatinskaya, N. G., Ageyeva, L. V., Yermakov, A. N., and Karyakin, A. V., "Chemical-Spectral Determination of Rare-earth Elements in Rocks of Various Types," Zh. anal. khimii (in press).

9. Belyayev, Yu. I., and Pchelintsev, A. M., "Estimation of Precision and Sensitivity of Atomic-Fluorescent Determination of Traces of Elements Using a Thermal Pulsed Atomizer of Solid Samples," Zh. anal. khimii 25(11), 2094 (1970).

N75 11835

ROCK-FORMING AND RARE ELEMENTS IN LUNAR SURFACE MATERIAL FROM THE SEA OF TRANQUILLITY AND THE OCEAN OF STORMS

/297

I. D. Shevaleyevskiy, and M. S. Chupakhin

Abstract

Methodological and analytical capabilities associated with spark mass-spectrometry and x-ray spectroscopy are presented in this study for the determination of the elemental composition of samples of lunar regolith returned to the Earth by Apollo 11 and Apollo 12. Using x-ray spectroscopy, the main constituents of samples of lunar surface material were determined, and using mass spectrometry -- the main admixtures. The principal difference of Apollo 11 samples from Apollo 12 samples was found for elements contained in microconcentrations. This is especially true of rare-earth elements.

The techniques of primary x-ray spectral analysis and spark mass spectrometry were used in investigating four samples of regolith from the cores of lunar surface material returned by the Apollo 11 expedition from the Sea of Tranquillity and the Apollo 12 expedition from the Ocean of Storms.

Samples 10005,34 and 10005,35 are fine-grained regolith sampled from a depth of 1.5 cm and 11 cm, respectively. Sample 12028,223 is also fine-grained regolith taken from a depth of 32-33 cm. Sample 12028,228 was selected from the coarse-grained layer at the depth 13-14.5 cm and consists of coarse fragmental material.

The quantitative analysis of the main constituents was made with a primary x-ray analyzer of model JPX-3 (JEOL company, Japan) with a planar crystal. The light elements (Na, Mg, Al, Si, P, and S) were analyzed with a KAP crystal at a voltage of 15 kV and a

current of 10 μA, and the heavy elements (K, Ca, Ti, Cr, Mn, and Fe) -- with a LiF crystal at 30 kV and 10 μA. The data collection time was 40 sec. The background was taken into account by the ordinary procedure. The experimental drift did not exceed 1 percent.

Preparation of the sample for analysis involved crushing it to a grain size <10 μm, distributing the weighed sample (10-15 mg) in an aluminum crucible, and pressing it to a compact state. The resulting table had an area of about 30 mm^2 (Ø6 mm) and, for x-ray spectral analysis, was sputtered in vacuum with a thin carbon layer. In the same way, reference standards W-1, JB-1, and BCR-1 were prepared and investigated. After the x-ray spectral analysis, the undisintegrated sample was sent for mass-spectral study. As a result, the same sample was analyzed by two different methods.

Mass-spectral analysis was conducted with an MX-3301 instrument. A new technique /1/ was developed specifically for investigating nonconducting geological objects; it permits making the determination with a mass spectrometer that has an ionic spark source without using conducting additives.

Essentially, the method involves the high-voltage, high-frequency breakthrough of a thin layer of dielectric by means of a field with intensity $\sim 10^7$ V/cm concentrated at the probe. The consumption of the sample in this method of analysis is 1.5-2 mg, and the number of elements determined simultaneously is as high as 75. /298

The results of the x-ray spectral analysis of four regolith samples are in Table 1.

From Table 1 it is clear that the Sea of Tranquillity regolith is well mixed at its depth, its composition is virtually identical, and it differs from the composition of the fine fraction of Ocean of Storms regolith by the considerably higher content of titanium oxide and the somewhat reduced content of the oxides of magnesium and silicon. Typical of the coarse material of the Ocean of Storms core is the high content of the oxides of iron and magnesium, and the low content of the oxides of aluminum and calcium.

From Table 2 it can be seen that the Sea of Tranquillity regolith, compared with the fine fraction from the Ocean of Storms, is significantly poor in zirconium and cesium, but rich in platinum, thallium, tungsten, and strontium.

In conclusion, it should be noted that this analysis for rock-forming and rare elements of regolith from different parts of the core and different regions reveals a wide diversity in compositions and makes it difficult to draw any specific conclusions. Obviously, a much larger number of determinations is needed for this purpose.

TABLE 1. RESULTS OF X-RAY SPECTRAL ANALYSIS OF REGOLITH (IN WEIGHT PERCENT)

Component	10005,34	10005,35	12028,233	12028,228
SiO_2	41,0	40,1	44,1	42,5
Al_2O_3	12,35	12,15	11,20	4,90
FeO	16,95	17,40	16,45	21,75
CaO	13,10	13,33	11,66	8,64
MgO	8,48	8,20	11,60	20,05
TiO_2	7,26	7,49	2,83	1,57
Na_2O	0,27	0,32	0,33	0,14
Cr_2O_3	0,25	0,25	0,31	0,83
MnO	0,22	0,22	0,22	0,[illegible]
S	0,21	0,24	0,17	0,05
K_2O	0,15	0,16	0,29	0,06
P_2O_5	0,14	0,16	0,27	0,04

TABLE 2. RESULTS OF MASS-SPECTRAL ANALYSIS OF REGOLITH (IN PPM)

Element	10005,34	10005,35	12028,233	12028,228	Element	10005,34	10005,35	12028,233	12028,228
V	0,50	0,74	1,12	0,64	Pd	0,060	0,073	0,019	0,008
Th	1,86	3,21	5,36	1,7	Mo	0,432	0,515	0,25	0,145
Bi	0,43	0,845	1,04	0,05	Nb	21,2	30	59,2	1,20
Pb	2,43	2,34	2,09	1,02	Zr	461,5	600	1410	22,6
Te	0,56	1,48	0,1	0,11	Y	168,3	212	115,2	71,4
Hg	0,059	—	0,066	0,097	Sr	252,5	192	68,9	115
Pt	2,19	1,93	0,05	0,015	Se	0,032	0,080	0,398	0,02
Ir	0,69	0,87	0,16	0,26	As	0,268	0,465	1,97	0,25
W	0,268	0,202	0,05	0,03	Ga	5,08	9,4	3,36	5,35
Hf	6,81	8,74	5,9	1,56	Sc	91,6		65	—
Cs	0,077	0,096	0,35	0,075	X	0,085	0,088	—	—
Sb	0,94	1,07	0,81	2,0	Ru	1,7	0,305	—	—
Sn	2,54	2,19	1,45	1,61	Rb	2,0	4,97	—	—
In	0,061	0,585	0,052	0,065	Br	0,84	1,60	—	—
Cd	0,315	0,413	0,16	0,024	Ge	1,02	1,01	—	—
Ag	0,155	0,193	0,17	0,025	Zn	27,6	110	—	—
					Cu	88,8	35,63	—	—
					Ni	100,25	150	—	—
					Co	18,65	28,4	—	—

REFERENCE

1. Chupakhin, M. S., and Polyakov, A. L., "Method of Mass Spectrometric Elemental Analysis of Geological Samples, Meteoritic Material, and Samples of Lunar Surface Material," Zh. Anal. khimii 27(3), 527 (1972).

Order of Lenin Institute of Geochemistry and Analytical Chemistry imeni V. I. Vernadskiy, USSR Academy of Sciences, Moscow

N75 11836

X-RAY ELECTRON STUDY OF LUNAR REGOLITH FROM THE SEA OF FERTILITY AND THE SEA OF TRANQUILLITY

/319

A. P. Vinogradov, V. I. Nefedov,
V. S. Urusov, and N. M. Zhavoronkov

Abstract

With a Varian IEE-15 spectrometer, x-ray electron spectra were obtained of the 2p-levels of Fe, Ti, Si, Al, and Mg, and of the 1s-level in lunar regolith from the Sea of Fertility (Luna 16) and the Sea of Tranquillity (Apollo 11). The spectra of the same elements were recorded for approximately 30 rock-forming minerals, oceanic gabbro, meteoritic-eucrite, and several iron meteorites. Analysis of the results based on line positions (chemical shifts) showed that all the elements studied have the usual degrees of oxidation, and that oxygen atoms are their nearest neighbors. The predominant coordination number of Al is 4.

In the Fe2p spectrum of regolith, besides the line of the oxide forms of Fe (from various iron-containing minerals), there is present a maximum relating to metallic iron and amounting, in intensity, to 10-15 percent of the intensity of the oxidized Fe. Analysis and comparison of the Fe2p spectra in regolith, various iron meteorites, and stainless steel leads to these conclusions: metallic iron in lunar regolith is in a highly dispersed state and is unusually stable with respect to oxidation by the oxygen of the Earth's atmosphere.

Introduction. Electron spectroscopy [1, 2] can provide data on the degree of oxidation of an element studied in the chemical compound, its nearest neighboring atoms, and other characteristics. Useful information can also be derived from investigating minerals [3-7], therefore it was quite natural to apply this new technique to the investigation of lunar regolith.

Essentially, the x-ray electron experiment amounted to the following. With an x-ray quantum of known energy R_γ applied to the material studied, an electron was ejected from one of the inner atomic levels. The kinetic energy E_{kin} of the ejected electron was measured in a spectrometer, and as a result, it was possible to calculate the bonding energy E_{bo} of the inner electron in the atom from the equality $E_{bo} = h_\gamma - E_{kin} - \phi$, where ϕ is the work function of the spectrometer material. E_{bo} depends directly on the various characteristics of the chemical bonding of the compound studied /1, 2/. The following notation was adopted for this quantity: first comes the symbol of the element studied, and next the optical designation of the corresponding level, for example, O1s, Fe2p, and so on.

Experimental section. The bonding energies of the inner electrons of O, Si, Al, Mg, Fe, and Ti were investigated in samples of lunar regolith from the Sea of Fertility returned by the Luna 16 automatic station, and from the Sea of Tranquillity returned by the Apollo 11 spacecraft, in the stony meteorite-eucrite Chervonyy Kut, and in oceanic gabbro (No. 12/4 from the collection of L. V. Dmitriyev)[1]. Also investigated were the bonding energies O1s in most of the minerals for which we earlier determined the bonding energies Mg2p, Al2p, Si2p, and the bonding energies Fe2p in iron meteorites, minerals, and the steel samples. Most of the most interesting spectra Fe2p are shown in Figs. 1-4.

The spectra were recorded on a Varian IEE-15 spectrometer. The samples were prepared by rubbing a finely ground powder[2] in a gold screen fitted on a metal cylinder enclosed with an organic film not containing oxygen, or by depositing the powder on an adhesive organic film. To record the spectra from metallic meteorites (with the exception of the Sikhote-Alin meteorite), turnings were prepared. The spectra of the Sikhote-Alin meteorite, as well as the various grades of steel, were recorded from intact samples turned in the form of a cylinder. All the spectra were obtained from several independent samples. In particular, three independent samples were prepared from the Sea of Fertility regolith, and /320
two independent samples from the Sea of Tranquillity regolith. Spectral excitation was carried out using AlK_α emission with the

---

[1] Iron gabbro containing titanomagnetite, Central-Indian Ridge of the Indian Ocean.

[2] The regolith from the Sea of Fertility was not ground, since the finest fraction was taken for analysis.

following x-ray tube loading regime: 8 kV, 80 mA, and a vacuum of 10^{-6} torr. The kinetic energy of the electrons I_{kin} reaching the analyzer in most cases was 100 eV, which ensured the maximum spectral intensity. The experimental technique is close to the method described earlier [3]. The results are in the Table.

Discussion. The spectra of the lunar regolith from the various points on the lunar surface are qualitatively close to each other, although in the Sea of Tranquillity regolith the Ti content (as follows from the spectrum and in accordance with the Table) is much higher. The spectra O1s, Si2p, Al2p, and Mg2p in the lunar regolith are very close to the corresponding spectra of the stony meteorite from Chervonyy Kut and oceanic basalts, and also to the spectra of several terrestrial minerals [3]. From this it follows that, in particular, the elements Mg, Al, and Si have the usual degree of oxidation in the regolith, and that oxygen atoms are the nearest neighbors of these atoms.

COMPOSITION OF LUNAR REGOLITHS, EUCRITE, AND OCEANIC GABBRO (IN WEIGHT PERCENT)

Component	Sea of Fertility regolith [4]	Sea of Tranquillity regolith [4]	Eucrite from Chervonyy Kut [5]	Oceanic gabbro
SiO_2	41.7	43	48.8	26.4
Al_2O_3	15.3	13	13.4	11.9
Fe_2O_3	--	--	--	14.1
FeO	16.8	16	18.7	17.5
CaO	12.2	12	11.5	4.9
MgO	8.7	8	7.0	10.3
TiO_2	3.4	7	0.7	7.9
Na_2O	0.37	0.5	0.5	0.6
K_2O	0.10	0.12	0.12	0.9
S	0.19	--	--	--
Ni	0.01	0.007	Not detected	--

The shifts of the lines Al2p and Si2p suggest the following qualitative conclusions on the mineralogical composition of the

regolith. Since the shift of the line Al2p in the regolith is 2.3 eV (relative to metallic aluminum), based on the results of the study [3] it can be concluded that in most minerals forming regolith the coordination number of the aluminum atoms is 4.

The line shift Si2p (relative to elemental silicon) is 3.4 eV. If we consider [3] that the shift of this line in silicates varies from 4.0 eV in SiO_2 to 3.0 eV in nephelin $NaAlSiO_4$, from this it follows that in the regolith there is virtually no extreme acidic and alkaline mineral constituents. These shift values agree well with the data from other methods [4] stating that the primary minerals in regolith are plagioclase, pyroxene, and olivines, in which the line shifts Al2p and Si2p are close to the shifts of these lines in the regolith [3].

Of greatest interest is a comparison of the spectra Fe2p in lunar and terrestrial samples. A total of three independent Fe2p spectra were obtained from two samples of Sea of Tranquillity regolith and seven independent Fe2p-spectra from three samples of Sea of Fertility regolith.

In all the regoliths spectra, lines of metallic iron were observed along with oxidic iron (see Figs. 1 and 2 where several spectra are presented). These lines are absent in the spectra of stony meteorite, oceanic gabbro (see Figs. 1 and 2) and in oxygen-containing terrestrial minerals (Fig. 3).

The line Fe2p from FeS_2 was observed in pyrite FeS_2 and pyrrhotite $Fe_{1-x}S$. In $Fe_{1-x}S$ it is probably due to the presence of FeS_2 in the surface layer, since in stoichiometric FeS, troilite (both in the synthetic material, as well as that extracted from the material of the Sikhote-Alin meteorite), this maximum is absent (see Fig. 3). By position, this line is close to the line of metallic iron (see Fig. 3). However, the additional maximum in the lunar samples is related specifically with metallic iron, and not with FeS_2. Actually, the sulfur content in the lunar regolith is low (tenths of a percent, see Table). FeS_2 and FeS were also not detected by the other techniques [4]. Also not observed was an appreciable rise in the intensity of the S2p-line. Therefore, the observed maximum evidently corresponds to metallic iron.

The presence of metallic Fe in lunar regolith was confirmed also by other techniques [4]. X-ray electron spectra revealed several not entirely usual properties of this iron. According to [4], based on the data of Mossbauer spectra of regolith it follows

that the content of metallic iron is about 2-5 percent of the total iron. At the same time, from the spectra (see Figs. 1 and 2) it follows that the intensity of the line from metallic Fe is no less than 10 percent of oxidized Fe. It must be taken into account that the x-ray electron spectra were obtained only from the surface layer (to a depth of 100 AU) of the sample, therefore the relative surface of the metallic iron atoms is about 10 percent of the surface of the/321 oxidized iron atoms, although its weight content is much less. But to this it must be added that some fraction of the surface of metallic particles are nonetheless oxidized. Hence it follows that metallic iron is in a finely dispersed state (compared with other iron-containing minerals).

Another unusual property of lunar iron is its stability with respect to the oxygen in the Earth's atmosphere. If, for example, we investigate the Fe2p line in stainless steel, it turns out that the surface layer is entirely oxidized: it has no metallic iron and in its spectrum only the line of oxidized iron (curve 8 in Fig. 4) is observed. Only after careful cleaning of the stainless steel sample does its spectrum disclose the line of metallic iron (curve 6 in Fig. 4); the exposure time of the sample to air oxygen is several minutes. After 24 hours' exposure of the sample in the air the intensity of the metallic iron maximum falls off sharply (curve 7 in Fig. 4), and in three weeks it virtually disappears (curve 8 in Fig. 4). Ordinary carbon iron behaves in similar fashion (the spectra are not presented).

Also investigated were Fe2p-spectra of several iron meteorites (see Fig. 4). In the freshly prepared turnings of kamacite from the Gressk meteorite (5.8 percent Ni) and taenite from the Santa Catarina meteorite (32 percent Ni), and freshly protected kamacite (6 percent Ni) from the Sikhote-Alin meteorite, the metallic iron line was observed. The intensity of this line in the Sikhote-Alin meteorite after two days' exposure of the sample in air decreased sharply (curves 4 and 5 in Fig. 4), however even after three weeks' exposure in air no appreciable further decrease in its intensity was observed.

Similar results were obtained for the Santa Catarina taenite: /322 the relative intensity of the maximum of metallic Fe after 10 days' exposure of the sample in air remained practically unchanged. Both these facts indicate that meteoritic iron is relatively stable to oxidation by atmospheric oxygen (although the surface of the samples was far from ideal).

The samples of Sea of Fertility regolith investigated were in the Earth's atmosphere for about half a year. Nonetheless, the ratio of the intensity maxima of metallic and oxidized iron in the lunar samples is the same as in samples consisting virtually of iron alone (see Fig. 4), although metallic iron in the regolith

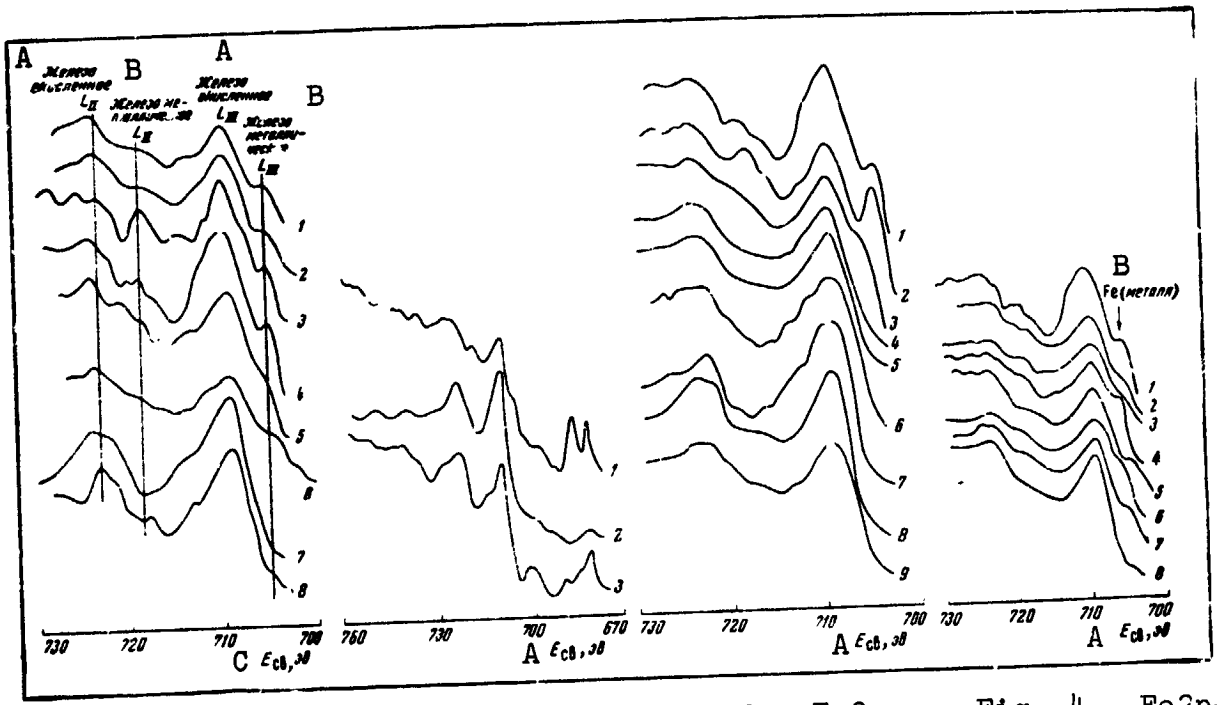

Fig. 1. Fe2p-lines
1,2. Sea of Tranquillity regolith
3-6. Sea of Fertility regolith
7. Oceanic gabbro
8. Eucrite of Chervonyy-Kut
KEY: A. Oxidized iron
B. Metallic iron
C. E_{bo}, eV

Fig. 2. Fe2p-lines (large spectral section)
1. Sea of Fertility regolith
2. Oceanic gabbro
3. Chervonyy-Kut eucrite
KEY: A. E_{bo}, eV

Fig. 3. Fe2p-lines
1. Sea of Fertility regolith
2. Pyrite, FeS_2
3. Pyrrhotite $Fe_{1-x}S$
4. Troilite FeS
5. Ilmenite, $FeTiO_3$
6. Olivine $(Mg,Fe)_2SiO_4$
7. Biotite $K(Mg,Fe)_3[AlSiO_4](OH)_2$
8. Hematite, Fe_2O_3
9. Magnetite, Fe_3O_4
KEY: A. E_{bo}, eV

Fig. 4. Fe2p-line
1. Sea of Fertility regolith
2. Kamacite, Santa Catarina meteorite
3. Taenite, Gressk meteorite
4. Kamacite, Sikhote-Alin meteorite (protected against air)
5. Kamacite, Sikhote-Alin meteorite, after two days' exposure in air
6. Stainless steel (protected against air)
7. Stainless steel, after 24 hours' exposure in air
8. Stainless steel after 3 weeks' exposure in air
KEY: A. E_{bo}, eV
B. Fe(metal)

represents a negligible part of the oxidized iron. It can be shown that these facts are consistent only if the lunar metallic iron is especially stable to oxidation by oxygen in the terrestrial atmosphere.

Actually, if it is assumed that lunar metallic iron is appreciably oxidized, the observed ratio of the maxima intensities of oxidized and metallic iron, given the negligible relative weight fraction of metallic iron, is possible only if the degree of dispersion of the metallic iron in the regolith is so high that the surface of the metallic iron is much greater than the surface of the oxidized iron. However, in this case one should expect an abrupt increase in the relative intensity of the line Fe2p from the oxidic forms of iron in the lunar samples, for example, with respect to the line Si2p, compared with the stony meteorite or oceanic gabbro, and this was not observed experimentally. Thus, the degree of surface oxidation of lunar metallic iron must be low.

The high stability of lunar iron with respect to atmospheric oxygen is afforded, evidently, by the strong thin oxide film forming on the surface of the metallic particles. The thin and strong film can form only if there are no surface defects present. Formation of a sufficiently thin film can also be promoted by the presence of metallic nickel in the iron, as is the case, for example, in meteorites. Our investigations of the Ni content in regolith showed that the nickel content is lower than the sensitivity of the method. Evidently, it can be concluded that the content of Ni in metallic Fe is low (since the high dispersion of the metallic phase suggested a relative rise in the intensity of the Ni line). The conclusion is in agreement with the Mossbauer investigations of iron in regolith [5].

Thus, our investigations showed that the regolith contains a very fine-grained fraction of metallic iron, resistant to corrosion, and evidently concentrated on the surfaces of the regolith particles (see also [8]). To account for the origin of the metallic iron of this type, we conducted an experimental simulation of the condensation of fine-dispersed Fe with various alloying additives and also in conditions of high vacuum, in a nonoxygen medium, and with a thorough study of the properties of this Fe [9].

The authors are grateful to Ye. L. Krinov and L. G. Kvash (Committee on Meteorites, USSR Academy of Sciences) for presenting the samples of meteorites, and to L. V. Dimitriyev for the sample of oceanic gabbro. We take this occasion to express our appreciation to L. M. Mitin for assistance in conducting the experiment.

REFERENCES

1. Siegbahn, K., et al., "Electron Spectroscopy for Chemical Analysis," Nova Acta Reg. Soc. Sci. Uppsaliensis, Ser IV 20, (1967).

2. Siegbahn, K., et al., Elektronnaya spektroskopiya /Electron Spectroscopy/, "Mir", 1971.

3. Siegbahn, K., et al., ESCA Applied to Free Molecules, North-Holland, Amsterdam, 1969.

4. Nefedov, V. I., Urusov, V. S., and Kakhana, M. M., "X-Ray Electron Study of Chemical Bonding in Minerals of Na, Mg, Al, and Si," Geokhimiya (1), 11 (1972).

5. Vinogradov, A. P., "Preliminary Data on Lunar Surface Material Returned by Luna 16 Automatic Station," Geokhimiya (3), (1971).

6. Chirvinskiy, P. N., and Sokolova, A. I., "Petrographic and Chemical Characteristics of Eucrite of the Chervonyy Kut, Falling on 23 June 1939," Meteoritika (3), (1946).

7. Maykuth, D. J., Product Engineering 24(11), 188 (1953).

8. Marov, I. N., Dubrov, Yu. N., and Yermakov, A. N., "Electron Paramagnetic Resonance of Several Lunar Rock Samples," present collection, p. 323.

9. Vinogradov, A. P., Nefedov, V. I., Urusov, V. S., and Zhavoronkov, N. M., "X-Ray Electron Studies of Metallic Iron in Lunar Regolith," Dokl. AN SSSR 207(2), 433 (1972).

Order of Lenin Institute of Geochemistry and Analytical Chemistry imeni V. I. Vernadskiy, USSR Academy of Sciences

Order of Lenin Institute of General and Inorganic Chemistry imeni N. S. Kurnakov, USSR Academy of Sciences, Moscow

N75 11837

ELECTRON PARAMAGNETIC RESONANCE OF SEVERAL LUNAR ROCK SAMPLES

/323

P. N. Marov, Yu. N. Dubrov, and A. N. Yermakov

Abstract

This report presents the results of investigating lunar rock samples from the sample returned by the Luna 16 automatic station, using electron paramagnetic resonance (EPR). The EPR technique makes it possible to detect paramagnetic centers and investigate their nature, with high sensitivity. Regolith (finely dispersed material) and five particles from it, 0.3 mm in size, consisting mostly of olivine, were investigated with EPR.

Experimental techniques. EPR spectra were recorded on a V-4502-15A spectrometer at the frequencies 9000 and 35,000 MHz (X- and Q-ranges). The V-4561 microwave bridge was used for work in the Q-range. The strength of the magnetic field was varied in the range 0-19,000 gs. Its value was determined with a IMI-2 nuclear meter with a ChZ-4 frequency meter. The microwave frequency was measured with a Ch4-5 heterodyne frequency meter in the X-range and with a resonator wavemeter built into the V-4561 bridge, in the Q-range. The results of frequency measurements were monitored by the value of the g-factor of diphenylpicrylhydrazyl (DPPH). The EPR spectra of the Q-range were recorded at room temperature, while the X-range spectra were recorded at the sample temperatures (-180) to (+ 40°) C, which were set with a V-4257 thermostat.

The regolith sample (sample 9-1d from the middle part of the lunar surface material) was investigated in nitrogen, and then in air, and the rock particles were studied in air. The samples were placed in quartz ampules.

The EPR line intensities were measured relative to the standard "Pitch" sample and known weighed amounts of the salt $Fe_2(SO_4)_3 \cdot 9H_2O$

and synthetic magnetite Fe_2O_3. Samples and standards were placed in once "half" of the double V-4352 resonator, and the DPPH sample in the other half, and from the intensity of the signal from this specimen the change in the Q-factor of the resonator was determined by the sample. The level of microwave intensity ensured that there was no saturation for all signals. The line intensities were calculated as the product of the square of the EPR line width between the points of maximum slope (ΔH) by the amplitude of the EPR signal (A). The line intensities were used in estimating the amount of metallic ferromagnetic iron by comparing the intensity of its EPR line with the intensities of the EPR lines of the paramagnets. Here one had to neglect the effects that are probably more substantial than the determination of the line intensities by this method.

Results. The EPR signals in the X- and Q-ranges consist mainly of a single asymmetric broad line I (Figs. 1 and 2). The effective value of the g-factor (g^*) measured from the point of intersection of the first derivative of the EPR signal with the zero line of the spectrum is close to the purely spin value of the g-factor. At room temperature $g^* = 2.12 \pm 0.3$ and 2.09 ± 0.01 for the X- and Q-ranges, respectively. The line width $\Delta\overline{H}$ is virtually independent of frequency, thus: $\Delta H = 820 \pm 80$ and 770 ± 80 gs for the X- and Q-ranges at room temperature. The dependence of the parameters of signal I on temperature is shown in the Table. The signal intensity conventionally measured as the number of paramagnetic particles with spin S = 1/2 and g = 2 based on the "Strong Pitch" standard with a number of unpaired spins $3 \cdot 10^{15}$ gave a value of the order of 10^{23} spins/g. The intensity expressed in the number of iron atoms of paramagnetic salt $Fe_2(SO_4)_3 \cdot 9H_2O$ and the ferromagnetic compound Fe_3O_4 is 10^{23} and 10^{21} atoms/g, respectively. /324

In the Q-range it was possible to observe also another, much less intense, EPR signal: line II (see Fig. 2) with $g \simeq 4.16$ and width $\Delta H \simeq 700$ gs.

The EPR spectra of individual rock particles are basically analogous to signal I (Fig. 3). The intensity of the signal per unit weight for the particles is approximately two orders of magnitude less than in the regolith, while for various particles it differs by several times. Exposure in air for several months did not lead, within the limits of experimental error, to a change in the intensity of the signals from the particles and the regolith. Alcohol treatment of the particle surfaces also did not reduce the intensity of the EPR signals. For sufficiently prolonged (longer than 30 minutes) treatment of the particle surfaces with hydrochloric acid at a concentration of ~7 mole/liter, the EPR signals were 70-80 percent reduced from their initial level. The dependence of the intensity of the signal from the time the particles were treated with acid is shown in Fig. 4.

DEPENDENCE OF EFFECTIVE g*-FACTOR AND LINE WIDTHS OF THE EPR SIGNAL OF REGOLITH ON TEMPERATURE, FOR THE X-RANGE

Temperature, °C	ΔH, gs	g*
40	800	2,12
20	820	2,12
−30	880	2,12
−80	930	2,14
−130	960	2,15
−180	1030	2,16
*Error of measurement	±80	±0,03

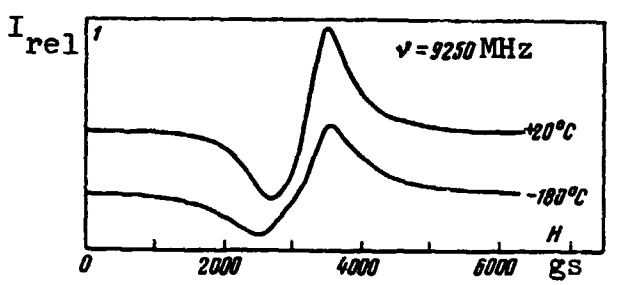

Fig. 1. EPR spectra of regolith in the X-range

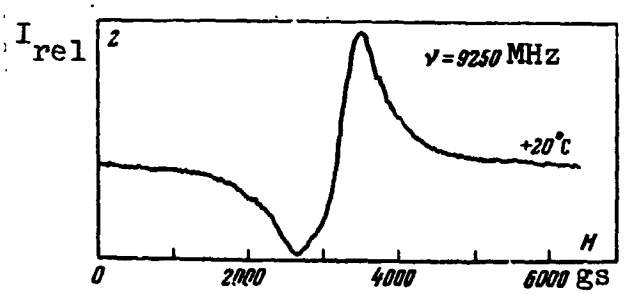

Fig. 2. EPR spectra of regolith in the Q-range at 20° C

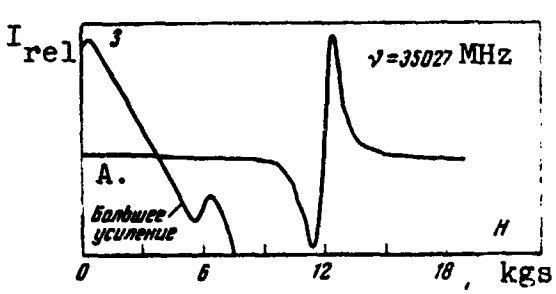

Fig. 3. Characteristic EPR spectrum of olivine particles in the X-range at 20°C
KEY: A. High amplification

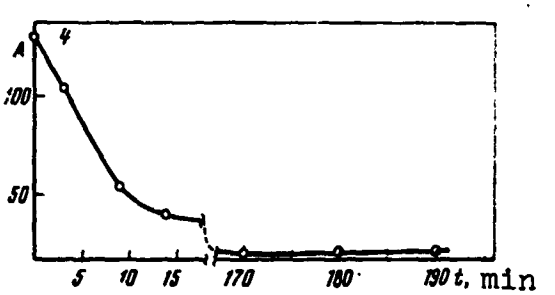

Fig. 4. Dependence of EPR intensity of olivine particle on time during which particle surface was treated with hydrochloric acid
A. Amplitude of EPR line in relative units

Discussion. Signal I cannot be interpreted as an EPR signal from any type of paramagnetic particles, since it exhibits an excessively high intensity. For example, in order to generate

signal I in regolith by Fe^{3+} ions (the most probable paramagnetic admixture, considering the amount of iron in the samples and the fact that the EPR of the Fe^{2+} ions was not observed in the temperature range used [1]), the amount of iron had to be one order of magnitude higher than the amount of the material in the samples investigated. The only reasonable explanation for the high intensity of the signal is to attribute the signal to ferromagnets or uncompensated, antiferromagnets (ferrimagnets). In ferromagnets the intensity of the signal is three (or somewhat more) orders of magnitude higher than in paramagnets at room temperature [2]. With reference to this, to account for the signal I in the regolith, it is sufficient to have an admixture of 0.1-1 percent finely dispersed metallic iron. This estimate of the amount of iron agrees with the results of the investigation of the sample returned by Luna 16 by Mossbauer spectroscopy [3], and with the data on the iron content in other samples of lunar material [4-6]. It should be stressed that signal I cannot be attributed to another most probable, strongly magnetic admixture, the ferrimagnetic Fe_3O_4. From a comparison of the intensities of signals I in the regolith /325 and in the synthetic magnetite, it follows that it is necessary to assume a 10 percent magnetite admixture in the regolith, which contradicts the data of other techniques [3, 6].

EPR signals of type I were observed in Apollo 11 samples [7, 8]. Our results confirm the point of view expressed by the authors of [7], who attribute this signal to metallic iron and reject attributing it to Fe^{3+} ions [8]. In [7], the attribution of the signal is based on a calculation of the line shape of the EPR spectrum (more exactly, of ferromagnetic resonance); but in the present study this same attribution is based on an investigation of signal intensity. Thus, different approaches leads to the same conclusion, which increases its reliability.

Evidently, signals of individual particles are also accounted for by metallic iron. In particular, this is confirmed by the decrease in the signal when the particles are treated with acid. Interestingly enough, most of the iron lies at the surface of the particles, since the signal decreases without appreciable decrease in particle size. It is probable that the iron is distributed over the surface in the form of thin films. Supporting this assumption is the linear dependence of the decrease in EPR signal intensity on the time during which the surfaces of particles were treated with acid during the initial period (Fig. 4). But if the iron were in the form of blebs, the dependence of the cubic root on signal intensity must be linear.

The nature of the EPR signal with a g-factor close to 4 is not entirely clear. Possibly, it is caused by Fe^{3+} ions; however, this problem requires additional study, which is extremely complicated owing to the presence of a broad and intense line I in the regolith.

Conclusion. 1. It was established that the intense EPR signal with $g \simeq 2$ is caused by the finely dispersed metallic iron, whose amount in the regolith is about 0.1-1 percent by weight, while for individual olivine particles it is two orders less.

2. It is shown that the iron lies at the surface of olivine particles and probably in the form of thin films.

3. An EPR signal with $g \simeq 4$ in the Q-range was detected. The nature of the signal is unclear, but probably it is caused by paramagnetic ions.

The authors are grateful to L. S. Tarasov and A. V. Ivanov for discussion and valuable information, and to S. V. Kozerenko for presenting the sample of synthetic magnetite.

REFERENCES

1. Low, W., Paramagnitnyy rezonans v tverdykh telakh /Paramagnetic Resonance in Solids/, Foreign Literature Pub. House, 1962.

2. Vonsovskiy, S. V., Magnetizm /Magnetism/, "Nauka", 1971.

3. Malysheva, T. V., and Kurash, V. V., "Mossbauer Spectroscopy of Lunar Samples Returned by Luna 16 Automatic Station," Geokhimiya (1), (1973).

4. Doell, R. R., Gromme, C. S., Thorpe, A. N., and Senftle, F. E., "Magnetic Studies of Apollo 11 Samples," Proc. Apollo 11 Lunar Sci. Conf., 3, (1970).

5. Greenwood, N. N., and Howe, A. T., "Mossbauer Studies of Apollo 11 Lunar Samples," Proc. Apollo 11 Lunar Sci. Conf., 3 (1970).

6. Herzenberg, D. L., and Riley, D. L., "Analysis of First Returned Lunar Samples by Mossbauer Spectrometry," Proc. Apollo 11 Lunar Sco. Conf., 3, 2221 (1970).

7. Manatt, S. L., Elleman, D. D., Vaughan, R. W., Chan, S. I., Tsay, F. D., and Huntress, Y. T., Jr., "Magnetic Resonance Studies of Lunar Samples," Science 167, 709 (1969).

8. Geake, J. E., Dollfus, A., Iarlick, G. F., Lamb, W., Walker, G., Steigman, G. A., and Titalaer, C., "Luminescence, Electron Paramagnetic Resonance and Optical Properties of Materials from Apollo 11," Proc. Apollo 11 Lunar Sci. Conf., 3, 2127 (1970).

Order of Lenin Institute of Geochemistry and Analytical Chemistry imeni V. I. Vernadskiy, USSR Academy of Sciences, Moscow

N75 11838

MOSSBAUER SPECTROSCOPIC STUDY OF LUNA 16 LUNAR REGOLITH /326

T. V. Malysheva

Abstract

Samples of bulk fractions of lunar regolith from the surface layer A and the deep layer V were measured by Mossbauer spectroscopy with the Fe^{57} nucleus. Metallic iron, ilmenite, olivine, pyroxene (mainly augite), and glasses were found. The iron distribution by mineral phases indicates that Luna 16 regolith differs from Apollo 11 regolith by a lower ilmenite content and a greater amount of olivine, and differs from Apollo 12 regolith by somewhat more olivine. No appreciable amount of iron was found in the trivalent state.

The lunar surface material returned by the Luna 16 automatic station is a 35 cm long core filled mainly with powdery material of black-brown color, the so-called regolith /1/. Iron-containing minerals give characteristic Mossbauer spectra, permitting identification of individual materials in the bulk regolith sample without any preliminary separation. By Mossbauer spectroscopy, the bulk fractions of regolith from different core layers were measured, as well as samples differing in grain size. Bulk samples 3-1 and 3-3a with grain size 0.2-0.4 mm from the surface layer 3 were analyzed. From the deep layers of the core, measurements were made of the bulk sample 8-2 and samples 9-4a, 9-5a, 9-6a, and 9-1r with grain size 0.200-0.450, 0.127-0.200, 0.083-0.127, and $\leqslant 0.083$ mm, respectively. The measurements were conducted on a time-based Mossbauer spectrometer operating in the constant-acceleration mode, in conjunction with a model LP 4050, 512-channel pulse analyzer. Co^{57} in a palladium matrix served as the source, its activity was 10 mCi. The lunar material was placed in the amount of 100-200 mg in a quartz cuvette Ø22 mm and measured for about 40 hours to collect 10^6 pulses in each analyzer channel. The measurements were processed by the method of least squares on BESM-3m and BESM-4 electronic computers.

Fig. 1 shows the Mossbauer spectra of sample 8-2 measured at room temperature at different rates of source movement relative to the absorber. Fig. 2 shows the absorption spectra of sample 3-1 measured at room temperature and at the temperature of liquid nitrogen. The spectrum of sample 3-3a is analogous to the spectrum of sample 3-1.

The peaks 1 and 1' were identified as a quadrupole doublet formed during resonant absorption of Mossbauer radiation in olivine. Table 1 gives a comparison of the chemical shifts, quadrupole splittings, and line widths Γ of the olivines in lunar samples with terrestrial and meteoritic olivines. From the table it is clear that the values of δ coincide with their values for terrestrial and meteoritic olivines, but Δ is closer to the values obtained for olivines with a larger f = FeO/(FeO + MgO) percent, which indicates a high iron abundance in lunar olivines /2/ (f = 50-80 percent). A somewhat lower abundance of 25 percent was found in the bulk fraction of the surface layer (sample 3-1). A tendency toward increased iron abundance in olivine with decrease in grain size is clearly evident. This can be associated with the increase in the iron content of olivine toward the middle of the olivine crystal (normal zonality of olivine) or with the fact that the more ferruginous olivine is more strongly affected by erosion. The narrower line width of the quadrupole doublets indicate rapid cooling of the lunar olivines after crystallization.

Absorption 2 and 2' relate to the pyroxene constituent of the regolith. Table 2 gives the parameters of the Mossbauer spectra of pyroxenes in meteoritic and terrestrial samples. The results /327 of measuring two samples of augites and glasses are also included in the table. Data from a chemical analysis of the augite samples are presented in Table 3. Table 4 gives the parameters of the Mossbauer spectra of the lunar samples. By comparing Tables 2 and 4 it is clear that the parameters of the Mossbauer spectra of the lunar pyroxenes coincide most closely with the results obtained for the augites and for the glasses. A value of δ somewhat larger than for glasses can be a consequence of depletion in alkalies. The lines of quadrupole splitting are significantly broadened. The results of attempting to resolve them into constituents corresponding to the two nonequivalent positions MI and MII in the lattice of pyroxenes are given in Table 5 and in Fig. 3. From these results it is clear that separation into constituents does not lead to satisfactory results. Evidently, this is associated with the presence of a large amount of glasses in the regolith.

Table 6 gives the parameters of the Mossbauer spectra for the quadrupole doublet with absorption lines 3 and 3' belonging to ilmenite. They are in good agreement with the data of /8/ on the measurement of terrestrial ilmenite. However, the right peaks of the quadrupole doublets of the lunar ilmenites are somewhat broader and more intense than the left, which can indicate the presence of some unidentified constituents in the lunar regolith. /331

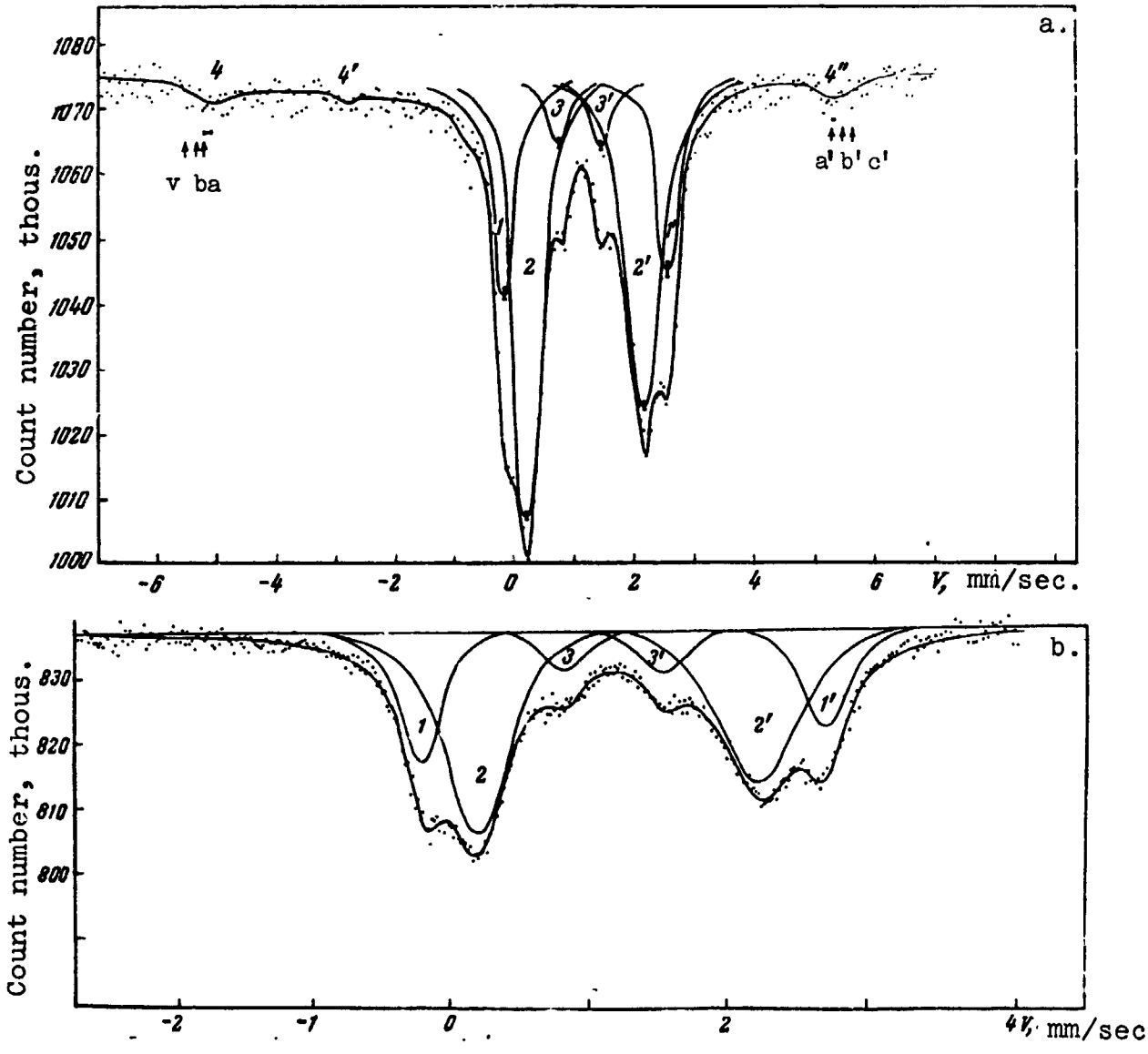

Fig. 1. Mossbauer spectra of sample 8-2.
a. Measured with a high travel rate of source relative to absorber
b. A lower travel rate (room temperature);
absorption peaks: 1 and 1'. olivine; 2 and 2'. pyroxene;
3 and 3'. ilmenite; 4, 4', and 4". metallic iron.

Measuring the samples at the temperature of liquid nitrogen did not enhance the resolution of the doublet lines characteristic of various iron-containing minerals (see Fig. 2 b). The absorption lines 4, 4', and 4" were identified as three peaks of magnetic splitting from six peaks of the hyperfine structure of metallic iron. The ratio of the peak intensities is characteristic of non-magnetized metallic iron with grain size not less than 15 AU /9_7.

TABLE 1. PARAMETERS OF MOSSBAUER SPECTRA OF OLIVINES (ROOM TEMPERATURE) /328

Sample	f	Chemical shift δ, mm/sec	Quadrupole splitting Δ, mm/sec	Line width, and Γ, mm/sec left peak		right peak	Reference
Terrestrial samples	7	1,28±0,002	3,02±0,02	0,58±0,02	—	0,58±0,03	[3]
	12,5	1,26	3,02	—	0,39	—	[4]
	46,6	1,25	2,93	—	0,40	—	[4]
	50	1,28±0,02	2,94±0,02	0,57±0,03	—	0,57±0,03	[3]
	60,9	1,27	2,90	—	0,40	—	[4]
	96,1	1,27	2,90	—	0,41	—	[4]
Pallas meteorite iron	10	1,30±0,02	3,04±0,02	0,28±0,02	—	0,40±0,02	[3]
Lunar regolith							
8-2	—	1,28±0,03	2,91±0,02	0,33±0,02	—	0,37±0,02	—
3-1	—	1,30±0,02	2,99±0,02	0,32±0,02	—	0,33±0,02	—
3-3a (0,2—0,4 mm)	—	1,26±0,02	2,90±0,02	0,29±0,02	—	0,42±0,03	—
9-4a (0,200—0,450 mm)	—	1,27±0,02	2,94±0,01	0,31±0,01	—	0,42±0,01	—
9-5a (0,127—0,200 mm)	—	1,26±0,02	2,92±0,01	0,36±0,01	—	0,42±0,01	—
9-6a (0,083—0,127 mm)	—	1,26±0,02	2,90±0,02	0,30±0,01	—	0,40±0,01	—
9-1r(—0,083 mm)	—	1,28±0,02	2,88±0,02	0,26±0,01	—	0,39±0,01	—

According to /10/, the effective magnetic field at the iron nuclei H_{eff} in an iron-nickel alloy differs from the H_{eff} for pure iron. In order to clarify the nature of iron in the lunar regolith, we measured the Mossbauer spectra of the iron meteorites Sikhote-Alin and Chinge, containing 6 and 16 percent nickel, respectively, based on the data of chemical analysis /11/, as well as the spectrum of pure metallic iron. The measurements are in Table 7 and in Fig. 4, from which it is clear that H_{eff} in meteorites is stronger than in pure iron. The Sikhote-Alin meteorite is virtually entirely kamacite, while the Chinge meteorite is a mixture of kamacite and taenite /11/. The determination of the iron abundance based on the data of Mossbauer spectroscopy in the meteorite samples measured is qualitative owing to the presence of a small amount of cobalt /332 (about 1 percent). However, the difference in the positions of the extreme peaks of the magnetic hyperfine structure for meteorites and pure metallic iron is clearly visible. Fig. 4 shows the positions 1 and 6 of the lines of the magnetic hyperfine splitting for pure iron (1), Sikhote-Alin meteorite (2), and Chinge meteorite (3). Clearly, within the limits of measurement precision, pure metallic iron is present in sample 8-2. An analogous result was obtained for all the samples investigated.

TABLE 2. PARAMETERS OF MOSSBAUER SPECTRA OF PYROXENES (ROOM TEMPERATURE)

Sample	δ, mm/sec		Δ, mm/sec		Γ, mm/sec		References
	M1	M2	M1	M2	M1	M2	
Rhombic pyroxenes	1,22—1,25	1,24—1,27	2,35—2,44	1,98—2,13	0,35—0,49	0,34—0,42	[4]
Johnston diogenite	1,28±0,04	1,28±0,04	2,31±0,05	2,10±0,04	0,35±0,03	0,33±0,03	[5]
Yurtuk howardite	1,27±0,04	1,30±0,02	2,62±0,03	2,15±0,01	0,35±0,01	0,34±0,01	[5]
Stonnarge eucrite	1,28±0,02	1,27±0,02	2,55±0,03	2,05±0,01	0,33±0,02	0,34±0,02	[5]
Augite 11638	1,20±0,03	1,21±0,01	2,58±0,03	2,02±0,01	0,46±0,03	0,40±0,03	—
Augite Dx379	1,22±0,02	1,20±0,02	2,68±0,03	2,13±0,02	0,46±0,03	0,40±0,03	—
Alkaline-iron-silicate glasses	1,18		2,11		0,40		[6]
	1,12±0,05		2,00±0,10		—		[7]

TABLE 3. RESULTS OF CHEMICAL ANALYSIS OF AUGITES* (IN WEIGHT PERCENT)

Component	11638	Dx379	Component	11638	Dx379
SiO_2	49,51	47,82	MnO	0,14	0,16
TiO_2	1,85	0,71	MgO	14,88	13,12
Al_2O_3	4,40	6,28	CaO	22,24	22,59
Fe_2O_3	3,43	4,70	Na_2O	0,74	0,80
FeO	3,20	3,07	K_2O	0,09	0,32

*The FeO/Fe_2O_3 ratio is understated compared with the results of the Mossbauer measurements.

The Mossbauer spectra of sample 9-4a (grain size 0.200-0.450 mm) and sample 9-5a (0.127-0.200 mm) are analogous to the spectra of samples 8-2 and 3-1. But in the spectra of sample 9-6a (0.083-0.127 mm) and 9-1r (-0.083 mm) lines of magnetic hyperfine splitting characteristic of troilite FeS (lines 5, 5', and 5" in Fig. 5) were found.

Within the limits of measurement precision, no trivalent iron was found. From the area of the corresponding hyperfine splitting peaks, the mineralogic composition of the iron-containing portion of the regolith was determined on the assumption that the values of resonant absorption for all the minerals are identical (Table 8). Presented here for comparison are the results obtained for samples of lunar regolith returned by Apollo 11 [12] and Apollo 12 [13].

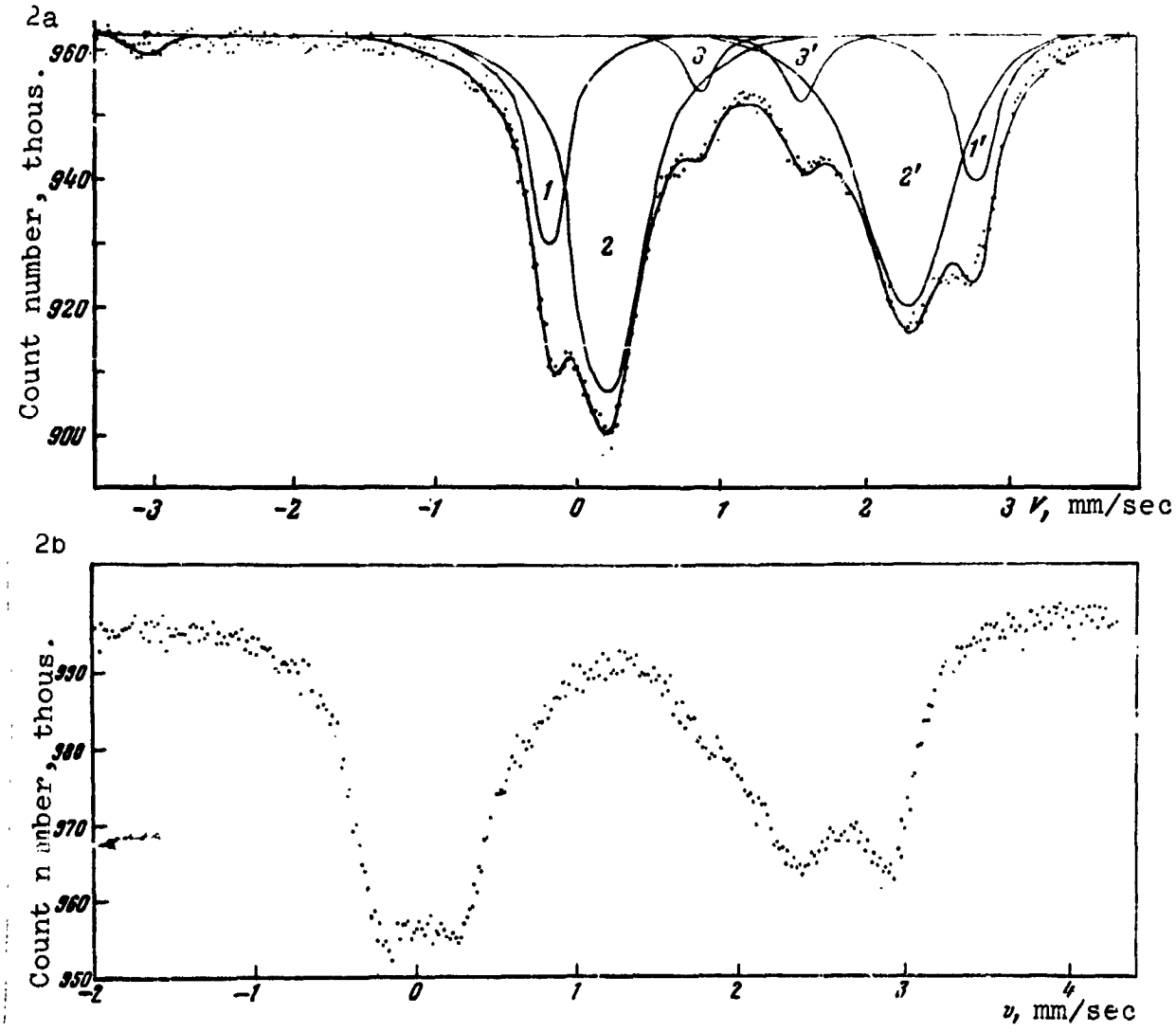

Fig. 2. Mossbauer spectra of sample 3-1
a. Measured at room temperature
b. Measured at temperature of liquid nitrogen. The symbols are the same as in Fig. 1.

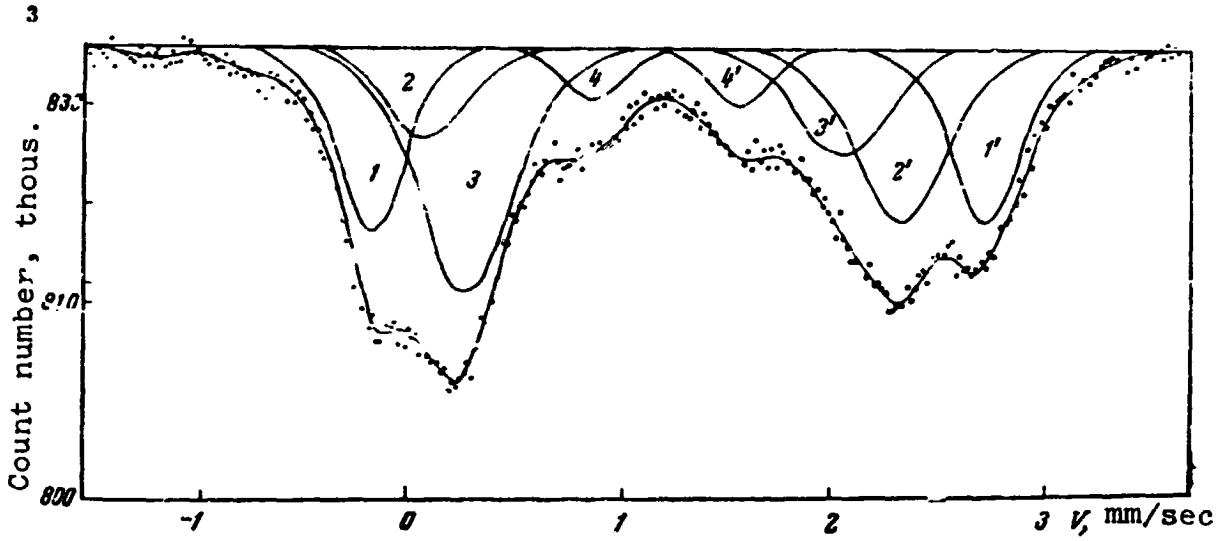

Fig. 3. Mossbauer spectrum of sample 8-2

TABLE 4. PARAMETERS OF MOSSBAUER SPECTRA OF PYROXENE CONSTITUENT OF LUNAR REGOLITH /330

Sample	Grain size, mm	δ, mm/sec	Δ, mm/sec	r, mm/sec: left peak low-velocity	r, mm/sec: right peak low-velocity
3-1	bulk sample	1,27±0,01	2,10±0,01	0,61±0,01	0,74±0,02
3-3a	0,2—0,4	1,22±0,01	2,02±0,01	0,61±0,02	0,64±0,04
8-2	bulk sample	1,23±0,02	2,02±0,01	0,56±0,02	0,68±0,03
9-4a	0,200—0,450	1,21±0,03	2,06±0,04	0,61±0,01	0,83±0,01
9-5a	0,127—0,200	1,24±0,01	2,05±0,01	0,61±0,01	0,82±0,01
9-6a	0,083—0,127	1,24±0,01	2,05±0,01	0,59±0,01	0,68±0,01
9-1 r	<0,083	1,26±0,02	2,04±0,02	0,62±0,01	0,73±0,01

TABLE 5. PARAMETERS OF MOSSBAUER SPECTRA FOR POSITIONS MI AND MII OF PYROXENE CONSTITUENT OF LUNAR REGOLITH

Sample	Grain size, mm	δ, mm/sec: I	δ, mm/sec: II	Δ, mm/sec: I	Δ, mm/sec: II	r, mm/sec: I left	r, mm/sec: I right	r, mm/sec: II left	r, mm/sec: II right
3-1	bulk sample	1,25±0,07	1,24±0,02	2,52±0,07	1,92±0,07	0,60±0,04	0,46±0,20	0,41±0,02	0,49±0,03
8-2	bulk sample	1,18±0,07	1,15±0,02	2,31±0,05	1,78±0,05	0,36±0,17	0,52±0,03	0,69±0,03	0,28±0,05
9-4a	0,200—0,450	1,18±0,01	1,16±0,01	2,28±0,01	1,77±0,01	0,35±0,03	0,45±0,01	0,45±0,02	0,45±0,01
9-5a	0,127—0,200	1,20±0,02	1,18±0,02	2,33±0,02	1,85±0,03	0,35±0,05	0,52±0,01	0,58±0,03	0,43±0,04
9-1r	<0,083	1,16±0,01	1,14±0,02	2,24±0,01	1,79±0,02	0,26±0,02	0,52±0,03	0,54±0,01	0,52±0,04

TABLE 6. PARAMETERS OF MOSSBAUER SPECTRA OF LUNAR ILMENITES

Sample	Grain size, mm	δ, mm/sec	Δ, mm/sec	Γ, mm/sec	
				left peak	right peak
8-2	bulk sample	1,22±0,02	0,69±0,02	0,29±0,04	0,31±0,04
3-3a	0,2—0,4	1,23±0,02	0,66±0,03	0,21±0,04	0,33±0,04
3-1	bulk sample	1,24±0,02	0,70±0,02	0,24±0,03	0,36±0,03
9-4a	0,200—0,450	1,24±0,02	0,70±0,02	0,22±0,01	0,29±0,01
9-5a	0,127—0,200	1,21±0,01	0,65±0,01	0,22±0,01	0,22±0,01*
9-6a	0,083—0,127	1,21±0,01	0,65±0,01	0,21±0,01	0,21±0,01*
8-1r	<0,083	1,20±0,04	0,65±0,01	0,21±0,01	0,21±0,01*

* Examined given the condition $\Gamma_{left} = \Gamma_{right}$.

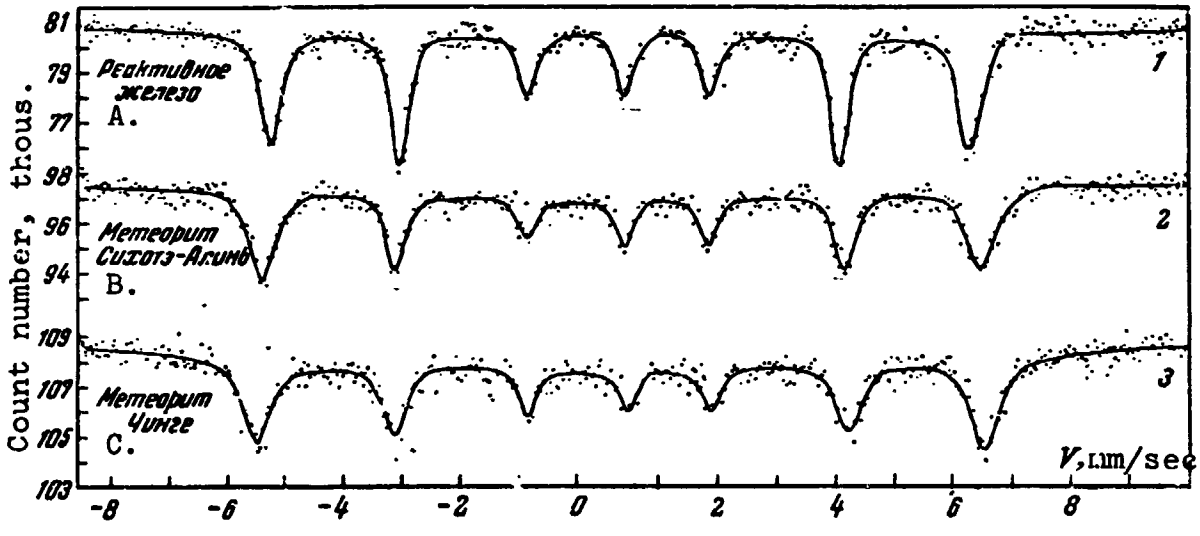

Fig. 4. Mossbauer spectra of iron meteorites of Sikhote-Alin and Chinge, and of pure metallic iron

KEY: A. Reagent, iron
B. Sikhote-Alin meteorite
C. Chinge meteorite

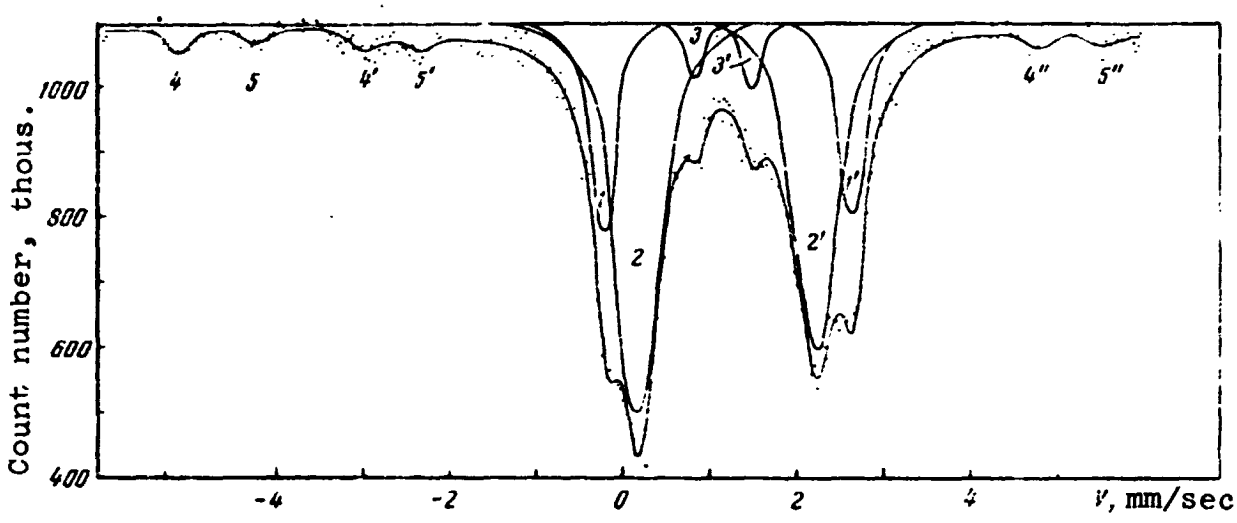

Fig. 5. Mossbauer spectrum of sample 9-6a
5, 5', 5". absorption lines of FeS; remaining symbols are as in Fig. 1.

TABLE 7. RESULTS OF MEASURING MAGNETIC HYPERFINE SPLITTING OF THE LINES IN MOSSBAUER SPECTRA OF SAMPLES OF IRON METEORITES /332

Sample	Left peak, channel nr	Right peak channel nr	Ratio of effective magnetic fields $\frac{H_{eff}(\text{meteorite})}{H_{eff}(\text{iron})}$	Amount of nickel, percent	
				Chemical analysis	Mossbauer measurements
Chinge meteorite	144,0±0,2	408,0±0,3	1,026±0,010	16	8±5
Sikhote-Alin meteorite	147,0±0,2	404,5±0,2	1,036±0,010	6	10±5
Reagent iron	149,0±0,2	401,1±0,2	1,00	0	0
Sample 8-2	150,0±1,4	401,5±0,9	1,00±0,01	—	0

From Table 8 and the figures it is clear that the silicate constituent (olivines and pyroxene glasses) is the bulk of the lunar surface material. As to the ilmenite content, the surface material returned by Luna 16 is closer to the surface material collected by Apollo 12. An increase in the area of the quadrupole doublets of the olivines along the core depth with decrease in grain size is probably associated with the increase in the fayalite constituent.

Thus, Mossbauer spectroscopy, based on the distribution of iron by mineral phases, makes it possible to characterize the type of magma in the sampling location of the lunar surface material.

TABLE 8. MINERAL COMPOSITION OF IRON-CONTAINING PORTION OF REGOLITH (IN PERCENT OF TOTAL AREA IN MOSSBAUER SPECTRUM)

Minerals	Luna 16							Apollo 11 /12/	Apollo 12 /13/
	3-1	3-3a, 0,2—0,4 mm	3-2	9-4a, 0,250—0,450 mm	9-5a, 0,127—0,250 mm	9-6a, 0,063—0,127 mm	9-1г —0,063 mm	1006	1206
Ilmenite	7,7	6,7	8,0	4,9	4,9	5,8	7,1	19,7	6,8
Pyroxene + glass	69,0	71,5	67,9	79,3	75,8	71,0	71,0	67,6	76,4
Olivine	18,3	16,7	25,1	15,8	16,2	22,6	21,9	4,4	11,6
Iron	4,5	5,1	4,1	4,2	3,3	5,1	3,1	5,8	4,3
Troilite	<1	<1	<1	<1	<1	2,8	2,0	1,1	0,9

In conclusion, I express my gratitude to all the laboratory coworkers participating in measuring the samples, and to L. M. Satarova for assistance in processing the spectra on the BESM-4 electronic computer.

REFERENCES

/333

1. Vinogradov, A. P., "Preliminary Data on the Lunar Surface Material Returned by Luna 16 Automatic Station," Geokhimiya (3), (1971).

2. Makarov, Ye. S., Il'in, N. P., and Ivanov, V. I., "Composition and Crystalline Structure of Minerals of Sea of Fertility Regolith," Paper No. K-24 at the 14th Session of COSPAR, June 1971, Seattle, United States.

3. Malysheva, T. V., Kurash, V. V., and Yermakov, A. N., "Gamma-Resonant Mossbauer Spectroscopic Study of the Isomorphic Replacement of Mg and Fe^{2+} in Olivines," Geokhimiya (11), 1405 (1969).

4. Bancroft, G. M., Maddock, A. G., and Burns, R. G., "Applications of the Mossbauer Effect to Silicate Mineralogy," Geochim. Cosmochim. Acta 31, 2219 (1967).

5. Malysheva, T. V., Kurash, V. V., Lavrukhina, A. K., and Akol'zina, L. D., "Mossbauer Spectroscopic Study of Pyroxene in Meteorites," Meteoritika (31), 101 (1972).

6. Gosselin, J. P., Shimony, U., Grodzins, L., and Cooper, A. B., "Mossbauer Studies of Iron in Sodium Trisilicate Glasses," Phys. Chem. Glasses 8(2), 56 (1967).

7. Belyustin, A. A., Ostanevich, Yu. M., Pisarevskiy, A. M., Tomilov, S. B., Bay-Shi, U., and Cher, L., "Mossbauer Effect in Alkaline Iron-Silicate Glasses," Fizika tverdogo tela 7(5), 1447 (1965).

8. Gibb, T. C., Greenwood, N. N., and Twist, W., "The Mossbauer Spectra of Natural Ilmenite," J. Inorg. Nucl. Chem. 31, 947 (1969).

9. Cleveland, B., Guarnieri, C. R., and Walker, J. C., "Magnetic Ordering in Very Thin Iron Films," Bull. Am. Phys. Soc. 15, 108 (1970).

10. Johnston, K., Ridu [transliterated], M., Cranshaw, T., and Madsen, P., "Field of Hyperfine Interaction and Magnetic Moment of Iron Atoms in Ferromagnetic Alloys," in the book: Effekt Messbauera [The Mossbauer Effect], Foreign Literature Pub. House, 1962, p. 367.

11. Zavaritskiy, A. N., and Kvasha, L. G., Meteority SSSR /Meterities of the USSR/, USSR Academy of Sciences Press, 1952.

12. Gay, P., Bancroft, G. M., and Bown, M. G., "Diffraction and Mossbauer Studies of Minerals from Lunar Soils and Rocks," Proc. Apollo 11 Lunar Sci. Conf. 1, 481 (1970).

13. Bancroft, G. M., Bown, M. G., Gay, P., Muir, I. D., and Williams, P. G. L., "Mineralogical and Petrographic Investigation of Some Apollo 12 Samples," Proc. Second Lunar Sci. Conf., 1971.

Order of Lenin Institute of Geochemistry and Analytical Chemistry imeni V. I. Vernadskiy, USSR Academy of Sciences, Moscow

N75 11839

MOSSBAUER ANALYSIS OF LUNA 16 LUNAR SURFACE MATERIAL /334

D. L. Nady, L. Cher, and K. Kulcsar

Samples of Apollo 11 lunar surface material were studied by the Mossbauer effect by numerous authors /1/. Owing to the small number of other resonant isotopes, all measurements were made with Fe^{57} nuclei. The principal constituents of the material were as follows: iron-containing silicates (olivine, pyroxene, and so on), ilmenite ($FeTiO_3$), and metallic iron.

The sample of Luna 16 lunar surface material we measured weighed 60 mg; its thickness was 40 mg/cm^2. The source of resonant gamma-quanta was 25 mCi Co^{57} in Cr. The measurements were made at room temperature on a constant-acceleration Mossbauer unit of the Central Institute of Physics Research, Academy of Sciences of the Hungarian People's Republic /2/. The spectrum was recorded with a model NTA 512-B 1024-channel analyzer.

The spectrum (figure) consists of one hyperfine sextuplet and three poorly resolved quadrupole doublets. The parameters of the spectrum were obtained by the method of least squares /3/ (see Table). They show that the components of the NHR /nuclear hyperfine resonants/ spectrum correspond to metallic iron, ilmenite, and to positions M1 and M2 of iron-containing silicates /1/. Though the statistics of the spectrum were relatively good, quadrupole splitting of ilmenite must be recorded with a value of 0.71 mm/sec /1/ to avoid correlations of the parameters.

Since the relative value of x^2 is 2.54, the sample probably also contains other constituents (troilite?).

The authors are extremely grateful to Academician A. P. Vinogradov for presenting the samples of lunar surface material.

Constituent	Atomic abundance, percent	Hyperfine magnetic field, kOe	Quadrupole splitting, mm/sec	Chemical shift*, mm/sec
Metallic iron	4.5±0.5	331.4±1.0	0.021±0.031	0.181±0.015
Silicates (M1)	28.5±0.9	—	2.748±0.006	1.321±0.002
Silicates (M2)	59.5±1.2	—	1.956±0.005	1.24±0.006
Ilmenite	7.5±0.4	—	0.7 (recorded)	1.202±0.006

* Relative to Co^{57} source in Cr.

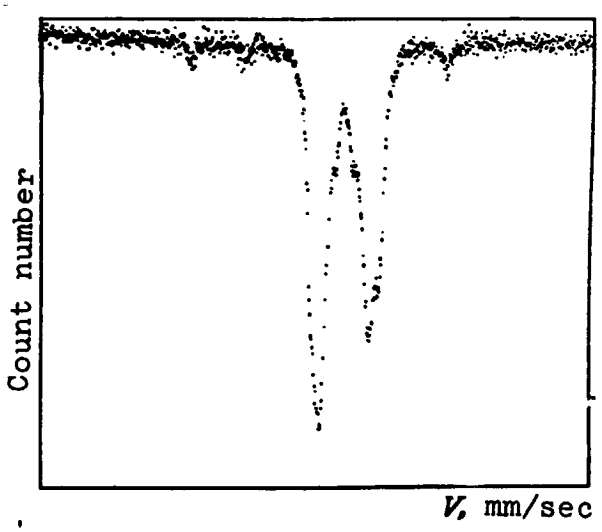

Mossbauer spectrum of sample of lunar regolith.

REFERENCES

1. Greenwood, N. N. and Hower, A. T., Proc. Apollo 11 Lunar Sci. Conf., 3, 2163; Herzenberg, C. L., and Riley, D. L., ibid, p. 2221; Housley, R. M., Blander, M., Agdel-Gawad, M., and Milir, A. H., ibid, 2251 (1970).

2. Serf, E., Varhalmi, L., and Kiss, E., to be published.

3. Nady, D. L., and Kulcsar, K., KFKI-71-66.

Central Institute of Physics Research, Academy of Sciences of the Hungarian People's Republic, Budapest, Hungary

N75 11840

ABUNDANCE OF MERCURY IN REGOLITH OF THE SEA OF FERTILITY, SEA OF TRANQUILLITY, AND OCEAN OF STORMS

/335

Yu. I. Belyayev, and T. A. Koveshnikova

Abstract

The direct determination of mercury by the atomic-fluorescent method is described, involving the pulsed thermal atomization of powdered samples when the mercury is vaporized in argon at normal pressure. The atomization temperature is 800-900° C, the working line of Hg is 253.7 nm, and the weighed regolith sample is 2 mg. The calibration curve was plotted from international reference standards. The detectability of the method estimated by the 3σ criterion is $8 \cdot 10^{-8}$ percent for a 5 mg weighed rock sample. The relative standard deviation at the level of detectability is 0.25; at the level of $1 \cdot 10^{-6}$ it is 0.1 percent. An increase in the mercury abundance in the regolith of the surficial layer with decrease in grain size and with variation in depth was noted, from $6 \cdot 10^{-6}$ in the surficial layer to $9 \cdot 10^{-6}$ percent at a depth of about 30 cm. It is shown that in conditions simulating lunar day, at temperatures of 130-150 C up to 15-20 percent of the mercury is vaporized from a 2 mg regolith weighed sample, and thus the hypothesis is advanced that mercury is adsorbed by the surface layers of the lunar surface material during lunar night and desorbed during lunar day. The assumption is advanced that there exists a meridional "mercury wind" between subsolar region of the Moon (heater) and the polar regions (cooler).

The problem of determining in regolith such a volatile element as mercury is of much interest. The results of determining the content of mercury to some extent permits tracing the thermal prehistory of regolith samples.

To determine mercury in the regolith returned by the Luna 16 station and the Apollo 11 and Apollo 12 expeditions, we developed a sensitive atomic-fluorescent method with pulsed thermal atomization involving vaporizing the mercury in argon at normal pressure from small weighed samples in powder form /1, 2/. The argon atmosphere was used to eliminate quenching of the resonant fluorescence of mercury by air oxygen.

A block diagram of the apparatus is shown in Fig. 1. Light from the excitation source of the fluorescence spectrum 1 is focussed to the side by a quartz lens 2 onto pairs of elements being determined over crucible 3 bearing the sample. The crucible with the sample is heated in the argon atmosphere with electric current to a specified temperature for the vaporization and atomization of the compounds of the elements being determined. Shield 4 makes it possible to reduce the effect of the scattered light. The fluorescence light is gathered by lens 5 onto the entrance slit of monochromator 6, and the photocurrents of the light detector 7 are amplified by a d.c. amplifier 8 and are recorded with automatic potentiometer 9. The layout of the atomic-fluorescent analyzer is shown in Fig. 2.

Heating the sample to the desired temperature leads to a single light pulse of the atomic fluorescence of mercury being produced. The amplitude of this pulse serves as the analytical signal. The resonant line of mercury 2537 AU was used as the working line, and the source of resonant radiation was a high-frequency electrodeless mercury lamp. The unit was calibrated based on international reference standards; the mercury content in these was assumed to be as follows /13/: AGV-1 (andesite) -- $4 \cdot 10^{-7}$ percent; DTS-1 (dunite) -- $8 \cdot 10^{-7}$ percent; GSP-1 (granodiorite) -- $2.1 \cdot 10^{-6}$ percent; G-2 (granite) -- $3.9 \cdot 10^{-6}$ percent; W-1 (diabase) -- $1.1 \cdot 10^{-5}$ percent; and G-1 (granodiorite) -- $2.45 \cdot 10^{-5}$ percent. The weighed sample used for single determination was 2 mg. The atomization temperature was 800-900° C, sufficient for complete and rapid distillation of the mercury from the rock. The detectability evaluated by the 3σ-criterion was $8 \cdot 10^{-8}$ percent. The standard deviation at the limit of detectability was 0.20-0.25, and at the level of $1 \cdot 10^{-6}$ percent -- 0.07-0.1. The calibration graph, the concentration dependence of the standard error, and the concentration dependence of the coefficient of variation are in Fig. 3.

Experimental data that we obtained allow us to estimate the content of mercury in the lunar surface material and also to trace some regularity of its distribution depthwise and by fractions. /336
In both the Luna 16 regolith and in the regolith returned by Apollo 11, Apollo 12, and Apollo 14, some increase in mercury abundance with depth is observed (Tables 1 and 2).

Interestingly, with variation in the size of particles of the fractions investigated, so also does the mercury abundance vary, which is reflected in the results listed in Table 3. Probably, one can speak of an approximately proportional relationship between the mercury abundance and the total surface area of particles (for the same mass of the sample). These same data allow us to assume that in any case, some of the mercury is adsorbed by particle surfaces: the greater the overall surface area, the higher the mercury content.

TABLE 1. DISTRIBUTION OF MERCURY CONTENT BY DEPTH OF REGOLITH CORE

Sampling site	Sample	Depth, cm	Mercury, percent
Sea of Tranquillity (Apollo 11)	10005,34-2	4,5	$1,3 \cdot 10^{-6}$
	10005,35-3	10—11	$7,1 \cdot 10^{-6}$
Ocean of Storms (Apollo 12)	12028,229-1	16	$7,6 \cdot 10^{-7}$
	12028,215*	18—19	$1,7 \cdot 10^{-6}$
	12028,233-2	33	$1,0 \cdot 10^{-6}$
	12028,216*	38—39	$2,0 \cdot 10^{-6}$
Fra-Mauro Formation (Apollo 14)	14148,13[2]*	Trench top	$7,2 \cdot 10^{-7}$
	14156,3[2]*	Middle	$8,6 \cdot 10^{-7}$
	14149,21[2]*	Bottom	$8,2 \cdot 10^{-7}$
	BCR-1		$3,75 \cdot 10^{-6}$

* Data of [4]. [2]* Data of [5].

It can be assumed that the lower mercury content values in the surficial layers compared with the deeper layers are associated with its desorption from the surface of the Moon during the lunar day when the temperature at the subsolar point is 130-150° C, and also with the diffusion of mercury into the deeper, cold layers. It can be assumed that mercury vapor diffuses from the hot lunar interior to the surface. Possibly, the minimum regolith temperature is at a depth of several tens of centimeters where diurnal temperature fluctuations do not penetrate. It is not to be precluded that the maximum mercury content values correspond to these depths.

When estimating the amount of mercury vaporized in conditions simulating the lunar day, we calcined 2 mg of regolith from the Sea of Fertility in a forevacuum (0.05 mm Hg) for 15 min at 135-140° C. As a result of calcining, the samples lost up to 15-20 percent of their initial mercury content. We obtained a similar result for terrestrial basalts. The authors of [4, 6] reached

the same conclusions. If we take the specific gravity of regolith in its natural bedding as 1.2 g/cm^3 /7/ and assume that during the lunar day the surface of the Moon at the subsolar point is uniformly heated to 120-140° C at a depth of 2 mm, then from one cm^2 of surface up to $1 \cdot 10^{-6}$ g mercury can be vaporized.

The question arises as to the fate of the mercury vapor. Probably, at night the mercury vapor condenses on the lunar surface cooled down to -150° C. It is not precluded that even during the lunar day mercury vapor can condense to some extent on the shadowed areas of the lunar landscape: in fractures, in shadow cast by rocks where the temperature can be quite low due to the absence of an atmosphere.

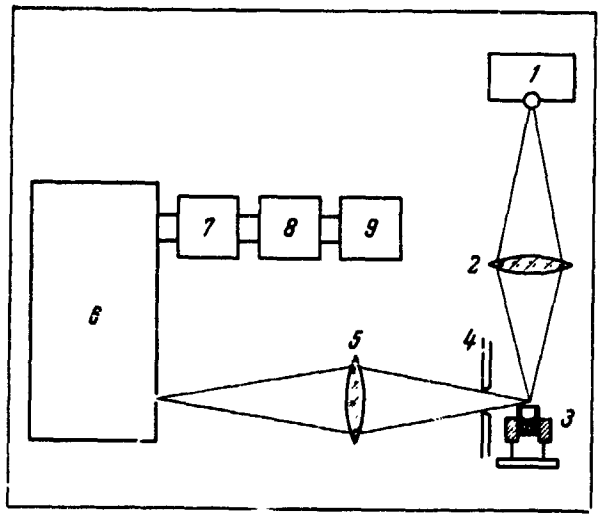

Fig. 1. Block diagram of layout
1. Light source
2, 5. Quartz lenses
3. Graphite crucible containing sample
4. Shield with opening
6. Monochromator
7. Photomultiplier
8. d.c. amplifier
9. Automatic potentiometer

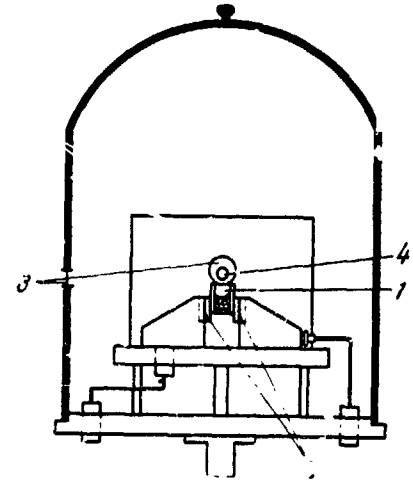

Fig. 2. Layout of atomizer
1. Crucible containing sample
2. Graphite brushes conducting current
3. Quartz windows in glass hood
4. Opening in shield

Considering the volatility of mercury, we can suppose the existence of a meridional "mercury wind" in the direction from the subsolar points (heater) where the Sun is at the zenith during the lunar day and the temperature reaches 140° C, toward the polar /337

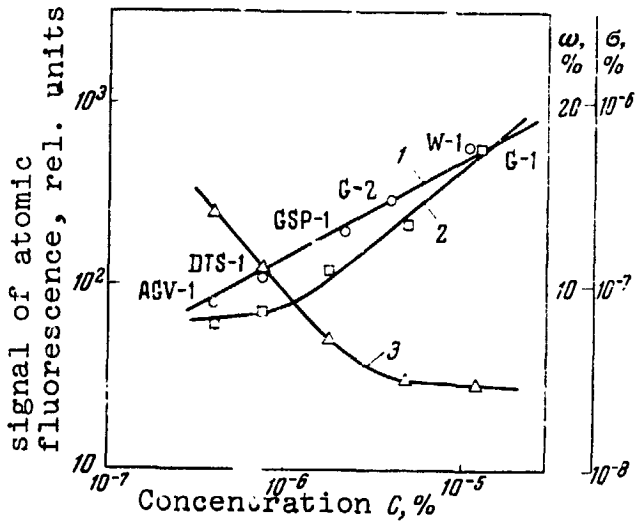

Fig. 3. Calibration graph for determining mercury (1), concentration dependence of standard error σ (2), and concentration dependence of coefficient of variation ω (3)

shadow zones (cooler) when the sunlight strikes the surface at very small angles and therefore the temperature of the regolith surface is close to -150° C, regardless of the time of the lunar 24-hour period. The distance from the heater to the cooler is longer than the length of the mean-free path of mercury atoms in the conditions of the lunar vacuum, and therefore the transfer of energy during collisions and condensation of mercury on the surface are possible. If this is so, then during the millions of years in which the meridional "mercury wind" existed on the surface of the regolith in the polar shadow zones, mercury was deposited in greater concentrations compared with the equatorial zones. Possibly, the weak "mercury wind" exists also between the day and night sides of the Moon.

TABLE 2. DISTRIBUTION OF MERCURY CONTENT BY DEPTH OF SEA OF FERTILITY REGOLITH (LUNA 16) FOR THE FRACTION < 0.083 mm

Depth, cm	Zone	Sample	Mercury, percent
0–8	A	3	$6.1 \cdot 10^{-6}$
8–15	B	6	$2.2 \cdot 10^{-6}$
28–33	G	7+8	$9.0 \cdot 10^{-6}$

TABLE 3. DISTRIBUTION OF MERCURY CONTENT BY DIFFERENT FRACTIONS OF SURFICIAL LAYER (DEPTH 0–8 cm) OF SEA OF FERTILITY REGOLITH (LUNA 16)

Particle size, mm	Mercury, percent
0.127–0.200	$2.2 \cdot 10^{-6}$
0.083–0.127	$4.6 \cdot 10^{-6}$
<0.083	$6.8 \cdot 10^{-6}$

We can also assume that there exists a meridional wind consisting of atoms of other volatile elements: fluorine, bromine, water vapor, and so on, that is, that in the surficial layers of the polar regions abundance of these elements is also somewhat higher compared with the equatorial zones and therefore sampling from the polar regions of the Moon is of interest.

Conclusion. The abundance of mercury in the regolith of the Sea of Tranquillity, Sea of Fertility, and the Ocean of Storms was determined by an atomic-fluorescent method developed (sensitivity $n \cdot 10^{-8}$ percent based on the 3σ-criterion, the coefficient of variation at the sensitivity level is 20-25 percent, and at the level of $1 \cdot 10^{-6}$ -- 7-10 percent). An increase in the mercury content with depth and with decrease in regolith particle size was noted. The assumption was advanced that there exists a meridional "mercury wind" between the subpolar region of the Moon (heater) and the polar regions (cooler). It is shown that in conditions simulating the lunar day, up to 15-20 percent of the mercury vaporizes from the surficial layer of the Sea of Fertility regolith.

The authors are grateful to Academician A. P. Vinogradov and to Candidate of Geologo-mineralogical sciences K. P. Florenskiy for consultation.

REFERENCES

/338

1. Belyayev, Yu. I., Pchelintsev, A. M., Zvereva, N. F., and Kostin, B. I., "Atomic-Absorption Determination of Traces of Elements in Rocks Using Pulsed Thermal Atomization of Solid Samples, Report 1. Determination of Cadmium," Zh. anal. khimii 26, 492 (1971).

2. Pchelintsev, A. M., Belyayev, Yu. I., Karyakin, A. V, and Koveshnikova, T. A., "Increasing the Sensitivity of the Atomic-Fluorescent Determination of Cadmium, Silver, Thallium, Mercury, and Bismuth in Graphite by Pulsed Selective Vaporization in Argon," Zh. anal. khimii 26, 1355 (1971).

3. Flanagan, F. G., "U. S. Geological Survey Standards II. First Compilation of Data for the New USGS Rocks," Geochim. Cosmochim. Acta, 33, 81 (1969); Fleischer, M., "U. S. Geological Survey Standards - I. Additional Data on Rocks G-1 and W-1, 1965-1967," Geochim. Cosmochim. Acta 32, 65 (1969).

4. Reed, G. W., Goleb, J. A., and Jovanovic, S., "Surface-Related Mercury in Lunar Samples," Science 172(3980), 258 (1971).

5. Jovanovic, S., and Reed, G. W., "Trace Element Profiles, Notably Hg, from a Preliminary Study of the Apollo 15 Deep-Drill Core," Earth Planet. Sci. Letters 16, 257 (1972).

6. Goleb, J., "The Determination of Mercury in Small Terrestrial and Nonterrestrial Rock Samples by Atomic-Absorption Spectroscopy, and the Study of Mercury Release at Elevated Temperatures," Appl. Spectrosc., 25, 522 (1971).

7. Vinogradov, A. P., "Preliminary Data on Lunar Surface Material Returned by Luna 16 Automatic Station," Geokhimiya (3), 261 (1971).

Order of Lenin Institute of Geochemistry and Analytical Chemistry imeni V. I. Vernadskiy, USSR Academy of Sciences, Moscow

N75 11841

DETERMINATION OF COPPER, SCANDIUM, MOLYBDENUM, TIN, LEAD, AND IRON GROUP ELEMENTS IN LUNAR SURFACE MATERIAL

/339

L. I. Pavlenko, L. V. Simonova,
and A. V. Karyakin

Abstract

Investigation of the distribution regularities of copper, scandium, molybdenum, tin, lead, and iron group elements in basaltoid rocks of lunar and terrestrial origin is necessary for the further study of the geochemistry of these elements.

To solve the geochemical problems based on the studies made to reduce the effect of the chemical composition of rocks on the results of spectral analysis, a quantitative method of simultaneous spectral determination of copper, scandium, molybdenum, tin, lead, cobalt, nickel, chromium, and vanadium in basaltoid rocks was developed. The sensitivity of the method is 10^{-5} - 10^{-4} percent, and the precision of the method is 10-20 percent.

Samples of various regolith zones taken in the area of the Sea of Fertility were analyzed, along with samples of basic and ultrabasic rocks of the East African Rift for their content of the trace admixtures listed.

The data obtained on the abundance of copper, scandium, molybdenum, tin, lead, cobalt, nickel, chromium, and vanadium in Luna 16 lunar surface material was compared with the abundance of these elements in samples of lunar rocks returned by Apollo 11, Apollo 12, and Apollo 14, with the exception of scandium; its content in the latter samples is considerably higher.

Study of the distribution regularities of copper, scandium, molybdenum, tin, lead, and iron group elements in the course of the evolution of magmatic melts is necessary to clarify the questions

of the depth and conditions of the genesis of these melts, the pathways and mechanism of their evolution, which is important both for lunar and terrestrial rocks.

To solve the geochemical problems posed, a spectral method of the simultaneous determination of these elements with enhanced sensitivity and precision is most promising.

In view of the fact that in the literature there are no studies on the simultaneous spectral determination of copper, scandium, molybdenum, tin, lead, and iron group elements (cobalt, nickel, chromium, and vanadium) in basic and acidic rocks, the aim of this study was to develop a method for simultaneous determination of these elements with high sensitivity and precision for the purpose of investigating the geochemistry of these elements.

The spectral determination of the elements listed in rocks rich in iron involves great difficulties, which leads to systematic errors when spectral determinations are made of their content of copper, scandium, molybdenum, tin, lead, cobalt, nickel, chromium, and vanadium /1-3/.

To increase the sensitivity of the determinations of these elements in basaltoid rocks of lunar and terrestrial origin (regolith, basalt, trachite, phonolite, and nephelinite), investigations were made on stabilizing the combustion of the arc and selecting optimal conditions of analysis; a study was also made of the effect of various additives and buffers. The investigation was conducted with a diffraction spectrograph with a high dispersion by the method of vaporizing samples from the channel of a carbon electrode in a d.c. arc.

Splashing of the samples during their vaporization in the arc was eliminated by using special electrodes and employing a buffer mixture consisting of carbon powder and 10 percent $BaCO_3$ /4, 5/.

The buffer used stabilizes the arc temperature and regulates the processes of sample vaporization during combustion of rocks having different chemical composition and with a high copper content.

The temperature was estimated from the change in the potential difference at the arc electrodes during the entire exposure when the test elements were being vaporized from basalts, trachite, picrite, and nephelinite with and without the buffer. Use of the buffer maintained the potential difference at the arc electrodes /341 at a certain (25-27 V) level, while in its absence, the voltage varied from 12 to 37 V.

TABLE 1. CONTENT OF ELEMENTS IN INTERNATIONAL STANDARDS (IN g/TON /6, 7/) /340

Element-Standard	BCR-1		BM		AGV-1		W-1		Sy	
	1	2	1	2	1	2	1	2	1	2
V	384	520	180	250	121	137	240	250	89,0	79,0
Cr	16,3	23,0	123	145	12,9	19,0	120	123	54,0	50,0
Ni	15,0	18,0	55,0	64,0	17,8	23,0	78,0	90,0	40,0	43,0
Co	35,5	35,0	31,0	44,0	15,5	17,0	50,0	62,0	19,0	17,0
Cu	22,4	33,0	48,0	57,0	63,7	89,0	110	135	23,0	25,0
Sc	36,5	33,0	34,0	38,0	13,3	17,5	34,0	38,0	15,0	13,0
Sn	1,4	2,3	1,2	0,9	3,2	3,6	—	—	—	—
Pb	18,0	19,0	12,0	15,0	35,4	53,0	—	—	—	—
Mo	3,9	4,2	0,7	0,9	3,7	3,3	0,5	1,1	—	—

1. Literature data; 2. Given method

Thus, buffering leads to the reduced influence of the tertiary constituents during the analysis of rocks having different chemical compositions on the trace admixtures listed (Fig. 1 a, b).

Fig. 1 presents the calibration graphs for the determination of V, and Fig. 2 -- for Sc and nephelinites, trachites, and basalts with and without buffer. As we can see from inspecting the figures, for scandium this influence is completely eliminated, while for vanadium the use of the buffer leads to a considerable reduction in the effect of tertiary constituents.

The method of three reference standards was used in the investigation; the calibration graphs were constructed in the coor inates lg R vs lg C. The following analytical lines were used in the investigation (in AU): V -- 3183.9; 3185.4; 3118.3; Cr -- 3014.8; Ni -- 3050.8; 3012.0; Co -- 3044.0; Sc -- 3368.9; 3353.7, and 3273.6; Cu -- 3273.9; Mo -- 3170.3; Pb -- 2833.0; and Sn -- 3175.0.

As part of the analysis of basaltoid rocks of lunar surface material and rocks from the East African massif, four series of reference standards were prepared compositionally analogous to the rocks being analyzed: basaltic, trachitic, phonolitic, and nephelinitic. The basaltic and nephelinitic series of reference standards were prepared on an unofficial basis; the basis for the phonolitic series was a sample of natural phonolite not containing the trace /342 elements being determined. In preparing the trachite base, use was made of natural feldspar to which iron oxide was added.

Selection of the optimal conditions of analysis, use of a high-dispersion spectrograph, and employing a buffer considerably increased

TABLE 2. CONTENT OF INDIVIDUAL ELEMENTS IN VOLCANIC ROCKS OF THE EAST AFRICAN RIFT ZONE (IN g/TON /8, 9/)

Rocks	Sample number	V	Ni	Sc	Cr	Cu	Co
I. Series of alkaline rocks							
Picrites (alkaline)	11034	42	280	13	700	—	—
Olivine melanephelinites	11197	180	167	21	445	—	—
	11064	165	150	28	560	—	—
	11091	200	59	21	140	—	—
	11092	165	35	25	54	—	—
Nephelinites	11001	185	4	5	8	—	—
	11027	160	4	6	17	—	—
	11086	100	6	10	10	—	—
	11113	56	3	1	1	—	—
Phonolites	11344	2	1	10,6	1	—	—
	51	4	1	4	4	3	4
	11196	81	2	0,7	7	—	—
	11198	59	2	0,6	4	—	—
	318	63	2	0,6	4	16	7
	11205	130	4	7	8	—	—
Pyroxenite--inclusions on intrusive rocks	11075	265	27	29	30	—	—
Ijolite	11266	120	5	6	8	—	—
II. Series of rocks of moderate alkalinity							
Picrito-basalts	11132	145	23	23	625	—	—
	11244	200	325	35	297	—	—
Olivine basalts	11320	210	147	35	217	—	—
	11323	450	54	28	39	—	—
	11331	300	80	35	100	—	—
Olivine andesito-basalts	11126	177	17	13	10	—	—
Trachites	11115	4	2	5	9	110	0,9
	206	12	2	5	6	11	2
	11121	16	2	4	5	3	2

Remark. In view of the contamination of the basalt basis with copper, its determination in the basalts did not appear possible.

the sensitivity of the determination of the above-listed elements to $1\text{-}5\cdot10^{-4}$ percent for Sc, Mo, Sn, Pb, Co, Ni, and Cr, and to $1\cdot10^{-5}$ percent for Cu and V when they were determined simultaneously.

The coefficient of variation was 10-20 percent, depending on the element being determined and its concentration. The correctness of the method was checked with the international standards (andesite AGV-1, basalt BCR-1, dunite DTs-1, peridotite PCC-1, granodiorite GSP-1, basalt BM, diabase W-1, and granite G-1).

TABLE 3. CONTENT OF ELEMENTS IN LUNAR SURFACE MATERIAL (IN g/TON [11, 12]) /341

Element	Apollo 11	Apollo 12	Apollo 14	Luna 16				Basalts of the East African Rift
				9-1a	9-1b	7-1g	interval of content values	
V	70—82	13—92	32—85	70	82	86	70—86	145—450
Cr	2760—3060	1050—3750	700—3000	1800	2100	2200	1800—2200	10—625
Sc	59—77	21—50	16—43	21	41	38	21—41	13—35
Co	30—32	13—42	19—56	26	30	27	26—30	
Ni	<5—200	80—350	14—320	210	240	250	210—250	17—325
Pb	1,2—6	—	—	3,1	2,3	2,6	2,3—3,1	—
Sn	—	—	—	<5	<5	13	<5—13	—
Mo	—	—	—	18	28	30	18—30	—

* Analysis of the regolith samples was based on the following weighed samples: 9-1a -- 20 mg; 6-1b -- 18 mg; 7-1g -- 18 and 20 mg.

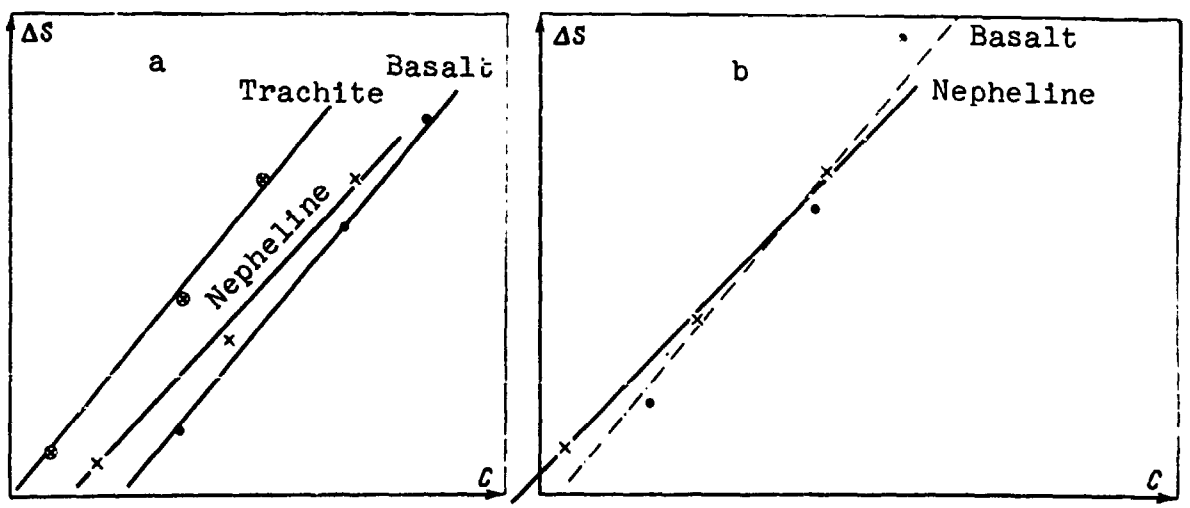

Fig. 1. Calibration graphs for the determination of vanadium.
a. In nephelinites, trachites, and basalts without buffer;
b. In nephelinites, trachites, and basalts with buffer; for vanadium, the analytical line is 3118.3 AU.

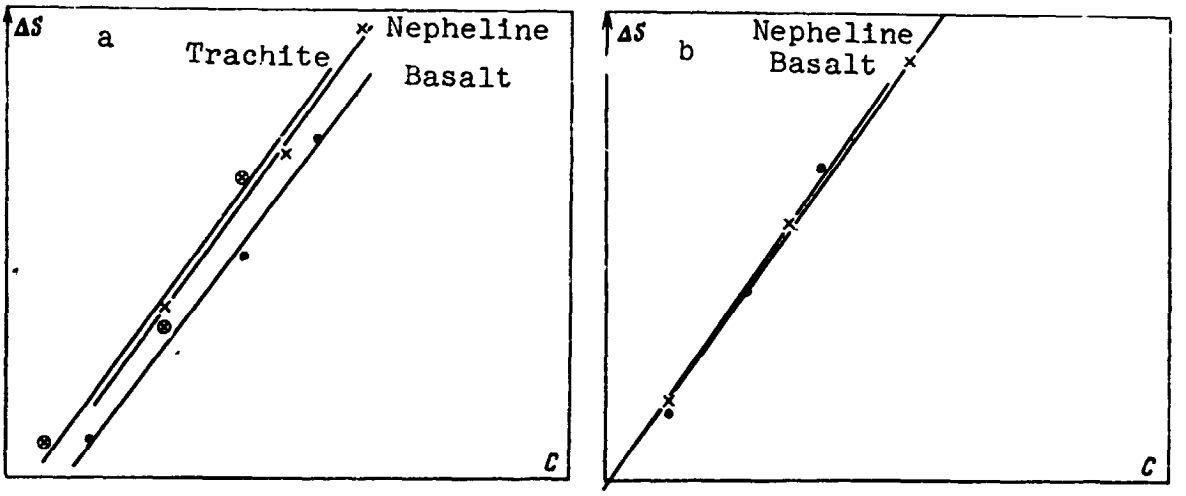

Fig. 2. Calibration graphs for the determination of scandium.
a. In nephelinites, trachites, and basalts without the use of buffer
b. In nephelinites, trachites, and basalts with buffer; the analytical line for scandium was 3273.62 AU.

These results agree well with the data cited in the literature for the above-listed standards (Table 1 /6, 7/).

The method developed was checked for samples of rocks of the alkaline-basaltic magma of the East African Rift Zone (see Table 2). The table gives data on the content of vanadium, nickel, scandium, chromium, copper, and cobalt in the volcanic rocks of the East African Rift Zone for the series of alkaline rocks and for the series of rocks with moderate alkalinity. As follows from the table, the maximum content values of vanadium, nickel, scandium, chromium, and cobalt in both rock series are confined to the most basic members of the series. With increase in the rock alkalinity, the concentrations of all five elements drops off sharply /8, 9/.

The proposed method was used in analyzing rocks of lunar origin returned by the Luna 16 station. Employed as reference standards for the determination of Cu, Sc, Mo, Sn, Pb, Co, Ni, Cr, and V in the lunar samples were rocks of basaltoid composition selected on the basis of a preliminary study of the mineralogic composition of the sample of lunar surface material and their semi-quantitative spectral analysis compared with analogous rocks of terrestrial origin /10/.

The data obtained dealing with the content of cobalt, nickel, chromium, vanadium, scandium, copper, molybdenum, tin, and lead in the various regolith zones taken from the area of the Sea of Fertility

are given in Table 3; this table also gives comparative data on the content of these elements in lunar rocks returned by Apollo 11, Apollo 12, and Apollo 14. The last column of the table presents the intervals of content values of the above-listed elements in the basaltoid rocks of the East African Rift.

From this table it follows that these results on the content of Mo, Sn, Pb, Co, Ni, Cr, and V in lunar surface material returned by Luna 16 are compatible with the results obtained for Apollo 11, Apollo 12, and Apollo 14, with the exception of scandium, whose content in the latter is considerably higher /10, 12/.

Conclusions. An investigation was made to diminish the effect of chemical composition of igneous rocks on the results of the /343
spectral determination therein of trace admixtures.

The action of a buffer aimed at stabilizing the plasma temperature and regulating the vaporization of samples containing a high amount of iron was studied. It was shown that adding a buffer mixture consisting of carbon powder and 10 percent $BaCO_3$ leads to a diminished influence of tertiary constituents in the analysis of rocks having different chemical composition.

A quantitative method for the simultaneous spectral determination of V, Co, Cr, Ni, Cu, Sc, Sn, Pb, and Mo in basic and ultrabasic rocks was developed, with a sensitivity of 10^{-5} to 10^{-4} percent and a coefficient of variation of 10-20 percent.

Study of vanadium, cobalt, nickel, chromium, copper, and scandium in the effusive rocks of the East African Rift made it possible to establish that the regularities of their distribution in the rocks studied are analogous to the regularities of the distribution of these elements in the series of rocks arising through crystallization differentiation of the parent magma.

The above-considered method of analysis proved suitable for investigating the lunar surface material returned by Luna 16. It was established that the content of iron group elements and of copper in the lunar surface material has the same values as in the lunar surface material returned by Apollo 11, Apollo 12, and Apollo 14 and analyzed by various instrumental techniques.

The authors express their gratitude to Professor V. I. Gerasimovskiy for offering the samples of rocks of the alkaline-basaltic magma of the East African Rift Zone and for valuable advice in discussing the article.

REFERENCES

1. Rusanov, A. K., Alekseyeva, V. M., and Khirtov, V. G., Kolichestvennoye spektral'noye opredeleniye redkikh i rasseyannykh elementov /Quantitative Spectral Determination of Rare and Disseminated Elements/, Gosgeoltekhizdat, 1960, p. 73.

2. Pyatova, V. N., Alekseyeva, V. M., and Rusanov, A. K., "Spectrographic Determination of Cobalt, Nickel, Vanadium, Chromium, and Titanium in Silicate Rocks and in Iron Ores" (Nauchnyy sovet po analiticheskim metodam, Instruktsiya No. 106-s /Scientific Council on Analytical Methods, Instruction No. 106-s/), VIMS[1], Moscow, 1971.

3. Serdobova, L. I., and Lizunov, N. V., in the book: Spektral'nyy analiz v geologii i geokhimii /Spectral Analysis in Geology and Geochemistry/, "Nauka", 1967, p. 173.

4. Rusanov, A. K., Spektral'nyy analiz rud i mineralov /Spectral Analysis of Ores and Minerals/, Moscow-Leningrad, 1948, pp. 63-64.

5. "Spectral Analysis in Geology," Materialy 4 seminara po spektral'nomu analizu dlya rabotnikov organizatsiy Ministerstva geologii SSSR /Materials of the Fourth Seminar on Spectral Analysis for Personnel in Organizations of the USSR Ministry of Geology/, 1971, p. 227.

6. Flanagan, F. J., Geochim. Cosmochim. Acta, 33, 81-120 (1969).

7. Fleischer, M.,Geochim. Cosmochim. Acta, 33, 65-79 (1969).

8. Gerasimovskiy, V. I., Geokhimiya 5, (1971).

9. Simonova, L. V., Raspredelniye elementov gruppy zheleza, medi i skandiya v protsesse evolyutsii shelochnobazal'tovoy magmy, Diplomnaya rabota /Distribution of Iron Group Elements, Copper, and Scandium During the Evolution of Alkaline-Basaltic Magma, Diploma Study/, Moscow, 1969.

[1] All-Union Scientific Research Institute of Mineral Raw Materials

10. Vinogradov, A. P., Geokhimiya 3, 261 (1971).

11. Chakles, S., Helz, A., and Helz, A. W., "Emission Spectrographic Determination of Trace Elements in Lunar Samples from Apollo 11," Proc. Apollo 11 Lunar Sci. Conf. 2, 991 (1970).

12. "Preliminary Examination of Lunar Samples from Apollo 14," Science 173, 681-693 (1971).

Order of Lenin Institute of Geochemistry and Analytical Chemistry imeni V. I. Vernadskiy, USSR Academy of Sciences, Moscow

N75 11842

DETERMINATION OF VOLATILE ANIONS -- PHOSPHORUS, SULFUR, FLUORINE, AND ALSO BERYLLIUM AND BORON IN LUNAR REGOLITH BY EMISSION SPECTRAL ANALYSIS

/344

Ye. N. Savinova, A. V. Karyakin,
and T. P. Andreyeva

Abstract

From studying processes occurring in the arc discharge and in the plasma jet, a new method of direct spectral determination was developed for the following anions: phosphorus, sulfur, fluorine as well as beryllium and boron in lunar surface material. The excitation source was a plasmotron with consumable electrodes. The plasma-forming gas was helium. The weighed sample for a single determination was 10 mg. The detectability (3σ-criterion) was: P -- $2.5 \cdot 10^{-3}$, S -- $5.0 \cdot 10^{-2}$, F -- $2.5 \cdot 10^{-3}$, Be -- $5.0 \cdot 10^{-5}$, and B -- $2.5 \cdot 10^{-4}$. The coefficient of variation for a single determination of phosphorus, sulfur, fluorine, beryllium, and boron was 5-10 percent.

In obtaining the most preliminary ideas of the lunar surface material returned by the Luna 16 automatic station, at the first stage of the investigation semiquantitative spectral analysis of several of its samples was carried out. The analysis followed the last-lines method, as well as the method of comparisons of the resulting spectra of lunar samples with the spectra of several rocks of terrestrial origin: granite, dunite, and basalt, and also meteorites.

Our results show that samples of lunar surface material do not differ markedly in chemical composition from terrestrial rocks and are very close to basalts with respect to the abundance of the principal rock-forming constituents.

Of major interest is the determination of the volatile element-anions (F, P, S, and so on) in lunar surface material. It is known that water and OH groups were not found in the regolith, therefore it was expedient also to trace the behavior of volatile anions.

We developed a method of determining fluorine in geological objects by using a plasmotron [1, 3]. For further improvement in the method permitting simultaneous determination of the above-indicated elements, we studied the conditions of vaporization and excitation of volatile elements, difficult to excite, in a plasma spectral source. A d.c. plasmotron with consumable electrodes was used as the source; a general view of the plasmotron is in Fig. 1. The proposed design of the plasma burner provided a stable plasma jet at a fairly high temperature (15,000°) with relatively low arc current ($\leqslant$ 50 A) and low gas volume flow (10 liters/min).

The properties and parameters of the plasma arc depend to a large extent on the properties of the plasma-forming gas, ordinarily argon, nitrogen, hydrogen, or their mixtures. In order to excite in the plasma jet the atoms of elements such as phosphorus, sulfur, and halogens (elements with high excitation potentials and, in addition, highly volatile), it is necessary not only to produce a high-temperature plasma, but also conditions under which the fullest vaporization of the elements of interest to us would become possible. Our investigations showed that only the use of helium, a gas with a very high ionization potential and high thermal conductivity permits obtaining the atomic spectra of fluorine, phosphorus, sulfur, and other elements.

The dependence of the intensity of spectral lines on the composition of the sample in analysis raises one of the main difficulties in spectral analysis. To reduce the effect of this factor, we used a buffer mixture consisting of carbon powder and potassium bromide, which also served as a thickener.

Experimental investigations showed that the effect of the base on the determination of fluorine, phosphorus, sulfur, boron, and beryllium is absent in our method. This is evidently accounted for by the constancy of the temperature of the discharge plasma, which in turn is due to the constancy of the effective ionization potential established by helium and potassium bromide, as well as the partial surface vaporization of the sample from the channel of the carbon electrode in a short exposure, leading to a sharp reduction in the fractional vaporization. /345

Based on a study of processes occurring in the arc discharge and the plasma jet, a fundamentally new method of the direct simultaneous determination of the following anions was developed: fluorine, phosphorus, sulfur, as well as boron and beryllium in lunar surface material.

TABLE 1. RESULTS OF DETERMINING SEVERAL ELEMENTS IN INTERNATIONAL REFERENCE STANDARDS AND THEIR COMPARISON WITH LITERATURE DATA

Element	Content in standard W-1, percent		Content in standard BCR-1, percent		Content in standard BM, percent	
	given method [5]		given method [4]		given method [6]	
P	$4.8 \cdot 10^{-3}$	$6.1 \cdot 10^{-2}$	$1.4 \cdot 10^{-1}$	$1.6 \cdot 10^{-1}$	—	—
F	$2.4 \cdot 10^{-2}$	$2.5 \cdot 10^{-2}$	$4.4 \cdot 10^{-2}$	$4.8 \cdot 10^{-2}$	$1.7 \cdot 10^{-2}$	$2.5 \cdot 10^{-2}$
Be	$1.7 \cdot 10^{-4}$	$1.5 \cdot 10^{-4}$	—	—	—	—
B	$1.6 \cdot 10^{-3}$	$1.5 \cdot 10^{-3}$	—	—	$1.3 \cdot 10^{-3}$	$1.5 \cdot 10^{-3}$

TABLE 2. SENSITIVITY OF DETERMINATION OF P, S, F, Be, AND B AND THE ABUNDANCE OF THESE ELEMENTS IN LUNAR SURFACE MATERIAL

Element	Analytical line, AU	Sensitivity of determination based on 3 σ, percent	Mean content in Earth's crust, percent	Content in lunar surface material, percent (regolith 9-1a, mg weighed sample)
P	I 2553.3	$2.5 \cdot 10^{-3}$	$9.3 \cdot 10^{-2}$	$4.4 \cdot 10^{-2}$
S	I 6757.1	$5.0 \cdot 10^{-2}$	$4.7 \cdot 10^{-2}$	$1.1 \cdot 10^{-1}$
F	I 6856.0	$2.5 \cdot 10^{-3}$	$6.6 \cdot 10^{-2}$	$1.1 \cdot 10^{-2}$
Be	II 3130.4	$5.0 \cdot 10^{-4}$	$3.8 \cdot 10^{-4}$	$1.0 \cdot 10^{-4}$
B	2496.8	$2.5 \cdot 10^{-4}$	$1.2 \cdot 10^{-3}$	$<1.0 \cdot 10^{-3}$

The sample of lunar surface material being analyzed (9-1a) was a fraction with grain size less than 83 μm (zone V, depth 20-28 cm). The light source (plasmotron) was focussed directly at the slit of an STE-1 spectrograph with a single-lens condenser. The power supply to the plasmotron came from a VARS-275-100 rectifier with a working voltage of 280 V and a current strength of 40-50 A. The plasmotron arc was fired with a high-frequency discharge. The /346
distance between the electrodes was 3.0 mm, the diameter of the opening in the lower electrode-anode was 4.0 mm, the depth 2.0 mm, the diameter of the nozzle in the carbon cathode 1.8 mm, the helium volume flow 10 liters/min, and the exposure time 15 sec. The sample mixed with the buffer was tamped tightly into the electrode opening. The sample consumption in a single analysis was 10 mg. The spectra were recorded on KN-4S motion picture film. The calibration graphs (Fig. 2) were plotted in the coordinates $\Delta S/\ell gC$. The internal

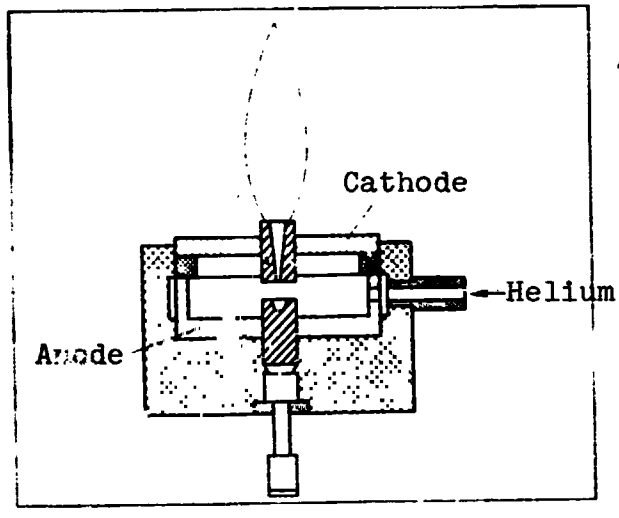

Fig. 1. General scheme of plasma burner

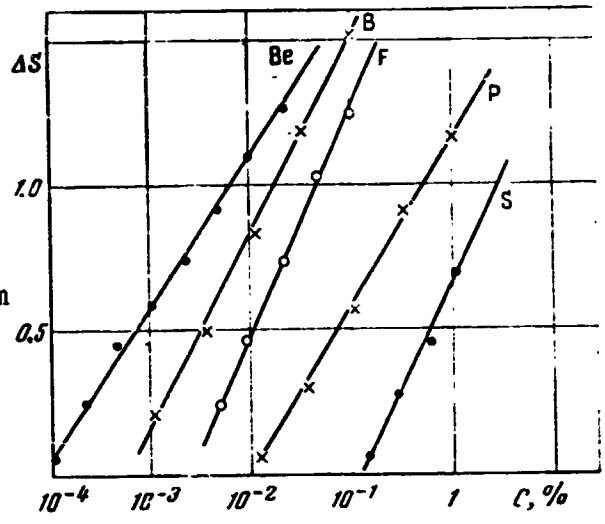

Fig. 2. Calibration graphs for determination of beryllium, boron, phosphorus, and sulfur in rock powders

standard was the background near the line. The following artificial reference standards were used (in percent): SiO_2 -- 60; Al_2O_3 -- 15; Na_2CO_3 -- 14; Fe_2O_3 -- 5; CaO -- 5; and MgO -- 1. The base was ground, calcined 12 hours in a muffle furnace, then reground in a vibratory mill, and then to the leading reference standard were added F, P, S, and Be in the form of NaF, KH_2PO_4, K_2SO_4, and BeO, and B was added in the form of datolite -- $Ca_2(BSiO_4)_2(OH)_2$. The remaining reference standards were prepared by subsequent dilution. The content of F, P, S, B, and Be in the reference standards was $1 \cdot 10^{-4}$ - 1 percent. The coefficient of variation of the single determination of fluorine, phosphorus, sulfur, boron, and beryllium was 5-10 percent.

The accuracy of the method was checked with standards of different rocks: granite, diabase, sulfide or syenite, and nephelinic syenite. As Table 1 shows, the results of our determinations and the literature data are in good agreement, indicating the reliability of the method. Table 2 gives the wavelength based on which F, S, P, B, and Be were determined in lunar surface material, along with the sensitivity of the method and the content of these elements in the lunar sample.

As follows from Tables 1 and 2, the content of volatile elements in the lunar regolith is considerably lower than in

TABLE 3. RESULTS OF VARIOUS AUTHORS ON THE DETERMINATION OF PHOSPHORUS, SULFUR, FLUORINE, BERYLLIUM, AND BORON IN LUNAR SURFACE MATERIAL RETURNED BY COSMONAUTS IN APOLLO 11, APOLLO 12, AND APOLLO 14, AND THEIR COMPARISON WITH THE RESULTS OF OUR DETERMINATIONS OF THESE ELEMENTS IN THE REGOLITH RETURNED BY THE LUNA 16 STATION

Element, g/ton	Apollo 11, sample 10084 [7-15]	Apollo 12, sample 12070 [16-19]	Apollo 14, sample 14163, 14259 [20-25]	Luna 16, sample No. 18 [21]	Luna 16, given method, sample 9-1a, regolith, 10 mg
P	213—1400	644—1376	1806-2236	—	440
S	770—1753	530—1104	800—900	—	1100
F	66—144	60—63	100—300	—	110
Be	1,6—4,0	3,2—4,3	3,1—4,4	1,2	1,0
B	1,0—8,0	9,0—11,0	7,0—20,9	2,6	1,0

terrestrial basalts. Table 3 gives the data on the determination of several elements in lunar surface material returned by the American cosmonauts in Apollo 11, Apollo 12, and Apollo 14, and by the Luna 16 automatic station. As follows from Table 3, the results of our determinations of phosphorus, sulfur, fluorine, beryllium, and boron, in regolith 9-1a are close to the results of the determinations of these elements in the regolith 10084 returned in Apollo 11 [7].

REFERENCES

1. Savinova, Ye. N., and Karyakin, A. V., "Spectral Method of Determining Fluorine in Rocks," Zh. anal. khimii 25, 7 (1970).

2. Karyakin, A. V., Savinova, E. N., and Zakharov, E. A., "The Use of Plasma Jet and Hollow Cathode Discharge for Fluorine Analysis in Rocks and Minerals," XV Colloquium Spectroscopicum Internationale, Madrid, 1969, Proceedings IV, 4 (1971).

3. Gerasimovskiy, V. I., and Savinova, Ye. N., "Fluorine Content in Volcanic Rocks of the East African Rift Zone," Geokhimiya 12 (1969).

4. Flanagan, F. I., "U.S. Geological Survey Standards -- II," Geochim. Cosmochim. Acta 31, 289 (1967).

5. Fleischer, M. N., "U.S. Geological Survey Standards -- I. Additional Data on Rocks G-1 and W-1. 1965-1967," Geochim. Cosmochim. Acta 33, 65 (1969).

6. Grassmann, H., "Report Four. Discussion on the Content of Several Principal Constituents Based on a New Analytical Technique," Z. Angew. Geol. 13, 473 (1967).

7. Annel, C. S. et al., "Emission Spectrographic Determination of Trace Elements in Lunar Samples from Apollo 11," Proc. Apollo 11 Lunar Sci. Conf. 2, 911 (1970).

8. Compston, W. et al., "The Chemistry and Age of Apollo 11 Lunar Material," Proc. Apollo 11 Lunar Sci. Conf. 2, 1007 (1970).

9. Engel, A. E. J. et al., "Lunar Rock Compositions and Some Interpretations," Proc. Apollo 11 Lunar Sci. Conf. 2, 1081 (1970).

10. Kaplan, I. R. et al., "Carbon and Sulfur Concentration and Isotopic Composition in Apollo 11 Lunar Samples," Proc. Apollo 11 Lunar Sci. Conf. 2, 1317 (1970).

11. Maxwell, J. A. et al., "Chemical Composition of Apollo 11 Lunar Samples 10017, 10020, 10072, and 10084," Proc. Apollo 11 Lunar Sci. Conf. 2, 1369 (1970).

12. Morrison, G. H. et al., "Elemental Abundances of Lunar Soil and Rocks," Proc. Apollo 11 Lunar Sci. Conf. 2, 1383 (1970).

13. Reed, G. W. et al., "Halogens, Mercury, Lithium, and Osmium in Apollo 11 Samples," Proc. Apollo 11 Lunar Sci. Conf. 2, 1487 (1970). /347

14. Smales, A. A. et al., "Elemental Composition of Lunar Surface Materials," Proc. Apollo 11 Lunar Sci. Conf. 2, 1575 (1970).

15. Wanke, H. et al., "Major and Trace Elements in Lunar Material," Proc. Apollo 11 Lunar Sci. Conf., 2, 1719 (1970).

16. Bouchet, M. et al., "Spark Mass Spectrometric Analysis of Major and Trace Elements in Six Lunar Samples," Proc. Second Lunar Sci. Conf 2, 1247 (1971).

17. Morrison, G. H. et al., "Elemental Abundances of Lunar Soil and Rocks from Apollo 12," Proc. Second Lunar Sci. Conf. 2, 1169 (1971).

18. Willis, J. P. et al, "Some Interelement Relationships Between Lunar Rocks and Fines and Stony Meteorites," Proc. Second Lunar Sci. Conf. 2, 1123 (1971).

19. Guttitta, F. et al., "Elemental Composition of Some Apollo 12 Lunar Rocks and Soils," Proc. Second Lunar Sci. Conf. 2, 1217 (1971).

20. Compston, W. et al., "Age and Petrogenesis of Apollo 14 Basalts," Third Lunar Sci. Conf., 1972, January 10-13. Abstract 136.

21. Eugster, O., "Li, Be, and B Abundances in Fines from the Apollo 11, Apollo 12, Apollo 14, and Luna 16 Missions," Third Lunar Sci. Conf., 1972, January 10-13. Abstract 226.

22. Hubbard, N. I., Gast, P. W., "Chemical Composition of Apollo 14 Materials and Evidence for Alkali Volatilization," Third Lunar Sci. Conf., 1972, January 10-13. Abstract 361.

23. Jackson, P.F.S. et al., "The Analysis of Lunar Material Returned by Apollo 14," Third Lunar Sci. Conf., 1972, January 10-13. Abstract 377.

24. Reed, G. W., et al., "Concentration and Liability of the Halogens, Platinum Metals and Mercury in Apollo 14 Samples," Third Lunar Sci. Conf., 1972, January 10-13. Abstract 559.

25. Wanke, H. et al., "Multi-element Analysis of Lunar Samples," Third Lunar Sci. Conf., 1972, January 10-13. Abstract 688.

Order of Lenin Institute of Geochemistry and Analytical Chemistry imeni V. I. Vernadskiy, USSR Academy of Sciences, Moscow.

N75 11843

GENESIS OF LUNAR REGOLITH

/348

A. P. Vinogradov

Abstract

From comparing the mineral and chemical composition of regoliths with the compositions of primary magmatic lunar rocks, it is shown that mare regolith is enriched in aluminum and depleted in iron, titanium, and chromium. This effect cannot be accounted for only by the admixture of highland anorthositic material. The entire array of geochemical data points to the considerable role of depthwise differentiation of the magmatic material in forming the composition of the primary lunar rocks and, naturally, the composition of the regolith. During regolith formation, processes of the effervescing of magma as it outflowed at the lunar surface were of primary importance. Impacts by micrometeorites represent another important factor.

Evidently, the entire surface of the Moon, both on the visible and the far side, is covered with a layer of loose inequigranular powder -- the regolith. From a study of sample of regolith returned at different times by Luna 16 and Luna 20, Apollo 11, Apollo 12, Apollo 14, and Apollo 15, we can see at least three different types of regolith, whose presence on the lunar surface is restricted to various provinces. The mare regolith is confined to the lunar maria which it covers and thus is distributed predominantly on the visible side of the Moon. The mare surface of the Moon is 16.10 percent of the entire lunar surface. And on the visible side it represents 29.76 percent, while on the far side -- 2.44 percent /10/. The thickness of the mare regolith has not been determined very strictly. Probably, it varies somewhat and increases from the coast of a mare to its center. Most investigators believe that the thickness of the mare regolith is somewhere in the range of up to several meters (in the central part of the maria). Some assume that the thickness is 30-50 m and, finally, from studying high-contrast photographs of the lunar surface, others accept even greater regolith thickness

values /11/, which are not very probable. From studying the morphology of Luna 16 regolith particles in the Sea of Fertility, we focussed on two main particle varieties. Regolith of dark color (nearly black) contains particles of magmatic rocks of the basalt type, with fresh appearance, similar to that observed on freshly crushed samples of unmodified terrestrial rock. They have no traces of roundedness; they exhibit angular shapes. The particles of the other type bear clear traces of fusion, among which are numerous sintered particles, complex shapes vitrified from the surface, considerable numbers of spherical fused formations, and spherules, obviously cooled from liquid in a state of rotation, in dynamic conditions. They have a glassy or metallic appearance. All these particles of gabbro, basalts, anorthosites, microbreccias, slag, sinters, glass, monograins, spherules, and others range in size from several millimeters to fractions of a micron. They are shown in the figure (see Color Plates II, Fig. 1, and Color Plate III, Fig. 1). A similar composition is found also for the mare regolith returned by Apollo 11 and Apollo 12, and also partially for the regolith returned by Apollo 15 from the Sea of Tranquillity, Ocean of Storms, and from the highland region of the Hadley Delta (see Fig. 1, text page 9, present collection). In other words, the mare regolith from the various maria is uniform in character. The principal minerals of this rock -- mare regolith -- are plagioclases, pyroxenes, ilmenite, and less often, olivine. Their content in the regolith from various maria, as we will see below, fluctuates somewhat. Regolith from the highland, terra regions of the Moon exhibits a quite paradoxical trend as to particle varieties. Most characteristic in this respect is the regolith returned by Luna 20 from a highland region, from the isthmus dividing the Sea of Fertility from the Sea of Crises (see Fig. 1, text page 9, present collection). It is important to note that /349 the Luna 20 sampling site was on highland 120 km directly north of the Luna 16 sampling site, or 35 km from the nearest point of the northern coast of the Sea of Fertility. The regolith from the highland province varies in color from gray to light-gray, that is, considerably lighter than Luna 16 mare regolith. The albedo of the highland regolith varies from 0.12 to 0.23, while the albedo is 0.107 for Luna 16 mare regolith. Among the Luna 20 sample particles, especially the large ones, a very high number of feldspar particles and particles of the anorthosite type, and infrequently troctolite, are noted. This is the principal fraction of the Luna 20 regolith, while in the Luna 16 material, and even in the regolith of Apollo 11, Apollo 12, and Apollo 15, the content of similar light particles is only a few percentages (1-5 percent). In Luna 20 regolith, particles of basaltic rocks and gabbro are present in considerably lesser amounts. There are incomparably fewer fused, slagged particles and, in particular, glass spherules than in the mare regolith. We can more properly speak of some roundedness of individual particles of the Luna 20 regolith. Among the anorthositic rocks, the presence of rocks of effusive appearance, of the anorthosite-basalt type, and so on, is characteristic.

As we will see below, the fine fraction of this regolith contains much feldspar material, little ilmenite, but somewhat more olivine and spinel-group minerals than does the Luna 16 regolith. Finally, we can anticipate that there is a third type of regolith from regions with complex geological situation where a shift of mare-formation rocks to highland rocks occurred, or vice versa. Regolith cores from these regions have stratigraphic differentiation /12/. An example of this can be the regolith returned by Apollo 14 from the highland region of Fra-Mauro, rich in clastic material. Most typical here is the high content in this regolith of Al_2O_3 and the low content of CaO ($Al_2O_3/CaO = 1.7$, while this ratio is about 1.4 for Luna 20 regolith). I wish to note that this ratio probably resulted from the displacement of material of mare and highland character, or their alternation. And still, this does not indicate a common intense process of displacement, since this type of regolith is confined to the spatially restricted complex regions of the lunar provinces. Regolith, mare and highland, have a well-defined boundary, for example, the line of contact of the Sea of Fertility regolith and the highland material from which the Luna 20 sample was returned. In the regolith returned by Luna 20 by weight the feldspar molecule is 50-60 percent, while it is no more than 5 percent in the mare regolith from the neighboring region of the Sea of Fertility returned by Luna 16. Thus, we can state at the outset that the regolith material arises in situ and is not transported like volcanic pumice on Earth from large distances. As most investigators assume, Luna 16 regolith is directly in contact with the mare basalt it overlies. The variegated regolith particles were studied very closely morphologically, for example, with respect to the stresses, traces of meteoritic impact, action of galactic radiation, temperature, and also with respect to their petrographic and mineralogic composition /13/. Therefore here we will not present these data, referring the reader to the original articles. Still, I wish to note that the phenomena of polymorphism of minerals arising under the effect of pressure, impacts, or heating was not noted.

Chemical and mineralogic composition of regolith. Regolith from the mare regions returned from the Sea of Tranquillity /7/, Ocean of Storms /8/, as well as the regolith from the Hadley Delta returned by Apollo 15 /12/ and, finally, the Sea of Fertility regolith returned by Luna 16 /13/ have a common character, typical of the mare regolith of the Moon. We present Table 1 as an illustration. The chemical composition can be learned about in greater detail in an article presented in this collection /15/ and, of course, from the numerous publications in the Proceedings of the Apollo 11 Lunar Science Conference, 1970, and the Proceedings of the Second Lunar Science Conference, 1971.

The composition of the mare regolith is characterized by a relatively high content of Fe, Ti, as well as Ni, and Cr. The content of all these elements in the regolith from the various maria fluctuates somewhat. Thus, the highest FeO content was noted in the regolith of the Ocean of Storms, and the maximum TiO_2 content -- in the Sea of Tranquillity regolith, and so on. Accordingly, for example, the material of the Ocean of Storms regolith contains greater amounts also of other mafic elements, more olivine, and less ilmenite, and so on. A low (compared with terrestrial tholeiitic basalt) content of alkalies in the regolith was noted. The view has been advanced that the alkalies were lost during formation of the regolith at high temperatures. The loss of alkalies during heating of rocks is well known. But there are very limited grounds to assume that alkalies dissipated from the /350
Moon, as some authors indicate. The low content of alkalies, specific for lunar magma, indicates in general the low content of volatiles as well. The content of other major elements such as, for instance, Ca, Mg, Si, and Al, in general fluctuates little in the mare regolith. The Luna 20 highland regolith is of an entirely different composition. In it there is a sharp increase in the anorthosite content, that is, the feldspar molecule, therefore it has a high Al_2O_3 content. In general, the regolith is represented by anorthositic rocks or their analogs. Therefore, at the same time the exceptionally high CaO content of 17.3 percent and the high Al_2O_3/CaO ratio of 1.4 is observed, while there is relatively very little FeO and MgO. The TiO_2 content is only a fraction of a percentage. The content of other mafic elements is also markedly reduced, TR does not follow CaO. Finally, the third type (its primary rocks are sometimes called nonmare basalts) is represented by the composition of the regolith, for example, from the region Fra-Mauro, in the highlands (see Fig. 1, text page 9, present collection). In it, in general the Al_2O_3 content is higher than in the typically mare regolith, with a relatively low CaO content (Al_2O_3/CaO is consequently high -- 1.64). The FeO content is considerably lower, while TiO_2 is about 1.8 percent. Noteworthy is the high content of Ni and the platinoids in all regolith types /157. I will discuss several elements encountered in small quantities when I compare the composition of the regolith with the composition of the crystalline rocks that are the sources of the regolith.

Composition of primary crystalline rocks of the Moon -- sources of inequigranular regolith material. In mare lunar regions, the regolith source is represented by igneous crystalline rocks of the class of basalts, differing structurally for the several mare regions, somewhat varying in composition, and also breccia from these rocks. Two types of basalts are described, mainly, for the Sea of Fertility:

TABLE 1. ABUNDANCE OF MAJOR ELEMENTS (IN PERCENT) AND SEVERAL TRACE ELEMENTS (IN PPM) IN LUNAR MATERIAL [7-9]

	Monolithic crystalline rocks						Regolith					
Constituent	Apollo 11, sample 10044	Apollo 12, sample 12063	Apollo 14, basalt 14053	Apollo 15, sample 15556	Luna 16 basalt (mean)	Luna 20, anorthosite	Apollo 11, sample 10084	Apollo 12, sample 12070	Apollo 14, (mean)	Apollo 15 sample 15601	Luna 16 (mean)	Luna 20 sample 4-1
SiO_2	42,8	44,5	48	45,11	42,95	44,2	41,9	45,8	48,0	45,05	41,90	44,4
Al_2O_3	11,84	9,3	12	9,43	13,88	19,1	12,97	12,6	18,0	10,20	15,33	22,9
FeO	17,15	21,6	16	22,25	20,17	6,91	15,48	16,38	10	19,79	16,66	7,03
TiO_2	10,5	4,67	1,5	2,76	5,5	0,52	7,9	2,6	1,8	1,98	3,36	0,56
MgO	6,47	8,4	8,4	7,73	6,05	13,37	7,97	9,86	9,9	10,89	8,78	9,70
CaO	7,34	13,6	120	10,82	10,8	13,3	11,34	10,64	11	9,79	12,53	15,2
NaO	0,48	0,30	0,38	0,20	0,23	0,48	0,42	0,42	0,57	0,29	0,34	0,55
K_2O	0,10	0,08	0,14	0,03	0,16	0,47	0,13	0,23	0,52	0,10	0,10	0,10
P_2O_5	—	—	—	0,08	0,14	0,17	—	—	—	0,11	0,12	0,14
Sr	151	130	180	107	433	86	174	140	206	109	220	108
Rb	(5,1)	1,1	2	—	1,3	3,7	3,0	8,7	13	3,1	1,9	4,0
Cr	1300	2580	3000	—	1640	1220	1830	2270	1400	3920	1910	720
Co	11	39	48	—	21,7	27	27,2	41,5	44	—	41	18
Ni	<10	49	14	—	113	189	280	200	304	—	171	194
Y	150	50	90	—	90,5	110	150	135	210	47	70,4	54
Ce	44	19	—	—	45	5,2	47	86	—	—	40,8	14
Pb	3	0,4	—	—	0,3	0,15	6	2,6	--	--	4	1,0
Th	0,98	0,82	2,24	0,5	—	—	1,61	5,52	14,5	4,2	0,80	1,5
U	0,28	0,24	0,64	0,15	—	—	0,35	1,69	3,9	1,0	0,2	0,5

fine-grained igneous crystalline rocks -- basalt and medium-grained basalts (gabbro). Fine-grained basalt including vesicles, and medium-basalt are differentiated in the Ocean of Storms.

Also encountered in the Sea of Fertility are two types of basalts with fine-grained structure and coarse-(medium) grained structure -- gabbro. Basalts of various types and maria differ somewhat in mineralogic and chemical composition, which is well known today [7-9]. As an illustration, we can use Table 1. All /351
the mare basalts are rich in mafic elements -- Fe et al., compared with the primitive basalts of the Earth. For example, the content of Fe is highest in the Ocean of Storms basalts, while the content of Ti is at a maximum in the Sea of Tranquillity basalt, and so on. Here it is important for us to note not the differences in the composition of basalts from the various maria, but the certain correspondence of composition between the local type of mare basalt and

the composition of the regolith overlying it. Actually, if we consider the content in basalts of various maria of mafic elements, for example, Fe, Mn, V, Mg, Cr, and so on, their content in the local regolith will be considerably lower than in crystalline rock. This is especially noticeable with respect to the FeO content. TiO_2 behaves entirely differently. Corresponding to the high TiO_2 content in the Sea of Tranquillity basalts is a TiO_2 content, which even though reduced, is still maximum for the regoliths of the moon. Still, to this regularity we must add yet another trend in the difference between the composition of crystalline rocks and regolith of a given mare, namely an increase in the regolith content, with respect to the local basalt of a given mare, of lithophilic elements, above all Al_2O_3, and then often R, and especially U, Th, and so on (see /15/).

This relatively brief examination of the composition of crystalline basalts and regolith of a given mare allows us to assume that 1) the regoliths of mare regions is genetically related to local basalts and 2) in the formation of regolith, some differentiation and variation of its composition occurred -- a reduction in its content of mafic elements and of TiO_2, and a considerable increase in Al_2O_3 and of several other lithophilic elements. Particularly interesting information is conveyed by the nature of the distribution of trace elements in the basalt-regolith system. Below we will again return to the method of regolith formation. At this point let us examine the question of what more material, besides local igneous crystalline rocks, participated in regolith formation. A constant presence of particles rich in the feldspar molecule -- -- anorthosites or their analogs, with high content of Al and Ca -- was noted in the composition of mare regolith. Doubtless, this material, as we have already seen, came from highland regions. But its content in the mare regolith is no more than 5 percent; it is assumed that, in addition to the directly visible fragments of anorthosite, it can also be contained to some extent in breccias. In addition, it can be said that nearly everything that pertains to the composition of regoliths can also be said of the composition of breccias. This is why the problem of whether the regolith is the basis of the formation of mare breccias arose.

Major interest was drawn to the question of the proportion of meteoritic material in regolith composition. The occurrence in mare regolith of meteoritic material was shown both by ourselves as well as many other investigators /5, 6/, above all as fragments of iron-nickel melt /3/ usually fractions of a millimeter in size, and also as segregations of Fe within glasses and other similar regolith materials. Analysis of these fragments showed that this is a FeNi melt with wide fluctuations in the Ni content, from 3 to

35 percent. We will dwell below on the causes of this phenomenon and on the role of micrometeorites. X-ray analysis showed that not infrequently two polymorphic forms of kamacite and taenite typical of meteoritic iron are present in the melt. Thus, the Ni content in taenite is as high as 35 percent /3/. A high Ni content was noted in all regolith samples, averaging up to 300 ppm compared with its content of about 50 ppm in igneous crystalline rocks (Table 2).

Still, present in the regolith in higher amounts (by one order higher than in crystalline rocks) is Au, Os, Ir, Pd, and other platinoids, that is, they can be used as labeled atoms. This made it possible to calculate the quantity of FeNi from meteoritic melt of chondritic material involved in the regolith (Table 3).

In the calculation, we adopted the mean content in the FeNi of the meteoritic melt of 8 percent Ni and, thus, the content of Fe, Au, Os, Ir, and Pd based on both calculations as well as our direct determinations of the platinoids in chondrites, in their principal phases /17/.

As we can see from these calculations, the regolith contains about 0.25 percent FeNi of the meteoritic melt, or about 2.5 percent of chondritic material. We must discuss the Fe in the regolith a little further. It is found in the form of FeO in compounds of the silicate phase of the regolith, as well as in $FeTiO_3$ and other phases. Here we encounter pieces of FeNi associated with the glass in the regolith, where the Ni content, as I stated above, markedly fluctuates in them. Finally, Fe is encountered in a finely dispersed form (30-100 AU) in the surface layer of regolith particles, detected by us through x-ray electron analysis /14/. The relative content in this layer of the dispersed iron, that is, the concentration, is considerably increased, and this was noted not only for Luna 16, Apollo 11, and Apollo 12 regoliths, but especially for Luna 20 regolith, that is, regolith of highland origin. This Fe evidently contains little Ni. But the most surprising fact was the discovery of its passivity with respect to O_2. This dispersed Fe is not oxidized by air oxygen at ordinary temperatures. Something similar was noted by Housley et al. /4/. Evidently, in the regoliths it is virtually free of Ni, which however requires an exact verification.

Thus far we do not know the source of the primary crystalline rocks of highland regolith. It is assumed that they are anorthositic rocks, since various fragments of the highland regolith are represented by diverse anorthositic rocks -- gabbro-anorthosites, anorthositic gabbro, and troctolite. There are hypotheses on the primary anorthositic crust of the Moon. However, strictly speaking, we do not know the origin of the anorthosites. The discovery of

TABLE 2. NICKEL CONTENT IN MARE ROCKS OF THE MOON (IN PPM) /352

Region	Crystalline rocks -- basalts	Breccias	Regolith	Author*
Sea of Tranquillity	10	370	280	Wänke
	54	200	200	Rose
	28	32	150	Compston
	4	162	117	Brown
	50	—	200	Haramura
	0.5 (A) 2.7 (B)	202	185	Annell
	42 (A) 75 (B)	60	170	Morrison
	15	100	150	Turekian
Ocean of Storms	19 (A) 15 (B)	230	190	Morrison
	57	—	164	Bouchet
	40	225	250	Taylor
	31	—	160	Willis
Sea of Fertility	79	—	180	Vinogradov
Mean	33	210	185	

*Proc. Apollo 11 Lunar Science Confer., 1970. Proc. Second Lunar Science Confer., 1971.

anorthosite in the highland provinces of the Moon resurrected the old ideas of the primary anorthositic crust of the Earth and, therefore, of the Moon. Anorthosites, as we know, on Earth are encountered in the Archean (age $3 \cdot 10^9$ years) and especially in the Proterozoic, predominantly as massive or stratiform rocks on shields. Windley /18/ described a third type of anorthosites on Earth in /353 regions of regional metamorphism. They all contain little of the mafic elements: Fe, Mn, and V, as well as little Ti, and so on, and much Al and Ca. Sometimes they contain much Cr, but in highland regolith Cr is encountered to a lesser extent than in mare regolith.

Anorthositic regolith also contains much Ni (about 200 ppm) and inclusions of metallic iron of different origins. It also contains even higher concentrations of passivated Fe on the surfaces of regolith particles. It appears to us that anorthosite is formed during crystallization differentiation of the primary gabbro-basaltic magma. The segregation of anorthosite at the surface of the Moon occurred during rapid outflowing of the magma, at high temperatures, and in conditions of the high vacuum on the lunar surface. However,

TABLE 3. CONTENT OF PLATINOIDS AND GOLD IN LUNAR ROCKS AND IN METEORITES (IN PPB)

Rocks and sampling site, sample number	Pd	Ir	Pt	Source
Lunar basalts				
Apollo 11, 10030	1,5	0,027	0,075	[21]
Apollo 12, 12063	1,0	(1,3)	(2,9)	[22]
Apollo 14, 14321	0,001	0,0011	0,0006	[24]
Apollo 15, 15597	—	0,0072	0,045	[23]
Anorthosite				
Luna 20, 2007-014				Present study
Apollo 15, 15415	13,0	0,010	0,117	[23]
Breccias				
Apollo 11, 10048	13,0	6,88	2,66	[21]
Apollo 12, 12073	10,2	8,8	2,7	[22]
Apollo 14, 14365	0,015	0,01	0,0057	[24]
Regolith				
Apollo 11, 10084	11,0	7,62	4,15	[21]
Apollo 12, 12073	9,0	11	2,6	[22]
Apollo 14, 14365	0,028	0,019	0,0061	[24]
Apollo 15, 15601	0,0062	0,0041	0,0016	[23]
Luna 16	<100	25	—	[13]
Luna 20 (anorthosite)	245	11	—	
Stony meteorites (chondrites)	696*	596*	161,6*	[25]
Fe-Ni phase of meteorites (chondrites)	370	280	100	[26]

* Mean values are calculated based on data given in [25].

as Yoder showed [19], this required a high content of water in the magma. During this process $FeTiO_3$ was segregated in the residue of the magma. Still, in the diopside-anorthite system, anorthite segregates even in the absence of H_2O or when its content is low, but at high temperatures (1274° C). Obviously, this problem of the formation of anorthosite from the primary magma now is attracting the attention of our petrologists. Finally, a few remarks are in order concerning the source of the materials of the regolith with high Al_2O_3 content, but not with high CaO content from the rocks of the highland regions of the Moon, for example, from the region Fra-Mauro (Apollo 14). The authors sometimes call these rocks "premare basalts." They are very similar to breccias, and their main feature is their clastic nature; they are very slightly sorted. It appears to us that these are intermediate mixed rocks of the clastic type, whose source was material from both highland and mare basalts.

Discussion and conclusions. In examining the endogenic processes on the Moon, we cannot go beyond a comparative analysis of events in the Earth-Moon system. We must reject the ideas that the Moon either

was segregated at some stage of its development from the material of the Earth, or else was moored to the Earth, for example, from the belt of asteroids or something similar. The Moon has a nearly circular orbit. In both of these hypotheses on the approach toward the Earth or retreat from it there was the factor of the deceleration of a smaller body, and under the laws of celestial mechanics the Moon would be in an elliptical orbit. But this did not happen. Therefore it can be assumed that the Moon was formed like many asteroidal bodies of lunar size by the accretion of cold matter from the protoplanetary cloud around the Earth, independently of the material of the Earth. The density of the Moon is 3.34, that is, lower than the density of chondrite-meteorites. The mass of the Moon (representing it by content similar to chondrites) is about 45 times less than the mass of the silicate phase of the Earth. The thermal conductivity of lunar rocks is noticeably lower than the thermal conductivity of the more oxidized crystalline rocks of the Earth containing more H_2O and other volatiles. The abundance of U, Th, and K in the lunar interior cannot be determined by their content in the basalts of the lunar crust. The flow of heat toward its surface is lower than for the Earth. Evidently, the history of the distribution of the heat generated by the radioactive process was affected by the absence of the metallic core in the Moon's center. This is indicated, in particular, by the FeO content in the fused rocks of the Moon that is appreciable compared with the rocks in the Earth's crust. Actually, on Earth basalts contain an average of 7 percent Fe, while the Fe content for the mare basalts of the Moon is up to 17 percent or higher. Therefore, during the outflowing of basalts on the Moon a considerable mass of Fe was utilized. It must be recalled that the mean composition of the chondrites has about 12 percent Fe in the form of FeO. Still, the incursion of FeO into the composition of silicate rocks fused at the surface of the Moon lowered their melting point. But the melting point of the mare basalts approaches 1100-1200° C. This evidently is associated with the low content of volatiles in the magma. We do not know the thickness of the fused crust of the Moon. It is assumed that these thickness values are 25-50 km and higher, which would be more than 3 percent of the thickness of the lunar rocks. On Earth the thickness of the melted layer -- the Earth's crust -- is less than 1 percent of the thickness of the mantle. This indicates that even under equal conditions of the content of volatiles in the Earth and Moon, for the latter their proportion per unit mass of the outflowing magma would be much less. Finally, however much of the volatiles H_2O, CO_2, H_2, and other compounds may have been released from the magma on the Moon, they easily dissipated into the vacuum of space. Many common gases were detected in the bubbles of the ancient lunar rocks and their pressure differed significantly (0.126 mm Hg) from the vacuum at the lunar surface [17]. All this

enables one to think that the outflowing of the magma on the Moon occurred at higher temperatures than on Earth, and its emergence at the lunar surface was accompanied by intense effervescence and possibly followed something like the process of eruptive volcanoes on Earth. A comparison of the abundance of Al, Ti, U, and other chemical elements in the basalts of the lunar crust with their probable abundance for the Moon as a whole indicates that the thickness of the lunar crust does not exceed 15-20 km. /354

The circular lunar maria are regions of depressions that were filled by lava flows. Upon examining the process of regolith formation, we can go further by starting from this simple truth. But as Muller and Sjogren have shown, an increase in gravitational force is associated with the circular maria. Beneath their surface at a depth of 50 km or deeper a rise in gravitational attraction, the so-called mascons, have been detected. This was shown for the lunar maria on the visible side facing the Earth, that is, on the side of the Moon that protrudes toward the Earth -- the Sea of Rains, Sea of Tranquillity, Sea of Moisture, Sea of Nectar, Sea of Crises, and Eastern Sea /20/. The only possible explanation for the appearance of the gravitational anomaly in the region of these lunar maria is the infall of meteorites, or which is even more plausible, the infall of satellites of the Moon during its early history. This of course is a hypothesis, however, it compels us to formulate a question of whether the formation of the mare regolith was associated with this process. The age of the regolith as a whole is about $4.6 \cdot 10^9$ years /16/. It is improbable that this single-step process was the cause of the formation of the regolith. But the depressions, if one assumes that satellites or meteorites did fall (protracted accretion) were prepared for their inundation in the future by basaltic lava. Now we can directly address ourselves to the formation of the regolith. The most central circumstance is represented by the differences in the composition of the entire regolith from the crystalline rock -- basalt -- genetically associated with it. These differences, as we have seen, for the mare regolith amount to the fact that in it the content of mafic elements, above all Fe, followed by Ti, Cr, and others, is reduced, and the content of Al and other lithophilic elements is considerably increased. This resembles the scheme of crystallizational differentiation of the bedrock. The decrease in the content of Fe or Ti and the increase in the content of Al or Th and U in the regolith as opposed to their content in the massive rocks on which they were formed amounts to 30 percent, and sometimes half or even one order of magnitude in content (for example, Th, U, and so on). Attempts have been made to explain this by the possible "dilution" of the mare regolith by the introduction of anorthosites. But quite simple calculations show that for the known anorthosite content and the mare regolith this is simply impossible. Further, attempts were made to account for the change in the regolith composition by the

proportion of meteoritic material. But, as we have already seen, this proportion adds extremely little material to the regolith. If we presuppose the differentiation of the regolith composition as resulting from the collision of meteorites with the basaltic rocks of the Moon and the fractionation of the basalts, forming a portion of the regolith poorer in the mafic elements, then where is the other portion of the material that was produced during this process, richer in the mafic elements? It appears to me that the process of the formation of mare regolith is the result of the differentiation of the magmatic material, the effervescing of the lava when it broke through the overburden and came to the surface of the Moon in the conditions of high vacuum. The outflowing of the lava was accompanied by its simultaneous boiling and fragmentation into fine particles, like explosions. On Earth the heat of the volcanoes is easily removed through the thermal conductivity of the atmosphere and so on. On the Moon there are no conditions for the rapid discharge of heat at its surface and therefore the heat of the magma and the lava is expended in melting the regolith particles. Differentiation and formation of the regolith were replenished by the enormous mass of the basaltic magma or lava. We were able to experimentally show the formation of fused particles if molten basalt rapidly appeared in conditions of high vacuum. Here the FeO was reduced to Fe and colored the spheroids, and so on, and particles of the "regolith" were formed which were observed for lunar material. It is probable that all the regolith cores must have had stratificational layers, which in general is clearly seen in the cores already taken from the lunar highlands /12/. Various layers of the regolith nonetheless were subjected to the action of the micrometeorites, to solar and galactic radiation, and the exposure age of the layers differs and is determined in the millions of years /13/. The content of neutral gases and tracks is also a function of exposure. All this together indicates that layers of regolith of different, but ancient age existed, in other words, these layers may have come from different lava flows. The formation of the highland (or anorthositic) regolith is an even more controversial question and we must await the time when crystalline lunar anorthositic rocks are made available to us. Doubtless, they have been degraded under the effect of the numerous lunar factors of "weathering" /13/.

Finally, a few more remarks about the role of meteorites in forming regolith. It appears to me that the impacts of meteorites against the surface of the Moon in the sense of a profound breaking up of its rocks is a significant additional effect. Mare regolith as well as highland (anorthositic) regolith were formed from different primary materials and, as I have indicated above, in different processes. Therefore the impacts of micrometeorites did not smooth over their morphological and other features. For example, the /355

exoelectronic emission of particles from the Luna 20 anorthositic regolith is an order of magnitude higher than the emission of particles from the Luna 16 mare regolith, and again the number of tracts in the minerals of the Luna 20 regolith is several orders of times higher than in the Luna 16 regolith, and so on. Besides some addition of material to the regolith, which it must be added evidently is identical both for the mare as well as anorthositic regolith, the impacts of micrometeorites (large chunks of meteorites have not yet been found) doubtless had a specific effect on the morphology of regolith particles owing to the thermal explosion, the formation of microcraters and openings in the particles, and shock effects. The behavior during this process of iron is quite diverse. Metallic iron with different Ni content appeared, and some proportion of the iron observed was reduced at elevated temperatures from the FeO of the silicates. It contains little Ni or none at all. Still, in the first place the Fe was easily oxidized. These complex chemical processes must be delved into in greater detail.

REFERENCES

1. Dolgov, Yu. A., and Shugurova, N. A., "Results of Investigating Gases from Inclusions in Lunar Glasses," present collection, p. 356.

2. Gievarry, J. J., "Thermal History of the Moon," Nature 225, 623 (1970).

3. Goldstein, J. I., and Jakowitz, N., "Metal Inclusion and Metallic Particles in the Apollo 12 Lunar Soil," Proc. Second Lunar Sci. Conf. 1, (1971).

4. Housley, R. M., Blonder, M., Abdel-Gaward, M., Grant, R. M., and Muir, A. H., Jr., "Mossbauer Spectroscopy of Apollo 11 Samples," Proc. Apollo 11 Lunar Sci. Conf. 3, 2251 (1970).

5. Il'in, N. P., Loseva, L. Ye., and Senin, V. G., "X-Ray Spectral Microanalysis of Composition of Individual Particles of Lunar Regolith," present collection, p. 209.

6. Makarov, Ye. S., Ivanov, V. I., Makeyeva, V. I., Tobelko, K. I., Bukin, V. I., Volkova, A. Ya., Kuznetsova, G. A., and Kuznetsov, L. M., "X-Ray Diffraction Identification of Minerals in Lunar Regolith Returned by Luna 16 Automatic Station," present collection, p. 148.

7. Proc. Apollo 11 Lunar Sci. Conf., 1970.

8. Proc. Second Lunar Sci. Conf., 1971.

9. "Preliminary Examination of Lunar Samples from Apollo 14," Science 173(3998), 681 (1971).

10. Rodionov, Zh. F., and Volkov, A. P., "Problems of Meteoritic Studies of the Lunar Surface," Tezisy Simpoziuma po fizike Luny i planet /Abstracts of Symposium on the Physics of the Moon and the Planets/, Kiev, 1968, p. 28.

11. Shoemaker, E. M., Hait, M. H., Swann, G. A., Schleicher, D. Z., Schaber, G. G., Goddard, E. N., Waters, A., Sutton, R. C., and Dahem, D. H., "Origin of Lunar Regolith at Tranquillity Base," Proc. Apollo 11 Lunar Sci. Conf. 3, 2399 (1970).

12. "The Apollo 15 Lunar Samples. Preliminary Description," Science 175(4020), 363 (1972).

13. Vinogradov, A. P., "Preliminary Data on Lunar Surface Material Returned by Luna 16 Automatic Station," Geokhimiya (3), 261 (1971).

14. Vinogradov, A. P., Nefedov, V. I., Urusov, V. S., and Zhavoronkov, N. M., "X-Ray Electron Study of Lunar Regolith from the Seas of Fertility and Tranquillity," Dokl. AN SSSR 207(2), (1972).

15. Vinogradov, A. P., Chupakhin, M. S., Shevaleyevskiy, I. D., and Belyayev, Yu. I., "Chemical Composition of Luna 16 Lunar Regolith," present collection, p. 264.

16. Vinogradov, A. P., and Artemov, Yu. A., "Absolute Age of Material of the Sea of Fertility Regolith," present collection, p. 455.

17. Vinogradov, A. P., Lavrukhina, A. K., Ganiyev, A. G., Sil'vanovich, Yu. A., and Rakhimov, Kh. R., "Distribution of Platinoids and Gold Among the Various Phases of Meteoritic Matter," Geokhimiya (3), (1972).

18. Windley, "Anorthosites on the Early Crust of the Earth and of the Moon," Nature 226, 333 (1970).

19. Yoder, H. S., "Phlogopite: Synthesis and Stability Range," Geochim. Cosmochim. Acta. 6, 157 (1954).

20. Muller, P. M., and Sjogren, W. L., "Mascons: Lunar Mass Concentrations," Science 161(3842), 680 (1968).

21. Ganapathy, R., Keays, R. R., Laus, J. C., and Enders, E., "Trace Elements in Apollo 11 Lunar Rock: Implications for Meteorite Influx and Origin of Moon," Proc. Apollo 11 Lunar Sci. Conf. 2, 1117 (1970).

22. Wanke, H., Wlotzka, F., Baddenhausen, H. et al., "Apollo 12 Samples: Chemical Composition and its Relation to Sample Location and Exposure Ages, the Two Component Origin of the Various Soil Samples and Studies on Lunar Metallic Particles," Proc. Second Lunar Sci. Conf. 2, 1187 (1971).

23. Morgan, J. W., Krahenbuhl, U., Ganapathy, R., and Anders, E., "Trace Elements in Apollo 15 Samples: Implications for Meteorite Influx and Volatile Depletion on the Moon," Proc. Third Lunar Sci. Conf. 2, 1361 (1972).

24. Wanke, H., Baddenhausen, H., Balacescu, A., et al., "Multi-element Analyses of Lunar Samples and Some Implications of the Results," Proc. Third Lunar Sci. Conf. 2, 1551 (1972).

25. Vinogradov, A. P., Lavrukhina, A. K., Ganiyev, A. G., Sil'-vanovich, Yu. A., and Rakhimov, Kh. R., "Distribution of Platinoids and Gold Among Various Fractions of Meteoritic Matter," Geokhimiya (12), (1972).

26. Vinogradov, A. P., "High-Temperature Protoplanetary Processes," Geokhimiya (11), (1971).

Order of Lenin Institute of Geochemistry and Analytical Chemistry imeni V. I. Vernadskiy, USSR Academy of Sciences, Moscow.

N75 11844

RESULTS OF INVESTIGATING GASES FROM INCLUSIONS IN LUNAR GLASSES

/356

Yu. A. Dolgov and N. A. Shugurova

Abstract

Common gases from inclusions in glass fragments and spherules of lunar surface material returned by the Luna 16 automatic station were investigated by the adsorption-volumometric method. Inclusions from eight particles were analyzed: the particle dimensions rarely exceeded 500 m, and those of the inclusions therein -- tens of microns. Eighteen analyses were made. A gas mixture from the inclusions had two- (CO_2 and H_2), three- (CO_2, H_2 and N_2 + inert gases), and (H_2S, SO_2, and NH_3), H_2,N_2 + inert gases, and four-component (H_2S, SO_2, and NH_3), CO_2, H_2, and N_2 + inert gases, compositions. The sulfur gases and the possible ammonia in 12 of the 8 analyses were up to 53.5 volume percent. The carbon dioxide in 12 analyses was 3-61 volume percent. Nitrogen and inert gases in 13 analyses were in the range 9.4 to 77 volume percent. Hydrogen in all (18) analyses was 10 to 95 volume percent. Diffusional exchange with the terrestrial atmosphere was absent (oxygen and nitrogen were absent in many vacuoles). An unexpectedly high density of gases in the vacuoles was obtained. The initial volume of the bubbles when the vacuoles were breached even rose 2.5 times and decreased in the limits of 2.3 to 54.5 times. This gas density did not correspond to the density of the terrestrial atmosphere. Various possibilities for the formation in the lunar surface material of glass fragments and spherules are discussed.

Fragments of clear greenish and brown glass smaller than 1 mm in size were found among the various particles of lunar surface material returned by the Luna 16 automatic station. Spherical and slightly deformed glass spherules of different colors and transparency and rarely exceeding 500 m in size were discovered in the medium and fine fractions of lunar surface material separated in the Institute

of Geochemistry and Analytical Chemistry imeni V. I. Vernadskiy. Spherical and several deformed vacuoles (see Figs. 1-3) were observed in the glass spherules and fragments of glasses, exhibiting transparency. The vacuoles were several tens of microns in size and were filled with a homogeneous substance (gas). Several vacuoles close to the surface were breached or had tiny cracks, invisible under the microscope, connecting them to the atmosphere. The gas inclusions in the spherical vacuoles of the lunar glasses and the lunar spherules externally strongly resembled inclusions in tectites and obsidians that we investigated earlier /5_/.

We were offered the possibility of selecting material containing gas-filled inclusions. Nine tiny particles from three samples were selected: five glass spherules, three glass fragments, and a gray fragment of fine-grained rock.

Description of particles of lunar surface material. Spherules. 1 sp. Light-yellow, translucent with numerous bubbles of different sizes (see Table, analyses 1-6). Three inclusions were clearly breached and have vacuole breaks visible under the microscope. The rest are hermetic. The surface of the spherule is slightly rough as if numerous fine particles had adhered to it. The shape is not ideally spherical, but flattened. In one section this is a circle with a diameter 350 μm, and in another -- an ellipse with a smaller diameter of 280 μm (Fig. 1).

2 sp. Light-brown, translucent, with a small number of fine gas bubbles with smooth even surface. The shape is ideal, spherical. The diameter is 400 μm (analyses 7-9) (Fig. 2).

3 sp. Dark-brown, weakly translucent. The surface is smooth, glistening. Gas bubbles can be seen with great difficulty with special illumination. There is one large bubble and several smaller ones. In shape regular spherical. The diameter is 400 μm (analysis 10).

4 sp. Ellipsoidal heterogeneous formation. Included in most of the yellow-green glass are angular particles of unfused opaque mineral. At the end of this droplike formation there is a "little /357 nose" of elongated clear glass with an angular upper fracture or separation section. Along the fractured part it resembles the narrow section of a "dumbbell". The size is 400 and 530 μm. No visible inclusions in transmitted light are contained.

5 sp. Dark, opaque, smooth spherule with several tiny holes at the surface. No inclusions were discovered owing to the opaqueness. Severely stressed, and when pressured no gas bubbles were observed to exist (analysis 11).

Glasses. 1 gl. Angular fragment of glass in transmitted light was scanned, disclosing a dark-brown to brown coloration. Contains numerous bubbles of different sizes. Vacuoles from bubbles lying in the spalling plane can be seen in chips. In external appearance and in color distribution the glass is homogeneous. The fracture is acute-angled, sometimes conchoidal. There are no fused surfaces, and the entire surface of the particle is one of spalling. The dimensions are 700 x 420 x 400 μm (analyses 12-13).

2 gl. Fragment of approximately rectangular shape. Dark-brown in color, slightly translucent along the margins. Glassy lustre. Its external surface is fine-granulose, rough, uneven; its interior surface has a marked curvature -- ideally smooth, even, and glistening. The fracture at the lateral surfaces is conchoidal and angular. The fragment resembles a spherical layer with dimensions 700-400 μm in the external surface and 550-420 μm in the internal, with a mean thickness of 200 μm. The glass is translucent only in a strong beam of transmitted light. Along the inner smooth surface can be seen isolated fine gas-containing inclusions.

3 gl. Fragment of light, clear, faintly yellow-green glass overfilled with spherical vacuoles containing gas. Some of the large vacuoles located at the surface have breaks in the walls and are filled with air. This fragment has a triangular cross section with dimensions 490 x 490 x 420 μm. It resembles the sectorial fragment of a large spherule. The external surface and internal spallings are even and glistening. On the spalling surfaces are numerous traces of breached spherical vacuoles (analyses 14-17; Fig. 3).

Fine-crystalline porous rock. Angular parallelepiped particle of gray, slaglike substance. Highly porous. Fine-crystalline structure is discernible (possibly this is basalt). Maximum dimensions more than 1000 μm.

Adsorption-volumometric method. In the preceding studies dealing with samples of lunar rocks returned by the American crew of Apollo 11, assumptions were made on the composition of the common gases. For example, in searching for carbon-containing compounds on the surface of the Moon, the authors of [13] indicated that most of the carbon in the form of CO_2 in the lunar material is contained in the gaseous state in bubbles present in the glass spherules. Semiquantitative data for nitrogen and hydrogen were obtained by micro-probing [15]. When the tracks were studied by vacuum heating, the following gases were found among the decomposition products:

H, He, Ne, Ar, N, and traces of Kr and Xe. The common gases CO_2, CH_4, H_2S, HCl, C_6H_6, and so on were also observed /14/. Vacuum and gas-containing inclusions of low density in lunar olivines were noted. However, their composition was not analyzed /17/.

Summing up the results of studying gases in lunar rocks, we can note that the inert gases in Apollo 11 samples were studied much more closely than the ordinary gases. There are numerous quantitative measurements of inert gases made for small quantities at high precision, while the ordinary gases are only assumed and at best determined qualitatively.

Use of the adsorption-volumometric method in studying gases from inclusions in terrestrial minerals has been mastered /4/ and applied in analyzing more than 3000 samples. Some experience has been accumulated in investigating samples of cosmic origin (tectites and cosmic dust). This permitted applying the developed scheme of analysis for small volumes of gas that may be present in inclusions in lunar glasses.

The adsorption-volumometric method was applied for analytical purposes by A. Croh (1911, 1913), I. Ens (1935), V. G. Voana (1937), V. T. Slavyanskiy and Ye. I. Krestnikova (1956), V. T. Slavyanskiy (1957), N. A. Pankova (1961), and by the authors of this present article (Yu. A. Dolgov and N. A. Shugurova, 1966; N. A. Shugurova, 1965) /16, 12, 1, 9, 10, 8, 11/. For demonstration purposes, without analyzing the composition of the gas mixture, it was used by G. Deysha (1950) and by E. Roedder (1970). Essentially, a variant of the method developed by the present authors consists of breaching an inclusion in a special miniature press with transparent lenses based on micromanipulation equipment under a microscope in a neutral liquid. The lower concave lens contains the neutral liquid, which covers the inclusion-containing sample. Gas /358 in the form of a separate phase of dissolved in the liquid leaves the inclusion and is located in the neutral liquid. From this point, the gas bubble by means of a micropipet undergoes selective absorption with various absorbers. Development of an efficient absorption scheme is the main advantage of this variant of the method.

The following constituents of the gas mixture were determined on the basis of the proposed scheme: 1) (H_2S, SO_2, NH_3, HCl, and HF); 2) CO_2; 3) hydrocarbons; 4) O_2; 5) CO; 6) H_2; and 7) N_2 + + inert gases. The sensitivity of the method is 0.5-1 percent, the arithmetic mean deviation is 4 percent, and the root mean square deviation is 0.4 percent.

After each of these gases or gas groups was absorbed, the volume of the gas bubble was measured and from the content of each constituent of the gas mixture was calculated in volume percentages. More detailed information on this method can be found in [4], [11]. The results of the analyses have been published in numerous articles. The investigation of gases in tectite glasses can be regarded as the closest to the investigation of gases from inclusions in lunar glasses [5], [7].

Breaching of gas-containing vacuoles and measurements in the neutral liquid. Before breaching, the vacuoles in all particles were usually specific (spheroidal) cavities. After breaching, in most cases the volume of gas was reduced in the range 2.32-54.5 times. In two cases the volume increased (2.64 and 2.50 times). If the crack transected the vacuole, the gas bubble exited into the neutral liquid without difficulty. If the crack only glanced the cavity without collapsing it, the liquid entered through the crack into the vacuole and the vacuole became two-phased (L_n - ?). The second variant required additional stresses in extracting the gas bubble for analysis.

When the fragment of brown glass was pressured (1 gl), besides the gas bubbles a clear light spherule 14 m in diameter, within the bulk of the glass, was disclosed in the glass fragments. The spherule contained one inclusion smaller than a micron. When the brown lunar spherule (2 sp) was pressured, in addition to the small gas inclusions, in the neutral liquid was observed an opaque black spherule 22.6 μm in diameter. In its behavior, the black spherule resembled some spongy material gradually releasing gas. In the free state a radial crack with a lumen was observed at the contour of the spherule in the neutral liquid. Along the perimeter of the spherule, opposite the origin of the crack, a tiny gas bubble began to grow, and in several minutes it was 16 μm in size and then was analyzed. Along its diameter at the other end of the bubble was formed a tiny, 2-3 μm bubble, which ceased growing. Pressing down on the press with the lenses deformed the black spherule and caused the new gas bubbles to exit into the neutral and, finally, after pressuring nine bubbles turned up in the neutral liquid.

Two samples were preserved and were not subjected to pressuring: a tiny fragment of basalt and glass (2 gl). One spherule was pressured into amazingly tiny fragments. Subsequent work with pressuring of the largest of the fragments did not lead to the release of gas bubbles. The spherule was dark, glassy, and inclusions could be scanned in it (6 sp). The spherule was heterogeneous, with dark disseminations; most of the glass also had no inclusions, and no gas bubbles were observed in the neutral liquid.

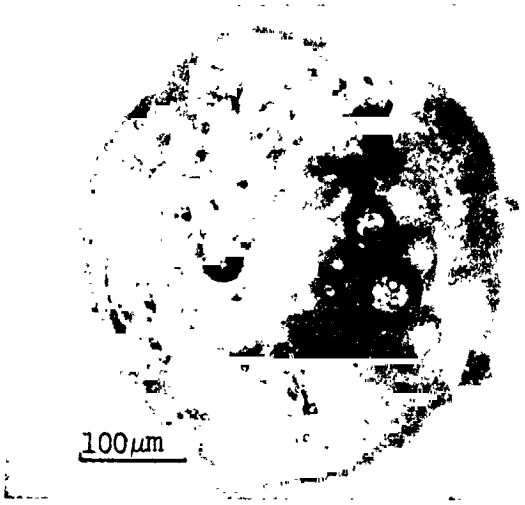

Fig. 1. Spherule (1 sp), glass, light yellow with numerous inclusions.

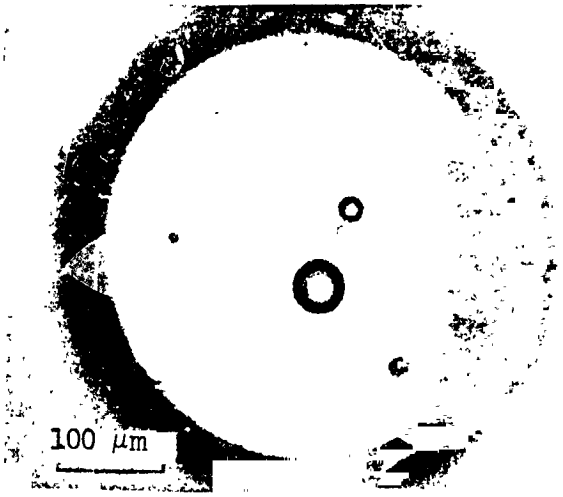

Fig. 2. Spherule (2 sp), glass, light-brown with fine gas bubbles

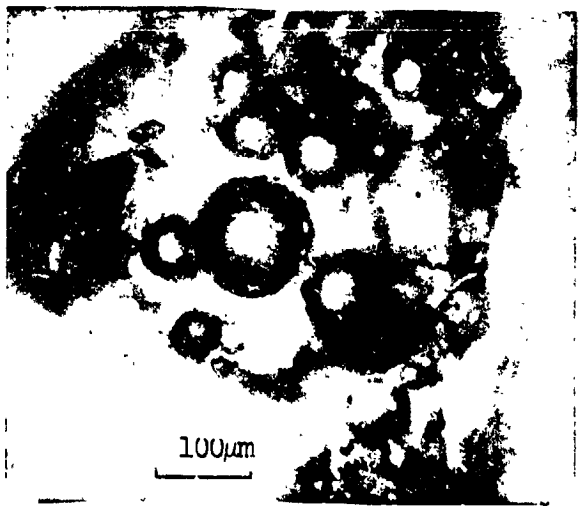

Fig. 3. Fragment (3 gl) of light-green glass with numerous inclusions.

Cut off ability of neutral liquids. The general remarks on the method are based on the assumptions that there are no liquids capable for a sufficiently long time of conserving a gaseous mixture without absorbing it. Studies were conducted to prepare nonabsorbing liquids exhibiting the required viscosity. Two liquids /359 resulted: in the first (L-1) a slight absorption begins after 25 minutes, and in the second (L-2) absorption begins after 20 minutes (Fig. 1). In principle liquids in which absorption will begin after several hours or longer can be formulated. The total time that a single gas bubble spends in a neutral liquid during the analysis does not exceed 5-15 minutes (measurements of diameters, and sometimes photography).

Possibility of diffusion into and out of a vacuole. In terrestrial minerals inclusions have pressures higher than the atmospheric owing to the presence of carbon dioxide gas. Therefore when inclusions are breached, the gas bubble always enlarges, with the

exception of infrequent cases of a slight reduction of gas bubbles from volcanic glasses (obsidians). In the assumed cosmic materials (tectites and cosmic dust) the gas mixture always reduces in volume after the vacuole has been pierced /5, 7/.

Thus, there are inclusions whose pressure exceeds the atmospheric and inclusions whose pressure is below the atmospheric volume. The rate of diffusion of gases through various solids can be the most varied, which raises the threat of disturbing the initial gas composition. Besides exact information on the question of the possibility and rate of diffusion in artificial materials for geological objects, this problem remains highly controversial, especially with respect to geologic time.

Let us present two examples that confirm the possibility of considerable diffusion of gases from inclusions through solids (minerals and glasses), reducing it to undetectable scales during fairly lengthy (geologic) time intervals.

1. Inclusions in moldavites (tectites) were investigated /5/. In these glasses of problematic origin are contained inclusions, spherical or ellipsoidal vacuoles containing gas. When the inclusions were pierced, the volume of gas was reduced by a maximum of 3000 times, and the composition of the gaseous mixture contained no air constituent and was made up of small amounts of sulfur gases (3-4 percent), carbon dioxide gas (50-70 percent), hydrogen (20-40 percent), and nitrogen (0.18-6.1 percent). The composition of the gaseous mixture from the inclusion differed appreciably from the composition of the air mixture and remained unchanged chemically through probable diffusion for 15 million years. The physical state of the gaseous mixture in inclusions is characterized by low density and high rarefaction, which during 15 million years also did not lead to equilibrium with air pressure.

2. Fine inclusions of liquid nitrogen have been detected in metamorphic rocks of the Southeast Altay /6/ in disthene (kyanite). At 20° C, the nitrogen in the inclusions has a pressure attaining and exceeding 1000 atm. The age of the rocks often exceeds 200 million years. Neither diffusion or time were able to bring the gases in these inclusions to a state that is equilibrium in chemical composition and physical state with the air or the rock gases of a different composition. It is not at all mandatory that the cases be generalized and used as arguments diffusion in general. However, they show that there are particular cases for which diffusion from the vacuole of an inclusion and into a vacuole is absent or so slight even on the scale of geologic time that it cannot be adequately measured. /360

Results obtained of the gas composition in glasses of lunar surface material. Presented in the table are the results of analyses

for six lunar particles, of these three are glass spherules and one is a black spherule from a glass spherule, and two are glass fragments.

Of the 18 pierced and analyzed inclusions, five were not measured before piercing (analyses 11-13). One gas bubble, as already noted, exited from an opaque internal spherule (analysis 9) and its initial volume was not measured. The other gas bubbles exited from vacuoles that were not intended for pressuring and were pressured together with the vacuole studied. For several gas bubbles the initial diameters were measured and their contraction established, however owing to a lack of time no analyses were made (they were in the cut-off liquid for more than 25 minutes). There were four of these measurements. They related to cases when the vacuole was filled with the cut-off liquid and the gas bubble, on contracting, remained within the inclusion.

Generalizations on the analyses reduce to the following.

1. Gas mixtures in inclusions having two-, three-, and four-component composition: CO_2, H_2, CO_2, H_2,N_2 + inert gases or H_2S, SO_2, NH_3), H_2, N_2 + inert gases, and H_2S, SO_2, and NH_3), CO_2, H_2, and N_2 + inert gases.

2. Sulfur gases and the ammonia that is possible in this group were present in 12 of the 18 analyses in amounts from 8 to 53.5 volume percent.

3. Carbon dioxide was also present in 12 analyses in amounts from 3 to 61 volume percent.

4. Hydrogen was present in all analyses (with the exception of the air bubble) in amounts from 10 to 95 volume percent.

5. Nitrogen and inert gases were present in 13 analyses in amounts from 9.4 to 77 volume percent.

6. The reproducibility of the analyses is characterized by two gas bubbles, completely identical in volume, from a single inclusion (analyses 4 and 5). The analyses show slight deviations. /361

7. The contraction of gas upon breaching of an inclusion is slight (much less than, for example, in certain tectites) and varies within the limits of 2.32 and 54.5 times.

8. Two gas bubbles (analyses 14 and 15) were in vacuoles at pressures above the atmospheric (2.5-2.64 /atm/).

RESULTS OF QUANTITATIVE ANALYSIS OF COMPOSITION OF GAS PHASE OF INDIVIDUAL INCLUSIONS

Analysis number	Sample	D of gas bubble after piercing, mm	Increase (+) or decrease (-) of bubble volume	Concentration, volume percent: CO_2	Hydrocarbons	O_2	CO	H_2	Total	Remarks
1	1 sp	0,126	—	15,9	0,0	—	0,0	0,0	74,4	9,7	100,0	—
2	1 sp	0,040	—	13,6	0,0	—	0,0	0,0	75,7	10,7	100,0	—
3	1 sp	0,042	1,59 (—)	23,0	28,2	—	0,0	0,0	28,4	20,4	100,0	—
4	1 sp	0,017	6,80 (—)	53,5	35,5	—	0,0	0,0	11,0	0,0	100,0	—
5	1 sp	0,017	—	53,0	35,0	—	0,0	0,0	12,0	0,0	100,0	—
6	1 sp	0,029	—	19,3	30,7	—	0,0	0,0	22,8	27,2	100,0	—
7	2 sp	0,018	14,80 (—)	11,0	61,7	—	0,0	0,0	Not analyzed			—
8	2 sp	0,035	—	0,0	29,8	—	0,0	0,0	14,9	55,3	100,0	—
9	2 sp	0,016	—	52,2	32,2	—	0,0	0,0	15,6	0,0	100,0	Black spherule 22.6 μm
10	3 sp	0,014	16,6 (—)	0,0	4,5	—	0,0	0,0	95,5	0,0	100,0	
11	5 sp	0,084	—	0,0	0,0	—	19,9	0,0	0,0	80,1	100,0	Dehermetized connection with air
12	1 gl	0,034	14,3 (—)	9,7	21,7	—	0,0	0,0	29,2	39,4	100,0	Sample 3
	1 gl	0,009	17,7 (—)	Not analyzed								
	1 gl	0,013	54,5 (—)	"								
	1 gl	0,021	4,67 (—)	"								Clear spherule 14 μm
13	1 gl	0,005	7,22 (—)	21,0	21,7	—	0,0	0,0	27,7	29,6	100,0	—
	1 gl	0,006	6,37 (—)	Not analyzed								
14	3 gl	0,156	2,84 (+)	0,0	3,9	—	0,0	0,0	15,4	80,7	100,0	Sample 12
15	3 gl	0,090	2,5 (+)	0,0	3,0	—	0,0	0,0	17,7	79,3	100,0	—
16	3 gl	0,080	—	0,0	13,0	—	0,0	0,0	10,0	77,0	100,0	—
17	3 gl	0,004	17,7 (—)	8,0	20,2	—	0,0	0,0	30,5	41,3	100,0	—
18	3 gl	0,030	20,7 (—)	19,9	45,3	—	0,0	0,0	34,8	0,0	100,0	—

9. One air bubble was analyzed extracted from an inclusion with a defective shell.

On the Moon, as well as on Earth, the most diverse cosmic material has fallen in which cometic, meteoritic, protoplanetary, and entirely lunar material can be presupposed.

Discussion of results. 1. The most unexpected result was the relatively high density of gases, differing sharply from the density of the lunar atmosphere. Whereas lunar glass spherules are the result of impacts of meteorites against the lunar surface, melting, and splashing of the lunar surface in the form of droplets, during melting intense outgassing of the melt can be anticipated.

However, inclusions in the lunar spherules were not subjected to this process. It can be assumed that spherules of different origins accumulated in the lunar surface material: lunar -- impactive without inclusions, extralunar -- cosmic, forming in an environment differing from the environment on the lunar surface, and spherules falling on the Moon from outer space. From the lunar surface material we purposely selected spherules with inclusions, although spherules not containing inclusions were in the vast majority.

Some analogies can be drawn for glass spherules that we found in deep-water sediments of the Pacific (the Tonga Trough). These spherules are also varied; most of them do not contain inclusions, and it is highly probable that these are spherules that arrived on the Earth's surface from the Moon.

A second group of spherules contain inclusions; for it a source other than the Moon is probable. When the inclusions in these spherules of extralunar origin were pierced, the rarefaction of the gas is also low.

2. The presence of hydrogen among the gases from the inclusions of all lunar spherules can be regarded as characteristic. The same feature is seen for certain spherules extracted from deep-water oceanic sediments and some of the spherules from the cosmic dust on the peat layer in the year of the fall of the Tungus phenomenon. Considerable amounts of hydrogen were found in several tectites (moldavites).

3. Very appreciable amounts of nitrogen and inert gases were observed among the gases from inclusions in lunar spherules. It must be added in qualification that we have no analytical data to substantiate the amounts of nitrogen or inert gases in this mixture. Its gases can be represented successfully only by inert gases or only by nitrogen, or by any of their quantitative combinations.

4. Some analyses reveal highly significant amounts of carbon dioxide and sulfur gases or ammonia.

As follows from these analyses and the diversity of the gas composition, various sources for the material in lunar surface material can be presupposed. The spectrometric investigation of comets shows the predominance of hydrogen. Hypotheses of the origins of the Moon from the terrestrial orb also take note of a certain role for hydrogen.

The most difficult problem is the possibility of the preservation of gases and the invariance of their composition. Some facts and examples have already been given above. Lunar material is in a special position. Its very rapid transition from lunar conditions to terrestrial bypassed the necessity of dealing with enormous

time intervals during which diffusion could occur to an appreciable extent. The time and place in which the glass lunar particles melted remains unknown. We can only note that all the investigated particles could scarcely have been formed recently. If among them there are particles that were formed in ancient times (millions of years), then it is doubtless true that diffusion from the lunar atmosphere did not occur. The short period of the terrestrial life of lunar rocks and the absence of an air component in the gas composition of lunar inclusions also do not make it possible to presuppose the diffusion through the glass shell with the terrestrial atmosphere. Inclusions with disturbed hermeticity quite clearly are revealed by the presence of an air component.

The study was carried out through the organizational cooperation of Academicians A. P. Vinogradov, A. A. Trofimuk, and V. S. Sobolev, as well as the practical assistance of coworkers at the Institute of Geochemistry and Analytical Chemistry imeni V. I. Vernadskiy Yu. I. Stakheyev, V. B. Naumov, and L. S. Tarasov, coworker of the Institute of Space Research A. V. Ivanov, and coworkers of the Institute of Geology and Geophysics (of the Siberian department of the USSR Academy of Sciences) G. M. Ivanova, N. M. Popova, and S. G. Motorin. The authors are deeply grateful to all these persons listed.

REFERENCES /362

1. Voano, V. G., "Modification of the Ens Analysis of Gases Trapped in Bubbles in Glass," Optiko-mekhanicheskaya Promyshlennost' (2), (1937).

2. Deysha, G., "Tests by Crushing Mineral Fragments to Find Gas Inclusions Under Pressure," in: Ocherki mineralogicheskoy monometrii /Mineralogic Monometry/, 1950.

3. Dolgov, Yu. A., and Shugurova, N. A., "Study of the Composition of Individual Gas Inclusions," in: Materialy po genetich. i eksperim. mineralogii /Materials on Genetic and Experimental Mineralogy/, Vol. 4, "Nauka", 1966.

4. Dolgov, Yu. A., and Shugurova, N. A., "Composition of Gases from Individual Inclusions of Various Minerals," in: Mineral. termometriya i barometriya /Mineralogical Thermometry and Barometry/, Vol. 1. "Nauka", 1968.

5. Dolgov, Yu. A., Shugurova, N. A., and Pogrebnyak, Yu. F., "Gas Inclusions in Tectites (Moldavites)," Dokl. SSSR 184(6), (1969).

6. Dolgov, Yu. A., Mal'gunov, S. V., and Shugurova, N. A., "Thermodynamic Conditions of the Formation of Metamorphic Rocks of the South Chuyskiy Range (Southeast Altay)," Dokl. AN SSSR 192(4), (1970).

7. Dolgov, Yu. A., Pogrebnyak, Yu. F., and Shugurova, N. A., "Composition of Gases and Their Pressures in Inclusions of Certain Tectites and Silica Glasses," Dokl. AN SSSR 198(1), (1971).

8. Pankova, N. A., "Precision of Measurement of Bubbles in the Analysis of Gases in Bubbles," Steklo. Byull. In-ta Stekla (1), (1961).

9. Slavyanskiy, V. T., and Krestnikova, Ye. N., Steklo i keramika 11, (1956).

10. Slavyanskiy, V. T., Gazy v stekle /Gases in Glass/, Oborongiz, 1957.

11. Shugurova, N. A., "Chemical Basis for the Method of Gas Analysis of Individual Inclusions in Minerals," Materialy II Vses. soveshch. po geotermobarometrii /Materials of the Second All-Union Conference on Geothermobarometry/, Novosibirsk, 1965.

12. Ens, I., "Analysis of Gases Contained in Glass Bubbles," Optiko-mekhanicheskaya promyshlennost' (2), (1935).

13. Burlingame, A. L., Calvin, M., Han, J., Henderson, W., Reed, W., and Simoneit, B. R., "Lunar Organic Compounds: Search and Characterization," Science 167(3918), (1970).

14. Fleischer, R. L., Haines, E. L., Hauneman, R. E., Hart, H. R., Jr., Kasper, J. S., Lifshin, E., Woods, R. T., and Price, P. B., "Particle Track, X-ray Thermal, and Mass Spectrometric Studies of Lunar Material," Science 167(3918), (1970).

15. Kirsten, T., Steinbrunn, F., and Zahringer, J., "Rare Gases in Lunar Samples: Study of Distribution and Variations by a Microprobe Technique," Science 167(3918), (1970).

16. Kroh, A., "Method of Microphysical Gas Analysis, Composition of Air in Insect Tracheas," Skand. Arch. Physical 25, (1911); 29, (1913).

17. Roedder, E., and Weiblen, P. W., "Lunar Petrology of Silicate Melt Inclusions in Apollo 11 Rocks," Proc. Apollo 11 Lunar Sci. Conf. 1, (1970).

18. Roedder, E., "Application of an Involved Crushing Microscope Stage to Studies of the Fluid Inclusions," Schweiz. Miner. Petrogr. 50/1, (1970).

Institute of Geology and Geophysics of the Siberian Branch of the USSR Academy of Sciences, Novosibirsk

N75 11845

ISOTOPIC COMPOSITION OF LITHIUM, POTASSIUM, RUBIDIUM, AND STRONTIUM IN LUNAR SURFACE MATERIAL

/363

V. G. Zaslavskiy, L. K. Levskiy, and A. N. Murin

Abstract

The isotopic composition of alkali and alkaline-earth elements in the Luna 16 regolith was investigated by the method of thermionic emission, without chemical separation.

The isotopic composition of the lithium in two regolith samples did not differ (within the limits 0.5 percent) from the mean for the terrestrial reference standard. At the same time, the observed difference (1 percent) in the isotopic composition of lithium between the samples requires further investigation and confirmation. The isotopic composition of K and Rb does not differ within the limits of experimental error from the isotopic composition of the reference standard.

Investigating the isotopic composition of elements in different objects of the solar system is vitally important in answering fundamental problems of the origin of the Earth, Moon, and the other planets. Identity of isotopic composition indicates their common origin, while a variation indicates the time and place at which the paths of the evolution of matter in the solar system diverged. One important problem in selenochemistry is the nature of the regolith [1]. A reliable establishing of the latter requires determination of the concentration and isotopic composition for as large as possible a number of elements. In this respect it is important to study the isotopic composition of lithium. The origin of lithium, just as for other light elements -- D, Be, and B -- remains puzzling thus far [2-4]. It should be noted that neither we [5] or some other investigators [6, 7] have detected any deviations or even local variations in the isotopic composition of lithium in meteorites of different types compared with terrestrial standards. It

is of interest to establish the identity of the isotopic composition (or its absence) also for other elements in the regolith and in the terrestrial reference standards.

Experiment. The isotopic composition of Li, K, Rb, and Sr was investigated for two samples of lunar surface material 9-1 and S-21 (the weighed sample was about 2 mg). Isotopic analysis (Li^7/Li^6), as well as experiments with the meteoritic material /5/ were conducted by the method of thermionic emission; this permits bypassing the chemical separation of the element and the use of an emitter /8/. Since the lithium content in samples is considerable ($10 \cdot 10^{-4}$ percent) /1/, the measurements were made with an electrometer; the sample weight did not exceed 0.1-0.2 mg. The lithium was burned completely and the number of cycles of measurement of the isotopic ratio was quite high (of the order of several hundred). The experimental data were processed on an electronic computer by the method of least squares, with allowance for the effect of fractionation of the lithium isotopes in the source.

To preserve the identity of the conditions during isotopic analysis of the individual samples, the measurements were made in a high vacuum ($2 \cdot 10^{-7}$ mm Hg) and with an invariant electronic-optical system. All samples were deposited with a teflon spoon on the same tantalum strip -- the heater of the ionic source with baked-in tungsten powder. After each experiment, the strip was fired until all traces of lithium and rubidium disappeared, and the potassium current did not exceed 0.1 percent of the working current. The measurements of the isotopic composition of Li, K, and Rb were made, respectively, on the same scales of the electrometric amplifier (for the reference standard and the samples). The isotopic composition of potassium (K^{39}/K^{41}) and rubidium (Rb^{85}/Rb^{87}) were measured at the beginning of the experiment (before the Li^7/Li^6) was measured). The K^{39}/K^{41} ratio was measured for several hours, and then the Rb^{85}/Rb^{87}. The measurements of the samples were alternated with the measurement of the terrestrial reference standard, the mineral olivine. The results of the measurements are in the table.

The isotopic analysis of lithium was carried out to high precision (0.1 percent), accounted for by the high content of lithium and by the large number of isotopic determinations of the Li^7/Li^6 ratio. The results for samples 9-1 and S-21 did not differ by more than 0.5 percent from the mean for the reference standard. /364
The observed difference in the isotopic composition for samples 9-1 and S-21 (about 1 percent) requires further careful investigation. The isotopic composition of potassium and rubidium, for which the mean values and the root mean square errors are given,

does not differ within the limits of 1-3 percent from the reference standard. It should be noted that the isotopic analysis data are not normalized relative to table data, although for Li and Rb they are close to these values. After the measurement of the isotopic composition of lithium was completed, the spectrum of the mass of isotopes was recorded with further increase in the temperature of the strip. In particular, the investigation showed that it is possible to measure the isotopic composition of the alkaline-earth elements Ba and Sr (the ionic current corresponding to Sr^{88} was 10^{-15} A). The need to enhance the sensitivity of the receiving section here compelled working with an ionic-electron multiplier. We note that rubidium does not interfere with the measurement of strontium, since it is completely burned up before measurement of the isotopic composition of strontium begins.

Preliminary data for strontium are given in the table. To construct the isochrons, besides Sr^{87}/Sr^{86}, one must establish the value of $Rb/^{87}/Sr^{86}$. To do this, at the present time the appropriate therionic emission method is underway.

Conclusions. 1. It has been shown possible to use thermionic emission in studying the isotopic composition of alkali and alkaline-earth elements in lunar regolith without chemical treatment of the material. The amount of material in a single experiment is 0.1 mg.

2. No variations in the isotopic composition of Li, K, and Rb were found in the regolith and the terrestrial reference standard.

3. Some regolith samples differed by 1 percent in their isotopic composition. However, careful study of the statistical dependence of this deviation is necessary.

In conclusion, we are happy to express our gratitude to A. G. Morachevskiy for assistance in organizing the experiment.

ISOTOPIC COMPOSITION OF LITHIUM, POTASSIUM, RUBIDIUM, AND STRONTIUM IN LUNAR REGOLITH

Sample	Date	Li^7/Li^6	Number of cycles	K^{39}/K^{41}	Number of cycles	Rb^{85}/Rb^{87}	Number of cycles	Sr^{87}/Sr^{86}	Number of cycles
9-1	31.10 70	12,13±0,01	164	14,25±0,30	98	2,61±0,08	72	—	—
	13.11 70	12,14±0,01	504	14,00±0,28	59	2,57±0,04	52	—	—
	23.01 71	—	—	13,50±0,10	37	—	—	—	—
	1.02 71	—	—	13,50±0,10	64	2,58±0,02	50	—	—
	4.02 71	—	—	—	—	—	—	0,702±0,005	15
	10.02 71	—	—	13,70±0,20	36	2,56±0,08	36	—	—
	13.02 71	—	—	—	—	—	—	0,707±0,007	20
S-21	3.11 70	12,25±0,01	258	14,00±0,40	90	2,59±0,05	81	—	—
	10.11 70	12,26±0,01	343	14,10±0,30	68	2,55±0,07	30	0,700±0,004	32
	28.01 71	—	—	14,20±0,10	49	2,59±0,03	17	—	—
Olivine (standard)	31.10 70	12,35±0,03	62	13,70±0,40	49	—	—	—	—
	9.11 70	12,21±0,02	52	14,00±0,18	54	—	—	—	—
	25.11 70	12,16±0,01	113	13,90±0,28	56	2,57±0,06	17	—	—
	1.12 70	—	—	13,70±0,21	47	2,58±0,04	8	—	—

REFERENCES

1. Vinogradov, A. P., "Preliminary Data on Lunar Regolith Returned by Luna 16 Automatic Station," Geokhimiya (3), 261-274 (1971).

2. Burnett, D., Fowler, W., and Hoyle, F., "Nucleosynthesis in the Early History of the Solar System," Geochim. Cosmochim Acta 29(12), (1965).

3. Bernas, R., Grandstajn, E., Reeves, H-, and Schatzman, E., "On the Nucleosynthesis of Li, Be, and B," Ann. Phys. (N.Y.) 44(2), (1967).

4. Audouse, J., "Some Nucleosynthetic Effects of Energetic Proton Fluxes on Stellar Surfaces and on the Solar System," Astronom. Astrophys. 8(3), (1970).

5. Levskiy, L. K., Murin, A. N., and Zaslavskiy, V. G., "Isotopic Composition of Lithium in Meteorites (Chondrites)," Geokhimiya (1), (1969).

6. Krankowsky, D., and Muller, D., "Isotopic Distribution and Abundance of Lithium in Stony Meteorites," Geochim. Cosmochim. Acta 28(11), (1964).

7. Balsiger, H., Geiss, J., Grogler, N., and Wyttenbach, A., "Distribution and Isotopic Abundance of Lithium in Stony Meteorites," Earth Planet. Sci. Letters 5(1), (1968).

8. Levskiy, L. K., Murin, A. N., and Zaslavskiy, V. G., "Thermionic Emission in the Isotopic Analysis of Lead and Lithium," Geokhimiya (6), (1969).

Leningrad State University imeni A. A. Zhdanov, Chemistry Division, Leningrad.

N75 11846

STUDY OF ISOTOPIC COMPOSITION OF HELIUM IN THE FINE FRACTION OF LUNA 16 LUNAR SURFACE MATERIAL

/365

B. S. Boltenkov, V. N. Gartmanov, E. I. Il'yasov, G. Ye. Kocharov, B. A. Mamyrin, Yu. A. Surkov, and L. V. Khabarin

Abstract

The content of He isotopes was measured in two samples of the lunar surface material returned by the Luna 16 automatic station.

Both samples consist of a fine fraction of lunar surface material and were samples from zone A_3 (sample 3-2k) and from zone V (sample 9-1r). The value of He^4/He^3 (2500 $\pm$ 100 for sample 3-2k and 2650 $\pm$ 100 for sample 9-1p) and the concentration of the He isotopes (0.229 cm^3 He^4/g for sample 3-2k, and 0.237 cm^3 He^4/g for sample 9-1r) are identical for both samples, within the limits of experimental error.

The content of the He isotopes in the magnetic fraction separated from sample 3-2k considerably exceeds the concentration of He isotopes in the nonmagnetic fraction of this same sample. Curves were plotted for the kinetics of separation of the He isotopes from the magnetic fraction of sample 3-2k. They are identical for both isotopes and are characterized by a series of features -- "peaks". Measurements of He in separate crystals selected from sample 3-2k show that the concentration of He varies from 0.23 cm^3 He^4/g to $5 \cdot 10^{-3}$ cm^3 He^4/g, but the isotopic ratio of He^4/He^3 lies within the range of the isotopic ratios characteristic of solar wind (1970-2650). A crystal with an anomalously high He^4/He^3 ratio of 9720 was found.

Interest in the study of the isotopic composition of inert gases in samples of extraterrestrial origin in recent years has climbed sharply owing to the new information obtained by artificial

satellites and interplanetary stations concerning the processes in near-Earth space and especially because the first samples of surface material returned from the lunar surface have been made available to investigators.

Study of the content of inert gases and their isotopic composition in lunar rocks and a comparison of these data with the measurements of inert gases in meteorites, terrestrial rocks, the Earth's atmosphere, and in the solar wind assists in solving problems such as the history of the Moon and the planets of the solar system, the physics and history of the Sun, and the conditions of the formation of the solar system.

The following processes represent the main possible sources for the formation of inert gases in samples of lunar surface material.

1. Direct capture of inert gas ions by the surface of a sample from fluxes of solar wind and solar cosmic rays. As shown by the first investigations of the samples of lunar surface material returned by Apollo 11, this process is dominant for the fine fraction of the lunar surface material -- lunar dust /1, 2/.

2. Formation of isotopes of inert gases resulting from nuclear reactions occurring in the material of the samples under the action of cosmic rays.

3. Formation of isotopes of inert gases owing to the disintegration of radioactive elements contained in the lunar rocks.

4. Capture of inert gases from the Moon's atmosphere during the cooling of molten lunar rocks at an early stage in the Moon's history.

Clarifying the role of these processes with respect to changes in the content of inert gases in lunar rocks is extremely difficult owing to the thermal diffusion, leading to the loss of inert gases by the sample, the phenomenon of saturation of the surface of a sample by inert gases during irradiation by corpuscular fluxes, and the complex chemical and mineralogic composition of the samples. Therefore detailed study of the dependence of the inert gas content on the composition of the sample and mineralogical structure is called for, along with the study of the kinetics of the segregation of gases from the sample, and the processes of diffusion and capture of gases by different areas of the sample. Preliminary results of work done by us in this direction are given in this article.

To carry out the experimental work with lunar surface material, we obtained two samples: sample 3-2k and sample 9-1p. Both /366 samples are a fine fraction of lunar surface material as a whole

(lunar dust) packaged in nitrogen atmosphere. Sample 3-2k was in the air during the investigation of the radioactivity of the lunar surface material. Sample 3-2k was sampled from zone [illegible], and sample 9-1r -- from zone V. All work in preparing the weighed samples from the general samples and separation by fractions was carried out in an air atmosphere.

The following samples were selected for analysis:

a) from general samples 3-2k and 9-1r, samples with mean composition (without separation into fractions); the weight of the weighed samples was 0.2-0.4 mg; and

b) from general sample 3-2k, weighed samples consisting of the magnetic and nonmagnetic fractions of the general sample. The separation into magnetic and nonmagnetic fractions was carried out under an MPS-2 microscope at a power of 100 in a microweighing bottle filled with acetone, using a steel needle with a permanent magnet secured to it. The acetone was used to reduce the force of cohesion between the particles of the surface material. The magnetic fraction consisted of fine opaque crystals adhering into conglomerates and represented the greater part of the general sample. The magnetic fraction consisted of coarser crystals of irregular shape, and also which were transparent.

TABLE 1. CHARACTERISTICS OF PARTICLES SELECTED FOR ANALYSIS FROM GENERAL SAMPLE 3-2k

Weighed sample number	Number of particles (Fig.2) included in weighed sample	Visual features of particles	Surface area of particles included in weighed sample, 10^{-4} cm^{-2}	Characteristic dimensions of particles in weighed sample, microns
1	5, 6, 7	Black, opaque, metallic appearance, particles of spherical shape	2.2	40
2	3, 8, 9, 10	Light-yellow, clear crystals of irregular shape	3.7	50
3	1	Green clear lamella	8.6	200
4	2, 4	Cloudy-yellow, translucent crystals of irregular shape	8.1	150
5	Separate crystal*	Clear, colorless crystal of irregular shape	3.6	100

*The crystal is not shown in the photograph. The volume of the crystal was $(0.3\text{-}0.4)\cdot 10^{-6}$ cm^2, and the weight at a density of 3 g/cm^3 $\simeq 10^{-6}$ g = 1 μg.

TABLE 2. CONTENT OF He ISOTOPES IN MEAN-COMPOSITION WEIGHED SAMPLES

Sample	Weight, mg	He^3, cm^3/g	He^4, cm^3/g	He^4/He^3
3-2k	0.2	$9.15 \cdot 10^{-5}$	0.229	2500 ± 100
9-1p	0.3	$8.95 \cdot 10^{-5}$	0.237	2650 ± 100

The size distribution of crystals in these fractions was determined by sampling. The size of crystals in each sampling was measured with a MBI-3 microscope at a power of 630. Histograms of the size distribution of crystals are shown in Fig. 1. Several weighed samples of these fractions having a weight of 0.2-0.4 mg were sampled. The coarsest crystals of various mineralogic fractions were sampled from general sample 3-2k. The general appearance of the sampled particles and the crystals is shown in Fig. 2. Five weighed samples were prepared from them. The characteristics of the weighed samples are in Table 1.

The release of helium from the prepared weighed samples was carried out by heating in a seamless metallic unit with purification by activated charcoal cooled to the temperature of liquid nitrogen, and with barium and titanium getters at T = 800° C.

The helium isotopes were analyzed on a dynamic resonant mass spectrometer with complete resolution of the doublet $(H^{3+} + HD^{+} - He^{3+})$ /3/. The background of a blank determination for He^3 did not exceed $1 \cdot 10^7$ atoms, and $8 \cdot 10^{10}$ atoms -- for He^4. The quantities of each isotope and the isotopic ratio in the weighed sample was measured by comparison with a reference standard mixture of isotopes similar in content and isotopic ratio to the weighed samples measured.

The degree of heating needed to release the helium from the sample of lunar surface material was verified in preliminary experiments. It was found that during degassing of the samples for one hour at T ≈ 200° C, approximately 1 percent of the total helium in the sample was released, with an isotopic composition differing only slightly from the isotopic composition of the helium in the sample. The remaining 99 percent of the helium was released at T ≈ 1200° C. It was shown that raising the temperature all the way to T ≈ 1500° C did not lead to an additional release of helium from the sample (to a precision of fractions of a percent of the total helium content). Therefore, to measure the content of helium in the various weighed samples of the lunar surface material, its release was carried out at T = 1200° C. The time of extraction was about one hour. /367

The results of measuring the He content in the selected weighed samples are given in Tables 2-4 (the volume of the gas is given in cm^3 under normal conditions, the weight of the weighed samples is in milligrams, and the particle size is in microns).

In addition to these experiments with the magnetic fraction of the lunar surface material, an experiment was conducted to determine the kinetics of the release of helium isotopes -- tempering. A sample weighing 0.3 mg was heated at a rate of 13° C per minute. Here the helium released from the sample was purified and sent directly into the chamber of the mass spectrometer in a regime of constant evacuation at a specified rate. The rate of evacuation of the analyzer chamber was selected so that replenishing 90 percent of the amount of gas in the chamber occurred in one minute. The amount of released isotopes was recorded continuously throughout the experiment.

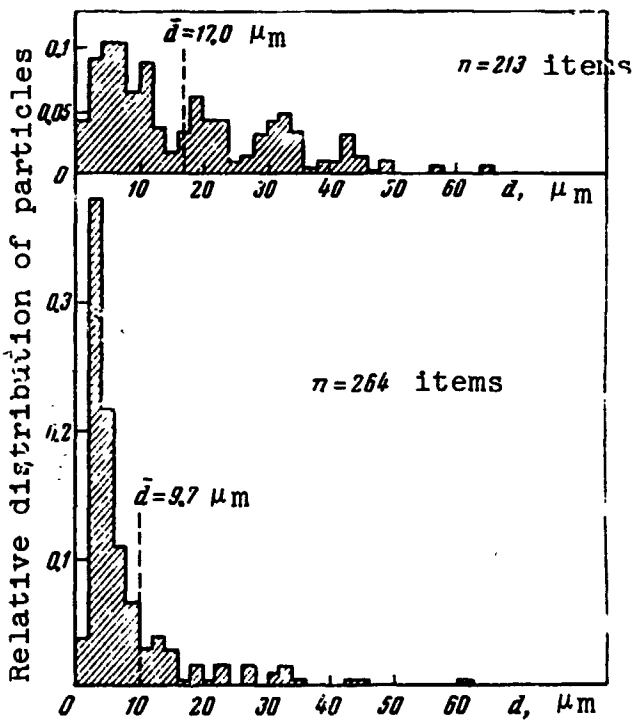

Fig. 1. Histograms of size distribution of particles in nonmagnetic (upper) and magnetic (lower) fractions of general sample 3-2k

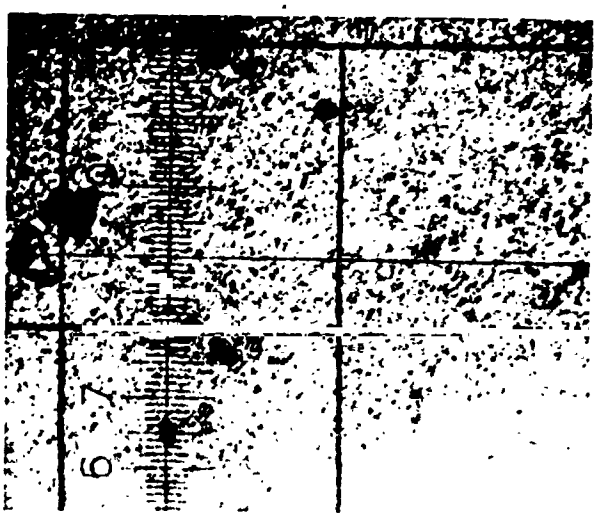

Fig. 2. Particles of lunar surface material sampled from general sample 3-2k. The finest scale division is 25 μm (see Table 1 for numbers)

When the blank determination was made for tempering, the background for each isotope remained constant throughout the experiment. The background level with respect to He^3 was 0.01 percent, and 0.1 percent for He^4, of the amount of the isotopes measured during the tempering of the magnetic fraction. The question of equipment stability during tempering is of some significance, since the duration of the entire experiment was of the order of 1.5 hours. During this time the instability of the measuring equipment and the operation of the mass spectrometer source, the inconstancy of the rate of helium evacuation from the mass spectrometer chamber, and variations in the rate of evacuation of getters in the helium purification system can lead to the appearance of false bursts on the curve of the release kinetics. To check the stability of these parameters, a special experiment was conducted with constant discharge of helium similar in amount and isotopic composition to the helium released from this sample. In an hour and a half of testing for stability, no abrupt fluctuations were observed either in the amount of the individual isotopes or in the isotopic ratio. The level of the fluctuations obtained in this experiment, both with respect to the amount of isotopes as well as with respect to the isotopic ratio, did not exceed ± 5 percent of the measured value, and the fluctuations during measurement of each isotope were random in nature and did not correlate with each other. /368

The results obtained in the experiment to determine the kinetics of the release of helium from the magnetic fraction of the lunar surface material are in Fig. 3.

Measurement of the mean-composition samples 3-2k and 9-1p taken from different depths on the Moon's surface (Table 1) give -- within the limits of experimental error -- identical values both with respect to the amount of isotopes as well as the isotopic ratio. This result can be accounted for either by processes of intensive mixing of the lunar surface material in zone V (for example, under the action of meteoric impacts), or else by the time-constancy of the mean flux of helium isotopes arriving from the Sun. The presence of intense mixing in the landing site of the Luna 16 automatic interplanetary station was confirmed by the excess of the content of cosmogenic radioisotopes in the samples of lunar surface material taken from a depth of several tens of centimeters, compared with the calculated values /4, 5/. We note that the saturation of the surface of the sample with helium ions captured from the solar wind flux occurred relatively rapidly and, according to the estimates by Eberhardt et al., the saturation time was 300 years /1_7/. These effects must be taken into account when interpreting the results of the depthwise trend of the concentration of helium isotopes.

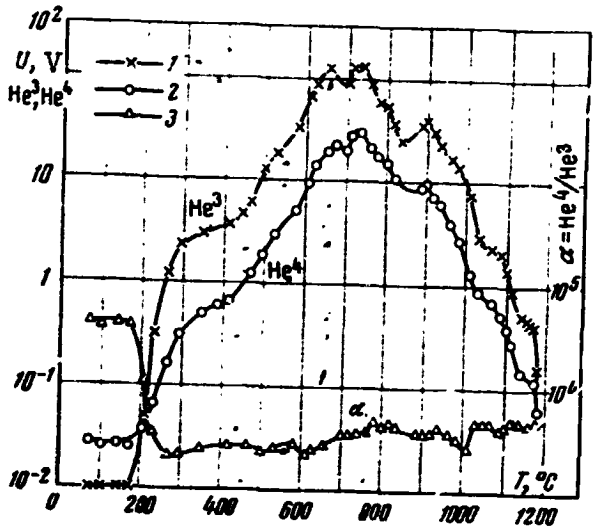

Fig. 3. Results of experiment on the kinetics of the release of helium isotopes from the magnetic fraction of the general sample 3-2k

1. He^3
2. He^4
3. $\alpha = [\bar{He}^4]/[\bar{He}^3]$

The content of helium isotopes in the magnetic fraction considerably exceeds the content of helium isotopes in the nonmagnetic fraction of the lunar surface material. In spite of the fact that the mean size of crystals in the magnetic fraction is less, that is, the overall surface area of all particles is greater than in the nonmagnetic fraction, the difference between the helium concentration in these fractions evidently cannot be determined only by the surface. As shown by measurements conducted on individual crystals for weighed samples 1 and 2 (Table 4), which are analogs of the magnetic and nonmagnetic fractions, the helium content values per unit surface area differ appreciably, which probably is due to the difference in the retention of helium by the crystal lattices of the minerals. This conclusion is also confirmed by the experiment on the kinetics of helium release. The general trend of the release curves of the He^3 and He^4 isotopes is identical, and in both curves a considerable number of incompletely resolved "peaks" corresponding to different temperature fractions can be clearly traced. Most of the helium was released in the temperature range 500-1000° C in the form of four "peaks". Outside this temperature range five more "peaks" of much lower intensity were observed. The large number of "peaks" in the high-temperature region evidently is accounted for by the different coefficients of the diffusion of helium in the lattices of the different minerals. The low-temperature "peaks" can be associated with the different capture sites of the helium atoms at depths of the order of several lattice constants from the surface of the minerals.

The isotopic ratio He^4/He^3 in the experiments on the release kinetics undergoes considerable fluctuation (by more than twofold) and monotonely increases with increase in temperature.

The isotopic ratio of helium in individual crystals in all the weighed samples, except for sample 4, lies within the range of isotopic ratios of helium in the solar wind (1800-2800). We note that

isotopic ratios recorded in different samples returned by the Apollo 14 expedition (14066,2; 14305,9; and 14321,13) were analogous and even exceeded the isotopic helium ratio we measured in sample 4 (9720) [6, 7]. One of the possible causes leading to the excess of the isotopic ratio He^4/He^3 in sample 4 (see Table 4) over the isotopic ratio characteristic of the solar wind can be the addition of radiogenic He^4 formed during the decay of radioactive elements. As shown by estimates, the content of radioactive elements in the sample 4 crystals (U^{238} of Th^{232}) required to account for this effect must be $(2\text{-}10)\cdot10^{-3}$ percent. At the same time it should be noted that /369 the content of uranium and thorium is one to two orders lower in the Sea of Fertility regolith [4].

TABLE 3. CONTENT OF HELIUM ISOTOPES IN MAGNETIC AND NONMAGNETIC FRACTIONS

Fraction	Weight mg	Mean diameter μm	Number of atoms in weighed sample		Concentration cm³/g		He^4/He^3
			He^3	He^4	He^3	He^4	
Magnetic	0,23	9,72	$3,28\cdot10^{11}$	$8,76\cdot10^{14}$	$5,28\cdot10^{-8}$	0,141	2680
Nonmagnetic	0,14	17,0	$0,49\cdot10^{11}$	$1,46\cdot10^{14}$	$1,29\cdot10^{-8}$	0,039	2990

TABLE 4. CONTENT OF HELIUM ISOTOPES IN PARTICLES EXAMINED

Sample number	Amount of isotopes in sample		Concentration, cm³/g		He^4/He^3
	He^3	He^4	He^3	He^4	
1	$52,3\cdot10^7$	$103\cdot10^{10}$	$118\cdot10^{-9}$	$232\cdot10^{-6}$	1970
2	$37\cdot10^7$	$76\cdot10^{10}$	$32,1\cdot10^{-9}$	$64,6\cdot10^{-6}$	2050
3	$3,7\cdot10^7$	$9,8\cdot10^{10}$	$2,4\cdot10^{-9}$	$5,46\cdot10^{-6}$	2650
4	$15,7\cdot10^7$	$153\cdot10^{10}$	$9,45\cdot10^{-9}$	$94,4\cdot10^{-6}$	9720
5	$15,4\cdot10^7$	$35,6\cdot10^{10}$	$15,9\cdot10^{-9}$	$36,8\cdot10^{-6}$	2310

In conclusion, we note that only further experimental investigation of the inert gas content in samples taken from different points on the lunar surface and from different mineralogic fractions, and special simulation experiments in laboratory conditions can provide us the information needed to interpret the history of the Moon.

The authors are deeply grateful to Academician A. P. Vinogradov for his close attention to this study.

REFERENCES

1. Eberhardt, P., Geiss, J., Graf, H., Grogler, N., Krahenbuhl, U., Schwaller, H., Schwarzmuller, H., and Steller, A., "Trapped Solar Wind Noble Gases, Exposure Age and K/Ar Agem Apollo 11 Lunar Fine Material," Proc. Apollo 11 Lunar Sci. Conf., Geochim. Cosmochim. Acta, Suppl. 1 2, 1037 (1970).

2. Kirsten, T., Steinbrunn, F., and Zahringer, J., "Rare Gases in Lunar Samples: Study of Distribution and Variations by a Microprobe Technique," Science 167(3918), 571 (1970).

3. Mamyrin, B. A., Tolstikhin, I. N., Anufriyev, G. S., and Kamenskiy, I. L., Geokhimiya (5), 595 (1969).

4. Surkov, Yu. A., Fedoseyev, G. A., and Sobornov, O. P., "Gamma-spectrometric Analysis of Sample of Luna 16 Lunar Surface Material," first Paper presented at the 15th Session of COSPAR, Madrid, Spain, 1972.

5. Lavrukhina, A. K., and Gorin, V. A., Paper presented at the 15th Session of COSPAR, Madrid, Spain, 1972.

6. Geiss, J., Eberhardt, P., Buhler, F., Meister, J., and Singer, P., J. Geophys. Res. 75, 5972 (1970).

7. Boltenkov, B. S., Gartmanov, V. N., Kocharov, G. E., Mamyrin, B. A., and Naidenov, V. O., Space Research 12, (1972) (to be published).

8. "Preliminary Examination of Lunar Samples from Apollo 14," Science 173(3998), 681 (1971).

Engineering Physics Institute imeni A. F. Ioffe, USSR Academy of Sciences, Leningrad.

N75 11847

CONTENT OF LITHIUM, BERYLLIUM, BORON, AND TITANIUM, AND THE ISOTOPIC COMPOSITION OF LITHIUM, BORON, AND MAGNESIUM IN LUNA 16 REGOLITH SAMPLE

/370

O. Eugster

Abstract

The abundance of the following elements in the L 16-19 No. 118 regolith sample, zone V (in μg/g) was determined by isotopic dilution using a mass spectrometer equipped with a scattering ion source: Li -- 9.8, Be -- 1.2, B -- 2.6, and Ti -- 1.92 percent. For comparison, these same elements were measured in samples of surface material returned by Apollo 11, Apollo 12, and Apollo 14, and in the terrestrial reference standard diabase W-1. The content of Li, Be, and B in the Luna 16 sample is nearly the same as in the Apollo 11 surface material. The surface material returned by Apollo 12 and Apollo 14 contains two to four times more of these elements. However, the abundance ratios of Li, Be, and B are remarkably similar in the surface materials from the four different lunar regions. The mean abundances of Li, Be, and B in lunar basaltic material agrees well with their abundances in the reference standard basalt BCR-1. With respect to basaltic achondrites and especially with respect to chondrites, the lunar basalts are enriched in Li, Be, and B up to 100 times. Thus, the lunar origin of basaltic achondrites is inconsistent with the abundance pattern of these elements in meteoritic and lunar material available at present. A strong correlation of Li and K was established for samples of lunar surface material collected in these four regions, which indicates the similarity of the chemical behavior of both alkali elements in different material from the lunar surface.

Introduction. Sample L16-19 No. 118 comes from zone V of the surface material core described by A. P. Vinogradov /157. The origin of this sample is 20-22 cm from the lunar surface. In the mass spectrometer, using isotopic dilution, measurements were made of the content of Li, Be, B, and Ti in a 51.6 mg sample of

the lunar surface material, from which the rock fragments larger than 1 mm were previously separated. The isotopic composition of Li, B, and Mg was determined in a sample consisting of three rock fragments 1-2 mg each in weight, and in a 1 mg sample, from a fraction with grain size 325-400 mesh. The goal of this work was as follows:

1. Study of the abundance of Li, Be, and B in lunar material. Owing to their different chemical behavior, large fluctuations in the abundances of these elements are noted in the samples of terrestrial, lunar, and meteoritic origins.

2. Measurement of the content of Ti as part of a study of the albedo of the lunar regolith conducted in collaboration with Maurette in our laboratory.

3. Measurement of the isotopic compositions of Li and B in the study of the action of cosmic rays or isotopic changes induced by solar wind. The Li^7/Li^6 ratio obtained in reactions of high energy fission is 2, and which can be anticipated in the solar wind, probably higher than the ratio for lunar or terrestrial Li. Thus far investigation of samples returned by Apollo 11 and Apollo 12 have not disclosed isotopic anomalies with respect to the terrestrial values /3/. The isotopic ratios of Mg were measured in samples used for the isotopic analysis of Li and B. The only possible factor that could cause isotopic anomalies of Mg was the additional component of radiogenic Mg^{26} resulting from the decay of Al^{26} ($T/2 = 7.4 \cdot 10^5$). However, considering the time of formation of the lunar material relative to the time of completion of nucleosynthesis, the detection of radiogenic Mg^{26} is extremely implausible. Also, the technique of isotopic dilution used in this study requires a knowledge of the isotopic composition of the elements investigated.

Experiment. Isotopic analyses of rock fragments. Three fragments of basaltic rocks with a total weight of 7 mg were mounted on a sample holder so that a very flat surface of about 2 mm in /371
extent was subjected, in the mass spectrometer source, to the action of a Cs^+ ion beam (9 keV) with an intensity of 10^{-6} to 10^{-9}. This ionic bombardment fractionated the atoms at the rock surface and scattered them in the form of positive ions, which then were separated in the mass spectrometer and recorded with an ion counter (16). This method is highly sensitive and well suited for direct analyses of Li, Be, B, Mg, Ti, and other elements, since interferences from neighboring elements are absent or very weak. Each analysis of the lunar material was immediately compared with the analysis of the terrestrial reference standard in order to reduce to the minimum the errors caused by fractionation. Since only the surface layer of several microns was consumed, the same rock fragments could serve for further investigations after this study.

Isotopic analysis of dust. A 1 mg dust sample was dissolved in concentrated HF using ultrasonic waves. A fraction of this solution containing less than 0.1 mg of the sample was placed on a precleaned and pretested gold disk and evaporated at 50° C. The isotopic composition of B was analyzed by the same procedure as that described for the surface of rock fragments. Then concentrated $HClO_4$ was added to the solution of the sample, which was then evaporated to dryness at 70-140° C in an enclosed teflon crucible under a stream of argon. Next, the sample was completely dissolved in 1 N HCl, part of the solution was deposited on the gold disk, and the deposited layer was analyzed for Li and Mg. The second step in the dissolving of the sample using $HClO_4$ and the higher vaporization temperature caused the nearly complete loss of B. Therefore B was measured before treatment with $HClO_4$.

Method of isotopic dilution. Known amounts of Li^6- and B^{10}-enriched tracers were added to a sample weighing 51.6 mg before dissolution After treatment in concentrated HF with ultrasonic waves, the residue, corresponding to about 10 percent of the initial sample, remained undissolved. Rechecking and comparison of the results obtained for terrestrial reference standard diabase W-1 with the literature data showed that B can be extracted quantitatively. The isotopic composition of B in the mixture of sample and indicator was measured as described above.

The technique of isotopic dilution could not be applied to Be, because this element is mono-isotopic and we did not have Be^{10}-enriched isotopic tracer in sufficient amounts. Therefore we measured the ratio of the limits of emission detection of Be and B with the mass spectrometer, which was found to be 1.6. After the B content and the ratios of the Be and B peak intensities were measured for the sample, it was possible to calculate the Be content. Li was determined after the complete dissolution of the sample, by using the $HClO_4$ treatment.

An aliquot of the final solution of the sample containing the known amount of the latter was mixed with the Ti^{47} tracer and the Ti was determined separately by isotopic dilution. During the entire experiment blank determinations were carefully conducted.

The correction for Be and Ti were < 1 percent and therefore negligibly small. Blank corrections for Li and Be of 0.5 and 5 percent were subtracted, respectively.

Isotopic abundances of Li, B, and Mg. Table 1 gives the isotopic ratios Li^7/Li^6, B^{11}/B^{10}, and Mg^{26}/Mg^{25} obtained for rock fragments, for surface materials, and for samples of terrestrial reference standards. Since the mass spectrometer introduces isotopic fractionation, the isotopic compositions of lunar samples

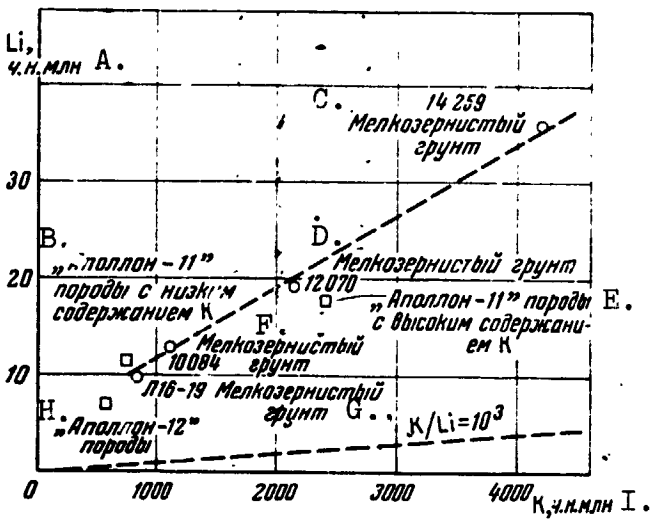

Fig. 1. Diagram of correlation of Li and K in lunar surface material and rocks. The data for K are taken from Vinogradov /15/, Tera et al. /14/, Hubbard et al. /7/, and from LSPET /8/. The data for Li and K for the rocks are taken from Tera et al. /14/ and from Annel et al. /1/.

KEY:
- A. ppm
- B. Apollo 11, rocks with low K content
- C. Fine-grained lunar surface material sample 14259
- D. Fine-grained surface material sample 12070
- E. Apollo 11 rock with high K content
- F. Fine-grained surface material sample 10084
- G. L16-19 fine-grained surface material
- H. Apollo 12 sample
- I. ppm

must be compared with those obtained for terrestrial samples under the same analytical conditions. It becomes obvious at once that there is no difference between the lunar and terrestrial isotopic compositions within the limits of experimental error, less than 2 percent. From these results we conclude that the lunar material was /372 subjected to the same homogenization as the terrestrial and meteoritic. Further, in spite of the prolonged exposure to bombardment of the material in the lunar surface by cosmic rays and solar wind, reactions of fission and the introduction of solar wind did not cause isotopic changes that could be detected in this investigation. Within the limits of experimental error of 1 percent, the measured ratios of lunar Mg^{26}/Mg^{25} do not indicate the additional component Mg^{26} caused by the decay of Al^{26} that could have existed in the early solar system.

Abundances of Li, Be, B, and Ti. Table 2 gives the concentrations of Li, Be, B, and Ti measured in the 51.6 mg sample L16-19 No. 118. The results of this Luna 16 sample reported here can be compared with the data in a preliminary report on the Luna 16 material by A. P. Vinogradov /15/. Excellent agreement was obtained for the concentrations of Li and Ti, although in this present study Li was measured in the "regolith V" fraction of the core of the surface material, while the data communicated by A. P. Vinogradov pertains to the "regolith B" and "regolith G" fractions. The concentrations of Be and B found in this work for the Luna 16 sample are below the values given in the

preliminary report /157. However, for Be the analytical errors can still be partially overlapped, since the experimental error of the determination of the abundance of Be in this work is ± 50 percent. The abundance found for B is 2.6 times less than that given in the preliminary report /157. It is probable that there are large inhomogeneities in the content of B, a fact which shows up in the fluctuations from 3.9 to 6 ppm within different layers /373
of the core. For comparison, also included are data obtained in our laboratory for lunar surface materials returned by Apollo 11, Apollo 12, and Apollo 14, as well as for the terrestrial reference standard diabase W-1.

TABLE 1. ISOTOPIC COMPOSITION OF Li, B, AND Mg IN ROCK FRAGMENTS WEIGHING 7 mg AND 1 mg OF FINE SURFACE MATERIAL FROM THE SEA OF FERTILITY

Sample	Li^7/Li^6	B^{11}/B^{10}	Mg^{26}/Mg^{25}
L16-19 No. 118, three rock fragments, total weight 7 mg	11.7 ± 0.17	3.73 ± 0.05	0.993 ± 0.010
Fragment of terrestrial muscovite	11.80 ± 0.20	3.69 ± 0.05	1.000 ± 0.010
L16-19 No. 118, 1.0 mg, fraction V surface material, 325-400 mesh	11.60 ± 0.15	3.54 ± 0.04	1.035 ± 0.010
Terrestrial diabase W-1, fine powder	11.30 ± 0.20	3.31 ± 0.04	1.045 ± 0.010
Difference between terrestrial and lunar material, mean (in percent)	(+0.35 ± 0.2)	(+1.0 ± 2.0)	(-0.9 ± 1.4)

This latter standard serves for verification of the experimental procedure used in this study, since the literature has numerous values for this standard drop. The content of Li, Be, and B measured in W-1 agrees well with the values reported by other investigators.

Ti was excluded from the discussion, since this element was measured as part of the investigations of the albedo by Maurette, who presents these results in another publication.

An examination of the data for the lunar samples given in Table 2 shows that the abundances of Li, Be, and B increase in the following order: Luna 16, Apollo 11, Apollo 12, and Apollo 14, with the exception of Be, which is more abundant in Apollo 12 fine surface material than in the Apollo 14 samples. For the fine

TABLE 2. CONTENT OF Li, Be, B, AND Ti IN THE SURFACE MATERIAL SAMPLE L16-19 No. 118 (REGOLITH, ZONE V), IN SURFACE MATERIALS RETURNED BY APOLLO 11, APOLLO 12, AND APOLLO 14, AND IN THE TERRESTRIAL STANDARD DIABASE W-1 /1, 3-5, 8, 12, 14/

Sample	Li, ppm	Be, ppm	B, ppm	Ti, percent
L16-19 No. 118, present study	9.8	1.2	2.6	1.92
Vinogradov /15/	10*	2	6	1.98
Apollo 11 surface material, 10084	12.8	1.6	3.2	4.36
Apollo 12 surface material, 12070	19.1	4.6	8.2	1.86
Apollo 14 surface material, 14259	35.6	4.4	17.2	1.08
Apollo 14 surface material, 14141	40.7	3.1	20.9	0.96
Terrestrial standard diabase W-1, present study	12.5	0.6	9.2	--
Other authors, latest analyses	12.7[3*]	0.63[5*]	9.0[2*]	--
	10-12[3*]	1.5[6*]	7.5[7*]	--
	10[4*]	0.623[8*]	12[4*]	--
Analytic imprecision (in percent), present study	13	50	5	3

*Regolith B and G

2*Quijano-Rico and Wanke /10/, fluorimetry

3*Gurney and Erlank /6, 7/, optical spectrography

4*Taylor et al., emission spectroscopy

5*Sievers et al. /12/, gas chromatography

6*Reilly and Shaw /11/, optical spectrography

7*Champ /2, 7/, optical spectrography

8*Sill and Willis /13/, fluorimetry

surface material of the four different lunar sections, the Li and K abundances correlate strictly with each other (Fig. 1), because both alkali elements behave chemically identically in the similar geochemically ambient media.

In Fig. 2 we have a comparison of the abundance schemes of Li, Be, and B normalized with respect to chondrite. At once it becomes obvious that for these elements intense enrichment is observed compared with chondritic quantities. This is because Li, Be, and B

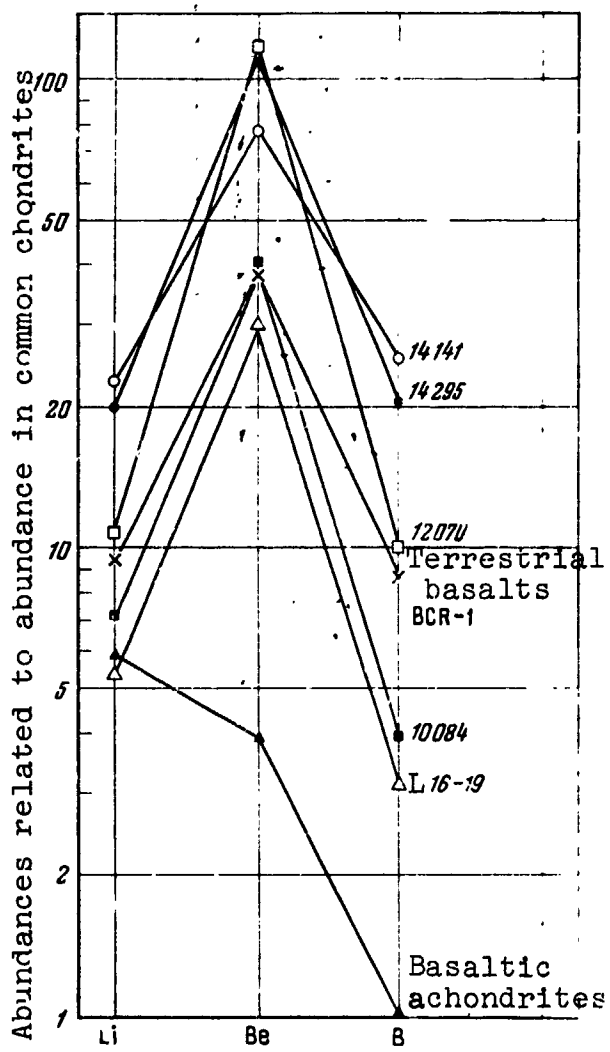

Fig. 2. Distribution of abundances of Li, Be, and B in lunar, terrestrial, and meteoritic samples normalized with respect to chondrite. The following chondrite values were used: Li -- 1.8 g/ton [9], Be -- 0.04 g/ton [13], and B -- -- 0.83 g/ton [10]. The data for basaltic achondrites are taken from Tera et al. [14], Sill and Willis [13], and from Kuijano-Rico and Wanke [10]. The data for BCR-1 was taken from a report by Flanagan [4] and Sievers et al. [12].

are lithophilic elements, which were concentrated in the residual liquid during magmatic crystallization. The same enrichment in the lunar material compared with the chondritic was found for the other lithophilic elements, such as W, Nb, Ta, U, Th, Cs, and the rare earths. The abundance schemes for Li, Be, and B are amazingly similar. In particular, the amounts of these elements in the fine surface material from Luna 16 and Apollo 11 are nearly identical, differing by only 1.2-1.3 times. Although Apollo 12 fine surface material comes from a typically mare region, as does the Luna 16 and Apollo 11 surface materials, the amount of Li, Be, and B in the fine surface material is approximately twice as high as in the fine surface material of the other regions of the mare. In a later study /3/ it is indicated that this comparative enrichment in the Apollo 12 fine surface material was caused by the admixture of fragments of rock with chemical composition differing widely from what was observed among the coarser samples of igneous rocks. This additional component was discovered and investigated by Gast et al. /7/ and was found to be considerably enriched in K, rare-earth elements, and in P (krip component). The possible sources of the krip component are the highland and near-mare regions. Actually, as can be judged from Fig. 2, the fine Apollo 14 surface material which was collected in the near-mare region shows a distribution of the abundances of Li, Be, and B that follows this hypothesis.

Fig. 2 also gives the terrestrial and meteoritic abundances. /374
The pattern of abundance in the terrestrial standard basalt BCR-1 is altogether similar with the mean lunar abundance. Basaltic achondrites contain similar amounts of Li, but nearly 10 times less Be and 3-20 times less B than the analyzed fine lunar surface material. Thus, the lunar origin of the basaltic achondrites is inconsistent with the abundance scheme of Li, Be, and B in lunar and meteoritic material if the samples from the four groups of the areas investigated are characteristic of the entire lunar surface.

This study was carried out as a result of discussion with Doctors R. Bernas, N. Grogler, and W. Krahenbuhl. I am especially grateful to H. Karl for technical assistance.

REFERENCES

1. Annel, C. S., Carron, M. K., Christian, R. P., Guttitta, F., Dwornik, E. J., Helz, A. M., Ligon, D. T., Jr., and Rose, H. J., Jr., "Chemical and Spectrographic Analyses of Lunar Samples from Apollo 12 Mission," Proc. Second Lunar Sci. Conf. 2, (1971).

2. Champ, W. H., Private communication, 1968. Quoted in Flanagan [4], (1969).

3. Eugster, O., and Bernas, R., "Li, Be, Mg, and Ti Isotopic Abundances and Search for Trapped Solar Wind Li in Apollo 11 and Apollo 12 Material," Proc. Second Lunar Sci. Conf. 2, (1971).

4. Flanagan, F. J., "U.S. Geological Survey Standards -- II. First Compilation of Data for the New USGS Rocks," Geochim. Cosmochim. Acta 33, 81 (1969).

5. Fleischer, M., "U.S. Geological Survey Standards -- I. "Additional Data on Rocks G-1 and W-1, 1965-1967," Geochim. Cosmochim. Acta 33, 65 (1969).

6. Gurney, J. J., and Erlank, A. J., "D.C. Arc Spectrographic Technique for Determination of Trace Amounts of Lithium, Rubidium, and Cesium in Silicate Rocks," Anal. Chem. 38, 1836 (1966).

7. Hubbard, N. J., Gast, P. W., and Meyer, C., "The Origin of the Lunar Soil Based on REE, K, Rb, Ba, Sr, P, and Sr^{87}/Sr^{86} Data," Proc. Second Lunar Sci. Conf. 2, (1971).

8. "LSPT (Lunar Sample Preliminary Examination Team). Preliminary Examination of Lunar Samples from Apollo 14," Preprint, 1971.

9. Nichiporuk, W., and Moore, C. B., "Lithium in Chondritic Meteorites," Earth Planet. Sci. Letters 9, 280 (1970).

10. Quijano-Rico, M., and Wanke, H., "Determinations of Boron, Lithium, and Chlorine in Meteorites," in: Meteorite Research, ed. P. Millmann (D. Reidel, Dortrecht), 132, 1969.

11. Reilly, G. A., and Shaw, D. M., "An Estimate of the Composition of Part of the Canadian Shield in Northwestern Ontario," Can. J. Earth Sci. 4, 725 (1967).

12. Sievers, R. E., Eisentraut, K. J., Johnson, D. G., Richardson, M. F., Wolf, W. R., Ross, W. D., Frew, N. J., and Isenhour, T. L., "Variations in Beryllium and Chromium Concentrations in Lunar Fines Compared with Crystalline Rocks," Proc. Second Lunar Sci. Conf. 2, (1971).

13. Sill, C. W., and Willis, C. P., "The Beryllium Content of Some Meteorites," Geochim. Cosmochim. Acta 26, 1209 (1962).

14. Tera, F., Eugster, D., Burnett, D. S., and Wasserburg, G. J., "Comparative Study of Li, Na, K, Rb, Cs, Sr, and Ba Abundances in Achondrites and in Apollo 11 Lunar Samples," Proc. Apollo 11 Lunar Sci. Conf. 2, 1637 (1970).

15. Vinogradov, A. P., "Preliminary Data on Lunar Ground Brought to Earth by Automatic Probe Luna 16," Proc. Second Lunar Sci. Conf. 1, 1 (1971).

16. Yiou, F., Baril, M., Dufaure de Citres, J., Fontes, P., Grandstajn, E., and Bernas, R., "Mass Spectrometric Measurements of Lithium, Beryllium, and Boron Isotopes Produced in O^{16} by High Energy Protons, and Some Astrophysical Implications," Phys. Rev. 166, 968 (1968).

Center for Nuclear Spectroscopy and Mass Spectroscopy of the National Center of Scientific Research, Orse, France.

N75 11848

NEUTRON ACTIVATION DETERMINATION OF THE OXYGEN CONTENT IN THE LUNA 16 LUNAR SURFACE MATERIAL

A. Nady, A. Chekke, E. Sabo, B. Forsag, and E. Zemplen

Abstract

The O_2 content in the No. 16/078 sample of lunar surface material returned by the Luna 16 automatic station was determined by activation using 14 Mev neutrons. The O_2 content in the sample is 42.1 $\pm$ 1.2 weight percent.

A sample studied in our laboratory is part of the sample of the powdered lunar surface material returned by the Luna 16 automatic station. The sample was taken from the region of the core 7 cm from the lunar surface, zone A where the mean grain size is 70 μm. The authors measured the O_2 content in a 77.2 mg sample taken from the general sample of lunar surface material No. 16/078, weighing 300 mg, containing grains of approximately identical size. This article gives the results of the analysis conducted in a neutron generator by irradiation with 14 Mev neutrons.

The sample of lunar surface material was obtained in a polished quartz ampule. During the measurement, transporting of the sample from the irradiation site to the measurement site was conducted in a capsule. The capsule, weighing 40 g and 50 mm^3 in volume, made of high-pressure polyethylene with a low O_2 content, was carefully cleaned, and then filled with the sample in a hermetic glove chamber. During filling, vibratory compaction was employed. The capsule was closed mechanically.

To determine the O_2 content, use was made of the reaction $O^{16}(n, p)N^{16}$, in which the activity of the product nucleus was compared

with the activity of a reference standard with known O_2 concentration. Employed as the reference standard, as well as the monitor of the neutron yield was extra pure SiO_2 placed in the very same capsule as the sample of lunar surface material. The weight of the reference standard was 40 g, and the weight of the monitor was 120 mg.

A Cockcroft-Walton, model Na-3 system built in the Central Institute of Physics Research /2/ was used as the neutron generator in irradiating the sample. The diameter of the active surface of the target was 17 mm. A target with an activity of 30 curies made of Soviet-produced tritium was employed, with the neutron yield of 10^{10} neutrons/sec. The sample and the monitor were placed one after the other, across from the target. The sample did not contain biaxial rotation.

A two-channel rabbit with electronic control was designed to transport the sample; the rabbit consisted of a cylindrical polyethylene tube with 5.5 mm inside diameter. The system made it possible to cyclicly repeat the transfer of the sample from the irradiation station to the measurement station and back again, automatically. The minimum rate of sample transfer was 30 m/sec. The pneumatic line was constructed without a bend.

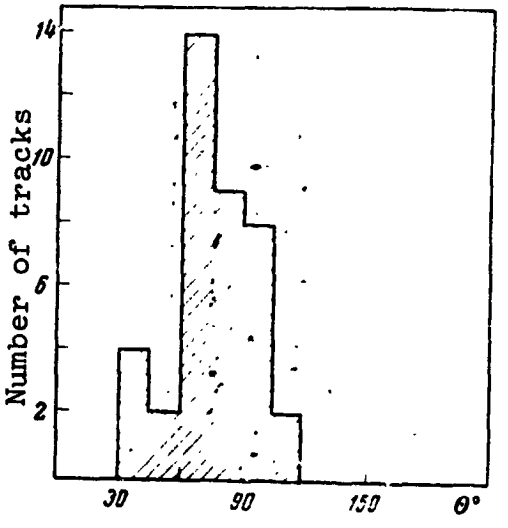

Histogram of 70 determinations of O_2 content in sample of lunar surface material 16/078. The relative error of measurement was 2-3 percent.

The measuring system consisted of an NaI/Tl detector 7.5 x 7.5 cm in size with a resolving power of 9 percent and a model NTA-512 B, 1024-channel analyzer, and the signals from this unit were integrated by a single-channel strobing analyzer in the energy range 4.5-8 MeV. The cycle time regulated with an electronic control block was 26 sec during the course of the analysis, 8 sec of which represented activation and 15 sec -- measurement. The specific activity of O_2 was 85 pulses/mg O_2. /378

Before the analysis, control measurements were made of natural and residual activity of the sample. In the energy range 100 keV to 2.5 MeV, no effects differing significantly from the background was observed.

OXYGEN CONTENT IN LUNAR SURFACE SAMPLES

Sample	Oxygen, weight percent	Literature source	Sample	Oxygen, weight percent	Literature source
Apollo 11			Apollo 11 and		
A	38,5±1,2	[3]	Apollo 12	41,4±2	[5]
B	39,4±1,0	[3]	As above	42,6±2	[5]
C	41,1±1,0	[3]	Apollo 12	45,2±0,6	[6]
Surface material	40,8±1,2	[3]	"	44,0±0,8	[6]
10017	40,87	[4]	"	40,4±0,9	[6]
10072	40,95	[4]			
10084	41,94	[4]			

In the measurement of the O_2 content, the amount of the reference standard and the sample was selected so that they represented an identical load with respect to Al^{28} of the Si for both gamma-spectra. Based on the literature /5/, the admixtures of F^{19} and B^{11} were assumed to be negligibly small so that they represented only several tens of milligrams per g.

Presented in the table are the literature data of the measurement of the O_2 content in the samples of lunar surface material. The results of measuring the oxygen content (in weight percent) carried out by us on the sample 16/078 are presented below:

39,9	43,6	38,5	41,4	42,9
41,6	44,1	37,9	40,4	41,2
40,6	40,1	44,2	42,9	42,9
39,4	39,7	39,8	39,8	42,5
42,2	40,8	42,2	45,4	39,6
43,2	40,0	41,4	38,2	38,0
41,5	43,0	38,5	41,8	37,6
40,6	38,6	44,8	37,8	39,4
43,9	41,2	44,3	39,8	41,7
37,4	38,5	42,2	40,8	43,5
43,6	42,4	42,3	42,6	38,6
42,3	38,5	38,0	40,9	42,3
43,6	40,1	43,2	43,9	39,5
42,4	43,8	37,7	42,3	41,9

Mean 42,1±1,2

The precision of the measurements in the studies indicated in the Table were determined on the basis of several (two to eight) parallel runs. Data on the sample 16/078 were obtained from 70 measurements conducted with the same sample. The precision of the measurement was characterized by the data shown in the histogram (see figure).

The authors express their gratitude to Sh. B. Nady, M. Shandory, and E. Jambor for assistance in the measurements and interpretation of the data.

REFERENCES

1. Vinogradov, A. P., "Preliminary Data on Lunar Surface Material Returned by Luna 16 Automatic Station," Geokhimiya (3), 261 (1971).

2. "Activation Analytical Laboratories Equipped with Neutron Generators," KFKI Report 3468/1968, Budapest.

3. Ehman, W. D., and Morgan, I. W., Science 167, 528 (1970).

4. Wirk, H. B., and Ojanpera, P., Science 167, 531 (1970).

5. Morrison, J. H., Anal. Chem. 43(7), 23A (1971).

6. Morgan, I. M., and Ehman, W. D., Earth Planet Sci. Letters 9, 164 (1970).

Main Division of Chemical Research of the Central Institute for Physics Research, Academy of Sciences of the Hungarian People's Republic, Budapest, Hungary.

N75 11849

INERT GASES IN SEA OF FERTILITY REGOLITH

/379

A. P. Vinogradov and I. K. Zadorozhnyy

Abstract

A study was made of the content and isotopic composition of inert gases -- He, Ne, Ar, Kr, and Xe -- in samples of lunar regolith returned by the Luna 16 automatic station. The samples were taken from depths of about 12 and 30 cm.

The high concentrations of inert gases were measured in the samples investigated, exceeding by several orders their concentrations observed in ordinary stony meteorites. The gases in lunar regolith are a complex mixture of gases of different origins: solar, cosmogenic, radiogenic, and so on. Solar wind gases predominate, distributed in the thin surficial layer (fractions of micron) of the regolith grains. The concentrations of these gases in the surficial layer is several cubic centimeters per gram. The isotopic composition of the inert gases of solar origin (with the exception of Ar^{40}) approaches their composition measured in gas-rich meteorites.

The composition of inert gases includes a slight admixture of cosmogenic component, which is masked by the solar gases in gross analyses and is disclosed only in high-temperature fractions of gases released by stepwise heating of the samples.

Excess Ar^{40} genetically associated with the decay of K^{40} in the rocks was detected in the regolith. This excess of Ar^{40} is a component of radiogenic argons released on the lunar rocks into the atmosphere and then impregnated back again into the surficial layer together with solar wind gases.

An investigation was made of the inert gases He, Ne, Ar, Kr, and Xe in samples of lunar regolith returned by the Luna 16 auto-

matic station. The lunar material was selected by the station with a drill at a depth of 35 cm.

The samples investigated were taken from two zones: zone B (sample 6-1v) at a depth of 8-15 cm and from zone G (sample 7-1a) at a depth of 28-33 cm. The surface material samples were sampled from material previously screened through sieve ($\leqslant 0.083$ mm) without any further distribution of the samples into fractions.

In four samples the inert gases were investigated by single-step total melting, and in one sample by the method of multistep degassing at intervals of 50-100° C in the 200-1500° C range. With stepwise increase in temperature, the complex multicomponent mixture of inert gases can be decomposed into components of different origins (cosmogenic, radiogenic, solar wind component, and so on). The data obtained in this fashion makes it possible to construct correlation graphs in the coordinates of isotopic ratios for the isotopes in gas fractions released at different temperatures. The two-component mixture of variable composition in this graph is represented by a straight line, whose extreme points correspond to the pure components of the mixture being analyzed. The position of any point on the graph will correspond to the relative content of the constituents of the mixture. The position of the point away from the straight line indicates the presence of a third component.

Experimental techniques. The analysis of the gases was conducted on an MI 13-11 mass spectrometer in a static regime with a resolution sufficient to separate the small hydrocarbon background present in the region of Kr. Samples of the general samples were dropped into a previously degassed molybdenum crucible and heated with a high frequency furnace to 1500° C. The temperature was measured with a platinum-rhodium thermocouple built into the crucible wall. The error of temperature measurement did not exceed $\pm$ 10° C. The gases released from the sample were purified with two successively operating Ti getters and one Cu-CuO furnace. The gas analysis was made for three fractions: He and Ne were analyzed jointly after the absorption of the heavy fraction of inert gases with activated charcoal at -196° C. Argon was released at -78° C, while Kr and Xe were desorbed at + 100° C and analyzed together. About 40 percent of the Kr was released together with the argon during its desorption, as a result of which its isotopes underwent fractionation. The Kr was analyzed after the Xe was subjected to analysis, and as a result the error of measurement rose even more. The results of analyzing Kr are omitted in this report.

The absolute amounts of the gases were measured by comparing the intensity of the ion peaks for an exactly calibrated portion of air gases. The error of measurement of the absolute gas content was 10-15 percent. The correction for discrimination by masses was

TABLE 1. CONTENT AND ISOTOPIC COMPOSITION OF INERT GASES IN REGOLITH /380

Sample	Weight, mg	Gas content, 10^{-8} nano-cm^3/g			Content 10^{-11} nanocm^3/g						
		He^4	Ne^{20}	Ar^{36}	He^4/He^3	Ne^{20}/Ne^{22}	Ne^{21}/Ne^{22}	Ar^{38}/Ar^{36}	Ar^{40}/Ar^{36}	Kr^{84}	Xe^{132}
6-1в	8,4	17 000 000	320 000	34 000	2625±80	12,46±0,08	0,0338±0,0004	5,26±0,05	1,06±0,02	1900±800	450±40
6-1в	5,1	18 000 000	340 000	35 000	2650±80	12,66±0,05	0,0340±0,0004	5,22±0,05	1,06±0,02	1820±750	330±50
7-1а	7,2	19 500 000	360 000	47 600	2670±50	12,70±0,06	0,0339±0,0013	5,27±0,06	1,02±0,13	2500±900	630±50
7-1а	5,7	18 000 000	340 000	46 000	2650±80	12,46±0,06	0,0332±0,0004	5,11±0,08	1,03±0,03	2670±900	590±60

	Xe^{124}/Xe^{132}	Xe^{126}/Xe^{132}	Xe^{128}/Xe^{132}	Xe^{129}/Xe^{132}	Xe^{130} Xe^{132}	Xe^{131}/Xe^{132}	Xe^{134}/Xe^{132}	Xe^{136} Xe^{132}
6-1в 8,4	0,00430±0,00028	0,00520±0,00028	0,0822±0,0024	1,034±0,004	0,1624±0,0010	0,8154±0,0052	0,3734±0,0032	0,3057±0,0022
6-1в 5,1	0,00507±0,00029	0,00564±0,00024	0,0817±0,0021	1,031±0,004	0,1599±0,0012	0,8148±0,0048	0,3752±0,0027	0,3062±0,0020
7-1а 7,2	0,00447±0,00015	0,00537±0,00021	0,0828±0,0020	1,029±0,008	0,1679±0,0013	0,8254±0,0042	0,3745±0,0037	0,3071±0,0019
7-1а 5,7	0,00501±0,00025	0,00574±0,00027	0,0823±0,0021	1,032±0,008	0,1681±0,0010	0,8272±0,0030	0,3721±0,0021	0,3023±0,0018

made for the isotopes of air gases. No correction for discrimination of helium isotopes was introduced. The blank run correction at 1500° C was as follows (in nanocm^3): $He^4 \leqslant 0.3 \cdot 10^{-8}$; $Ne^{20} \leqslant 0.1 \cdot 10^{-8}$; $Ar \approx 4 \cdot 10^{-8}$; $Kr^{84} \approx 8 \cdot 10^{-12}$; and $Xe^{132} \approx 6 \cdot 10^{-12}$. The background of the isobaric admixtures did not exceed the following values: $He^3 \leqslant 5 \cdot 10^{-10}$; $Ne^{21} \leqslant 1 \cdot 10^{11}$; and $Ne^{22} \leqslant 2 \cdot 10^{11}$ nanocm^3.

Results of analysis and discussion. The composite data /381 obtained in elemental and isotopic analysis of inert gases in the samples of the lunar surface material are in Tables 1 and 2.

The regolith samples investigated, taken from different depths, contain high concentrations of all inert gases, exceeding by several orders their concentrations measured in most stony meteorites. The isotopic composition of inert gases (except for Ar^{40}) approximate their composition measured in gas-rich meteorites [1].

The high concentrations and isotopic composition of the inert gases in the regolith indicate that only the solar wind can be the source of their origin. Similar concentrations of inert gases were

TABLE 2. CONTENT AND ISOTOPIC COMPOSITION OF INERT GASES IN THE TEMPERATURE FRACTIONS OF REGOLITH SAMPLE 7-1a, WEIGHT 44.6 mg

Temperature °C	200	300	400	500	600	650	700	750	800
He^4, 10^{-4} nanocm³/g	0,60	14,0	680	510	320	230	48,2	36,5	8,2
He^4/He^3	2240±100	2300±100	2670±150	2580±80	2600±80	3050±100	2500±100	2400±100	2250±100
Ne^{20}, 10^{-4} nanocm³/g	0,006	0,05	13,18	10,10	6,32	5,34	0,92	0,86	0,40
Ne^{20}/Ne^{22}	—	13,50±0,12	12,91±0,06	12,85±0,06	12,70±0,05	12,74±0,05	12,78±0,06	12,70±0,08	12,24±0,06
Ne^{21}/Ne^{22}	—	0,0373±0,0006	0,0324±0,0003	0,0324±0,0001	0,0325±0,0001	0,0323±0,0002	0,0333±0,0002	0,0329±0,0002	0,0338±0,0004
Ar^{36}, 10^{-4} nanocm³/g	—	0,007	0,09	0,34	0,70	1,11	0,67	0,56	0,42
Ar^{38}/Ar^{36}	—	—	5,66±0,06	5,45±0,04	5,32±0,05	5,27±0,03	5,29±0,03	5,26±0,05	5,26±0,04
Ar^{40}/Ar^{36}	—	4,00±0,05	1,80±0,03	1,48±0,03	0,74±0,01	0,78±0,01	0,77±0,01	0,81±0,01	0,87±0,01
Xe^{124}	—	—	0,408±0,050	0,548±0,042	0,513±0,030	0,510±0,027	0,505±0,031	0,517±0,025	0,512±0,022
Xe^{126}	—	—	0,502±0,055	0,469±0,040	0,498±0,031	0,485±0,028	0,492±0,027	0,480±0,023	0,521±0,019
Xe^{128}	—	—	8,41±0,40	8,16±0,32	8,05±0,27	8,16±0,16	8,17±0,12	8,45±0,09	8,35±0,09
Xe^{129}	—	—	1,020±0,040	1,003±0,038	1,024±0,018	1,026±0,012	1,019±0,009	1,051±0,009	1,047±0,007
Xe^{130}	—	—	15,60±1,80	15,67±1,40	15,95±1,20	16,10±0,30	15,92±0,75	16,61±0,32	16,64±0,21
Xe^{131}	—	—	83,04±2,20	81,82±2,00	81,71±1,80	82,45±1,10	81,90±0,90	82,73±0,80	82,52±0,63
Xe^{132}	—	—	100	100	100	100	100	100	100
Xe^{134}	—	—	36,31±0,90	36,73±0,85	36,23±0,80	36,16±0,64	35,81±0,41	36,93±0,36	37,10±0,30
Xe^{136}			34,00±0,80	33,45±0,80	32,14±0,54	31,52±0,50	30,50±0,42	30,10±0,30	30,24±0,23
Xe^{129}, 10^{-10} nanocm³/g			3,85	7,06	30,10	31,05	35,80	60,20	96,16

/Table 2 continued on following page/

measured earlier in samples of lunar surface material returned by Apollo 11 /2/. Detailed results of the analyses were reported in /3-8/.

All the inert gases contain a minor, but well-defined cosmogenic component, formed through the accumulation of products of nuclear fission reactions under the effect of galactic and solar cosmic rays. An apprcximate estimate of the cosmogenic component /383 of He^3 and Ne^{21} can be obtained in the general gross analysis with stepwise melting of the sample by introducing the correction for the content of the component of trapped gases with respect to their isotopic composition measured in gas-rich meteorites.

TABLE 2. CONTENT AND ISOTOPIC COMPOSITION OF INERT GASES IN THE TEMPERATURE FRACTIONS OF REGOLITH SAMPLE 7-1a, WEIGHT 44.6 mg
(CONCLUSION)

Temperature °C	850	900	950	1000	1100	1200	1300	1400	Total
He^4 10^{-4} nanocm^3/g	2,4	9,1	2,3	0,70	—	—	—	—	1852±200
He^4/He^3	2500±100	3100±150	2200±150	1400±180	—	—	—	—	2670±100
Ne^{20} 10^{-4} nanocm^3/g	0,05	1,37	0,14	0,09	0,08	0,06	—	—	39,6±4,5
Ne^{20}/Ne^{22}	12,44±0,09	12,12±0,08	12,05±0,11	11,80±0,13	10,67±0,15	10,63±0,19	—	—	12,76±0,08
Ne^{21}/Ne^{22}	0,0352±0,0006	0,0367±0,0005	0,0429±0,0011	0,0484±0,0010	0,0674±0,0017	0,0728±0,0018	—	—	0,0327±0,0004
Ar^{36} 10^{-4} nanocm^3/g	0,32	0,21	0,18	0,13	0,03	0,05	0,007	0,003	4,53±0,65
Ar^{40}/Ar^{36}	5,21±0,05	5,12±0,06	5,20±0,06	5,02±0,05	5,12±0,07	4,95±0,07	4,82±0,07	4,69±0,09	5,26±0,05
Ar^{38}/Ar^{36}	0,86±0,01	0,94±0,01	0,92±0,01	1,10±0,02	1,50±0,02	2,30±0,03	3,00±0,25	—	0,94±0,02
Xe^{124}	0,517±0,017	0,568±0,016	0,553±0,009	0,607±0,011	0,605±0,017	0,627±0,016	0,746±0,029	0,722±0,044	0,493±0,022
Xe^{126}	0,551±0,018	0,592±0,018	0,565±0,009	0,638±0,013	0,640±0,016	0,737±0,019	0,893±0,031	0,906±0,038	0,512±0,021
Xe^{128}	8,57±0,18	8,67±0,05	8,82±0,05	8,71±0,07	8,67±0,17	8,79±0,11	8,95±0,19	8,64±0,28	8,50±0,11
Xe^{129}	1,050±0,005	1,065±0,005	1,066±0,004	1,052±0,008	1,035±0,011	1,050±0,009	1,051±0,012	1,033±0,018	1,050±0,009
Xe^{130}	16,64±0,18	16,81±0,12	16,92±0,11	16,78±0,17	16,58±0,27	16,86±0,25	16,92±0,82	16,72±0,35	16,62±0,24
Xe^{131}	83,41±0,34	83,23±0,28	84,34±0,20	84,12±0,25	84,47±0,34	85,26±0,82	85,73±1,20	84,86±2,10	83,74±0,38
Xe^{132}	100	100	100	100	100	100	100	100	100
Xe^{134}	37,01±0,22	36,97±0,18	37,31±0,17	36,91±0,27	36,63±0,55	36,98±0,48	37,43±0,85	33,17±0,90	37,00±0,22
Xe^{136}	29,78±0,18	29,95±0,15	30,20±0,20	30,12±0,17	30,26±0,34	29,83±0,31	29,61±0,65	29,87±0,90	31,43±0,20
Xe^{132}, 10^{-10} nanocm^3/g	104,00	112,86	107,00	76,88	18,10	23,13	1,77	0,60	700,0±90,0

The concentration and isotopic composition of inert gases measured in regolith samples taken at different depths are practically identical. The variations observed can be accounted for by the inhomogeneity of the material. The ratio $He^4/He^3 = 2650 \pm 100$, as well as the ratio $He^4/Ne^{20} = 53 \pm 10$, measured in both samples at different depths, differ somewhat from the results of the analysis of lunar regolith returned by Apollo 11 [9, 10].

The curves of the rate of gas release as a function of temperature, shown in Fig. 1, clearly indicate that the release of inert gases occurs not simultaneously, but as a function of the atomic weight of the element: with increase in the atomic number of the element, its degassing temperature rises. Evidently, the intro-

/382

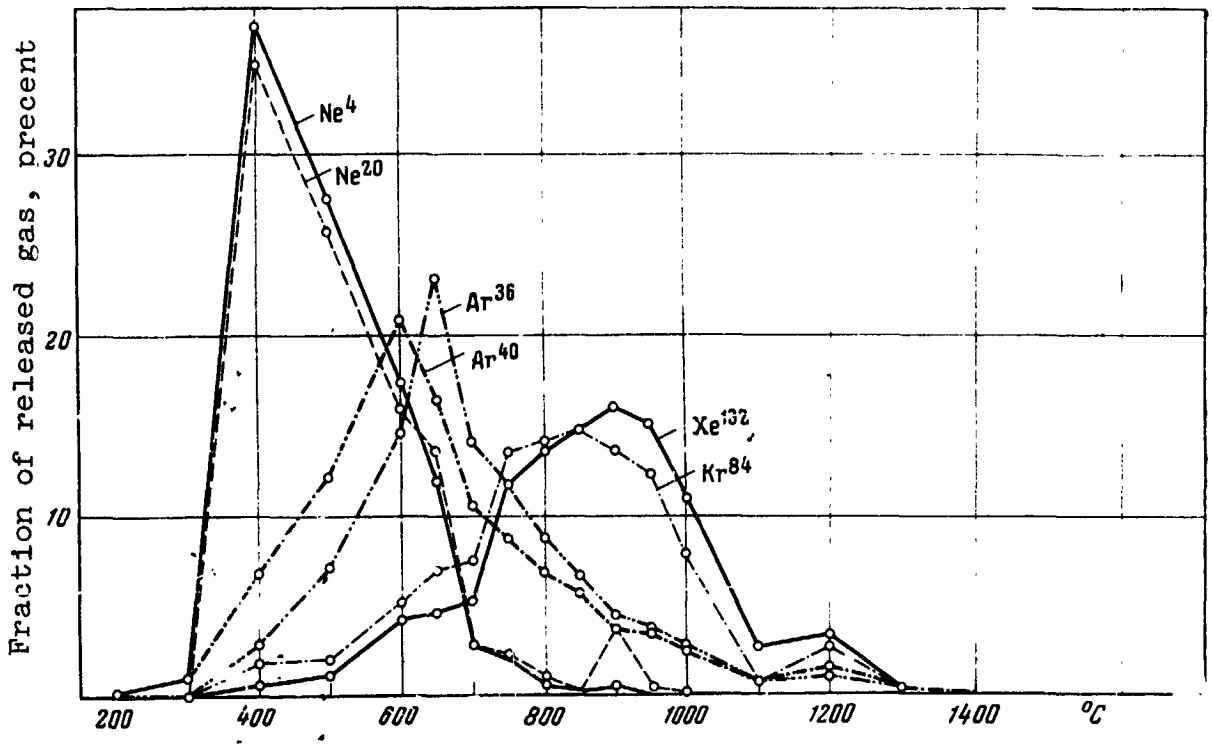

Fig. 1. Release of rare gases in stepwise degassing of sample 7-1a. The amount of gas released in each temperature fraction is expressed in percent of its total content in the sample.

duction of heavier gases (probably, also of isotopes) occurs at a greater depth in the surficial layers of the regolith grains, leading to an increase in the bonding energy and fractionation of the gases during their subsequent degassing in laboratory experiments.

The dominant constituent of He and Ne in regolith is the constituent of the trapped solar gases. With stepwise degassing of the sample, significant variations are observed in the isotopic composition of He and Ne (Table 2). The ratio He^4/He^3 increases from 2240 at 220° C to 3050 at 650° C, and then drops to 1400 at 1000° C.

The Ne^{20}/Ne^{22} ratio varied appreciably at the same time as /384 a nearly constant Ne^{21}/Ne^{22} ratio in the regions of low and medium temperatures. In the graph, most points in the coordinates of isotopic ratios (Fig. 2) are grouped in a region with a mean Ne^{20}/Ne^{22} ratio of 12.74 ± 0.05; only in the region of high temperatures do some of the points shift in the direction of increasing content of the cosmogenic component. The line drawn through these points in the direction of the cosmogenic component runs below the

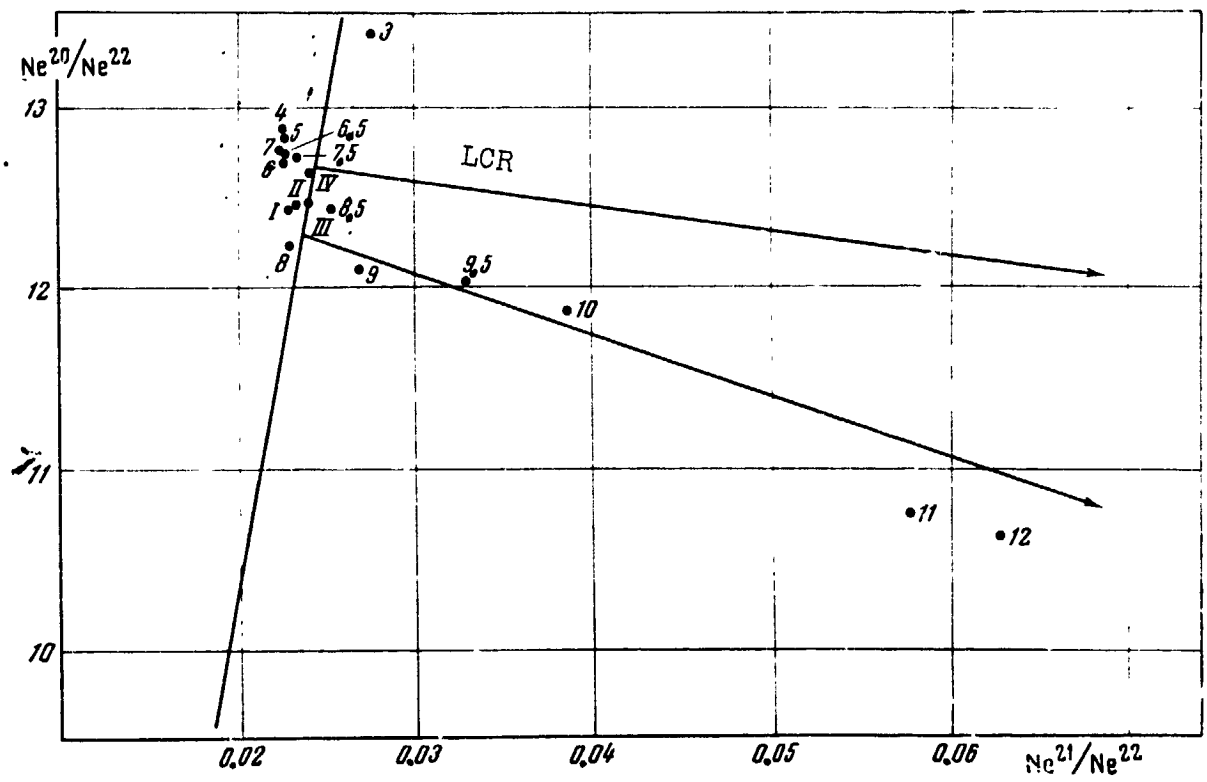

Fig. 2. Isotopic composition of Ne in gas fractions released during stepwise heating of sample 7-1a. The numbers denote the degassing temperature, expressed in a 100° scale.
I - IV. Isotopic ratios in the regolith for a single-act complete melting of sample.
LCR. Line of crystalline lunar rocks from large samples

correlation line corresponding to the lunar rocks (rock l...) /11/, but does not run through the point corresponding to the composition of the cosmogenic component of stony meteorites and the crystalline lunar rocks. This indicates a different composition of the cosmogenic component in the regolith. The data obtained do not contradict the results of the analysis of Ne in the regolith from the Apollo 11 collection /11, 12/.

Variations in the isotopic ratio Ne^{20}/Ne^{22} measured in temperature fractions of sample 7-1a indicate a certain regularity as a certain regularity as a function of temperature: high Ne^{20}/Ne^{22} ratios observed at low temperatures monotonely decrease with increase in temperature.

In gas-rich meteorites, the Ne^{20}/Ne^{22} ratios vary over a wide range. This makes it possible to advance the hypothesis that two components of primary neon are present in meteorites /13, 14/.

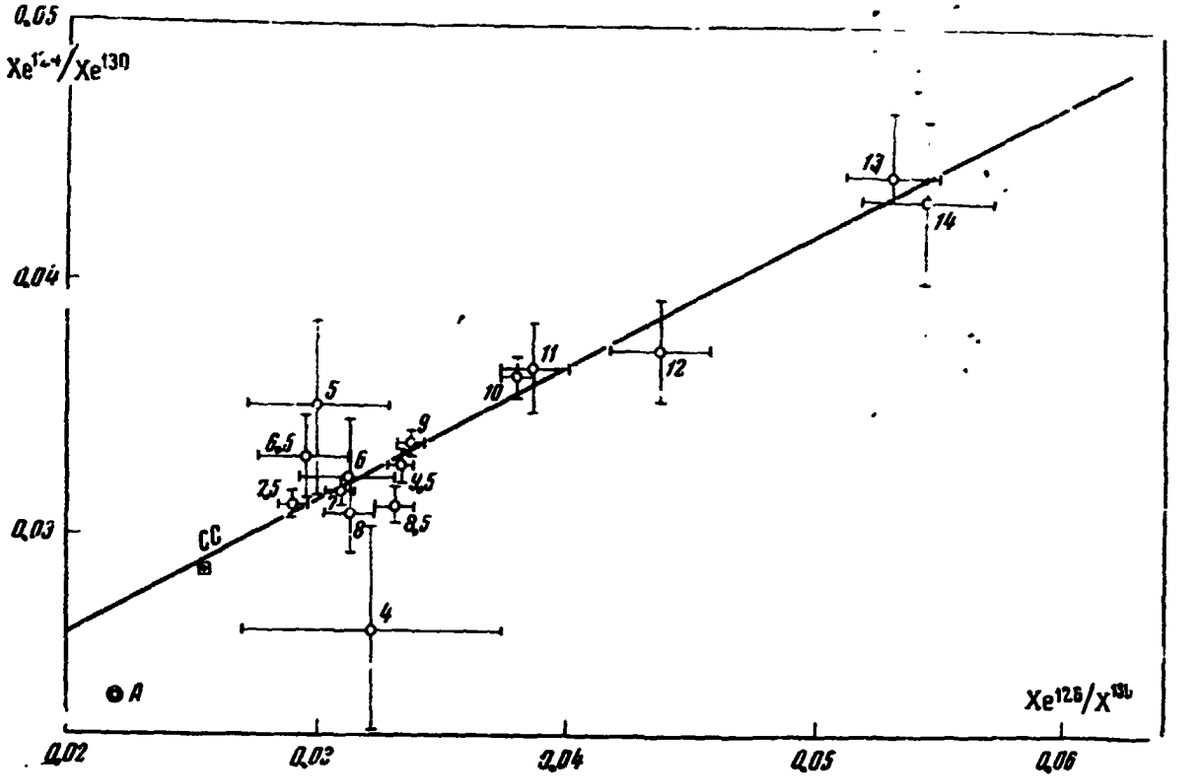

Fig. 3. Correlation graph for light isotopes of xenon released during stepwise heating of sample 7-1a. The numbers correspond to the degassing temperature expressed in a 100° scale.
A. Isotopic ratios of atmospheric xenon
CC. Mean value of isotopic ratios of xenon in carbonaceous chondrites

However, the existence of two components of trapped neon one of which differs from the composition of solar-wind neon, appears improbable for lunar regolith. The authors of /12/ reject the idea of the two-component composition of trapped Ne, interpreting the observed variations as a consequence of the diffusional fractionation with respect to masses of an isotopically single constituent of trapped solar neon caused by the different depths at which the various isotopes penetrate the surficial layer of the regolith grains. Lighter isotopes (He^3 and Ne^{20}) introduced upon irradiation by solar wind to a lower depth and with a lower bonding energy are released preferentially at lower temperatures, and as a result the effect of isotopic fractionation arises. The observed variations of the isotopic composition of He and Ne at low temperatures in the regolith samples we investigated satisfactorily agree with the idea of a two-step model of isotopic fractionation.

Argon in the regolith is represented by a complex mixture of components of different origins. The curves for argon degassing and variations in the ratio of its isotopes in gas fractions released during stepwise degassing of the sample are shown in Fig. 1. The Ar^{36}/Ar^{38} ratio monotonely decreases from the maximum 5.66 at 400° C to 4.69 at 1400° C. In the temperature range (600-950° C) at which a maximum release of the component of trapped Ar^{36} is observed, the Ar^{36}/Ar^{38} ratio is retained quite constant, averaging 5.27 ± 0.05. The resulting reduction in this ratio is caused by the release of the cosmogenic component. During single-step analysis of samples, the mean ratio Ar^{36}/Ar^{38} = 5.22 ± 0.06. It can be assumed that for the solar-wind argon component, the ratio Ar^{36}/Ar^{38} = 5.26 ± 0.05. This ratio is somewhat lower than its value in the terrestrial atmosphere, which possibly is accounted for by the presence of traces of the cosmogenic component. As in the case of neon, in stepwise degassing in the low-temperature argon fractions, an excess of the light isotope Ar^{36} is observed, which is probably caused by the same mechanism of selective impregnation of the solar-wind argon isotopes.

The concentration $Ar^{40} = 4.7 \cdot 10^{-4}$ nanocm^3/g appears to be excessively high: its content is approximately four times greater than its possible amount capable of accumulating during the decay of K^{40} in situ in 4.5 billion years. The mean ratio Ar^{40}/Ar^{36} = = 1.06 ±0.02, measured in single-step analysis of the samples. In the argon samples released during multistep analysis, it drops to 0.74 at 600° C, where the maximum release of the solar-wind component Ar^{36} is observed. The value of this ratio determines the upper limit of the Ar^{40} content in the solar wind. Its excess above this limit in conjunction with the concentration of K measured in the regolith (0.11 percent) [15] gives the K/Ar age ≈ 5.3 billion years, which appears to be clearly overstated.

The age of the regolith calculated in [5] under similar assumptions, proving to be ⩾ 4.65 billion years, also appears to be overstated. Moreover, the true Ar^{40}/Ar^{36} ratio in the solar-wind argon must be considerably lower. According to the nuclear systematics, the abundance of Ar^{40} in the solar atmosphere does not exceed $\sim 10^{-4}$ [16]. In the achondrite Novo Urei, the Ar^{40}/Ar^{36} ratio was measured and found to be ⩽ 0.35 [17]. In stepwise degassing of gas-rich meteorites, an even lower ratio ⩽0.05 was observed [18]. Obviously, a component of Ar^{40} is present in the regolith not belonging to solar-wind argon and not associated with the decay of K^{40} in situ. /385

It is shown in /3/ that the Ar^{40} content in regolith correlates with the surficially distributed Ar^{36}, indicating a relationship between the mechanism of Ar^{40} introduction and the solar wind.

The most probable source of the excess Ar^{40} must be regarded as precisely the lunar atmosphere, in which radiogenic Ar^{40} diffused from lunar rocks and then was impregnated again under the action of the interplanetary magnetic and electrical field induced by the solar wind /9, 10/. Ar^{40} ions accelerated in the electromagnetic field will have a much lower energy by the moment of collision with the lunar surface (~ 1 keV) compared with the energy of solar-wind Ar^{36} ions (~ 40 keV), as a result of which the Ar^{40} will be more weakly bound in the surficial layer of the regolith and more easily released upon degassing.

Variations in the isotopic ratio Ar^{40}/Ar^{36} observed in the temperature fractions of argon and the appearance of two maxima corresponding to the different rates of release of these isotopes (Fig. 1) confirm the hypothesis that there are different sources for the origin of these isotopes and that the nature of their penetration into the regolith is impregnational /20/.

High concentrations of Kr and Xe were measured in the regolith samples. Xenon released from the sample in single-step melting is enriched in the light isotopes Xe^{124}, Xe^{126}, and Xe^{128} and depleted in the heavy isotopes Xe^{134} and Xe^{136} with respect to their abundances in carbonaceous chondrites and in Xe of the terrestrial atmosphere. Enrichment in light isotopes is caused by the presence of the cosmogenic component. Xenon measured in the samples of regolith returned by Apollo 11 has the identical composition /10-12/.

Analysis of Xe by the method of stepwise degassing revealed several details in the composition of Xe. The relative abundance of its light isotopes in the low-temperature fractions differs nearly not at all from their abundance in the component of primary Xe in stony meteorites and in different temperature fractions reveals a linear correlation that corresponds to a two-composition of Xe. Fig. 3 shows the correlation graph in the coordinates of isotopic ratios Xe^{124}/Xe^{130} and Xe^{126}/Xe^{130}. The points corresponding to the different temperature fractions define a straight line, which runs through the point corresponding to the mean composition of Xe in carbonaceous chondrites /22/. Most of the points from the low-temperature fractions are grouped near this point. The point corresponding to the terrestrial-atmosphere Xe lies to one side. From these data it only follows that the abundances of the light isotopes of the trapped Xe component are extremely similar or

correspond to their values in the Xe in carbonaceous chondrites. We can take as the approximate estimate of the composition of the Xe component of solar wind the point that lies closest to the point of the carbonaceous chondrite (from the 750° C Xe fraction), although it is not precluded that present in it are traces of the cosmogenic component.

The relative abundances of the heavy Xe isotopes in the regolith are analogous to their abundances measured in the Xe fraction released at 1000° C from the Staroye Pes'yanoye achondrite /21/.

The results of analyzing Xe in the lunar regolith confirms the hypothesis /21/ that the solar Xe and the component of the trapped meteoritic Xe are analogous in composition. The difference observed in the composition of the Xe in lunar regolith and in carbonaceous chondrites is attributed to the presence in carbonaceous chondrites of a fissile Xe component /22/. An Xe component from the fission of U^{238} is present in the regolith, and its contribution does not exceed 8-10 percent.

Conclusions. Inert gases observed in the lunar regolith are a complex mixture of gases of different origins.

The dominant components are the solar-wind gases distributed in the thin surficial layer (fractions of a micron) of the regolith grains, whose concentration in the layer is as high as several cubic centimeters per gram.

Through the nuclear reactions occurring under the effect of galactic and solar cosmic rays, cosmogenic isotopes of inert gases accumulate in the regolith. Separate analysis of the content and isotopic composition of both components is a complicated problem and thus far no unambiguous answer has been obtained.

The high concentration of Ar^{40} measured in the regolith cannot be accounted for by the decay of K^{40} in situ. The considerable fraction of Ar^{40} present in the regolith is a component of the argon diffusing into the lunar atmosphere from the rocks and then impregnated back again by the mechanism of ionic bombardment together with solar-wind gases. The solution of this problem is a matter for the immediate future.

REFERENCES

1. Pepin, R. O., and Signer, P. "Primordial Rare Gases in Meteorites," Science 149, 253-265 (1965).

1a. Eberhard, P., Geiss, J., and Grogler, N., "Further Evidence on the Origin of Trapped Gases in the Meteorite Khor Temiki," J. Geophys. Res. 70, 4375-4378 (1965).

2. "LSPET (Lunar Sample Preliminary Examination Team)," Science 165, 1211-1227 (1969).

3. Heyman, D., Yaniv, A., Adams, J. A. S., and Frier, G. E., "Inert Gases in Lunar Samples," Science 167, 555-558 (1970)

4. Funkhouser, J. A., Schaeffer, O. A., Bogard, D. D., and Zahringer, J., "Gas Analysis of the Lunar Surface," Science 167, 561-563 (1970).

5. Marti, K., Lugmair, G., and Urey, H. C., "Solar Wind Gases, Cosmic Ray Spallation Products, and the Irradiation History," Science 167, 548-550 (1970).

6. Reynolds, J. H., Hohenberg, C., Lewis, R., Davis, P., and Kaiser, W. A., "Isotopic Analysis of Rare Gases from Stepwise Heating of Lunar Fines and Rocks," Science 167, 545-548 (1970).

7. Pepin, R. O., Nyquist, L., Phinney, D., and Black, D. C., "Isotopic Composition of Rare Gases in Lunar Samples," Science 167, 550-553 (1970).

8. Hintenberger, H., Weber, H. W., Voshage, H., Wanke, H., Begeman, F., Vilsek, E., and Wlotzka, F., "Rare Gases, Hydrogen and Nitrogen: Concentrations and Isotopic Composition in Lunar Material," Science 167, 543-545 (1970).

9. Heyman, D., and Yaniv, A., "Inert Gases in the Fines from the Sea of Tranquillity," Geochim. Cosmochim. Acta 1, 1247-1259 (1970).

10. Marti, K., Lugmair, G. W., and Urey, H. C., "Solar Wind Gases Cosmic Ray Spallation Products, and Irradiation History of Apollo 11 Samples," Geochim. Cosmochim. Acta 1, 1357-1367 (1970).

11. Pepin, R. O., Nyquist, L. E., Phinney, D., and Black, D. C., "Rare Gases in Apollo 11 Lunar Material," Geochim. Cosmochim. Acta 1, 1435-1454 (1970).

12. Hohenberg, C. M., Davis, P. K., Kaiser, W. A., Lewis, R. S., and Reynolds, J. H., "Trapped and Cosmogenic Rare Gases from Stepwise Heating of Apollo 11 Samples," Geochim. Cosmochim. Acta 1, 1283-1309 (1970).

13. Pepin, R. O., "Trapped Neon in Meteorites," Earth Planet Sci. Letters 2, 13 (1967).

14. Black, D. C., and Pepin, R. O., "Trapped Neon in Meteorites - II." Earth Planet. Sci. Letters 6, 395 (1969).

15. Vinogradov, A. P., "Preliminary Results of a Study of Lunar Regolith Returned by the Luna 16 Automatic Station," Geokhimiya (3), 261-273 (1971).

16. Bernstein, W., Fredricks, R. W., Vogel, J. L., and Fowler, W. A., "The Lunar Atmosphere and the Solar Wind," Icarus 2, 233-248 (1963).

17. Marti, K., "Trapped Xenon and Classification of Chondrites," Earth Planet. Sci. Letters 2, 193-196 (1967).

18. Black, D. C., "On the Origins of Trapped Helium, Neon and Argon Isotopic Variations in Meteorites-1. Gas-Rich Meteorites, Lunar Soil, and Breccia," Geochim. Cosmochim. Acta 36, 347-375 (1972).

19. Eberhardt, P., Geiss, J., Graf, H., Grogler, N., Krahenbuhl, U., Schwaller, H., Schwarzmuller, J., and Stettler, A., "Trapped Solar Wind Noble Gases, Exposure Age, and K/Ar Age in Apollo 11 Lunar Fine Material," Geochim. Cosmochim. Acta 1, 1037-1039 (1970).

20. Manka, R. H., and Michel, F. C., "Lunar Atmosphere as a Source of Ar^{40} and Other Lunar Surface Elements," Science 169, 278 (1970).

21. Marti, K., "Solar-Type Xenon: A New Isotopic Composition of Xenon in the Pesyanoe Meteorites," Science 166, 1263-1265 (1969).

22. Pepin, R. O., "Neon and Xenon in Carbonaceous Chondrites," in: Origin and Distribution of the Elements (editor, L. H. Ahrens), (30), 379-386, Pergamon Press, 1968.

Order of Lenin Institute of Geochemistry and Analytical Chemistry imeni V. I. Vernadskiy, USSR Academy of Sciences, Moscow.

N75 11850

PROBLEM OF NATURE OF INERT GASES IN LUNAR SURFACE MATERIAL

L. K. Levskiy

Abstract

The origin of isotopes of inert gases in lunar surface material was investigated from the standpoint of the isotopic two-component status of inert gases in the solar system.

The deviation of the curve of atomic abundances of inert gas isotopes in lunar surface material from the curve of cosmic abundances must be attributed either to the predominant retention of heavy gas isotopes (krypton and xenon) by the material of the regolith, or to the different genesis of the heavy and light gases. The last possibility is supported by the experimental study of the isotopic composition of inert gases in regolith.

Helium and neon represent the solar wind component (unfractionated gases of type B), while krypton and xenon are planetary gases (fractionated gases of type A).

Type A gases are trapped by the material of the regolith in the early stages of the existence of the solar system and were brought to the lunar surface together with dust. The material of the regolith therefore cannot be considered as the product of the erosion of the crystalline rocks of the Moon and in this sense are extralunar. The regolith material containing type A gases must be identified with the high-temperature minerals of the carbonaceous chondrites.

This study discusses the validity of a fact that at first glance is indisputable: the origin of inert gas isotopes in lunar surface material (regolith) derived from the solar wind.

The high concentration of gases in the regolith and the atomic abundances of individual gases, near the cosmic values, support this fact. At the same time it should be noted that in all cases either a deficit of light gases (helium and neon) or an excess of heavy gases (krypton and xenon) relative to cosmic abundances is noted. Of course, this anomaly must be attributed to the unsatisfactory retention of the expelled atoms of the light gases by the surfaces of the regolith particles. However, it is observed even in the case of ilmenite particles, supposedly quite satisfactorily retaining solar gases /1/.

Considering the anomaly and focussing on the isotopic composition of the inert gases, we will consider gases contained in regolith, in order of increasing atomic weight[1].

A. Neon. The isotopic structure of neon (but not its origin) is now represented as quite reliably established from the study of meteorites /2, 3/. It is characterized by a high Ne^{20}/Ne^{22} ratio for achondrites (up to 13-13.5). This is "solar" neon, or type B neon. Characteristic of carbonaceous chondrites (in any case for individual temperature fractions) is a low Ne^{20}/Ne^{22} ratio $\approx$ 3-4. This is "planetary" neon, or type A neon. Neon of the terrestrial atmosphere with $Ne^{20}/Ne^{22} = 9.8$ is intermediate. The foregoing is illustrated by Fig. 1.

Lunar surface material neon doubtless corresponds to type B. In particular, some data for the stepwise annealing of regolith in the Luna 16 landing site are given in Table 1. Also given here are data for the Ar^{38}/Ar^{36} ratio.

Judging from the atomic abundance, helium in the lunar regolith can be classified as type B.

Capture of type B gases by the material in the lunar surface occurred relatively recently. This is indirectly confirmed by the proximity of the Ne^{20}/Ne^{22} ratio in the regolith and in aluminum foil -- a direct detector of solar wind /4, 5/. Evidently, in most achondrites, type B gases are also relatively "young". /406

---

[1] Helium is excluded from consideration owing to unreliable data concerning the isotopic composition of solar and planetary helium.

TABLE 1. RESULTS OF STEPWISE ANNEALING OF REGOLITH FROM THE LUNA 16 LANDING SITE

Temperature, °C	Ne^{20}/Ne^{22}	Ne^{21}/Ne^{22}	Ar^{36}/Ar^{38}
500	—	—	0,189±0,003
600	12,86±0,12	0,030±0,003	0,177±0,009
700	12,20±0,09	0,039±0,002	0,196±0,002
800	13,70±0,40	—	0,195±0,003
900	13,10±0,21	—	0,193±0,008
1000	12,05±0,09	—	0,200±0,004
1100	11,15±0,21	—	0,199±0,003

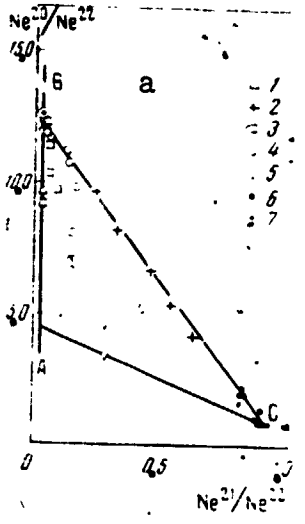

Fig. 1. Identification of planetary (A) and solar (B) neon; C. spallogenic neon
1. Neon of terrestrial atmosphere
2. Achondrite Khor Temiki. Temperature fractions of neon in meteorites:
3. Fayetteville chnodrite
4. Staroye Pes'yanoye
5. Migei (S2)
6. Kainzas (SZ)
7. Mean value for neon in lunar surface material

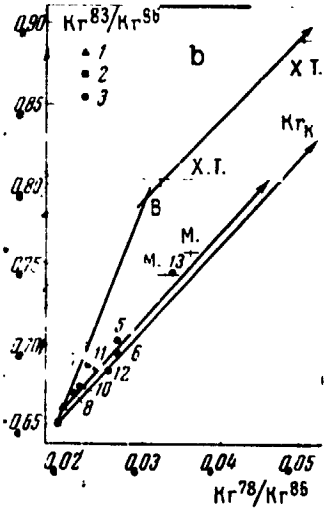

Fig. 2. Identification of planetary and solar (B) krypton
1. Krypton of terrestrial atmosphere
2. Krypton of carbonaceous chondrites
X.T. Achondrite Khor Temiki
M. Moux chondrite
3. Temperature fractions of krypton in lunar surface material, numbers refer to the gas release temperatures in a 100° scale (5 ≡ 500°, 7 ≡ 700°, and so on)
Kr_K. Spallogenic krypton (the Stannern achondrite)

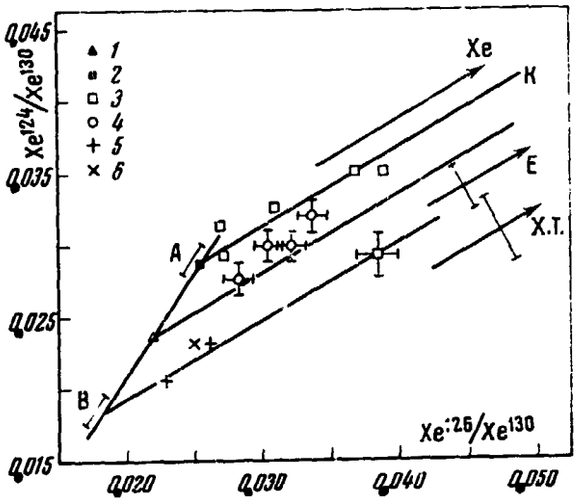

Fig. 3. Identification of planetary (A) and solar (B) xenon
1. Xenon of terrestrial atmosphere
2. Xenon of carbonaceous chondrites
Xe_K. Spallogenic xenon (Stannern achondrite)
3. Chondrite (sign with direct intervals of variation: 400° C fraction)
4. Staroye Pes'yanoye
5. Shallowater achondrite (400° C and 600° C fractions)
6. Schalk achondrite
E. Esterville mesosiderite
X.T. Khor Temiki achondrite

B. Argon. As we know [3, 6, 7], variations in the isotopic composition of primordial argon is not as significant as for neon. Nonetheless, the predominance of Ar^{36} is characteristic of type B argon:

$$\frac{\left(\frac{Ar^{38}}{Ar^{36}}\right)_A - \left(\frac{Ar^{38}}{Ar^{36}}\right)_B}{\left(\frac{Ar^{38}}{Ar^{36}}\right)_A} \approx 0{,}05.$$

Lunar argon does not have this feature. Judging from the data in Table 1, only for 600° C can one note a decrease in Ar^{38}/Ar^{36} (relative to terrestrial argon and argon of carbonaceous chondrites). The minimum value of Ar^{38}/Ar^{36} in the regolith was noted earlier by Hohenberg at the Apollo 11 landing site, 0.1784 ± 0.0016 [8]. It is characteristic of the low-temperature fractions of the argon released. Evidently, solar argon corresponds to these fractions. At the same time, most of the lunar surface material argon has a high Ar^{38}/Ar^{36} value, which only to a small extent can attributed to the admixture of spallogenic argon with a high Ar^{38}/Ar^{36} ratio (1.5-1.7). The relative proportion of A and B argon can be estimated from the following equality:

$$x \cdot 0.1784 + y \cdot 1.600 + z \cdot 0.1900 = 0.1925,$$

where x is the fraction of B argon and 0.1784 is the Ar^{38}/Ar^{36} ratio in type B argon [3, 8]; y is the fraction of spallogenic argon and 1.600 is the mean Ar^{38}/Ar^{36} ratio for spallogenic argon; z is the fraction of the type A argon and 0.1900 is the mean value of the Ar^{38}/Ar^{36} ratio for the type A argon [3].

The quantity y/x can be estimated from the corresponding spallogenic excess of Ne^{21}, since $Ne^{21}/Ne^{22} = 0.0332$ compared with $Ne^{21}/Ne^{22} = 0.0300$ for primordial type B neon. Considering that /407 y/x for neon and argon are approximately the same, we get: y/x = = 0.1. Finally, after uncomplicated calculation we get: x = 0.05 z. Thus, argon in lunar surface material is ~95 percent planetary argon. This fact, generally speaking, does not contradict the hypothesis that Ar^{40} accumulated in the lunar surface material through the ionization of neutral atoms of the lunar atmosphere followed by their introduction into the regolith /9/, since both Ar^{36} and Ar^{38} can be present in the lunar atmosphere.

C. Krypton. Fig. 2 shows the structure of the isotopic composition of krypton. The isotopic ratios for type B krypton are determined by the point of intersection of the line corresponding to the experimental data for the Khor Temiki achondrite /10/ (the inert gases in this meteorite are best represented by solar gases) and the line drawn through the point corresponding to the krypton in carbonaceous chondrites and in the terrestrial atmosphere. Krypton in the Stannern achondrite was selected as the spallogenic krypton /10/.

An examination of the data for the temperature fractions of lunar krypton /11/ shows that some of the lunar krypton is type A krypton (the temperature points of 600, 900, and 1200° lie in the curve; the krypton in the carbonaceous chondrites is spallogenic krypton), some have an admixture of B krypton (the temperature points of 500, 800, 1000, and 1100° lie in the curves; the krypton in the terrestrial atmosphere is spallogenic krypton, but the points of 700 and 1300° are somewhat higher than this line). However, since the admixture of type B krypton in the atmospheric krypton is small, the fraction of solar krypton in the lunar soil /sic/ krypton is also slight and, considering the absolute content of isotopes in the temperature fractions, is about 5 percent of the total krypton content. Thus, the krypton in the lunar surface material is mainly type A krypton.

D. Xenon. In most meteorites, it has the beginning of the carbonaceous-chondrite xenon, evolving from this point to spallogenic xenon (characteristic of the Stannern achondrite). Slight variations are observed for the isotopic composition of spallogenic xenon in the lunar surface material; however, these variations are not essential for the present study.

Some experimental values are lowered beneath the curve; the carbonaceous chondrite xenon is spallogenic xenon, and even below the atmosphere line -- spallogenic xenon. Typically, xenon in the achondrite Khor Temiki (the uniqueness of this meteorite has been noted above) belongs precisely to the last group (Fig. 3). It is quite natural to assume that the coordinates of point B in Fig. 3 determine the isotopic composition of solar xenon.

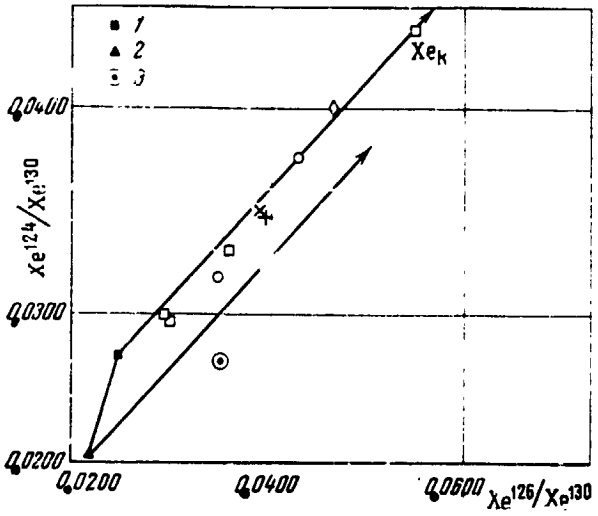

Fig. 4. Isotopic composition of xenon and lunar surface material based on the data of various authors.

1. Xenon in carbonaceous chondrites
2. Xenon in the terrestrial atmosphere
3. 500° C fraction /8/, Xe_K. spallogenic xenon. The other symbols are the data of the various investigators.

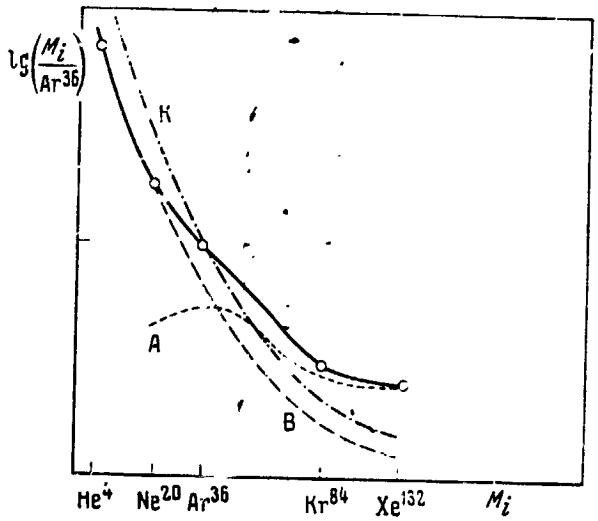

Fig. 5. Schematic composition of inert gases in regolith Circles. Experimental values of the abundances of inert gases

K. Curve of cosmic abundance (after Suess-Urey)

B. Curve corresponding to solar gases (drawn through the points He^4 and Ne^{20} parallel to curve K)

A. Curve corresponding to planetary gases (corresponds to the atomic abundances of inert gases in carbonaceous chondrites)

From Fig. 3, in particular, it follows that the identification of xenon in the achondrite Staroye Pes'yanoye as solar xenon /12/ is incorrect. /408

Data for lunar xenon are represented separately in Fig. 4. At the present time the number for experimental points in Fig. 4 can be considerably increased, and they all confirm the fact that lunar surface material xenon is practically all type A gas.

The point denoted in Fig. 4 by a circle with a point in its center corresponds to the 500° fraction of lunar xenon /8/, which based on isotopic composition corresponds to type B xenon. However, the content of xenon in this fraction is slight (0.01 percent of the total content).

Table 2 gives the summary information on the inert gases in the lunar surface material.

TABLE 2. COMPOSITION OF GASES OF TYPES A AND B IN REGOLITH

Gas	A, %	B, %
He	—	100
Ne	—	100
Ar	95	5
Kr	95	5
Xe	100	—

Confirmation of these considerations concerning the complex composition of lunar surface material gases can also be found in the atomic abundances of the inert gases.

The atomic abundances of type B gases are close to the cosmic values and, conversely, the abundances of type A gases are characterized by an acute deficit of light inert gases (helium and neon) and a predominance of the heavy (krypton and xenon) gases.

It remains to take the next step and to represent the gases in the lunar surface material, based on the atomic abundances, as consisting of type B gases (helium and neon) and type A gases (argon, krypton, and xenon). Curve B in the illustrative Fig. 5 is drawn through points corresponding to helium and neon parallel to the curve of atomic abundances (K). Obviously, in this concept the relative excess of heavy gases is accounted for by the considerable contribution made by type A gases and not predominantly by the loss of helium and neon.

If the "charging" of the lunar material by type B gases occurred in the not distant past, at what moment did type A gases accumulate? Obviously, this occurred in the early stages of the existence of the solar system during the consolidation and crystallization of the primordial material[1].

Since the crystalline rocks of the Moon do not contain type A primordial gases, the conclusion follows that most of the regolith is of extralunar origin. The erosion of crystalline rocks leads to the comminution of the material, an increase in specific surface and, as a consequence, to the accumulation of type B gases from the solar wind. The accumulation of type A gases cannot occur in this fashion.

[1] In this study we do not consider the causes that can lead to the formation of types of inert gases that differ so appreciably in isotopic composition.

The extralunar origin of the lunar dust is also supported by other considerations, in particular, by the investigation of tracks /13/ and the content of rare earths /14/.

As we know /15/, establishing the identity of the lunar surface material with any material known to us is difficult. It is most probable, from the standpoint of the isotopic composition of the heavy inert gases, that the lunar surface material is close to the material of carbonaceous chondrites. On the other hand, based on the content of volatile elements in the lunar soil the admixture of the latter is estimated to be low (1-2 percent) and cannot account for the composition of inert gases that has been discovered.

It appears to us, however, that we should not seek direct genetic relations between the content of volatiles and the concentrations of inert gases in the material of carbonaceous chondrites. Inert gases are evidently associated with the high-temperature fraction of the material in carbonaceous chondrites and were trapped at the moment of its crystallization.

Lunar surface material should be identified precisely with this fraction.

REFERENCES

1. Eberhardt, P., Geiss, J., Graf, H., Grogier, N., Krahenbuhl, V., Schwaller, H., Schwarzmuller, J., and Stettler, A., "Trapped Solar Wind Noble Gases, Kr^{81}/Kr Exposure Ages and K/Ar Ages in Apollo Lunar Material," Science 167(3918), (1970).

2. Pepin, R. O., "Trapped Neon in Meteorites," Earth Planet. Sci. Letters 2(1), (1967).

3. Levskiy, L. K., "Isotopic Composition of Primordial Argon," Geokhimiya, (1970) (in press).

4. Buhler, F., Eberhardt, P., Geiss, J., and Schwarzmuller, J., "Trapped Solar Wind Helium and Neon in Surveyor 3 Material," Earth Planet. Sci. Letters 10(3), (1971).

5. Geiss, J., Eberhardt, P., Buhler, F., Meister, J., and Signer, P., "Apollo 11 and 12 Solar Wind Composition Experiments: Fluxes of He and Ne Isotopes," J. Geophys. Res. 75(31), (1970).

6. Black, D. C., "Trapped Neon-Argon Isotopic Correlations in Gas Rich Meteorites and Carbonaceous Chondrites," Geochim. Cosmochim. Acta 35(2), (1971).

7. Mazor, E., Heymann, D., and Anders, E., "Noble Gaes in Carbonaceous Chondrites," Geochim. Cosmochim. Acta 34(7), (1970).

8. Hohenberg, C. M., Davis, P. K., Kaiser, W. A., Lewis, R. S., and Reynolds, J. H., "Trapped and Cosmogenic Rare Gases from Stepwise Heating of Apollo 11 Samples," Proc. Apollo 11 Lunar Sci. Conf. 2, (1970).

9. Manka, R. H., and Michel, F. C., "Lunar Atmosphere as a Source of Ar^{40} and Other Lunar Surface Elements," Science 169(3942), (1970).

10. Eugster, O., Eberhardt, P., and Geiss. J., "Isotopic Analyses of Krypton and Xenon in Fourteen Stone Meteorites," J. Geophys. Res 74(15), (1969).

11. Pepin, R. O., Nyquist, L. E., Phinney, D., and Black, D., "Rare Gases in Apollo 11 Lunar Material," Proc. Apollo 11 Lunar Sci. Conf. 2, (1970).

12. Marti, K., "Solar-type Xenon: a New Isotopic Composition of Xenon in the Pesyanoe Meteorite," Science 166(3910), (1969).

13. Barber, D. J., Hutcheon, J., and Price, P. B., "Extralunar Dust in Apollo Cores?" /no source given/

14. Gast, P. W., and Hubbard, N. J., "Rare Earth Abundances in Soil and Rocks from the Ocean of Storms," Earth Planet. Sci. Letters 10(1), (1971).

15. Ganapathy, R., Keys, R. R., Laul, I. C., and Anders, E., "Trace Elements in Apollo 11 Lunar Rocks: Implications for Meteorite Influx and Origin of Moon," Proc. Apollo 11 Lunar Sci. Conf. 2, (1970).

Leningrad State University imeni A. A. Zhdanov, Chemistry Division, Leningrad

N75 11851

COSMOGENIC Al^{26} AND Na^{22} IN LUNA 16 LUNAR REGOLTIH /410

A. P. Vinogradov, A. K. Lavrukhina, V. D. Gorin,
and G. K. Ustinova

Abstract

The activities of cosmogenic isotopes Al^{26} and Na^{22} in two samples taken from different depths of the lunar regolith core returned by the Luna 16 automatic station were measured. The measurements were conducted with a low-background scintillation gamma-spectrometer in the gamma-gamma coincidence mode. The measured activities, when recalculated to the time of sampling of the lunar surface material, are (in disintegrations·min^{-1} kg^{-1}): Al^{26} - 62 ± 8 and 54 ± 9; Na^{22} - 42 ± 8 and 48 ± 9. Depthwise distributions of the activities of these isotopes in lunar rocks of different types were calculated; the distributions indicate the presence of a considerable depth gradient of activity near the surface caused by the fall off in the fluxes of primary and secondary cosmic radiation. The absence of this gradient in the measured samples, along with data on the tracks and content of inert gases, as well as the granulometric characteristics of the regolith indicate that the surficial layer of the regolith at the sampling site underwent mixing. Comparison with the data from a study of regoliths from other areas of the lunar surface affords grounds for anticipating the prevalence in the evolution of the lunar regolith of its layerwise alteration resulting from ejecta during bombardment of the surface by meteorites and cosmic particles.

The Moon devoid of atmosphere and magnetic field is an invaluable arena for the study of nuclear reactions caused by cosmic rays. But the lunar surface is not stable. As a result of the continuous process of crater formation under the impacts of meteoric bodies, the surface has evolved: layers of the lunar dust have been mixed, fragments of rocks have been rolled changing their orientation on

the surface, some of them have become heaped, while others in contrast have become exposed, on being ejected onto the surface from deeper-lying layers. Measurement of the activity of cosmogenic isotopes formed by cosmic rays at different depths in the lunar rocks of different types can disclose the nature of the evolution of the lunar surface, in particular, the history of the accumulation of regolith -- lunar dust /1_7.

At the present time samples of rocks from four extensive regions on the visible side of the Moon have been investigated in Earth laboratories: Sea of Tranquillity (Apollo 11 samples), Ocean of Storms (Apollo 12 collection), Sea of Fertility (Luna 16 samples), and the area of the Fra-Mauro Crater (Apollo 14 collection). These are magmatic rocks of at least two types, breccia and regolith. The rocks do not differ widely in chemical composition /1-3/, but the crystalline rocks in the regolith have different densities (1.2 g/cm^3 for the regolith and 3.1 g/cm^3 for the crystalline rocks). We calculated the depthwise distribution of Al^{26} and Na^{22} in rocks of the following types: A (10057,40), B (10017,33) (volcanic rocks), C (10018,22) (breccias), and D (10084,18) (regolith) from the Apollo 11 sample, in regolith of type (12070) from the Apollo 12 samples (D'), and in the regolith returned by Luna 16 (D"). The calculation was carried out based on a previously suggested and developed analytical method that permits calculating the depthwise distribution of primary cosmic radiation and secondary nuclear-active particles, as well as cosmogenic isotopes in spherical cosmic bodies of different size and composition /4-8/. The effectiveness of the method was confirmed by numerous calculations of radioactivity in meteorites /9_7. Fig. 1 a and b gives the calculated curves of the depthwise distribution of Na^{22} and Al^{26} in lunar rocks of different types. From the figure it follows that the difference in the distribution of the same isotope in rocks that have approximately the same density and differ slightly in chemical composition is slight. But the density of dust rocks is nearly three times lower. Since /411 ionization losses and losses in nuclear interaction depend strongly precisely on density, the fall off in the fluxes of cosmic radiation with depth in rocks with low density will be less, therefore the activity of the cosmogenic isotopes they formed will be greater at greater depths (the activity of Al^{26} in D rocks is 2.2 times higher than in A rocks at a depth of 50 cm from the surface). In contrast, the difference between the activity in the regolith D, D', and D" determined only by chemical composition again is low. The Sea of Fertility regolith contains somewhat more aluminum, which is one of the main contributors to the formation of the activity of Al^{26} (15.33 percent as against 13 and 14 percent in the regoliths of the Sea of Tranquillity and the Ocean of Storms), therefore, in Luna 16 samples the activity of Al^{26} is somewhat higher. But in

the formation of Na^{22}, the main contribution is made by magnesium and silicon, whose abundance in the Sea of Fertility is lower than in the regolith from the other areas of the Moon, therefore, even the activity of Na^{22} in Luna 16 samples is lower. As a whole, the depthwise distributions of both cosmogenic isotopes are characterized by a sharp fall off in activity down to a depth of 5-6 cm from the surface caused by an abrupt fall off of the low-energy flux of solar protons, rapidly losing their energy owing to intense ionization losses, and then a gradual decrease with depth corresponding to a change in the flux of the secondary nuclear-active particles from the galactic component of cosmic rays.

The Sea of Fertility regolith was taken with a core, which penetrated 35 cm into the rock. Deeper, it touched solid rock or large fragments of rock. Thus, the thickness of the regolith in the Sea of Fertility at the sampling point is small and possibly 0.5-1 m or somewhat more than a meter, similar to the thickness of the regolith in the Ocean of Storms (of the order of 1-3 m), while it is assumed to be up to 6 m for the Sea of Tranquillity. The true mean thickness of the regolith is still unknown.

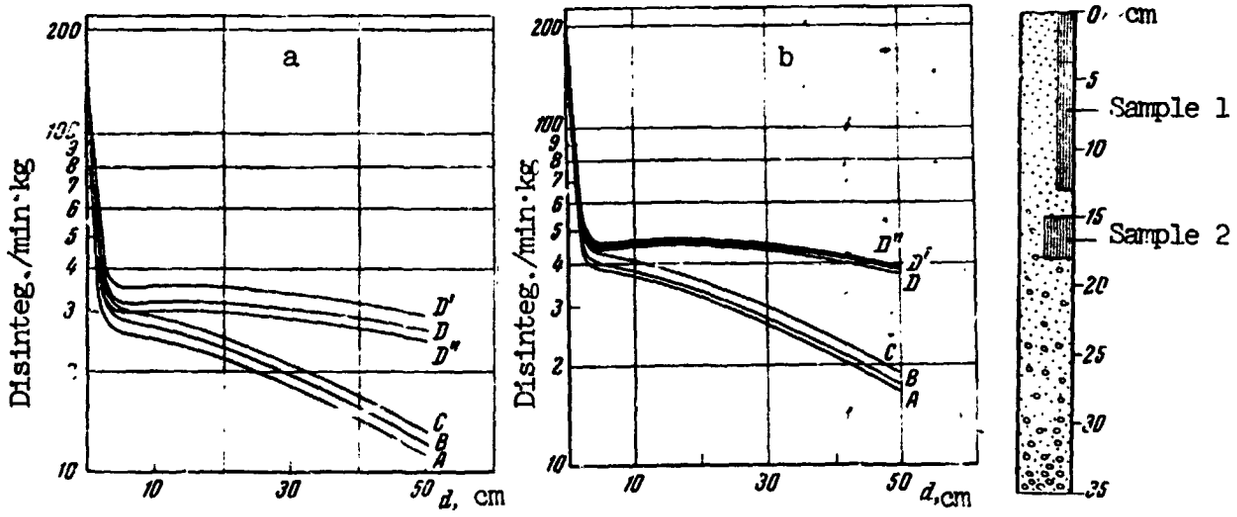

Fig. 1. Depthwise distribution of activity of Na^{22} (a) and of Al^{26} (b) in lunar rocks of different types (d is the distance from the lunar surface)

Fig. 2. Schematic core of lunar surface material.

Two samples were taken for the analysis of the activities of Al^{26} and Na^{22}: sample 1 weighing 18.87 g from the core, from the surface layer to a depth of 13 cm, and sample 2 weighing 10.396 g, from a depth of 15-18 cm (Fig. 2). It should be noted that thus

far no measurements have been made of the depthwise gradient of the activity of cosmogenic isotopes in samples of lunar dust. This is associated with the measurement technique used that permits measuring the activities only in samples of large volume (of the order of 50-100 g), which -- given the small diameter of the drill with which the surface material was collected -- leads to determining only some mean activity over wide depth intervals, that is, to blurring of the depth effect and thus to a loss of valuable information both with respect to cosmic ray intensity as well as the history of the samples investigated. We built a special unit to measure the activity in small weighed samples (10-20 g) without destruction of the sample. The measurements were conducted with a low-background scintillation gamma- /412
spectrometer in the gamma coincidence mode /10/. The material investigated was packed hermetically into miniature plexiglas cups, with inside dimensions 40 x 10 mm (sample 1) and 40 x 5 mm (sample 2) and placed between two spectrometric transducers equipped with low-background NaI(Tl) scintillators 120 x 100 mm in size. To reduce the background, the transducers were placed in the axial channel of the protective anticoincidence transducer based on a 500 x 650 mm plastic scintillator. The entire system of transducers was placed within a massive protective steel chamber with 300-400 mm thick walls. To suppress the neutron component of the background, on the chamber walls was laid a layer 100-150 mm thick made of a mixture of 75 percent paraffin and 25 percent boric acid. Use of this passive and active shielding reduced the integrated background of the spectrometric transducers by more than 200 times in the 0.1-3.0 MeV range /11/.

The measurements were made in cycles of 5 hours; the cycles of lunar sample measurement were alternated with the cycles of background measurement. Between the cycles, a check was made of the efficiency of the system based on the control source Na^{22} in standard geometry, as well as a correction for drift in the amplifier line; the shift of the Na^{22} photopeak during the 5-hour cycle did not exceed $\pm$ 0.5 percent. Samples of powdered dunite in the same amounts and in the same packaging as lunar samples 1 and 2 were used in the background measurements. The comparative background measurements were made with an empty plexiglas cup of the same dimensions. The results, within the limits of the statistical precision of the measurements, proved to be identical, indicating that the dunite samples used do not produce an addition to the natural background of the spectrometer. The total time for measuring sample 1 was 200 hours, and for sample 2 -- 250 hours, and thus the same amount of time for the background. The resulting spectrograms of the lunar surface material and of the background for sample 1 are shown in Fig. 3 (the corresponding spectrograms for sample 2 are analogous in shape). Preliminary results of these investigations were published in /12/. The present report gives

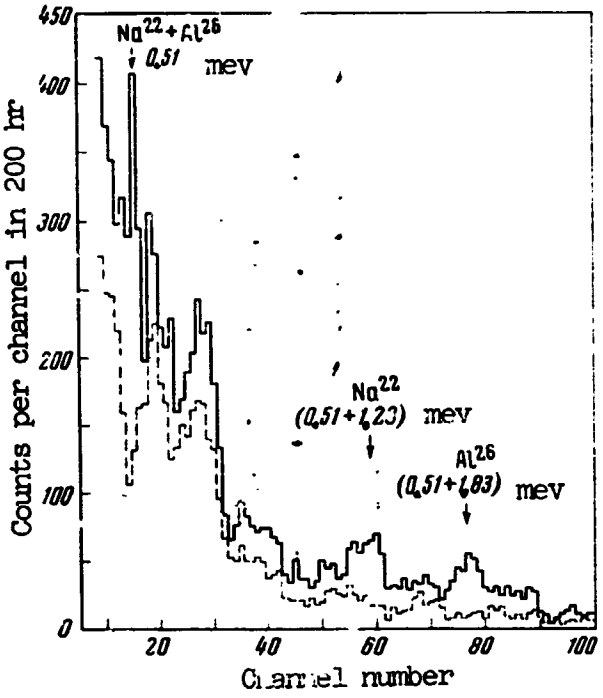

Fig. 3. Spectrogram of lunar sample 1 (solid line, total measurement time 20 hours) and corresponding spectrogram of background (dashed line)

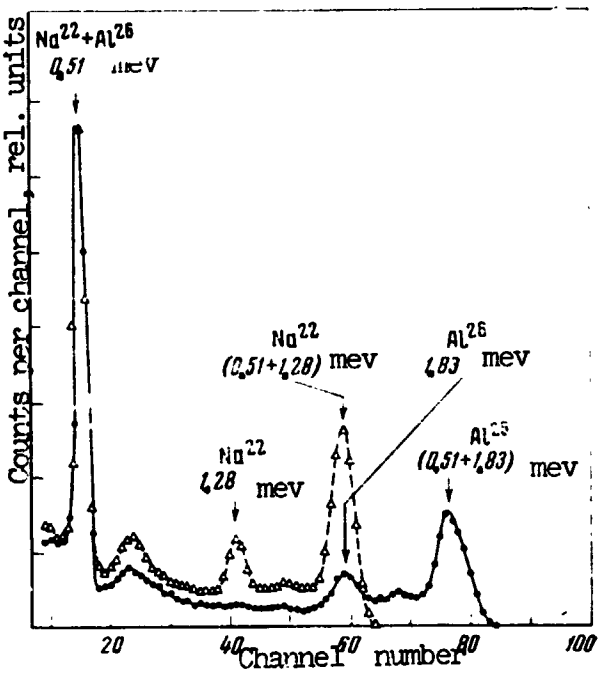

Fig. 4. Spectrograms of molds for sample 1 containing Al^{26} (solid curve) and containing Na^{22} (dashed line)

revised data obtained after more careful calibrations and more exact allowance for the contribution made by U and Th. The activity of Al^{26} was calculated based on the composite photopeak with E_γ = = (511 + 1830) keV (channels numbers 73-79 of the spectrogram) with a background of 0.35 pulse/hour and 0.38 pulse/hour and efficiency of 1.4 and 1.6 percent, respectively, for samples 1 and 2. The corresponding excesses of the effect over the background amount to 1.17 pulses/hour and 0.62 pulse/hour. The excess over the background in channels 80-89 are due to the presence of U and Th in the lunar surface material. To allow for the contribution of U and Th to the Al^{26} and Na^{22} photopeaks, additional measurements were made of terrestrial basalt in similar conditions. The contributions of U and Th to the Al^{26} photopeak thus determined were 12 and 7 percent, respectively, for samples 1 and 2. The Na^{22} activity was calculated based on the composite photopeak with E = (511 + 1275) keV (channels 55-62 of the spectrogram) with a background of 0.84 and 0.95 pulse/hour and efficiencies of 2.3 and 2.85 percent, respectively, for samples 1 and 2. The corresponding excesses over the background were 1.53 and 1.08 pulses/hour and the contribution of U and Th -- 5 and 3 percent. /413

To calibrate the spectrometer, special castings were made of samples 1 and 2. The casting mixture was composed of quartz powder SiO_2 (66 percent by weight) and the powder of ferro-ferric oxide $Fe_3O_4 \cdot 4H_2O$ (34 percent by weight). With this ratio of constituents, the casting parameters $\Sigma_i N_i Z_i$, $\Sigma_i N_i Z_i^2$ and $\Sigma_i N_i Z_i^3$ were equal to the corresponding parameters of the samples of lunar surface material investigated, where N_i is the number of atoms of the i-th element in the casting or the lunar sample, and Z_i is the atomic number of the corresponding element. In this way the identity of the conditions of gamma-quantum scattering and absorption in the lunar sample and in the casting was achieved. To portions of the casting mixture equal in weight to samples 1 and 2 were added known amounts of radioactive solutions $Al^{26}Cl_3$ of $Na^{22}Cl$; after careful mixing, the calibration mixture was hermetically packed in the same plexiglas cups as samples 1 and 2. Calibration of the $Al^{26}Cl_3$ and $Na^{22}Cl$ solutions was made with a low-background, flow-through $4\pi - \beta$ counter to a precision of not less than 5 percent. The castings were measured in the same regime and in the same conditions as the lunar samples. The spectrograms of the castings for sample 1 are shown in Fig. 4. The measurements are given in the Table.

The measured activities recalculated to the moment of sampling of the lunar surface material by the Luna 16 craft are as follows (in disintegrations$\cdot min^{-1} \cdot kg^{-1}$): Al^{26} -- 62 $\pm$ 8 and 54 $\pm$ 9, Na^{22} -- -- 42 $\pm$ 8 and 48 $\pm$ 9, and likewise for samples 1 and 2 (Fig. 5 a and b, bold-faced crosses 1 and 2). Given in the same figures, alongside the calculated curves, are the activities corresponding to them, which should have been observed in the samples selected for measurement (dashed crosses). The anticipated and measured activities in sample 1 (which was a mixture of surface material in the layer 0-13 cm from the surface) coincided within the limits of error, but the measured activities in sample 2 was higher than the anticipated values by 1.2 times for Al^{26} and 1.6 times for Na^{22} and close to the corresponding activities in sample 1. This enables us to assume that the surface material in sample 2 is also a mixture analogous to the mixture of surface material of different layers /414 in sample 1, that is, the surficial layer of the lunar regolith experienced mixing at least to a depth of 18 cm during a period of the order of 4 years (for Na^{22}, 1.5 $T_{1/2}$ is 4 years). This conclusion is confirmed by results on measurement of inert gases whose content does not contain on the regolith depth /1/.. Granulometric characteristics of regolith returned by Luna 16 and the scatter of the granulometric curves recorded for different depths /13/ also indicate that evidently the core investigated was taken from a surface that had been formed through repeated (but perhaps not many times)

RESULTS OF MEASURING ACTIVITIES OF LUNAR SURFACE MATERIAL

Sample number	Sample 1		Sample 2	
Weight of sample, g	18.87		10.396	
Position in core of lunar surface material, cm from the surface	0 - 13		15-18	
Measuring time, hr	200		250	
Isotope measured	Al^{26}	Na^{22}	Al^{26}	Na^{22}
Calculated photopeak, keV	511+1830	511+1275	511+1830	511+1275
Background in photopeak, pulse·hr^{-1}	0.35	0.84	0.38	0.95
Net effect over background, pulses·hr^{-1}	1.17	1.53	0.62	1.08
Contribution of U and Th, percent	12	5	7	3
Recording efficiency, percent	1.4	2.3	1.6	2.85
Activity at time of sampling of surface material /Illegible/ September 1970 (disintegrations·min^{-1}·kg^{-1})	62±8	42±8	54±9	48±9

ejection of lunar dust from neighboring areas. Mixing of a layer about 15 cm thick can also be caused by a 2 mm diameter micrometeorite. Mixing is indicated also by the data of L. L. Kashkarov who investigated tracks; at a depth of about 13 cm he discovered particles on whose surfaces a high gradient of track density from low-energy nuclei of iron-group elements included in solar cosmic rays was observed. /415

Different characteristics were obtained for the regoliths of the Sea of Tranquillity and the Ocean of Storms. A sharp gradient of track density on the surface of crystals taken from different depths and an absence of a gradient of track density in the crystal bulk were observed in the regolith core 10004-26, 13.2 cm in length /14/. A discontinuous change from layer to layer in track density /15/ and in the content of solar-origin He^4 and Ne^{20} /16/ were detected in the regolith core 12025-28, 60 cm in length. Thus, we have an example of an unmixed layer of regolith 10004-26,

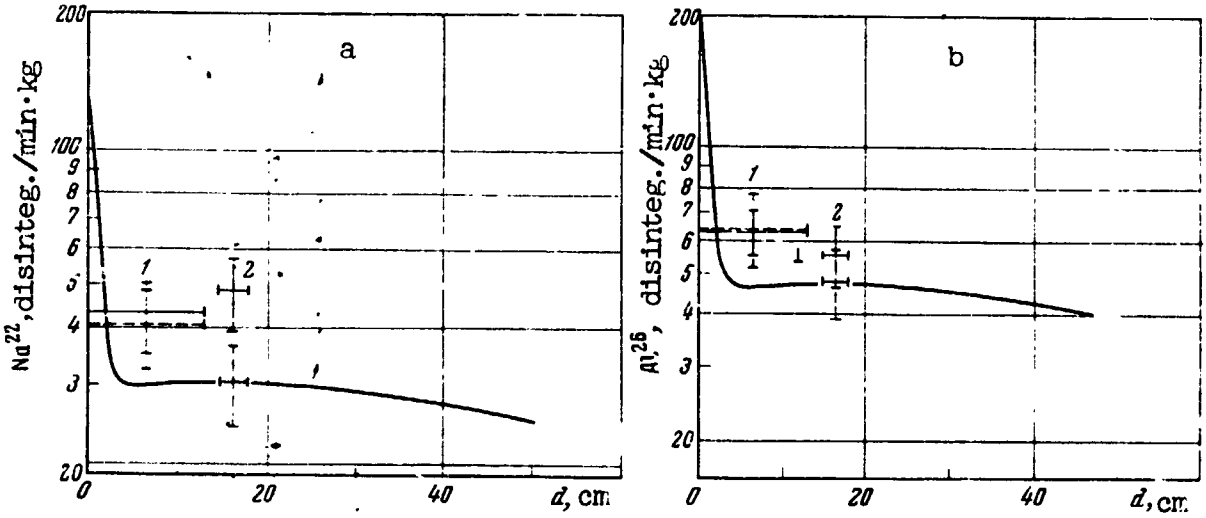

Fig. 5. Distribution of activity of Na^{22} (a) and of Al^{26} (b) in lunar regolith returned by Luna 16.
Solid curves represent measured values, and dashed curves represent the anticipated values in samples 1 and 2.

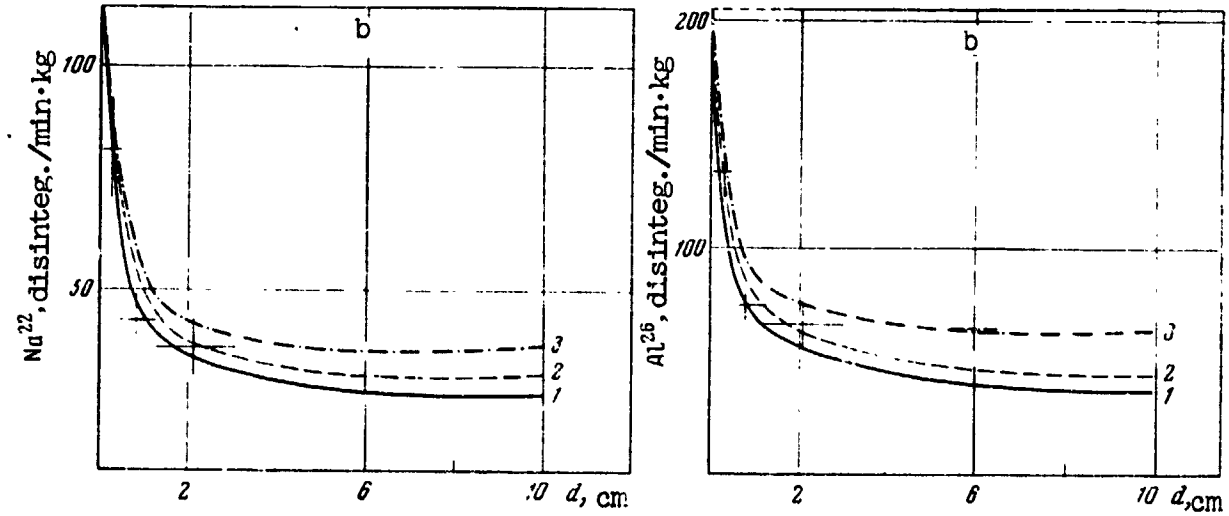

Fig. 6. Distribution of activity of Na^{22} (a) and of Al^{26} (b) in sample 10017, if the rock lies
1. in the plane of the lunar surface having the same composition
2. in the plane of the surrounding regolith
3. on the surface plane

indicating the long absence of ejecta from the neighboring surface areas; an example of mixing occurred during a period of time of less than 4 years before the sample was taken; and an example of

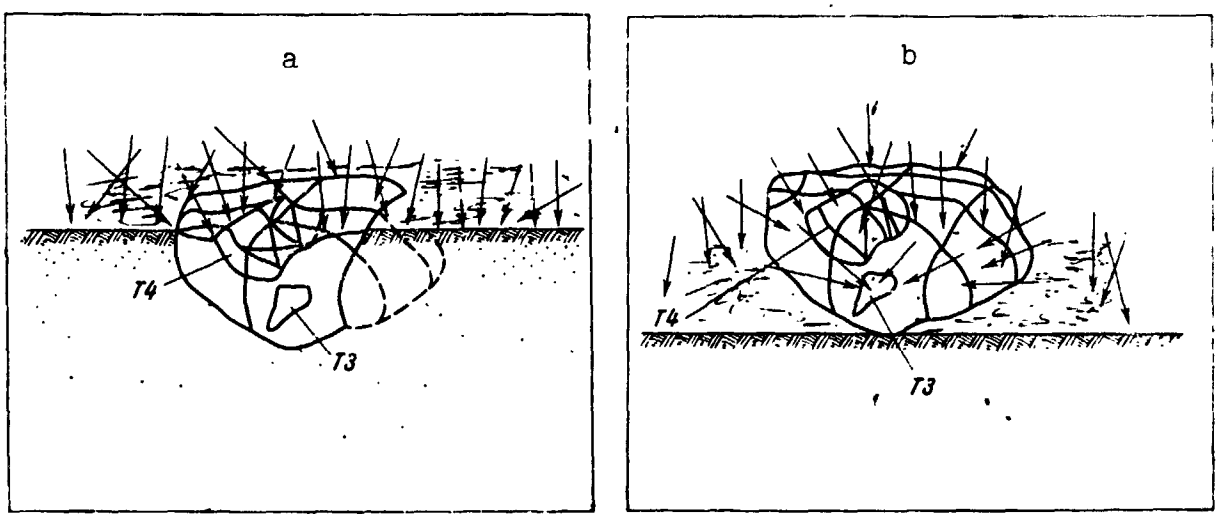

Fig. 7. Schematic representation of different conditions of irradiation of sample 10017
a. in the plane; b. in the plane of the surrounding surface

alternation of mixed and unmixed layers in the Ocean of Storms regolith with the most diverse radiation ages for the different layers (from 0 to 100 million years /15/) was also recorded.

All these data indicate at least the prevalence of processes of layerwise evolution of the regolith resulting from ejecta during constant bombardment of the lunar surface by bodies and particles from space over the constant processes of alteration of regolith resulting from erosion, whose rate is less than 10^{-7} cm/year /16/, or due to the influx of material from space. This conclusion was confirmed also by our calculations of the activities of cosmogenic isotopes in sample 10017 (crystalline rock of type B), for which measurements were obtained of Na^{22}, Al^{26}, Mn^{53}, Mn^{54}, and Fe^{55} in sample T-4 from a depth of 0-3 cm and from the irradiated surface, and in sample T-3 from a depth of 6 cm /17/. Fig. 6 a and b give the calculated curves and the data of the measurements /17/ for Na^{22} and Al^{26}. The observed activities of radioisotopes in equilibrium conditions were accumulated during a time equal to 1.5 $T_{1/2}$ of these isotopes before they were removed from irradiation. Thus, for Na^{22} and Al^{26} one can compare processes occurring during the last million years and the last approximately 4 years. Earlier, by analyzing the calculated and measured data for Na^{22} and Al^{26} at the surface of sample T-4 in sample 10017, constancy of the flux of solar protons for the last million years was shown /18/. A similar analysis in the depth sample T-3 made it possible to trace the history of sample 10017. Solid and dashed curves in

Fig. 6 a and b describe the distribution of activity in sample 10017 if it lies entirely in the plane of the lunar surface having the same composition, and in the lunar dust, respectively, so that only its upper surface was irradiated (Fig. 7 a). The same dash-dot curves describe the distribution of activity in the sample if it lay on a surface elevated over it and irradiated thus from all sides except the lower (see Fig. 7 b). From an analysis of the figure it follows that during the last 4 years a layer of lunar dust was heaped around the rock, while for the most of the past million years it lay on an open surface. Exactly the same curves were obtained for Fe^{55}, Mn^{54}, and Mn^{53}. Thus, to the already known history of sample 10017 (age of solidification 3.6 billion years /19/, cosmic age based on Kr^{81}-Kr^{83} 450-500 million years /20/, /416 and track-data age -- 9-10 million years /14/), it can be added that about 500 million years ago the rock was thrust up from deeper-lying layers to a level of 15-50 cm from the surface, and about 10 million years ago it was ejected onto the surface /14/; besides this we can state that during the last million years the rock continued to lie on the open surface, and the constant processes in the surrounding regolith was so negligible that they were not reflected in the conditions of its cosmic ray irradiation, but during a period > 4 years before the stone was taken from the lunar surface, in the course of one or several events a layer of lunar dust 6 cm thick was heaped around it. Supplementing the data obtained with Luna 16, this once again indicates that the decisive factor in the evolution of the lunar regolith is its layerwise alteration resulting from ejecta during bombardment from space.

REFERENCES

1. Vinogradov, A. P., Geokhimiya (3), 261 (1971).

2. Wanke, H., Begemann, F., Vilcsek, E., Rieder, R., Teschke, F., Born, W., Quijano-Rico, M., Vochage, H., and Wlotrka, F., Science 167, 523 (1970).

3. "Preliminary Examination of Lunar Samples from Apollo 12," Science 167, 1325 (1970).

4. Lavrukhina, A. K., and Ustinova, G. K., Astron. zh. 44, 1081 (1967).

5 Lavrukhina, A. K., Ustinova, G. K., and Ibrayev, T. A., in the collection: Kosmicheskiye luchi /Cosmic Rays/, No. 11, "Nauka", 1969, p. 100.

6. Lavrukhina, A. K., and Ustinova, G. K., Dokl. AN SSSR 179, 1448 (1968).

7. Lavrukhina, A. K., Ustinova, G. K., Ibraev, T. A., and Kuznetsova, R. I., Meteorite Research, Dordrecht, Holland, 1969, p. 227.

8. Lavrukhina, A. K., and Ustinova, G. K., Astron. vestnik 5(3), 144 (1971).

9. Lavrukhina, A. K., and Ustinova, G. K., Geokhimiya (9), 1083 (1972).

10. Gorin, V. D., Tezisy dokladov XXII Soveshchaniya po yadernoy spektroskopii i strukture atomnogo yadrya /Abstracts of Papers Presented at the 22nd Conference on Nuclear Spectroscopy and the Structure of the Atomic Nucleus/, Part 2, Kiev, 1972, p 91.

11. Gorin, V. D., Doklad na VI Vses. konf. po sintezu, proizvodstvu i ispol'zovaniyu stsintillyatorov /Paper Presented at the 6th All-Union Conference on the Synthesis, Production, and Uses of Scintillators/, Kharkov, 1971.

12. Vinogradov, A. P., Lavrukhina, A. K., Gorin, V. D., and Ustinova, G. K., Dokl. AN SSSR 202, 193 (1972).

13. Florenskiy, K. P., Ivanov, A. V., Stakheyev, Yu. I., and Tarasov, L. S., Space Research XII, Berlin, 123 (1972).

14. Lal, D., Macdougall, D., Wilkening, L., and Arrhenius, G., Proc. Apollo 11 Lunar Sci. Conf. 3, 2295 (1970).

15. Bhandari, N., Bhat, S., Lal, D., Rajagopalan, G., Tamhane, A. S., and Venkatavaradan, V. S., Report on Second Lunar Sci. Conf., Houston, 1971.

16. Funkhouser, J., Bogard, D., and Schaeffer, D., Report on Second Lunar Sci. Conf., Houston, 1971.

17. Proc. Apollo 11 Lunar Sci. Conf. 2, 1503 (1970).

18. Lavrukhina, A. K., and Ustinova, G. K., Nature 232, 472 (1971).

19 Albee, A. L., Burnett, D. S., Chodos, A. A., Eugster, O. J., Huneke, J. C., Papanastassiou, D. A., Podosek, V. A., Russ II, G. P., Sanz, H. G., Tera, F., and Wasserburg, G. J., Science 167, 463 (1970).

20. Marti, K., Lugmair, G. W., and Urey, H. C., Science 167, 548 (1970).

Order of Lenin Institute of Geochemistry and Analytical Chemistry imeni V. I. Vernadskiy, USSR Academy of Sciences, Moscow.

C-5

N75 11852

GAMMA-SPECTROMETRIC ANALYSIS OF LUNA 16 SAMPLE OF LUNAR SURFACE MATERIAL

/417

Yu. A. Surkov, G. A. Fedoseyev, O. P. Sobornov, G. B. Nazarkina, and L. P. Bachina

Abstract

Using a low-background scintillation gamma spectrometer with shielding against anticoincidences, the content of the natural radioelements (K, U, and Th) and long-lived cosmogenic radioisotopes (Al^{26}, Na^{22}, and Mn^{54}) in a sample of Sea of Fertility regolith was determined:

K = 0.095 ± 0015 percent,

U = (2.50 ± 037)·10^{-5} percent,

Th = (0.80 ± 0.36)·10^{-4} percent,

Al^{26} = 63 ± 27 disintegrations/min·kg;

Na^{22} = 45 ± 11 disintegrations/min·kg;

Mn^{54} = 41 ± 15 disintegrations/min·kg.

The analysis was carried out on a 10 g sample (inequigranular material with inclusions of rock fragments and other particles) taken from the middle part of the core of the lunar surface material returned by the Luna 16 automatic station.

Based on the content data of natural radioelements, an attempt was made to classify this sample in the scale of petrochemical types of terrestrial rocks arranged in accordance with their silicic content and alkalinity. Within the frame of reference of calcium-uranium systematics of lunar samples, a comparison was made of the K/U ratio obtained for the Sea of Fertility sample with analogous data for other regions of the Moon. Also discussed are problems on the depthwise distribution of cosmogenic radioisotopes along the regolith profile.

As is known, the first direct determinations of the radioactivity of the lunar surface were made in 1966 by the Luna 10 and Luna 12 automatic stations. Based on information arriving directly from space, for the first time the type of rocks covering the surface of the Moon was determined. Analysis of the data of a gamma-spectrometric survey made possible, in particular, the conclusion that lunar rocks correspond to terrestrial tholeiitic basalt [1].

Laboratory investigations of the radioactivity of lunar samples returned to Earth by spacecraft considerably extended the range of questions associated with lunar radiation, in particular, with its evolution, formation of rocks, history of regolith accumulation, radiation environment on the Moon in the past, and so on.

To solve these problems further investigations of the radioactivity of lunar rock in different regions and at different depths are needed. Still, already the information on the radioactivity of lunar rocks obtained in recent years makes it possible to consider it in the level of modern concepts on the radioactivity of terrestrial rocks (natural radioactivity) and of meteorites (radioactivity induced by cosmic rays).

Investigations of the natural radioactivity of terrestrial rocks, lunar regolith, and stony meteorites made it possible to establish several regularities in the distribution of radioelements, which in turn at the present time permits solving also the inverse problems -- giving the characteristics of rocks by their content of radioelements.

For example, in [2] approximate diagnostics of rocks is given, using gamma-spectrometric surveying, based on correlations revealed in the distribution of radioelements in terrestrial magmatic rocks in relation to their mineralogic and chemical composition.

Recently, in several studies [3, 4] analyzing data on the content of radioactive elements in lunar rocks, the potassium-uranium (K/U) systematics of the samples studied proved highly useful. Suggested by Wasserburg et al. [5] for comparison of data on the radioactivity of chondrites and terrestrial rocks, this systematics is based on differences in the behavior of potassium and uranium in processes of magmatic differentiation and suggest several conclusions on the history of the formation and evolution of planets and meteorites. /418

Finally, the special character of the information derives from an analysis of radioactivity induced by cosmic rays. This information deals primarily with the history of regolith formation as well as the role of cosmic rays and solar wind in this process.

This present study examines the results of an analysis made of the radioactivity of the sample of lunar surface material returned by Luna 16 from the area of the Sea of Fertility and discusses the data from the standpoint noted above.

Measurements of radioactivity of lunar sample. The content of natural radioelements and cosmogenic radioisotopes in the 10-gram regolith sample taken from zone V of the core of lunar surface material [6] was determined by the method of low-background scintillation gamma spectrometry. The papers [7, 8] describe the gamma spectrometer with shielding against anticoincidence designed for measuring low activities in samples of relatively low weight and volume and used in the present investigation.

When the lunar material was measured, the main detector was a spectrometric NaI/Tl crystal of cylindrical shape Ø 100 x 100 mm, with a well Ø 30 x 60 mm, exhibiting in a pair with an FEU-82 [photomultiplier-82] a resolution of 10.5 percent based on the Cs^{137} line.

The specifics of the measurement of samples in a 4π geometry consist of redistribution of the information in the observed spectrum occurring in the region of higher energies owing to summation of cascade gamma quanta. Therefore the use of the large-volume analytical crystal permits quite effective determination of the activity of several isotopes from the areas of the composite peaks against the lower background of the hard spectral region.

Preliminary studies conducted with simulated samples made it possible not only to examine the most convenient measurement geometry (a crystal Ø 100 x 100 mm with a well), but also to select for each isotope being determined the optimal energy interval in the spectrum, with maximum excess of effect over background. The simulated sample with content of natural and long-lived cosmogenic radioisotopes proportional to the values found in preliminary investigations [8-11] was made by adding the appropriate radioactive salts to radiation-free Na_3PO_4 salt. With it, a method was developed for the simultaneous measurement of the lunar sample both in the regime with the protective scintillator in the anticoincidence mode, as well as in the ordinary regime of a single-crystal spectrometer. All preparations (lunar and simulated samples, reference standard sources, and the background simulator were radiation-free material with electronic and physical densities analogous to the lunar values) were placed in hermetic teflon beakers and measured in identical geometry. The content of radioisotopes in the reference standard sources was determined by various methods, to a precision from 2 to 5 percent. For comparison, use was made of the international BCR-1 standard [12]. The technique of prolonged measurements of the radioactivity of lunar samples is given in [8].

Analysis of the experimental gamma spectra was made on an electronic computer using a method described in [13]. The content three natural (K^{40}, U^{238}, and Th^{232}) and three cosmogenic radioisotopes (Na^{22}, Al^{26}, and Mn^{54}) was determined. The remaining cosmogenic radioisotopes either had decayed by the time the lunar sample was measured, or else their content was beyond the limits of equipment sensitivity. As a result of the continuous measurements for a month, the statistical error of the determination of the radioactivity of these radioisotopes in the lunar sample ranged from 15 to 45 percent.

Content of natural radioelements in Sea of Fertility regolith. As a result of the gamma-spectrometric analysis of the sample of regolith taken from a depth of 15-18 cm from the Moon's surface (inequigranular material with inclusions of rock fragments and other particles not more than 3 mm in size [6]), the following content values were obtained for the natural radioelement (the results are given with statistical errors):

$$K = 0.095 \pm 0.015 \text{ percent},$$
$$U = (2.50 \pm 0.37) \cdot 10^{-5} \text{ percent},$$
$$Th = (0.80 \pm 0.36) \cdot 10^{-4} \text{ percent}.$$

These results on the K content agree with the data of the x-ray analysis in [6], while those for the U and Th content are intermediate between the corresponding data of a preliminary analysis conducted by mass spectrometry [6] and gamma spectrometry [8].

Table 1 gives the data on the content of K, U, and Th in regolith samples collected in four regions of the Moon. From the table it follows that the Sea of Fertility regolith differs in its content of natural radioelements from the regolith of the Sea of Tranquillity, Ocean of Storms, and Fra-Mauro and has lower concen- /419 trations of potassium, uranium, and thorium. While the Th/U ratios for all the four cases coincide within the limits of error, the K/U ratios differ and can serve, as indicated in [4], as the basis for the systematics of lunar samples.

Fanale and Nash, on examining the diagram of K/U ratios for chondrites, lunar samples, and terrestrial rocks, noted that these three family types differ by their correlation inclined lines connecting different points in each series of samples. In the authors' view, the large distance between the inclined lines of the family of chondrites ($K/U \sim 10^5$), and families of lunar and terrestrial samples ($K/U \sim 10^3 - 10^4$) evidently reflects an essential difference in the early history of the material of chondrites of the Earth and the Moon.

TABLE 1. CONTENT OF NATURAL RADIOELEMENTS IN REGOLITH SAMPLES FROM DIFFERENT REGIONS OF THE MOON

Element	Sea of Fertility	Sea of Tranquillity /9/	Ocean of Storms /10/	Fra-Mauro /11/
K, %	0,095	0.11	0,206—0,44	0,40—0,48
U, 10^{-4}%	0,25	0,59	1,5—3,4	3,8—4,1
Th, 10^{-4}%	0,80	2,24	6,0—13,2	13,4—14,9
Th/U	3,2	3,8	4,0	3,6
K/U	3800	2000	1400—1500	1100

At the same time, without denying in principle the possibility of the formation of the Moon and the Earth from material with an identical primordial K/U ratio, the authors stress the systematic decrease in this ratio for the families of samples from the Sea of Tranquillity and the Ocean of Storms ($K/U \sim 10^3$) compared with the terrestrial samples ($K/U \sim 10^4$).

We note, however, that the $K/U = 3.8 \cdot 10^3$, obtained for the Sea of Fertility regolith, is comparable with the corresponding data for terrestrial rocks. Thus, from /14/ it follows that a series of terrestrial rocks (dunites, peridotite inclusions in basalts and kimberlites, and so on) have the same ratios as for lunar samples ($K/U \sim 3 \cdot 10^3$).

On the other hand, new data on the K/U ratios for the Sea of Fertility regolith and samples of Fra-Mauro rocks, supplementing the array of correlational inclined lines for the known families of rocks of the Sea of Tranquillity and the Ocean of Storms rocks indicate differences in the nature of magmatic differentiation and, in particular, confirm the conclusion that the formation of regolith in different regions of the Moon was local /4/.

As already noted, the values of radioelement content in lunar rock can be used as an indicator of the petrochemical type of the igneous rocks. For this purpose, it is expedient to use a classificatory key diagram /2/ making it possible to present in the coordinates of two main petrochemical characteristics -- silicic content and alkalinity -- the approximate diagnostics of magmatic rocks. Loading this diagram with the gamma-spectrometric information in /2/ assists in distinguishing in diagnostics the limestone-alkaline series of differentiation from the alkaline series, as well as distinguishing the main representative rocks in these series.

An analysis based on the classificatory key diagram suggests this conclusion. The initial material of the Sea of Fertility regolith compositionally is evidently the product of the cooling of melts of the limestone-alkaline series, which can be qualified with a probability of about 60 percent as basalt, and as andesite-basalt with a probability of about 40 percent (in the key diagram this regolith sample lies near the boundary of the fields of petrochemical parameters of the basalts and andesite basalts. This conclusion does not contradict the data of the direct petrochemical analysis given in /6_7.

Cosmogenic radioisotopes in the Sea of Fertility regolith. By the gamma-spectrometric analysis of the regolith sample, the following data on the content of long-lived cosmogenic radioisotopes were obtained (recalculated to the moment of sampling of the surface material by Luna 16):

$$Al^{26} = 63 \pm 27 \text{ disintegrations/min·kg;}$$
$$Na^{22} = 45 \pm 11 \text{ disintegrations/min·kg;}$$
$$Mn^{54} = 41 \pm 15 \text{ disintegrations/min·kg.}$$

For comparison, in Table 2 are given the data on the radioactivity of Al^{26}, Na^{22}, and Mn^{54} in samples taken from other regions of the Moon.

The data given in /9-11_7 dealing with the mean content of cosmogenic radioisotopes in regolith samples from the Sea of Tranquillity, Ocean of Storms, and Fra-Mauro lie in fairly broad limits and on the average have somewhat higher values than in the Sea of Fertility sample. This can be partially explained by the fact that the sample used in our measurements was taken from a depth of 15-18 cm (zone V of the core of lunar surface material /6_7) and, thus, did not contain the most radioactive surficial layer.

Even preliminary investigations showed that all of the regolith to a depth of 35 cm bears signs of solar wind influence. This /420
conclusion was made after detecting large amounts of neutral solar gases throughout the volume of the core all the way to zone G, and also based on analyzing the structure of the infrared spectrum of the regolith /6_7. Additional information on this problem can be obtained in a discussion of the induced radioactivity data.

As we know, the formation of cosmogenic radioisotopes in the surficial layer of the Moon, on the one hand, depends on the flux intensity and the space-time variations of solar corpuscular and galactic cosmic radiation (SCR and GCR), and on the other hand -- -- on the chemical composition of the lunar material. In several

TABLE 2. CONTENT OF COSMOGENIC RADIOISOTOPES IN REGOLITH SAMPLES FROM DIFFERENT REGIONS OF THE MOON (DISINTEGRATION/MIN·kg)

Element	Sea of Fertility	Sea of Tranquillity /9/	Ocean of Storms /10/	Fra-Mauro /11/
Al^{26}	63	86—137	58—140	78—220
Na^{22}	45	51—61	27—80	45—84
Mn^{54}	41	29	40	—

papers /15, 16/ are presented calculations of the depthwise distribution of cosmogenic isotopes in lunar rocks. In these calculations, considering all the details of the nucleon-meson cascade that accompanies the interaction of cosmic rays with the nuclei of rock-forming elements, use was made of data on the actual chemical composition and density of the Sea of Tranquillity regolith, as well as corresponding data on the contribution made by GCR and SCR to the total intensity of particle flux. The resulting distributions (for Al^{26}, Na^{22}, and Mn^{54}) are characterized by a steep drop in activity near the lunar surface, which is associated with the intense absorption of the low-energy component of the SCR in the upper layer of the regolith (0-5 cm) and then by a smooth fall off in activity at greater depths due to the absorption of the high-energy component of SCR and GCR, accompanied by secondary active particles. According to the calculations, at a depth of about 15 g/cm^2 /sic/ the specific activity of the layer is 25-40 disintegrations/min·kg for Al^{26} and Na^{22}, and about 5-20 disintegrations/min·kg for Mn^{54}.

Since the main rock-forming elements in lunar samples from the Sea of Tranquillity and the Sea of Fertility is approximately identical, in particular, for both cases the content of Na, Mg, Al, Si, Mn, and Fe are close, these elements being mainly responsible for the formation of the radioisotopes we examined in nuclear reactions of the type (p, pn), (p, 2pn), and (n, 2n), we can compare these experimental data with the calculation results.

This comparison shows that the experimental data on the content of Al^{26}, Na^{22}, and Mn^{54} somewhat exceeded theoretical estimates. Obviously, the fullest pattern yielding an idea of the history of regolith formation can be obtained only by studying the layerwise distribution of the products of nuclear reactions. However, even the results of measuring the activity of cosmogenic isotopes formed in the regolith layer at a depth of 15-18 cm indicate the necessity of allowing for mixing of the regolith under the effect of external factors.

REFERENCES

1. Vinogradov, A. P., Surkov, Yu. A., Chernov, G. M., Kirnozov, F. F., and Nazarkina, G. B., Geokhimiya (8), 891 (1966).

2. Surkov, Yu. A., Yermolayev, N. P., and Sobornov, O. P., Mezhdunarodnyy geokhimicheskiy kongress, SSSR, Moskva, iyul' 1971 g. Tezisy dokladov /International Geochemical Congress, USSR, Moscow, July 1971, Abstracts of Papers/, p. 171.

3. Tera, F., Eugster, O., Burnett, D. S., and Wasserburg, G. I., Proc. Apollo 11 Lunar Sci. Conf. 2, 1637 (1970).

4. Fanale, F. P., and Nash, D. B., Science 171, 282 (1971).

5. Wasserburg, G. I., MacDonald, G. I.F., Hoyle, F., and Fowler, W. A., Science 143, 465 (1964).

6. Vinogradov, A. P., Geokhimiya (3), 261 (1971).

7. Sobornov, O. P., and Fedeoseyev, G. A., Vsesoyuznaya konferentsiya po sintezu, proizvodstvu i ispol'zovaniyu stsintillyatorov, Khar'kov, 1971 g. Tezisy dokladov /All-Union Conference on the Synthesis, Production, and Uses of Scintillators, Khar'kov, 1971, Abstracts of Papers/.

8. Surkov, Yu. A., Shtan', A. S., Kirnozov, F. F., Ivanov, I. N., and Moskaleva, L. P., Trudy XIV sessii KOSPAR /Transactions of the 14th Session of COSPAR/, Seattle, United States, 1971.

9. "Preliminary Examination of Lunar Samples from Apollo 11," Science 165, 1211 (1970).

10. "Preliminary Examination of Lunar Samples from Apollo 12," Science 167, 1325 (1970).

11. "Preliminary Examination of Lunar Samples from Apollo 14," Science 173, 681 (1971).

12. Flanagan, F. I., Geochim. Cosmoch. Acta 33, 81 (1969).

13. Iudilevich, D., and Martin, P. I., Appl. Rad. Isot. 14(11-12), (1963).

14. Fisher, D. E., Science 172, 1166 (1971).

15. Armstrong, T. W., and Alsmiller, R. G., Proc. Apollo 12 Lunar Sci. Conf., (1971).

16. Lavrukhina, A. K., and Ustinova, G. K., Astron. vestnik 5(3), 144 (1971).

Order of Lenin Institute of Geochemistry and Analytical Chemistry imeni V. I. Vernadskiy, USSR Academy of Sciences, Moscow.

N75 11853

SOME RESULTS OF TRACK METHOD OF INVESTIGATING LUNA 16 LUNAR MATERIAL

L. L. Kashkarov, A. K. Lavrukhina,
and L. I. Genayeva

Abstract

Preliminary data from an investigation of tracks in olivine crystals separated from the five zones of a lunar surface material core are reported. The gradients of track densities, their lengths, and their angular distribution were measured with an optical microscope. Throughout the core depth (35 cm) crystals bearing traces of exposure to low-energy solar cosmic rays were found, indicating the occurrence of mixing processes in the surficial layer of lunar surface material. The age of the occurrence of the samples investigated on the lunar surface, calculated from the track density, is in the interval 0.7-16 million years.

The sample of lunar surface material, or regolith, returned by the Luna 16 automatic station, as indicated in /1/, is a friable loose powder, whose granularity increases from the surface into the core depth. In this same study it is noted that the main process of regolith formation is the fragmentation of the initial rock occurring under the effect of falling meteorites. Still, the regolith material was continually subjected to solar wind and also solar and galactic cosmic rays. Solar wind protons with energies up to several kilo-electron-volts /2/ may have been the cause of the disintegration and erosion only of the thinnest upper layers of the material. Particles of cosmic rays, exhibiting high energies, acted on the material at some depth from the surface. From the typical depthwise distribution of the activity of the cosmogenic isotopes, whose regularities were examined in /3/, it follows that close to the surface (at depths to 5 cm) the intensity of the low-energy (down to 100 MeV) protons of solar cosmic rays is reduced by 100 times. The intensity of the higher-energy galactic cosmic rays is reduced only by several times after traversing the upper

layer of material about 50 cm in thickness. In addition, if it is considered that the composition of cosmic rays includes nuclei of heavier elements and that under the effect of protons in the primary cosmic rays secondary nuclear-active radiation is formed in the material, the complexity of the entire array of factors that have different effects on regolith formation becomes evident.

To clarify several problems of the history of regolith formation at the sampling site of the Luna 16 automatic station, we investigated tracks in olivine crystals segregated from different core depths. This present study gives several preliminary results of these identifications.

Silicate minerals at the surface of the Moon, throughout the geological time of their existence, have been integrated detectors recording in the form of traces of ionization damage to their crystal lattices heavy nuclei of solar and galactic radiation. In particular, olivine is capable of thus bearing record of nuclei with charges $Z \gtrsim 23$ [4]. With further increase in the charge, the crack length grows, which makes it possible to investigate the chemical composition of elements forming tracks from the distribution of track lengths [5, 6].

The main source of tracks in silicate materials on the surface of the Moon are these: a) nuclei of iron-group elements (VH-group) of solar cosmic rays with energies in the range from unity to several mega-electron-volts per nucleon; b) VH-group of nuclei of the galactic cosmic rays, whose energies exceed hundreds of mega-electron-volts per nucleon; c) recoil nuclei -- products of the interaction of high-energy protons and alpha-particles of cosmic /422
rays with the material of the crystals irradiated; and d) fragments of spontaneous and induced fission of uranium and thorium, as well as transuranium elements that have died out by the present time. The identification of tracks belonging to a particular group of sources was made using a series of characteristics, the principal of which are: track length, variation in track density with increase in depth from surface of the center of the crystals investigated, and also as a function of the bedding depth of the sample in the core of lunar surface material, and the spatial orientation of tracks in individual crystals. The main problem in this investigation was to study the history of the formation of the surficial layer of the lunar material and, in particular, to clarify the role of such possible processes as the successive heaping of individual layers of fragmented lunar material and its mixing.

The samples investigated -- olivine crystals 200-400 μm -- were segregated from all five zones [1] of the core of lunar surface material to depths of 35 cm. Using a special accessory,

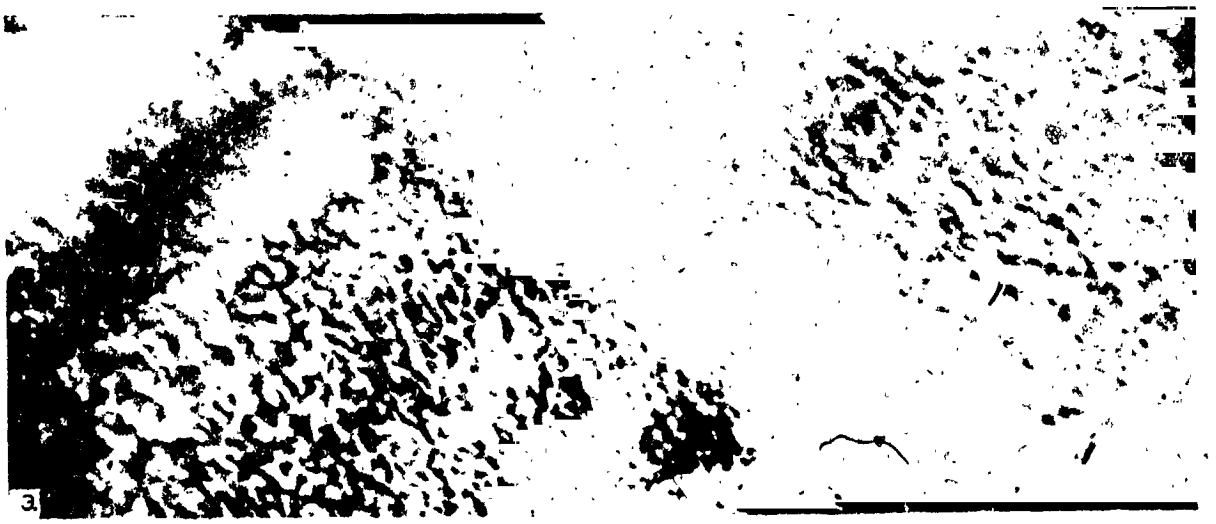

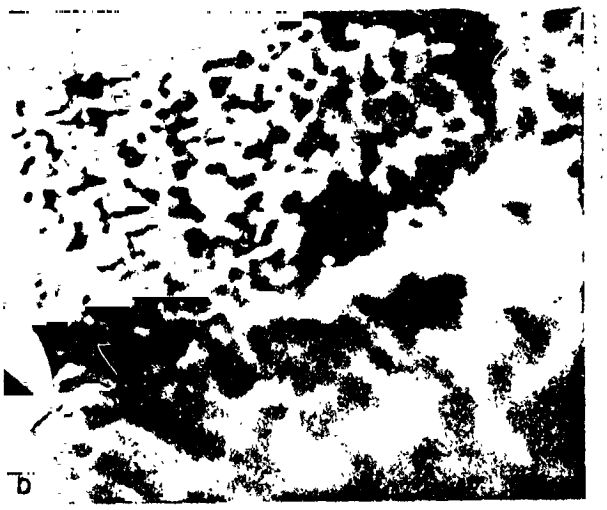

Fig. 1. Microphotographs of tracks on the surfaces of an olivine crystal ($R < 5$ μm)
Track density: a. $\rho > 7 \cdot 10^7$ cm^{-2}
b. $\rho \approx 10^7$ cm^{-2}

the crystals were cleaved into several parts, clear thin chips suitable for further track investigations. To etch the tracks, the olivine pieces were placed at room temperature in the following solution for 45 sec: two parts HF:one part H_2SO_4: four parts H_2O. The tracks thus etched were counted and measured with an optical microscope at a power of 1000 in transmitted light. Figs. 1, 2, and 4 present microphotographs of tracks observed in different olivine crystals.

At the present time, a total of 25 individual olivine samples were studied, for which the following quantities were measured: a) density (ρ) of short tracks in the length interval $2 \lesssim R \lesssim 5$ μm on the surfaces of each crystal; b) variation in the density of these tracks in the transition from surface to crystal bulk; c) distribution of lengths and the density of the longer tracks with $R \gtrsim 5$ μm; and d) angular distribution of tracks. The measurements are given in the table.

In nearly all the samples studied, the track density at the /423
crystal surface (ρ_{sur}) was close to or exceeded the maximum that can be calculated in the optical microscope. In our conditions, $\rho_{max} \simeq (5\text{-}7)\cdot 10^7$ tracks/cm^2 and was determined by the geometrical dimensions of the tracks etched. The change in the density of short tracks ($R \lesssim 5$ μm) with depth of immersion (D) in crystals revealed some characteristic features. Three regions can be distinguished: a) the region close to the crystal surface ($D \lesssim 10$ μm) with a maximum track density, for different samples lying in the range $(2\text{-}7)\cdot 10^7$ g/cm^2; b) the region following it ($D \simeq 10\text{-}70$ μm) in which the track density is reduced by 2-3 times; and c) the region with virtually constant track density differing for different samples by tenfold.

Fig. 3 shows the track density gradients in several samples. For comparison, also presented in the graph are the data of Fleischer /7/ for an augite crystal returned by Apollo 11.

From the calibration data /5, 6/ we know that the maximum etched length of tracks formed by iron nuclei with energies $\epsilon \gtrsim 2$ MeV/nucleon is 7-8 μm in olivine and corresponds to a nuclear mean-free path of about 10 μm. The mean length of tracks observed by us in the surficial layer (region a) is 2-5 μm, which corresponds to low-energy iron-group nuclei of the solar cosmic rays with $\epsilon \lesssim 2$ MeV/nucleon. With increasing distance from the crystal surface (regions b and c) tracks up to 10-14 μm in length are encountered, which can be formed by iron-group nuclei with energy $\epsilon \gg 2$ MeV/nucleon. A distinguishing feature of the long tracks is the well-defined spatial asymmetry of the direction of tracks within crystals (Fig. 5). This is additional proof that the tracks observed were formed by low-energy iron-group nuclei penetrating to this depth from the side of the nearest surface. The absolute track density observed in the surficial layer (up to 100 μm) of each crystal characterizes the time (T) during which the given sample was on the Moon's surface and was subjected to the direct /426
action of low-energy solar cosmic rays. Based on the mean flux of iron-group nuclei determined by independent methods for different energy ranges, we can estimate the time of accumulation of the measured track density.

The table gives the ages obtained for olivine based on the track density at the surface of crystals and at a depth of about 100 μm. Since in most cases the track density for $D \simeq 10$ μm was considerably higher than the maximum density that can be calculated in the optical microscope, the estimate of the time of irradiation at the surface of the Moon, when ρ_{sur} values were used, gives only the lower limit to the age. Based on the track density observed at

Fig. 2. Microphotographs of tracks whose density decreases with depth of immersion in the olivine crystal
a. The gradient extends approximately to 70 μm
b. The gradient extends approximaterly to 30 μm

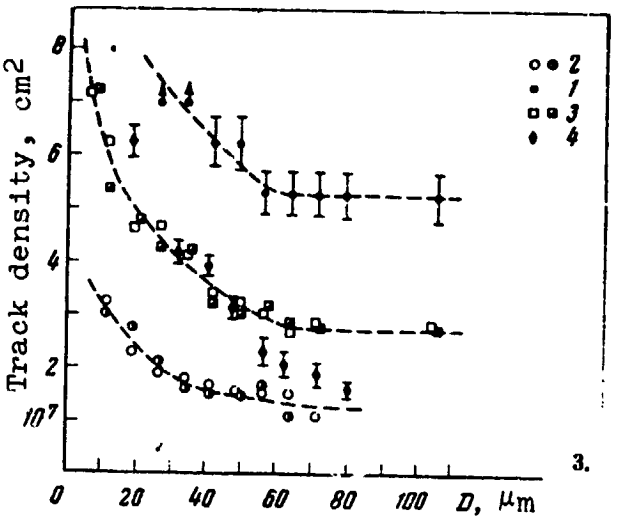

/424

Fig. 3. Change in track density from surface to center of crystals. The results of the present study for olivine from zones A and B
1. Sample 1-B
2. Sample 3-A
3. Sample 3-B
4. Fleischer's data /7/ for augite (Apollo 11)

Fig. 4. Tracks greater than 5 μm in length observed in olivine crystals with an optical microscope at a magnification of 1000

a depth of about 100 μm, age values were obtained in the range 2-16 million years (although for one of the samples, 3-V, a lower age of ≃ 0.05 million years was obtained). To determine the age T, use was made of theoretical calculations /8/ of the rates at which tracks were formed by iron-group nuclei. We note that the contribution from the fission fragments of heavy elements for olivine with uranium content $\sim 10^{-9} - 10^{-10}$ g/g is negligibly small. The density of tracks from the spontaneous fission of U^{238} accumulated in $4.6 \cdot 10^9$ years is about 10^2 tracks/cm^2.

Data on the distribution of track length and density in individual olivine crystals, owing to the limited statistics,

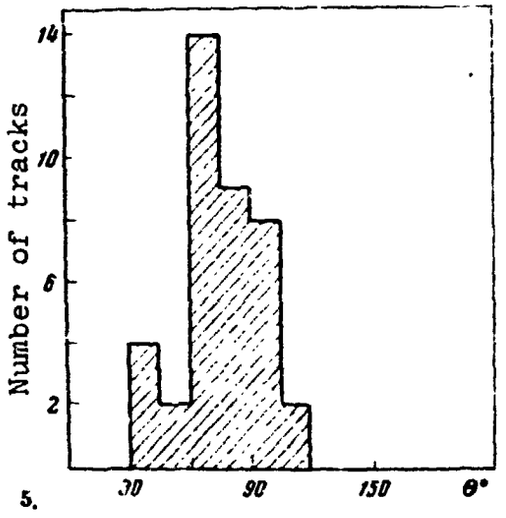

5.

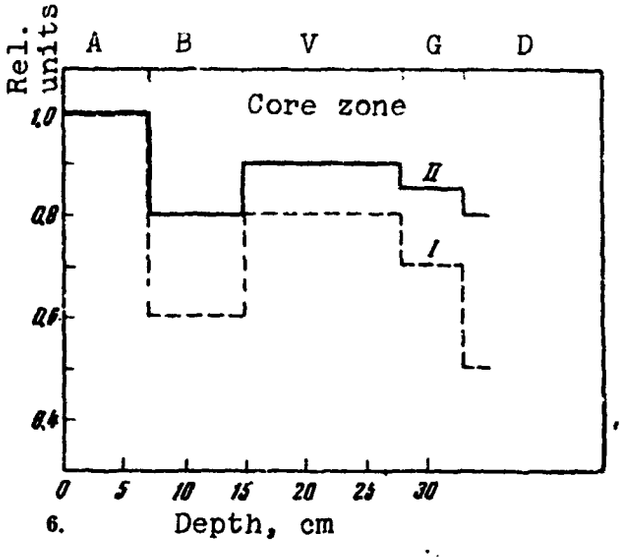

6.

Fig. 5. Angular distribution of tracks with length >5 μm in several Luna 16 olivine crystals

Fig. 6. Relative variation with depth of immersion in Luna 16 column of lunar surface material.
I. Number of olivine crystals with track density gradient
II. Mean-weighted density of tracks observed within crystals taken from the indicated depth of surface material core.

do not yet permit any quantitative conclusions, however some preliminary conclusions can be drawn.

As can be seen from the table, in all five zones of the core there are crystals with maximum surficial track density (Fig. 6). Some trend toward a decrease in the relative number of these crystals with increase in depth of the core was noted, which can indicate the reduction in the mean irradiation time of crystals at the lunar surface for zones G and D compared with the overlying layers. The discovery throughout the core depth of individual crystals bearing traces of exposure to low-energy solar cosmic rays indicates that they were present for several millions of years at the surface of the lunar surface material. The irradiation time varied within wide limits (from tens of thousands to several millions of years). Based on this it can be assumed that participating in forming the surficial layer of the Moon, simultaneously with a possible process of the successive layering of the fine-crystalline material, constant mixing of this material was also highly significant, occurring under the effect of collisions of micrometeorites at the lunar surface.

RESULTS OF MEASURING TRACKS IN OLIVINE CRYSTALS FROM LUNAR SURFACE MATERIAL RETURNED BY LUNA 16 AUTOMATIC LUNAR STATION

Depth*, cm	Sample	Tracks $2 \leq R \leq 5$ μm: ρ_{sur}, 10^7 g/cm^2	Tracks $2 \leq R \leq 5$ μm: gradient ρ, 10^7 g/cm^2	Tracks R > 5 μm: ρ, 10^6 g/cm	Tracks R > 5 μm: R, μm	T, millions of years based on tracks with $R \geq 5$ μm: $R \geq 10$ μm	T, millions of years based on tracks with $R \geq 5$ μm: $R > 100$ μm
0–7.5	1-A	>7	(7–1.9)	—	—	>2	10
	2-A	>7	(7–2.3)	3.5	5.8–9.3	>2	11.5
	3-A	>7	—	(14–5)	5–7.2	>2	—
	4-A	>7	(7–2.3)	—	—	>2	12.5
	5-A	>7	(7–3.2)	—	—	>2	16
7.5–15	1-B	>7	(7–5)	—	—	>2	—
	2-B	>5	(7–2.8)	—	5–9.1	>1.6	14
	3-B	~3.5	(3.5–2.3)	5–7	5.2–5.8	~1.2	12
	4-B	~7	(7–2.8)	5	6.8	>2	14
	5-B	4.3	(4.3–3.2)	—	—	1.4	16
15–27	1-V	~7	(7–2)	7.6	8–11	~2	9
	2-V	~7	(7–0.5)	2.1	7–14	~2	2.6–9
	3-V	5	(5–0.01)	—	—	1.7	0.05–15
	4-V	~7	(5–2.8)	—	5.6	~2	15
	5-V	~7	(7–0.9)	(14–0.8)	5–9	~2	11.5
27–33	1-G	>7	—	—	—	>2	—
	2-G	>7	(7–1.4)	—	—	>2	10.5
	3-G	>7	(7–2)	—	—	>2	9
	4-G	>7	2)	—	5.5–7.3	>2	10.5
	5-G	~2	(2–0.01)	(15–3.5)	6–10.2	~0.7	—
	6-G	~6	(6–1.4)	—	7.5–10.2	~2	7–9
33–35	1-D	~6	(6–2.1)	—	5.4	~2	11–13
	2-D	5.2	(5–2.1)	3.5	5.9–9.1	1.7	3.5–8
	3-D	4.8	(4.8–1.8)	—	—	1.6	9–11.5
	4-D	~6	(6–3.2)	—	—	2	15

* Depth from surface of lunar surface material is indicated.

The authors are thankful to A. V. Ivanov and L. S. Tarasov for much assistance in selecting and identifying the minerals studied from the Luna 16 lunar surface material.

REFERENCES

1. Vinogradov, A. P., "Preliminary Data on Lunar Surface Material Returned by Luna 16 Automatic Station," Geokhimiya (3), (1971).

2. Solnechnyy veter /The Solar Wind/, "Mir", 1968.

3. Lavrukhina, A. K., and Ustinova, G. K., "Regularities of the Depthwise Distribution of Cosmogenic Isotopes in Lunar Rocks," Astron. vestnik 5(3), (1971).

4. Fleischer, R. L., Price, P. B., and Walker, R. M., "Solid-State Track Detectors: Applications to Nuclear Science and Geophysics," Ann. Rev. Nucl. Sci. 15, 1 (1965).

5. Price, P. B., Fleischer, R. L., and Moak, C. D., "Identification of Very Heavy Cosmic-Ray Tracks in Meteorites," Phys. Rev. 167(2), 277 (1968).

6. Kashkarov, L. L., Genaeva, L. I., Malishev, V. V., Satarova, L. M., and Lavrukhina, A. K., "Investigation of Cosmic Ray Induced Tracks in Meteoritic Minerals," Acta Phys. Acad. Sci. Hungarical 29 (suppl. 1), 449 (1970).

7. Fleischer, R. L., Haines, E. L., Hart, H. R., Jr., Woods, R. T., and Comstock, G. M., "The Particle Track Record of the Sea of Tranquillity," Proc. Apollo 11 Lunar Sci. Conf. 3, 2103 (1970)

8. Bhandari, N., Bhat, S., Lal, D., Rajagopalan, G., Tamhane, A. S., and Venkatavaradan, V. S., "Fossil Track Studies in Lunar Materials," Rep. Second Lunar Sci. Conf., 1971.

Order of Lenin Institute of Geochemistry and Analytical Chemistry imeni V. I. Vernadskiy, USSR Academy of Sciences, Moscow.

N75 11854

RADIATION DAMAGE AND STRUCTURE RECORDED AT HIGH RESOLUTION IN GRAINS FROM FINE FRACTIONS OF LUNA 16 SURFACE MATERIAL

/430

L. Durrieu, C. Jouret, J. P. Bibring, R. Meunier, and M. Maurette[1]

Abstract

In the finest particles of a sample (total weight about 1 mg) taken from the samples returned to Earth by Luna 16, their ultramicroscopic features were studied with a high-voltage electron microscope. The investigations were carried out in the Institute of Electron Optics of the National Center for Scientific Research of France and then the results were compared with those obtained by similar methods for dust particles of the Apollo 11, Apollo 12, and Apollo 14 collections. The following amazing features were noted in particles of surface material returned in all the lunar trips: a very high density of tracks of nuclear particles, ultrathin amorphous shells, highly rounded forms, and amazingly good ordering of crystal lattice. These features were used along with calibration experiments in solving the following problems: 1) determining the energy spectrum and, where possible, the chemical abundances of the very heavy nuclei in the solar wind and in the solar cosmic rays with low energies ($E < 1$ MeV/a.e.m.)[2]; 2) studying the past activity of the Sun; 3) obtaining data on the lunar dynamic processes affecting dust particles; 4) analyzing composite effects caused by the penetration of solar wind into the lunar surface material in the past, and 5) establishing the existence of the "ancient" lunar atmosphere and magnetic field.

---

[1] The article was prepared by M. Maurette.

[2] E < 1 MeV/a.e.m /atomic energy mass/ is the frequency per MeV expended per atomic unit of nucleon mass. -- Editor's note.

Introduction. Samples from the surface of the planets that have no atmosphere and are deprived of a magnetic field, like the Moon, have been irradiated by galactic and solar cosmic rays and solar wind particles, and were also subjected to different types of dynamic lunar processes, such as impacts of meteorites, thermal cycles, and the powdering of material by the solar wind. As a result, tracks of nuclear particles and other damage to crystal lattices must exist in grains of lunar surface material, and their structure and shape must reflect their complex history, including shock and thermal effects and erosion in the lunar regolith.

In this article we attempt to illustrate the correctness of these assumptions first by describing the radiation damage and structure recorded with high resolution. We observed them with a 1 MeV electron microscope in micron-sized grains extracted from 1 mg of the L-16-19 sample from the surface material returned by Luna 16. This study was carried out with the instruments of the Institute of Electronic Optics of the National Center for Scientific Research in Toulouse. Then we discuss the possible initial factors producing this complex pattern by comparing it with the patterns and factors noted either in the dust grains of Apollo 11, Apollo 12, and Apollo 14, or else in fragments of micron size obtained from fragmentation of lunar and meteoritic rocks, which were then subjected to artificial irradiation and heat exposures. Finally, we consider several new methods that we have developed for carrying out various problems in cosmophysics.

These new methods were specially developed by us for their successful use in working with very small amounts ($\lesssim 1$ mg) of fine fractions of the sample. Therefore they were especially suitable for preliminary investigations, for example, very small amounts of samples of martian soil. In addition, by using them we obtained good information for lunar investigations, in particular, in studying fine fractions of surface material from different areas of the Moon and from different depths of the lunar core. Therefore we will present or discuss the results for Luna 16 in comparison with the data we already obtained for Apollo 11, Apollo 12, and Apollo 14. /431

Experiment. From the finest fractions of the samples of lunar surface material returned by Luna 16, Apollo 11, Apollo 12, and Apollo 14, micron-sized grains were extracted and then transferred with a platinum wire to Fukami-Adachi type substrates. Before being extracted, several of the grains were etched chemically or heated to 900° C, as described in /2_7.

Then the preparations were studied with 1 MeV and 100 keV electron microscopes in the Institute of Electronic Optics. By

studying the same Luna 16 preparations on the two microscopes, we concluded that a high-voltage electron microscope had to be used. And for the study of the intergrain cement and the very weak contrasty structures in the crystalline grains as, for example, amorphous shells (Fig. 1) and not etched or "hidden" tracks of nuclear particles (Fig. 3), the observations were carried out in dark-field conditions. The 100 keV electron microscope was used only for studying the external appearance of the grains and their size distribution, observations of very weakly etched tracks, and for determining the ratio between the amorphous and crystalline grains.

COMPARATIVE ULTRAMICROSCOPIC STUDY OF THE FINEST GRAINS EXTRACTED FROM FRACTIONS OF VARIOUS SAMPLES OF LUNAR DUST FINER THAN 400 MESH

Sample number	Automatic station or spacecraft	Grains covered entirely with film, percent	Amorphous grains, percent	Fraction of particles with track density of 10^{10} tracks/ /cm^2, percent
L-16-19	Luna 16	90	13	20
10084	Apollo 11	90	11	20
12070	Apollo 12	63	23	22
12032	"	24	--	--
14259	Apollo 14	80	19	8
14141	"	6	11	1

Results. The following features, partially reflected in the table, were observed for Luna 16 and several Apollo 11, Apollo 12, and Apollo 14 samples.

1. In the dark-field of microphotographs taken with the 1 MeV electron microscope (Figs. 1 and 2) it can be seen that a considerable fraction of the grains are surrounded with a surface coating of amorphous material, that appears as a dark shell about the grains. Grains with the coating are a very common phenomenon. Thus, the examples given in the table pertain to grains extricated from Luna 16 and Apollo samples. Preliminary measurements of the coating thickness show that it is in the limits from the minimum size of about 200 AU for grains extracted from the samples L-16-19 and Apollo 11 -- 10084 up to about 1000 AU for grains from the Apollo 12 sample 12070. The proportion of coated grains fluctuates markedly from one sample to another, and the largest values were observed for the samples L-16-19, 10084, and 14259. The coated grains disclose highly rounded forms.

2. Most of the grains (~90 percent) in the samples L-16-19 and 10084 disclose a high density of nuclear particle tracks, which can be seen in Fig. 3 as contrasting lines. These tracks are present in grains in both Luna 16 and Apollo samples.

In all these samples, after short etching, tracks show up in the grains in the form of narrow etching channels, which are observed with the 100 keV electron microscope.

3. The proportion of entirely amorphous grains (glass?) we found in the finest fractions (finer than 400 mesh) of all the samples of surface material in general was much less than in the coarser fractions studied by other authors /3/.

4. The pattern of the electronic diffraction of crystalline grains beneath the amorphous shells reflected good ordering of the crystal lattice and showed that the fraction of grains with a high degree of disorder was uncommonly low (~1 percent) in all the samples of the fine fractions of surface material.

5. Only the Luna 16 grains contained, prior to artificial heating, inclusions similar to those observed in artificially heated grains of surface material or in micron-sized fragments extracted from the lunar breccias 10046 and 10059 of Apollo 11. Therefore the Luna 16 sample is classified in a subgroup that embraces the samples 10084 and 14259 of Apollo and disclosing the highest proportion of grains coated with the amorphous layer, the highest density of hidden tracks of nuclear particles, /432 and the most rounded, as if "eroded" shapes. But the Luna 16 grains differed quite definitely from the Apollo 11, Apollo 12, and Apollo 14 grains in that they contained "thermal-like" inclusions superimposed on the tracks.

Discussion of results. Ultrathin shells, hidden tracks, and past solar activity. Amorphous shells. To establish the origin of the thin amorphous shells found on the particle surfaces, we made a series of calibration experiments.

Initially a fragment from the inner part of the lunar igneous rock sample 12021 returned by Apollo 12 was crushed to micron size. These fine fragments, entirely protected against low-energy solar nuclear particles, as to be expected, had very angular shapes and did not disclose either amorphous shells or hidden tracks. Irradiation of this preparation with a high dose (~10^{16} ions/cm^2) of xenon ions at an energy of 1 keV/a.e.m /atomic unit of mass/ using a heavy isotope separator in our Institute /4/ led simultaneously to the formation of well-defined roundedness of the microcrystals and amorphous shell on grains very similar to those observed in grains of natural dust (Fig. 1).

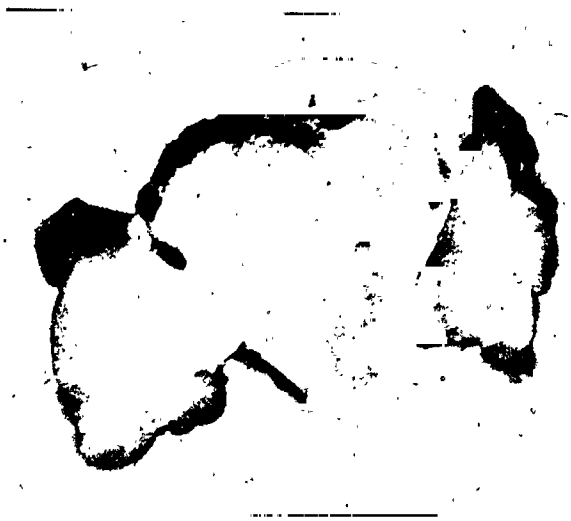

Fig. 1. Dust particles 1 micron in size from core of lunar surface material returned by Luna 16. Microphotograph taken in dark field conditions with an electron microscope (1 MeV).

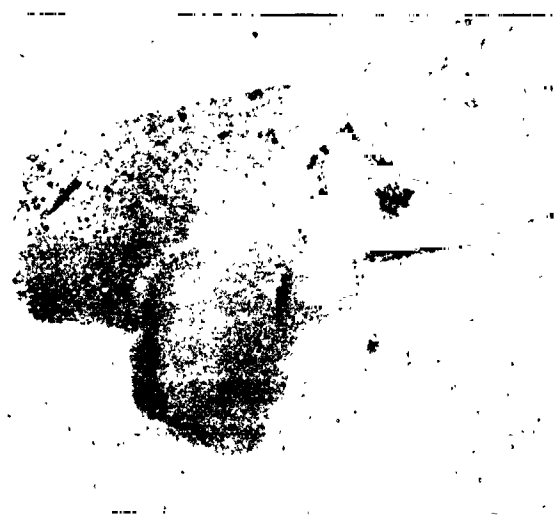

Fig. 2. High ($\geqslant 10^{10}$ tracks/cm^3) density of ancient tracks in the form of contrasty lines from observed nuclear particles in dust grain from core of Luna 16 lunar surface material. Microphotograph was taken in dark field conditions with an electron microscope (1 MeV).

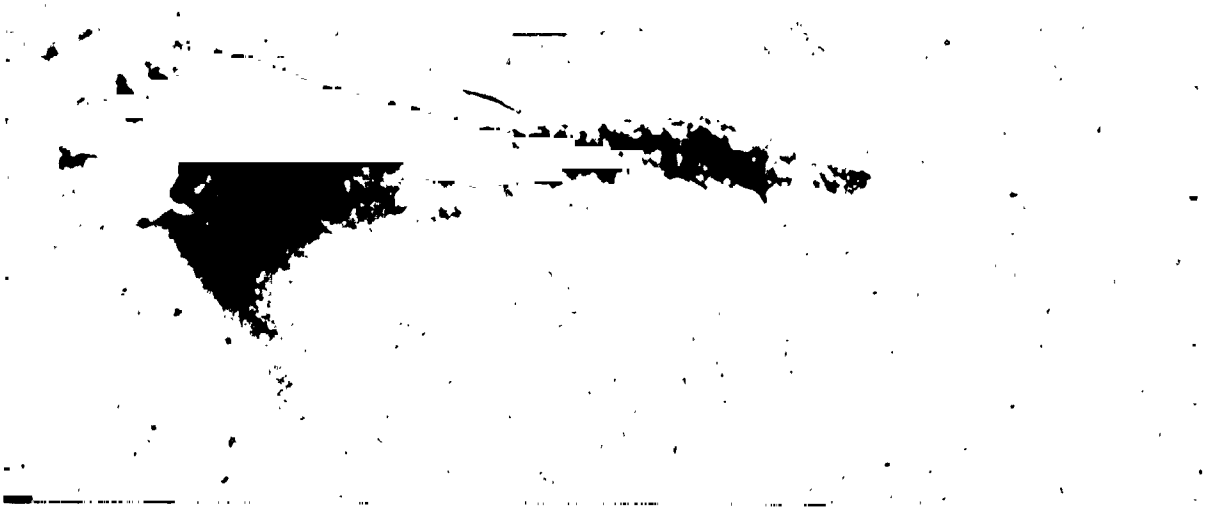

Fig. 3. Microphotograph in dark field conditions taken with an electron microscope (1 MeV) of dust grain from Luna 16 core. Visible are inclusions that most likely are phase transformations induced by radiation.

Then we studied the thermal stability of natural shells and hidden tracks observed in the same grains, by heating the dust grains 2 hours at different temperatures. It was found that the shells and tracks disappeared nearly roughly at the same time at 800° C, being converted into inclusions (see Fig. 3) very similar to those observed by Price and Walker /5/ in mica artificially irradiated with fission fragments and then heated. We assume that this experiment with annealing quite convincingly showed that the material of the crystal shells by nature are similar to what is the radiation-damaged track core. Finally, by measuring the distribution of shell thickness we determined that it agrees entirely with the anticipated depth of penetration (about 500 AU) of heavy ions of the solar wind type with energy approximately 1 keV/a.e.m /6/.

Based on these observations, we concluded that the ultra-thin shells are surface films damaged by radiation, "metamictized" during a period of ancient penetration of solar wind type ions into dust particles when they were at the very surface of the lunar regolith. The fact that these ions most likely are solar wind ions and not the products of the α-decay of a hypothetical radon atmosphere settling downward /7/ is shown by the following /433 data.

1. Zircon is metamictized in nature by recoil α-particles, extremely similar to those obtained during the α-decay of atmospheric radon, and the minimum metamictizing dose is about 10^{13} recoils/cm^2 /8/. If it is assumed that this "minimum dose" also caused the surface metamictization of lunar dust grains, we get the present-day Po^{210} activity of lunar surface material ~4 disintegrations/cm^2, approximately 10^3 times higher than the value recently determined by Lindstrom et al. /7/. Therefore it appears implausible that the radon atmosphere was the cause of the formation of the amorphous shells of grains.

2. There is a strict correlation between the fractions of grains covered with the amorphous shell and the content of solar wind inert gases in samples of lunar surface material /9/. At the same time we did not observe any correlation with the content of the precursor-elements of radon (U and Th); the Apollo 14 surface material contains roughly ten times more U and Th than does the Luna 16 surface material, but the fraction of the coated grains in the former is usually less /9/.

The thickness of the Luna 16 grain shells is approximately half that of the shells of the grains in sample 12070 from the Apollo 12 material. This can reflect a change in the effective radius of action of the solar wind ions and, therefore, a change in their energy by the time of penetration. If this is so, then

obviously we can study the activity of solar processes accompanied by the ejection of solar wind nuclei into cosmic space in the past, by means of detecting the distinct changes in the thickness of the grain shells as a function of their bedding depth in the well-stratified lunar cores. However, it would be necessary to carry out artificial ionic irradiation in order to verify whether the thickness of the shells depends on ion energy. Moreover, it is necessary to be certain that the depth in the cores actually gives the time scale of grain irradiation at the very surface of the lunar regolith.

Tracks of lunar particles. We have already advanced the hypothesis /10/ that the particles forming the tracks may have been very heavy "suprathermal" ions ($Z \gtrsim 20$) of solar origin with energies lying in the interval between the energies of the solar wind nuclei ($E \sim 1$ keV/a.e.m) and the more energetic solar cosmic rays ($E \gtrsim 1$ MeV/a.e.m). This hypothesis rests on the following arguments.

1. Our preliminary measurements show that the distribution of the total mean-free paths of particles $N (R \gtrsim R_0)$, where N is the number of tracks with particles greater than R_0, is best described by selecting a momentum-like differential energy spectrum for particles with energies in the range 10 keV/a.e.m $\lesssim$ $\lesssim E \lesssim$ 100 keV/a.e.m. This spectrum agrees with what has been recently reported by Frank /11/ for "suprathermal" protons in the same energy limits and differs altogether from the spectrum of the power dependence of the kinetic energy $E^{-\gamma}$, which is commonly reported for high energy solar cosmic rays. Based on the foregoing, we can conclude that particles forming the tracks may have been "suprathermal" heavy ions.

2. Since these low energy ions penetrate into solids to a shallow depth ($\lesssim 1$ μm), they must be noted in the surface, one-micron layer of coarser grains of surface material. From studying Luna 16 dust grains, we actually observed the amazing effect of grain dimensions, which shows up in the abrupt falloff in the number (γ) of grains with tracks when we pass from the finest dust grains ($\gamma \sim 90$ percent) to small fragments obtained by crushing grains with diameter of about 100 μm ($\gamma \sim 5$ percent). /434

If this hypothesis will be subsequently confirmed, including artificial irradiation with low-energy Ni /sic, Ne is probably what is meant/ obtained in an elastic scattering chamber in our institute, then we can expect: a) to obtain the energy spectrum of the flux of solar ions that in cosmic space could not have been detected by ordinary techniques; b) to study the activity of solar processes accompanied by the ejection of "suprathermal" nuclei into space in the past, by measuring the distribution of

track lengths, reflecting the energy spectrum of random particles as a function of the grain bedding depth in a well-stratified core of lunar surface material. This study would supplement the data on the activity in the past obtained by measuring the distribution of the shell thickness of grains located at the same depths.

Other conclusions from the present results pertaining to cosmophysics. Dynamic lunar processes. From the astonishing similarity between the rounded shape of dust grains from Luna 16, Apollo 11, and artificially irradiated fragments of regolith, we concluded that the pulverization of material by solar wind was a smooth erosional process acting on dust grains in the lunar regolith of the Seas of Fertility and Tranquillity. By measuring the relative number of coated grains and the thickness of the shells, as well as the distribution characteristics of hidden tracks in grains extracted from different depths with the double core returned by Earth by Apollo 12, we obtained detailed stratographic profiles. We are continually developing the counting techniques in order to use these profiles in selecting different models of lunar soil displacement. We very much wish to compare these models at the landing sites of Luna 16 and Apollo 12, since the sites according to estimates differ from each other by the density of craters, which is an important starting parameter in the theory.

Crystalline inclusions in Luna 16 grains. Luna 16 dust grains differ from those returned to Earth by the Apollo expeditions in that they very often disclose a high density of very small crystalline inclusions. These inclusions are very similar to those observed either in artificially heated dust grains of surface material, or in the grains of breccias 10046 and 10059 from the collections of the Apollo 11 expedition. Therefore, since lunar brecciation quite probably includes also thermal metamorphosis /13/, it is possible that the "ancient" inclusions in Luna 16 grains are the "remnant" of tracks of nuclear particles and that the remnant may have partially undergone annealing during the period of metamorphosis causing the moderate heating of the grains.

From our investigations it follows that the history of the dust grains of Luna 16 regolith would apparently be more complex than the history of Apollo dust grains. At the present time we do not have a good model that could be proposed for this complex history. It may be the following: 1) the dust grains initially were freed from lunar igneous rocks under the effect of micrometeorites impacting against their surface, and then a high density of "solar" tracks was formed in them; 2) then the "individually" irradiated dust grains were compacted into breccias under the effect of a process including metamorphosis, accompanied by moderate heating and transformation of tracks

into inclusions; and 3) finally, the metamorphosed grains, with increasing erosion of the breccias, were released a second time.

Albedo of the regolith. Most of our work consisted in correlating ultramicroscopic characteristics of the finest regolith grains with various properties of the lunar surface material as a whole. Earlier various aspects of these investigations had already been presented /14/. Here we only discuss several new, to our understanding, aspects of the origin of specific features of the lunar albedo based on measurements recently made by A. Dollfus for the same samples of lunar surface material, including also Luna 16 samples that we studied.

The albedo of a lunar surface material sample a priori is a function of four parameters: 1) the proportion of glass /15/; 2) the content of such intensely absorbing ions as titanium /15/; 3) the existence of shells on grain surfaces /16/; and 4) the mineralogic composition of the samples, since pyroxenes absorb more than do feldspars /15/. In collaboration with Doctor O. Eugster /17/, in our laboratory were measured the effect of the first three parameters and discovered only a very decided reduction in the albedo in different samples of surface material returned by the Apollo craft and by Luna 16 with increase in the proportion of grains covered with shells. In this work we also calculated the reflectance of crystalline grains with index of refraction n_1 coated with a layer damaged by irradiation, with index of refraction n_2. Work done by Hines and Arndt /18/ on artificially irradiated crystals and by Pellas /8/ on naturally metamictized zircons showed that in this multidielectric structure $n_1 > n_2$. We showed that this structure can be effective in the absorption of incident radiation due to internal reflection, which leads to a reduction in the reflectance and thus in the albedo in the visible range. Therefore the albedo of samples of surface material taken at four different landing sites apparently correlates with the history of the irradiation of their constituent grains by the solar wind, as was first posed by Gold /16/. This is important for telescopic observations of atmosphereless planets with no magnetic field, like the Moon. /435

Ancient lunar atmosphere and magnetic field. If it is assumed that the "minimum" (approximately 200 AU) thickness of the shells observed in grains of surface material returned by Luna 16 characterizes the reduction in the effective mean-free path of solar wind ions due to their slowing down in the "thin" lunar atmosphere, we get the upper limit of $\sim 10^{-9}$ torr for the mean lunar atmosphere during a period of time in which the grains were subjected to the solar wind on the surface of the Moon at the Luna 16 landing site.

The upper limit of the mean magnetic field (about 100 g) active during the same period of irradiation of the grains on the Moon's surface could be obtained if it is assumed that the thickest shells (approximately 800 AU) on some grains of Luna 16 surface material arose under the effect of high-energy (~3 keV/a.e.m) solar wind ions traversing the possible lunar magnetic field.

We stress that these methods for the study of the "ancient" lunar atmosphere and magnetic field are in the most preliminary stage of development, since they are based on the hypothesis that ultrathin shells on dust particles are layers metamictized under the effect of solar wind, and that the thickness of the coating depends on the energy of the solar wind ions during their penetration. We have discussed them only in order to show their broad possibilities in a study of the "ancient" ambient medium of the Moon or Mars, by employing unusually small samples -- -- weighing approximately 1 mg.

REFERENCES

1. Vinogradov, A. P., "Preliminary Data on Lunar Ground Brought to Earth by Automatic Probe Luna 16," Proc. Second Lunar Sci. Conf. 1, 1 (1971).

2. Borg, J., Durrieu, L., Jouret, C., and Maurette, M., Geochim. Cosmochim. Acta, (1971).

3. "LSPET (Lunar Sample Preliminary Examination Team)," Science 165, 1211 (1970); Science 167, 1325 (1970).

4. Alexandre, K., Camplan, J., Ligonniere, M., Meunier, R., Sarrouy, J. L., Smith, H. J., and Vassent, B., Orsay, Nucl. Inst. Meth. 84, 45 (1970).

5. Price, P. B., and Walker, R. M., J. Appl. Phys. 33, 3400 (1962).

6. Winterbon, K. B., Sigmund, P., and Sanders, J. P., Mat. Fys. Medd. Dan. Vid. Selsk. 37(14), (1970).

7. Kraner, H. W., Schroeder, G. L., Davidson, G., and Carpenter, J. W., Science 152, 1235 (1966); Tarkevich, A. L., Patterson, J. H., Franzgrcte, E. J., Sowinski, K. P., and Economou, T. E., Science 167, 1722 (1970); Lindstrom, R. M., Evans, J. C., Finkel, R. C., and Arnold, J. R., Earth Planet. Sci. Letters 11, 254 (1971).

8. Pellas, P., Mem. Museum Nat. Hist. Nat. 12, 227 (1965).

9. Durrieu, L., Jouret, C., and Maurette, M., "Symposium on Physics, Chemistry and Shape of the Moon," Communication No. 13, Unpublished Proceedings, 1971.

10. Borg, J., Durrieu, L., Jouret, C., and Maurette, M., Earth Planet. Sci. Letters 8, 379 (1970).

11. Frank, L. A., J. Geophys. Res. 75, 707 (1970).

12. Stone, E., Caltech preprint, 1971.

13. Mason, B., and Melson, W., The Lunar Rocks, Wiley-Interscience Pub., 1970; Dran, J. C., Durand, J. P., and Maurette, M., Proceedings of the IAU Symposium No. 47 on "The Moon", 1971.

14. Berg, J., Durrieu, L., Jouret, C., and Maurette, M., Geochim. Cosmochim. Acta, (in press), (1971); Durrieu, L., Jouret, C., Lerculley, J. C., and Maurette, M., Jernkont. Ann. 155, 65 (1971); Bibring, J. P., Durand, J. P., Durrieu, L., Jouret, C., and Maurette, M., submitted to science, 1971.

15. Conel, J., and Nash, D., Proc. Apollo 11 Lunar Sci. Conf., and Geochim. Cosmochim. Acta, Suppl. 1 3, (1970); Adams, J. B., and McCord, T. B., Geochim. Cosmochim. Acta, (1971).

16. Gold, T., Campbell, M. J., and O"Leary, B. T., Proc. Apollo 11 Lunar Sci. Conf., and Geochim. Cosmochim. Acta, Suppl. 1 3, 2149 (1970); Hapke, B. W., Cohen, A. J., Cassidy, W. A., and Wells, E. N., ibid., 2199; see also reference [2].

17. Bibring, J. P., Durrieu, L., Eugster, O., Jouret, C., and Maurette, M., submitted to Earth Planet. Sci. Letters, (1971).

18. Hines, R. L., and Arndt, R., Phys. Rev. 119, 623 (1960).

Center of Mass Spectrometry, Orse

National Center of Scientific Research and Institute of Electronic Optics, Toulouse

National Center of Scientific Research, France

N75 11855

STUDY OF SAMPLE OF SEA OF FERTILITY LUNAR SURFACE MATERIAL BY THE TRACK METHOD

/436

G. Poupeau, G. C. Chatrit, and P. Pellas

Abstract

Tracks in crystals of feldspars, olivines, pyroxenes, and in several fragments of basalts from a sample of Luna 16 lunar surface material was studied. A high track density, exceeding 10^8 cm^{-2}, was found. The tracks were produced mainly by iron-group nuclei of cosmic galactic and solar rays.

Introduction. A study was made of less than 5 mg of fragments of crystals in rocks from sample of L-16-19 regolith No. 118. The material was selected from the layer located at the depth of 20-22 cm (zone V) of the core of Luna 16 lunar surface material.

The size of particles selected for the investigation was limited to the range 100-500 μm. The object of the investigation were initially feldspars, which from the mineral phase-indicators apparently are the best track recording media. Subsequently, other minerals, especially olivines and several pyroxenes, were studied. The track method can be employed only in crystalline indicators whose lattice has not yet been subjected to impact effects or annealing. Thus, feldspars, differing by optical anomalies characteristic of impact metamorphism (with fibrous or more or less glassy structure) are not track indicators. In addition, these same observations were made on several crystals in rocks returned by Apollo 14. It must be emphasized that even in the event that "good" indicators are selected, the results are not indicative for the sample as a whole. This is the first limitation. The second limitation is the maximum track density (cm^{-2}) that we could resolve instrumentally. It is as high as $5 \cdot 10^9$ cm^{-2} when an electron scanning microscope is used.

Results. Individual crystals of feldspars. About 100 crystals were selected for the study. Of these, 20-30 percent could not be indicated owing to defects resulting from impacts. All the rest of the crystals showed a track density higher than 10^8 cm^{-2} (see Figure). This high density was measured in the internal zones of the crystals (after polishing). Actually, most crystals revealed track densities from $0.5 \cdot 10^9$ to $2 \cdot 10^9$ cm^{-2}, in addition, we observed differences in the effectiveness of the manifestation of tracks given the same etching time; these differences showed up in the change of track density as a function of the position of the crystallographic planes in the same oriented surface. This observation apparently indicates that twinning planes often encountered in feldspars must be checked with respect to their effectiveness of track recording.

Pyroxene and olivine crystals. In several clinopyroxene crystals (probably augite) and of olivine the same results were obtained as for feldspars. Actually, track densities for these always exceeded 10^8 cm^{-2}. The highest incidence (as far as we can judge this from the small number of observations) of crystals reflecting gradients of track density could be caused by the zonality of the chemical composition of these minerals, that can locally change the conditions in which the tracks were formed and manifested in these indicators.

Rock fragments. In order to compare the coefficients of irradiation of individual crystals and rock fragments from the same granulometric fraction, the tracks were studied in 34 fragments of basaltic rocks. Some of these fragments were selected because they had angular shapes. The indicators used in all these rocks were feldspars, which in opposition to those taken from the surface material in the form of individual grains prove to be very good crystal indicators.

The cracks were studied in fragments of basalts either in the internal section (after polishing) or in the entire fragment after /437 crushing of the rock. Just as for feldspars taken from the surface material, the track density did not fall below 10^8 cm^{-2} (in the most central zones of fragments) and in most cases were approximately constant within the same fragment. Still, changes in density from 10^8 to $3 \cdot 10^9$ cm^{-2} were observed in some fragments. In particular, for one basalt fragment (500 μm in diameter), a track density exceeding $3 \cdot 10^9$ cm^{-2} was established (at an external facet), but etching, even though very brief, damaged the plane of observations to the extent that no good estimates could be obtained.

Conclusion. Owing to the small content of uranium ($\leq$ 1 ppb) in the mineral phases studied: feldspar, olivine, and pyroxene,

most of the tracks observed must be attributed to iron-group ions of cosmic galactic and solar rays. However, neither can we leave unmentioned the by no means negligible contribution made by the spontaneous decay and the induced radioactivity as a consequence of prolonged irradiation by cosmic rays, traces of this radioactivity being observed in crystal cracks. We also noted that the gradients of track densities, very easily determined in meteorites enriched with inert solar gases, in contrast is very difficult to disclose in severely irradiated lunar fragments.

On the other hand, the fact that each crystal or fragment studied had a density exceeding or equal to 10^8 cm^{-2} compel us to assume that all these grains underwent irradiation to a shallow depth (less than 1 cm) in the lunar surface material. Therefore, the sample of surface material studied could be one of the most irradiated regoliths if it is compared with the regoliths obtained from other lunar regions studied thus far. Actually, among the numerous samples of surface material taken by Apollo 12, only two: 12028,51 [1] and 12042,43 [2] have the same content of crystals with track density $\geqslant 10^8$ cm^{-2}.

Our observations agree with those by Maurette [3], who, based on a study of the finest grains ($\leqslant 10$ μm) of the same Luna 16 sample, concludes that it must be one of the most irradiated. From this standpoint, it is of interest to note the geographical location of the Luna 16 landing. In contrast to Apollo 11 that landed far from the highlands, or even the Apollo 12 section, which is much closer to the highland territories, the Luna 16 landing site is in a bay of the Sea of Fertility surrounded by a highland locale. Therefore, a the Luna 16 landing site the highland influxes must have been more significant. The results obtained for sample No. 118 of Luna 16 by Allegre et al. [4] show that most of the fine surface material must have been of "exotic origin". Finally, the content of elements in surface materials analyzed by A. P. Vinogradov [5], Allegre et al. [4], and Eugster [6] are characteristic of bedrock and apparently reflect the primary character of the highland rocks near the Luna 16 landing site.

Tracks of cosmic rays in feldspar crystal from basalt fragment in Luna 16 core.

REFERENCES

1. Arrhenius, G. et al., Proc. Apollo 12 Lunar Sci. Conf., Preprint, 1971.

2. Crozaz, G., Walker, R. M., and Wolum, D., ibid.

3. Maurette, M., "The High Resolution Irradiation Record of the Finest Luna 16 Duct Grain," Preprint, 1971.

4. Allegre, C. J., Birck, J. L., Loubet, M., and Provost, A., "Rb^{87}/Sr^{87} Age and the Content of K, Rb, Sr, Ba and Solar Wind Rare Earths in the Sea of Fertility (Moon), Reported on the Luna 16 Soviet Expedition," C. R. Acad. Sci., Paris 273 D, 779 (1971).

5. Vinogradov, A. P., "Preliminary Data on Lunar Ground Brought to Earth by Automatic Probe Luna 16," preprint, Proc. Apollo 12 Lunar Sci. Conf., 1971.

6. Eugster, O., "Concentrations of Li, Be, and Ti, and Isotopic Composition of Li, B, and Mg," Preprint, 1971.

National Center of Scientific Research and Mineralogic Laboratory of Museum, Paris, France.

N75 11856

STUDY OF RADIATION DAMAGE AND STRUCTURE OF LUNA 16 SAMPLE PARTICLES USING HIGH-RESOLUTION ELECTRON MICROSCOPES

/444

J. Borg, D. Durrieu, C. Jouret, L. L. Kashkarov, M. Maurette, and P. Moris

Abstract

Using an electron scanning microscope and a high-voltage microscope, a study was made of the radiation damage and structure of micron-sized grains and grains separated from the 200-mesh fraction of the L-16-19 surface material sample. Then the structural features were compared with those found by studying with the same techniques grains separated from 20 different samples of lunar dust taken from the Apollo 11, Apollo 12, Apollo 14, and Apollo 15 collections.

The L-16-19 sample is similar to the most intensely irradiated samples returned to Earth by Apollo craft, since it contains:

1) very rounded grains of micron-sized dust with very high track density (Fig. 1), coated with ultrathin layers of amorphous material (Fig. 2), most likely formed under the effect of the "ancient" solar wind on these grains; and

2) a large number (about 70 percent) of feldspar grains in the 200-mesh fraction characterized by a density of etched tracks of more than 10^9 tracks/cm^2 on the internal surfaces obtained after polishing; these tracks were observed either directly by examination under the scanning electron microscope, or by the preparation of surface replicas and their study at 100 keV with an electron microscope (Fig. 3).

With the exception of these features of similarity, the grains of the sample L-16-19 evidently differ altogether from the grains isolated from Apollo dust samples. Here the characteristic features are:

1) a large fraction of the micron-sized grains either with small crystallites from ~ 50 to ~ 1000 AU in size, or else yielding electron diffraction patterns characterized by a small number of diffraction centers (Fig. 4); and

2) a large fraction (~50 percent) of grains in the 200 mesh fraction revealing amorphous properties when observed in polarized light. Nonetheless, investigations in a scanning electron microscope revealed that these grains actually are aggregates of small crystals and glass fragments (Fig. 5), and observations in a high-voltage electron microscope of micron-sized fragments formed when these grains are crushed from the 200 mesh fraction often disclosed very high track densities ($\gtrsim 10^{10}$ tracks/cm^2) throughout the grain volume.

/445

Fig. 1. Microphotographs of micron-sized grains of lunar dust taken at 1 MeV by dark-field method. The grains in Fig. 1 a-d were isolated from samples 1084, 12070, 14259, and L-10-19, respectively. These grains are characterized by a high density of nuclear particle tracks, often exceeding 10^{11} tracks/cm^2, and appear as sharp lines.

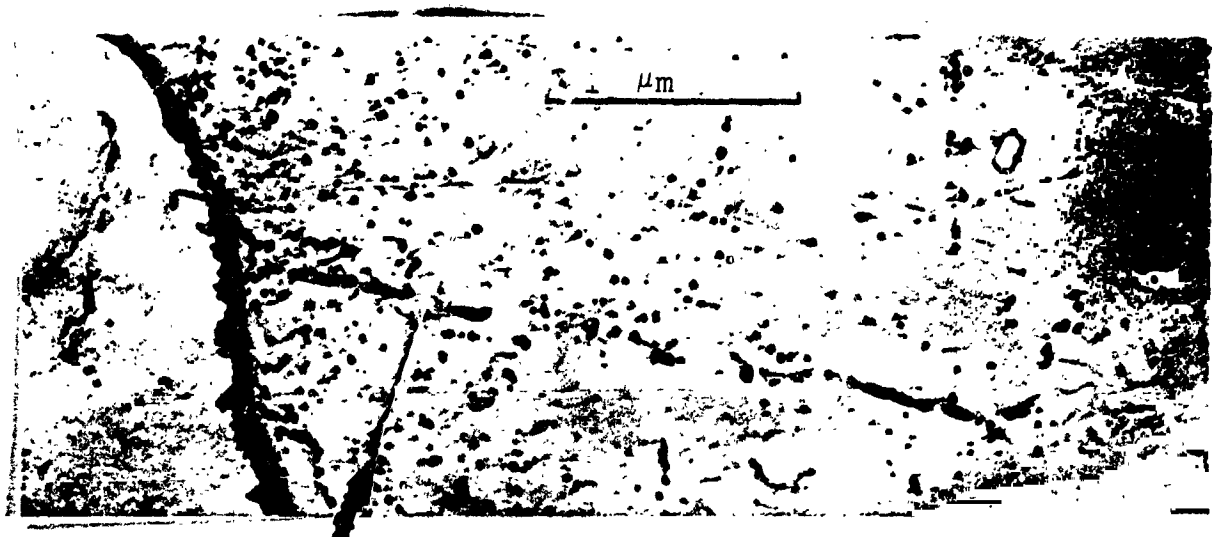

Fig. 2. Microphotograph of carbon replicas with leached section of feldspar grain from the 200 mesh sample of the lunar dust sample L-16-19, taken at 100 keV by dark-filled method. The leached tracks appear as thin openings with entering black arrows. Study of the dependence track density in the grain on depth shows its marked drop at a depth of about 2 μm. This drop generally indicates the existence in cosmic space of low energy nuclei ($E < 300$ keV/a.e.m), which have a very short path in silicates.

Calibration experiments show that crystallites in the finest-grained fraction of L-16-19 surface material generally are thermally metamorphized tracks [thermally annealed tracks] and artificially radiation with high doses ($\gtrsim 10^{16}$ ions/cm^2) of low-energy α-particles ($E \lesssim 30$ keV/a.e.m) and argon ions show that the well-defined lattice disturbances observed in micron-sized grains from the L-16-19 sample and the Apollo 14 sample 14249 can be caused by their more intense radiation by fluxes of low energy nuclear particles. Finally, qualitative analysis conducted by means of an electromicron analytic attachment to a scanning electron microscope suggested that the grains comprising "amorphous" aggregates from the 200 mesh fraction have analogous composition, thus indicating that these aggregates are most likely devitrifed glasses, and not "lunar microbreccia" formed through the sintering of lunar dust particles.

Thus, it appears possible that the sample L-16-19 dust consists of two surface material constituents: the "ordinary" constituent representing about 50 percent of the grains very similar to the most irradiated and eroded samples of surface material returned at present time to Earth by the Apollo spacecraft, and an "exotic" constituent consisting of grains characterized by even higher concentration of radiation disturbances and a more complex history

/446

Fig. 3. Microphotographs of micron-sized grains of lunar dust coated with a very thin layer of amorphous substance, represented by dark crusts around the grains, taken at 1 MeV by dark-field method. Dust particles in Fig. 2 /Fig. 1 is what is intended -- translator/ a-d were isolated from samples 10084, 12070, 14259, and L-16-19, respectively. /447

Fig. 4. Electron diffraction pattern of dust grain of Luna 16 sample, at 1 MeV. Picture shows serious disturbances in crystal lattice of grain, leading both to sharp decrease in total number of electron diffraction centers, as well as in total scatter of diffusing electrons, imposed on the diffraction centers.

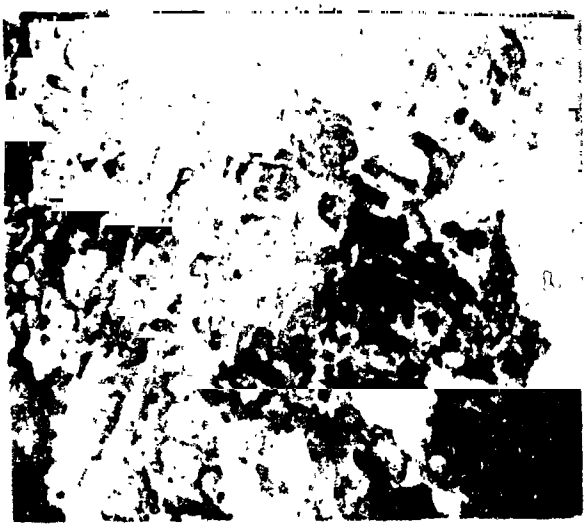

Fig. 5. Polished section of "amorphous" grain from 200 mesh fraction of sample L-16-19 observed in scanning electron microscope after weak chemical etching of grain. This grain doubtless is an aggregate of small crystals and glass fragments, and its constituent grains are characterized by very high track densities of nuclear particles

of thermal metamorphism. Our preliminary observations, with the exception of Apollo 14 sample 14259, showed that this constituent is usually considered less widespread in samples of surface material from the Apollo landing sites.

These different characteristics of dust collected in the Sea of Fertility region must first of all be confirmed, by investigation of samples taken from different depths in the core of Luna 16 surface material, and by an attempt to more carefully find the possible "exotic" constituent in the Apollo samples, as well as by attesting that the "amorphous" aggregates from the 200 mesh sample are actually devitrified glasses. Then these features must be used to interpret the very complex history of the regolith by study of Luna 16 grains. It is probable that they are characterized by a considerably longer time of occurrence in the surface layers of the regolith, as well as by the broader transformation of the grains

into lunar breccia. The latter was subsequently eroded during the bombardment of the surface by micrometeorites or by being "reground" during mixing.

The proof that low-energy particles exist in space must be found, that is, particles with energies intermediate between E = = 1 keV/a.e.m (characteristic of solar wind ions) and E ≈ 300 keV/a.e.m (characteristic of the lowest-energy nuclear particles in cosmic rays). Particles of the latter type have thus far been found in cosmic rays during solar flares examined with satellite-mounted instruments.

Center for Mass Spectrometry, Orse, and the Institute of Electronic Optics, Toulouse

National Center for Scientific Research, France

Order of Lenin Institute of Geochemistry and Analytical Chemistry imeni V. I. Vernadskiy, USSR Academy of Sciences, Moscow

Institute of Physical Chemistry of the Committee on Atomic Energy, Saclay, France

N75 11857

ABSOLUTE AGE OF LUNAR REGOLITH MATERIAL FROM THE SEA OF FERTILITY

A. P. Vinogradov, and Yu. M. Artemov

Abstract

By averaging the absolute age of lunar regolith materials from the Sea of Fertility for the fine regolith fraction (finer than 0.083 mm) from the core zone V, an age of $4.65 \cdot 10^9 + 0.4 \cdot 10^9$ years (2 σ) was obtained, employing as the primordial Sr^{87}/Sr^{86} ratio 0.69884 (ADOR). Also close to this age value is the age estimate based on the Pb^{207}/Pb^{206} ratio. Using the value 0.69898 (BABI) as a primordial Sr^{87}/Sr^{86} ratio reduces the calculated age of the fine regolith fraction to $4.25 \cdot 10^9$ years. The fine fraction of lunar regolith from the Sea of Fertility is also characterized by a minimum addition of radiogenic Sr^{87}, a minimum Rb/Sr ratio, and a maximum K/Rb ratio compared with analogous lunar material from other points.

For the fraction of inequigranular gabbro and the more feldspathic portion of the material separated from this same fraction, the age of $3.5 \cdot 10^9 \pm 0.6 \cdot 10^9$ years (2 σ) was obtained by the Rb-Sr isochronic method (for rock and mineral from rock), with the primordial value of the Sr^{87}/Sr^{86} ratio of 0.6991 (0). This age corresponds to the time of crystallization of individual mineral phases of rock. Based on the studies made, it was concluded that the age of $4.4 \cdot 10^9 - 4.7 \cdot 10^9$ years corresponds to the time of differentiation of primordial lunar material and that the age of about $3.5 \cdot 10^9$ years corresponds to the age of the maximum melting of the bedrock of the mare lunar crust. The regolith of mare provinces, as apparently also the regolith of the highland regions, was formed mainly from the local rock on which it lies.

From lunar materials returned by the Luna 16 automatic station, we investigated several individual samples. A sample of the fine regolith fraction was taken from zone V of the drill core (the fraction finer than 0.083 mm) [1, 2]. The gabbro fraction (composite, inequigranular) was assembled from different sections of the core. From it, without crushing, the lighter, predominantly feldspathic particles with dark-colored inclusions were visually separated, having a total weight of about 10 mg.

The chemical treatment of these samples was carried out by the usual scheme [3-6]. The samples were decomposed with a mixture of HG and $HClO_4$ acids; in one instance a parallel decomposition was also carried out with one of the weighed samples of fine regolith using a mixture of HF and HCl, with appropriate cautionary measures [7], which yielded, from an estimate of results, an identical completeness of decomposition. All decomposition operations were carried out in teflon apparatus. Enriched isotopic tracers Sr^{84}, Rb^{87}, and K^{41} were used to determine the amounts of Sr, Rb, and K by isotopic dilution; the tracers were usually added before decomposition of the samples. The tracers were not added to aliquot weighed amounts of the samples in those cases when strontium were separated from them for the purpose of measuring the isotopic ration Sr^{87}/Sr^{86} in order to ensure the highest possible experimental purity.

For the ion exchange-chromatographic separation of the elements analyzed, use was made of Dowex 50BX8 ion exchange resin, 200-400 mesh. The total length of the system of columns was about 50 cm. Elution was performed with HCl solutions of different normalities, by washing the fractions in separate columns; in different cases 0.6 N HNO_3 and 1.0 N HCl were used. The reagents employed for analytical purposes were previously purified.

The mean value of the blank determinations for the total volume of the analytical procedures, when calculated on a weighed sample of 100 mg, was $1.5 \cdot 10^{-8}$ g for Sr, $4 \cdot 10^{-9}$ g for Rb, and $2 \cdot 10^{-6}$ g for K.

The isotopic ratios Sr^{87}/Sr^{86} were measured with a model MI-1311 mass spectrometer, with a central trajectory radius of 300 mm, using the single-beam method, followed by interpolation of the measured ion currents [8, 9]. Continuous sweep of the magnetic field at a variable rate was used; the time to record the region of the maximum (plateau) ion current was more than 9 τ in all cases. The exit slit of the ion source was 0.05 mm. Strontium was ionized with a preconditioned central tantalum strip. A d.c. amplifier with an input impedance of $5 \cdot 10^{11}$ Ω was used in measuring the ion current. The measurements were taken at a fixed

/456

Sr^{87} ion current level $\simeq (6\text{-}5)\cdot 10^{-13}$ A $\pm$ 10 percent. A model ETsPV-3 digital voltmeter was used for recording. The inclusion in the instrument of a parallel amplification channel with an input impedance of $1\cdot 10^{12}$ Ω permitted additional monitoring during the experimental period of the spectrum for Rb at the level of 1:4000 relative to Rb^{85}/Sr^{87}. In the working measurement mode, the Sr ion beam was virtually free of other ions. Vacuum conditions in the working mode were not poorer than $3\cdot 10^{-8}$ mm Hg from the readings of calibrated magnetic-ionization transducers; in the steady working regime, the vacuum indicators were unaffected by the operation of the ion source or by heating of some sections of the instrumental system. The level of resolution, relative to the possibility of imposing an additional signal on Sr^{87}, was checked by measuring the ion current level in a prepared preparation of the isotopes Sr^{86} and Sr^{84}, segregated at the level of working intensities, and the Sr^{88}/Sr^{86} ratio in ordinary strontium in the vicinity of mass 85. This level, under the working conditions of measurement, was better than 1:9900 with respect to the possible level of the ion current for the mass 85 to the half-sum of the intensities of the neighboring peaks. The linearity of the final result for the Sr^{87}/Sr^{86} ratio normalized to the Sr^{86}/Sr^{88} ratio of 0.1194 was checked by the method of additions (by comparing the Sr^{87}/Sr^{86} values calculated from the weighted values of mixing, with the measured Sr^{87}/Sr^{86} values) for the range of values from 0.7032 to 0.7144. This verification showed that the linearity in this region is not poorer than the reproducibility of the measurements. The result of a direct verification of the linearity by mixing an aliquot sample of the fine regolith fraction with a weighed amount of a solution containing strontium, Aymer and Amund standard, is shown in Fig. 1. The estimate of the reproducibility of our measurements of Sr^{87}/Sr^{86} (normalized) can be based on six independent measurements of this standard, made during this study. It is at the level $\pm$ 0.0002 (2σ) in units of the Sr^{87}/Sr^{86} ratio for an individual independent measurement. The mean value we adopted for Sr^{87}/Sr^{86} normalized for the Aymer and Amund standard was 0.70800 $\pm$ 0.00007 (2σ) with a 95 percent confidence interval, where our uncorrected instrumental value was somewhat less, but virtually within the limits of this error. For the Sr^{86}/Sr^{88} ratio our mean instrumental value was close to the adopted value of 0.1194 ($\simeq$ 0.11945). For the Sr isolated from coral (Mariana Island), the value of Sr^{87}/Sr^{86} was 0.7090 $\pm$ $\pm$ 0.0001. It should also be noted that the experimental verification showed in our case that the variation of the measuring-complex

parameters in the direction of a further rise in sensitivity is reflected in the reproducibility of the results. In the MI-1311 mass spectrometer used to measure the isotopic composition of Sr, no preparations that could have contained Rb of mixed isotopic composition had been introduced and the measurements were taken only at a signal for the mass 85 not different from the zero level. During the period preceding the measurements, the mass spectrometer was checked for all parameters, as well as being adjusted, and several changes were made in some assemblies aimed at optimizing the analytical characteristics. The ion source was adjusted in the series circuit with experimental selection of the optimal conditions of focussing for the geometry of the ion beam, axial focussing, and the like /9/. /457

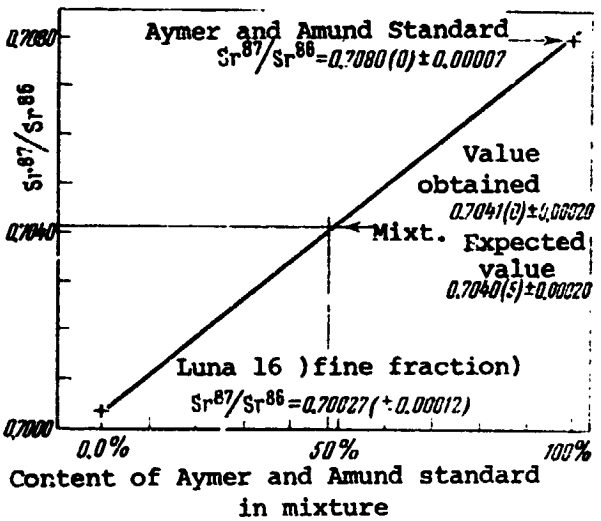

Fig. 1. Plot of check of linearity of Sr^{87}/Sr^{86} (normalized) measurements

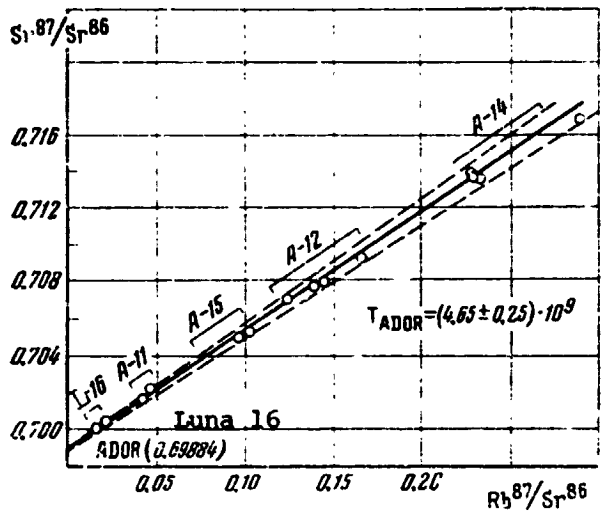

Fig. 2. Plot of correlation dependence of K/Rb on measured Sr^{87}/Sr^{86} ratio for fine regolith fraction from various lunar territories (Luna 16, Apollo 11, 12, 14, and 15)

We used a modernized, model MS-4 mass spectrometer (with a 200 mm radius) in measuring the isotopic ratios of K, Rb, and Sr in the isotopic dilution method; Sr was ionized with a central tantalum strip, and K and Rb -- with a tungsten strip. The ion sources with built-in strips were preconditioned and then checked for purity for these elements in a mass spectrometer. Our reproducibility of the measurements of the amounts of K, Rb, and Sr by the isotopic dilution method was 1.5-2.5 percent for Sr and Rb, and 2-3.5 percent for K within the limits of a 95 percent confidence interval. The precision of the Rb and Sr determinations was poorer for the analysis of the sample from the essentially feldspathic fraction (Table 1), since the measurement was made on a minimum amount of the material (most of the sample was used in

the aliquot, from which the Sr^{87}/Sr^{86} ratio was measured) in conditions of shortened chemical procedures and appreciable incompleteness of separation.

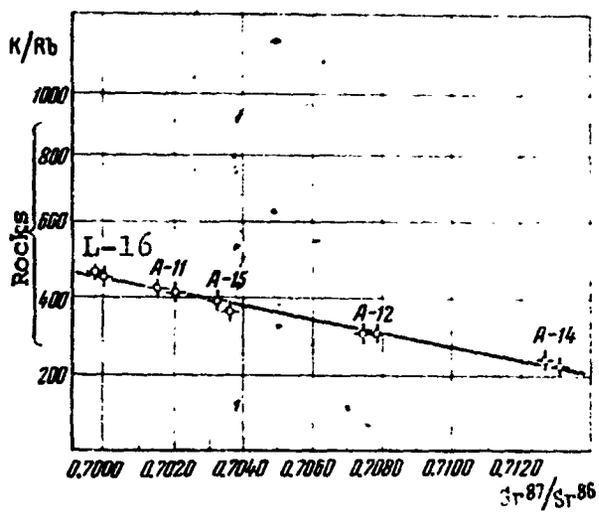

Fig. 3. Isochronic Rb-Sr plot for fine fraction of lunar regolith from different lunar territories (Luna 16, Apollo 11, 12, 14, and 15)

The isotopic ratios we adopted in the calculations for the method of isotopic dilution for which the correction was made are as follows: $K^{39}/K^{41} = 13.53$; $Rb^{85}/Rb^{87} = 2.591$; and $Sr^{84}/Sr^{88} = 0.006748$. Our instrumental value of K^{41}/K^{40} for the reagents was 561 ± 11 (2σ). The sample of the Aymer and Amund standard was obtained by us from the laboratory of the Geological Service of Canada through V. A. Grinenko.

Content of K and Rb. K/Rb ratio and the primordial Sr^{87}/Sr^{86} ratio. An examination of several problems associated with the variation of K/Rb ratio and the content of K and Rb in different lunar materials is important for an understanding of processes leading to the formation of the regolith and rocks encountered on the lunar surface. The Rb content in samples of the fine regolith fraction as a rule is higher than in the samples of basalts and gabbro returned from these same regions. An exception to this is represented by the basalts of the high-potassium group (Apollo 11) and rock samples, provisionally denoted as krip, differing by their high relative content of K, Tr, and P [6, 10-13].

From the various possible correlation constructions, in the plot (Fig. 2) we showed the variation in the K/Rb ratio relative to the measured ratio Sr^{87}/Sr^{86} in samples of the fine fraction of the lunar regolith from different situations (Luna 16 and Apollo collections) based on the results of a generalization of the corresponding data [12-18]. The correlation between these values is quite appreciable. The general range of the K/Rb ratios in the fine regolith fraction is 260-470. The range of the K/Rb ratios for the lunar rocks investigated gives an interval of values 260-900, including for the group of lunar basalts and gabbro, among which as we know there are two types of rock with a ratio of about /459

750-900 (mare basalts of Luna 16 and the Apollo collections) and with a value of about 400-500 (nonmare basalts of Apollo 14 and Apollo 12 and high-K basalts of Apollo 11) /6, 10, 12, 14, 19/. Lower values of the K/Rb ratio are found for several other rocks, for example, of the krip type.

TABLE 1. RESULTS OF MEASURING SAMPLES RETURNED BY LUNA 16 AUTOMATIC STATION

Sample	Content in parts per million			K/Rb	Rb/Sr	Sr^{84}/Sr^{86}	Rb^{85}/Rb^{87}	K^{41}/K^{40}	Rb^{87}/Sr^{86}	Sr^{87}/Sr^{86} *	Sr^{87}/Sr^{86}, primordial	age, billions of years
	K	Rb	Sr									
1. Fine fraction												
a) regolith (layer V)	1015	2.2	.278	460±20	0.0079	0.00678± ±0.00010	2.59±0.02	550±18	0.02310± ±0.00090	(0.7004± ±0.0002)	0.69884	4.65±0.40
b) as above	993	2.08	283	475±12	0.0073	–	–	–	0.02154± ±0.00060	0.7003 0.7002 0.7003 Cp. 0.7002(7) ±0.00012	0.69836	4.25±0.40
2. Composite fraction of inequigranular gabbro	1250	1.65	315	800±90	0.0052	0.00680± ±0.00010	–	–	0.01510± ±0.00060	0.6999 0.6998 0.6998 Cp. 0.6998(5) ±0.00012	0.6991(0) 0.6991(0)	3.5±0.6 3.5
3. Light, predominantly feldspathic portion, segregated from the inequigranular gabbro fraction	–	1.01	750	–	0.0013		–	–	0.00400 ±0.00060	0.6993(0) ±0.00015		

* All ratios are given with the 95 percent confidence interval. The age is calculated based on the value $\lambda_{Rb^{87}} = 1.39 \cdot 10^{-11}$ years^{-1}.

/Footnotes to Table 1 continued on following page./

/Continuation of footnotes to Table 1 on preceding page./

2* The errors in the determination of elemental content are totaled and are reduced to the errors of the corresponding ratios for K/Rb and Rb^{87}/Sr^{86}. The content of K for the gabbro fraction is taken from a preceding paper /1/; the K/Rb ratio for this fraction was calculated in accordance with a 10 percent content of the light-colored portion in the unseparated gabbro fraction.

3* The Sr^{87}/Sr^{86} ratios were normalized with respect to Sr^{86}/Sr^{88} = = 0.1194. Sr^{87}/Sr^{86} for the Aymer and Amund standard = 0.7080(0). For the light-colored part of the gabbro fraction, the error in the Sr^{87}/Sr^{86} ratio is statistical.

Remark. This study was prepared for publication in the collection by 10 March 1972.

The examination of questions concerning the Rb-Sr age estimates for the fine regolith sample and in general outline concerning the age aspects of lunar petrology is associated with a preliminary fundamental decision on the initial (primordial) Sr^{87}/Sr^{86} ratio used in the calculations for the one-stage model.

As we know, based on a high-precision study determining the Rb-Sr age by the method of seven achondrites /20/, the primordial Sr^{87}/Sr^{86} ratio was found, 0.69898 ± 0.00003 (revised estimates by the authors), subsequently referred to by the acronym BABI. This value is used at present as the initial, essentially universal point in calculating the Rb-Sr age characteristics of the lunar regolith in numerous studies /6, 10, 17, 21-23/. It should be pointed out that the primordial Sr^{87}/Sr^{86} ratio was determined also for several other meteoritic materials /24/, and values differing from the BABI value were found. In this respect, we must examine even though briefly, our attitude toward this problem.

To estimate the validity of adopting BABI (or, alternatively, the possibility of adopting any other specific value obtained from data on other meteorites) as the primordial value corresponding to the time of accretion of protoplanetary material, the following are essential:

a) the isochronic age for seven achondrites with the primordial BABI value of 4.39 ± 0.26 (2) billion years /20/. This value agrees with the age of 4.6-4.7 billion years as the present-day estimate of the time of accretion, at the limit of confidence;

TABLE 2. CONTENT OF CERTAIN ELEMENTS IN VARIOUS SAMPLES OF THE FINE LUNA 16 FRACTION (BASED ON DATA OF DIFFERENT AUTHORS)

Author	Layer, sample	Content in ppm					Ratio			T_{BABI}^{Rb-Sr}, billions of years
		K	Rb	Sr	Pb	U	K/Rb	$\frac{Rb}{Sr} \cdot 100^*$	Sr^{87}/Sr^{86} *	
1. Papanastassiou and Wasserburg, Tera et al. [12,21,32]	A-2, A2-3								0,70009	
	A-39	844	1,79	271	0,95; 1,15	0,34	470	66,1	0,70015	
	G-2,G-50	—	1,89	272	0,78	0,24	—	69,5	0,70016	4,17
2. Allegre et al [23]	V	1047	2,45	294	—	—	440	83,3	0,70042	4,20
3. Vinogradov and Artemov (present study), Vinogradov [1, 2]	V	1015	2,2	278	1,0	0,25	460	79,4		4,25
		993	2,08	283			475	73,2	0,70027	
4. Nyquist et al. [31], Hubbard et al. [13,31]	A-3, A-37	976	1,82	280	—	0,31				
			1,87			0,38			0,70011	
							520	65,1		4,33
	G-3, G-47	935	1,90	296						
		1077	1,94	304	—	0,39			0,70015	
5. Philpotts et al. [14]	A-4	850	1,85	244	—	—	460	75,8	—	—
	G-4	880	1,90	271	—	—		70,1		
Mean estimates		950	2,0	280	—	0,32	475	72,0	0,70020	4,25

* Sr^{87}/Sr^{86} ratios were corrected according to the estimates made by authors for the values compared.

b) depending on the sample grouping of data on the seven achondrites, values of the primordial Sr^{87}/Sr^{86} ratio were obtained both coinciding with BABI, as well as differing from it. For example, for the three achondrites with a maximum Rb content this value is larger than BABI;

c) in disagreement with the BABI value, the primordial Sr^{87}/Sr^{86} ratio was found for the rare achondrite Angra do Reis (abbreviated as ADOR), also differing in that in spite of the extremely low K and Rb content values, the K/Rb ratio for it is close to the chondritic value [25, 26];

d) the analyses of isotopic ratios with respect to oxygen for the achondrites do not agree with the representation of their typical primordial level [27, 28]; and

e) we should also note that using meteoritic data for these purposes involves the assumption that there was no effect of any kind when they came into contact with our planet, which can be reflected in the parameters of the study, which in the general case is not obvious.

From the foregoing it more likely follows that there are no adequate grounds for the predominant acceptance of the primordial Sr^{87}/Sr^{86} values being equal to BABI, even if it is in the interval of values satisfactorily agreeing with the estimates for a specific factual situation.

We also must pose the question of whether there are grounds for accepting some Sr^{87}/Sr^{86} ratio as the initial value for all the subsequent processes and a single ratio characterizing the system (solar) or some of it, with a possibility of reducing the corresponding data to it. In other words, whether there are grounds for accepting a value that is essentially taken as the universal constant for the above-given scope, where it is not important based on the consequences whether this assumption is made explicitly or whether introduced by our calculations. We assume, without here going into further details that are essentially hypothetical, but limited to indicating the possible duration of the stage -- the stage of the protoplanetary cloud-accretion, that the existence of a single ratio as a function of the corresponding chemical homogeneity in the last point is more likely to be improbable. As for the problem concerning the level of the portion of the system, for example, meteorites-Earth-Moon, or at the limit, a separate body, this problem remains open, and only with perspective of further investigations can it find its solution. An interesting consequence from the nonhomogeneous model for a separate body with allowance for its mass would be the possible focal primordial development of the melting process. For a body with the mass of the Moon, the preservation of relicts of this inhomogeneity can be possible to a certain extent.

Quantitatively, the foregoing discussion touches on the level /460 of variation in the value of Sr^{87}/Sr^{86}, most likely not more than three units in the fourth decimal place, that is, at the level of 0.3-0.5 percent and smaller.

Age data. Turning to an examination of these results, in the light of the foregoing we would wish to note that by subsequently using the values of BABI and ADOR as the primordial (in the general sense) Sr^{87}/Sr^{86} ratio in our calculations, we have in mind principally the alternative nature of the age estimates as a function of the primordial Sr^{87}/Sr^{86} values adopted in the calculation

already widely utilized in the literature, but in the general case we do not assume that any of these specific ratios used as being definitively established in advance as the primordial value.

From the data given in Table 1 for the fine fraction of the Luna 16 regolith and plotted also on the composite graph (Fig. 3), it can be concluded that this material as the lowest radiogenic admixture Sr^{87}, the minimum values of K and Rb content, the maximum K/Rb ratio, and the Sr content that is the maximum for the fine regolith. These factors make the material of the fine fraction of the Luna 16 regolith critical for estimates of the lunar regolith in the system age-primordial Sr^{87}/Sr^{86} ratio. Actually, for the fine regolith, the variation in the primordial Sr^{87}/Sr^{86} ratio within the range 0.6990-0.6988, from data based on Apollo materials, does not significantly change the age estimates. At the same time, adopting BABI or ADOR for the fine Luna 16 regolith is reflected in the calculated age in a significant way, especially if one considers that the alternative age estimates for this comparison will have a lower error than the tabulated values, since the actual BABI and ADOR values can be used as point values. We should also not fail to note the good agreement between the results of age determination in the measurement of the fine Luna 16 regolith (Fig. 3) based on the independent data of four laboratories. Our data for the fine regolith now discussed in greater detail, has already been reported by one of the authors [1, 2], where the age estimate of $4.25 \cdot 10^9$ years was made for the case of adopting the primordial BABI value, and where $4.85 \cdot 10^9$ years was the maximum value from a calculation based on ADOR, on the assumption that our results for Sr^{87}/Sr^{86} from measuring the Aymer and Amund standard could be understated by $\simeq 0.1$ percent compared with certain other laboratories [29, 30]. It should also be pointed out that the recent discussion [21] on the possible discrepancies between interlaboratory comparisons is doubtless valid overall in this situation, however it is scarcely essential owing to the virtual identity of the age characteristics obtained by the different laboratories, and for material with variable content values of Rb, Sr, and several other elements in different sections of the verification [1, 2, 21, 23, 31]. From this there derives the noncomparability of the results obtained for the fine Luna 16 sample with respect to the age values based on the primordial Sr^{87}/Sr^{86} ratio equal to BABI, both with Rb-Sr age estimates for the fine Apollo regolith, as well as with the data of the U-Th-Pb method for the fine Luna 16 regolith, including age data from our laboratory for the Pb^{207}/Pb^{206} ratio. The latter was obtained from analyzing filtrates of the same material, from which the Rb-Sr parameters were determined. The Pb^{207}/Pb^{206} ratio is close to $4.5 \cdot 10^9$ years [1, 2]

and is characterized by low, somewhat less than 60, corrected Pb^{206}/Pb^{204} ratio. Even higher age estimates within the range $(4.7\text{-}4.8)\cdot10^9$ years were obtained in another, high-precision study [32].

Data collected in Table 2 show that differences in the content values of various elements in the fine Luna 16 regolith exist both between layers as well as between samples in the same layer, and also with respect to data obtained from the same laboratory, that is, the observed differences in the elemental content values given in the table cannot be accounted for by a discrepancy only in procedures. Variations in the Rb/Sr ratio for samples of the fine Luna 16 regolith are definitely larger than, for example, for sample 12070 (Apollo 12), where of the six regolith samples examined by laboratories, only the results from one (Papanastassiou and Wasserburg) differed from the others [10, 19, 22, 33-35]. We should also specifically note the high level of agreement between the results of calculated age determinations by the Rb-Sr method, with a scatter in values within the limits of 4 percent, with a mean $T_{BABI} = 4.25\cdot10^9$ years. All this indicates most of all that the Luna 16 regolith is a system chemically mixed, but exhibiting a quite homogeneous age characteristics.

Our age determinations made by the Rb-Sr method in rock (inequigranular gabbro) and the predominantly feldspathic portion, examined as a mineral fraction, separated from the same gabbro fraction gave an isochronic age of $(3.5 \pm 0.6)\cdot10^9$ years. The inequigranular gabbro fraction was assembled from different core sections and in this sense is an averaged material to some extent. The lighter-colored, essentially feldspathic fragments, but containing dark-colored inclusions, with a total weight of about 10 mg were separated from the gabbro fraction by hand sorting, without crushing, and considering this circumstance, the gabbro fraction must be considered to some extent, in spite of the sampling carried out, as representative (matrical) for its interpretation as a rock overall. Naturally, the material selected in this manner can admit of different interpretations on the interrelatedness of constituents, however this circumstance was substantially verified by the analytical data as such, and the possible averaging of the material to some extent can prove useful for interpretation. In finding the primordial Sr^{87}/Sr^{86} ratio in this case, we used both auxiliary estimates of this ratio made for the low-potassium group of Apollo 11 basalts similar in situation, and several other parameters [29, 35, 36]. /461

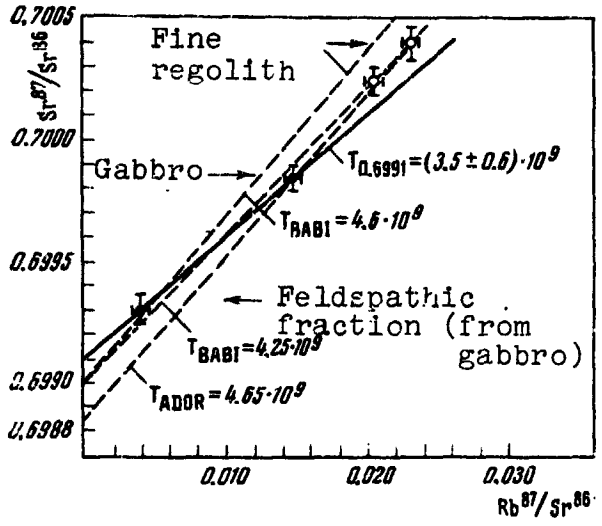

Fig. 4. Isochronic Rb-Sr plot for the fine regolith fraction, gabbro fraction, and feldspathic fraction of gabbro (materials of the Luna 16 station). The route mean square errors of measurement are indicated in the graph.

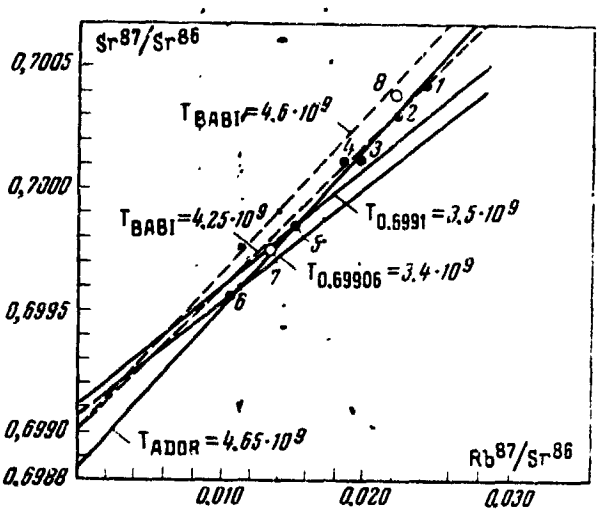

Fig. 5. Isochronic Rb-Sr plot for Luna 16 station materials studied, based on different data
1. Fine Luna 16 regolith /23/
2. Fine Luna 16 regolith (present study)
3. Fine Luna 16 regolith /21/
4. Fine Luna 16 regolith /31/
5. Luna 16 gabbro (present study)
6. Luna 16 basalt /21/
7. Apollo 11 basalts of low-potassium group /26, 29/, mean of four
8. Apollo 12 basalts with K/Rb ratio ≃480 /22, 35/, mean of six.

This permitted estimating, with a smaller error, the possible fluctuation in the primordial Sr^{87}/Sr^{86} ratio that was found (0.69910 ± 0.00006). By comparing the age value we found with data obtained by other authors by the K-Ar and Rb-Sr isochronic methods for the minerals ($3.45\cdot10^9$ and $3.42\cdot10^9$ years, respectively), we can conclude that the level of agreement of these data is satisfactory /21, 37/. Also quite close are the estimates of the primordial Sr^{87}/Sr^{86} ratios (0.69910 and 0.69906). These data are shown in Figs. 4 and 5 for the rocks. Calculation of the age for the Luna 16 rocks based on the BABI primordial value yielded age estimates of $(4.0\text{-}4.1)\cdot10^9$ years. These estimates are lower than those for the situation of Apollo 12 and Apollo 14, and are more closely comparable with the estimates for several Apollo 11 basalts. At the same time, as can be seen from Fig. 5, agreement relative to the isochrons is observed for the primordial Sr^{87}/Sr^{86} ratio close to ADOR, and with the age of about 4.6 billion years, between the

data for the Luna 16 fine regolith and rocks, and also for the low-potassium Apollo basalts and its fine regolith (the latter is beyond the limits of the graph). Fig. 5 is plotted from the data of different authors with appropriate corrections /10, 15, 22, 23, 26, 29, 31, 33-35/. The interpretation of all these data reduces to the following. If the regolith was formed during local /462 processes of melting syngenetic to the formation of the rocks, the age estimates obtained for the regolith must be in agreement with the corresponding data for the rocks. In view of the differences in the data /32, 45, 50/ based on the U-Th-Pb method for rocks and fine regolith, as well as the age data for rock minerals relative to regolith, it is meaningful to resort to selective volatility of certain elements (for example, Rb and Pb) /38-41/ in the rock-regolith direction to account for this. But in the case of Rb selective volatility must lead to a decrease in the Rb-Sr age estimates for the regolith (if the Rb is accumulated in it) compared with the syngenetic rocks. The condition of predominant volatility of lead /38-40/ is necessary principally in order to account for the low U-Th-Pb age for rocks as a whole relative to the regolith, for example, in the Apollo 11 situation, but for the regolith this condition is not mandatory, since the Rb-Sr isochron for the regolith-rock system with the primordial Sr^{87}/Sr^{86} ratio close to ADOR can indicate the earlier separation from the substrate of the matrices of the corresponding materials with an age corresponding to this event (this is not tantamount to the existence from this time of certain constituents as physical substances currently in existence). If in this same system of argumentation we use the primordial BABI value, assuming that the deviations of the point from the corresponding isochron are associated with events that are difficult to correlate, then the time of substrate separation could have been later, and the age of the volatile Pb admixture in the regolith increases.

By way of a general comment it should also be noted that for processes of the type of Rayleigh vaporization isotopic fractionation must have occurred for lead, difficult to estimate in magnitude, while for the Sr^{87}/Sr^{86} ratio (but not with respect to Rb), due to acceptance of the normalization of results this effect will be eliminated /41/. If the fine regolith is a mixed, inhomogeneous array where both local (with a matrix corresponding in individual situations to the rocks under investigation), as well as an introduced constituent, where the latter evidently must have supplied the regolith with most of the Rb and the radiogenic Sr^{87} and Pb, the resulting age effect for the regolith could have been expressed in a greater age, and the parallel possible condensation of the volatile lead from the rocks also would have worked in this direction.

In general, the logical significance of the operation of this addition (homogeneous in age) would be manifested in the leveling of the age estimates for the fine regolith, and in the limiting case attributing to it age and certain other (for example, the K/Rb ratio) parameters intrinsic to the material of the addition. However, certain limitations in the interpretation, in the sense of attributing a number of properties to the addition, are related to the fact that in this variant evidently in all the situations a considerable amount of Rb was introduced to the regolith (the admixture was enriched in Rb compared with the corresponding mean matrices for local rocks), but not K and Sr (the admixture must have contained different amounts of these elements compared with the mean matrix in each situation).

If the regolith was essentially the most ancient material (for example, the most ancient mantle of the planet's surface), essentially weakly or in general undifferentiated and corresponding in composition to some, principally primary level of inhomogeneity, the age characteristics for it would have been of a reconciling nature (Rb-Sr data calculated based on ADOR, and U-Th-Pb data). For the rocks as phases that experienced to differing degrees and, possibly, at different times, differentiation and melting, both visible satisfactory agreement as well as certain deviations with respect to the Rb-Sr isochrons for regolith could have been observed, with the primordial ADOR ratio. In supplement, we wish to indicate that the estimate of the age based on Rb-Sr data of mineral isochrons and K-Ar dates may not have always been fully unambiguous, since we cannot preclude the possibility of the effect of processes defined as metamorphic, although the level of their possible influence evidently is low.

Discussion. The model construction (working hypothesis) concerning the age, occurrence, and the systematics of lunar formations is associated for fine regolith with the necessity of adopting an alternative solution: whether the actual age of the regolith or some material constituent of it is the same as was obtained from the Rb-Sr estimates and the U-Th-Pb age data, or whether these same values are fictitious, being the result of events distorting the age, for example, the loss of more volatile materials during heating a vacuum or the effect of cosmic radiations. In the latter case an analogy can be drawn with the aromalous values based on K-Ar data [59, 60].

In examining this alternative, we should note that the U-Th-Pb estimate ages of mare regolith lie in the interval of 4.4-4.85 billion years [32, 43, 45, 50, 54] with the mean of 4.65 billion years, while the Rb-Sr data (the primordial ADOR ratio as in best agreement for all situations) determine the age interval of 4.4-4.75 billion years with the mean of 4.6 billion years. The level of agreement of the age estimates is quite satisfactory. /463

Supplementing the earlier discussion of this alternative situation, we can add that the mean U-Th-Pb age estimate for lunar rocks as a whole is close to the value of 4.2-4.4 billion years (mean $\simeq 4.3 \cdot 10^9$). An exception is represented by the high-potassium Apollo 11 rocks, for which this age will be less, but interestingly, for these rocks close agreement based on the Pb^{206}/Pb^{207} method can be obtained with the Rb-Sr age of rocks as a whole if the latter is reckoned from the time of separation of the high-potassic differentiate from the low-potassic matrix. But the same agreement can be obtained for the conditions specified with an age $\simeq 4.3 \cdot 10^9$ years by interpreting the Rb-Sr data for several fragments of sample 12013. The presence of ancient lead is also established for the samples of two Apollo 14 basalts [32]. These cases can cast some doubt on the effectiveness of the overall sublimation of the lead from the rocks prior to their stabilization, since the age of the essentially solid phase of these samples (based on the Rb-Sr mineral isochron and K-Ar data) is 0.2-0.3 billion years less. The Rb-Sr age for the rocks as a whole, calculated from the ADOR value, gives a mean estimate of $4.6 \cdot 10^9$ billion years in agreement with the Rb-Sr age of fine regolith.

We also noted that if the material constituent of the regolith responsible for its age characteristics and bearing certain chemical characteristics emerged, for example, at an early stage in the formative planetary body, then subsequently local material must have been added to the regolith (and the local material on a volume basis must have represented most of the regolith). And in general it is not fundamentally as important for the case of maria whether this constituent was introduced from the highland regions or remained from the time preceding the last outflowings of mare basalts. The principal of the addition of local material to the regolith is necessary in order not to contradict the actual chemistry of the regolith and rock sample in particular situations. However, there is some difficulty in compiling the age balance in this system. It stems from the insufficiency of the age of lunar rocks (not regolith) based on U-Th-Pb data (our mean estimate for them is ~4.3-4.4 billion years, Table 3) with respect to the Rb-Sr and U-Th-Pb regolith age being placed in agreement, since we must answer the question of where, if not in the regolith, to assign the Pb that accumulated furing the interval of 4.7-4.3 billion years, that is, we must indicate the receiver for storing the excess radiogenic Pb lost by the rocks, but nonetheless not established essentially in the regolith. We have already indicated the material of the krip type or the type of anorthosites from the lunar highland regions as such a receiver [31, 32], whence it could even have entered in some quantities into the regolith of maria, causing the corresponding age effects. In the limiting case if the U-Th-Pb age of the regolith, with the fluctuations in the above-indicated range, were entirely determined by some mechanism of "relatively precise proportioning"

of the addition of this material storing the excess radiogenic Pb into regoliths from different situations, then one can reject the correspondence of the actual age of the regolith or of some constituent of it with the age of 4.6-4.7 billion years. This follows from the fact that the maximum actual age of any regolith constituent must be $\simeq 4.3 \cdot 10^9$ years, in accordance with the U-Th-Pb scheme. Many variants of intermediate constructions, whose significance lies in preserving the correspondence of the age of some constituent of the regolith material with the age of 4.6-4.7 billion years, have already been discussed [32, 53]; some premises from this type of construction appear to us satisfactory in several features. However, owing to the importance of the consequences for the model construction it is still necessary to discuss the possibility of a fundamentally different solution, while preserving agreement with available data. We can, for purposes of discussion, presuppose that most of the regolith bearing the principal age and some chemical load is (in the sense of a material phase) the result of a somewhat later event than the time of planetary accretion. This may not be entirely identical to the meteoritic origin, since the cloud of cosmic material could have been in the gravity field of the formative planetary body and the encounter of the material with the surface of the body may not have been of the "meteoritic" type.

In the proposed case, this material can bear information on /464
some stage of the protoplanetary state (concerning the planet of the Moon). In terms of chemistry, this material is logically assumed to be more homogeneous (which is important) than in the other cases, and it can differ from the material actively participating in the accretion, for example, as to the K/Rb ratio that must be close to the chondrite ratio ($\simeq$ 300). The most important thing is that in this variant a timewise separation can be made for the events corresponding to the calculated age of this "most ancient regolith constituent" and to the age of the accretion of the planet of the Moon, during the process of which nearly all the Pb accumulating in the protostage was either lost or not captured (from the gaseous phase?). It is also possible that the loss of some, relatively small, amount of Pb in this process occurred.

All the foregoing, as well as several other similar constructions will be in agreement with the age data if the age of the accretion of the Moon corresponds to the level of $\simeq 4.4$ billion years. This conclusion, of course, is not so much inapplicable, as unaccustomed and, of course, hypothetical, but it could eliminate numerous difficulties. First of all, the difficulties with respect to lead are eliminated. The U-Th-Pb ages of the lunar rocks in general will correspond to the age of the beginning of the reckoning for the Moon, and the possible fluctuations associated with the operation of various mechanisms, including the sublimation of Pb will become quite appropriate quantities of a

TABLE 3. DATA ON THE AGE OF LUNAR ROCKS FOR DIFFERENT SECTIONS OF THE MOON (IN BILLIONS OF YEARS)

Section, sample	Isochronic Rb-Sr age for rock minerals	K-Ar age	U-Th-Pb age for rocks	References
1. Apollo 11, mare basalts				
a) high-potassic basalt group	3,6—3,7	3,6—3,7	3,9	[6, 26, 29, 35, 43, 44, 45, 46]
b) low-potassic basalt group	3,6—3,7	3,6—3,7	4,2	
2. Apollo 12				
a) sample 12013 (with granitoid material)	4,0—4,1 (4,3—4,5)	4,0—4,1	4,35	[10, 22, 33, 34, 35, 47, 48, 49, 50, 51, 52, 57]
b) basalts, mainly with K/Rb ≃ 480	3,2—3,4	3,2—3,3	4,0—4,2	
3. Apollo 14				
a) nonmare type basalts	4,0—4,2	3,9—4,1	4,1—4,4	[15, 17, 31, 52, 53, 54, 55, 56, 57]
b) krip material	4,0; 4,5; (5,0)	3,77		
4. Apollo 15				
a) mare type basalts	3,2—3,5	3,2—3,4	Presence of excess Pb relative to Rb-Sr and K-Ar data	[15, 17, 32, 52, 55, 57, 58]
b) anorthosite		3,92; 4,09		
5. Luna 16				
Basalt and gabbro of mare type	3,4—3,5	3,4—3,5		[21, 23, 31, 32, 37]

* In the cases of discordant ages, the advantage is given in the estimation to age data based on the Pb^{206}/Pb^{207} ratio.

relatively small order. Secondly, some loss of Rb in general negligibly affects the pattern of the ages for the rocks as a whole, as well as in view of the low Rb/Sr ratio for the lunar rocks (not for the case of krip type rocks), where the accumulation of radiogenic Sr^{87} for the material of the planetary rocks can commence from the level of the primordial Sr^{87}/Sr^{86} ratio, as already being close to BABI at this time, and possibly with some scatter (the effect of inhomogeneity of the residual type, if it occurred). Thirdly, it is precisely in this variant that the age of seven basaltic achondrites with a primordial Sr^{87}/Sr^{86} ratio equal to BABI (or variants of its construction) found in a study by Papanastassiou and Wasserburg /20/ takes on new significance.

Overall, the hypotnesis in the form presented must presuppose the absence of dates for lunar rocks based on the Rb-Sr and U-Th-Pb mineral isochrons and the K-Ar values, definitely larger than $4.4 \cdot 10^9$ years. It is important that this can be verified. As a result of the foregoing, we conclude that in this present study /465 we cannot give a correct answer to the question of the processes producing the regolith and we can only indicate the doubtless mixed character of the regolith material and that the accretion of the planet ended no later than 4.4 billion years ago.

There is one more specific question that is central for model constructions, dealing with certain initial aspects of the chemistry of lunar rocks (basalts) of the mare and nonmare types, and we consider their differences in the K/Rb ratio important, since the K/Rb ratio is a good indicator for several processes, and to assume for it a variable orientation in different situations is much more difficult than in the cases of pairs such as, for example, Rb and Sr, and K and U. The nature of the data we have examined on lunar materials is extremely complex and ambiguous and evidently here we can now only conclude that at different time stages in the development of the material of the lunar crust (nonmare formations are older than the mare) processes of differentiation reached different levels.

The satisfactory agreement of the Rb-Sr mineral isochron ages with the K-Ar data (and with the data for several mineral isochrons for the U-Th-Pb method) affords grounds for evaluating these parameters as corresponding to actual events in the lunar history.

Conclusion. As a result of examining the data on age determination based on the Rb-Sr and U-Th-Pb methods for the fine fraction of the lunar regolith from the Sea of Fertility, and also from comparing them with the data for other mare of the lunar surface, it can be concluded that they agree well in a quite narrow

range of values (4.4-4.7) billion years with respect to the Rb-Sr method and in the same interval (4.4-4.8) billion years based on the U-Th-Pb method. On the other hand, determinations of the age of monolithic rocks, gabbro-basalts of the Moon, based on the Rb-Sr isochron method for the rocks as a whole, also with some exceptions, gives the same calculated, model age within the range 4.3-4.7 billion years, and the U-Th-Pb method in this case gives estimates somewhat smaller, but close together for several cases, 4.3-4.4 billion years. Thus, the data obtained for lunar rocks, generally for both monolithic rocks as well as for the fine regolith fraction, are close to the value of 4.4-4.6 billion years. This age, in our understanding, corresponds to the time of differentiation of the primordial material of the Moon (by melting) and the formation of the lunar crust /1, 2, 61/. The average age of about 3.5 billion years obtained for the gabbro-basalts of the mare type by both the Rb-Sr isochron method for rock minerals, as well as by the K-Ar method, corresponds to the time of crystallization of individual mineral phases of the rocks. Still, we assume that the age of about 3.5 billion years is the age of the maximum development of melting of individual rocks in the lunar mare crust.

The regolith of the mare provinces as, apparently, also is true of the regolith of the highland regions, was formed principally from local rocks on which they lie. In the lunar mare these are gabbro-basalts of a given province.

This follows from the corresponding comparisons of the composition of basalts and regolith. However, the composition of the fine fraction of the lunar mare regolith differs by a somewhat lower content of femic elements compared to the gabbro-basalts. The process which produced the mare regolith is not exactly known to us. In this process the distribution and ratio of several elements compared to their content and ratio in the monolithic rocks of the corresponding province in the given mare, without considerable changes in the gross composition, underwent a disturbance. This disturbance also, in particular, can have occurred through mixing with a small amount of highland material and meteoritic matter. However, this mixing most likely could not have in any manner affected the composition of the regolith, in the system of the possible age change (its increase), since this would require two-thirds of the corresponding regolith material to have been brought in from other sources not intrinsic to the given mare province. But this did not occur, as indicated by comparative mineralogic and chemical analysis of the regolith of the mare regions. It is also difficult for us to imagine the possibility of the regular and selective nature of the loss of Rb and the influx of radiogenic Pb as being the cause for the high value of the age of the fine regolith fraction. Still, there is no doubt of this possibility, which we as well as many

other investigators know well and have more than once verified experimentally predominantly by comparing with Sr the loss of Rb by heating rocks in a vacuum, as well as the considerable loss of Pb from rocks in this process.

Finally, there remains a certain indeterminacy in all the determinations based on the Rb-Sr method of the age of rocks (as a whole) and of lunar regolith, owing to the primordial Sr^{87}/Sr^{86} ratio and the question of the universality of this ratio, whose value was used by us as well as other investigators in calculating the age. However, it must be pointed out that here the data obtained by the Rb-Sr method are not in contradiction with the data of the U-Th-Pb method for mare regolith.

REFERENCES

/466

1. Vinogradov, A. P., "Preliminary Data on Lunar Surface Material Returned by Luna 16 Automatic Station," Geokhimiya (3), (1971).

2. Vinogradov, A. P., "Preliminary Data on Lunar Ground Brought to Earth by Automatic Probe Luna 16," Proc. Second Lunar Sci. Conf., Geochim. Cosmochim. Acta, Suppl. 2 1, (1971).

3. Gerling, E. K., and Artemov, Yu. M., "Absolute Gecchronology of Southern and Central Regions of the Yeniseyskiy Mountain Range," Geokhimiya (7), (1964).

4. Burnett, D. S., and Wasserburg, G. J., "Evidence for the Formation of an Iron Meteorite at $3.8 \cdot 10^9$ Years," Earth Planet. Sci. Letters 2(3), (1967).

5. Hamilton, E. I., Prikladnaya geokhronologiya /Applied Geochronology/ Leningrad, "Nedra", 1968.

6. Gast, P. W., Hubbard, N. J., and Wiesman, H., "Chemical Composition and Petrogenesis of Basalts from Tranquillity Base," Proc. Apollo 11 Lunar Sci. Conf., Geochim. Cosmochim. Acta, Suppl.1 2, (1970).

7. Dolezhal', Ya., Povondra, P., and Shul'tsek, Z., Metody Razlozheniya gornykh porod i mineralov /Methods of Decomposing Rocks and Minerals/, "Mir", (1968).

8. Rafal'son, A. E., and Shereshevskiy, A. M., Mass-spektrometricheskiye pribory /Mass Spectrometric Instruments/, "Atomizdat", (1968).

9. Artemov, Yu. M., "Mass Spectrometric Determination of Isotopic Composition of Strontium and Conditions of Optimizing Measurement Results," Vtoroy Vsesoyuznyy simpozium po primeneniyu stabil'nykh izotopov v geokhimii, Tezisy dokladov /Second All-Union Symposium on the Use of Stable Isotopes in Geo-Chemistry, Abstracts of Papers/ Moscow, (1968).

10. Hubbard, N. J., and Gast, P. W., "Chemical Composition and Origin Nonmare Lunar Basalts," Proc. Second Lunar Sci. Conf., Geochim. Cosmochim. Acta, Suppl. 2 2, (1971).

11. Urey, H. C., Marti, K., Hawkins, J. W., and Lin, M. K., "Model History of the Lunar Surface," Proc. Second Lunar Sci. Conf., Geochim. Cosmochim. Acta, Suppl. 2 2, (1971).

12. Albee, A. L., Chodos, A. A., Gancarz, A. J., Haines, E. L., Papanastassiou, D. A., Ray, L., Tera, F., Wasserburg, G. J., and Wen, T., "Mineralogy, Petrology, and Chemistry of a Luna 16 Basaltic Fragment Sample B-1," Earth Planet. Sci. Letters 13(2), (1972).

13. Hubbard, N. J., Nyquist, L. E., Rhodes, J. M., Bansal, B. M., Wiesman, H., and Church, S. E., "Chemical Features of the Luna 16 Regolith Sample," Earth Planet. Sci. Letters 13(2), (1972).

14. Philpotts, J. A., Schnetzler, C. C., Bottino, M. L., Schuman, S., and Thomas, H. H., "Luna 16: Some Li, K, Rb, Sr, Ba, Rare Earth, Zr, and Hf Concentrations," Earth Planet. Sci. Letters 13(2), (1972).

15. Cliff, A., Lee-Hu, C., and Wetherill, G. W.,"K, Rb, Sr Measurements in Apollo 14 and 15 Materials," Three Lunar Sci. Conf. Abstracts, Houston, 1972.

16. Mason, B., Henderson, E. P., Jarosewich, E., Melson, W. G., and Nelen, J., "Composition of Luna 16 - G52 and Apollo 14 - Apollo 15 Fines," Three Lunar Sci. Conf. Abstracts, Houston, 1972.

17. Murthy Rama, V., Evensen, N. M., Jahn Bor-ming, and Coscio, M. R., "Rb-Sr Ages, Trace Elements and Speculations on Lunar Differentiation," Three Lunar Sci. Conf. Abstracts, Houston, 1972.

18. Morgan, J. W., Krahenbuhl, H., Ganapathy, R., and Anders, E., "Volatile and Siderophile Elements in Apollo 14 and 15 Rocks," Three Lunar Sci. Conf. Abstracts, Houston, 1972.

19. Schnetzler, C. C., and Philpotts, J. A., "Alkali, Alkaline Earth, Rare-Earth Element Concentrations in Some Apollo 12 Soils, Rocks, and Separated Phases," Proc. Second Lunar Sci. Conf., Geochim. Cosmochim. Acta, Suppl. 2 2, (1971).

20. Papanastassiou, D. A., and Wasserburg, G. J., "Initial Strontium Isotopic Abundances and the Resolution of Small Time Differences in the Formation of Planetary Objects," Earth Planet. Sci. Letters 5(6), (1969).

21. Papanastassiou, D. A., and Wasserburg, G. J., "Rb-Sr Age of Luna 16 Basalt and the Model Age of Lunar Soils," Earth Planet. Sci. Letters 13(2), (1972).

22. Compston, W., Berry, H., Vernon, M. J., Chappell, B. W., and Kaye, M. J., "Rubidium-Strontium Chronology and Chemistry of Lunar Material from the Ocean of Storms," Proc. Second Lunar Sci. Conf., Geochim. Cosmochim. Acta, Suppl. 2 2, (1971).

23. Allegre, C. J., Birck, J. L., Loubet, M., and Provost, A., "Rb^{87}-Sr^{87} Age and Content of K, Rb, Sr, Ba, and Rare Earths of the Solar Wind from the Sea of Fertility (of the Moon) Reported by the Soviet Luna 16 Mission," C. R. Acad. Sci. Paris 273-D, 779 (1971).

24. Sanz, H. G., Burnett, D. S., and Wasserburg, G. J. "A Precise Rb^{87}/Sr^{87} Age and Initial Sr^{87}/Sr^{86} for the Colomera Iron Meteorite," Geochim. Cosmochim. Acta 34(6), 1227 (1970).

25. Tera, F., Eugster, O., Burnett, D. S., and Wasserburg, G. J., "Comparative Study of Li, Na, K, Rb, Cs, Ca, Sr, and Ba Abundances in Achondrites and in Apollo 11 Lunar Samples," Proc. Apollo 11 Lunar Sci. Conf., Geochim. Cosmochim. Acta, Suppl. 1 2, (1970).

26. Papanastassiou, D. A., Wasserburg, G. J., and Burnett, D. S., Rb-Sr Ages of Lunar Rocks from the Sea of Tranquillity," Earth Planet. Sci. Letters 8(1), (1970).

27. Ahrens, L. H., and Danchin, R. V., "The Chemical Composition of the Basaltic Achondrites," Phys. Earth 8, (1970).

28. Taylor, H. P., Jr., and Epstein, S., "O^{18}/O^{16} Ratios of Apollo 11 Lunar Rocks and Minerals," Proc. Apollo 11 Lunar Sci. Conf., Geochim. Cosmochim. Acta, Suppl. 1 2, (1970).

29. Compston, W., Arriens, P. A., Vernon, M. J., and Chappel, B. W., "Rb-Sr Chronology and Chemistry of Lunar Material," Science 167(3918), (1970).

30. Gast, P. W., and Hubbard, N. J., "Abundance of Alkali Metals, Alkaline, and Rare Earth and Sr^{87}/Sr^{86} Ratios in Lunar Samples," Science 167(3928), (1970).

31. Nyquist, L. E., Hubbard, N. J., and Gast, P. W., "Rb-Sr Relationship for Some Chemically Defined Lunar Materials," Three Lunar Sci. Conf., Abstracts, Houston, 1972.

32. Tera, F., and Wasserburg, G. J., "U-Th-Pb Analyses of Soil from the Sea of Fertility," Earth Planet. Sci. Letters 13(2) (1972).

33. Cliff, R. A., Lee-Hu, C., and Wetherill, G. W., "Rb-Sr and U-Th-Pb Measurements on Apollo 12 Materials," Proc. Second Lunar Sci. Conf., Geochim. Cosmochim. Acta, Suppl. 2 2, (1971).

34. Murthy Rama, V., Evensen, N. M., Jahn Bor-ming, and Coscio, M. R., Jr., "Rb-Sr Isotopic Relations and Elemental Abundances of K, Rb, Sr, and Ba in Apollo 11 and 12 Samples," Lunar Sci. Conf. Thesis. Houston, 1971.

35. Papanastassiou, D. A., and Wasserburg, G. J., "Lunar Chronology and Evolution from Rb-Sr Studies of Apollo 11 and 12 Samples," Earth Planet. Sci. Letters 11(1), (1971).

36. Albee, A. L., Burnett, D. S., Chodos, A. A., Eugster, O. J., Heneke, J. C., Papanastassiou, D. A., Podosek, F. A., Russe Price, G., Sanz, H. G., Tera, F., and Wasserburg, G. J., "Ages Irradiation History and Chemical Composition of Lunar Rocks from the Sea of Tranquillity," Science 167(3918), (1970).

37. Huneke, J. C., Podosek, F. A., and Wasserburg, G. J., "Gas Retention and Cosmic-Ray Exposure Ages of Basalt Fragment from Mare Fecunditatis," Earth Planet. Sci. Letters 13(2), (1972).

38. Huey, J. M., Ihochi, H., Black, L. P., Ostic, R. G., and Kohman, T. P., "Lead Isotopes and Volatile Transfer in the Lunar Soil," Proc. Second Lunar Sci. Conf., Geochim. Cosmochim. Acta, Suppl. 2 2, (1971).

39. Silver, L. T., "Lead Volatilization and Volatile Transfer Process on the Moon," Three Lunar Sci. Conf., Abstracts, Houston, 1972.

40. Doe, B. R., and Tatsumoto, M., "Volatilized Lead from Apollo 12 and 14 Soils," Three Lunar Sci. Conf., Abstracts, Houston, 1972.

41. Gibson, E. K., and Hubbard, N. J., "Volatile Element Depletion Investigations on Apollo 11 and 12 Lunar Basalts Via Thermal Volatilization," Three Lunar Sci. Conf., Abstracts, Houston, 1972.

42. Artemov, Yu. M., "Possibilities of the Interpretation of Data on the Isotopic Composition of Lead /Nuclides/," Geokhimiya (10), (1970).

43. Silver, L. T., "Uranium Thorium-Lead Isotopes in Some Tranquillity Base Samples and Their Implications for Lunar History," Proc. Apollo 11 Lunar Sci. Conf., Geochim. Cosmochim. Acta, Suppl. 1 2, (1970).

44. Tatsumoto, M., and Rosholt, J., "Age of the Moon: An Isotopic Study of U-Th-Pb Systematics of Lunar Samples," Science 167(3918), (1970).

45. Tatsumoto, M., "Age of the Moon: An Isotopic Study of U-Th-Pb Systematics of Apollo 11 Lunar Samples II," Proc. Apollo 11 Lunar Sci. Conf., Geochim. Cosmochim. Acta, Suppl. 1 2, (1970).

46. Turner, G., "Agron-40/Agron-39 Dating of Lunar Rock Samples," Proc. Apollo 11 Lunar Sci. Conf., Geochim. Cosmochim. Acta, Suppl. 1 2, (1970).

47. "Lunatic Asylum. Mineralogic and Isotopic Investigations on Lunar Rock 12013," Earth Planet. Sci. Letters 9(2), (1970).

48. Turner, G., "Ar^{40}-Ar^{39} Age Determination of Lunar Rock 1213," Earth Planet. Sci. Letters 9(2), (1970).

49. Tatsumoto, M., "U-Th-Pb Age of Apollo 12 Rock 12013," Earth Planet Sci. Letters 9(2), (1970).

50. Tatsumoto, M., Knight, R. J., and Doe, B. R., "U-Th-Pb Systematics of Apollo 12 Lunar Samples," Proc. Second Lunar Sci. Conf., Geochim. Cosmochim. Acta, Suppl. 2 2, (1971).

51. Turner, G., "Ar^{40}-Ar^{39} Ages from the Lunar Maria," Earth Planet. Sci. Letters 11(2), (1971).

52. Wasserburg, G. J., Turner, G., Tera, F., Podosek, F. A., Papanastassiou, D. A., and Huneke, J. C., "Comparison of Rb-Sr, K-Ar, and U-Th-Pb Ages," Three Lunar Sci. Conf. Abstracts, Houston, 1972.

53. Papanastassiou, D. A., and Wasserburg, G. J.,"Rb-Sr Ages of Igneous Rocks from the Apollo 14 Mission and the Age of the Fra Mauro Formation," Earth Planet. Sci. Letters 12(1), (1971).

54. Tatsumoto, M., Hedge, C. E., Doe, B. R., and Unruch, D., "U-Th-Pb and Rb-Sr Measurements on Some Apollo 14 Lunar Samples," Three Lunar Sci. Conf., Abstracts, Houston, 1972.

55. Huneke, J. C., Podosek, F. A., Turner, G., and Wasserburg, G. J., "Ar^{40}-Ar^{39} Systematics in Lunar Rocks and Separated Minerals of Lunar Rocks from Apollo 14 and 15," Three Lunar Sci. Conf. Abstracts, Houston, 1972.

56. Silver, L. T., "U-Th-Pb Abundances and Isotopic Characteristics in Some Apollo 14 Rocks and Soils and an Apollo 15 Soil," Three Lunar Sci. Conf. Abstracts, Houston, 1972.

57. Stettler, A., Eberhardt, P., Geiss, J., and Grogler, N., Ar^{39}/Ar^{40} Ages of Apollo 11, 12, 14, and 15 Rocks," Three Lunar Sci. Conf. Abstracts, Houston, 1972.

58. Wasserburg, G. J., and Papanastassiou, D. A., "Age of an Apollo 15 Mare Basalt; Lunar Crust and Mantle Evolution," Earth Planet. Sci. Letters 13(1), (1971).

59. Kaiser, W. A., "Rare Gas Studies in Luna 16-G-7 Fines by Stepwise Heating Technique," Earth Planet. Sci. Letters 13(2), (1972).

60. Heymann, D., and Yaniv, A., "Ar^{40} Anomaly in Lunar Samples from Apollo 11," Proc. Apollo 11 Lunar Sci. Conf., Geochim. Cosmochim. Acta, Suppl. 1 2, (1970).

61. Vinogradov, A. P., "Origin of Lunar Rocks," Geokhimiya (1), (1970).

Order of Lenin Institute of Geochemistry and Analytical Chemistry imeni V. I. Vernadskiy, USSR Academy of Sciences, Moscow.

N75 11858

Rb-Sr AGE AND CONTENT OF POTASSIUM, RUBIDIUM, STRONTIUM, BARIUM, AND RARE EARTHS IN SURFACE MATERIAL FROM THE SEA OF FERTILITY

/468

C. J. Allegre, J. L. Birck, M. Loubet, and A. Provost

Abstract

The Luna 16 automatic station returned from the Sea of Fertility a 35 cm long column of lunar surface material. According to the French-Soviet space research plan, 1 g of the Luna 16 lunar surface material, taken at a depth of 22 cm, was given to a group of French investigators working in this field. As already indicated by Soviet investigators /1/, this sample consists of fine material: surface material and fine fragments of rocks from 1 to 4 mm in diameter. The present article deals with analyses made on 17 mg of the fine lunar surface material, from which all the rock fragments were sampled (but without sieving).

Integrated methods that we had to use will be described in detail in two special articles /2, 3/. K, Rb, Sr^{84}, Ba, and rare-earth traces were added prior to dissolving. The decomposition was carried out with 1 cm^3 HF and 0.5 cm^3 HNO_3 in a teflon bomb at 150°. After adding the HCl, the solution was eluted on on Dowex X 8200 400 mesh resin. Thus, we successfully obtained the fractions corresponding to K, Rb, Sr, Ba, (La, Ce, Nd), (Sm, Eu, Gd, Dy), and (Er, Yb, Lu). The entire chemical treatment was carried out in a teflon dish in an ultraclean room /2/ with twice-distilled reagents prepared from ultrapure products of the Merck Company. The contents of K, Rb, Ba, and rare earths were determined by six series of measurements on a modified, model 206 K THN mass spectrometer /3/ by isotopic dilution. Here the blank correction for the elements was as follows: K -- 0.1 μg; Rb -- 0.1 ng; Ba -- 2 ng; and rare earths -- less than 0.1 ng. The precision of determination for K and Rb was 1.5 percent, and

for Ba and TR -- from 2 to 5 percent. The Sr^{87}/Sr^{86} ratio and the Sr content was measured with the mass spectrometer using programmed magnetic sweep scanning, digital recording, and automatic totaling with respect to the ordinates (model 206 THN, modified). The precision obtained for the MIT standard was 0.708023 ± 0.000035. In this experiment, the blank correction for Sr was 1 nanogram owing to the inadequate purity of the rare earth tracer. It was ten times greater than our usual correction.

The results obtained for the Luna 16 surface material are plotted on the diagram of the isotopic evolution of strontium (Fig. 1) and show that this surface material is most depleted of radiogenic Sr^{87} of all the known lunar surface materials and that the point characterizing Luna 16 lies somewhat to the right of the line corresponding to an age of 4.6 billion years, which was determined by Papanastassiou and Wasserburg for other surface materials [4].

Rb^{87}/Sr^{86}	Sr^{87}/Sr^{86}
0,02407	0,700442 ± 0,000063 (1)
	0,700384 ± 0,000150 (2)

Although the age of Sea of Fertility rocks has not yet been determined, it is probable that this will be done. We know that the "visible ages" determined for lunar surface materials are somewhat greater than the ages of the mare rocks which they overlie [4, 5]. This circumstance makes it possible to assume that the lunar surface material is a mixture with the predominance at least of one "exotic" constituent with an age of 4.6 billion years, rich in K, Rb, and rare earths [4]. Seemingly, Sea of Fertility surface material will not be an exception to this rule. Various authors assume that this exotic constituent must be rich in K, Rb, and rare earths. It can be noted that, if the surface material is rich in K, Rb, and rare earths, like Apollo 12 regolith, the points corresponding to it will lie below the isochrons /469
at 4.6 billion years. The exotic constituent rich in K is, in our view, less than 4.6 billion years old, but doubtless there exists an exotic constituent poor in K and Rb, and rich in Sr, which predominates in Luna 16 surface material, and possibly in Apollo 11 surface material and is 4.6 billion years old.

By comparing our results (in ppm) with those obtained for the Apollo 11 and Apollo 12 regoliths [6, 7], it can be stressed that the Luna 16 surface material is the poorest in the content of K, Rb, and rare earths and the richest in the Sr contents:

K	Rb	Sr	Ba
1047	2,4478	294,2	266

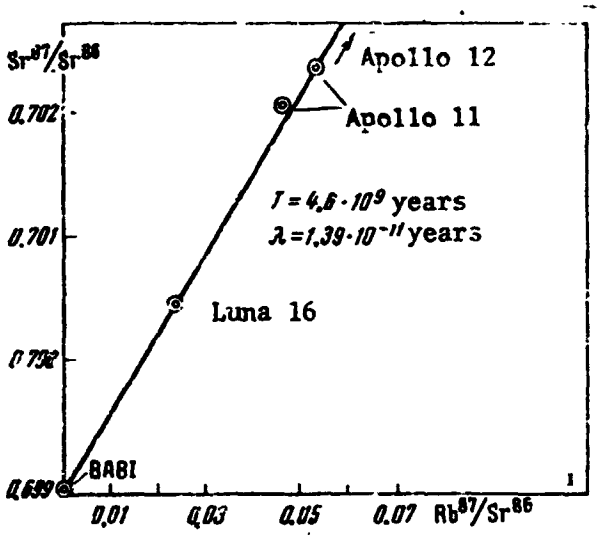

Fig. 1. Plot of Sr^{87}/Sr^{86} -- -- Rb^{87}/Sr^{86} for lunar surface material.

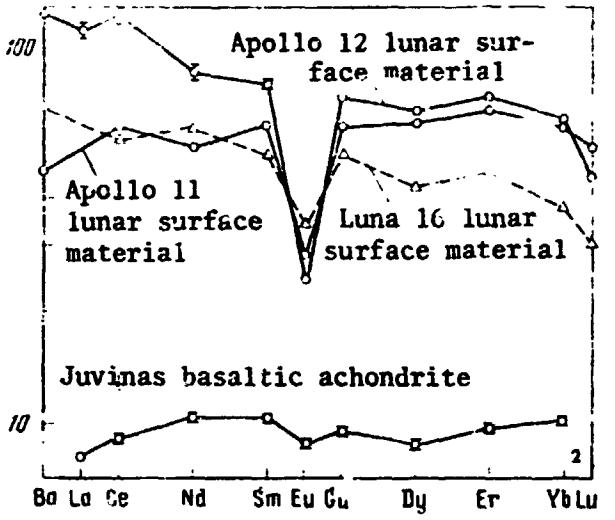

Fig. 2. Distribution of rare-earth elements in lunar surface material.

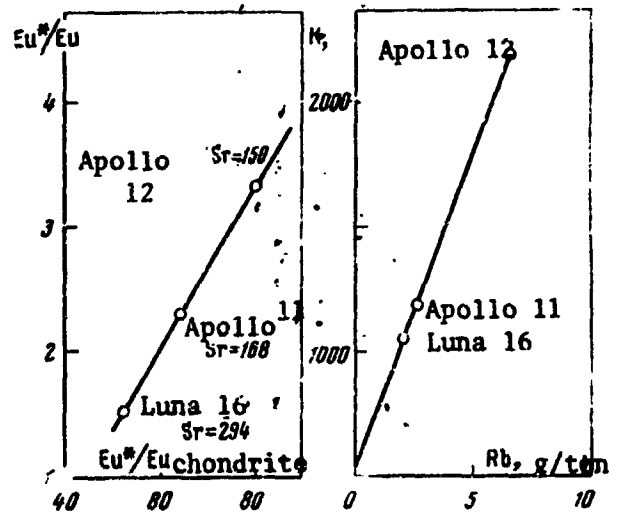

Fig. 3. Anomaly of europium ratio in lunar surface material.

Fig. 4. K/Rb ratio in lunar surface material.

The abundance diagram of rare earths log [(abundance in surface material)/ abundance in chondrites)] vs atomic number makes it possible to compare Luna 16 surface material with the surface materials of Apollo 11 and Apollo 12 [6, 7], and with the basaltic Juvinas achondrite, which was also analyzed in our laboratory (Fig. 2). The results of all the analyses are also given below (in ppm):

	Ce	Nd	Sm	Eu	Gd	Dy	Er	Yb	Lu
Luna 16	46	42,2	10,5	2,4	13,5	12,7	8,62	6,20	0,92
Juvinas	7,12	6,72	2,14	0,62	2,30	2,62	1,79	1,80	—
Various chondrites	0,787	0,652	0,208	0,071	0,256	0,303	0,182	0,188	0,031

The europium anomaly decreases linearly with decrease in the mean content (Sm-Gd). This decrease, according to Gast /7/, lies in an anticorrelation with an increase in the Sr content (Fig. 3). The contents of K and Rb change identically, while the K/Rb ratio is inconstant (Fig. 4). These ratios, apparently, indicate the same genetic and magmatic relations between different lunar regoliths. /470

Lunar soils returned by Apollo 11 and Apollo 12 do not fit on the above-determined lines. These facts can be easily interpreted if we assume that the lunar surface materials are mixtures of exotic constituents differentiated in the same epoch and during the same process. This process may have been the primordial lunar differentiation taking place 4.6 billion years ago. The contents of the dispersed elements here also indicate the exotic origin for most of the fine surface material (and not only for a minor portion of it).

This study was possible only thanks to the assistance of the National Center of Scientific Research and the National Center for the Study of Space of France. Organization of the clean laboratories and the use of the latest methods in this study were to a large extent facilitated due to material assistance obtained from the National Center of Scientific Research and from the Faculty of Sciences at Paris University. The cooperation and continual assistance shown us by H. Curien, the general director of the National Center of Scientific Research, G. Jaubert, at that time scientific director, and P. Pellas, director of research at this center, was a great support to us.

M. Tatsumoto gave us extremely ultrapure hydrofluoric acid, and G. J. Wasserburg assisted us with his counsel on the isotopic analysis of strontium. We received much assistance from the discussion of the work with R. Montinier and G. Manes, and by the help they provided us. R. Dars and A. Lepage allowed us to prepare the manuscript in difficult conditions of the university vacation.

REFERENCE

1. Vinogradov, A. P., "Preliminary Data on Lunar Ground Brought to Earth by Automatic Probe Luna 16," Proc. Second Lunar Sci. Conf. 1, 1 (1971).

2. Allegre, C. J., Birck, J. L., Provost, A., and Gilles, J., "Analysis of the Isotopic Composition of Strontium from a Rock Sample to a Precision of 5/100,000," (in press).

3. Loubet, M., and Allegre, C. J., "Microanalysis of Rare Earths by Isotopic Dilution and Mass Spectrometry," (in press).

4. Papanastassiou, D., and Wasserburg, G. J., "Lunar Chronology and Evolution from Rb-Sr Studies of Apollo 11 and 12 Samples," Earth Planet. Sci. Letters 11, (1971).

5. Tatsumoto, M, "Age of the Moon: U-Th-Pb Systematics of Apollo 11 Lunar Sample," Proc. Apollo 11 Lunar Sci. Conf. 2, (1970).

6. Gast, P. W., Hubbard, N. J., and Weismann, H., "Chemical Composition and Petrogenesis of Basalts from Tranquillity Base," Proc. Apollo 11 Lunar Sci. Conf. 2, (1970).

7. Gast, P. W., and Hubbard, N. J., "Rare Earth Abundances in Soil and Rocks from Ocean of Storms," Earth Planet. Sci. Letters 10, (1970).

Group of Geochemical Investigation of Louis-Barrabet, Institute of Earth Physics, Paris University, Paris, France.

N75 11859

OPTICAL CHARACTERISTICS OF REGOLITH FROM THE SEA OF FERTILITY, SEA OF TRANQUILLITY, AND OCEAN OF STORMS

/496

I. I. Antipova-Karatayeva, Yu. I. Stakheyev, and K. P. Florenskiy

Abstract

Presented are the results of investigations of the diffuse reflection spectra of regolith returned by the Luna 16 automatic station and by the Apollo 11 and Apollo 12 expeditions, the indicatrix of scattering, and the spectra of the specular reflection of Sea of Fertility regolith, as well as the spectra of diffuse reflection from polished sections of lunar rocks from the Sea of Tranquillity and the Ocean of Storms. The spectra of diffuse reflection of the samples investigated have no well-defined structure and are close to each other. The lowest reflectivity is exhibited by the Sea of Tranquillity regolith, and the highest -- by the Ocean of Storms regolith. A weak absorption band with a maximum near 1 nm is noted in the spectra, corresponding to the Fe^{2+} ion in the octahedral position in the lattice of regolith mineral constituents. Its position and intensity are distinguishable in the spectra of different samples, which is due to their different mineralogical composition. When the indicatrix of scattering of the regolith was recorded, a specular component was detected; its spectrum differs somewhat from the spectrum of diffuse reflection. This difference evidently accounts for the visually observed change in the hues of the regolith from brown to greenish when it is illuminated and observed at different angles.

Samples of regolith returned by the Luna 16 automatic station were investigated. The samples were taken from zone A, that is, from the depth of 0-8 cm from the surface /1 7. They consist of a fine-grained powder with low total coefficient of reflection. The particle size varied from 2 to 1500 μm and their mean median

size was 60 μm. Morphological examination established that at least half of all particles are fused or slagged from the surface. Here both slag-like vesicular melting, as well as a smooth glazed vitrification were encountered. More than 1 percent of the particles were glass spherules. Both the sample overall as well as its individual fractions by particle size underwent measurements: -83; + 83 - 127; + 127 - 200; and + 200 - 450 μm.

Also investigated were regolith samples returned by Apollo 11. Sample 10005,34-5 was taken from the core at a depth of 1.5 cm, and sample 10005,35 was taken from a depth of 10-11 cm.

The regolith samples returned by Apollo 12 are also samples from the drill core. Sample 12028,229 was situated 16 cm from the surface, and sample 12028,233 -- at a depth of 33 cm.

The diffuse reflection spectra of the samples were recorded with a Hitachi EPS-3T spectrophotometer with an integrating sphere with respect to a standard plate sputtered with magnesium oxide. The wavelength range was 220-1800 nm.

The indicatrices of light scattering were investigated with a photometer that provided measurements of the reflected light in the angle range 0-80° with respect to both sides from the normal to the sample. The angle of incidence of the light was recorded in the limits 0-80°. The minimum phase angle was 22°. The sample was illuminated with point-type tungsten, iodine, or deuterium lamps. Monochromatization of the reflected light was achieved with a monochromator with a Fasti diffraction grating; a model 1 R 28 photomultiplier was mounted outside the exit slit. The sample was illuminated and the reflected light recorded without condenser systems.

The diffuse reflection spectra of all the samples measured had no well-defined structure and were very close to each other. A slow rise in the albedo was observed in the wavelength range 250-1800 nm (Fig. 1), and its mean values for the Sea of Fertility regolith (spectrum 4) were as follows: 0.086 for the 260-400 nm region; 0.107 for the 400-750 nm region; 0.126 for the 750-950 nm region; and 0.128 for the 950-1800 nm region [2]. In the 0.8-1 μm region, the spectra of all samples disclosed a broad absorption band, which was identified with the d-d transition in the Fe^{2+} ion, part of the crystal lattice of the regolith mineral constituent. From the data of chemical analysis, the iron content in the sample returned by Luna 16 was 13.1 percent [1]. /497

The lowest reflectivity was shown by the Sea of Tranquillity regolith (spectra 3 and 5, Fig. 1), and the highest -- by the Ocean of Storms regolith (spectra 1 and 2, Fig. 1). The difference in the spectra of the samples taken from different levels, but from

the same drill core was small in all cases; it did not exceed 2 percent over the entire range of wavelengths studied. Nonetheless, regolith reflectivity clearly increases in the direction from the surface to the depth (spectra 2 and 1, spectra 3 and 5, Fig. 1). The diffuse reflection spectrum of the Sea of Fertility regolith (spectrum 4, Fig. 1), with respect to the integral coefficient of reflection, is intermediate between the spectra of regolith from the Sea of Tranquillity and from the Ocean of Storms. It has the least pronounced structure, approximating in character the spectrum of regolith from the surficial layer of the Sea of Tranquillity.

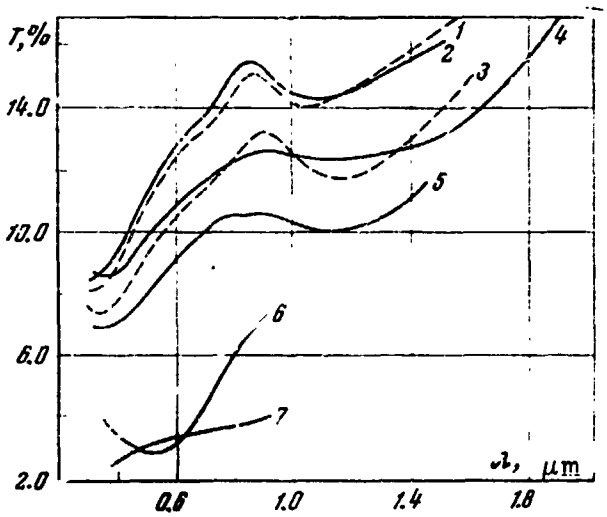

Fig. 1. Diffuse reflection spectra of regolith from different parts of the Moon
1. Sample 12028,229
2. Sample 12028,233
3. Sample 10005,35
4. Sample L-16-A
5. Sample 10005,34-5
6. Spectrum of specular reflection of sample L-16-A; angle of incidence of light 60°; coefficient of reflection in arbitrary units
7. Reduced spectrum of diffuse reflection of sample L-16-A; coefficient of reflection at 0.5 μm is equal to the coefficient of specular reflection.

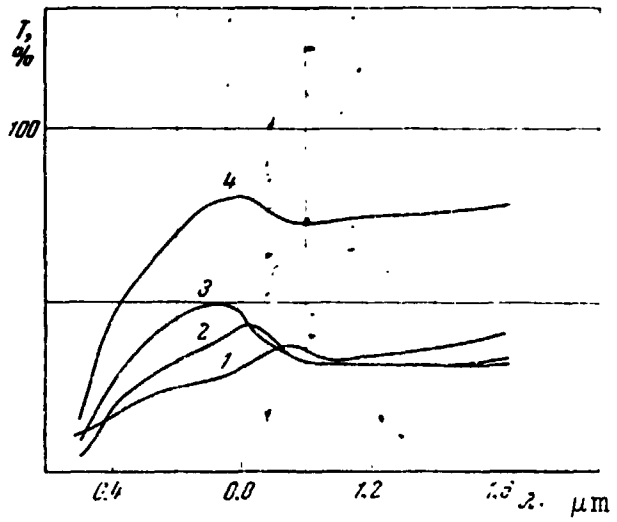

Fig. 2. Spectra of diffuse reflection of polished sections of lunar rocks
1. Breccia, sample 10048,53
2. Coarse-grained basalt, sample 10047,25
3. Fine-grained basalt, sample 12018,80
4. Breccia, sample 12034,34

The experimental data we obtained is in good agreement with the data from the measurement of the diffuse reflection spectra of other regolith samples [3-7]. The numerical value of the recorded albedo

for samples from the Sea of Fertility is somewhat higher than the albedo for the Moon as a whole. However, telescopic data obtained for the area of the Sea of Fertility virtually agrees with the data of direct measurement.

For a more detailed analysis of the diffuse reflection spectra of regolith from different areas of the Moon, the spectra of four polished sections of samples of lunar rocks returned by Apollo 11 (10047,25 and 10048,53) and by Apollo 12 (12034,34 and 12018,80) were recorded. The spectra were recorded in the same conditions as the regolith spectra.

An adequate similarity was observed in the general trend of the spectra of the samples of regolith and polished sections investigated (Fig. 2): a rise in the intensity of reflected light with increase in wavelength and the presence of an absorption band in the region of about 1 μm. However, the intensity of the spectra of all polished sections was considerably higher; the absorption band of bivalent iron was more well defined, and the difference between the samples of polished sections from different parts of the Moon with respect to the spectra was less than between regolith samples. Thus, the diffuse reflection spectra of the polished sections 10048,53, 10047,25, and 12018,80 are similar to each other, especially in the region 0.8-1.8 μm, while the spectrum of sample 12034,34 differed markedly from them. /498
In addition, the dependence of the intensity of light diffusely reflected from the polished sections, on wavelength in the 250-800 nm range, was much more strongly pronounced than in the regolith spectra, and in the longer-wave region (0.8-1.8 μm), this dependence becomes markedly weaker.

All these properties poorly distinguish the spectra of polished sections from regolith spectra.

For Sea of Fertility samples, the characteristics of light scattering were investigated. The indicatrix of scattering, reducing to measurements of the intensity of light at different angles, was recorded for a fixed position of the light source, namely with normal incidence of light and when the angles between the normal to the sample surface and the direction of the incident light were 20, 30, 40, and 60°.

With normal incidence of light on a sample, a rapid rise in the intensity of reflected light with decrease in the phase angle is observed (Fig. 3). This corresponds to data on the scattering of light by the lunar surface as well as data obtained for samples from the Sea of Tranquillity /8/. The curvature of the curve changes somewhat with the wavelength of the incident light: with decrease in the wavelength a more rapid rise in the intensity of the reflected light is observed, where the differences in the curvature of the curve become more appreciable at phase angles less than 50°.

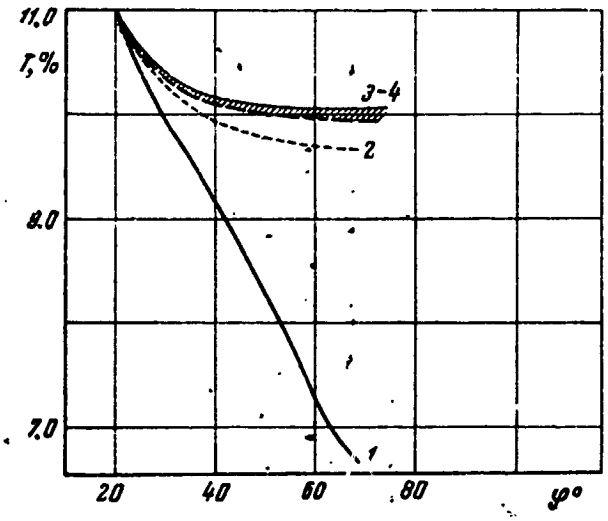

Fig. 3. Scattering indicatrices for normal incidence of light
ϕ. Phase angle
T. In arbitrary units reduced to the same value for ϕ = = 22°
1. Wavelength 0.4 μm
2. Wavelength 0.436 μm
3-4. Wavelength 0.6-0.9 μm

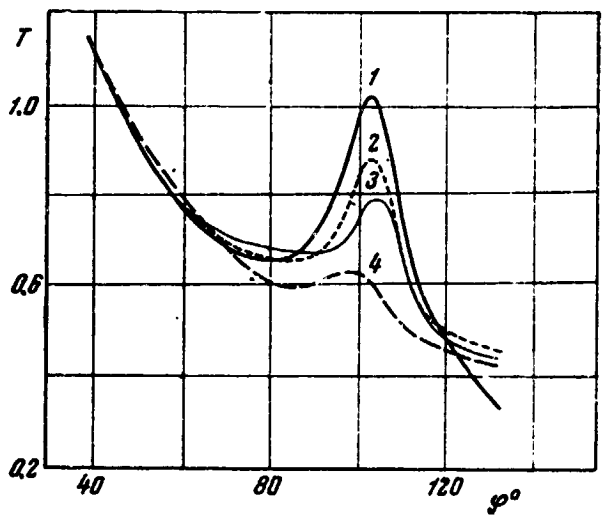

Fig. 4. Indicatrices of scattering for the angle of light incidence 40°
ϕ. Phase angle
T. In relative units, in all cases reduced to the same value at ϕ = 22°
1. Wavelength 0.33 μm
2. Wavelength 0.40 μm
3. Wavelength 0.60 μm
4. Wavelength 0.80 μm

When samples were illuminated at other angles, the nature of the indicatrix is somewhat changed. Except for an increase in the intensity of the reflected light, with decrease in the phase angle a low-intensity reflected light maximum is observed in the region of the phase angles corresponding to specular reflection of the source light from the sample investigated. The maximum of specular reflection becomes appreciable at angles of incidence of light exceeding 30°.

At smaller angles, the specularly reflected component cannot be detected against the background of scattered light, evidently owing to its low intensity. The relative intensity of the specular constituent depends markedly on the wavelength of the incident light, decreasing with an increase in this wavelength. Typical indicatrices of scattering for different spectral regions and for an angle of light incidence of 40° are shown in Fig. 4. In the wavelength range 330-950 nm, the relative intensity of the specular component is reduced by approximately five times.

As we can see from Fig. 4, the interval of angles at which the specular component is recorded is approximately 40°, that is the half-width of the effect is 20°. Here the maximum intensity is somewhat shifted toward the side of large angles with respect to the position of the exact specular reflection. When the sample was replaced with a mirror, an effect having an angular half-width of 2.5° was recorded at an angle exactly equal to the angle of light incidence. /499

The appearance of a maximum in the specular reflection against the background of the indicatrix of scattering was recorded for samples of Sea of Fertility regolith differing in particle size. This effect proved to be well pronounced for samples consisting of particles with dimensions in the range + 83 - 127 μm, where the surfaces of the samples during measurements were rough (a free heap was formed in the cuvette).

When the surface was smoothed, the intensity of the specular components rose markedly (smoothing was carried out by pressing a glass plate to the surface of the sample), and the interval of angles at which it was observed was narrowed.

The presence of a reflection maximum for the specular component in the indicatrix of scattering is evidently a specific feature of samples of lunar surface material, and the cause of its appearance evidently is the modification of the surfaces of regolith particles under the effect of secondary processes specific to the Moon. An analogous effect for powders of terrestrial rocks and meteorites was not noted in the literature and was not recorded by us. Measurements of the indicatrix of scattering of several powders of basalts, dunites, gabbro-diabase, and stony meteorites made with the same device yielded results that agreed with literature data /9/. The resulting indicatrices showed that the intensity of the reflected light increased sharply with decrease in the phase angle; the coefficients of reflection of all the samples investigated was much less than the coefficient of reflection of the samples returned by Luna 16.

A specular component specific to terrestrial-origin samples with rough surfaces, as well as to a sample of the Yefremovka chondrite did not show up even at angles of light incidence greater than 60°. Intense smoothing of the surface of samples (by rubbing a polished glass plate) led to the appearance of a very weak specular effect.

The angular half-width of the specular reflection effect here was more than 30°, and its intensity was very low.

The presence of specular reflection (along with diffuse reflection characteristic of rock powders) from samples of lunar

surface material evidently is due to features of the morphology of the surfaces with secondary-origin particles. Their characteristic property is the presence of vitrified surfaces in 40 percent of particles larger than 450 μm [1] and large number of glass spherules in the fine-grained fractions.

Some of these particles can have been oriented so that specular areas appeared on the sample surface. This consideration is confirmed also by a visual observation of regolith powder, in which the characteristic lustre distinguishing it from simulating powders of terrestrial-origin rocks is noted.

We measured the reflection spectrum of the specular constituent in the wavelength range 0.35-0.90 μm (spectrum 6 in Fig. 1). This spectrum differs somewhat from the diffuse reflection spectra of the samples investigated. Its main features, namely, structurelessness and monotonic increase in the coefficient of reflection with increase in wavelength persist in this case as well. However, the coefficient of reflection in the spectrum of the specular constituent, beginning with the wavelength of approximately 0.6 μm rises much faster than in the spectrum of the diffuse constituent, and it is somewhat lower in the region 0.5-0.6 μm.

Possibly, this difference in the reflection spectra of the diffuse and specular constituents accounts for the oft-noted difference in the hues of the regolith color, which have been judged by different observers to be both brown and greenish. Evidently, this is due to the differences in the conditions of illumination and observation, all the more so in that these differences were noted in the region of maximum visual sensitivity of 500-600 nm.

The above-indicated effects showing up upon examination of the optical characteristics of the regolith differentiated with respect to these parameters from terrestrial rocks. This is important, especially when we note that they are partially closely related in chemical composition. It is not precluded that these effects in the following can find use in telescopic observations in determining the relative content of particles of primary and secondary origin or the degree to which secondary processes have acted on various regions of the Moon.

REFERENCES

1. Vinogradov, A. P., "Preliminary Data on Lunar Surface Material Returned by Luna 16 Automatic Station," Geokhimiya (3), 261 (1971).

2. Antipova-Karataeva, I. I., Stakheyev, Yu. I., and Florenskiy, K. P., "The Optical Parameters of Mare Fecunditatis Regolith," Space Research XII, Life Science and Space Research X, Paper 19, 1971.

3. Hapke, B. W., Cassidy, W. A., Wells, E. N., Cohen, A. J., and Hodge, E., "Analyses of Optical Coatings on Apollo Fines," J. Geophys. Res. (in press).

4. Birkebak, R. C., Cremers, C. J., and Dawson, J. P., "Spectral Directional Reflectance of Lunar Fines as a Function of Bulk Density," Proc. Second Lunar Sci. Conf. 3, 21-97 (1971).

5. Garlick, G. F. J., Lamb, W. E., Steigmann, G. A., and Geake, J. E., "Thermoluminescence of Lunar Samples and Terrestrial Plagioclases," Proc. Second Lunar Sci. Conf. 3, 2277 (1971).

6. Nash, D. B., and Conel, J. E., "Luminescence and Reflectance of Apollo 12 Samples," Proc. Second Lunar Sci. Conf. 3, 2235 (1971).

7. Bershov, L. V., Borsuk, A. M., Vinogradov, V. I., Kondakov, A. A., and Chrenyshev, I. V., "Makeup of the Moon Based on Apollo 11 Materials," VINITI, seriya Itogi nauki. Geokhimiya, mineralogiya, petrografiya 150, (1971).

8. Gold, T., Campbell, M. J., and O'Leary, B. T., "Optical and High-Frequency Electrical Properties of the Lunar Samples," Science 167, 707 (1970).

9. Hapke, B. W., "Lunar Surface. Composition Inferred from Optical Properties," Science 159, 76 (1968).

Order of Lenin Institute of Geochemistry and Analytical Chemistry imeni V. I. Vernadskiy, USSR Academy of Sciences

Institute of Space Research, USSR Academy of Sciences, Moscow.

N75 11860

LIGHT SCATTERING INDICATRICES OF LUNAR SURFACE MATERIAL RETURNED BY LUNA 16 AUTOMATIC STATION

/501

N. P. Barabashov /deceased/, and L. A. Akimov

Abstract

Measurements are made of the indicatrix of scattering of lunar surface material with a special instrument -- an indicatometer -- with a spread of the illuminating beam of less than 0.5° and of the detected beam of about 1.5°. The results are compared with the indicatrices for the lunar mean obtained by terrestrial telescopic measurements. It is concluded that the main features of the reflection of light by the Moon (rapid rise in brightness with approach to the full Moon) are accounted for by the microrelief caused principally by grains smaller than a millimeter.

At the present time when the Soviet automatic station has returned to Earth samples of lunar surface material it has become possible to subject it to laboratory investigations.

Of interest to us is the study of the photometric properties of the lunar surface material taken from the upper part of the drill core.

The sample investigated was heaped onto a flat support 2 x 3 cm in size. The measurements were carried out with an indicatometer, specially designed for this purpose, with an illuminating light-beam spread of less than 0.5° and about 1.5° spread of the detected beam. The minimum angle of the phase was 2°. The maximum angle of the incidence and reflection was 60°. The measurements were conducted in a single vertical plane for angles of incidence i = 0, 30, 45, and 60°.

The results of measuring the brightness $B(i, \epsilon, \alpha)$ as a function of the angle of light incidence i and the angle between

RESULTS OF MEASURING BRIGHTNESS (B) OF LUNAR SURFACE MATERIAL

i	0°	30°		45°		60°	
α°	ε = α	ε = i + α	ε = i − α	ε = i + α	ε = i − α	ε = i + α	ε = i − α
2	1,000	1,000	0,970	0,980	0,937	0,938	0,882
5	0,867	0,875	0,832	0,870	0,790	—	0,705
10	0,743	0,750	0,673	0,751	0,638	—	0,560
15	0,676	0,692	0,597	0,687	0,543	—	0,474
20	0,630	0,651	0,545	—	0,475	—	0,415
30	0,560	0,570	0,475	—	0,400	—	0,330
40	0,520	—	0,436	—	0,361	—	0,277
50	0,492	—	0,418	—	0,338	—	0,241
60	0,470	—	0,410	—	0,328	—	0,230
70	—	—	0,410	—	0,335	—	0,225
80	—	—	0,424	—	0,350	—	0,232
90	—	—	0,462	—	0,381	—	0,250
100	—	—	—	—	0,450	—	0,283
110	—	—	—	—	0,540	—	0,353
120	—	—	—	—	—	—	0,512

the incident and reflected beam α are shown in the Table. The brightness for the phase angle $\alpha = 2^{\circ}$ and $\epsilon = 0$ was taken as 1.

Of major interest was the possibility of comparing these results with the indicatrices for the lunar average obtained by telescopic observations from the Earth.

Given in the figure are the indicatrices for the lunar surface material and the lunar mean found by N. P. Barabashov by interpreting the V. A. Fedorets catalog /1/.

From a comparison of these measurements, it can be concluded that the main feature of the reflection of light by the Moon (rapid rise in brightness with approach to the full Moon and attainment of the brightness maximum of details in the full Moon independently of the position on the disk) are accounted for by the microrelief, represented mainly by grains smaller than a millimeter. This confirms the conclusion made by us earlier based on an analysis of panoramas of the lunar surface taken by the Luna 9 station /2/.

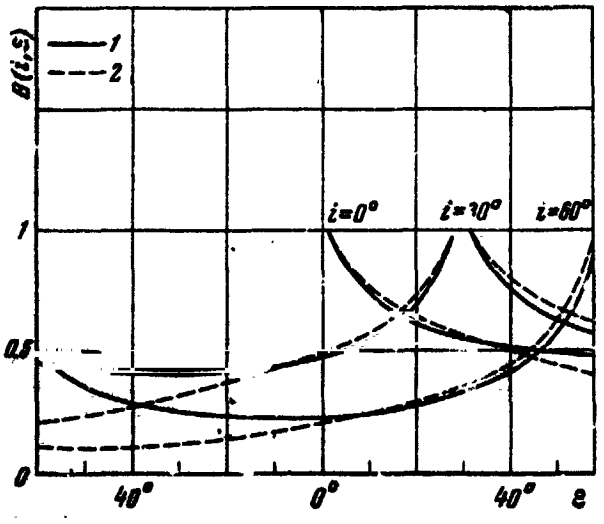

Indicatrices of scattering for lunar surface material (1) and lunar average (2)

The differences between /502 the indicatrices of the lunar surface material and the lunar average observable at large phase angles and large angles of incidence and reflection of light are evidently due to the diffraction of light by microrelief particles and by scattering within them. When the Moon is observed from the Earth, this rise is concealed owing to the averaging over large and more or less inhomogeneities constituting the meso relief from the lunar surface.

This phenomenon can be used for classifying regions on the Moon by degree of saturation with large inhomogeneities, through analysis of photographs of the lunar surface near the terminator at large phase angles.

In conclusion, the authors are indebted to Academician A. P. Vinogradov for giving them the opportunity to perform this study, and to I. I. Antipova-Karatayeva and to Yu. I. Stakheyev for assistance in carrying out the experiment.

REFERENCES

1. Fedorets, V. A., Trudy Astronomicheskoy observatorii Khar'kovsk. un-ta 12, 49-172 (1952).

2. Barabashov, N. P., and Akimov, L. A., Vestnik Khar'kovsk. un-ta (52), seriya astronomicheskaya (5), 18-28 (1970).

Astronomical Observatory
Khar'kov State University

N75 11861

INFRARED SPECTROSCOPY OF LUNAR MARE REGOLITH

/503

M. V. Akhmanova, B. V. Dement'yev, A. V. Kartashev, A. V. Karyakin, M. N. Markov, and M. M. Sushchinskiy

Abstract

Spectra of reflection, emission, and transmission of regolith returned by the Luna 16 automatic station were investigated in the 1.8-13 μm region. A reflection maximum (up to 30 percent) was shown to be present in the region 3-5 μm, along with a corresponding minimum in the emission coefficient. The spectra were interpreted based on a comparison of the optical properties with the chemical and structural properties of the regolith. The regolith in the entire array of properties in the infrared region differs appreciably from terrestrial objects. It was established from the scattering indicatrices that the specular effect of the increase in reflection at normal observation occurring in the visible and near IR regions disappears by 6-8 μm. In addition, the spectra of diffuse reflection and the spectra at angles of incidence 0° and angles of reflection 15 and 30° were investigated with samples of the regolith returned by the Apollo 11 and Apollo 12 missions. A comparative examination revealed a similarity of the infrared reflection characteristics of the regolith from different lunar mare regions. This is associated with similar dispersion properties of the surface material of lunar maria, the identical microporous structure of particles comprising the regolith, and also the closeness of the types of rocks, and their gross and mineral compositions.

The material from lunar mare regions investigated in samples returned by Luna 16 as well as by the Apollo 11 and Apollo 12 missions conducted with various techniques revealed that the regolith from the Sea of Fertility, Sea of Tranquillity, and the Ocean of Storms has many features in common as to rock type, gross chemical and mineral compositions of the rocks, similar dispersion properties, quite low and similar albedo values, and so on.

The investigation of the optical properties of lunar material in the infrared spectral region is of interest in refining the thermal regime of various regions of the lunar surface.

Also, the data can be used in finding the chemical and structural features of the regolith and for clarifying its nature.

In this present work, the study centered on a regolith sample returned by the Luna 16 station (zone Z based on the data in [1], weight 360 mg). This sample consisted of inhomogeneous particles with a mean size of 70 μm. Relatively large particles comprising most of the surface material were coated with smaller particles, 5-10 μm in size. Data on the chemical and mineral composition are in [1]. Also, the dust samples returned by the Apollo 11 mission (No. 10005,35-6, weight 142 mg) and the Apollo 12 mission (No. 12028,229-4, weight 114 mg) were analyzed. The samples were loose, with no tamping, heaped in a cuvette, and their porosity was 40 percent.

The reflection characteristics of the Moon in the infrared spectral region were obtained earlier for sections 100 km in extent and for the entire Moon by astronomical methods [2]. Future investigations will rely on remote measurements. These circumstances determined the formulation of the experiment in the present study. In particular, the beam spread when the reflection and emission spectra were investigated in illumination and observation did not exceed 1°. The thickness of the regolith layer was selected as quite high -- 1 mm. Investigation with near-parallel beams permits observing the effect of increase in reflectivity in specular angles.

The apparatus for obtaining the reflection and emission spectra included an illuminator, where a parallel beam was formed and the emission was modulated: an IKS-21 monochromator with an NaCl prism in a Littrow scheme and a special detector-amplifier system. Photocells of germanium doped with gold and mercury were used as the radiation detectors, with cooling down to the temperatures of liquid nitrogen or helium.

For observation at different angles and for construction of [504] the indicatrix, a mobile П-shaped mirror system was built in the illuminator; the axis of rotation of the mirror system coincided with the surface of the sample. Collimation and focussing of the emission at the monochromator slit was carried out with KCl lenses. The device for producing the reflection spectra and the indicatrix is shown in Fig. 1. The regolith spectrum was recorded at the points relative to the spectra of the etalon scattering scattering plate-diffusor. The diameter of the working area of the sample and the diffusor was 20 mm for the Luna 16 and 15 mm for the Apollo 11 and Apollo 12 samples. A matte-finish

coated with aluminum by vacuum vaporization served as the diffusor. This diffuser is virtually nonselective in the 1.8-13 μm region studied. However, its indicatrix varied over the section 7-13 μm, requiring special consideration. Use of a semitransparent KRS-5 plate in the Π-shaped device permitted the recording of reflection spectra at a strictly normal incidence and normal reflection. The illuminator made it possible to record the spectra at angles of incidence and reflection of 0-3 and 15-75°.

The diffuse reflection spectra were analyzed with an integrating sphere (Fig. 2). The 100 mm diameter sphere was made of copper, electrolytically coated with a matte silver layer. There were 20 mm diameter openings at the poles of the sphere for the entrance of the beam and the housing of the sample. The emission was recorded through an opening in the equator of the sphere without a focussing system between the sphere and the monochromator slit.

When the emission spectra were recorded, the modulator [chopper] was secured at the monochromator slit; only part of the mirror system was used in the illuminator (Fig. 3). The sample and the etalon [reference standard] irradiator (a disk coated with a thick layer of gold enamel) was heated by 30° with respect to the ambient medium to produce a thermal contrast.

Fig. 4 shows the design of a cuvette containing the regolith sample and the reference standard irradiator (or diffusor). The cuvette was provided with sylvite covers sealed with lead inserts to protect the sample against external influences.

In all cases, when the spectra and the indicatrix were measured, the sample was in air at room temperature. Within the limits of measurement precision, no changes were noted in the spectra in a time interval of 3 months for the Luna 17 regolith sample.

Fig. 5 a presents the reflection spectra of the regolith in the region 1.8-13 μm obtained with normal illumination of the sample and for observation angles of 0-15°. Some difference can be seen in the spectra in going from 0 to 15°. The spectra at observation angles of 15-75° are similar and are distinguishable only in intensity. In all cases the resolution in the spectrum was 0.25 μm (spectral width of the monochromator slit).

The reflection spectra of the regolith samples from Apollo 11 and Apollo 12 at angle of incidence 0° and angles of reflection 15 and 30° are shown in Fig. 5 b. Fig. 6 shows the indicatrices of scattering of the regolith for the selected regions 2.2, 4.5, and 7.5 μm. The spectra of diffuse reflection recorded

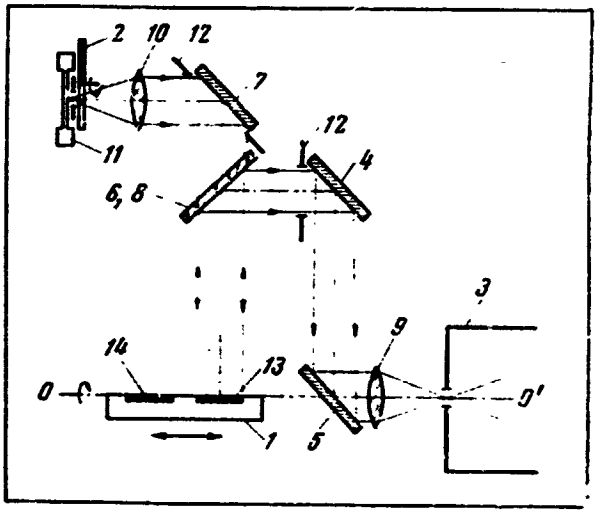

Fig. 1. Optical scheme of unit for obtaining reflection spectra and the indicatrix of scattering
1. cuvette
2. modulator [chopper]
3. monochromator
4-7. rotating mirrors
8. KRS-5 plate
9,10. lens
11. globar
12. diaphragms
13. sample
14. reference standard reflector

with an integrating sphere are [505] shown in Fig. 7 a and b. Fig. 8 presents the spectral trend of the coefficient of emission.

Let us discuss the experimental data obtained. We will examine first the spectrum of diffuse reflection obtained with the integrating sphere. The coefficient of reflection obtained for $\lambda = 1.8$ μm is 18 percent, close to our data for the Apollo 11 and Apollo 12 samples, and also the data in [3-5]. In the region 3-5 μm there is a flat maximum with a reflection coefficient of 30 percent. Then the reflection drops off virtually to zero at 9-10 μm. The trend of the spectral curves of the Apollo 11 and Apollo 12 samples as a whole is similar to the trend of the Luna 16 sample spectral curve, but with somewhat smaller albedo values. These spectra can be compared with astronomical data for the reflection properties of the moon in the infrared region (Fig. 9). As can be seen from the figures, the spectral trend of the curves is similar, but the albedo based on spectral data of the mare region regolith (Luna 16), as well as the Apollo 11 and Apollo 12 regoliths is smaller than the mean obtained by astronomical methods for the entire Moon (about 0.3 as compared with 0.4). The small albedo values for the visible region (~ 0.1) are evidently associated with the specific (hole-porous) structure of the particles comprising the regolith and with the presence therein of strongly absorbing elements. Thus, for example, divalent iron constituting part of various particles in minerals and rocks yields a very intense and broad electronic absorption band with a maximum at about 1 μm. The drop in the intensity of this band toward the infrared region can even lead to a rise in the reflection coefficient, reaching at the maximum 30 percent in the case of Luna 16 samples. The falloff in reflection toward the longer-wavelength direction is associated with the beginning of an intense absorption band characteristic of silicate rocks and minerals (absorption band of the vibrations of SiO_4 groups, isolated and bound).

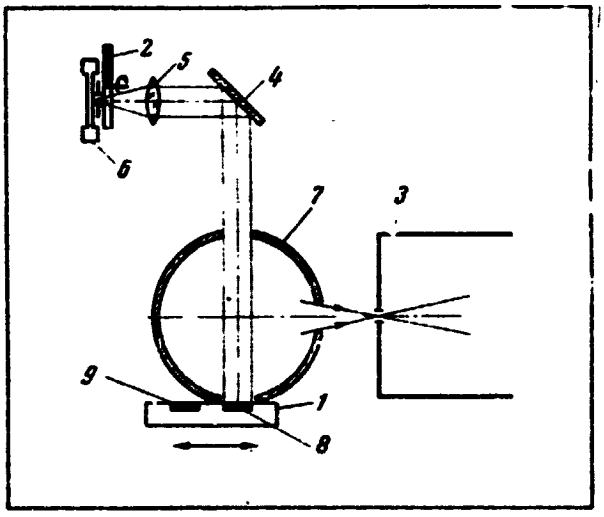

Fig. 2. Optical scheme of unit with integrating sphere
1. cuvette
2. modulator [chopper]
3. monochromator
4. rotating mirrors
5. lens
6. globar
7. integrating sphere
8. sample
9. reference standard

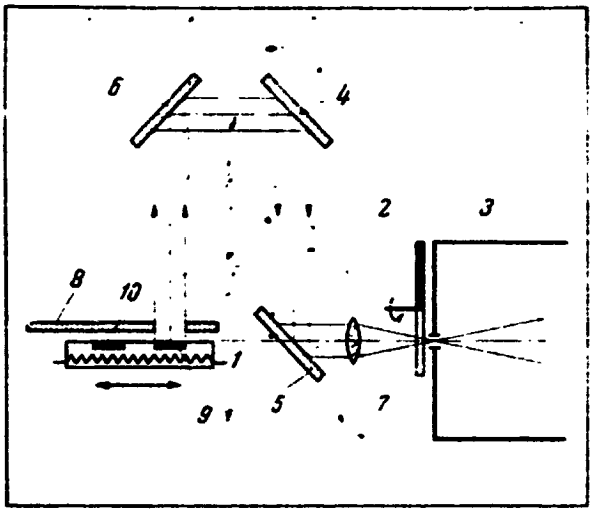

Fig. 3. Optical scheme of unit for measuring emission
1. cuvette
2. modulator
3. monochromator
4-6. rotating mirrors
7. lens
8. diaphragm
9. sample
10. reference standard emitter

The absorption maximum in this band, measured for thin layers, lies at 9.8 μm. But no increase in reflection is observed in this region, as for example, for quartz [6], when for large values of the absorption coefficient (much larger than 1000 cm^{-1}) the sample surface can function as a "metallic" sample. In the case of regolith, it does not reach such high values and "metallic" reflection is absent in this region.

As indicated above, regolith is a specific formation of particles neterogeneous in composition, size, properties, and -- in particular -- in optical properties. The nature of reflection by this material is unclear. Additional experiments with powdered materials with various sizes and absorbing and transparent in the region have been conducted to explain reflection. These experiments aimed at distinguishing, qualitatively, the effects of scattering and absorption for different disperion values of the material. For this purpose, the spectra of basalt, obsidian (particle 8-10 μm), and quartz (fractions with particle size 8.80-100 μm and 0.25-1 mm) were investigated. These materials show intense absorption in the same regions as does the regolith.

/506

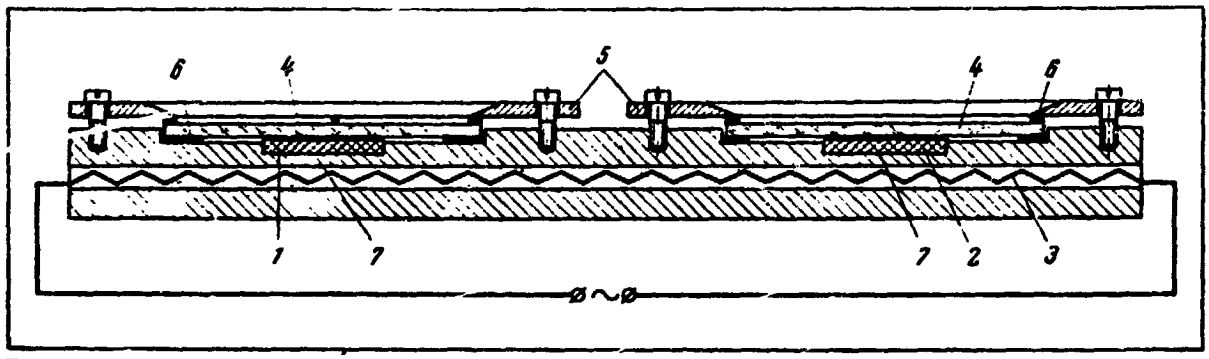

Fig. 4. Cuvette

1. sample
2. reference standard
3. heater
4. sylvite (KCl) windows
5. covers
6. lead spacers
7. thermocouples

Also analyzed was barium fluoride, with particle size smaller than 8 μm and 0.25-1 mm. It is completely transparent in this region. /507

The diffuse reflection spectra of the materials investigated are shown in Fig. 10. All these materials in the powdered form have reflection coefficients larger than that of the regolith. Upon inspection of the spectra, three regions can be distinguished: a region of transparency of the material, a region of the onset of absorption, and a region of intense absorption. The reflectivity of the materials depends weakly on particle size, remaining relatively high for all wavelengths, for example, for samples of BaF_2 powder the reflection coefficient in the 2-13 μm region is 70 percent. For the absorbing materials, the drop in reflection associated with the onset of absorption begins earlier for the coarser particles. Finally, in the region of intense absorption the intensity of "metallic" reflection falls off as one approaches the finer fractions (let us examine, for example, the reflection spectra of quartz in Fig. 10). A decrease in reflection for the absorbing materials is also associated with the onset of an absorption band. This means that the reflection recorded in the regolith spectra essentially is Fresnel reflection at particles transparent in this region.

The flat maximum in reflection in the 3-5 μm region is the result of the decrease in the intensity of absorption from two sides, from the side of the visible and from the side of the mid-infrared region. Depending on the chemical and the mineral composition, the position and intensity of this maximum can change.

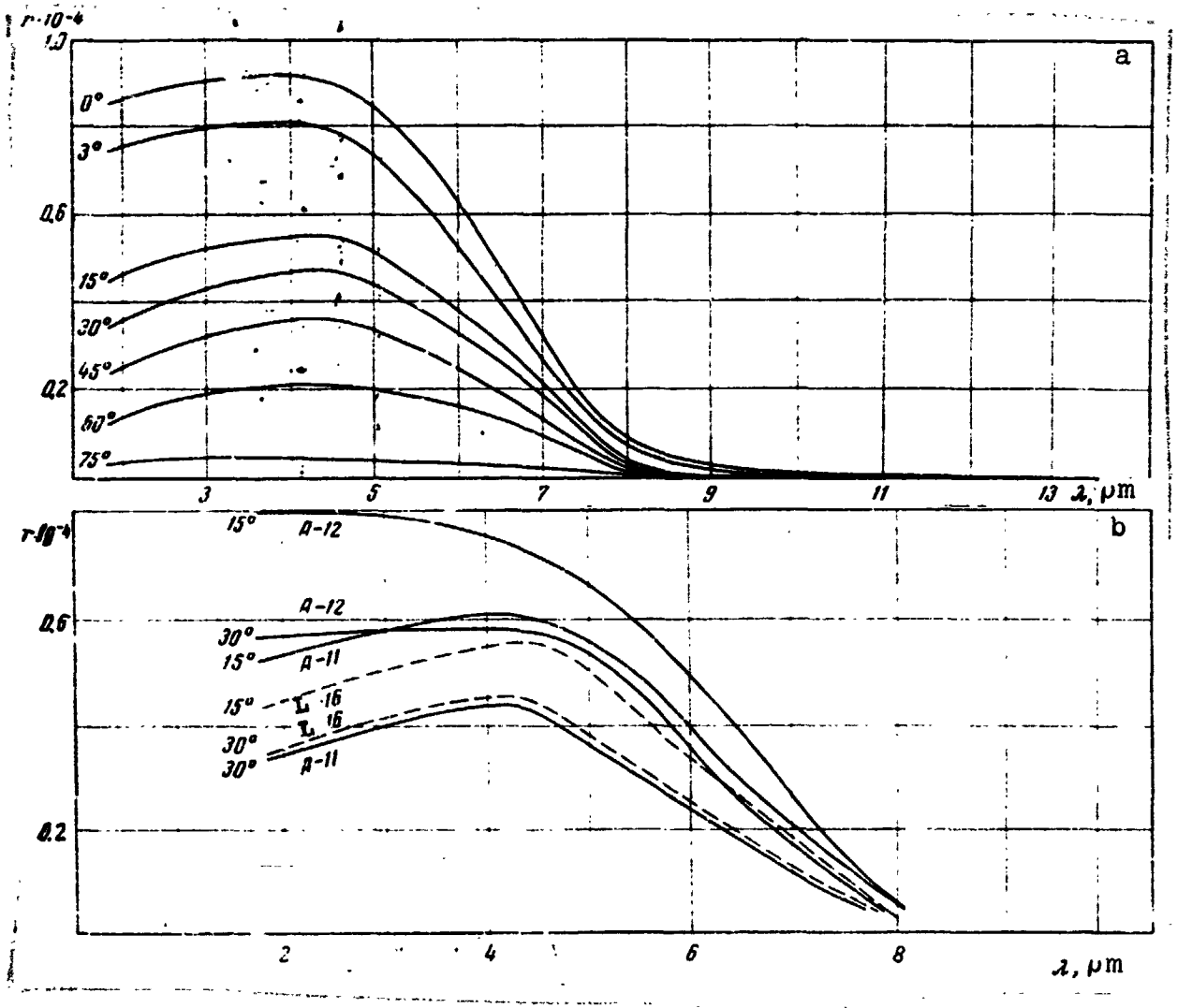

Fig. Regolith reflection spectra
a. at normal angle of incidence and at angles of observation from 0 to 75° (Luna 16)
b. at angles of incidence of 0° and of reflection of 15 and 30° (Apollo 11 and Apollo 12)

Thus, for example, the presence of carbonate minerals in rocks can shift this maximum toward the shorter wavelengths, and in the 4.5 μm region a minimum would appear in the reflection typical of carbonates (in particle, for calcites). Thus, in principle the reflection spectra -- as has long since been shown -- can be used for the gross determination of composition. Thus, in Fig. 10 it is clear that in the 3 μm region there is the characteristic manifestation of the absorption bands of water (basalt and obsidian). But in regolith, even following prolonged storage in air no water absorption bands show up, evidently indicating

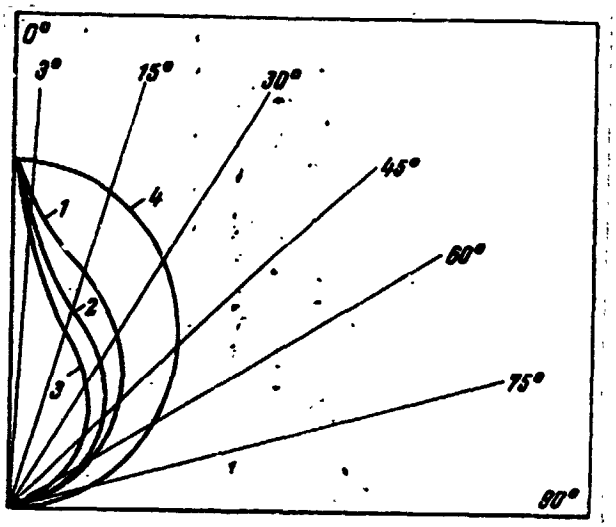

Fig. 6. Indicatrices of scattering of regolith (Luna 16)
1. λ = 7 μm
2. λ = 4.5 μm
3. λ = 2.2 μm
4. $I/I_0 = \cos\theta$ (θ = angle of reflection, I_0 = incident radiation, I = reflection radiation

that the regolith does not adsorb either water or carbon dioxide in detectable amounts. It is precisely in this fact that we have the uniqueness of the IR reflection spectra of regolith and their distinction from the spectra of terrestrial objects. The similarity of the reflection spectra of regolith samples from Luna 16, Apollo 11, and Apollo 12 evidently is linked with the dispersion properties of the surface of surface material from the various mare regions with identical microporous structure of the particles comprising the regolith and also with the closeness of the gross and rock composition.

Let us turn to the results of measuring the indicatrices of scattering of Luna 16 samples. In this case, the reflection spectra were measured for near-parallel beams and at normal incidence and observation angles 0-75° (see Fig. 5). A specular effect was noted at observation angles close to 0° (or a back-scattering effect), and relatively isotropic scattering at the angles 15-75°. As can be seen in Fig. 5, the specularity depends on wavelength, appearing most distinctly in the 2.2-4.5 μm interval. A decrease in the "specularity" at wavelengths longer than 4.5 μm can be attributed to a rise in the absorption of materials with a simultaneous change in the nature of scattering: scattering in the 4.5 μm region becomes more isotropic. This follows both from the nature of the indicatrix (see Fig. 6) as well as from a comparison of the spectra recorded with parallel beams and with the integrating sphere.

Investigation of the specular effect at the wavelengths 2.2 and 4.5 μm was also carried out on various terrestrial objects: basalt, obsidian, quartz, and barium fluoride. The table presents, at two angles of observation (0 and 15°) the coefficients of reflection at λ = 2.2 and 4.5 μm for regolith and terrestrial materials. The specularity is most pronounced in the case of the regolith at 2.2 μm. /508

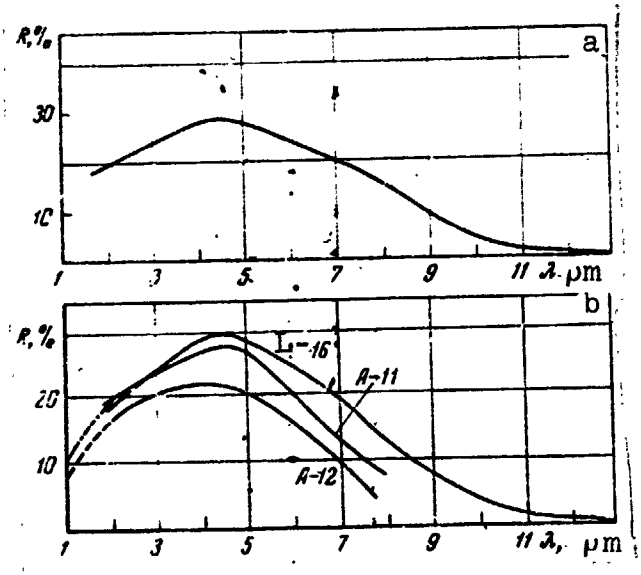

Fig. 7. Diffuse reflection spectrum of regolith
a. Luna 16 b. Apollo 11 and Apollo 12

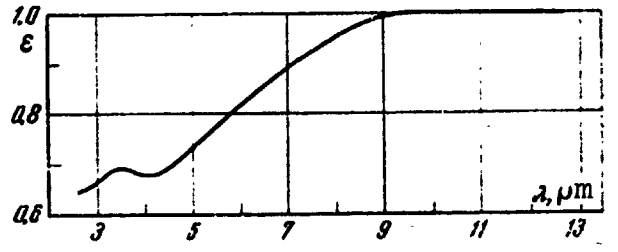

Fig. 8. Emission spectrum of regolith (Luna 16)

RATIO OF COEFFICIENTS OF REFLECTION OF POWDERS AT 0° ANGLE OF OBSERVATION TO THE COEFFICIENTS OF REFLECTION AT 15° ANGLE OF OBSERVATION. ILLUMINATION ALONG THE NORMAL TO THE SURFACE

Material	2.2 μm	4.5 μm
Basalt	1.4	1.6
Obsidian	1.1	1.2
Quartz, grain size 8 m	1.1	1
BaF_2 grain size 8 m	1.1	1
Quartz, grain size 0.25–1 mm	1	1
Luna 16 regolith	2	1.6

The coefficient of reflection at the 0° observation angle is nearly twice the reflection coefficient at the 15° observation angle. This excess is 1.5 for basalt and 1.2 for obsidian. For barium fluoride and quartz the specularity effect is absent. The sizes of the particles of terrestrial materials studied were

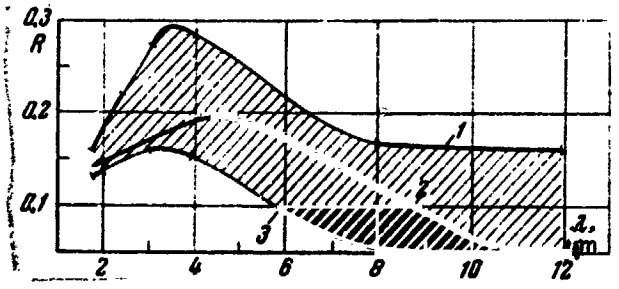

Fig. 9. Lunar albedo
1,3. limiting values of albedo, averaged for disk, obtained by astronomical methods
2. albedo of regolith sample from the Sea of Fertility

less than 8 μm. For terrestrial objects, the specularity at 2.2 and 4.5 μm is approximately the same. For the regolith the specularity effect at 4.5 μm decreases, becoming equal to the effect for basalt and virtually disappearing at the wavelengths close to 8 μm. Evidently, the dispersion of the material, its absorbing properties, as well as the presence in this material of a certain amount of fused "lustrous" material play a role in the occurrence of specular reflection in the regolith. Upon examination of the dispersion properties, it should be noted that for the entire visible region, the particle size remains greater than the wavelength of the incident radiation all the way to the near-infrared region. In the region beginning at 5 μm, some of the regolith material has particle sizes comparable with the wavelength and, further, toward the longer wavelengths some of the particles become smaller than the wavelength of the incident radiation. Accordingly, the ratios between scattering, transmission, and absorption undergo changes. Evidently, the relative role of absorption must climb, which can produce a drop in the specular reflection in the infrared region. The role of absorption in the visible region is not associated with particle size and therefore the specular effect in the visible region does not depend on absorption. On the other hand, if we assume that the specular reflection is produced by fused particles, these particles will also reflect where they do not absorb, or where they absorb very strongly. And the intense absorption of these particles, mainly fused silicate material, begins at 8 μm. But further on, at the maximum this absorption is not sufficiently intense so as to yield metallic reflection. /509

The reflection spectra of the Apollo 11 regolith at angles of incidence 0° and of reflection 15 and 30° practically coincide with those for the Luna 16 sample. Reflection of the Apollo 12 sample is somewhat stronger at these angles than for the Luna 16 and Apollo 11 samples. So we can conclude that the indicatrices of scattering of the regolith in the IR region for the Sea of Tranquillity and the Sea of Fertility are similar, and the indicatrix of scattering for the Ocean of Storms regolith is less extended.

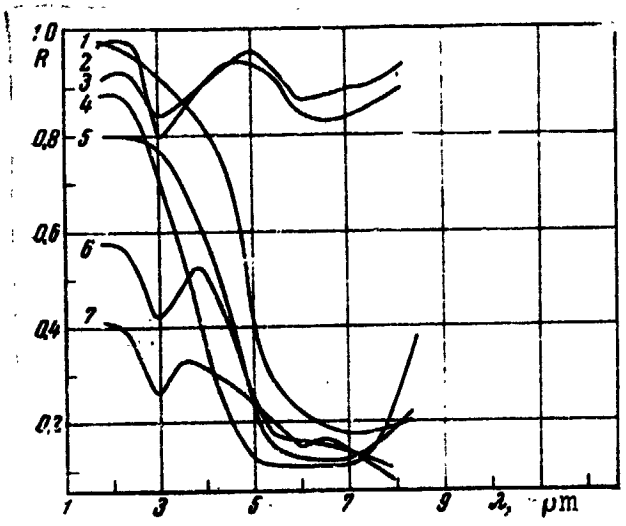

Fig. 10. Diffuse reflection spectra of powders
1. quartz (grain size < 8 μm)
2. BaF_2 (grain size < 8 μm)
3. BaF_2 (grain size 100 μm - 1 mm)
4. quartz (grain size 0.25-1 mm)
5. quartz (grain size 80-100 μm)
6. obsidian 7. basalt

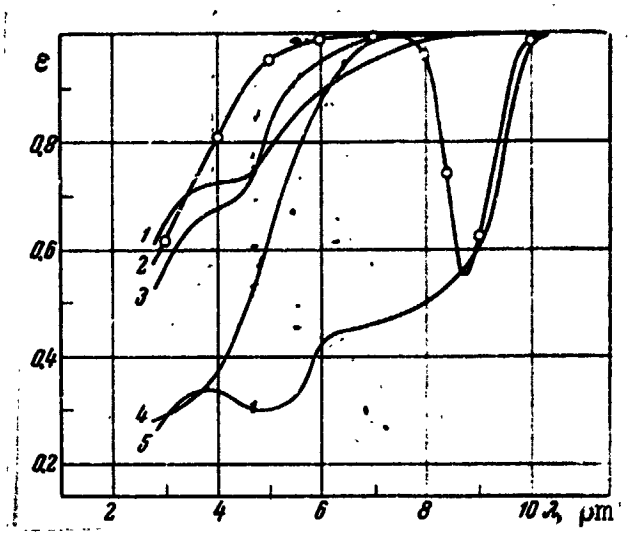

Fig. 11. Emission spectra of powders
1. basalt
2. quartz (grain size 0.25--1 mm)
3. obsidian
4. quartz (grain size < 8 μm)
5. BaF_2 (grain size 100 μm--1 mm)

In examining the intrinsic emission of lunar surface material, the problem was to obtain absolute values of the emissivity. A key factor here was the maintenance of constancy and equality of the temperatures of the emitting surfaces of the regolith and the reference standard irradiator (in our case, gold enamel). This can be achieved if the cuvette and the samples are in conditions that are close to thermodynamic equilibrium. In our scheme the conditions were close to equilibrium: the rate of influx of heat to the emitting surface was kept at the required level. The spectral dependence of the emission coefficient is shown in Fig. 8. It should be noted that on the average the spectral trend of the emission coefficient corresponds to the trend of the reflectivity obtained from the experiment with the integrating sphere. An exception is represented by the 2.8-4.5 μm region, where present in the emission spectrum is a structure indistinguishable in the reflection spectrum. The interpretation of this "singular" point is unclear. In this region, a maximum was obtained in measurement of the reflection and emission spectra of the far side of the Moon from Zond 3 [7]. The emissivity of the region of intense absorption, where "metallic" reflection is possible, can fall off, and -- for example -- this occurs in the investigation of coarse-grained quartz (Fig. 11). In the case of the regolith, no decrease

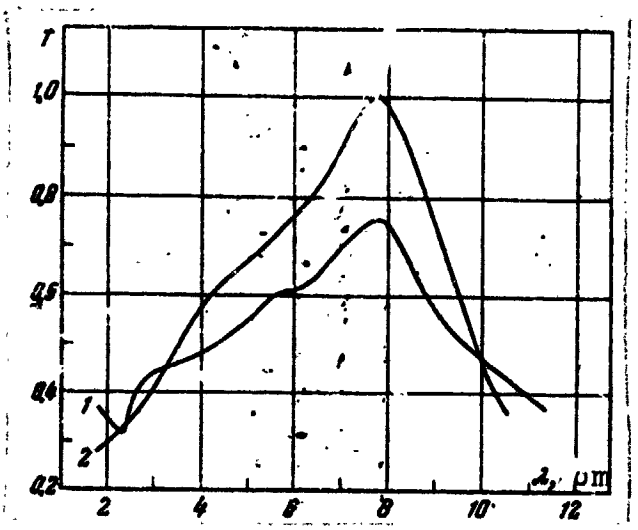

Fig. 12. Transmission spectrum of terrestrial basalt (1) and fine fraction of Luna 16 regolith (2) (thick layer)

in emission in the 9-10 μm region was observed. The emission spectrum of basalt (see Fig. 11) is similar to the regolith spectrum, but does not have a "singular" point in the region 2.8-4.5 μm.

To find the more detailed structure in the emission spectra, it would be desirable to place a sample in altogether different conditions, that is, to produce essential nonequilibrium conditions at its surface. For this purpose, the sample must be placed in a vacuum and its surface heated by emission from another source. This experiment was conducted with terrestrial samples, for example, in [8]. However, in this experiment it was virtually impossible to know or to equate with the reference standard the surface temperature and so no absolute emissivities could be obtained. /510

Highly interesting are the results of an analysis of the transmission spectra of regolith powder (Luna 16). The principal coarse fraction (particle size ~80 μm) was virtually opaque in the 2-13 μm region (its transmission t ~0.1 percent). Therefore, we investigated the fine fraction (particle size 3-5 μm) and found a sharp maximum of transmission in the 7-8 μm region (Fig. 12). The position and shape of this maximum are similar to those for basalt.

Such a sharp rise in transmission in this region is associated with the familiar Christiansen effect, occurring near an absorption band. The rise in transmission occurs at the wavelength at which the refractive index of the material and that of the dispersing medium coincide. In our case the dispersing medium is air with a refractive index close to 1. The position of the transmission peak, its half-width, and its intensity can be affected by particle size and by the absorption coefficient. The refractive index of regolith at 7-8 μm evidently becomes close to 1, which then causes the rise in transmission. Transmission drops rapidly in the 8-9 μm region -- the region in which the SiO_4 groups begin to absorb strongly.

Of definite interest is a characterization of the surfi ial layer of the lunar surface material (regolith) in terms of the model of a scattering and absorbing medium with two parameters κ and σ.

Naturally, these parameters cannot in this case be assigned to a specific regolith constituent and they must be regarded as being certain effective characteristics of the medium. As is known, the coefficient of reflection R from an infinitely thick layer in this model is of the form [9]:

$$R = (1 + \kappa/\sigma) - 1/\sigma\,(\kappa^2 + 2\kappa\sigma)^{1/2},$$

where κ is the absorption coefficient and σ is the scattering coefficient. At the same time, the transmission t of the thin layer with thickness l_0 is

$$t = (1-R^2)\exp\left[-l_0(\kappa^2+2\kappa\sigma)^{1/2}\right]/1 - R^2\exp\left[-2l_0(\kappa^2+2\kappa\sigma)^{1/2}\right].$$

An experimental (very rough) estimate for the transmission of a regolith layer with thickness l_0 = 0.2 mm in the 2-8 μm region (with allowance for scattering) the value t = 10^{-3}. Since on the average R ~ 10^{-4}, by solving the two equations jointly we find κ_{ef} ~ 100 cm^{-1} and σ_{ef} ~ 400 cm^{-1}. Thus, the regolith is a medium whose effective coefficients of scattering and absorption in the 2-8 μm region do not differ very widely.

The upper limit to the coefficient of absorption can be obtained from the transmission spectrum of a thin regolith layer. The transmission spectrum of the regolith sample in the 2-8 μm region, prepared by pressing a 3 mg sample with KBr powder, was recorded with a Zeiss UR-20 instrument (GDR). The thickness of the sample layer was assumed to be 10 μm. The absorption coefficient calculated from the expression $I = I_0\exp(-\kappa x)$ was of the order of 400 cm^{-1}.

Investigation of the radiation, reflection, and absorption properties of the regolith showed that we are dealing with a material differing widely in its properties from terrestrial rocks that can be compared with them (basalt, obsidian, meteorites, and so on).

The infrared spectra show that this uniqueness can scarcely be attributed solely to the regolith composition and the properties of its constituents.

On the other hand, a comparison of the regolith spectra with the spectra of materials known to us opens up the possibility of using the reflection spectra for analytical purposes, bearing in mind that the methods of infrared spectroscopy make it possible to conduct the analysis on a global scale. IR transmission spectra, with allowance for the Christiansen effect, also can

be of analytical application, for example, in investigating the /511 transmission of dust clouds.

Of no small importance is the fact that the infrared reflection and emission spectra of the surficial fraction of the regolith in general outline coincide with the first and very gross model of the spectrum obtained from terrestrial observations. Besides the already familiar example of determining the properties of the Venusian atmosphere, this case testifies to the adequacy of the physical methods in astronomy. As for the study of the natur of the regolith, it appears to us that this investigation is just the first step on this path.

In conclusion, the authors are deeply appreciative to the Vice President of the USSR Academy of Sciences A. P. Vinogradov, with it whose active cooperation this work could not have been done. The authors are indebted to K. K. Vul'fson for giving them the samples of the terrestrial rocks and minerals, and also to A. V. Ivanov, Yu. I. Stakheyev, and L. S. Tarasov for valuable conversations, advice, and assistance.

REFERENCES

1. Vinogradov, A. P., Priroda (3), (1971).

2. Markov, M. M., "Moon and Planets Session," Seventh International Space Science Symposium, Vienna, 1966, North-Holland Pub. Co., Amsterdam, 1967, pp. 53-59, edited by A. Dollfus.

3. Adams, J. B., and Jones, R. L., Science 167(3918), 737 (1970).

4. Johnson, T. V., Science 167(3918), 855 (1970).

5. Hapke, B. W., Cassidy, W. A., and Wells, E. N., Proc. Second Lunar Sci. Conf. 2, (1971).

6. Leconte, J., Infrakrasnoye izlucheniye /Infrared Radiation/ Fizmatgiz, 1958.

7. Moon and Planets II Session of Open Meeting of Working Groups I, II, and V of the Plenary Meeting of COSPAR, London, July, 1967, Amsterdam, North-Holland Pub. Co., edited by A. Dollfus, p. 55, 1968.

8. Loyd, Logan M., Science 169(3948), 865 (1970).

9. Ivanov, A. P., Optika rasseivayushchikh sred /Optics of Scattering Media/, Minsk, "Nauka i tekhnika," 1969.

N75 11862

PHOTOMETRIC AND POLARIMETRIC ANALYSIS OF SAMPLES OF LUNAR SURFACE MATERIAL RETURNED BY THE LUNA 16 AUTOMATIC STATION

/512

A. Dollfus, and E. Bowell

Abstract

Polarimetric properties were determined for the L-16-19-1-116 samples, weighing 0.087 g. The measurements were made for five wavelengths between 3540 and 5850 AU. In addition, the normal albedo was determined for each of these wavelengths. The albedo for the measured sample was slightly lower than for the typical material of the dark lunar maria (8.5 percent for orange light) and in addition, there was a well-developed branch of negative polarization, which resembles the branch obtained for carbonaceous chondrites crushed into powder, and the branch obtained for the powders of several terrestrial basaltic and ultrabasic rocks. It is not precluded that the polarimetric and photometric properties observed for the lunar sample impartially arose under the effect of solar wind irradiation which the lunar surface was subjected to.

Characteristics of sample. The sample given the Laboratory of the Physics of the Solar System by the Academy of Sciences of the Soviet Union is regolith powder sampled in zone V of the core between depths 20 and 22 cm. It was given to the laboratory on 22 April 1971 by the President of the National Center Space Research.

The sample, packed in weighing bottle No. 116, had a total weight of 0.177 g and was designated L-16-19-1-116. On 24 April 1971 it was transferred to a new plastic ampule provided with a label bearing the same code and was delivered in this form to the laboratory in Medon; on 22 May, 0.087 g was removed from the ampule. This fraction was the object of the investigation described below.

Measurements made. The same method which was used by Dollfus, Bowell, and Titulaer for terrestrial samples was used in the measurements. The sample was placed in a capsule on the horizontal stage of a goniometer with the horizontal axis. One of the sleeves of this goniometer housed a light source depolarized with quartz plates, and a collimator producing a parallel beam. In the other was a high-sensitivity photoelectric polarimeter, which was capable of detecting a faint beam of polarized light (up to 0.5 m/lumen from 0.2 cm^2 of sample surface).

The surface of the sample was first loosened up with a stainless steel pointing tool in order to make it rough and porous. This is precisely the structure that actually corresponds to the structure of the lunar surface.

The goniometer levers can be installed so that they cover the phase angles (the angles between the direction from the source to the sample and the polarimeter axis) between 3 and 12°. The polarization measurements were made at each half-degree between 3 and 125°, and then at 3° intervals for angles larger than 26°. The measurements were made successively with five color filters, whose wavelengths are indicated in Fig. 1.

The polarization curves obtained from these measurements are shown in Figs. 1 and 2 in the coordinates of the intensity of the polarized light versus the phase angle V.

The albedo measurements were also made with five light filters; the phase angle V was 5°, and the measurements were made for light reflected perpendicularly to the surface; the sample was compared with a MgO diffuser occupying the same position. A gray matte neutral screen was used to monitor the proportionality of the instrument readings and the light intensity.

Results and conclusions. The polarization curves shown in Fig. 1 are interesting in many respects; some of their sections yield information on the optical and physical properties of the sample.

Negative branch of polarization curve. The corresponding /513
results are given in a magnified scale in Fig. 2. The results are identical for all filters in this region of phase angles.

A comparison of the curve obtained from investigating the Soviet sample L-16-19-1-116 with the results of terrestrial telescopic measurements for a number of lunar surface materials shows that the negative branch of the curve is more developed, the minimum polarization P_{min} is relatively smaller, and the inversion angle V(0) is smaller.

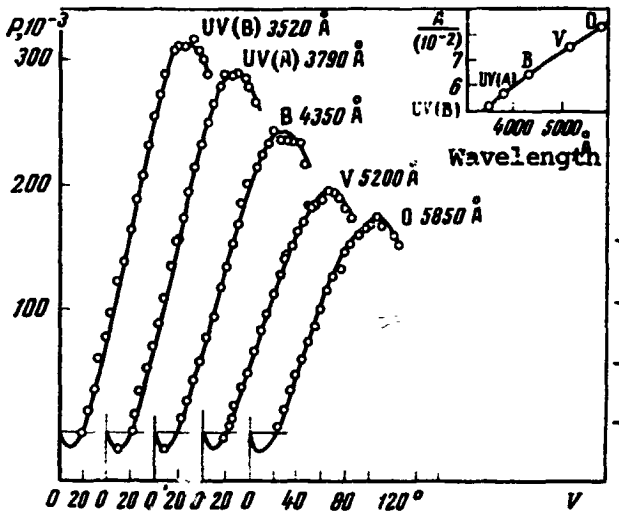

Fig. 1. Curve of polarization of the Luna 16 lunar sample L-16-19-1-116 for five wavelengths. Given in the insert in the upper right are the measurements of the albedo as a function of wavelength, related to measurements of the scattering magnesium oxide screen.

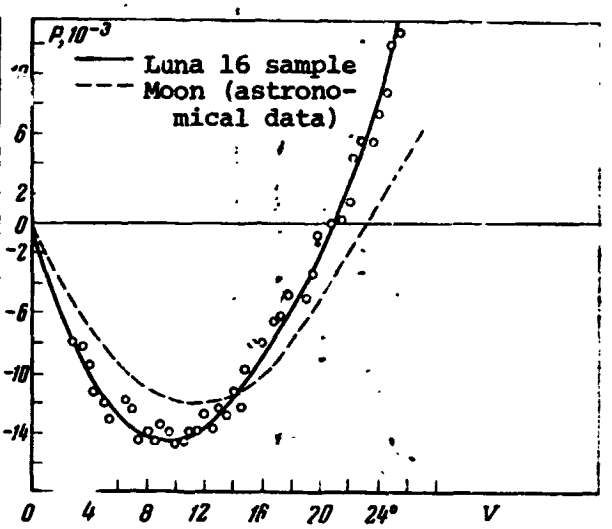

Fig. 2. Negative branch of polarization curve for the Luna 16 lunar sample L-16-19-1-116, measured in the laboratory, and for the lunar surface observed through telescope

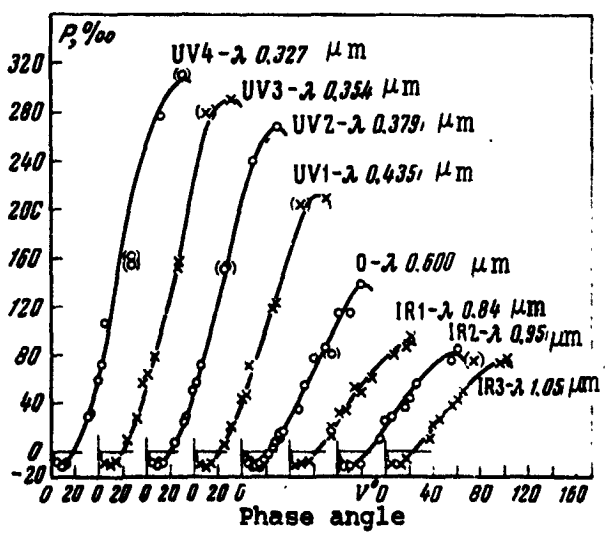

Fig. 3. Polarization curves of the region in the Sea of Rains obtained with a telescope.

These differences between the curves obtained in the laboratory for the Luna 16 sample and for the Moon by telescopic observations can depend on different factors, in particular, on the structure and compactness of the powdered material, the optical opaqueness of the grains, and the granulometry of the powder.

In the case of the Luna 16 sample, the difference evidently is accounted for by the opaqueness; the grains apparently absorb light much more strongly than on the average do the other lunar samples. However, we cannot preclude also a difference in granulometry. The sample was taken from a depth between 20 and 22 cm below the surface. In addition, during the sampling

OPTICAL DATA FOR LUNA 16 REGOLITH FROM THE SEA OF RAINS

Filter	L-16-19-1-116		Sea of Rains	
	P_{max}, °/₀₀	$V_0(P_{max})$	P_{max}, °/₀₀	$V_0(P_{max})$
Orange	173	106±3	128	105±5
Green	197	107	—	—
Blue	242	107	216	105
Ultraviolet (A)	289	105	257	105
Ultraviolet (B)	314	108	293	110

time or during manipulations in the laboratory, changes in the granulometric composition may have occurred. It should be noted that the Luna 16 sample is unique: its negative branch considerably deviates from the curve obtained from telescopic observations.

Positive branch of polarization curve. Fig. 1 shows that this portion of the curve depends strongly on wavelength. For this reason it is useful to determine the value P_{max} -- the polarization maximum, and also the phase angle $V(P_{max})$ corresponding to it, for different wavelengths.

We must compare the measurements made on the Luna 16 sample /514
in the laboratory with those obtained by telescopic observation of the neighborhood of the landing site in the Sea of Rains (see Table). Telescopic observations are reproduced in Fig. 3.

The values of $V(P_{max})$ agree with each other, but the values of P_{max} are systematically higher for the Luna 16 sample than those that correspond to the Sea of Rains samples. This difference shows that the sample taken (from between 20 and 22 cm from the /515
surface) is not characteristic with respect to the polarization properties for the entire region of the Ocean of Storms, whose data were obtained with a telescope.

Albedo for five spectral regions for $V = 5^{\circ}$.

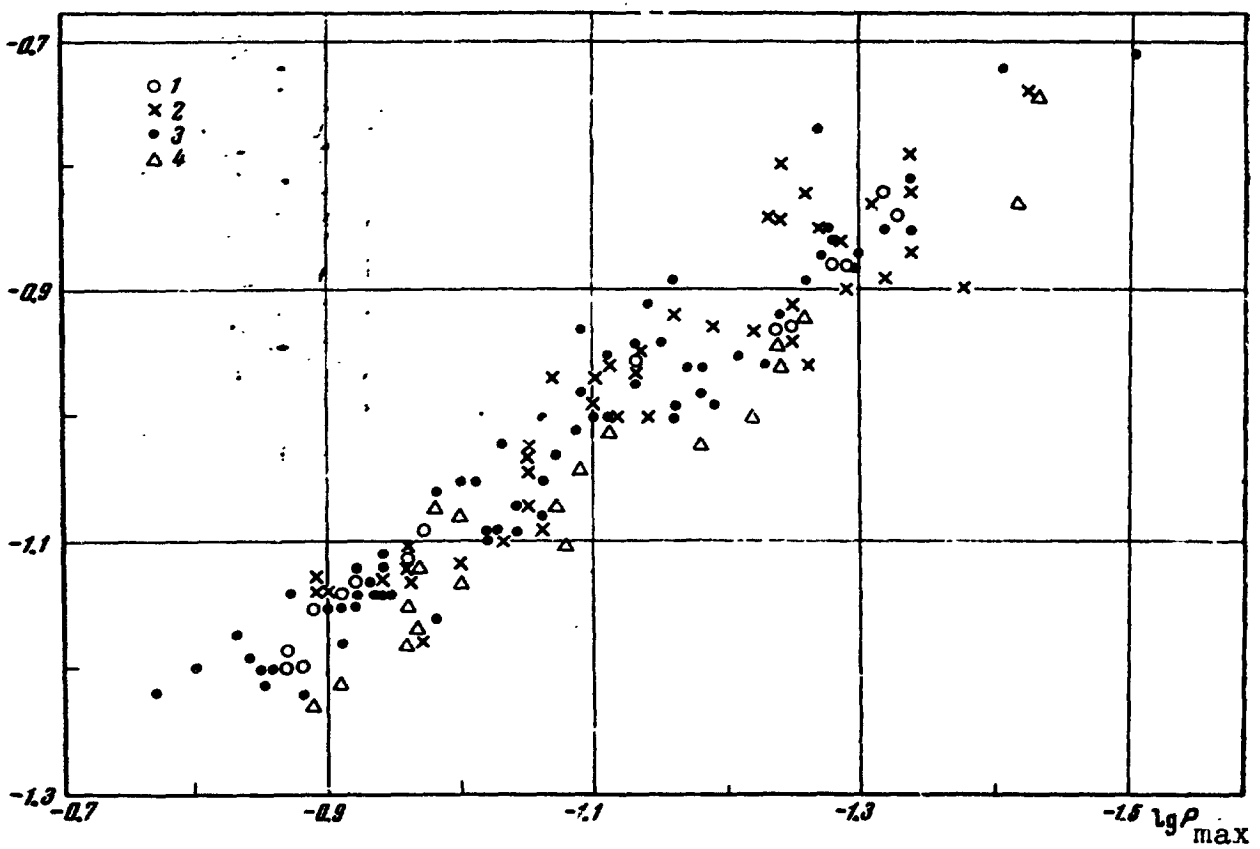

Fig. 4. Diagram relating albedo of lunar surface A with maximum polarization P_{max} expressed in logarithmic scale, for 144 lunar sections (orange light, λ = 5850 AU)

Measurements:
1. Dollfus (65")
2. Dollfus (5")
3. Bowell (5")
4. Wilhelm (15")

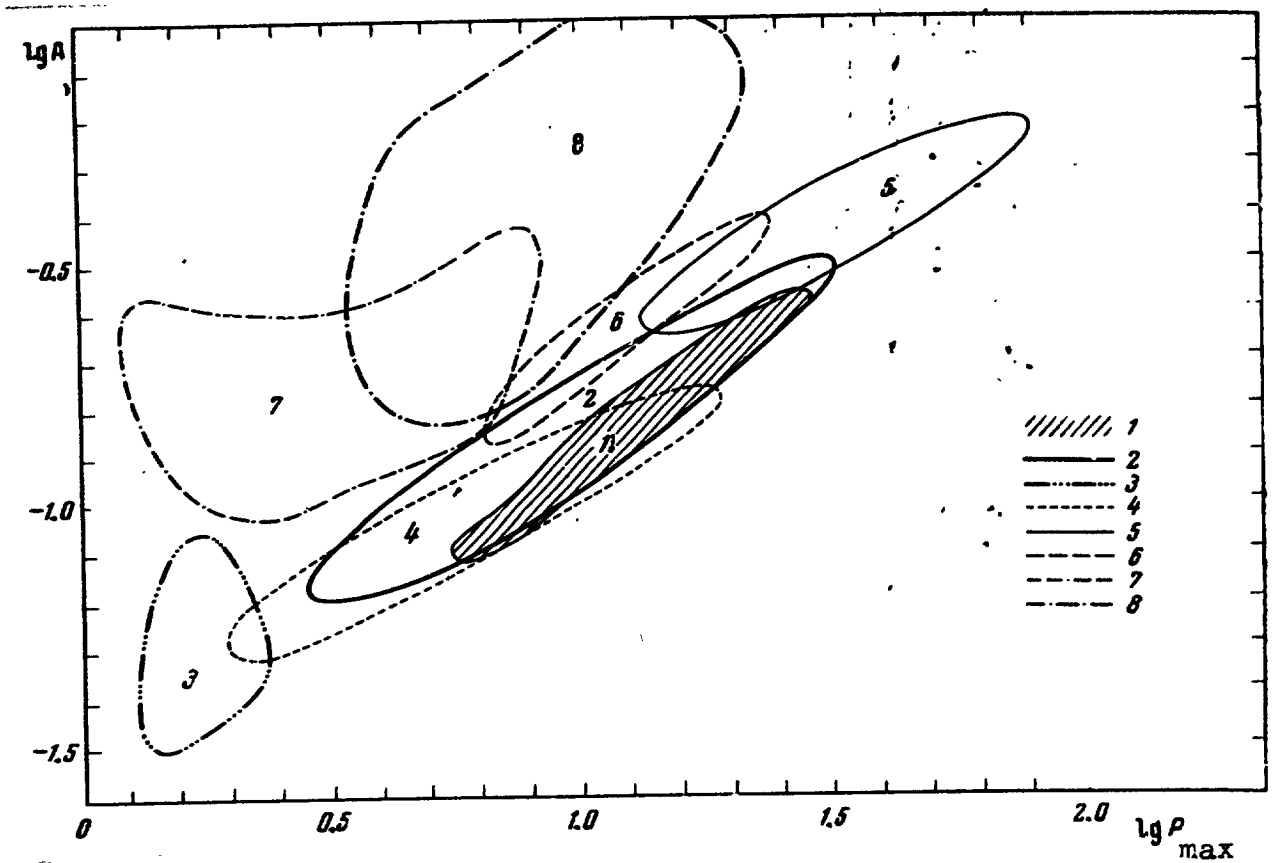

Fig. 5. Diagram of log A as a function of log P_{max} for different samples of terrestrial crushed minerals and for lunar measurements derived from Fig. 4.

1. Lunar measurement
2. Powders of basaltic lavas
3. Powder of glassy basalt
4. Volcanic pumice
5. Powder of ignimbrite
6. Meteoritic powder
7. Coarsely crushed rock grains
8. Sands, clays, chalk

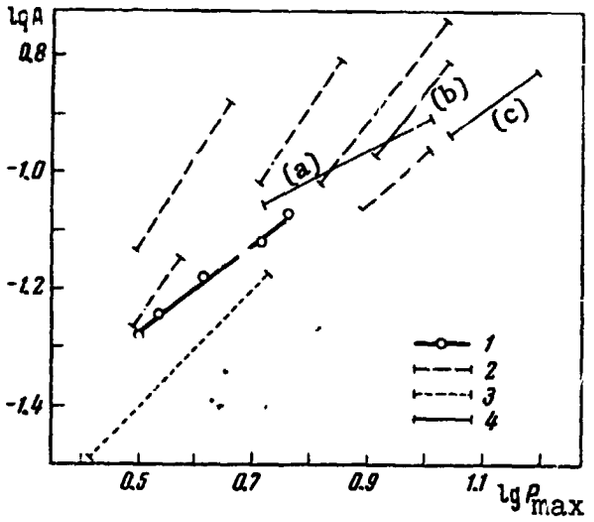

Fig. 6. Diagram of log A as a function of log P_{max} for different wavelengths. The right and left cutoff boundaries correspond to wavelengths of 5850 and 3540 AU. Results of measurements for each of the filters used are presented for the Luna 16 sample. The corresponding segment is at the left cutoff of the region characterizing the Moon in orange light. Therefore, the sample corresponds especially to the dark lunar material.

1. Luna 16, sample L-16-19-1-116
2. Terrestrial basalts
3. Carbonaceous Orgeueil chondrite
4. Apollo 12

a. Sample 12-28-204
b. Sample 12-28-299
c. Sample 12-032

The values measured are given in Fig. 1 and in the following: /516

Filter	Albedo A, percent
Orange	8.5
Green	7.6
Blue	6.6
Ultraviolet (A)	5.1
Ultraviolet (B)	5.3

Diagram in the coordinates log A as a function of log P_{max}. The data of telescopic observations of P_{max} and A obtained for different regions of the Moon are plotted in the diagram with the log A along the X axis and the log P_{max} along the Y axis. They occupy an intermediate region with the linear dependence of log A on log P_{max}. Fig. 4 gives the results of 144 measurements of small lunar regions obtained by us in 1971. They were made at the wavelength 6000 AU. In addition, P_{max} and A varied with wavelength.

Data of analogous laboratory measurements of crushed terrestrial specimens treated by the same method form different characteristic regions in the log A vs log P_{max} plot. Fig. 5 summarizes the results obtained for numerous laboratory samples by Dollfus and Titulaer in 1971. The region embracing the data of the telescopic measurements of the Moon (see Fig. 4) is also plotted in the diagram. Fig. 4 shows that the photometric and polarimetric characteristics of the lunar surface material are simulated best by finely crushed basalts. /516

This simulation can be even more refined if we take note of the variability of the properies of P_{max} and A as a function of wavelength. Fig. 6 gives in the coordinates log A and log P_{max} the data obtained for the lunar sample L-16-19-1-116, for lunar samples returned by Apollo 12, for crushed terrestrial basalts, and for the carbonaceous chondrite Orgueil. For the Luna 16 samples the different points in the plot correspond to different wavelength for which the measurements were made. The corresponding segments are the longer, the more intensely covered is the sample, and their position in the diagram depends on the general optical properties of the material.

Judging from the polarization criteria as well as albedo and coloring, we can conclude from the diagram that the Luna 16 sample is characteristic of the darkest materials that can be found in the lunar maria. From this standpoint, and also from the data on the singular form of the negative polarization branch (see Fig. 2), the lunar sample returned by the Soviet Luna 16 automatic station is of special interest; it reveals unusual optical properties.

REFERENCES

1. Dollfus, A., and Bowell, E., "Polarimetric Properties of the Lunar Surface and Its Interpretation, Part 1: Telescopic Observations," Astronom. Astrophys. 10, 29 (1970).

2. Dollfus, A., and Titulaer, C., "Polarimetric Properties of the Lunar Surface and Its Interpretation, Part 2: Terrestrial Samples in Orange Light," Astronom. Astrophys 10, 450 (1971).

3. Dollfus, A., and Titulaer, C., "Polarimetric Properties of the Lunar Surface and Its Interpretation, Part 3: Volcanic Samples in Several Wavelengths," Astronom. Astrophys. 12, 199 (1971).

Laboratory of the Physics of the Solar System,
Paris Observatory, Medon, France.

N75 11863

PHOTO-POLARIZATION STUDY OF LUNAR SAMPLES -- NEGATIVE BRANCH

/517

A. Dollfus and E. Bowell

Abstract

The program of polarization measurements conducted in the Medon Observatory was divided into two parts: measurement with a telescope of the degree of polarization of light reflected by planetary surfaces; comparative measurement of terrestrial minerals, meteorites, and the returned lunar samples. The polarization curve-plots of the dependence of the degree of polarization on the phase angle V (the angle: source -- sample -- observer) are plotted and compared with each other to determine the optical characteristics of the planetary surfaces.

All the solid surfaces of planet have polarization curves, for which P is negative given small V ($\lesssim 30°$) and positive for large V; the maximum P_{max} is attained in most cases when $V \approx 100°$. Positive branch (large angle V) and P_{max} vary with wavelength, but in most cases the negative branch remains unchanged. There is a linear /519 correlation between albedo A (reflectivity) and P_{max} for the moon (see plot in logarithmic scale, Fig. 1, in studies of the Third Houston Conference). P_{max} depends on the optical opaqueness of the sample: intensely opaque samples reproduce the results obtained for the Moon, while opaque and translucent samples do not reproduce them (Figs. 1 and 2). Most terrestrial minerals and meteorites do not follow this relation; some extrusive basalts and meteorites correspond to it. The same values were obtained for all samples of lunar surface material and several breccias measured as for the lunar surface for observations taken with the telescope, but the values deviate widely for several breccias and for all crystalline lunar rocks.

The negative branch of the polarization curves was obtained mainly through multiple scattering at contiguous facets of submicron-sized particles. For the Moon, the negative branch remains unchanged

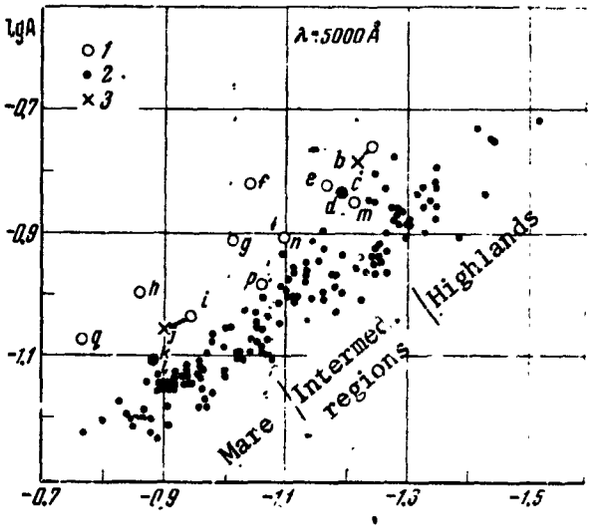

Fig. 1. Dependence of albedo A on maximum degree of polarization P_{max} (logarithmic scales) for 144 lunar regions and 16 samples of lunar surface material; the low A/high P_{max} is in the lower left hand corner of the diagram.
1. regolith returned by Apollo spacecraft (laboratory investigations)
2. lunar surface (astronomical investigations)
3. samples irradiated with protons. The sample number in the graph is indicated by the following letters: a. 12033; b. 12033 irradiated; c. 12032; d. 12032 irradiated; e. 12028,155; f. 12028,90; g. 12028,203; h. 12038,55; i. 12070; j. 12070 irradiated; k. 10084; l. 10084 irradiated; m. 14163,29; n. 14003,12; p. 14259,39; q. Luna 16, sample 16-19-1-116

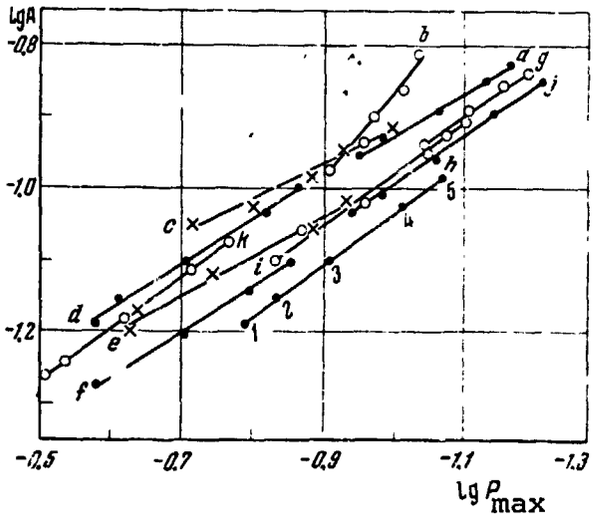

Fig. 2. Diagram of log A/log P_{max} and variations of these parameters for 11 lunar samples as a function of wavelength. The wavelengths 3520, 3790, 4300, 5200, and 5800 AU were used. The measurements for each sample are joined by the same line, on which the points are arranged according to the indicated series of wavelengths, like points 1-5 on line h. The points in the lower left hand of each line correspond to measurements at shorter wavelength. Usually, the longer the line, the more red the sample. The sample numbers in the graph are denoted with letters: a. 12028,155; b. 12028,98; c. 12028,203; d. 12028,55; e. 12070; f. 10084; g. 12032; h. 14259,39; i. 14003,12; j. 14163,29; k. Luna 16.

from place to place in telescopic observations, and we conclude that the lunar surface is everywhere reworked to the same microstructure. Terrestrial rocks are highly diverse and sometimes do not have a negative branch. Individual lunar samples disclose some changes in the polarization curves, and we are attempting at present to relate the shapes of their negative branches with a microstructure disclosed in electron microscopy.

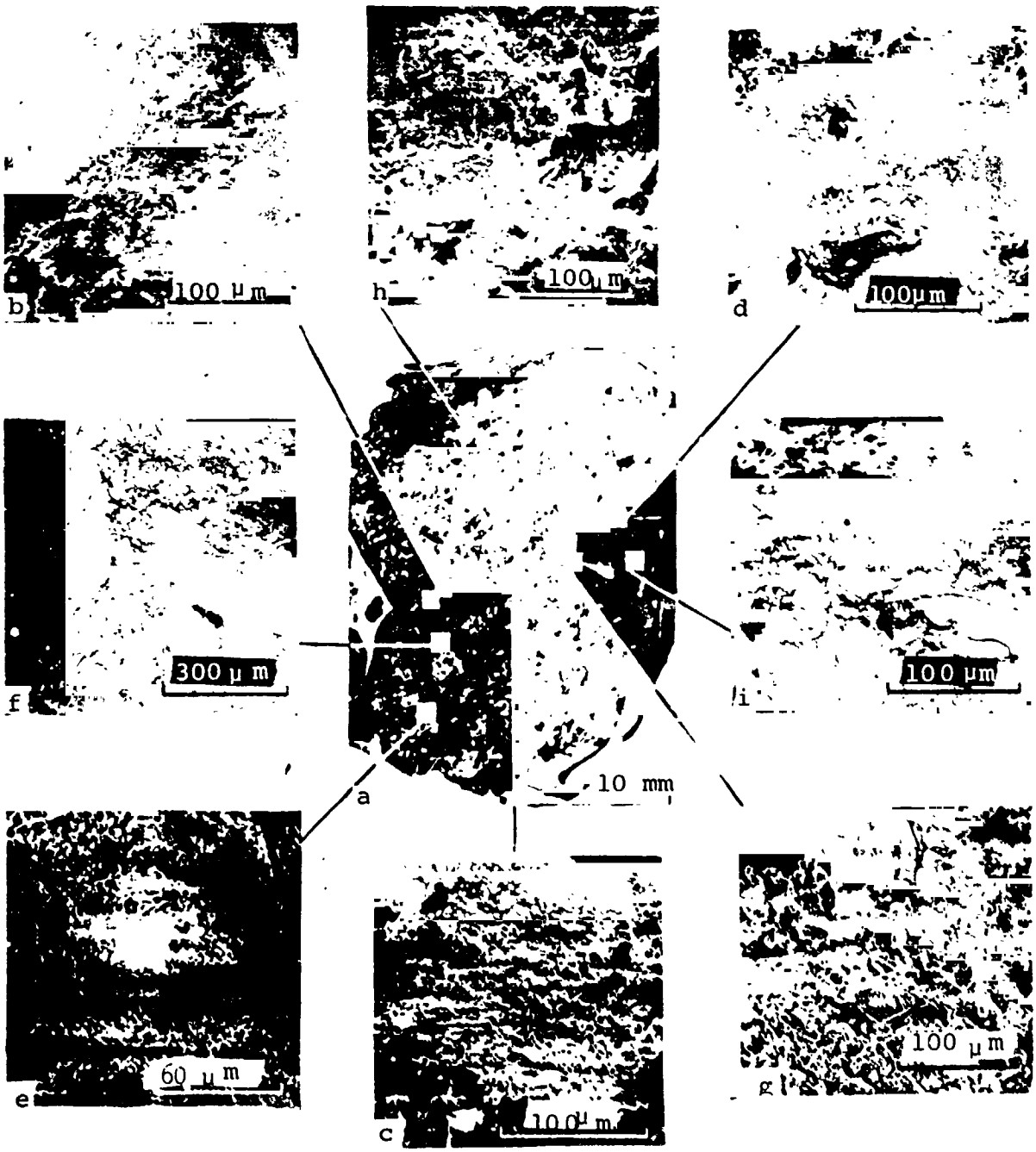

Fig. 3. Breccia 14267. Surface fragment in center (a) and images of fragment sections taken with a scanning electron microscope. Sections c and d are covered with dust, sections b, e, f, g, h, and i are covered with glass

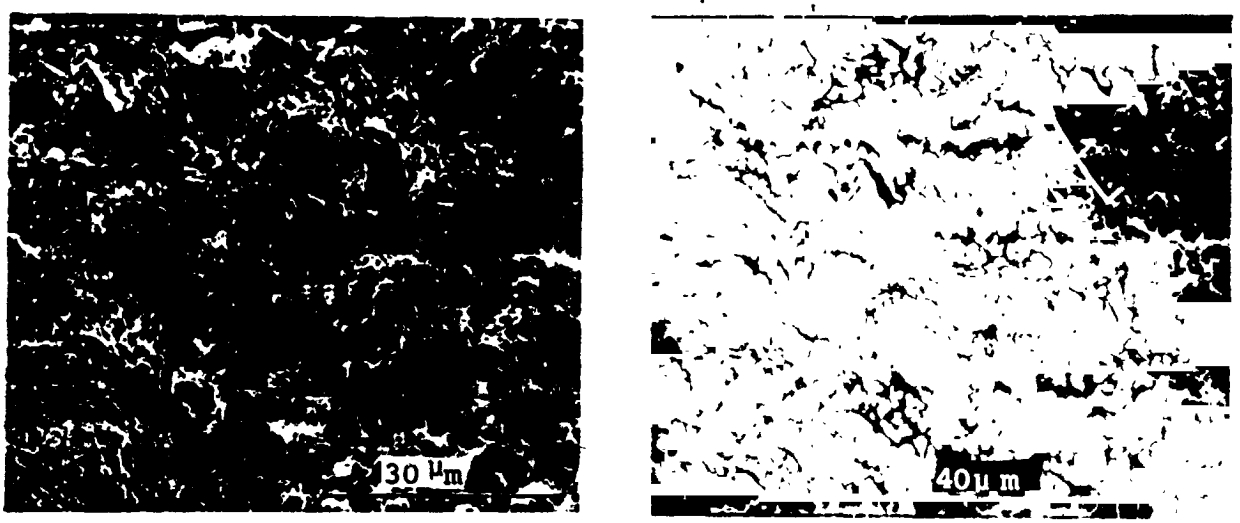

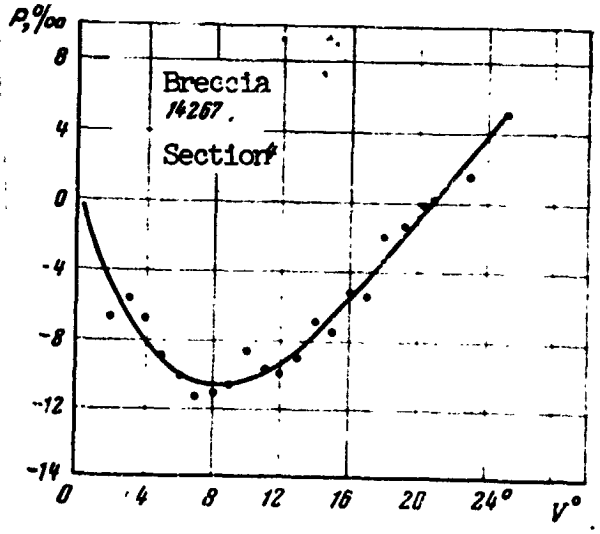

Fig. 4. Breccia 14267, region a, covered with dust. The two energies of the surface in the scanning electron microscope are as follows: left at a magnification of 1100, right -- 1350, and polarization curve

The photographs in this article pertain to a sample of the fine fraction of Luna 16 lunar surface material, to the breccia 14267 of the European Consortium, and to the Orgueil meteorite. We investigated three surface types for the breccia: freshly exposed surface, surface covered with glass film, and surface covered with dust. The Luna 16 surface material and the powdered material of the Orgueil meteorite were dusted with gold and mounted on aluminum stages for electron micrography. Below are given descriptions of the photographs.

Breccia 14267. In the center (Fig. 3) arrows indicate the appearance of the exposed surface of the rock and the location of the regions investigated. Typical microphotographs of all the areas investigated are shown (magnifications from 70 to 350). Below is presented the description of the most important sections. The surfaces of all regions are covered with fine particles.

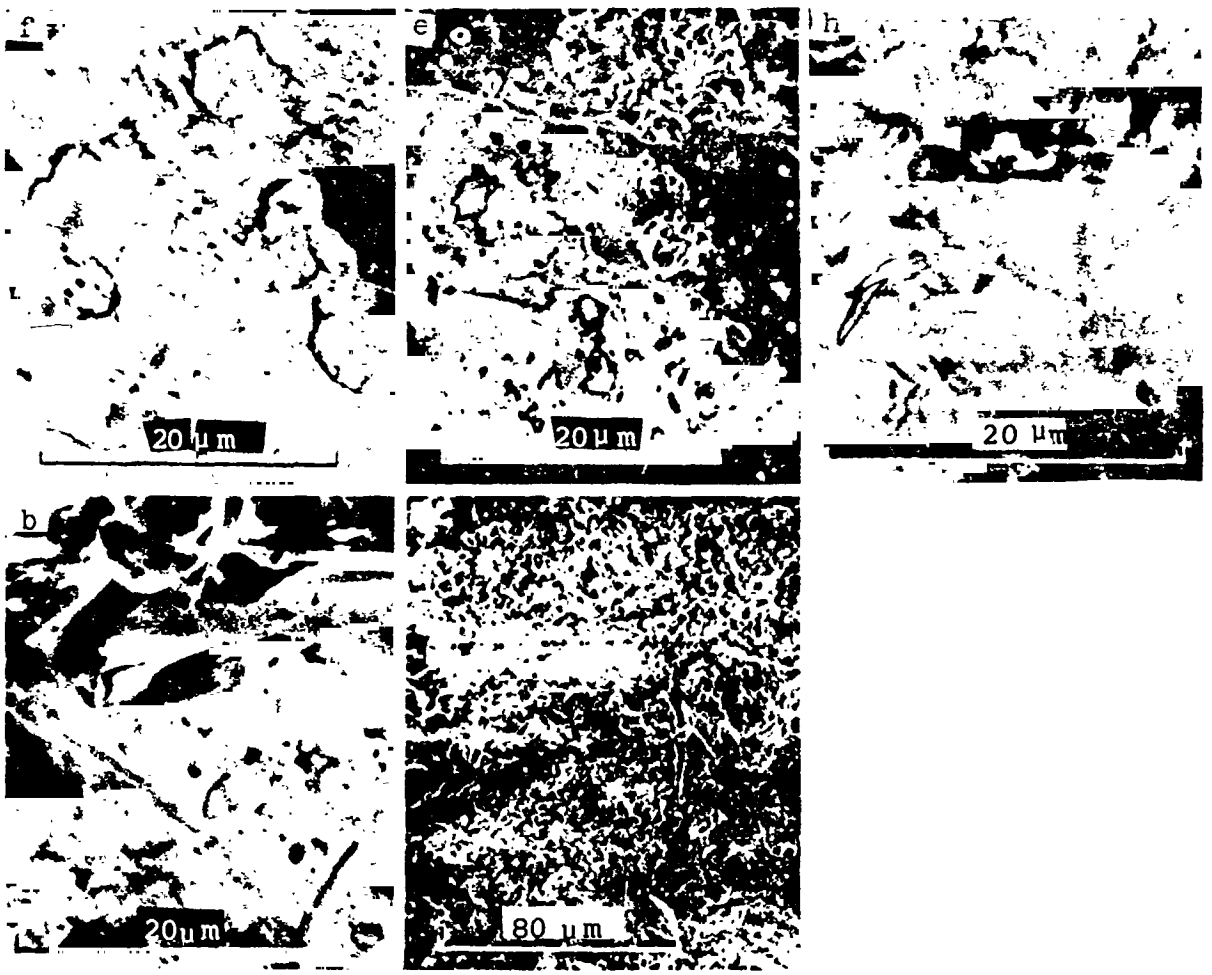

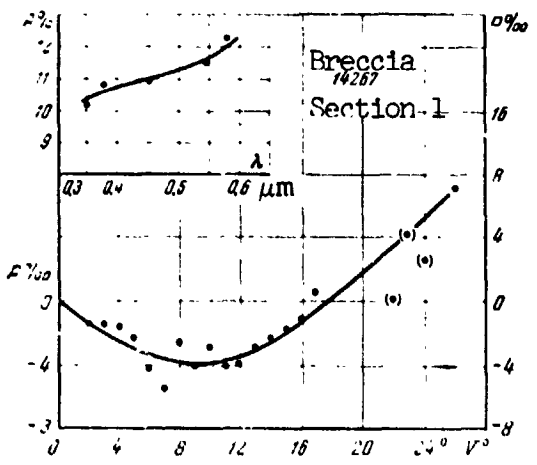

Fig. 5. Breccia 14267, regions b, e, f, and j covered with glass. The images of the surface of the four sections are taken with a scanning electron microscope at a magnification of 2000 (three photos) and 2500 (the photo in the upper right) and the appearance with moderate magnification (425) is in the middle row, right. Below are the polarization and albedo curves for the vitrified section.

* corresponding to a change in the photographs. The photo of section b is erroneously designated c [correction has been made by translator]

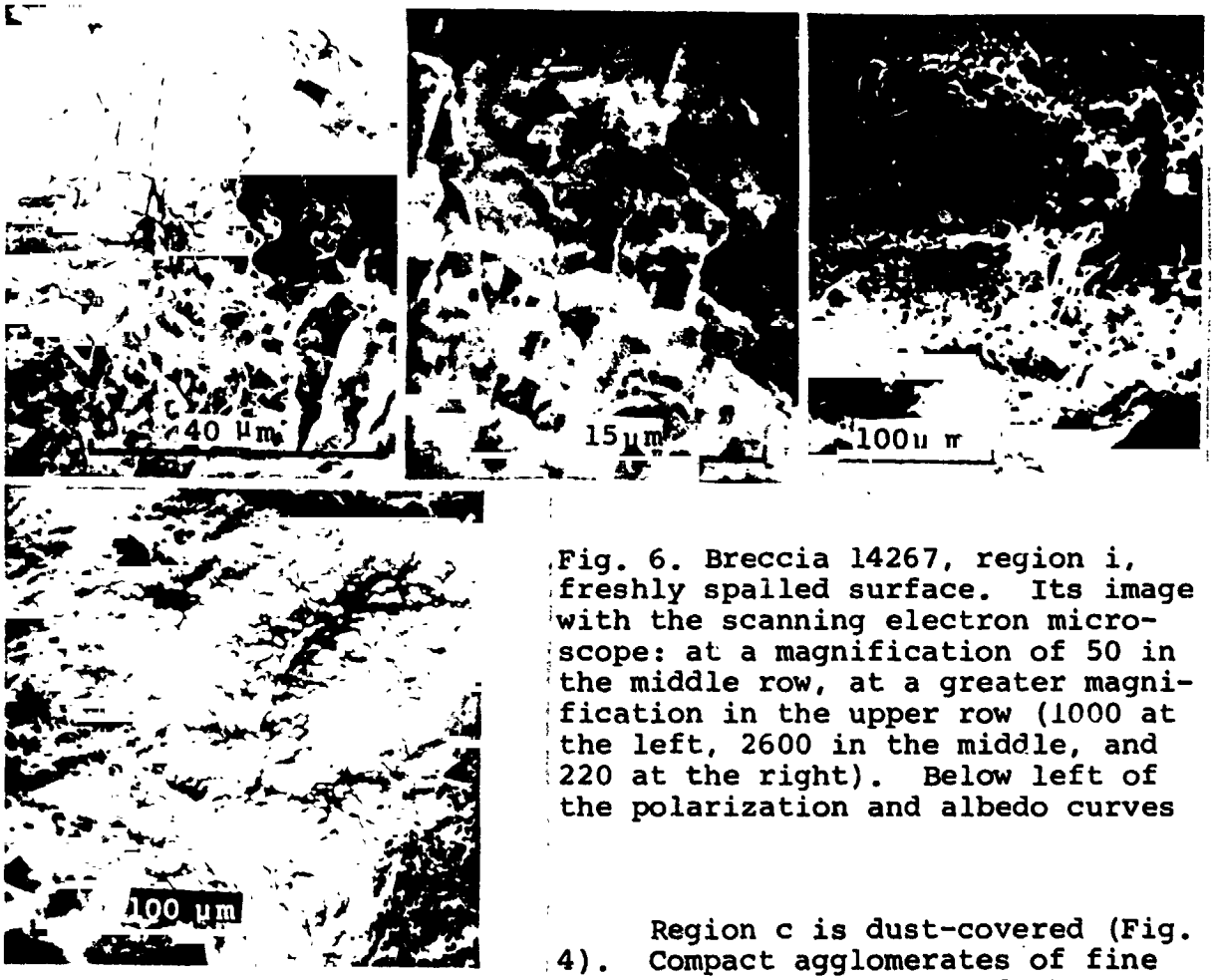

Fig. 6. Breccia 14267, region i, freshly spalled surface. Its image with the scanning electron microscope: at a magnification of 50 in the middle row, at a greater magnification in the upper row (1000 at the left, 2600 in the middle, and 220 at the right). Below left of the polarization and albedo curves

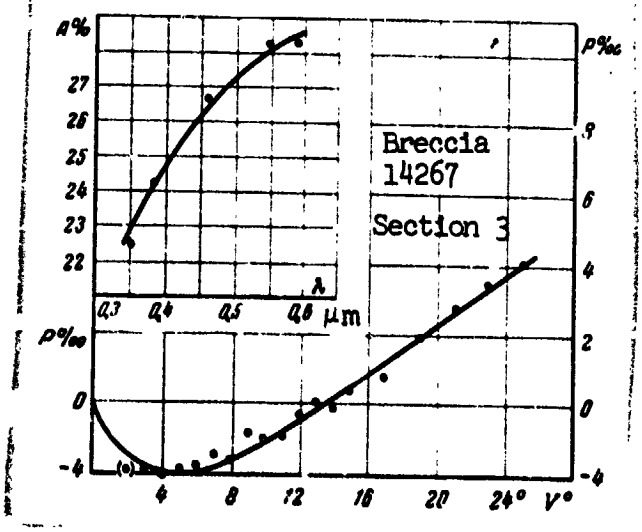

Region c is dust-covered (Fig. 4). Compact agglomerates of fine particles can be seen and the photo at a magnification of 1350. The complex surface structures were formed through interphase adhesion, and most of the individual grains are approximately of micron size. The curve of the negative polarization blend dips to 11 per mil at about V = 9°, and inversion angle V(0) = 20°. The negative branch obtained through telescopic measurements of the Moon reveals P_{min} = -12 per mil when V = 10°, V(0) = 23°. Based on these data, region c is very close to lunar surface on a large scale, as well as to lunar surface material.

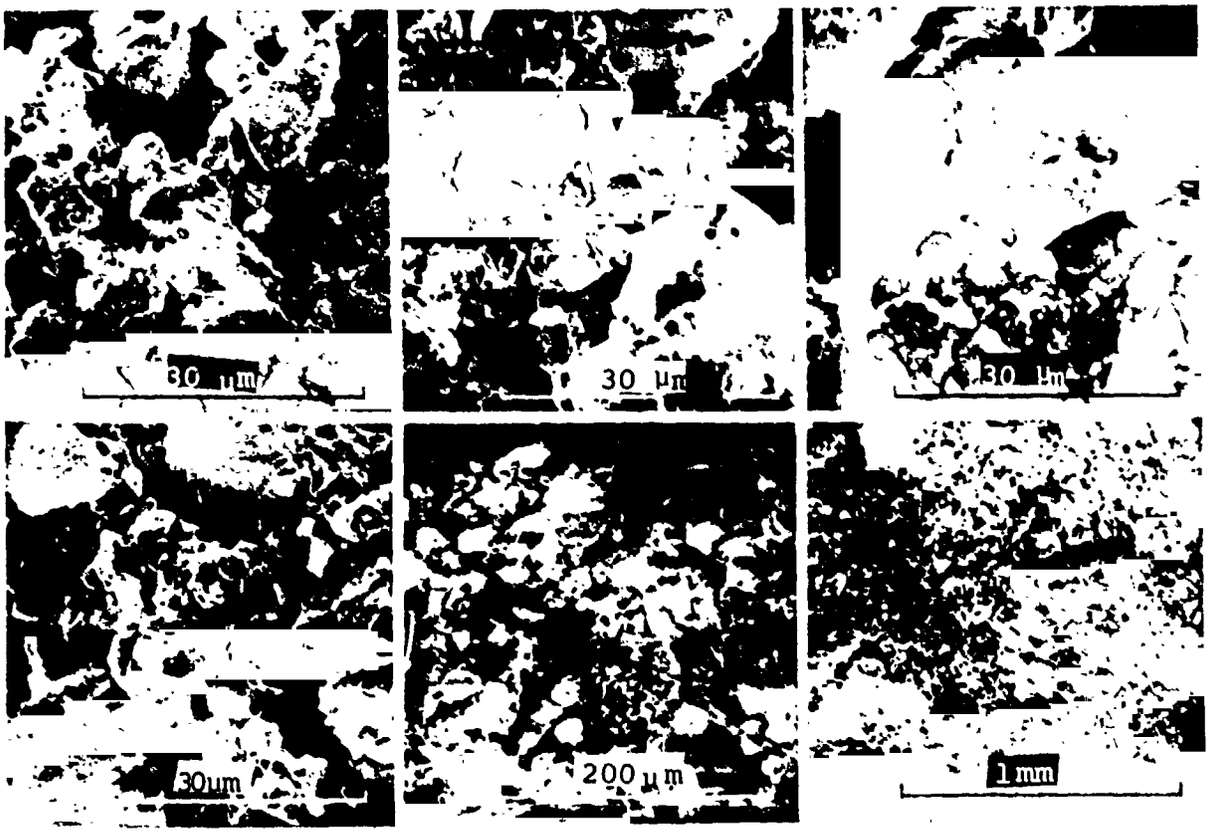

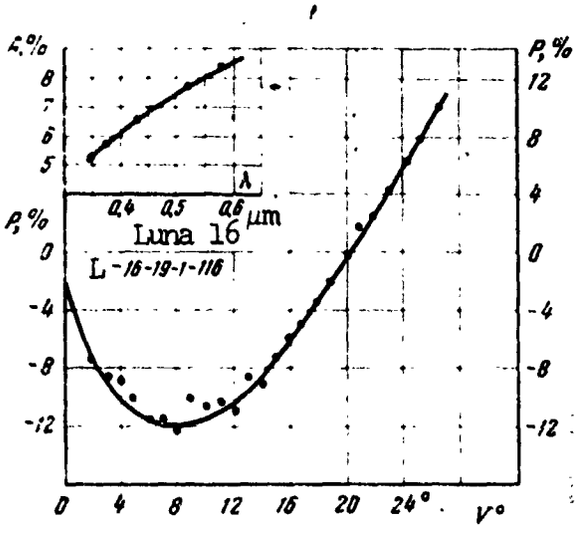

Fig. 7. Luna 16 lunar surface material, sample L-16-19-1-116. Surface images taken with scanning electron microscope (highest magnification of 1300 for the four photos) and absorption and albedo curves (below)

Regions b, e, f, and j are vitrified (Fig. 5). In four photographs (f, e, j, and b) with magnification of 2000, and one with magnification of 400 we can see a complex of fine particles lying on a relatively smooth surface. Photographs b and e disclose individual grains on a very smooth glass-like surface and an agglomerate of relatively smooth grains. The negative branch of the region covered with glass is not at all like the negative

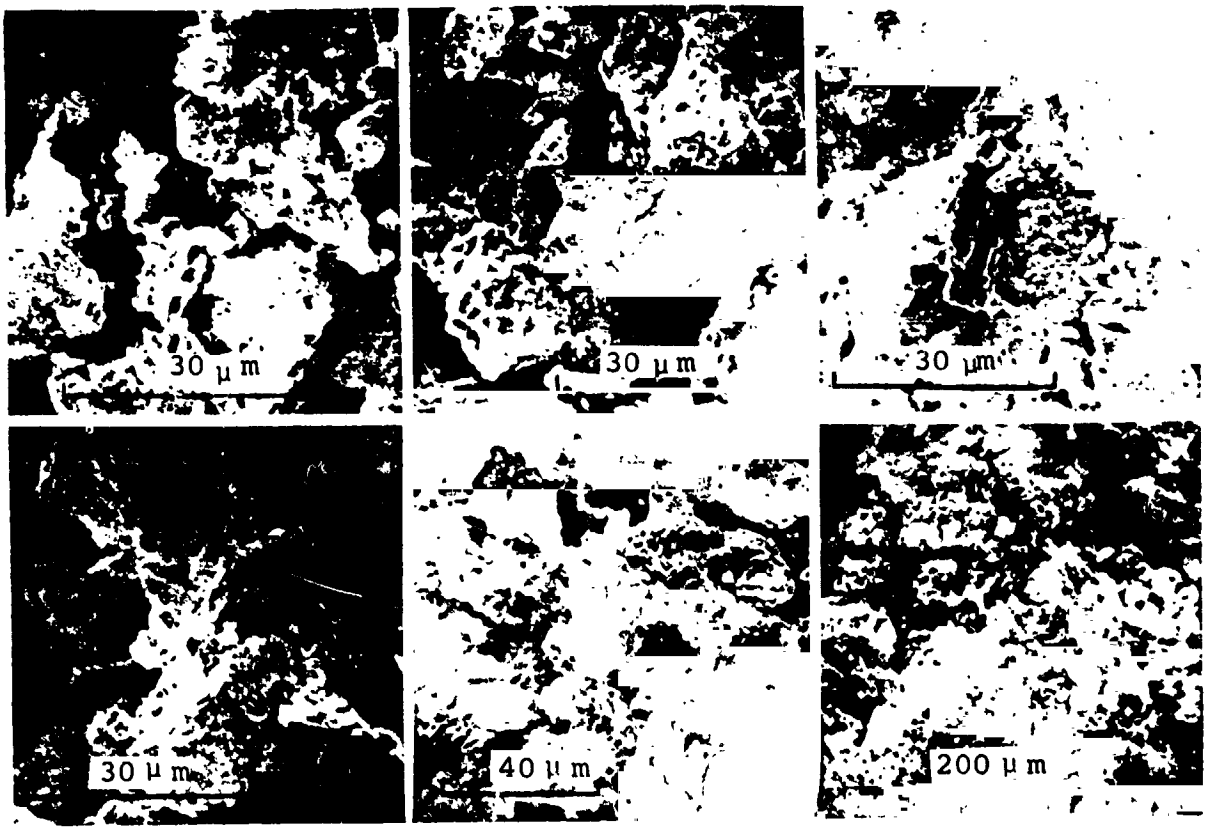

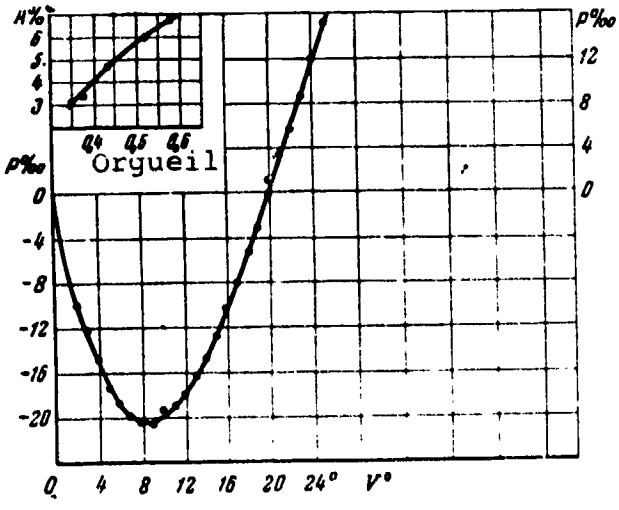

Fig. 8. Orgueil meteorite. Surface images with a scanning electron microscope (magnification 1000) and polarization and albedo curves (below)

region of the Moon. It dips only to P_{min} = -4 mil when V = 9° with V(0) = 17°. The effect of multiple scattering in this case is greatly weakened, since there are few complex structures present or none at all, and the polarization curve is close to the one for a flat dielectric surface.

Region i is a freshly spalled area (Fig. 6). In the photograph (magnification from 50 to 2600) can be seen in the surface on which infrequent fine particles lie. The negative branchshows that the surface cannot entirely reproduce the nature of the lunar polarization. The albedo curve given in the insert is characteristic of the color and albedo of lunar highland regions.

Sample L-16-19-1-116. Sample from core tube (Fig. 7) and from a depth of 20-22 cm (magnification from 40 to 1300). Complex interphase adhesion and the clumping of fine particles into clods are responsible for multiple scattering, which gives the results that agree with the telescopic lunar measurements. The albedo curve of the sample is similar to the lunar albedo curve.

Orgueil meteorite. This is a powdered carbonaceous chondrite (Fig. 8) externally similar to the Luna 16 sample. In the microphotographs the albedo is lower than for the albedo of the lunar material. However, the negative branch dips to $P_{min} = -20$ per mil, that is, it is more developed than any we measured. We will once again investigate this sample in order to attempt to confirm this property.

Laboratory of the Physics of the Solar System
Paris Observatory, Medon, France

N75 11864

INFRARED TRANSMISSION SPECTRA OF SEA OF FERTILITY REGOLITH

/524

M. V. Akhmanova, A. V. Karyakin
and L. S. Tarasov

Abstract

Transmission spectra in the 2-25 μm region were obtained for samples of lunar regolith returned by the Luna 16 automatic station. A comparison of investigation of the Luna 16, Apollo 11, and Apollo 12 samples showed that the infrared transmission spectra of regolith samples from the mare regions are similar and characteristic of basic basaltic rocks. The absorption bands show up in the vibration region of the SiO_4 groups. No water and OH groups were found in the samples based on the spectrum. Spectra of regolith samples calcined at 1000°C showed changes that can be interpreted as changes in the spectra of irradiated crystals (especially distinctly for the Luna 16 samples).

This study was made to determine, from the transmission spectra in the infrared region, possible changes in lunar rocks and minerals during the formation of regolith and to discover effects that derive from irradiation and crushing. Accordingly, crystallization and recrystallization of terrestrial rocks and lunar samples with heating and cooling were investigated; changes in the spectra of spherules obtained by calcining basalt powder through a plasma jet were determined. The lunar samples were compared with terrestrial samples for purposes of identification and discovery of differences[1].

---

[1] Experiments on simulating regolith formation processes, in particular in obtaining spherules, were carried out by Yu. I. Stakheyev (Geochemistry Institute, USSR Academy of Sciences).

The lunar material as present is being studied so closely and in such great detail by all possible methods that it is worthwhile to specify more precisely for which problems IR spectropy is most effective as a technique. These problems include investigating the "glassy" material: particles of glass, spherules, slags, and sinters. Are the glass formations "rock" or monomineralic? What is the mineral composition of the slags? How crystalline are the glasses? Are centers of crystallization present and if so, in which minerals? These questions are associated with the origin of the regolith and the dynamics of the processes occurring therein. Another important problem is finding water and OH groups in lunar material. A special problem is determining the degree of order and crystallinity of lunar material.

Lunar material has been subjected to "external" (solar wind and cosmic radiation) and "internal" (decay of radioactive elements and spallation nuclei) irradiations. The results of the action of these factors on the crystalline material vary. Experiments in terrestrial conditions showed that internal irradiation causes vastly greater changes in a crystal than external [21]. The greatest damage is caused by heavy recoil nuclei of the family (U, Th) [2, 3]. However, in laboratory conditions when artificial corpuscular irradiation was carried out, it was also possible to cause metamictization and the X-ray amorphousness of several compounds, in particular, silicate minerals [4]. Bombardment with micrometeorites to some extent can cause damage in a lattice analogous to exposure to heavy recoil nuclei. In principle can we differentiate materials losing crystallinity when impacted by micrometeorites from those subjected to prolonged irradiation?

In this sense, the following comparison can prove of interest: in the study [5] samples of lunar surface material were arranged in the following series based on their content of glass-containing material: Apollo 15 (Cone Crater) -- 10 percent, Apollo 12 -- 20 percent, Apollo 11 -- 50 percent, Apollo 14 -- 40-75 percent, and Luna 16 -- 80 percent[2].

In the report [6], the lunar samples were arranged in nearly /525
the same sequence, but this sequence depended on the number of damage sites in the lattice of individual particles (electron microscopy), beginning with the least: Apollo 15, Apollo 11, Apollo 14, and Luna 16. But the irradiated crystals (we have in mind terrestrial material) are not necessarily glass. Metamictic minerals subjected to radioactivity often preserve their external crystalline appearance, but reveal diffuseness in the X-ray diffraction patterns, and in the case of heavy damage -- X-ray amorphousness, increasing volume, cracking, loss of birefraction, and

---

[2] The data are from [7] for the Luna 16 samples.

so on [2, 8]. These crystals are microblock formations [8]. It can be assumed that also within the blocks the interatomic distances and the angles between bonds have been modified [9, 10]. Calcining restores to metamictic minerals their crystallinity, sharpness of X-ray diffraction patterns, and so on.

X-ray amorphous samples can be investigated by IR spectroscopy and the changes in samples that are ideally crystalline from the standpoint of X-ray structural analysis can be disclosed. True, this investigation requires monomineralic crystals.

By the method of vibrational spectroscopy, studies can be conducted to identify individual rock and mineral particles and to make comparisons with the corresponding terrestrial minerals. The following main problems in investigating lunar surface material were solved in [11-13]: specifics of the spectra of lunar materials, finding the spectral dependence on concentration for a number of elements (for example, Ca in pyroxenes), determining on this basis the degree of contamination of mare-region surface material by other material, and identification of glasses. An advantage of IR spectroscopy as a method is the possibility of investigating highly crushed material. The actual method presupposes studying samples in powdered form with particle size less than the wavelength of the incident light (2-5 μm).

For the investigations, the authors had available samples of dust, rock fragments, and slag particles from Luna 16, Apollo 11, and Apollo 12, as well as samples of meteorites and terrestrial rocks (see Table). The lunar and terrestrial samples underwent heat treatment in the 300-1000°C temperature range.

The spectra were recorded on a Zeiss UR-20 instrument from the GDR in the 2-25 μm region (5000-400 cm^{-1}). The samples were investigated in the form of tablets pressed from the 2 mg of material and 100 mg of KBr powder. The resulting spectra are shown in Figs. 1-6.

There were two broad absorption bands with smooth structure in the regions 1200-900 and 600-400 cm^{-1} present in the spectra of the regolith samples (see Figs. 1-3), characteristic as a whole for silicate compounds in the region of absorption by SiO_4 groups. The spectra of the regolith from different core levels were virtually identical (zones A and G) [7]. The absorption bands of the samples of lunar regolith are similar in their position to the spectra of terrestrial basalts, however there is a different, somewhat smooth contour present. The spectra of terrestrial basalts from different regions, as a rule, are different both in the number and in the shape of the absorption bands (see Fig. 4). This cannot be said of samples of regolith taken from different mare regions of the lunar material. The spectra of surface material samples of Luna 16, Apollo 11, and Apollo 12 are

CHARACTERISTICS OF SAMPLES INVESTIGATED

Sample	Origin
Luna 16	
Fine fraction, -0.083 μ m	1. Layer A, 3-2 d
	2. Layer A, 3-2 m
	3. Layer A, 3-1 zh
Slag particles	Layer B, sample 6
Gabbro particles	Layer V, sample 9
Apollo 11, regolith	No. 10005, 34-4
	No. 10005, 35-5
Apollo 12, gabbro	No. 12028, 229-3
Basalts, terrestrial	
Picritic, gray	1034, Kamchatka
Gabbro-diabase, gray	Armenia
As above	1791, Karelia
Gabbro-dark brown	Karelia
Tholeiitic	Indian Ocean
Meteorite	Chondrite, Saratov

quite similar to each other. The most blurred spectra are those exhibited by Luna 16 surface material samples. Absorption bands of water and OH groups were recorded in the spectra of all terrestrial basalts. No bands of this kind were found in the spectra of the regolith samples. Absorption by lunar dust from mare regions occurs in the same interval as the absorption of basic volcanic rocks. When the regolith spectrum was compared with the spectrum of a lunar rock sample, it was found that the dust spectrum is more blurred and has a somewhat different redistribution of intensity. But even the spectrum of the rock fragment is the spectrum of a nonholocrystalline formation (see Fig. 2). Further, let us compare the spectra of a piece of lunar basalt with the spectra of terrestrial rocks and meteorites, and tectites. The spectrum of oceanic tholeiitic basalts (containing about 90 percent glass) was closest to the spectrum of lunar basalt, but even it did not wholly coincide with the lunar basalt spectrum (Fig. 4). The IR spectrum of lunar basalt is a spectrum characteristic of a silicate material containing much glass. It is interesting to compare the spectra of the same materials isolated from highland rock and from the fine regolith fraction. According to the data in [11], the spectra of pyroxenes, plagioclases, and olivines taken from dust and from a rock fragment are similar, but differ from the spectra of the corresponding terrestrial minerals. This

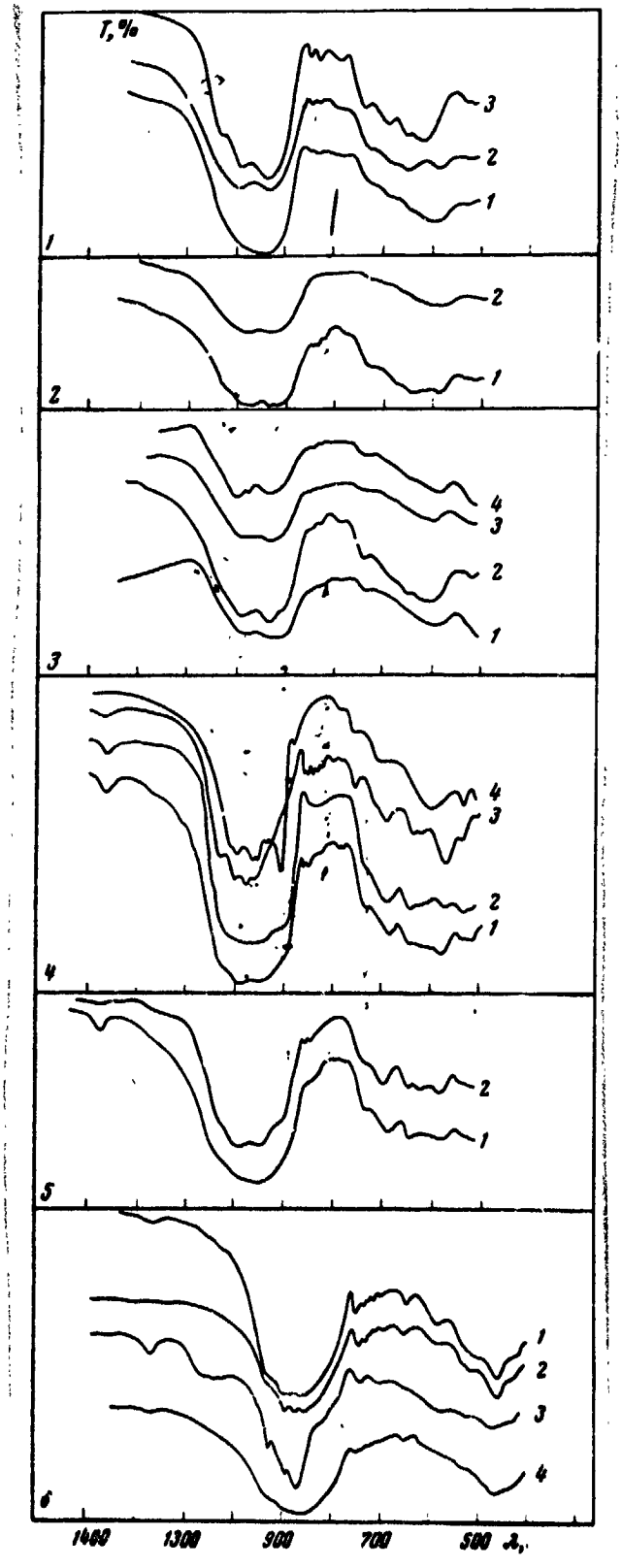

Fig. 1. IR transmission spectra /526
of Luna 16 regolith
1. uncalcined sample, layer A, sample 9-1d
2. sample calcined in air at 1000°C
3. sample calcined in argon at 1000°C

Fig. 2. IR transmission spectra
1. rock fragments
2. slag fragments

Fig. 3. IR transmission spectrum
1. sample of Apollo 12 dust
2. calcined Apollo 12 sample (argon, 1000°C)
3. Apollo 11 dust sample
4. calined Apollo 11 sample (argon, 1000°C)

Fig. 4. IR transmission spectra
1. terrestrial basalts, gray, 1034, Kamchatka)
2. terrestrial basalt (dark brown, Karelia)
3. terrestrial basalt (gray, Armenia)
4. meteorite

Fig. 5. IR transmission spectra of oceanic tholeiitic basalt (Indian Ocean)
1. uncalcined sample
2. sample calcined in argon at 1000°C

Fig. 6. IR transmission spectra
1. terrestrial gabbro-diabase and various fractions of spherules obtained by passing this gabbro-diabase through a plasma jet
2. -0.370 + 0.100 mm fraction
3. -0.100 + 0.045 mm fraction
4. -0.045 mm fraction

is particularly characteristic of the spectra of pyroxenes and olivines, where the spectra of lunar olivines differ from the spectra of meteoritic olivines. Evidently, this is associated with the conditions of crystallization and with the presence of micro-admixtures. The greatest similarity due to terrestrial materials is shown by lunar plagioclases. From data in [11], the spectrum of the plagioclase sample investigated (10085/46) is closest to the An_{100} plagioclases. Based on the same spectra of data, ilmenites from the Moon have several characteristics (spectral differences in the region outside the working region of the UR-20 instrument). Investigation of IR spectra of glass-spherules and fragments of different shapes conducted in [11-13] showed that many light glasses are plagioclase, and dark glasses /527
are pyroxene. At the same time, the spectra of all lunar glasses differ sharply from tectite spectra. Also investigated were heterogenous glasses [13].

Only one broad blurred absorption band in the region 1000 cm^{-1} was present in the IR spectra of slag particles -- the absorption region of the valency vibrations of the SiO_4 groups. Slag particles consist either of substantially remelted material, or remains of a slag persisting from the time of lava outflowing.

To study changes and the recovery of the structure particles forming lunar dust, after heat treatment the IR spectra of samples calcined in air at 300, 500, 800, and 1000°C, and only in argon at 1000°C were recorded. The resulting spectra are shown in Figs. 1 and 3. The spectra of samples of Luna 16 dust calcined at 300, 500, and 800°C in air not reveal changes in the absorption region of the SiO_4 group. The samples taken on a reddish hue, which is associated with the oxidation of the Fe^{2+} present in the material to Fe^{3+}, indicating some change of absorption in the region 500 cm^{-1} where the vibration of the Fe-O bond is manifested. In the spectrum of a sample calcined in air at 1000°C there appears a fine structure both in the absorption band characteristic of the valency vibrations of the SiO_4 groups, free and bond (1200-900 cm^{-1}), as well as in the region of the deformed vibrations of the SiO_4 groups and the vibrations of the metal-oxygen polyhedra (700-400 cm^{-1}). The changes in the spectra are analogous for the sample calcined in argon, but much more distinct. In addition, in argon the samples did not become oxidized and no Fe^{3+} - O bands appeared in the spectrum. The spectra of samples subjected to heat treatment again do not coincide with any of the spectra of terrestrial basalts. The changes in the spectra of calcined Apollo 11 and Apollo 12 samples are analogous, and perhaps somewhat less distinct. The spectra of calcined samples resemble the spectrum of the rock fragment. Calcining causes virtually identical changes in the spectra of samples taken from different core zones.

Changes occurring in the spectra of samples during calcining can be interpreted as the restoration of the structure of metamictic minerals -- minerals subject to irradiation, and as crystallization during heat treatment of the uncrystallized "glassy" material. In favor of the former is the attainment of a stepwise (at 1000°C) effect after unprolonged heating (1 hour) and rapid cooling (30 min). Processes of crystallization, for example, of synthetic glasses are much more prolonged. However, the change in the IR spectra is an indication of the action of radiation on crystals, a feature that perhaps is obligatory, but by no means sufficient. Complete proof requires a combined study of the properties of an irradiated crystal. The appearance of microblock status and further comminution of the material without internal changes do not introduce changes into the infrared spectrum, in particular, in the region of valency and deformation vibrations of the SiO_4 group. And in general it is difficult to imagine how the microblock status could have developed in crystals as the result of irradiation and impacting.

On the other hand, we can assume the possibility of the glass in the regolith crystallizing during heat treatment. Terrestrial basalts, with the exception of tholeiitic, do not reveal changes in the spectra upon heating. Possibly, they are entirely crystallized during processes of repeated heating and cooling in natural conditions. Fine structure appears in spectrum of oceanic tholeiitic basalt after calcining (see Fig. 5). This basalt, from petrological data[3], consisting of 90 percent glass (age 10 million years) extruded in water and rapidly cooled, was no longer heated. Changes in the spectra of lunar dust during heating are somewhat different in nature, but it is possible that lunar basalts as well were not subjected to general heating to 1000°C after formation and solidification of the maria.

An investigation of the spectra of spherules (see Fig. 6) obtained by calcining powdered terrestrial basalt through a plasma jet was undertaken as part of experiments on simulating the processes of regolith formation. The starting material was gabbro-diabase from Karelia. The spectra of spherules larger than 370 μm in size did not differ from the spectra of the initial basalt. The smaller the spherules, the greater the changes observed in the spectra. Different spectra can be recorded for spherules of identical size. Evidently, during crushing and melting rock can be separated into mineral grains. The spectra of the smallest spherules (45 μm in this experiment) were blurred, characteristic of glass. The large spherules could not be melted completely, but only fused, while /528 the fine spherules melted completely. An examination of the spectrum of powdered basalt passed through a plasma jet in conditions

---

[3] Samples were kindly made available by L. V. Dmitriyev (Geochemistry Institute of the USSR Academy of Sciences).

in which a small number of spherules was formed (close to Luna 16 samples) revealed that the spectrum of the resulting material is very close to the spectrum of the initial material.

The main conclusions are these.

1. The spectra of regolith samples of Luna 16, Apollo 11, and Apollo 12 in the 2-25 μm region are very similar and characteristic of the basic igneous rocks of the basaltic type.

2. Spectra of samples calcined at a temperature close to 1000°C revealed changes that can be interpreted as changes in the spectra of irradiated crystals. This appears especially distinctly in the samples of the Luna 16 surface material.

3. The infrared spectra showed no water or hydroxyl groups to be present in the regolith samples.

The authors are grateful to Academician A. P. Vinogradov, without whose cooperation this work could not have been done. The authors are also indebted to A. V. Ivanov and Yu. I. Stakheyev for their continual assistance in the work.

REFERENCES

1. Akhmanova, M. V., and Mikhaylenko, I. Ye., "Infrared Spectroscopy for Investigating Solid Radioactive Inorganic Compounds," Dokl. AN SSSR 177, 1120 (1967).

2. Dins, D., and Vinyard [transliterated], D., Radiatsionnyye effekty v tverdykh telakh [Radiation Effects in Solids], IL, 1960.

3. Ginzburg, A. I., Gorzhevskaya, S. A., Yerofeyeva, Ye. A., and Sidorenko, G. A., Geologiya mestorozhdeniya redkikh elementov [Geology of Deposits of Rare Elements], No. 10, Gosgeoltekhizdat, 1960.

4. Primak, W. A., "The Metamict State," Phys. Rev. 95, 837 (1954).

5. Adams, B., "Optical Evidence for Regional Cross-contamination of Highland and Mars Soils," Third Lunar Sci. Conf., January 10-13, 1972, Abstracts, 1.

6. Phakey, P. P. et al., "Radiation Damage in Soils From Five Lunar Missions," Third Lunar Sci. Conf., January 10-13, 1972, Abstracts, 534.

7. Vinogradov, A. P., "Preliminary Data on Lunar Surface Material Returned by Luna 16 Automatic Station," Priroda (3), 8 (1971).

8. Barsanov, G. P., "Principles of Systematics and Classification of Metamictic Titanoniobates," Trudy Min. muzeya AN SSSR [Transactions of the Mineral Museum, USSR Academy of Sciences], No. 10, 1959.

9. Akamanova, M. V., and Leonova, L. L., "IR Absorption Spectral Study of Metamictic Decomposition of Zircons," Geokhimiya (5), (1961).

10. Akamanova, M. V. and Leonova, L. L., "IR Spectral Study of Metamictic Decomposition of Silicates," Mineraly SSSR 4(14), (1963).

11. Estep, P. A., et al., "Infrared Vibrational Spectroscopic Studies of Structural Variations in Minerals From Apollo 11, and 12 Lunar Samples," Proc. Second Lunar Sci. Conf. 2, (1971) (preprint).

12. Estep, P. A., et al., "Infrared and Raman Spectroscopic Studies of Structural Variations in Minerals From Apollo 11, 12, and 14 Samples," Third Lunar Sci. Conf., January 10-13, 1972, Abstracts, 223.

13. Perry, C. H., et al., "Far Infrared and Raman Spectroscopic Investigations of Lunar Materials," Third Lunar Sci. Conf., January 10-13, 1972, Abstracts, 531.

Order of Lenin Institute of Geochemistry and Analytical Chemistry imeni V. I. Vernadskiy, USSR Academy of Sciences, Moscow.

N75 11865

ORIGINAL CONTAINS
COLOR ILLUSTRATIONS

CATHODOLUMINESCENCE OF REGOLITH RETURNED BY LUNA 16 AUTOMATIC STATION

/529

G. V. Spivak, M. K. Antoshin, N. P. Il'in, and G. V. Saparin

Abstract

Observations of local variations in the intensity and spectral composition of the cathodoluminescence of lunar regolith are described. These variations are caused by structural features, by the kind and quantity of the material and the admixtures. In addition, cathodoluminescent emission is also associated with a change in the temperature of the lunar surface. Periodic "diurnal" illumination and darkening of the Moon is responsible for a temperature gradient normal to the lines of longitude.

These observations made of regolith, using a scanning electron microscope with an attachment for temperature variation, simulate the indicated thermal changes of the cathodoluminescent properties of lunar material.

Colored cathodoluminescence was produced by us with a fast neutron beam in a scanning electron microscope. Naturally, in actual conditions cathodoluminescence and its variations are determined by other cosmic factors as well (solid wind, cosmic rays, X-ray radiation, ultraviolet, and so on).

However, the temperature factor, regardless of the cause producing cathodoluminescence, will always be operative and simulate the spectral composition. By the end of the lunar "day" the intrinsic lunar cathodoluminescent glow shifts (owing to overheating) toward the side of shorter wavelength.

If the Sun becomes "turbulent", then an intense fluctuation in external exciting radiation will produce in the regolith even more bright and diverse colored cathodoluminescence.

Introduction. It is known that when bombarded with an electron beam [1, 2], several objects can show intrinsic radiations -- cathodoluminescence (CL). This radiation is associated with the production in the material of electron and whole pairs, with interzone transitions of the carriers produced in a solid, in particular, with the replenishment of the zone of free electrons and their exiting from the valency zone. After excitation of the charge system of a solid, the externally obtained energy can be returned by conversion to heat or radiation. In the latter case a spectrum can be produced over a wide wavelength range, including also in the visible region. Thus, cathodoluminescent emission associated with the production of an electron and a hole, on culminating their reunion (recombination), can appear as recombination emission.

In this study, CL was produced in a scanning electron microscope (SEM) by electron bombardment. The CL signal served as a video signal and by means of an appropriate detector was used to produce an image. The contrast of the pattern was determined by several factors: structural inhomogeneities, the presence of admixtures, their density, nonlinearity of the detector, noise, and so on.

Local glow in the case of CL may not correspond to the place which corresponds to the point of encounter of the electron beam and the object. Penetrating fast electrons producing pairs diffuse and scatter in the bulk of the body. This diffusion is noted also for the pairs generated -- electrons and holes. Recombination takes place at the locations where there are the above-noted inhomogeneities whose presence also favors the release of stored potential energy.

Given a sufficient density of inhomogeneities in such natural materials as lunar regolith, all formations on the Earth, minerals with large number of structural disturbances, and others, we have highly favorable conditions for high localness of CL emission.

In contrast to the familiar method of determining composition (atomic number) by micro X-ray analysis, CL responds not only to /530
the chemistry of the material, but also to its small quantities. We note that the possibility of recording small amounts of an admixture naturally is due to the considerably higher yield of cathodoluminescence compared with X-ray emission.

Still, micro X-ray analysis makes it possible to obtain quantitative data, while CL emission is used as a qualitative factor. Obviously, it is desirable to employ both methods when investigating multiconstituent objects.

Lunar regolith subjected for long time to alloying by solar-wind particles, intensive exposure to high energy quanta, impacts by micrometeorites, and abrupt temperature fluctuations, as explained above, is a favorable material for CL experiments.

Experiments with lunar regolith. The anticipated and typical feature of the CL of lunar regolith must be the periodicity of the intensity and spectral composition associated with the temperature variation produced by the rotation of the Moon. We note that a typical feature of CL is its strong dependence on temperature [1, 2].

The Moon is illuminated by the Sun for 14 Earth days and is heated, and for the same number of days is cooled during the lunar "night". For example, from the data in [3], it is possible to record on its surface along the lunar latitudes the distribution of the infrared brightness temperature from -50 to +120°. It can be assumed that the amplitude of the temperature fluctuations can even be greater, therefore it is of interest to reproduce, even in laboratory conditions, the effect of temperature on the CL emission of the lunar regolith. In natural conditions the regolith is bombarded by cosmic particles and high energy quanta, while in our conditions -- with an electron beam having an energy up to 20 keV. Thus, one of the possible cosmic exposures of lunar material was reproduced.

We built an accessory for the Stereoscan instrument [4], permitting samples to be observed at temperatures from -196 to +500°C and thus for local thermal phenomena to occur in the temperature interval of interest to us.

The regolith returned by Luna 16 has already been studied with respect to its morphology [5] and in greater detail with a SEM [6]. In this report we emphasize the possibility of observing the quite faint CL in the form of a distribution pattern not with a black-and-white contrast, but with a color contrast, i.e., as it would appear to an observer on the Moon and with access to a fairly sensitive spectral apparatus capable of detecting, amplifying, discriminating, and synthesizing the CL signal.

In order to obtain color photographs of the regolith, we use a number of devices based on the SEM: 1) an accessory for suppressing noise and discriminating weak video signals [6], an accessory for maintaining the temperature of the sample within the required limits [4], a device for protecting the sample against deposit of hydrocarbon vapor, leading to the formation of contaminating polymeric films on it, a device for charge removal [8], and a multichannel device for simultaneous reception and transmission of an arbitrary large number of video signals from microgeometry and color. Interestingly, a useful combination of all these devices permits observing not only the static pattern of the CL, but also its rapid or periodic temporal trend.

REPRODUCIBILITY OF THE ORIGINAL PAGE IS POOR.

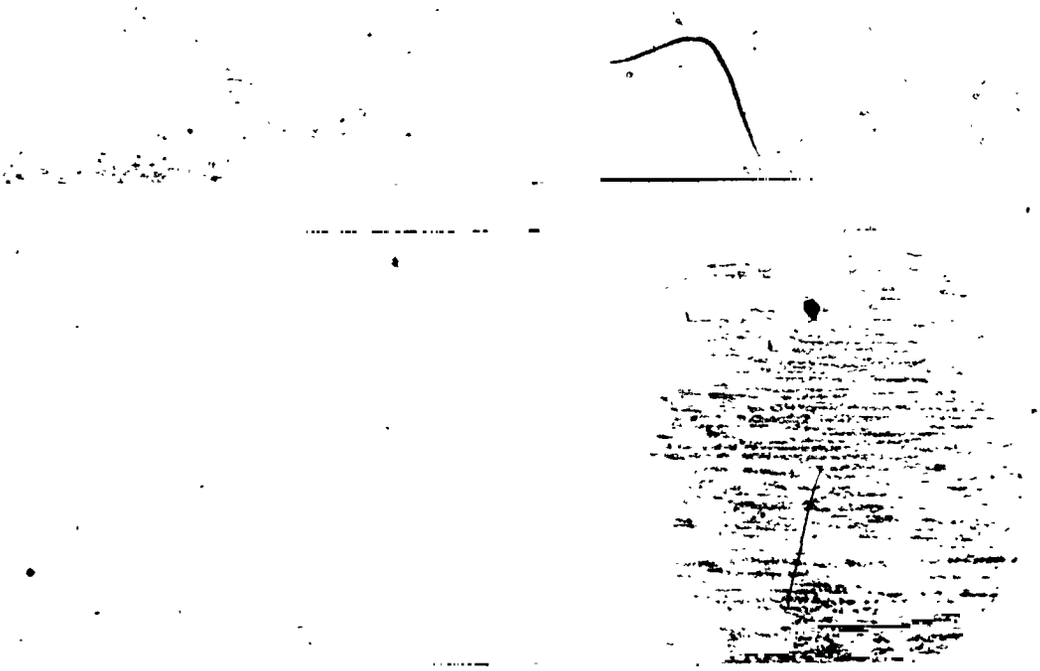

COLOR PLATE IX

1. Cathodoluminescence of regolith at 300° K; magnification of 50 for all photographs in color plate IX.
2. Cathodoluminescence of regolith at 170° K.
3. Cathodoluminescence of regolith at 500° K.
4. Optical image at room temperature

The results we obtained are shown in four photographs (Color Plate IX. 1-4). The lunar regolith was investigated in a SEM using the CL method at different object temperatures, from low to high. Fig. 1 was taken at T = 170° K, Fig. 2 -- 300° K, and Fig. 3 -- 500° K. The fourth photograph was presented for comparison and was taken at room temperature, but not in CL, rather with a light microscope.

A comparison of the first three photographs makes it possible to visually trace some features of emission in different spectral sections corresponding to the three points on the temperature dynamics of CL. In Fig. 1 we can observe the quite intense and uniform glow of the entire region of the object in the blue spectral region with a sharp luminosity at particles scattered over its surface. This can be easily seen in the central part of the photograph. The glow occurs not less intensely in the red and green regions, however in this case no characteristic selectivity associated with morphology is observed. With increase in temperature (see Figs. 2 and 3) the density of the luminescence drops off in the blue spectral region and only bright spots can be easily seen, whose source arc is represented by the surface grains of the regolith. The intensity of the glow weakens appreciably in the red spectral region. Thus, it can be concluded that in the integrated color cathodoluminescent photograph, emission in the red spectral region rises with increase in temperature, and the proportion of blue luminescence predominates, /531 although based on luminescent density it also drops off. It should be noted that with rise in temperature the luminescent intensity of some particles does not decrease. The foregoing possibly corresponds to the fact that regolith particles have different phase states. It can be noted that in contrast to crystalline particles, in the case of amorphous particles in radiation depends weakly on temperature. Figs. 1 and 4 show an amazing difference in photographs taken in CL and with illumination by ordinary visible light.

We are grateful to A. P. Vinogradov for useful guidance, cooperation, and close attention to the study.

REFERENCES

1. Thornton, P. R., Scanning Electron Microscopy, Chapter X, Chapman and Hall, London, 1968.

2. Spivak, G. V., Saparin, G. V., and Bykov, M. V., "Scanning Electron Microscopy," Uspekhi fizicheskikh nauk 99(4), 635 (1969); Soviet Physics Uspekhi, USA Translation 12, 756 (1970).

3. Bakulin, P. I., Kononovich, E. V., and Morov, V. I., Kurs obshchey astronomii [Course in General Astronomy], chapter X, section 132, "Nauka", 1970.

4. Spivak, G. V., and Antoshin, M. K., "Observations in a Scanning Electron Microscope of Ferroelectric Domain Structures Modulated by Phase Transition," Radiotekhnika i elektronika 16, 1742 (1971).

5. Vinogradov, A. P., "Preliminary Data on Lunar Surface Material Returned by Luna 16 Automatic Station," Geokhimiya (3), 261 (1971).

6. Antoshin, M. K., Il'in, N. P., and Spivak, G. V., "Scanning Electron Microscopy of Lunar Regolith Returned by Soviet Luna 16 Automatic Station," Geokhimiya (5), 661 (1972).

7. Spivak, G. V., Saparin, G. V., Antoshin, M. K. et al., "Study of Cathodoluminescence of Gallium Antimonide in Modulating SEM," Fizika i tekhnika poluprovodnikov 2, 1791 (1968).

8. Spivak, G. V., Bykov, M. V., Saprain, G. V., and Andreyenko, Yu. A., "Observation of Dielectrics in SEM," Radiotekhnika i elektronika 16, 1530 (1971).

Moscow State University imeni M. V. Lomonosov

Order of Lenin Institute of Geochemistry and Analytical Chemistry imeni V. I. Vernadskiy, USSR Academy of Sciences, Moscow

N75 11866

MAGNETIC PROPERTIES OF LUNAR SAMPLES RETURNED BY LUNA 16 AUTOMATIC STATION

/532

E. S. Gorshkov, Ye. G. Gus'kova,
and V. I. Pochtarev

Abstract

Results of measuring the specific magnetic susceptibility of regolith are presented. The data indicate that regolith samples from the Sea of Tranquillity and the Sea of Fertility are similar in order of magnitude of the specific magnetic susceptibility. Several stony meteorites of subgroup L have a similar value of this quantity.

After comparison with artificial analogs, it can be concluded that the bulk content of ferromagnetic minerals in regolith samples is 3-4 percent.

A complex of investigation of various magnetizing processes was carried out on the regolith samples. The uniqueness of the regolith is manifested in the possibility of magnetic texturizing, indicating the marked effect of shape anisotropy of the ferromagnetic particles. Studies conducted for different types of magnetization by the method of comparing stability characteristics reveal that the ratios between the kinds of magnetization in the regolith are retained at the same values as for rocks and stony meteorites.

After a study of the magnetic properties of the regolith, the phenomenon of the time-based drop in magnetization was found: a constant value for magnetization of any kind was established only 5-6 minutes after exposure to the magnetizing field. Further study of various regolith fractions and artificial analogs will assist in establishing the nature of the time-based drop in magnetization and the degree to which it can be applied in explaining the structural features of the regolith.

Investigation of the magnetic properties of lunar samples can help in solving several problems associated with the origin and history of the Moon. In particular, investigation of the regolith returned by the Luna 16 automatic station makes it possible to estimate the percent content of the ferromagnetic constituent, by which the main magnetic characteristics are determined -- specific magnetic susceptibility χ and saturation field H_S. In addition, it is useful to establish several correlations of magnetizing processes and to compare them with the corresponding correlations known for rocks and stony meteorites. It must be borne in mind that structurally regolith has practically no terrestrial analog.

Three samples of the general sample from the overall rock (regolith) having a total weight of 533 mg was presented in sealed capsules for the investigation of magnetic properties. The characteristics of the fraction and weight of each sample are shown in the Table.

CHARACTERISTICS OF SAMPLES

Sample number	Fraction, mm	Weight, mg	χ, 10^3 sec·gs/g
3-2p	-0.083	175.3	5.1
9-1s	-0.083	188.1	4.9
3-5a	+0.083 -0.127	169.6	5.0

The specific magnetic susceptibility χ was determined in a terrestrial magnetic field of 0.48 oersted. The measurements were made with a high-sensitivity MA-21 astatic magnetometer. As repeatedly noted in the press, the regolith powder has the property of high compaction [1-3]. By compaction, the volume of the regolith is changed and its cohesiveness increased, permitting a change in the position of the sample in the instrument, as required by the measurement technique. All data on magnetic susceptibility relate to the maximum compaction of the regolith, that is, the density was taken as 1.8 g/cm^3 in calculations of the specific magnetic susceptibility. The mean values of χ are also given in the Table; the error in the measurement of χ was 10 percent. When the magnetic susceptibility of the lunar dust returned by Apollo was investigated, the χ values obtained were $(10\text{-}40)\cdot10^{-3}$ sec·gs/g [4] and $1.13\cdot10^{-3}$ sec·gs/g [5] in a field ~1 oersted. /533

These results indicate that regolith samples from the Sea of Tranquillity and Sea of Fertility are similar in order of magnitude of χ and, therefore, to some extent also with respect to the content of ferromagnetic material.

To estimate the possible content of ferromagnetic minerals in regolith samples, an attempt was made at a quantitative reproduction (simulation) of the dependence of specific magnetic susceptibility χ on the ferromagnetic content. Data of chemical and mineralogic analyses indicate the presence in lunar samples of native (Fe) and nickelous iron (FeNi, kamacite) [1, 5], therefore the analogs were prepared from a mixture of powdered nickelous iron with an Fe content 93.32 percent, and Ni content 5.94 percent (the iron meteorite Sikhote-Alin [6]) or electrolytic iron with 99.99 percent pure Fe and quartz sand. The magnetic properties of the material depend strongly on the sizes of the ferromagnetic grains, therefore in preparing these standards powders were used in which 70-80 percent of the grains were 120 μm or smaller in size, as in the case of the regolith samples investigated (see Table). The density of the analogs also averaged 2 g/cm^3.

Fig. 1 shows the experimentally obtained dependence of specific magnetic susceptibility χ on the bulk content of the ferromagnetic (Fe or FeNi). Based on this function it can be assumed that the value χ of the regolith can corresponds to ~ 4 volume percent of the ferromagnetic. We note that these values of the specific magnetic susceptibility are exhibited by a large number of stony meteorites of the subgroup L with the same bulk content of nickelous iron [7], also reflected in Fig. 1, but in this case undisturbed samples of stony meteorites underwent measurement, and not powdered samples. Their are no natural analogs for the native iron.

In addition to the quantitative agreement of the χ values, we can judge the possible ratio of the analogs and the samples investigated also from the curve of residual magnetization I_r in a constant magnetic field H. Fig. 2 gives the curve $I_r = I_r(H)$ to H = 100 oe for the samples and three analogs similar in χ. As can be seen, the curves $I_r = I_r(H)$ for the samples lie between the corresponding curves for the analogs III and IV containing 3.7 and 2.9 volume percent nickelous iron; curve $I_r = I_r(H)$ for the analog Fe-10 (3.7 percent Fe) lies considerably higher. The trend of the curves confirms the assumption of the possible content of a ferromagnetic in the regolith samples in the amount of 3-4 volume percent.

Fairly well founded conclusions on the content of the ferromagnetic can be made from studying the saturation magnetization of the samples investigated. Fig. 3 presents the dependence of the residual magnetization I_r on the magnetizing field for the samples and for two analogs with similar values of specific magnetic susceptibility χ. It should be noted that the curves

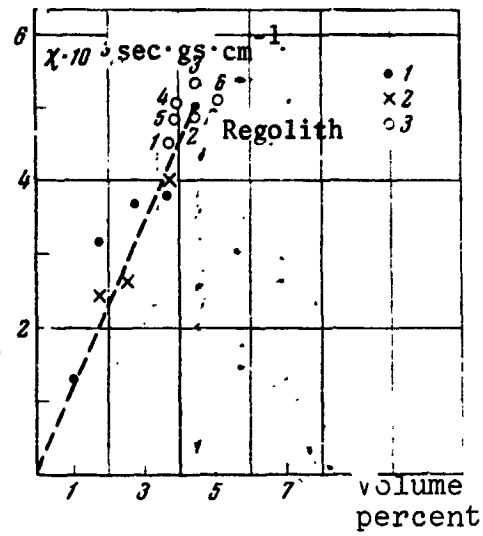

Fig. 1. Dependence of specific magnetic susceptibility on bulk content of ferromagnetic material

1. FeNi
2. Fe
3. Stony meteorites (1 -- -- Lundsgarden, 2, 3 -- -- Saratov)
4. McKinney
5. Pinto Mountains
6. Dalgety Downs

$I_r = I_r(H)$ for samples 9-1s and 3-2p coincide, while for sample 3-5a the residual saturation magnetization has a smaller value ($300 \cdot 10^{-3}$ and $230 \cdot 10^{-3}$ sec·gs·cm^{-3}, respectively); here saturation is attained in the same field H_S of the order of 3000 oersteds. It is possible that the difference in the value of I_{rs} can be associated with the large size of the ferromagnetic particles in sample 3-5a compared with the rest (see Table), since it is known that the coercitive force, and therefore, the residual magnetization rises especially appreciably for magnetic particles with sizes less than 80-100 μm. The fact that the curves $I_r = I_r(H)$ for the samples lie between the curves for the analogs Fe-7 (2.5 volume percent Fe) and III (3.7 volume percent FeNi) obviously also indicates the possible content of the ferromagnetic in regolith samples up to 3-4 volume percent.

The resulting magnetization H = 100 oersteds was demagnetized /534 in an alternating magnetic field $\tilde{H}$ with an amplitude falling to zero in order to determine by the method of comparing stability characteristics the ratio I_r of the analogs and regolith samples. From Fig. 4 it can be seen that I_r of the samples was entirely demagnetized only in $\tilde{H}$ = 120-150 oersteds (and not in 100 oersteds in which it was produced) and is much more stable than the analogs: in the field $\tilde{H}$ = 50 oersteds, 90 percent of the I_r of the analogs was demagnetized, while only 40 percent of the I_r of the samples. This dependence shows evidently that the analogs (mechanical mixture of nickelous or native iron and quartz sand) do not wholly reflect the magnetization processes occurring in samples, in spite of the quantitative agreement of the values of the specific magnetic susceptibility χ. It is altogether possible that the difference in the behavior of the samples in the analogs observed in this case is associated with the inadequate representation in the analogs of the silicate constituent, which is enriched in iron in the regolith.

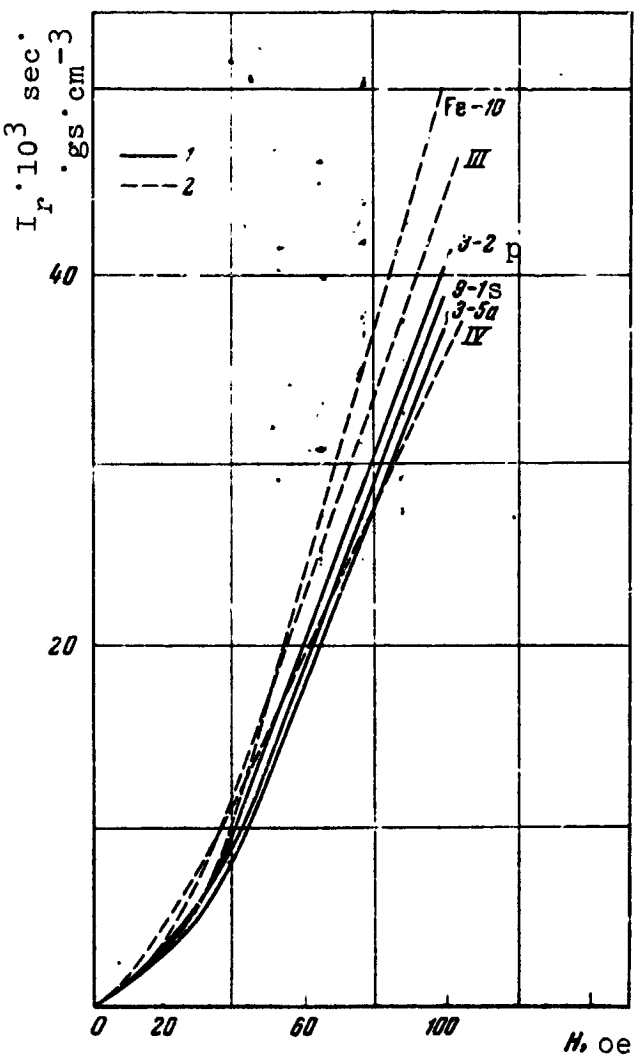

Fig. 2. Initial sections of curves of residual magnetization I_r for samples and analogs
1. Samples
2. Analogs (explanation of numbers in text)

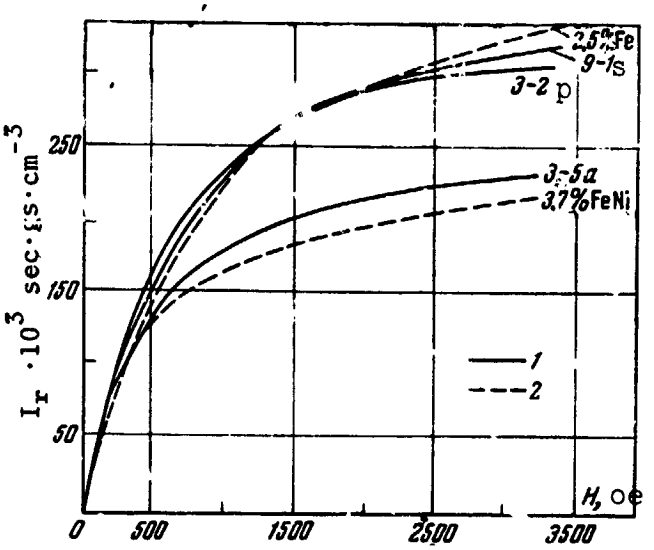

Fig. 3. Dependence of residual magnetization on magnetizing field for samples and analogs
1. Samples
2. Analogs

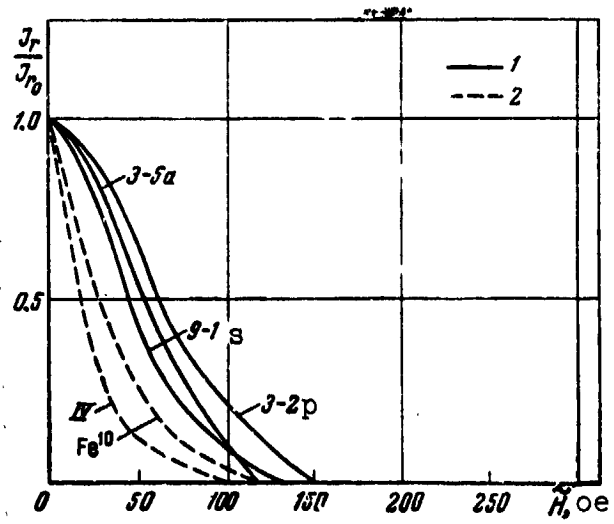

Fig. 4. Demagnetization curves of residual magnetization I_r using alternating magnetic field
1. Samples
2. Analogs

The uniqueness of the regolith from the investigation of magnetization processes shows up in the possibility of magnetic texturizing. Mechanical compaction of regolith samples in a magnetic field for a period of time led to a rise in the value and stability of the resulting residual magnetization, which we denoted by I_{rm}. For sample 9-1s this texturizing in a field of 100 oersteds for 1 minute boosted the magnetization 1.4 times (Fig. 5 a); a further increase in the texturizing time weakly affected a rise in magnetization, so that after 5 min a state close to saturation in this field was attained. Stability of magnetization I_{rm} rises compared with normal magnetization I_r obtained in a field of 100 oersteds (see Fig. 5 b). Cyclic magnetization was produced in sample 9-1s -- a constant magnetic field of 100 oersteds was successively superimposed in several cycles; for sample 9-1s the saturation of cyclic magnetization was observed after 29 cycles, and for analog III (3.7 volume percent FeNi) -- after 39 cycles (see Fig. 5 c), where the limiting values of magnetization I_{rm} and I_{rz} after 29 cycles in this field were practically the same ($5.3 \cdot 10^{-3}$ and $50 \cdot 10^{-3}$ sec·gs·cm^{-3}, respectively). The stability of cyclic magnetization I_{rz} after 29 cycles also increased compared with I_r and approximated the stability of the magnetization I_{rm}. Interestingly, the magnetization I_r produced in a field of 130 oersteds coincided both in value and in stability with the cyclic magnetization I_{rz} after 29 cycles and with the magnetization I_{rm} obtained in a field of 100 oersteds for 5 minutes. The manifestation of magnetic texturizing in regolith samples indicates the marked effect of shape anisotropy of the ferromagnetic particles and the fact that the process of regolith magnetization (given any method of magnetizing) is necessarily accompanied by texturizing; here we can establish equivalent ratios between the magnetic field H, magnetization time, number of cycles, and so on. /535

As we know, among the various types of magnetization the most stable are thermoresidual magnetization produced by cooling from the Curie temperature in a magnetic field, and ideal magnetization, which is produced in a constant magnetic field in the presence of an alternating magnetic field. Since heating of the regolith samples investigated was not assumed, an ideal magnetization I_{ra} was produced in sample 9-1s, equal in value to the normal magnetization I_r in a field of 100 oersteds (this value I_{ra} was obtained in a constant magnetic field of 6.2 oersteds and an alternating magnetic field of 400 oersteds). Demagnetization in H shows that stability rises compared both with I_r as well as I_{rm} (Fig. 6 a). /536

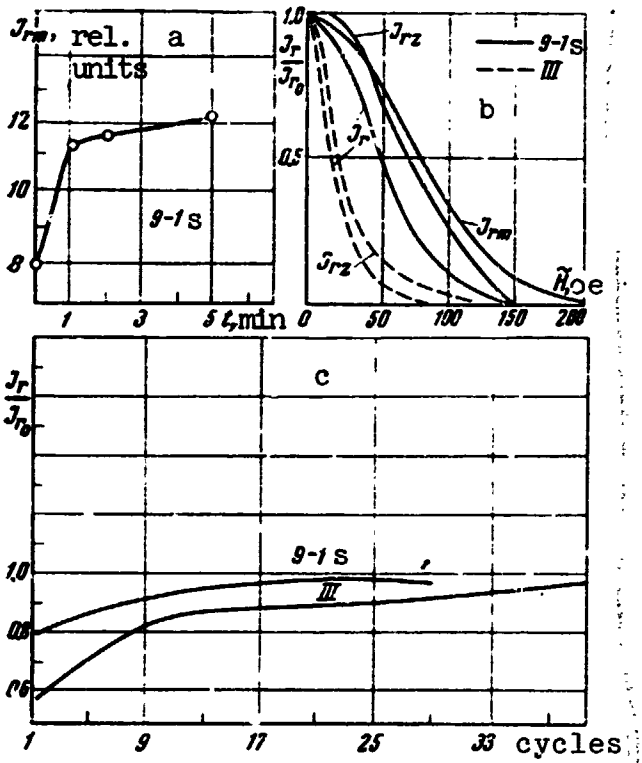

Fig. 5. Characteristics of magnetization

a. Rise in magnetization I_{rm} as a function of texturizing time

b. Comparison of demagnetization curves in an alternating magnetic field for the magnetization values I_r, I_{rz}, and I_{rm}

c. Rise in cyclic magnetization with number of cycles

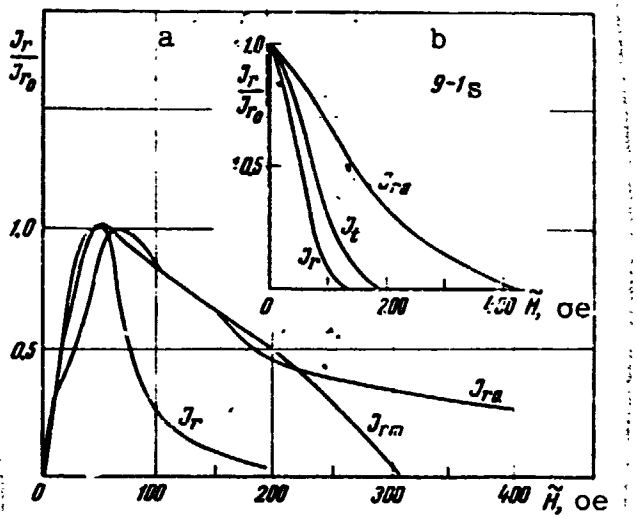

Fig. 6. Demagnetization curves in alternating field (a) and coercitive spectra (b) of different kinds of magnetization for sample 9-1s

This is also indicated by the coercitive spectra of the different kinds of magnetization -- -- normal I_r and I_{rm} obtained by mechanical compaction in a field, and ideal magnetization I_{ra} (see Fig. 6 b): in the transition from I_r to I_{ra}, more highly coercitive particles became involved in producing the magnetization, increasing the stability of the magnetization (it is probable that the finer particles did not participate in the texturizing due to their isometric shape). This indicates that the ratios between the different kinds of magnetization in regolith are retained at the same values as for rocks and stony meteorites [8].

/537

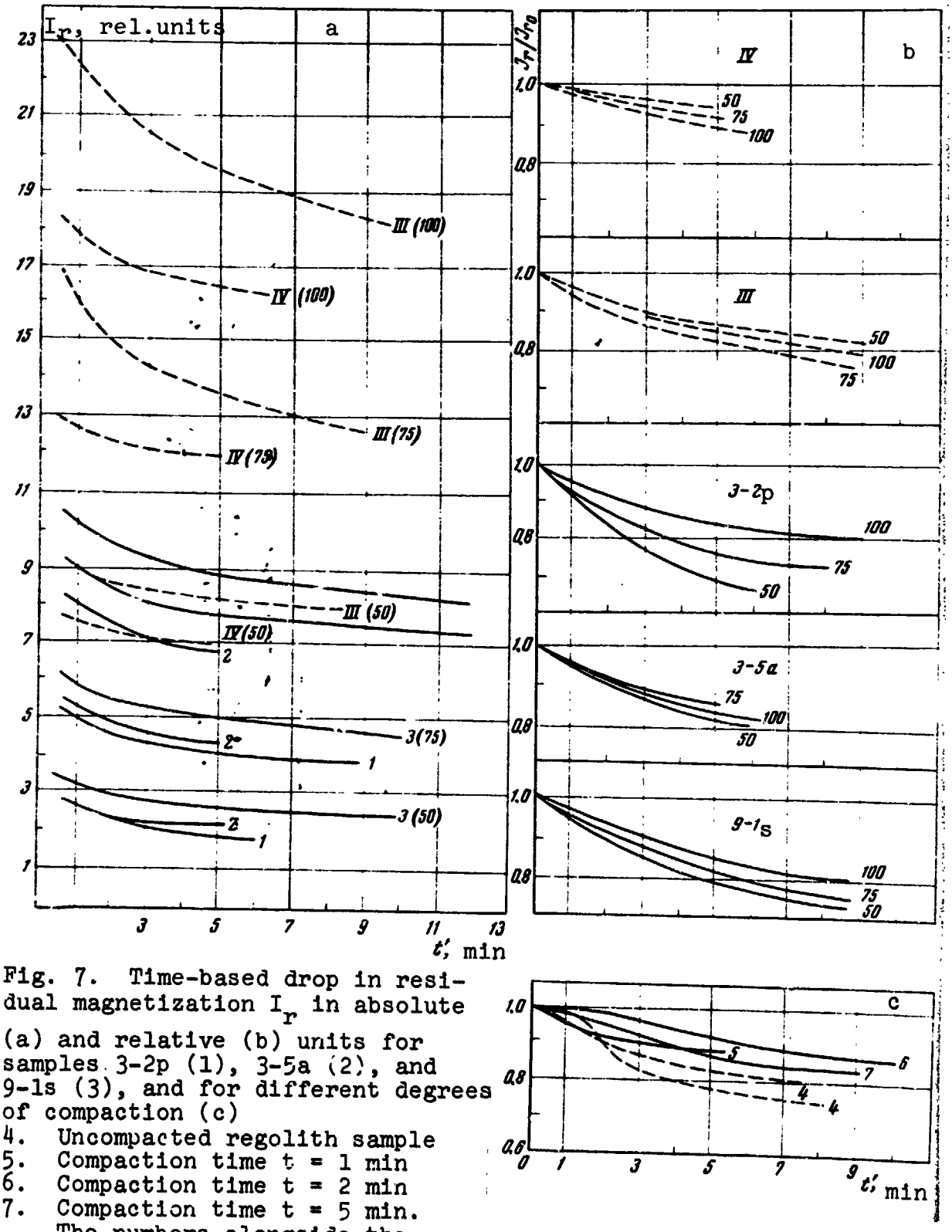

Fig. 7. Time-based drop in residual magnetization I_r in absolute (a) and relative (b) units for samples 3-2p (1), 3-5a (2), and 9-1s (3), and for different degrees of compaction (c)

4. Uncompacted regolith sample
5. Compaction time t = 1 min
6. Compaction time t = 2 min
7. Compaction time t = 5 min.

The numbers alongside the curves are the magnetic fields (in oersteds).

From studying the magnetic properties of the regolith, the phenomenon of the time-based falloff of magnetization was found: the constant values of magnetization of any kind was established only after 5-6 minutes following exposure to the magnetizing field, therefore in the measurements the time elapsing since the switching off of the field was used.

Fig. 7 presents the time-based falloff of normal magnetization for samples and analogs in absolute (Fig. 7 a) and relative (see Fig. 7 b) units; the numbers alongside the curves denote the magnetizing field strength. As we can see, the absolute value of the time-based falloff is nearly independent of the field applied (the curves for each sample or analog run parallel), but for the samples 9-1s and 3-2p a tendency toward a decrease in the relative size of this effect with increase from 50 to 100 oersteds is noted. The time-based falloff is observed over a wide interval of field values (all the way to the saturation field H = 3000 oersteds); the value of the time-based drop in magnetization in fields stronger than 200 oersteds averages 5-10 percent.

The observed phenomenon of time-based drop in magnetization does not reduce to relaxation processes of the type seen in the time-based drop in viscous magnetization in rocks, since time-varying exposure in the same field of 75 oersteds (from 1 to 30 min) did not change the absolute value of the resulting magnetization. It can be assumed that the time-based drop is determined by the powdered structure of the samples: this assumption is confirmed to some extent by the fact that the time-based drop is not observed in artificial samples consisting of a mixture of nickelous iron and modeling clay. At the same time, the different degree of compaction also is meaningful: Fig. 7 c gives the time-based falloff curves for the normal magnetization of an uncompacted sample 9-1s and the magnetization I_{rm} obtained in a field of 100 oersteds for different texturing times (1, 2, and 5 min). Evidently, we can conclude that there is some trend toward a reduction in the time-based falloff, a kind of stabilization of magnetization with increase in sample compaction. We note that the phenomenon of time-based falloff is not observed in artificial samples consisting only of a ferromagnetic constituent (100 percent nickelous or native iron), that is, it is intrinsic only to multicomponent powdered mixtures, one of which is silicate. We have found no reference to this phenomenon in the literature, which obviously is accounted for by the fact that the magnetic properties as a rule are studied with cemented or pressed ferromagnetic powders, and not in the free state. Further study of regolith and analogs will help to establish the nature of the time-based falloff in magnetization and its applicability in accounting for the structural features of regolith. With a specific method of regolith sampling, it is possible also to study the natural residual magnetization and therefore to determine the time and nature of the action of the field that magnetized lunar rocks.

REFERENCES

1. Vinogradov, A. P., "Preliminary Data on Lunar Surface Material Returned by Luna 16 Automatic Station," Geokhimiya (3), 261-274 (1971).

2. Ivanov, A. V., Stakheyev, Yu. I., and Tarasov, L. S., "Regolith from the Sea of Fertility," Nauka i zhizn' (1), 60-64 (1971).

3. Avduyevskiy, V. S., and Ekonomov, A. P., "Hot "Fur Coat" of the Moon," Priroda (3), 73-74 (1971).

4. "Preliminary Examination of Lunar Sample from Apollo 11," Science 165, 1211-1227 (1969).

5. Strangway, D. W., Larson, E. E., and Pearce, G. W., "Magnetic Properties of Lunar Samples," Science 167, 691-693 (1970).

6. D'yakonova, M. I., "Chemical Composition of the Sikhote-Alin Meteorite," in Sikhote-Alinskiy zheleznyy meteoritnyy dozhd' /Sikhote-Alin Iron Meteoritic Shower/, USSR Academy of Sciences Press, 1963, pp. 345-351.

7. Gus'kova, Ye. G., "Nature of Natural Residual Magnetization of Meteorites," Meteoritika 26, 60-65 (1965).

8. Gorshkov, E. S., Gus'kova, Ye. G., and Pochtarev, V. I., "Comparative Analysis of Magnetic Properties of Lunar Rocks and Meteorites," Kosmicheskiye issledovaniya (in press).

Leningrad Branch of the Institute of Terrestrial Magnetization, Ionosphere, and Propagation of Radiowaves, USSR Academy of Sciences, Leningrad.

N75 11867

METALLOGRAPHIC STUDY OF METALLIC FRAGMENT OF LUNAR SURFACE MATERIAL

/538

R. I. Mints, T. M. Petukhova,
and A. V. Ivanov

Abstract

A high precision investigation of a metallic fragment from the lunar material returned by the Soviet Luna 16 automatic station revealed three characteristic temperature intervals with different kinetics of solid solution decomposition.

The following were found in the structure of the metal, which is an iron-nickel-cobalt alloy:

a) δ-phase and α-ferrite of diffusional, displacement origin in the grain-boundary and acicular forms; and

b) martensite of isothermal and athermal nature, acicular, lamellar, massive, and dendritic.

The diversity of the shapes of structural constituents is associated with the effect on their formation of elastic distortions and various mechanisms of deformation-relaxation processes, which accounted for, respectively, the nature of the decomposition of the solid solution and the transformation kinetics in volumes that are commensurable with the subgrain.

Until recently, the only solid body of extraterrestrial origin that could be studied by man was a meteorite landing on Earth. In several fundamental investigations it was shown that meteorites as one of the forms in which matter exists in our solar system to a large extent preserves in their composition and structure data on the early stages in the development in the planetary system. However, the extraterrestrial prehistory of a meteoritic body is complicated by the effect of dynamic contact with the atmosphere. In

addition, only several bodies can withstand the conditions (high pressures and temperatures) of passage through the atmosphere. The foregoing enables us to assume that the samples landing on the Earth in the form of meteorites probably do not represent all the kinds, types, and structural states of solids encountered in interplanetary space. Accordingly, study of the phase and structural composition of individual fragments of lunar surface material opens up great possibilities in penetrating the extra-terrestrial prehistory and the specific of the action of the cosmic environment on the structure and properties of solids.

The investigation was conducted on the metallic particle M104 from the + 0.20-0.45 mm fraction of zone A of the column of regolith returned by the Luna 16 automatic station, using optical microscopy (see Figs. 1-7). To determine the chemical composition, use was made of a model JXA-5M electronic microanalyzer. The x-ray structural analysis was carried out with a URS-55 ionization unit in a Debye chamber using $FeK_{\alpha,\beta}$-emission following the standard technique. The microhardness was determined with a PMT-3 instrument.

The metallic particle of irregular shape resembling a "crown" is shown in Fig. 1. Upon visual inspection of its surface, traces of thermal and mechanical exposure in the form of fused sections and a considerable number of pits and craters of diverse shape, depth, and location were found. After etching or upon removal of the surface layer by polishing, the characteristic metallic lustre appeared.

Chemical analysis showed that the object investigated is an alloy consisting of the following principal elements: Fe-Ni-Co (Ni = 4.8-5.5 percent; Co = 0.5; Fe is the remainder).

X-ray structural analysis revealed the fine-grained (grain size from 1.5-2 to 20-30 μm) structure. On the x-ray diffraction patterns, besides the lines relating to the α-phase (kamacite), some patches somewhat shifted relative to the principal lines were observed, which did not preclude the presence of δ-ferrite considerably differing in lattice parameters from the α-phase. The results of microhardness measurements are shown in the Table.

The scatter of the microhardness values is probably due to /539 the inequigranularity, as well as to the chemical and structural inhomogeneity of the sample. The hardness values obtained are characteristic of an alloyed solid solution (of the ferrite type) subjected to deformation exposure.

Fig. 2 a shows the microvolumes in which are visible traces of deformation in the form of slip lines and mechanical twinning.

MICROHARDNESS OF METALLIC PARTICLE

Load, g	Microhardness, kg/mm^2										
5	257	257	189	189	—	—	—	—	—	—	—
10	229	229	229	185	229	229	229	229	185	229	185
20	189	220	189	258	—	258	—	—	—	—	—
50	257	257	—	—	—	—	—	—	—	—	—
Limiting values	189-229-257 kg/mm^2										

Mechanical twinning by narrow bands intersect individual grains and lie closer to the boundary of the sample. In the center of the polished section investigated they disappear, and only deformation lines remain, grading into slip bands.

Deformation action can be either the result of phase transitions (phase work hardening) as well as the consequence of relaxation-recrystallization processes. Thermal cycling plays a great role here. These kinds of deformation can lead to the stabilization of the solid solution and the passage of the deformation along different planes, which shows up in the form of intersecting slip lines (see Fig. 2 b). Neither is it precluded that from the side of the sample where the mechanical twinning can be seen there was a cleavage of the particle resulting from impact. The metallographic nature of the structure of the deformation indicates that the distribution of stresses caused by dynamic loads is marked by localness and intense nonuniformity. Stresses and deformations arose in individual microvolumes quite independently of what occurred in any other section. In this type of loading, the metal reveals properties which do not occur in ordinary loading. The idea of the stability of the solid solution and the capacity of the metal to undergo plastic deformation and disintegration change in these conditions [1, 2]. This is indicated by the ϵ-phase detected in the structure of the metallic fragment (Fig. 3). In ordinary conditions, this phase does not form in alloys having this composition. The presence in the particle investigated of a structure similar to the ϵ-phase can be viewed as the result of impulsed dynamic exposure providing the conversion of the α-modification to the denser hexagonal packing in conditions of stabilized solid solution.

Chemical analysis of the test object and the presence of the δ-ferrite indicate the possibility, in suitable conditions of the environment, of a $\delta \rightarrow \gamma$-transformation. The subsequent products

of the decomposition of the γ-solid solution (taenite) can be the α-modification (kamacite) whose shape depends on the kinetics and the temperature conditions of the transformation. The introduction of defects due to deformation, thermal, and radiation exposure can account for the change in the deformation transformation by displacement transformation, in which from the γ-solid solution is formed an α-solution having the same concentration.

Fig. 4 shows the structure consisting of grains of homogeneous ô- and α-solid solutions differing in colors. In some grains acicular segregations of the α-phase (kamacite) are observed, the spaces between which are filled with the α-phase that does not have an acicular shape. Thin lamellae of kamacite either are grouped into colonies or else lie at angles of 30-60° relative to each other. Grains are encountered that apparently are cross-hatched with kamacite needles. It is probable that the transformation developed in this sequence. First grain-boundary ferrite appeared, then needles of Widmanstatten ferrite appeared, characterized by the displacement mechanism of transformation. The gaps between them were filled with the products of the normal diffusion transformation. The characteristic difference of structure even in a single grain is the basis for assuming that two mechanisms of transformation existed: the normal and the displacement mechanism, in competition with each other.

One feature of the metallographic structure of the metal /541
particle of the lunar surface material is the presence of diverse shapes of martensite structure. Massive martensite (Fig. 5 a), acicular martensite -- in the form of "ferm-molnium" (see Fig. 5 b), lamellar martensite -- in the form of parallel and intersecting lamellae (see Fig. 5 c), and dendritic martensite (see Fig. 5 d) were detected. Fig. 5 a shows the isothermal and athermal martensite from the standpoint of a middle midrib line that is the proof of the spontaneous formation of the crystals. The diversity of the martensite shapes indicates that during the formation of the metallic particle the kinetics of phase transformation changed. In several studies it is shown that with the shift in the kinetics there is a change in the morphology of the structural of transformation /3, 4/. Characteristic of martensite are two kinetics: isothermal and athermal. In the case of the isothermal process, there is the dependence of the transformation rate on temperature, and the dependence of the temperature interval on the cooling rate. In the case of the athermal transformation, the position of the martensitic point does not depend on the cooling rate, while the amount of the martensite is determined only by temperature.

A characteristic of the environment and external factors is as follows: on the one hand, fast reactions stimulated by impact loading, and on the other hand, the possibility of slow

Fig. 1. External appearance of particle.

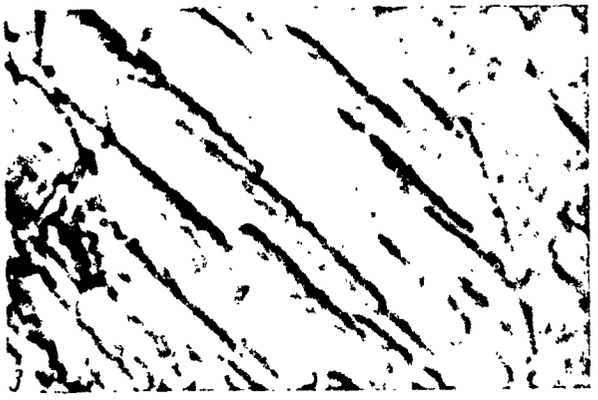

Fig. 3. Segregations of close-packed modification.

cooling at rates of the order of 1-10° per million years [5]; this feature suggests the realization of the processes of atom displacement by the following three mechanisms [4]: a) nondiffusion cooperative displacement; b) nondiffusion noncooperatuve displacement; and c) diffusion.

Fig. 2. Mechanical twinning and slip lines.
a. Deformation twinning
b. Deformation lines

Fig. 4. Different shapes of α-phase segregations.

Fig. 5. Types of martensite.
a. Massive
b. Acicular
c. Lamellar
d. Dendritic

Fig. 6. Martensitic relief

The degree to which the mechanism of nondiffusion cooperative displacement of atoms is manifested depends on the difference in the lattices of the two phases participating in the transformation. For the transformation of a nucleus if the difference between the lattices is large, a high energy of activation and considerable supercooling are required. But since the displacement of atoms can occur cooperatively so that between the new and old phases the crystallographic relationship is preserved, an unusually high

Fig. 7. Stratification of solid solution.

growth rate of the nuclei formed is attained. At the surface distortions in the form of relief are formed, and in the fine structure -- twinning, packing defects, and dislocations. This structure is martensite (Fig. 6), since the presence or absence of lattice defects in the crystal can serve as a criterion for martensitic structure.

The mechanism of nondiffusional noncooperative displacement is characteristic of high temperature. In the case of high temperatures, the probability that nuclei will form is high, and the required supercooling is small. But since displacement of atoms is not cooperative, the energy of activation of growth must not be as low as for martensitic conversion. In addition, due to the smallness of the supercooling the driving force of the conversion disappears at once following a rise in temperature owing to the heat given off during the transformation time, and the growth rate is not as high as in the martensitic conversion. Since in this case there is no need for the diffusion of atoms, the transformation rate is much higher than in the case of the formation of phase decomposition products. A consequence of this mechanism is the formation of massive structure (see Fig. 5 a). /542

The diffusional mechanism plays the principal role in the formation of the phase decomposition products -- ferrite (kamacite). The development of diffusional processes is manifested in the presence of a ferritic matrix, δ-ferrite, segregations of the α-phase along grain boundaries, and phenomena of stratification of homogeneous α-solid solution (Fig. 7). The latter is due to the fact that the energy of activation for the diffusion of nickel in iron in both the γ- as well as the α-state is very high, of the order of 70,000 cal/mole, and in the decomposition of the solid solution into equilibrium constituents, the equalizing of concentrations must occupy a long period. At the same time, in Fe-Ni alloys, beginning at 4.9 percent Ni, with prolonged annealing in the critical region (600-700° C), stratification is observed, manifested in the decomposition of the homogeneous α-solid solution.

Evidently, there is no well-defined boundary between the three mechanisms listed above, which can alternately be imposed on each other or act simultaneously, competing at stages of transformation.

This investigation shows that in spite of the limited dimensions of the object, in it are represented in all their diversity the products of both diffusional and nondiffusional transformations. It is probable that multiple heatings, repeated deformation and radiation exposures, and constant heat cycling were responsible for the thermal and deformation decomposition of the solid solution, producing phase and structural metastability.

Conclusions. 1. Features of the phase composition and structure of the test object are determined by the kind of kinetics of the transformation -- the decomposition of the solid solution in conditions of ultrahigh vacuum, radiation environment, and deformation exposure.

2. The different kinetics of decomposition and the specific phase composition of the solid solution ($\delta \rightarrow \gamma \rightarrow \alpha$) of the iron-nickel-cobalt alloy produced the following structures: a) ferrite (kamacite) of diffusional and displacement origin in the grain-boundary and acicular forms; and b) massive martensite, as well as martensite in the form of "lerm-molnium", Widmanstett, and dendrites. Thermal and athermal martensite were found.

3. Slip lines and deformation twinning indicate the possibility of the deformational mechanism of the decomposition of the solid solution. This is also indicated by the cellular structure of the matrix and the presence of a close-packed phase, the result of dynamic pulsed exposure converting the α-modification to the more dense hexagonal packing.

4. The diversity of the structural constituents is associated with the effect on their formation of elastic distortions and different mechanisms of relaxation-recrystallization processes caused by deformation and forward and reverse conversions.

5. The specific features of the environment and chemical composition account for the coexistence within the limits commensurable with the subgrain of different mechanisms of solid solution decomposition (diffusional-nondiffusional, thermal-athermal).

REFERENCES

1. Mints, R. I., Problema prochnosti i printsip vybora metallicheskikh splavov v usloviyakh mikroudarnogo nagruzheniya /Problem of Strength and Principle of Selection of Metallic Alloys in Conditions of Micro-Impactive Loading/, Moscow, 1964.

2. Reinhardt, D., and Pearson, D., Povedeniya metallov pri impul'snykh nagruzkakh /Behavior of Metals in Pulsed Loading/, IL, 1958.

3. Georgiyeva, I. Ya., and Maksimova, O. P., FMM 2(32), 364 (1972).

4. Nishiyama, D., Nikhonkindzoku gakkai kaiho 8(5), 328 (1969).

5. Axon, H., Metallurgy of Met orites 13(4), 215 (1968).

Ural Polytechnic Institute imeni S. M. Kirov, Sverdlovsk

Institute of Space Research, USSR Academy of Sciences, Moscow.

N75 11868

EXOELECTRONIC EMISSION OF PARTICLES OF LUNAR SURFACE MATERIAL

/543

R. I. Mints, V. I. Alimov, V. P. Melekhin, I. I. Mil'man, V. I. Kryuk, L. L. Kunin, and L. S. Tarasov

Abstract

Using a specially designed setup employing a secondary-electron multiplier, a study was made of the thermostimulated exoelectronic emission of particles of lunar surface material returned by the Soviet Luna 16 automatic station. The "natural" exoemission from fragments of slag, glass, anorthosite, and a metallic particle was recorded in the isochronic and isothermal thermostimulation regimes. The temperature of emission onset depends on the type of regolith fragment. For the first three particles the isothermal drop in emission is described by first-order kinetic equations. For the anorthosite fragment, exoemission at constant temperature is characterized by a symmetric curve with a maximum.

These data indicate the presence in the regolith fragments studied, above all for anorthosite, of active surface defects, whose nature can be due to the prehistory of the particles.

Study of the exoelectronic emission of individual particles of rocks and minerals that are part of the lunar regolith is of particular interest.

Earlier /1/, using a Geiger Mueller counter, data on the exoelectronic emission of lunar rocks returned by Apollo 12 were obtained. The experimental results enabled the authors of /1/ to conclude that there is a relationship between the exoelectronic emission parameters and the energy accumulated in the "natural" defects of lunar materials. However, the study made of the chemical and mineralogic composition, as well as the electrophysical properties of samples of the lunar surface material returned by

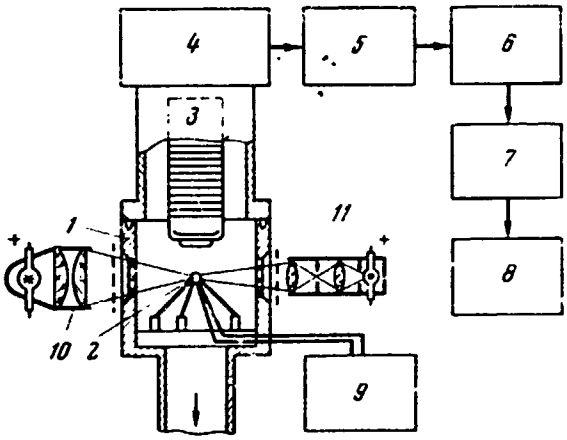

Fig. 1. Setup for study of exoelectronic emission of regolith particles

Apollo 11 and Apollo 12 showed that the most interesting results were obtained not from massive samples, as would be expected, but from the fine regolith fractions /2/. This is accounted for by the fact that the "lunar dust" in contrast to the massive samples contains numerous fragments whose origin and evolution differ: particles of meteorites, samples of rocks beneath the lunar surface, and rocks significantly changing in structure under the effect of various external factors. Evidently, it is precisely the regolith particles that are responsible for the unusual properties of the lunar surface material (increased tendency to electrification, anomalous cohesiveness, low thermal conductivity, and so on). The small size of these particles requires development of a special method of studying them.

To re ord the exoelectronic emission from objects less than 0.2 mm in size, we designed and built a special experimental setup (Fig. 1).

The test sample (2) of lunar surface material was secured within the working chamber (1) in molybdenum needles with a tip diameter less than 1 μm. Used as the exoelectron detector was a secondary-electron multiplier (3), with a low intrinsic background (0.1 electron/sec) and a high sensitivity (10^{-20} A); it was placed over the sample within a removable seal column. /544

The secondary-electron multiplier /SEM/ was supplied with stabilized voltage from a separate high-voltage source. The counting characteristic of the secondary-electron multiplier had a plateau in the voltage region 3.3-3.7 kV. Voltage pulses produced when exoelectrons struck the first dynode of the SEM were recorded from the load resistance of the multiplier and sent successively to the preliminary (4) and the wide-band (5) amplifiers. In order to bypass the pulses produced by the noises of the preliminary amplification cascades, connected in series after the wide-band amplifier was an amplitude discriminator (6), whose discrimination threshold somewhat exceeded the amplitude of the noise pulses. From the amplitude discriminator, the signal was sent through a counting-rate meter (7) and a recorder

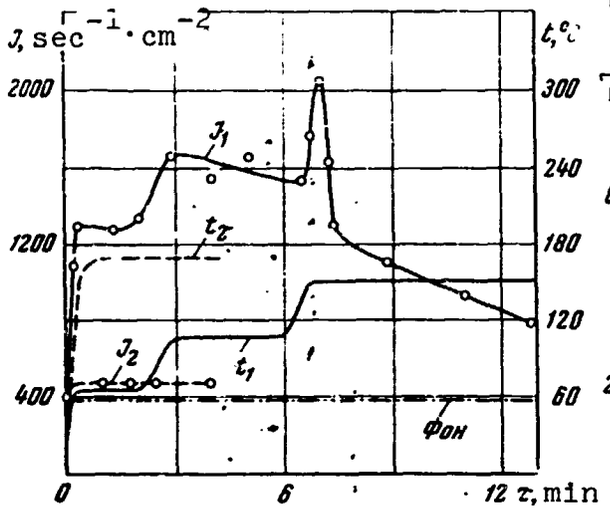

Fig. 2. Exoelectronic emission of slag particle; subscripts 1 and 2 refer to the first and second sample heating, respectively.

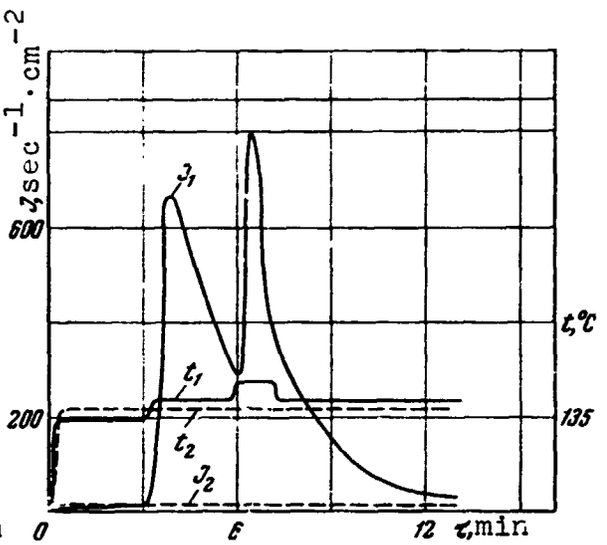

Fig. 3. Exoelectronic emission of metallic particle

(8), with which the change in the intensity of the exoelectronic emission was automatically recorded. The exoemission was measured in a vacuum $5 \cdot 10^{-6}$ torr. To prevent oil vapor from the diffusion pump entering the working chamber, the vacuum system of the setup was provided with a nitrogen trap.

Thermal stimulation of the emission current was provided by heating the sample with a focussed light beam from a DRSh-500 lamp (10). The hard component of the light flux was cutoff with a filter transmitting only the red and infrared rays.

The sample temperature was measured with a thermocouple of copper and constantan wire 30 μm in diameter. The measurement results were recorded on a graph tape of the recorder (9). The setup was also provided with additional photostimulation of exoemission by means of a light source (10) and an objective composed of quartz lenses (11). Before the beginning of the experiment, the light filter was selected so that the cold sample did not yield photoemission.

The object of the investigation was the characteristic regolith particles returned by the Soviet Luna 16 automatic station. The specifics of the lunar regolith are that the processes leading to

the formation of individual fragments differed. For particles of igneous rock this was a process of crystallization from molten magma in conditions of prolonged or relatively lengthy cooling. Glasses and slags experienced pulsed heating, melting, or fusing and very rapid cooling. Breccias were the result of fragmentation and agglomeration of material. Considerable impact and explosive actions led to shock effects, also contributing to the complex history of the formation of lunar surface material particles.

The experiments were conducted on the following particles: slag, metallic, glass, and anorthosite. Exoelectronic emission was recorded upon thermostimulation from 20 to 160° C in regimes /545 that were near-isothermal or near-isochronic. The limitation of the upper limit to the heating temperature of these regolith fragments was aimed at avoiding as far as possible any structural or phase transformations, that is, preserving their initial properties. In this temperature range, exoelectronic emission whose intensity rose with increase in temperature was observed from the surfaces of all the particles selected (see Figs. 2-5).

These data are of interest above all from the standpoint of the actual fact of recording quite a significant low-temperature "natural" exoemission from particles of lunar surface material. In this case recording the exoelectrons must indicate the presence in the surface layers of the samples of surface material investigated of defects to which electronic traps with shallow energy levels correspond.

These energy states of geological objects, which as a rule are extremely difficult to disclose by ordinary methods (for example, thermoluminescence), can be associated with the high concentration of relatively unstable defects in the surficial and near-surface layers, for example, of vacancies and their complexes, arising either through a mechanical deformation, irradiation with protons of various energies, and ultraviolet light, or through deformation caused by thermal stresses /3/. The nature of the surface states depends both on the particle material, as well as on the conditions of its formation. This finds confirmation in the data obtained on the temperature of exoemission onset. In the temperature range investigated, exoelectronic emission from the slag surface developed already at 60° C, from the glass surface at 80-100° C, and from the surface of the metal particle at 140° C.

Another characteristic feature of the exoelectronic emission of the particles of lunar surface materials studied was the fairly well-defined change in the nature of the process with time for particles of different types. The intensity of the exoelectronic emission from the surfaces of the samples of slag and glass, and

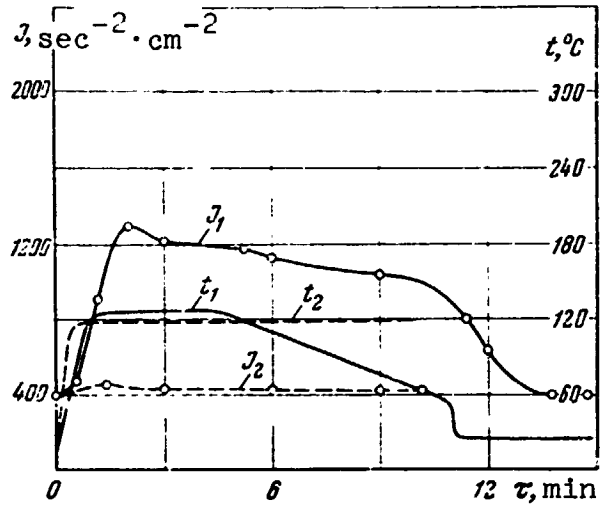

Fig. 4. Exoelectronic emission of glass particle

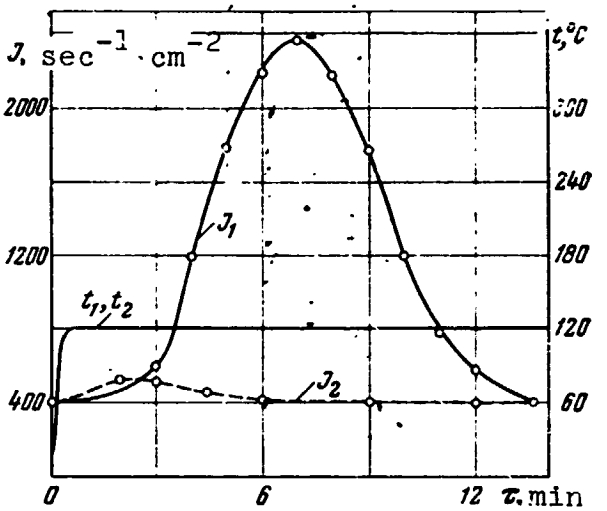

Fig. 5. Exoelectronic emission of anorthosite particle

the metallic particle with increase in temperature rose sharply, reaching a maximum value for the given temperature. With subsequent isothermal exposure, a falloff of the emission was observed, which for these particles can be described by first-order kinetic equations that are usual for exoemission measurements. A rise in the stimulation temperature led to a rise in exoemission (Figs. 2 and 3), while a temperature drop led to a decrease in exoemission (Fig. 4). Estimating the energy of activation of the process for the slag particle and for the metal particle gave markedly differing values: 0.10 and 0.6-0.8 kV, respectively. Reheating of the particles from room temperature caused practically no exoemission.

Altogether untypical both for the rest of the particles of lunar surface material as well as for known data on the exoemission of terrestrial minerals was the kinetics of exoelectronic emission from the anorthosite surface (Fig. 5). Roughly a minute after attainment of the emission excitation temperature (120° C), a smooth rise in the intensity of the emission current is observed; another 6 minutes resulted in the exoemission reaching a maximum, and then its decline began, that is, the general trend of exoemission is characterized by a symmetric curve indicating two combined processes, one of which is evidently associated with the liberation of emission centers and is preparatory for the next stage directly responsible for electron ejection. This kinetic relationship (along with the relatively high intensity of exoemission) can probably be accounted for by the increased "activity"

/546

of the surfaces of the anorthosite particles, leading to the appearance of sorptive bonds, which in turn "freeze" the active emission centers and require thermal stimulation[1] for their breakdown.

The singular state of the anorthosite surface, reflected in these results on exoelectronic emission has been noted more than once in the investigation of mineralogic fragments of regolith. Thus, the studies [4, 5] on the surface of lunar materials examined by luminescent methods established that the main carrier of natural thermoluminescence and cathodoluminescence is plagioclase. It is precisely in the anorthosite particles and in the specifically feldspathic particles that in several cases the strongest shock effects were noted, manifested in recrystallization and vitrification of the material, its brecciation, and the like. The anomalous exoemission (as well as luminescence) from the surfaces of particles of this type is possibly also caused by a set of processes leading to the production of metastable states both on the surface as well as in the bulk of individual particles.

---

[1] The effect of "blocking" of active emission centers through the sorption of the constituents of the terrestrial atmosphere was observed by us also in experiments on exoemission with fresh chips of silicate rocks close to lunar surface material in composition.

REFERENCES

1. Becker, K., and Gammage, R. B., "Exoelectron Emission and Surface Characteristics of Lunar Materials," Proc. Second Lunar Sci. Conf. 2, 1401 (1971).

2. Wood, G., Meteority i proiskhozhdeniye Solnechnoy sistemy /Meteorites and the Origin of the Solar System/, "Mir", 1971.

3. Lewis, D. R., Bull. Geol. Soc. Amer. 7[illegible], 761-770 (1966).

4. Dalrymple, D. B., and Doell, R. P., Science 167(3918), 713 (1970).

5. Sippel, R. F., and Spencer, A. P., Science 167(3918), 677 (1970).

Ural Polytechnic Institute imeni S. M. Kirov, Sverdlovsk

Order of Lenin Institute of Geochemistry and Analytical Chemistry imeni V. I. Vernadskiy, USSR Academy of Sciences, Moscow.

N75 11869

TEMPERATURE EMISSION SPECTRUM OF EXOELECTRONS OF LUNAR REGOLITH

/547

R. I. Mints, V. I. Alimov, V. P. Melekhin,
I. I. Mil'man, V. I. Kryuk, T. M. Petukhova,
L. L. Kunin, and L. S. Tarasov

Abstract

By linear heating in a vacuum of 10^{-6} torr, a study was conducted of thermostimulated exoelectronic emission of eight fragments of regolith returned by the Soviet Luna 16 automatic station. The nature of the exoemission "glove-curves" is determined by particle type. Fragments of breccia, sinter, slag, anorthosite, glass plate, and leucocratic gabbro after the first heating disclosed a single exoemission maximum, whose temperature position is in the range 115-200° C. Two emission maxima (at 130 and 200° C) were noted for the glass spherule and three maxima (50, 170, and 300° C) for the olivine particles. With the exception of the olivine particles, exoemission peaks after contact with the atmosphere were observed for all samples.

The estimate of the effective energy of activation (E) of exoemission, based on the Balazin-Zetzsche estimate, shows that for particles disclosing a single maximum after the first heating, E is in the range 0.25-0.35 eV. Considerably higher E values are characteristic of the high-temperature peaks of olivine (0.55 and 1.30 eV) and the glass spherule (0.55 and 1.40 eV).

The data obtained indicate the complex and inhomogeneous energy structure of some regolith fragments. The presence of surface states capable of forming sorptive bonds can be assumed for most particles. The exoemission of anorthosite, olivine, and the glass spherule is due to the presence of the formation defects at their surfaces, which is confirmed by visual appraisal of the particles.

Recording "natural" exoelectronic emission from some regolith particles of lunar surface material in the isothermal and isochronic regimes of thermostimulation makes it necessary to study the exoelectronic emission at different temperatures. Obtaining the temperature spectrum of exoemission permits drawing conclusions as to the nature of the centers responsible for the ejection of electrons, which can serve as a source of information on the prehistory of the material investigated.

The most convenient from the standpoint of interpreting the results is the constant-rate heating regime. In this case characteristic temperature positions of the maxima of the emission "glove-curves" (analogous to the curves of thermoluminescence) appear and it becomes possible to estimate the effect of energy of activation of exoemission. The method of calculating the energy of activation proposed by Balazin-Zetzsche /1/ makes it possible for processes occurring under first-order reaction kinetics to use the entire extent of the curve in the calculations. The main working equation is

$$\frac{d \ln(-\ln c)}{d(1/T)} = -E K,$$

where E is the energy of activation, T is temperature, $^{\circ}$K, K is Boltzmann's constant, and c is the relative fraction of sinters responsible for the process kinetics.

The experimental method and the apparatus techniques (with the exception of thermostimulation) remained the same as for the investigation of exoemission in the isothermal and isochronic regimes. To study the temperature dependence of the exoelectronic emission of regolith samples, the setup described for investigating the exoemission of small objects was supplemented with a special heater providing a linear rise in the temperature of samples at a rate of 0.03-1.0° C/sec (the heating took place at 0.3° C/sec).

The exoemission of various regolith particles returned by the Soviet Luna 16 automatic station was studied. Included among the fragments examined were both particles from primordial magmatic rocks (anorthosite M105, sample No. 13, olivine M108, sample No. 3, leucocratic gabbro M125, samples No. 6), as well as particles of /548
secondary formations (breccia M101, sample No. 13, sinter M102, sample No. 13, slag M103, sample No. 13, glass plate M114, sample No. 3, glass spherule M122, sample No. 9). The mean size of the fragments was 0.1-0.2 mm. The experimental results are given in Figs. 1-8. All the particles, even after the first heating, disclosed exoelectronic emission markedly exceeding the background level.

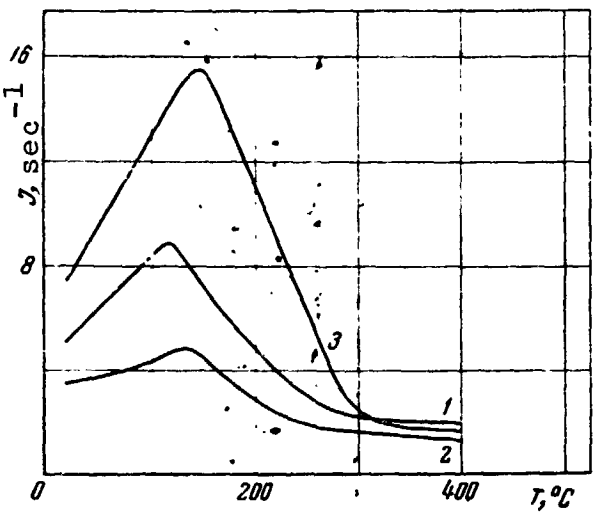

Fig. 1. Exoelectronic emission in breccia surface in the first (1) and second (2) cycles of thermostimulation and with heating after contact with the atmosphere (3).

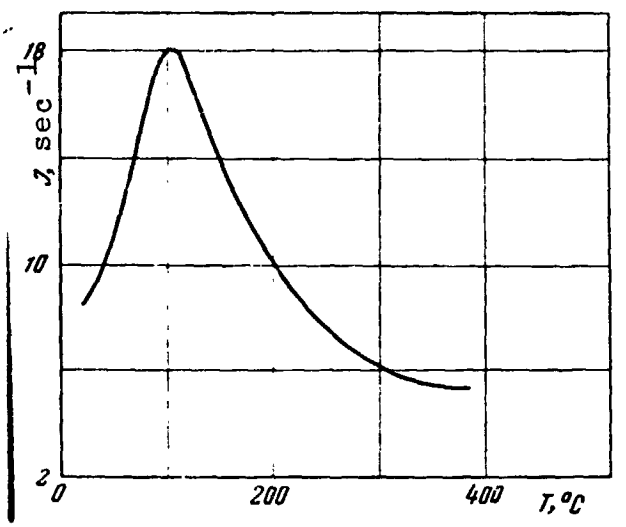

Fig. 2. Exoelectronic emission from surface of sinter.

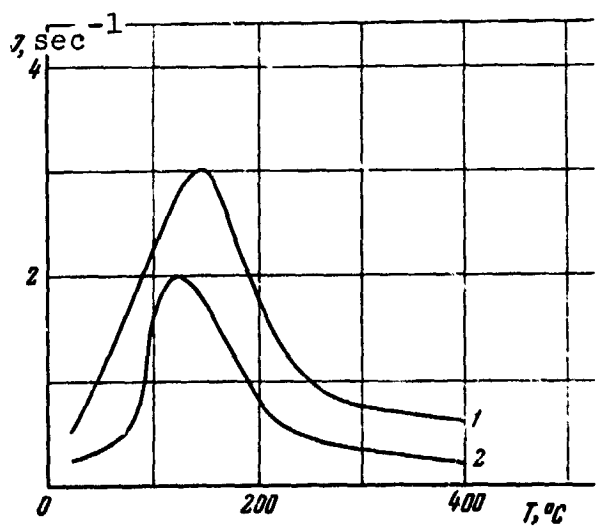

Fig. 3. Exoemission of glass plate after first heating (1) and after contact with atmosphere (2).

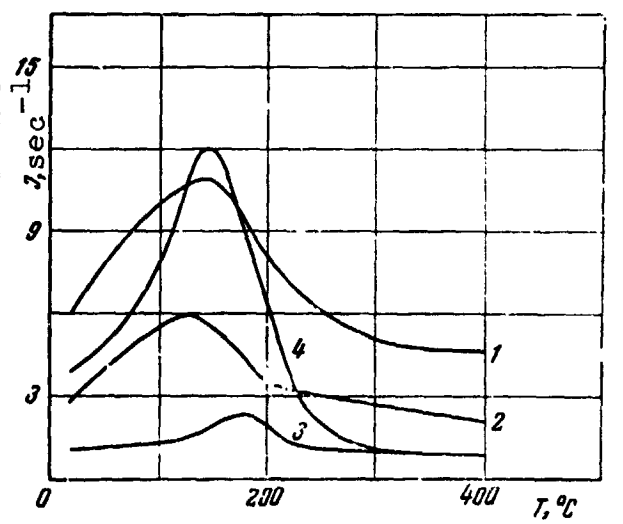

Fig. 4. Exoemission of anorthosite after first (1), second (2), and third (3) heating cycles, and after contact with the atmosphere (4).

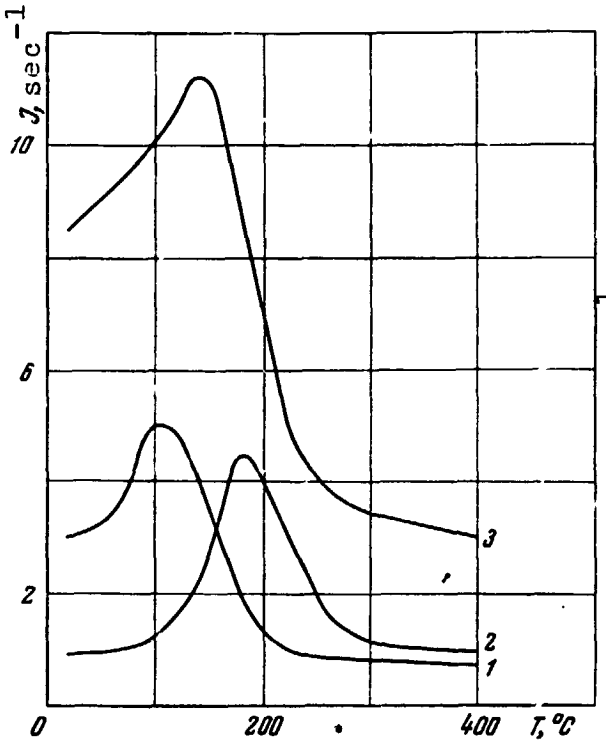

Fig. 5. Exoemission of slag particle after first (1) and second (2) heating cycle, and after heating following contact with the atmosphere (3)

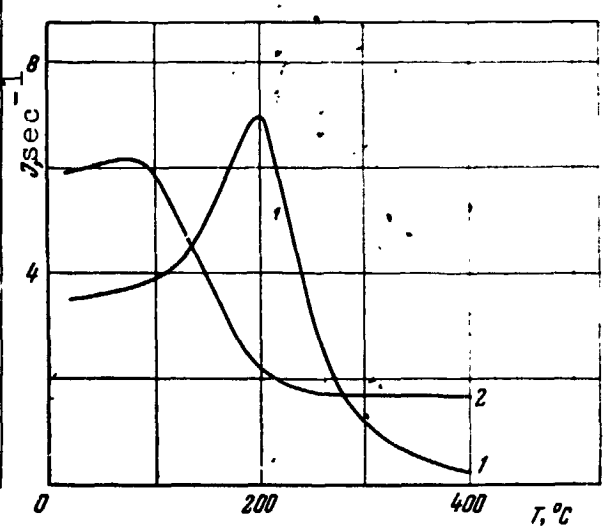

Fig. 6. Exoemission of particle of leucocratic gabbro after first heating (1) and following contact with the atmosphere (2).

Two types of exoelectronic emission curves characteristic of the first heating of the samples can be distinguished. First, these are curves with a single emission maximum (see Figs. 1-6). The temperature position of the maxima is different for the different particles and lies in the range 115-130° C (± 5° C) for the breccia, sinter, and slag, 140° C for anorthosite, 155° C for the glass plate, and 200° C for the gabbro.

The thermostimulation exoemission is of a different kind for the olivine sample and the glass spherule (see Figs. 7 and 8): they show three and two emission peaks, respectively, differing in temperature position (50, 170, and 300° C for the olivine, 130 and 200° C for the glass spherule).

Reheating of the particles examined without disturbing the vacuum (10^{-6} torr) either did not cause emission, or led to a decrease in its intensity followed by its disappearance upon the third heating (samples of breccia and slag). An exception is represented by an anorthosite fragment, from whose surface the exoemission is observed both in second as well as in third heatings. /549

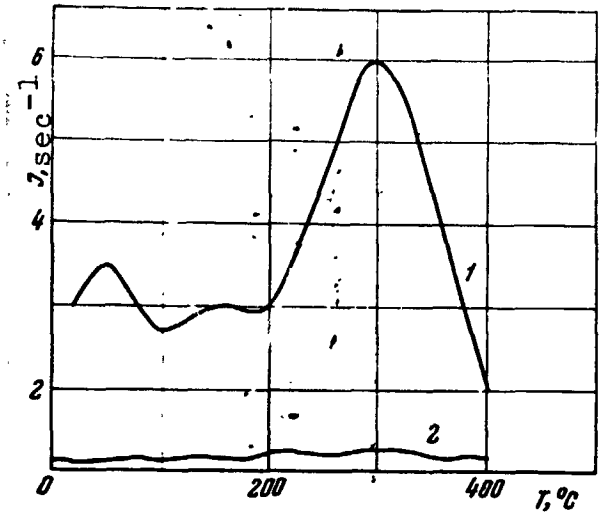

Fig. 7. Emission of exoelectrons from olivine fragment after first heating (1) and after contact with the atmosphere (2).

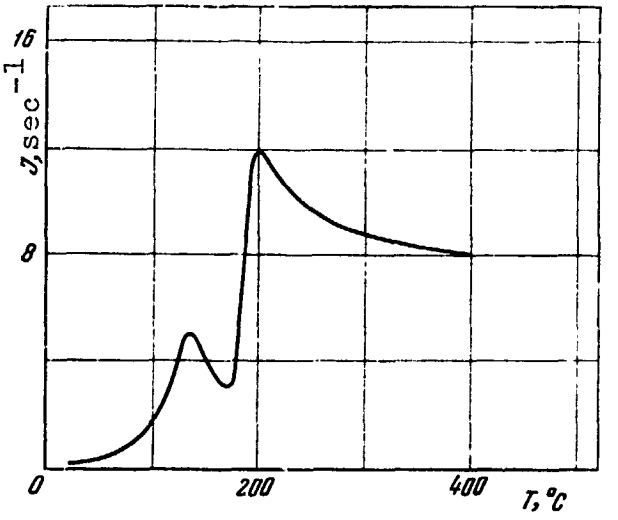

Fig. 8. Exoemission from surface of glass spherule.

In the case when the heating without disruption of vacuum no longer excited emission, the samples were thermostimulated by admitting atmospheric air into the chamber. After a 5-minute contact with the atmosphere, emission peaks were observed for most samples. The temperature positions of these peaks for breccia, slag, glass plate, and anorthosite are quite close to the temperatures for the exoemission maxima observed after the first heating. For the leucocratic gabbro particle, a substantial shift in the emission maxima (by 100° C) was observed. Olivine particles did not disclose emission after contact with the atmosphere.

The Balazin-Zetzsche method was used in estimating the effect of energy of activation of exoemission E. Characteristic calculated plots are shown in Fig. 9.

It was noted that for particles disclosing one emission maximum after the first heating, E is in the range 0.25-0.35 eV ($\pm$ 0.05 eV). Calculation yielded the same energies of activation for the exoemission peaks after the second heating of breccia and sinter, and also for peaks showing up after the samples had been brought into contact with the atmosphere.

The considerably larger E values for the exoelectronic emission process are characteristic of the high-temperature maxima of olivine (first peak -- 0.30 eV; second peak -- 0.55 eV; and third peak -- 1.30 eV), glass spherule (0.55 and 1.40 eV, respectively, for the first and second peaks), and also for the peak arising after the third heating of anorthosite (0.70 eV).

These data indicate the complex and inhomogeneous nergy structure of the surfaces of individual lunar regolith particles.

A developed structure is characteristic of particles that are aggregated formations resulting from "lunar weathering" and subsequent sintering of rocks (Fig. 10). The closeness of the curves and the agreement of the energies of activation of the exoelectronic emission processes obtained after the first heatings and after contact of samples with the atmosphere indicates evi- /550
dently that surface states capable of forming sorptive bonds even in a vacuum of 10^{-5} - 10^{-6} torr are present in these particles. Thus, contact of the lunar regolith with the atmosphere revealed the activity of the particle surfaces. Activation of the exo-emission of nonmetallic materials in conditions of contact with an oxidizing medium is possible through a reduction in the surface potential barrier when oxygen diffuses into the bulk of the defective surface layers of the particles. Exoemission from oxidized lunar materials was observed by Becker and Gammage /2, 3/ in samples returned by Apollo 11 and Apollo 12.

These results indirectly agree with the data on the natural thermoluminescence of breccias /4_7, which yield a luminescent peak near 100° C.

The exoelectronic emission of the glass plate particle is analogous, disclosing a substantial maximum after the first heating and a rise in the emission intensity after contact with the atmosphere. The order of magnitude of the energy of activation (0.25-0.35 eV) can indicate that the limiting stage in the kinetics of exoemission is either the sorptive processes as such or processes associated with the surface migration of defects.

The different nature of the exoelectronic emission of the particles of anorthosite, slag, olivine, and glass spherule is probably predetermined by the defect structure of these fragments.

Anorthosite reveals emission properties even after three heating cycles in vacuum. The first two peaks, as well as the peak arising after contact with the atmosphere are similar in temperature position (130-145° C) and in the energy of activation (0.30-0.35 eV). The emission maximum corresponding to the third heating peak is shifted into the high-temperature region (165° C) and is characterized by a large value of $E \approx 0.70$ eV. Traces of diverse shock effects noted upon examination of the surface properties of anorthosites /4, 5/ can lead to the appearance of a developed defect surface. Probably, the exoelectronic emission of anorthosite is due to the presence of at least two different types of defects. It is not precluded that emission after the

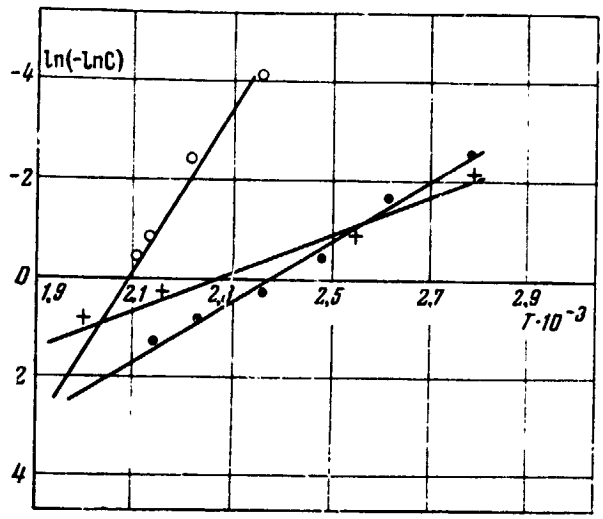

Fig. 9. Plots for calculating energy of activation of emission from sinter particle (+), of first (o) and second (o) maxima of exoemission from surface of glass spherule.

third heating cycle is limited by the diffusion kinetics of the migration of defects (vacancy type) into the near-surface layers, and for it to be manifested requires preliminary depletion of the surface sorptive centers. The latter factor is also indicated by the results of studying the exoemission of anorthosite in the isothermal regime. The presence of feldspathic minerals in the sample M125 (leucocratic gabbro) possibly accounts for the emission properties of this particle.

Data on the exoelectronic emission of the slag particle (Fig. 11:see Fig. 5) can be viewed analogously with results obtained from studying the anorthosite fragment. The emission peaks arising after heating and after contact of the slag sample with the

10a 10b

Fig. 10. Fragments of breccia (a) and sinter (b).

atmosphere are characterized by closely similar energies of activation (0.35 and 0.30 eV) and do not differ very widely in the temperature maximum. This indicates that the surface states responsible for both exoelectronic maxima are similar in nature. and that their activation can be caused by sorptive processes. /552

11

Fig. 11. Slag particle.

12a

12b

Fig. 12. Particles of olivine (a) and glass spherule (b).

Displacement of the exoemission peak after the second heating into the high-temperature region (185° C) and a rise in the energy of activation (E ≈ 0.5 eV) can indicate that here a different mechanism of electron ejection is realized, whose kinetics is probably limited by the diffusion of defects into the near-surface layers.

Of special interest are the results of studying the temperature dependence of the exoelectronic emission of olivine. The absence of emission after contact of the sample with the atmosphere (just as the value E) can indicate that in this case the exoemission is caused by the presence only of deformation defects, whose annealing terminates already after the first heating cycle and probably occurs according to diffusion kinetics. The three types of defects whose annihilation leads to three exoemission maxima evidently arose through the combination of deformation damage, among which can be included, for example, proton bombardment (low-temperature peaks) and micrometeoritic bombardment.

The two types of defects whose production is probably caused by thermal stresses and impact are disclosed also upon investigating the glass spherule (emission peaks with temperatures of 130 and 200° C and, thus, with E ≈ 0.55 and 1.40 eV).

The presence of a considerable number of deformation defects in olivine and in the glass spherule revealed by exoelectronic

measurements is confirmed by a visual evaluation of the state of the surface of these particles (Fig. 12). Spalling with characteristic deformation striation steps is clearly discernible on the olivine surfaces; traces of micro-impact can be easily seen on the surfaces of the glass spherule.

As noted by A. P. Vinogradov [6] one of the urgent problems in lunar research is studying the structure and composition of the surface of the Moon and their transformation, as well as history and evolution which resulted in the present lunar surface. The results obtained here suggest that the possibility of recording the exoelectronic emission of regolith particles and estimating the activation parameters of the process reveal certain prospects in the investigation of the prehistory of lunar materials. In addition, since the exoemission characteristics bear information about the energy changes in the properties of the material in the form of an electrical signal that can be coded and transmitted via telemetry, it is possible to use the effect of exoelectronic emission in studying deformation measurements of lunar surface material directly at the surface of the Moon.

REFERENCES

1. Balazin, M., and Zetzsche, A., Phys. stat. sol. 2, 1670 (1962).

2. Becker, K., and Gammage, R. B., Proc. Second Lunar Sci. Conf., 1971.

3. Gammage, R. B., and Becker, K., Earth Planet. Sci. Letters 12(2), 155 (1971).

4. Dalrymple, G. B., and Doell, R. K., Science 167(3928), 713 (1970).

5. Wood, J. A., Dickey, J. S., Jr., Marvin, W. B., and Powell, B. N., Izv. AN SSSR, seriya geol. (6), 33 (1970).

6. Vinogradov, A. P., Geokhimiya (1), 3 (1970).

Ural Polytechnic Institute imeni S. M. Kirov, Sverdlovsk

Order of Lenin Institute of Geochemistry and Analytical Chemistry imeni V. I. Vernadskiy, USSR Academy of Sciences, Moscow.

N75 11870

HEAT-PHYSICAL PROPERTIES OF LUNAR SURFACE MATERIAL RETURNED TO EARTH BY THE LUNA 16 AUTOMATIC STATION

/553

V. S. Avduyevskiy, N. A. Anfimov, M. Ya. Marov, Yu. A. Treskin, S. P. Shalayev, and A. P. Ekonomov

Abstract

A study was made of the density, specific heat capacity, and coefficient of thermal conductivity of a sample of lunar surface material taken from the sample returned by the Luna 16 automatic station. The study was carried out in a helium-filled chamber. The density of the surface material when freely heaped was 1.2 g/cm^3, and when shaken down -- 1.7 g/cm^3. The specific heat capacity was 0.177 ± 0.010 $cal \cdot g^{-1} \cdot deg^{-1}$. The coefficient of thermal conductivity in the material was $4.8 \cdot 10^{-6} \pm 1.2 \cdot 10^{-6}$ $cal \cdot cm^{-1} \cdot sec^{-1} \cdot deg^{-1}$.

During the last 20 years, the investigation of the heat-physical properties of the surficial layer of the Moon was carried out by analyzing the data of optical infrared measurements and radio astronomical observations. This analysis makes it possible to determine in the first case the complex parameter $\gamma = (k\rho c)^{-0.5}$, and in the second case -- to establish a correspondence between the depth of heating and the depth of penetration of electromagnetic waves, dependent on the electroconductivity of the lunar surface material and its dielectric and magnetic permittivities.

The construction of spacecraft of the Apollo and Luna 16 type made it possible to return to Earth samples of lunar rocks, permitting the use of direct experimental methods in their study. In the present article are described the methods and results of measuring the density, specific heat capacity, and the coefficient of thermal conductivity of the lunar material returned to Earth by the Luna 16 station.

Laboratory equipment. A special laboratory with a research booth and the requisite complex of auxiliary systems and services was built to investigate the heat-physical properties of the lunar material. From the central receiving laboratory, the portion of lunar surface material was brought in a hermetic container. The main work with the surface material involved opening the container, weighing it, taking samples for various studies, filling and hermeticizing the ampules for investigation of heat capacity, pouring the surface material into the receiving vessels of the instruments for investigation of thermal conductivity and electrical properties -- -- all these operations were carried out in the "glove box" in helium (Fig. 1). To avoid contamination of the samples of surface material, the objects introduced into the chamber through the hatch were first sterilized. Strict observance of the purity of the helium atmosphere was maintained.

Housed in the helium chamber was an analytical balance and an array of instruments specifically built for handling lunar surface material. In addition, placed within the helium chamber was a vacuum bell connected with an evacuating system providing a vacuum down to 10^5 mm Hg. Within the bell were housed instruments for investigating thermal conductivity and electrical characteristics. Large observation windows in the glass chamber areas and in the bell cover provided convenience for the operators. Auxiliary instruments of the measuring system were placed near the chamber and connected via electric plugs with the transducers housed therein.

The auxiliary services of the laboratory included groups of chemical analyses, microscopic investigations, x-ray structural analysis, and technical services.

Material investigated. The investigated portion of the lunar material consisted of the upper part of a core of surface material about 350 mm in length taken by the surface-sampling device of the Luna 16 station from the surficial layer of the Moon in the region of the Sea of Fertility. Structurally, this section of the core (zone A /1/) is regolith -- a loose dispersed material consisting of particles of two types: primary magmatic rocks (of the basalt type) and lunar rocks subjected to appreciable transformations in processes of disintegration under the effect of the cosmic factors active on the Moon (sintered, partially surfacewise fused particles, and melted formations of nearly spherical shape). The arithmetic-mean particle size in the portion of surface material investigated was about 25 μm, and the mean-gravimetric size was 160 μm. /554

Density. The results of the measurements showed that when the lunar surface material was heaped freely in helium its density

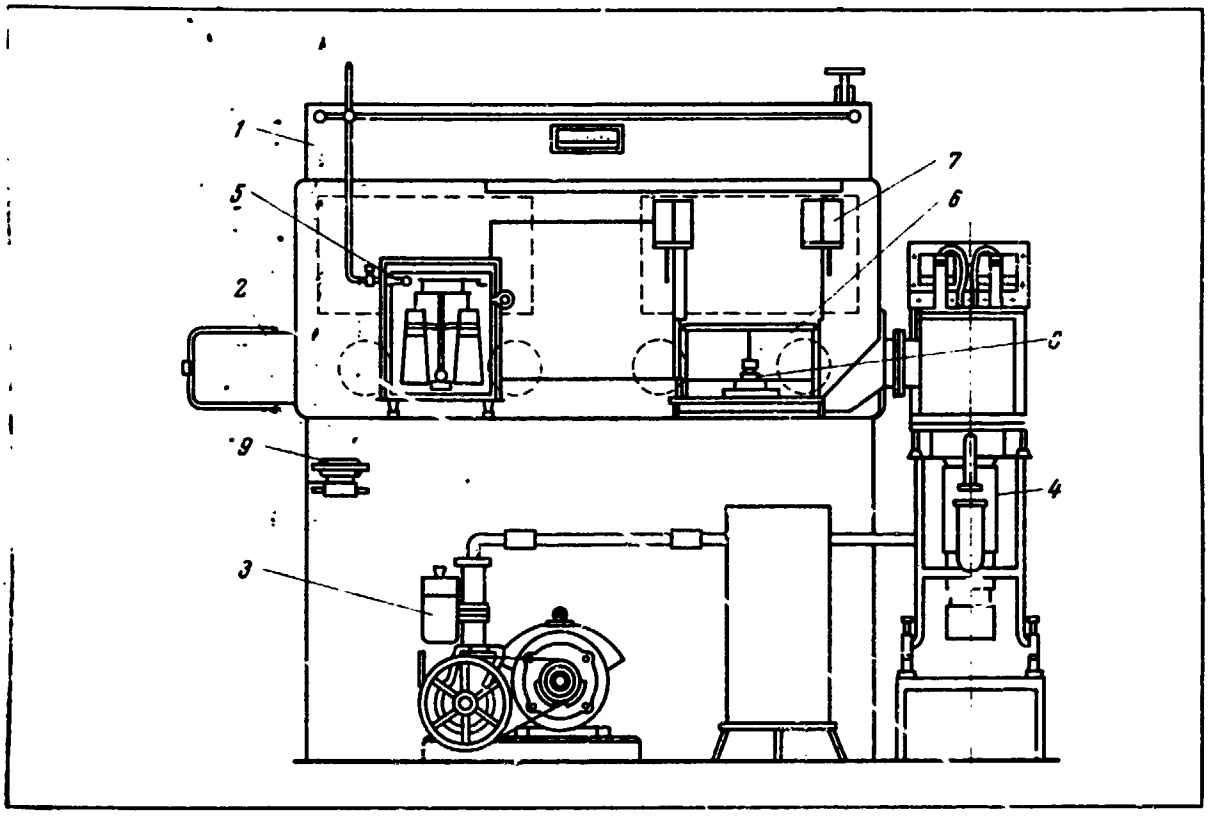

Fig. 1. Chamber for working with lunar material.

1. 2KA-NZh chamber
2. Hatch
3. Forevacuum pump
4. Diffusion pump
5. Analytical balance
6. Vacuum bell
7. Bell elevating system
8. Conductimeter
9. Automatic device for maintaining excess helium pressure

was about 1.2 $g \cdot cm^{-3}$. By vibro-compaction, the density of the surface material can be raised to 1.7 $g \cdot cm^{-1}$. The maximum density of the lunar surface material was achieved in the instrument for measuring the coefficient of thermal conductivity (ρ = = 2.25 $g \cdot cm^{-3}$). Here the dirt was placed in a thin layer 1 mm thick, and a load was applied to its upper surface. The specific pressure on the surface material was varied from 0.015 to 0.8 $kg \cdot cm^{-2}$, which did not change the density of the lunar material.

Specific heat capacity. To measure the specific heat capacity of the lunar material c, use was made of an isothermal ice calorimeter, whose operating principle is based on a change in the volume of the ice-water system when applied heat is brought to it. The constant of the ice calorimeter was 1.136 $mm^3 \cdot cal^{-1}$.

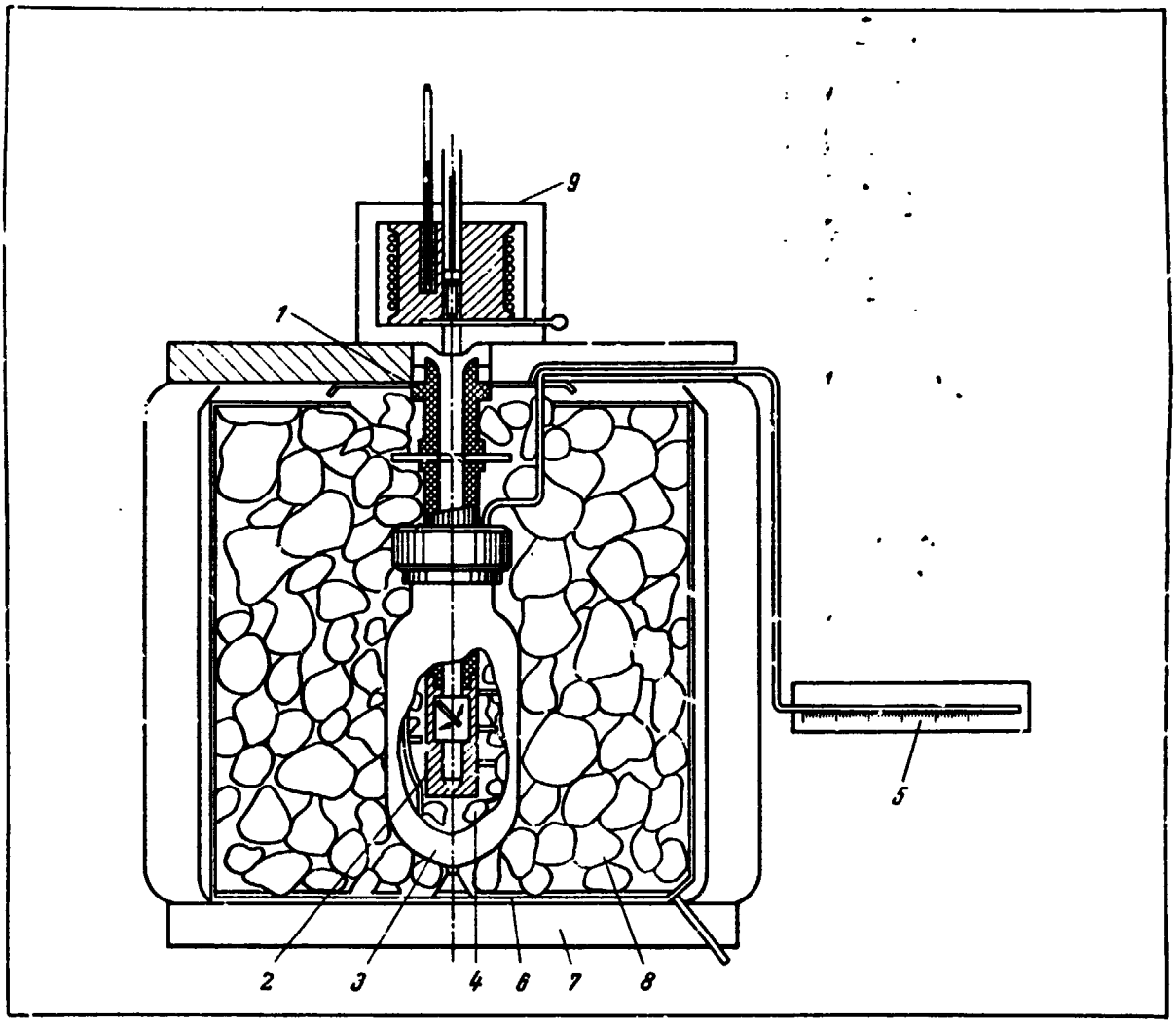

Fig. 2. Ice calorimeter

The calorimeter used for this study was a modernized version of the scheme described in [3]. The calorimeter scheme is shown in Fig. 2. The receiving part of the calorimeter consisted of two parts: the upper part (1) was made of an insulation material, the lower part (2) was made of copper. A slidegate was provided at the connection of the upper and lower parts. The receiving part was inserted hermetically into a Dewar vessel (3), whose volume was filled with ice (prepared from distilled, degassed water) and with water (4). From this vessel there was an outlet terminating in a horizontal measuring capillary (5) 0.78 mm in diameter. The Dewar vessel was placed in a metal box (6) covered externally with thermal insulation (7). The internal volume of the box was filled with ice (8) to reduce to the minimum the influx of heat within the calorimeter.

An approximately 1.5 g portion of the surface material was placed in the helium atmosphere in a specially constructed thin-walled metal ampule, whose internal volume was 1.1 cm^3, and whose empty weight was 0.85 g. The ampule was hermeticized. It was heated in a special heater-thermostat (9), consisting of a massive copper cylinder with electric heating winding; here the temperature was monitored to $\pm$ 0.1° C. After being kept in the thermostat at constant temperature for an hour, the ampule containing the surface material was discharged into the receiving part of the calorimeter, which made it possible to measure its total enthalpy. When the specific heat capacity of the lunar material was determined, an allowance was made for the intrinsic heat capacity of the ampule and the heat losses when the ampule was discharged from the heater-thermostat into the receiving part of the calorimeter. /555

The total methodological error in the determination of c was estimated to be $\pm$ 5 percent. The specific heat capacity of the lunar material in the temperature range 0 to 100° C, as the mean of a series of five experiments, was $c = 0.177 \pm 0.010$ cal·$\cdot g^{-1} \cdot deg^{-1}$.

Thermal conductivity. A special instrument was used to measure the coefficient of thermal conductivity of the lunar material -- a conductimeter, in which the one-dimensional flow of heat through a thin layer of the material investigated was achieved. The design scheme of the conductimeter is shown in Fig. 3. The lunar material investigated was poured into a cavity (1) 30 mm in diameter and about 1 mm in height. The height of the layer of material δ when freely heaped was determined with a calibrating ring (9), and after assembly the instrument was monitored with a cathetometer. The working electric heater (heat source) (8) was surrounded with a protective heater (6) separated from the main heater (8) by a gap of 0.2 mm. The heat receiver (caolrimeter) (12) was surrounded with a protective ring (8), separated from it also by a gap of 0.2 mm. Thus, the layer of the material investigated can be conditionally regarded as divided into two zones -- the working zone (beneath heater 8) and the protective zone (under the heater 6). The protective ring (3) rested on porcelain supports (4), whose lower ends were secured in the protective heater (11). The shield-vacuum insulation (2) and (7) was used to eliminate radiative heat transfer from the instrument components. The surface material sampler (5) served to reduce the losses of material during charging of the instrument. The difference of the temperatures between the parts (8) and (6) and also the parts (11) and (3) was maintained at a sufficiently low value (less than 0.1° C) by automatic regulation of the current in the heaters. The temperatures were measured /556

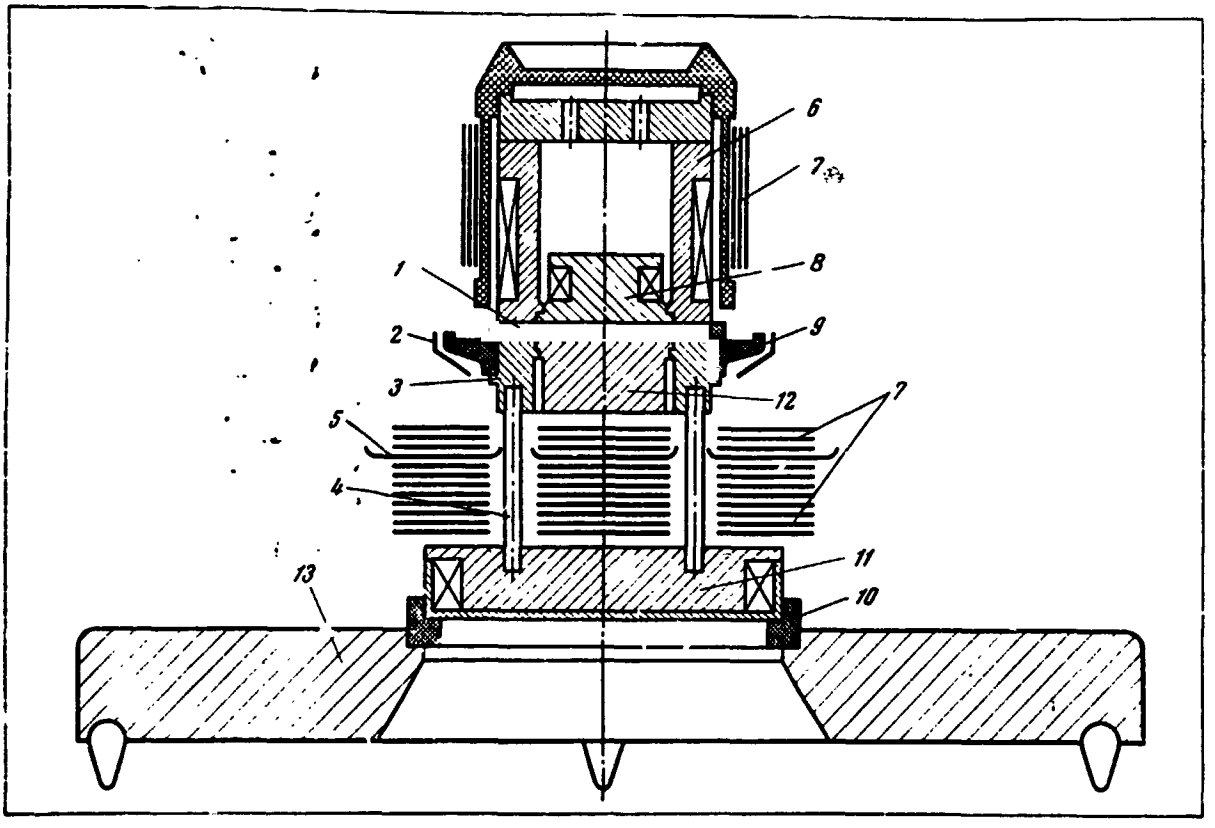

Fig. 3. Schematic of conductimeter

with cnromel-constantan thermocouples, and the signal from these was amplified with electronic microvoltmeters of the modulator-amplifier-demodulator type, and then recorded by automatic recorders. The precision of recording was 0.1° C.

The conductimeter was placed within the vacuum hood in helium. By evacuation, the pressure was brought to $4 \cdot 10^{-1}$ -- 10^{-5} mm Hg. The temperature in the layer of the lunar material virtually linearly depended on the transverse coordinate x. The difference between the temperatures at the opposite surfaces of the layer ΔT was kept constant for a sufficiently long time and was approximately 20° C. The thermal flux from the main electric heater (8) in contact with the upper surface of the layer of the material passed through the material investigated to the heat receiver (12), whose temperature T was steadily increased. However, the mass of the heat receiver was selected as sufficiently large so that the derivative of the receiver temperature with respect to time T'_τ was sufficiently small, and the change in the derivative with

respect to the coordinate $\Delta T'_x$ across the sample was negligible compared with the mean value of this derivative $T_x' : \Delta T_x' = \rho c \delta T_\tau'/k \ll T_x'$.

In this case, the coefficient of thermal conductivity of the material investigated was as follows: /557

$$k = \frac{q\delta}{\Delta t}, \quad (1)$$

where the thermal flux q can be determined from the electrical power given off in the heater, as well as from the heating rate of the heat receiver. The total error in measuring the coefficient of thermal conductivity was not greater than $\pm$ 25 percent.

The results of the experiments to determine the coefficient of thermal conductivity of the lunar surface material in the 20-40° C temperature range for different gas (helium) pressures P_{He} and for different specific pressure on the surface material p_g are shown in Fig. 4.

Clearly, the coefficient of thermal conductivity of the lunar surface material in vacuum within the limits of experimental precision does not depend on the specific pressure on the surface material (within the range 0.015-0.8 $kg \cdot cm^{-2}$). Averaging of all the results yields for this coefficient the value of $k = 4.8 \cdot 10^{-6} \pm 1.2 \cdot 10^{-6}$ $cal \cdot cm^{-1} \cdot sec^{-1} \cdot deg^{-1}$ for $\rho = 2.25$ $g \cdot cm^{-3}$ and T = 20-40° C ($P_{He} \sim 10^{-3}$ mm Hg).

Evaluation of the effective size of surface material pores. The effect of helium pressure on the coefficient of thermal conductivity of the surface material begins to show up markedly when $P_{He} = 4 \cdot 10^{-1}$ mm Hg (at this pressure a twofold rise in k is observed, that is, the contribution of the thermal conductivity of helium k_{He} is approximately equal to the thermal conductivity of the surface material in the vacuum). This factor must be used in estimating the effective pore size d in the surface material. The mean-free path of the helium atoms in these conditions is 0.4 mm, that is, it markedly exceeds the characteristic pore size. In this case, the thermal flux through the gas q_{He} is [9]:

$$q_{He} \approx \frac{3}{8} P_{He} \sqrt{\frac{3R}{4t}} T' d,$$

where R is the gas constant.

COMPARISON OF HEAT-PHYSICAL PARAMETERS OF LUNAR SURFACE MATERIAL

Method of determination	Characteristics			References
	c, cal·g^{-1}·deg^{-1}	k, cal·cm^{-1}·sec^{-1}·deg^{-1}	ρ, g·cm^{-3}	
Laboratory analysis				
Luna 16	0,177±0,01	(4,8±1,2)·10^{-6}	2,25	Present study
Apollo 11	0,185	5,5·10^{-6}	1,265	[4]
	0,20±0,02			[5]
Optical and radio-measurements		1,25·10^{-5}	0,5	[6]
		3,50·10^{-5}	0,5	[7]
		1,2·10^{-6}		
		1,7·10^{-5}	4,9–0,35	[8]
Calculations	Based on known composition 0.188			

Hence follows an estimate for the effective pore size: $d \approx 0.2$ mm. This size agrees with the data of the statistical measurements made of the size of lunar surface material particles.

Discussion of results. In the optical and radio astronomical observations of the Moon, use was made of complex heat-physical characteristics, which are a combination of the above-determined quantities -- the coefficient of thermal diffusivity $a = k/\rho c$, the depth of of heating of the lunar surface $\ell_T = (2a/\Omega)^{0.5}$, where $\Omega = 2.46 \cdot 10^{-6}$ rad·sec^{-1} is the angular rate of rotation of the Moon, as well as the parameter $\gamma = (k\rho c)^{-0.5}$.

These values are as follows for specific mean values of c, k, and ρ: $a = 1.2 \cdot 10^5$ cm·sec^{-1}; and $\gamma = 725$ cm^2·deg·sec$^{0.5}$·cal^{-1}.

The values obtained for the specific heat capacity, the coefficient of thermal conductivity, and the density of the lunar material from the core taken by Luna 16 can be compared with the estimates of the values of c, k, and ρ obtained by employing the parameters a, ℓ_T, and γ from terrestrial observations, as well as with values determined for the regolith in the analysis of the Apollo 11 samples. The results of this comparison are given in the Table.

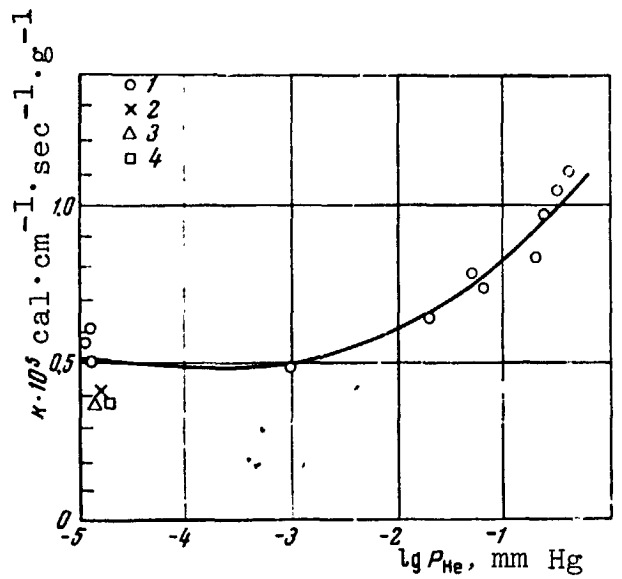

Fig. 4. Dependence of coefficient of thermal conductivity on helium pressure for different specific pressures on the surface material (in kg/cm^2)
1. 0.015
2. 0.2
3. 0.4
4. 0.8

From the Table it follows /558 that the values of c and k determined in the direct laboratory experiment on the Luna 16 and Apollo 11 samples are in good agreement. The specific heat capacity agrees satisfactorily also with the calculations of this characteristic for the known chemical composition of surface material samples /1, 10/, defined as

$$c = \sum_i c_i x_i,$$

where x_i is the gravimetric concentration of the i-th constituent in the sample. In the estimates of the coefficient of thermal conductivity based on optical and radio astronomical measurements, the discrepancy is marked. However, it should be noted that k depends strongly on the composition and structure of the surface material, and for granular dispersed materials -- also on its density, and therefore can vary over the lunar surface.

The experimental confirmation of the accuracy of the very low values of the coefficient of thermal conductivity of the surfucial layer of the Moon given its relatively high density is a result of this study.

The low values of the coefficient of thermal conductivity are significant for the thermal regime of the surficial layer of the Moon, responsible for the rapid drop in the amplitude of the temperature fluctuations with depth. As we know, the amplitude of temperature fluctuations in the surficial layer of the Moon can be 280° C /11/. If the heat-physical properties of the lunar material determined in the present study remain constant in a sufficiently thick surficial layer, at the depth of 7 cm the amplitude of temperature fluctuations can drop to 30°, and at a depth of 14 cm it will not be more than 3° C.

The absence of the explicit dependence of the coefficient of thermal conductivity of the lunar material on the specific pressure on the surface material (at relatively low pressures) suggests that the transfer of heat through this material occurs mainly via radiation. The coefficient of the radiative thermal conductivity in dispersed materials is described by the Loeb formula [12]:

$$k_r = 4\sigma d \varepsilon \Gamma T^3. \qquad (2)$$

where σ is the Stefan-Boltzmann constant, d is pore size, ϵ is degree of blackness, and Γ is the shape factor ($\Gamma = 2/3$ for spherical pores). Inserting the resulting coefficient of thermal conductivity of lunar material into Eq. (2) shows that the characteristic pore size must be of the order of 0.5 mm. This estimate markedly exceeds the actual pore size in lunar material, which permits the conclusion that contact thermal conductivity makes an appreciable contribution to the total heat transfer process through the surficial layer of the Moon.

REFERENCES

1. Vinogradov, A. P., "Preliminary Data on Lunar Material Returned by Luna 16 Automatic Station," Geokhimiy (3), 261 (1971).

2. Avduyevskiy, V. S., Anfimov, N. A., Marov, M. Ya., Shalayev, S. P., and Ekonomov, A. P., "Heat-Physical Properties of Lunar Material Returned to Earth by the Luna 16 Automatic Station," Dokl. AN SSSR 196(4), 801-804 (1971).

3. Popov, M. M., Termometriya and kalorimetriya /Thermometry and Calorimetry/, MGU, 1954.

4. Robie, R. A., Hemingway, B. C., and Wilson, W. H., Science 167(3918), 749-750 (1970).

5. Bastin, J. A., Clegg, P. E., and Fielder, G., Science 167(3918), 728-730 (1970).

6. Troitskiy, V. S., Novoe o Lune /Progress in Moon Research/, USSR Academy of Sciences Press, 1963.

7. Salomonovich, A. Ye., Novoe o Lune, USSR Academy of Sciences Press, 1963.

8. Sen'or, T. V., Zigel', F. M., and Zhiro, A., Novoe o Lune, USSR Academy of Sciences Press, 1963.

9. Graber, G., and Ercke, S., Osnovy ucheniya o teploobmene /Fundamentals on Heat Transfer/ IL, 1958.

10. Peck. L. C., and Smith, V. C., Science 167(3928), 532 (1970).

11. Sytinskaya, N.N., Priroda Luny /Nature of the Moon/, Fizmatgiz, 1959.

12. Loeb, A. L., J. Appl. Phys. 22(3), 282-285 (1951).

N75 11871

RESULTS OF INVESTIGATING THERMAL AND ELECTRICAL PROPERTIES OF LUNAR SURFACE MATERIAL AND ITS ANALOGS

/559

A. R. Golov[illegible], N. Dmitriyev, Ye. A. Dukhovskoy, G. Ya. Nov[illegible] R. G. Petrochenkov, V. V. Rzhevskiy, A. A. Silin, and V. V. Shvarev

Abstract

Presented are the results of investigating the thermal and electrical properties of lunar surface material returned to Earth by the Luna 16 automatic station and its terrestrial analogs in a 10^{-6} torr vacuum and in a helium atmosphere. Study of the lunar surface material and its analogs showed that their specific heat capacity and electrical properties are similar in value but the coefficients of thermal conductivity differ. The results are compared with data on the thermal and electrical properties of the surface layer of the Moon obtained by indirect radiometric methods, and with results obtained for samples of lunar surface material returned to Earth by the crew of the Apollo 11 spacecraft.

Indirect radiometric methods of determining the physical properties of the lunar surface material [1-4] showed that lunar surface materials are dielectrics and have very low thermal conductivity.

The Moscow Mining Institute and All-Union Scientific Research Institute of Physical Optical Measurements conducted investigations of the thermal and electrical properties of lunar surface material returned to Earth by the Luna 16 automatic station and its terrestrial analogs: andesite-basaltic sand and finely crushed basalt. The study of the thermal and electrical properties of lunar surface material was conducted at 20°C in a 10^{-6} torr vacuum and in an atmosphere of chemically pure helium at normal pressure in the special chamber, and the study of analogs was additionally conducted also in an air atmosphere. To determine how correct the

methods developed for studying material in small samples in vacuum conditions that we used, the thermal and electrical properties of the analogs were determined also on standard devices in an air atmosphere and in vacuum.

The specific heat capacity c, the coefficient of thermal diffusivity a, and the coefficient of thermal conductivity λ were determined by a combination method, uniting the technique of the instantaneous heat source (determination of a) and the method of the periodic input of heat [5] (determination of c). The coefficient of thermal conductivity was calculated as the products of a, c, and surface material density δ.

The device for determining the thermal properties with small samples (see Fig. 1) consisted of a teflon beaker with thin walls, 10 mm in diameter and 20 mm in height (1): a thin graphite rod 2 in the center of the beaker serving as a line source of heat; thermocouples 3 installed at a distance of 2 mm from the heat source; and thermocouple 4 installed close to the beaker wall. The temperature from each thermocouple was recorded on two model PS-1 electronic recorders 5 operating synchronously.

The coefficient of thermal diffusivity in vacuum was determined by measuring the time required to reach the temperature maximum at the thermocouple 3, and was monitored in the helium atmosphere and air atmosphere, in addition, with thermocouple 4. The specific heat capacity was calculated based on the ratio of the amount of heat given off by the line heat source per unit mass of surface material, after subtracting the thermal losses into the ambient medium (teflon beaker, current-conducting leads, and so on) to the temperature of the system after it had attained thermal equilibrium. The latter was determined from the equality of the temperatures recorded by both thermocouples.

The pulse duration was regulated with a mechanical time relay 6. It was 0.5 sec for the determination of a, and 10-20 sec for the determination of c. The strength of the current source was regulated with a model RNO-250-5 a.c. transformer 7 and was 5-10 W /561 for the determination of a, and 1-2 W for the determination of c. The thermal losses were determined by conducting experiments on materials with known heat capacity. The error in the determination of a was $\pm$ 4 percent, $\pm$ 5 percent -- in the determination of c, and $\pm$ 10 percent -- in the determination of λ.

The determination of a, c, and λ was carried out by freely heaping previously loosened test material. Here the density of the lunar surface material, andesite-basaltic sand, and the finely crushed basalt were 1.38, 1.14, and 1.22 g/cm^3, respectively (Table 1).

TABLE 1. RESULTS OF DETERMINING THERMAL PROPERTIES OF LUNAR SURFACE MATERIAL AND ITS ANALOGS /560

Rock	Parameter determined	Experimental conditions: vacuum, 10^{-6} torr	Atmosphere: helium	Atmosphere: air, small	Atmosphere: air, standard instrument
Lunar surface material	c	0,74	0,76	—	—
	a	0,27	14,7	—	—
	λ	2,76	155	—	—
Andesite-basaltic sand	c	0,735	0,75	0,735	0,74
	a	0,51	6,3	4,45	4,3
	λ	4,27	53,8	37,2	36,3
Finely crushed basalt	c	0,79	0,81	0,8	0,8
	a	0,725	9,8	6,4	6,25
	λ	0,98	97,0	62,4	61,0

$c\left[\frac{J}{g.deg}\right]$; $a\left[10^{-4}\frac{m^2}{sec}\right]$; $\lambda\left[10^{-3}\frac{W}{m.deg}\right]$.

TABLE 2. DEPENDENCE OF ϵ, ρ, AND $\mathrm{tg}\,\Delta$ ON FREQUENCY

Frequency, Hz	Rock	Experimental conditions: vacuum, ϵ	vacuum, $\mathrm{tg}\,\Delta\cdot10^{-3}$	vacuum, ρ	helium, ϵ	helium, $\mathrm{tg}\,\Delta\cdot10^{-3}$	helium, ρ
10^5	Lunar surface material	3,36	1,6	$3,2\cdot10^6$	3,39	1,65	$3,32\cdot10^6$
	Andesite-basaltic sand	3,35	1,24	$4,9\cdot10^6$	3,37	1,1	$4,7\cdot10^6$
	Finely crushed basalt	3,94	0,94	$4,15\cdot10^6$	3,97	1,1	$4\cdot10^6$
$4\cdot10^5$	Lunar surface material	3,32	1,36	$8,3\cdot10^5$	3,35	1,3	$8\cdot10^5$
	Andesite-basaltic sand	3,35	1,18	$1,2\cdot10^6$	3,35	1,05	$0,9\cdot10^6$
	Finely crushed basalt	3,9	0,92	$1\cdot10^6$	3,92	1	$1,1\cdot10^6$
10^4	Lunar surface material	3,3	1,24	$4\cdot10^5$	3,33	1,2	$4,2\cdot10^5$
	Andesite-basaltic sand	3,4	1,03	$4,8\cdot10^5$	3,42	1,1	$4,7\cdot10^5$
	Finely crushed basalt	3,81	0,9	$4,2\cdot10^5$	3,87	0,98	$4,4\cdot10^5$
$4\cdot10^4$	Lunar surface material	3,2	1,12	$1\cdot10^5$	3,28	1,1	$1,1\cdot10^5$
	Andesite-basaltic sand	3,25	1,10	$1,15\cdot10^5$	3,26	1,2	$1,15\cdot10^5$
	Finely crushed basalt	3,7	0,88	$0,98\cdot10^5$	3,73	1,1	$1\cdot10^5$
$10\cdot10^6$	Lunar surface material	3,17	1,02	$4,4\cdot10^4$	3,22	1,1	$4,5\cdot10^4$
	Andesite-basaltic sand	3,16	0,9	$4,4\cdot10^4$	3,2	1	$4,3\cdot10^4$
	Finely crushed basalt	3,5	0,86	$4\cdot10^4$	3,5	0,95	$4,1\cdot10^4$
$12\cdot10^6$	Lunar surface material	3,15	0,98	$3,6\cdot10^4$	3,2	0,89	$3,8\cdot10^4$
	Andesite-basaltic sand	3,13	0,88	$3,7\cdot10^4$	3,17	0,9	$3,8\cdot10^4$
	Finely crushed basalt	3,45	0,86	$3,3\cdot10^4$	3,47	0,89	$3,5\cdot10^4$

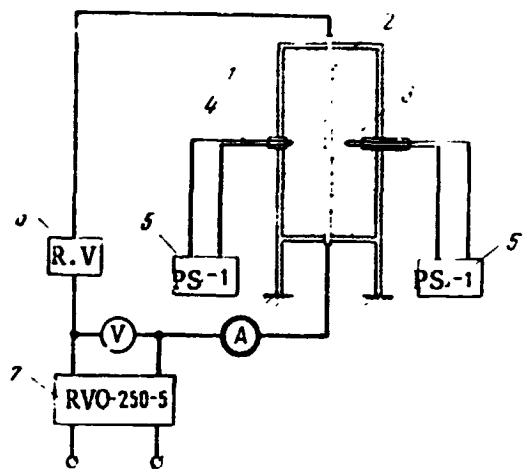

Fig. 1. Block diagram for the determination of thermal properties

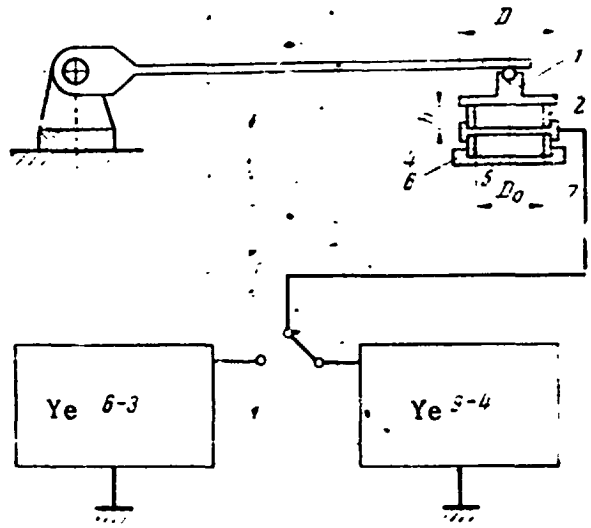

Fig. 2. Scheme for measuring electrical parameters

The relative dielectric permittivity ϵ, the dielectric loss tangent $\tan\Delta$, and the specific electrical resistance ρ of the lunar surface material and its analogs were studied in the frequency range 100 kHz-12 MHz using a Ye-9-4 Q-meter. The correctness of the method of determining ϵ, $\tan\Delta$, and ρ with a small sample was checked with the analogs in an air atmosphere and in vacuum on the specially developed measuring capacitor (Fig. 2) and a standard instrument (cylindrical capacitor). The difference in the values of the parameters determined was not more than $\pm$ 7 percent. The measuring scheme (see Fig. 2) included a measuring capacitor placed in a vacuum chamber, the Ye-9-4 Q-meter located outside the chamber, and leads connecting the Q-meter with the measuring capacitor. The body of the vacuum chamber connected to the body of the Q-meter served as the return lead.

To measure the electrical properties of the small samples of friable materials, use was made of a flat disk type three-electrode capacitor with partial filling of it with the test rock. The measuring capacitor (see Fig. 2) consisted of the upper grounded plate 1, protective ring 2, metal plate 4, lower circular insulator 5, and lower grounded plate 6.

Plate 1 was secured to a rotating lever with a hand drive externally, permitting raising, lowering, and adjustment of its force of clamping against the protective ring 2. The working chamber of the capacitor was formed by the plates 1 and 4 and by the protective ring 2. The lower chamber 7 was formed by the

plates 4 and 6 and by the ring 5. The voltage from the Q-meter was brought to the central plate 4 by means of copper leads securely attached to teflon insulators.

The height of the working chamber h and the diameter of the plates D_0 was selected on the basis of the volume and maximum diameter of the grains of the test material, and also from the conditions of reducing and stabilizing the "parasitic" capacitances of the measuring capacitor.

The design dimensions of the capacitor (see Fig. 2) were: D = 28 mm; D_0 = 20.1 mm; and h = 2.72 mm. Here the capacitance of the working chamber c_0 = 1.03 pf. The capacitor plates were made of stainless steel. The protective and insulating rings were made of alumdum.

The calculation of ϵ, ρ, and tg Δ was conducted with allowance for the "parasitic" parameters of the connecting leads and the measuring capacitor.

The final working formulas were as follows: /562

$$\varepsilon = \frac{C_3 - C + C}{C_0}, \qquad (1)$$

$$\rho = \frac{\pi D_0^2 R_k R}{4h(R_k - R)}, \qquad (2)$$

where R_h is the calculated resistance of the alumdum ring; R is the total resistance of the capacitor filled with the test material; C and C_3 are the total capacitance of the empty and rock-filled capacitor.

$$\operatorname{tg}\Delta = \frac{R_k - R}{2\pi f (C_3 - C + C_0) R_k R}, \qquad (3)$$

where f is the line frequency.

The results of studying ϵ, ρ, and tg Δ as a function of frequency are given in Table 2.

The specific heat capacities of the lunar surface material and the analogs, as to be expected, proved to be very close. The values of the coefficients of thermal conductivity of the lunar surface material and the analogs different significantly both in vacuum and in helium. The ratio of the coefficient of thermal conductivity of the lunar surface material in helium and in vacuum was 55. The coefficient of thermal conductivity of the lunar surface material in vacuum was approximately 1000 times lower than the coefficient of the thermal conductivity of the compact rocks of analogous composition.

The values of the electrical properties (ϵ, ρ, and tg Δ) of the lunar surface material and its analogs in the frequency range

studied were close to each other. The variation in ϵ, ρ, and $\mathrm{tg}\,\Delta$ of the lunar surface material as a function of frequency was analogous to the variation of these parameters for terrestrial rocks of similar composition.

A comparison of the resulting data with the results of studies conducted from the Earth's surface [1-3] showed that the values of the coefficient of thermal conductivity of lunar surface material in vacuum lie within the range of values determined in the studies [1-3]. The values of ϵ, $\mathrm{tg}\,\Delta$, and ρ differed from the values obtained by indirect methods owing to the differences in the frequency used in the determination [1, 2].

Data on the thermal properties of lunar surface material in vacuum [6] obtained for samples of surface material returned to Earth by the Apollo 11 crew agree with our data, if we allow for certain differences in the composition and heaped weight. When the specific weight of the lunar surface material and its analogs is increased, the coefficient of the thermal conductivity in vacuum rises, but decreases in the helium atmosphere. Differences in the values of ϵ that we obtained also for the samples returned by the Apollo 11 crew [7] are also accounted for by the differences in the heaped weight and the frequencies at which the measurements were made.

REFERENCES

1. Krotikov, V. D., and Troitskiy, V. S., Uspekhi fizicheskikh nauk 81(4), 588 (1963).

2. Troitskiy, V. S., Izvestiya vysshikh uchebnikh zavedeniy, Radiofizika 10(10), 1266 (1967).

3. Pettit, E., and Nicolson, S. B., Astrophys. J. 72, (1930).

4. Evans, I. V., J. Res. Nat. Bur. Standards 69 D(12), (1965).

5. Euchen, R. A., Phys. 10, 586 (1909).

6. Robbil, R. A., Hemingway, B. S., and Wilson, W. H., Science 167, 749 (1970).

7. Gold, I., Campbell, M. I., and O'Leary, B. I., Science 167(3918), 707 (1970).

All-Union Scientific Research Institute of Physical-Optical Measurements

Moscow Order of Labor Red Banner Mining Institute

N75 11872

RESULTS OF INVESTIGATING THE PHYSICOMECHANICAL PROPERTIES OF A SAMPLE OF LUNAR SURFACE MATERIAL IN A RESEARCH CHAMBER IN NITROGEN

/563

A. K. Leonovich, V. V. Gromov, A. D. Dmitriyev, V. A. Lozhkin, P. S. Pavlov, A. V. Rybakov, and V. V. Shvarev

Abstract

Presented are the results of an investigation of the mechanical properties of the lunar surface material sample returned by the Luna 16 automatic station. The study included determination of the specific weight of the surface material, the nature of its disintegration, and the determination of its compressibility characteristics, shear resistance, and bearing capacity. The article presents quantitative data on mechanical properties of the lunar surface material, many of which are determined for the first time. The instruments and experimental techniques are described.

Name and program of investigation. The aim of the investigation of the mechanical properties of the lunar surface material was to obtain information needed to evaluate its construction engineering qualities, the possibilities of moving transportation facilities, and building of models of the lunar surface material, as well as to solve other problems associated with the study and conquest of the Moon.

The program of the investigation of the mechanical properties included determining the specific weight of the surface material in the loose and compacted states, studying the nature of the disintegration of the surface material, and determining the characteristics of compressibility, shear resistance, and bearing capacity.

Instruments and experimental techniques. The investigation of the mechanical properties of the lunar surface material was based on direct measurements of the characteristics of the surface material by the techniques adopted in soil mechanics. To do this, use was made of specially built instruments capable of use in investigating small samples of surface material, as well as precluding the possibility of contaminating the surface material with foreign admixtures.

Fig. 1 shows the following: the SPLG-1 shearing instrument for determining compressibility and the shear resistance of the surface material, a micropenetrometer for determining bearing capacity, and a Coulomb instrument with which the disintegration of the surface material was studied. The layout of the shearing instrument and the micropenetrometer are shown in Fig. 2.

The shearing instrument is in the class of planar single-cutoff instruments with a fixed shear surface. The dimensions of the lunar surface material sample for testing in this instrument was as follows: diameter 25.2 mm and height 12 mm. The micropenetrometer was capable of determining the resistance to indentation in the surface material of stamps of different shapes. The Coulomb instrument (Fig. 3) had a movable partition; when it was moved it was possible to visually observe through transparent walls of the instrument the deformation of the surface material. The surface material was investigated in the research chamber of the receiving laboratory of the Geochemistry Institute of the USSR Academy of Sciences in a nitrogen atmosphere.

Sample of lunar surface material for investigation of mechanical properties. For the investigation of the mechanical properties, a sample was taken from the upper part of the sample of lunar surface material returned to Earth by the Luna 16 station. This corresponded to the uppermost layer of the surface material in its natural bedding at a depth of 100 mm. The sample consisted mainly of small mineral particles of the most diverse shapes. The color of the sample material overall was dark-gray. The particles easily clumped together, forming clods; sharp impressions persisted on the surface of the material. In spite of the appreciable adhesiveness, the surface material was readily passed through a sieve. The predominant fraction in the surface material consisted of particles 0.08-0.1 mm in size.

Results of the investigation. Determination of specific weight. The specific weight was determined by weighing surface material heaped into a weighing bottle with a volume of 3 cm^3, and also by conducting experiments on the shearing instrument and the micropenetrometer. Twenty measurements were made for the most friable state of the surface material. The mean value of the specific weight was 1.115 g/cm^3, with a root mean square deviation of 0.02 g/cm^3.

The most compact state of the surface material was obtained /564 by its layerwise compaction in the weighing bottle by the vibro-impact method and by hand tamping. The specific weight of the surface material in the state was 1.793 g/cm^3. The coefficient of porosity, gives them the specific weight of the surface material 3.0 g/cm^3, was 1.7 for the friable state, and 0.67 for the compact state.

Investigation of the disintegration of the surface material in the Coulomb instrument. The experiments in the Coulomb instrument were carried out for two states of the surface material: maximum friable state and the state compacted to the specific weight of 1.6 g/cm^3. The following results were obtained from the experiments with the friable surface material. When the partition was shifted from the surface material, a vertical wall formed at the contact area. With light rapping on the instrument, the surface material fell into a heap and formed a stepped surface. It was quite difficult to determine the angle of natural repose of the surface material from this surface.

When the partition was shifted toward the surface material, it was compacted. When pressed along horizontal by 10.5 mm, the height of the sample increased 2.5 mm.

For surface material compacted to a specific weight of 1.6 g/cm^3 the following were observed: a vertical wall persisted after the partition was moved away from the surface material; and

with lateral pressure against the sample, a well-defined straight line of slippage was formed, and then a prism of the surface material splitted off from the bulk of the sample. The slope of the line of slippage was 22° to the horizontal axis. This corresponds to an angle of internal friction of 46° for the surface material [1].

Investigation of compressibility. The compressibility of the surface material was determined during its preliminary compaction prior to shearing testing. The experiments were conducted in conditions in which it was impossible for the surface material to laterally expand, with the uniform distribution of stresses along the thickness of the sample of surface material.

The sample of surface material was placed in an instrument in the most friable state. A compressive force was applied by stages of 0.1 kg/cm^2 with exposure at each stage until the deformations had completely attenuated.

In several experiments the loading was unremoved and the reverse branch of the compressibility curve was determined.

Fig. 4 shows the averaged dependence, based on 16 experiments, of the relative vertical shrinkage of the surface material sample

TABLE 1. COEFFICIENT OF COMPRESSIBILITY

Range of compressive pressures, kg/cm^2	0—0.1	0.1—0.2	0.2—0.3	0.3—0.4	0.4—0.5
Coefficient of compressibility, kg/cm^2	3.9	3.0	1.0	0.3	0.2

on the compression pressure. In the range of compression pressure 0-0.32 kg/cm^2, a virtually linear relationship was observed between deformation and pressure. With further compaction, there was an abrupt drop in the compressibility of the surface material, and the deformation values approached some maximum-compacted state of the surface material.

The changes in the deformation of the sample with time after the application of the successive stages of loading that were recorded showed that the process of stabilization of surface material shrinkage occurs quite rapidly, in several seconds. When the sample was unloaded, the deformations in the surface material that were restored proved to be very small (see Fig. 4).

Fig. 5 shows the compressibility curve plotted in the coordinates of porosity coefficient versus compression pressure, as is customarily in soil mechanics. The specific weight of the surface material here was taken as 3.0 g/cm^3.

The coefficient of compressibility of the surface material defined as the ratio of the increment of the porosity coefficient to the pressure increment varies strongly with increasing compaction of the surface material. The averaged values of these coefficients for different intervals of the compressive pressures are given in Table 1.

An analytical expression for the compressibility curve was selected for the calculation of the deformations in the surface material over the entire range of the compression pressures.

The method of equalizing the experimental data was used to obtain the finding that an exponential function of the following form corresponds most fully to the trend of the compressibility curve:

$$\varepsilon = \varepsilon_\infty + (\varepsilon_0 - \varepsilon_\infty) \cdot \exp(-kp), \qquad (1)$$

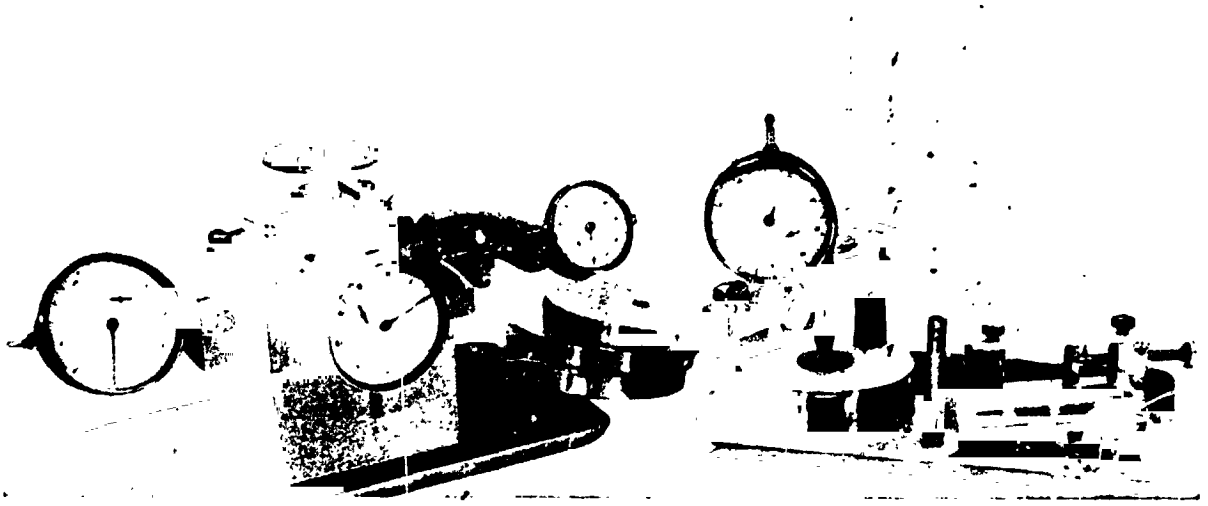

Fig. 1. Instruments for investigating the mechanical properties of lunar surface material

where ϵ is the porosity coefficient of the surface material; ϵ_∞ is the porosity coefficient of the surface material when it was compacted with a maximum blow; ϵ_0 is the porosity coefficient in the most friable state of the surface material; k is a constant; and p is the compression pressure.

As applied to the plot in Fig. 4, the following values were obtained for the coefficients of Eq. (1): $\epsilon_0 = 1.7$; $\epsilon_\infty = 0.85$; and $k = 8.5$ cm^2/kg. A comparison of the experimental compressibility curve and the curve calculated by Eq. (1) with the above-presented values of the coefficients showed a good agreement. The compressibility coefficient for any point on the compressibility curve will be as follows: /565

$$a = \frac{d\epsilon}{dp} = -(\epsilon_0 - \epsilon_\infty) k e^{-kp} = -k(\epsilon - \epsilon_\infty). \qquad (2)$$

In the maximum friable state $\epsilon = \epsilon_0$, and the compressibility coefficient is: $a_0 = -k(\epsilon_0 - \epsilon_\infty)$.

Substituting this value into Eq. (2) and carrying out the transformation, we get:

$$a = \frac{d\rho}{dp} = a_0(1 - D), \qquad (3)$$

where $D = \frac{\rho_1 - \rho}{\rho_1 - \rho_\infty}$ is a coefficient of the relative density of the soil.

If we introduce the notation $R = \frac{\varepsilon - \varepsilon_0}{\varepsilon_{max} - \varepsilon_0}$, Eq. (3) becomes as follows:

$$a = a_0 R. \tag{4}$$

The coefficient R has an opposite significance with respect to the coefficient of relative density and can be called the coefficient of relative friability.

When R = 1, the surface material is in the maximum friable state, and when R = 0 the surface is in the most compact state. Then the coefficient of compaction of the test sample of lunar surface material in the range of compression pressures up to 0.5 kg/cm^2 will be equal to the coefficient of compaction for the surface material in the maximum friable state multiplied by the coefficient of relative friability.

Investigation of shear resistance of surface material. Resistance to shear was determined by the method of overcompacted surface material. For this, the preliminary compaction of the surface material was carried with a maximum loading, which was applied to plot the resistance to shearing.

The intermediate points in the plot were determined at lower loadings. This method of testing permitted obtaining plots of the resistance to shearing at a virtually constant specific weight (porosity coefficient) and permitted tracing the variation in the shear parameters of the surface material as a function of its compaction.

The precision of the determination of the shear resistance and the normal pressure in shearing is 0.003 kg/cm^2. The deformation of the surface material sample was measured to 0.01 mm. After completion of the experiment, the sample of surface material well preserved the shape of the working chamber of the shearing instrument. The shearing surface was distinctly visible.

Fig. 6 gives the results of the experimental determination of the resistance to shearing of surface material compacted with a pressure of 0.5 kg/cm^2 to a specific weight of 1.61 g/cm^3.

The experimental points fitted quite well on a straight line, which can be described by the Coulomb equation for the resistance of surface materials to shearing:

$$\tau = c + p \operatorname{tg} \varphi, \tag{5}$$

where τ is the shear stress (kg/cm^2),
c is adhesion (kg/cm^2),
p is the normal pressure in the shear plane (kg/cm^2), and
ϕ is the angle of internal friction of the surface material.

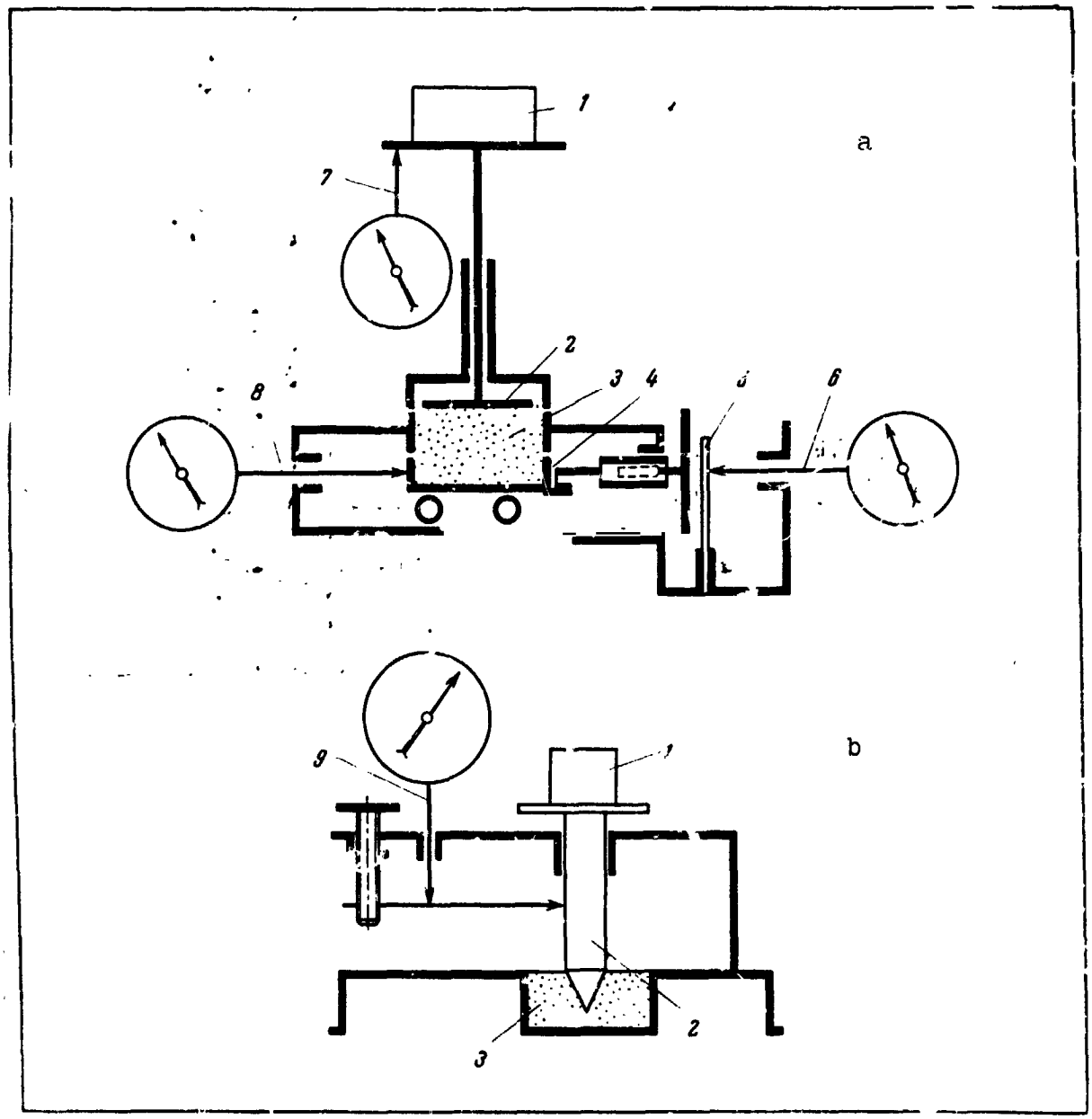

Fig. 2. Scheme of shearing ir trument (a) and micropene rometer (b)/566
1. weight producing vertical load
2. stamp transmitting vertical load
3. sample of lunar surface material
4. sliding carriage
5. elastic beam
6. indicator of diflection of elastic beam
7. indicator of vertical deformation
8. indicator of horizontal deformation
9. indicator of stamp displacement

In addition, the experiments in the Coulomb instrument with surface material of the same density yielded an angle of internal friction of 46°.

For the linear section of the plot, the parameters in the Coulomb equation has the following values: $c = 0.052$ kg/cm^2 and $\phi = 25°$. The cohesion in the absence of normal pressure is 0.04 kg/cm^2. With decrease in the compaction of the surface material, its resistance to shearing becomes less. /567

For compaction with the loading of 0.2 kg/cm^2 (specific weight 1.51 g/cm^3), the angle of internal friction is 22°, and with compaction produced by a loading of 0.1 kg/cm^2 (specific weight 1.29 g/cm^3), the angle of internal friction is lowered to 10-12° (Fig. 7).

A graphical representation of the effect of surface material compaction (specific weight) on its resistance to shearing is given in the plot in Fig. 8.

Laid out along the vertical axis in this plot are the values of the shear coefficients at a normal pressure of 0.1 kg/cm^2, and along the horizontal axis -- the specific weight of the surface material. The shear coefficient is the ratio of the shear stress to the normal pressure.

As we can see from Fig. 8, with increasing compaction of the surface material, its resistance rises sharply. An especially intense rise occurs when the surface material is compacted to a specific weight of 1.5-1.6 g/cm^3.

A very interesting trend is shown in the curve of resistance of shearing obtained when the surface material is compacted only by exposure to normal shear pressure (Fig. 9). In this case a well-defined nonlinear trend results between the shearing and normal loading in the zone of normal pressures 0-0.2 kg/cm^2. At pressures greater than 0.2 kg/cm^2, the curve levels off and approaches the shear resistance curve obtained by the method of overcompacted surface material. For this section, the coefficients in Eq. (5) will have the following values: $c = 0$ and $\phi = 30°$.

Eq. (5) is inapplicable for the initial section, since a fairly substantial slope of the curve (up to 45°) a negative value of cohesion ($c < 0$) results, which lacks any physical meaning.

This trend in the shear curve obtained for different densities of the surface material can be accounted for by the fact that with increasing compaction of the surface material a considerable change occurs in the cohesion and angle of internal friction, especially in the range of compression pressures 0-0.4 kg/cm^2.

TABLE 2. SPECIFIC WEIGHT AND MODULUS OF DEFORMATION OF LUNAR SURFACE MATERIAL

Spec. wt. of surface material, g/cm^3	1.12	1.29	1.45	1.62
Mod. of deformation, kg/cm^2	0.156	0.29	0.85	2.4

The shearing limiting stress reaches the maximum for some value of the shear deformation rising with increase in normal loading. With further increase in deformation, the shear stress becomes smaller.

A change occurs in the volume of the sample of surface material in the shearing process. If the normal pressure during shearing is absent, loosening of the surface material occurs, and its specific weight is less. At a normal pressure of 0.1 kg/cm^2, the specific weight of the surface material remains practically unchanged. At pressures higher than 0.1 kg/cm^2, during the shearing time this surface material becomes compacted, and its specific weight rises.

The variation in the surface material volume proceeds especially intensely during the time of buildup of the shearing stress.

Determination of bearing capacity of surface material. The bearing capacity of surface material was estimated from the curve of indentation into the surface material of a flat and cone-shaped stamp. The experiments were conducted at different surface material compaction values.

Fig. 10 gives the curves for indentation of a flat stamp, 8 mm in diameter, into soil with different density.

When inserted into soil in the most friable state (specific weight 1.12 g/cm^3) the stamp leaves a well-defined impression, along which shallow circular cracks are formed. No bulging of the surface material around the stamp was observed. When the stamp was lowered to a depth of more than 5-6 mm, the indentation curve begins to be markedly affected by the bottom of the instrument in which the test sample of surface material is situated.

With increase in surface material density, the resistance to stamp penetration markedly rises. Also changing is the nature of the deformation of the surface material; zones of bulging appear around the press, and radial and concentric cracks are formed.

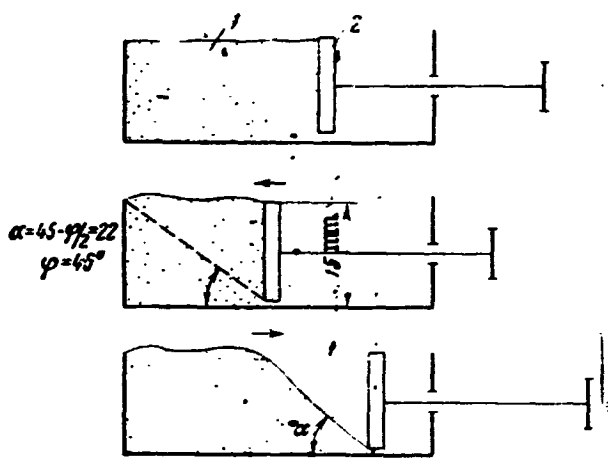

Fig. 3. Layout of Coulomb instrument
1. sample of surface material
2. movable partition

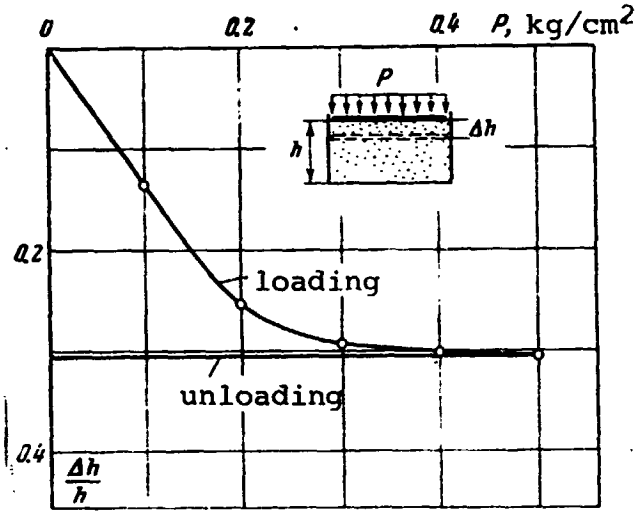

Fig. 4. Relative shrinkage (Δh/h) of sample of service material when acted on by compression pressure (p)

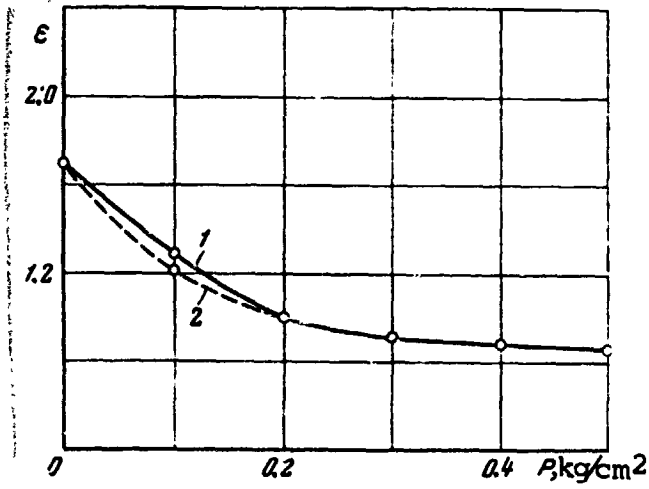

Fig. 5. Curve of compressibility of surface material in the coordinates of porosity coefficient (ε) versus compression pressure (p)
1. experimental
2. calculated from Eq. (1)

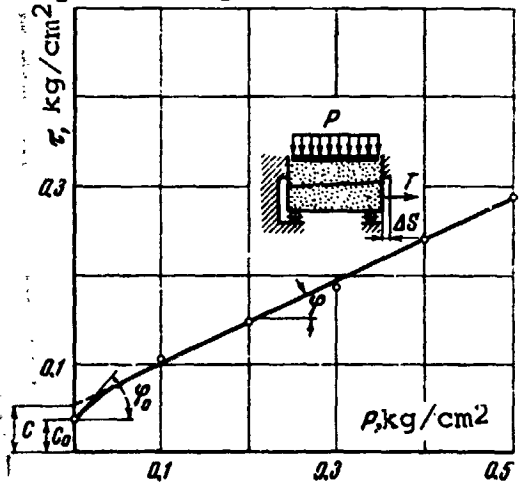

Fig. 6. Plot of shear resistance of surface material compacted with the pressure of 0.5 kg/cm^2 (specific weight 1.61 g/cm^3)

Table 2 gives the values of the modulus of deformation determined for the initial branch of the curve of flat stamp introduction.

The modulus of deformation was calculated based on the formula:

$$E = pD/H,$$

where p is the specific pressure of the stamp on the soil (kg/cm^2), D is the press diameter (cm), and H is the depth to which the press was immersed (cm).

A cone-shaped press with a tip angle of 30° penetrated into the soil with a specific weight up to 1.5 g/cm^3 to the full depth of the surface material layer (12 mm) under its own weight (32 g). Penetration of the cone-shaped press into the surface material compacted to a specific weight of 1.75 g/cm^3 occurred with a relatively constant pressure on the press, transmitted to its cross section at the surface material level, and was 0.65-0.8 kg/cm^2. /568

To estimate the effect of the confined volume of the surface material on the penetration of the stamp, special experiments were conducted with artificially formulated surface material that were close to the lunar surface material in granulometric composition. It was found that owing to the effect of the limited volume of the surface material, the resistance to the indentation of the flat press rose by about two times. For a cone-shaped press this effect was poorly detectable.

Analysis of results. The results of these experiments provided the first idea of the mechanical properties of the test sample of lunar surface material and a comparison with earlier data.

Lunar surface material from the Sea of Fertility is a fine-grained material, whose specific weight can have values from 1.1 to 1.8 g/cm^3. The specific weight of surface material returned by the Apollo 11 spacecraft was 1.36 g/cm^3 in the friable state and 1.8 g/cm^3 in the compact state. Here, in both cases the surface material for the investigation was taken from the uppermost layer at a depth of 100-120 mm. If in the compact stage the specific weight values are quite close, in the friable state a substantial difference was observed. On this basis, it can be assumed that surface material from the Luna 16 landing site will have greater compressibility than the surface material returned by Apollo 11. /569

The lunar surface material is highly compressible. The coefficient of compaction has a variable value and depends on the relative density of the surface material. Upon compaction, the compressibility of the surface material becomes less. In the range of compression pressures investigated (up to 0.5 kg/cm^2), the compressibility curve can be described by very simple relations. The shear characteristics of the lunar surface material depends strongly on its compaction.

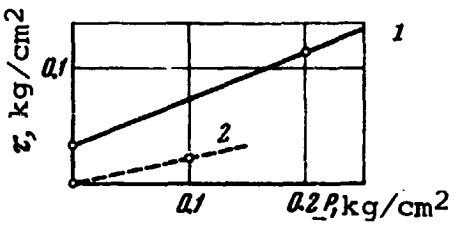

Fig. 7. Plots of shear resistance of surface material
1. surface material compacted with a pressure of 0.2 kg/cm^2 (specific weight 1.51 g/cm^3)
2. surface material compacted with a pressure of 0.1 kg/cm^2 (specific weight 1.29 g/cm^3)

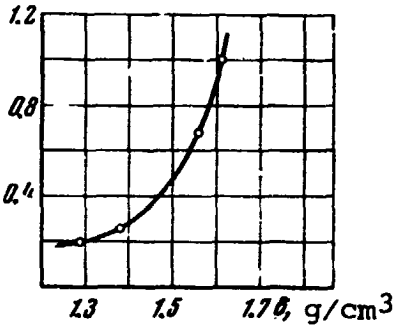

Fig. 8. Dependence of shear coefficient (ϕ) on compaction of surface material (specific weight δ)

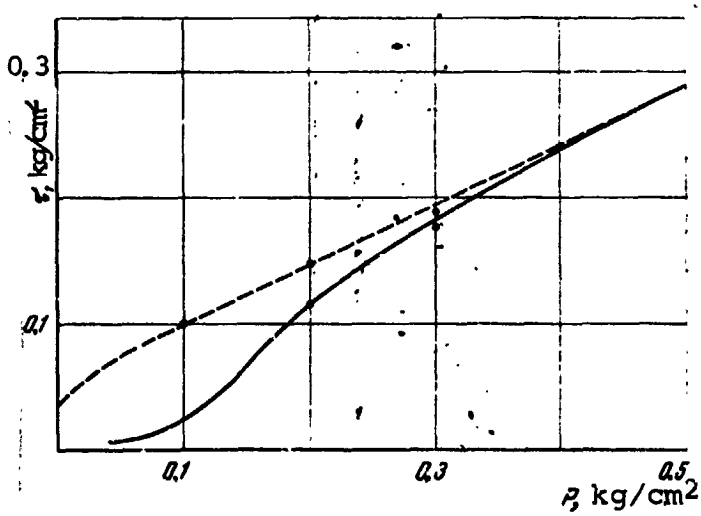

Fig. 9. Plot of shear resistance for surface material compacted by normal shear pressure. Dashed line indicates plot corresponding to the plot in Fig. 5.

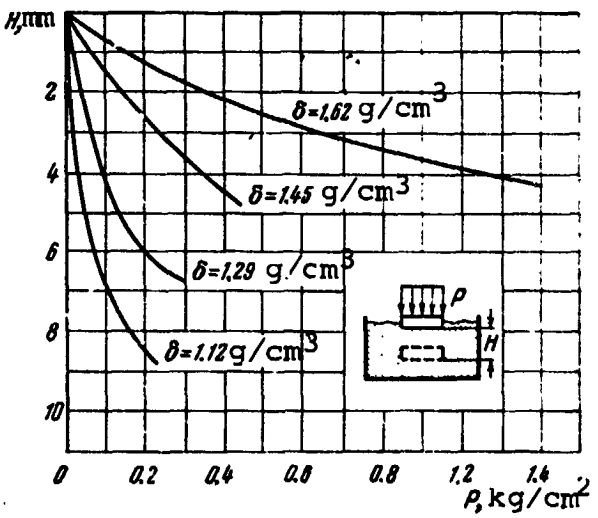

Fig. 10. Curves of penetration of flat stamp into surface material with different specific weight

The surface material in the friable state has slight cohesion and a small angle of internal friction. With increasing compaction of this surface material (specific weight up to 1.5 g/cm^3), resistance to shearing rises both owing to an increase in the forces of

greatness as well as through an increase in the angle of internal friction. With further compaction (specific weight of 1.5 g/cm^3), the angle of internal friction approaches 25°, and a further rise in resistance to shearing occurs mainly through an increase in the forces of cohesion. The dependence of the mechanical properties of the lunar surface material on its compaction can be utilized to increase its mechanical strength the artificial preliminary compaction. Adequate compaction can be attained by application of a static load of 0.4-0.5 kg/cm^2; here its shear resistance is /570 appreciably increased, especially for small normal pressures (0.1-0.2 kg/cm^2), the modulus of deformation reaches 2-2.5 kg/cm^2, and the compressibility of the surface material decreases markedly.

The values obtained by direction measurements for the angle of internal friction and for cohesion differ markedly from the values that were known earlier. For example, in report materials in the Surveyor program [2], the angle of internal friction was assumed to be 35-37°, and the cohesion 0.003-0.007 kg/cm^2. In an article dealing with an investigation of samples of surface material returned by Apollo 11 [3], surface material cohesion was determined to be 0.003-0.014 kg/cm^2.

The nearest data to these results were obtained by the Luna 13 automatic station [4], with the angle of internal friction found to 32°, and cohesion 0.005 kg/cm^2. This difference can be caused by the difference in the properties of the surface material in the regions investigated, and also possibly by the different techniques of their determination. It should be noted that determination of the compressibility and resistance to shearing of the lunar surface material returned by Luna 16 for the first time was carried out by direction measurements adopted in soil mechanics. Until now, these parameters had been determined by indirect methods from the nature of the deformation of surface material when external bodies acted on it. Obviously, to obtain comparable data on mechanical properties of lunar surface material taken from different regions of the lunar surface, they must be investigated by a single technique and using identical instruments. Comparison of the mechanical properties of lunar surface material from the landing site of the Luna 16 station with terrestrial surface materials and artificially formulated materials shows that dusty volcanic sand is a close analog of lunar surface material. A mixture composed of fractions of ground basalt and close to lunar surface material in granulometric composition can be used as a possible model of the lunar surface material.

REFERENCES

1. Tsytovich, N. A., Mekhanika gruntov [Soil Mechanics], "Vysshaya shkola," 1968.

2. "Surveyor Project Final Report, Part 2, Scientific Results," California Institute of Technology, Pasadena, California, Technical Report No. 32-1262, 1968.

3. "Preliminary Examination of Lunar Samples From Apollo 11," Science 165(3899), (1969).

4. Pervyye panoramy lunnoy poverkhnosti [First Panoramas of the Lunar Surface], "Nauka", 1968.

N75 11873

INVESTIGATION OF MECHANICAL PROPERTIES OF LUNAR SURFACE MATERIAL AND ITS ANALOGS IN DIFFERENT ATMOSPHERIC CONDITIONS AND IN VACUUM ON THE TOR-1 UNIT

/571

A. I. Vedenin, Ye. A. Dukhovskoy, V. V. Markachev, A. A. Silin, I. I. Cherkasov, and V. V. Shvarev

Abstract

A description is given of the design of measuring assemblies in the TOR-1 instrument along with methods for determining the specific resistance to penetration, compressibility, and the resistance to rotational shearing of lunar surface material and its analogs. Investigations were conducted in helium at normal pressure, as well as in vacuum $5 \cdot 10^{-6}$ torr in the temperature range + (20-140)° C. Values of the specific resistance to penetration of the lunar surface material, coefficients of relative compressibility, and the parameters of the resistance to rotational shearing were obtained for three kinds of compaction of the lunar surface material.

Characteristics of materials investigated. Lunar surface material from the Sea of Fertility returned by the Luna 16 automatic lunar station, and two terrestrial analogs of lunar surface materials were investigated. The first of these is andesite-basaltic volcanic sand from the settlement of Klyuch (Central Kamchatka), and the second is crushed basalt from the Berestovetskiy deposit in the Ukrainian SSR. The data on the chemical, mineralogic, and granulometric composition of all three materials are in Tables 1 and 2.

Under the classification of surface materials SNIP-PB-162 adopted in the USSR, both analogs are categorized as silty sands.

The mineralogic composition of the materials investigated was as follows: the lunar surface material, based on the data of A. P. Vinogradov /1/ contains as the principal minerals plagio-

clases, ilmenite, pyroxene, and olivine, as well as feldspathic rocks (anorthosite). Among the fine grains are encountered monomineralic grains, in which plagioclase, olivine, pyroxene, and ilmenite were identified, as well as spherules and minute dumbbell-shaped objects of volcanic glass. The andesite-basaltic volcanic sand contains disseminations and microlites of plagioclase, pyroxene, hornblende, and ore mineral. The crushed basalt consists of plagioclase, pyroxene, and ore minerals -- magnetite and ilmenite.

The specific weight of the mineral grains of the lunar surface material was assumed to be γ_y = 3.2 g/cm^3; the mean specific weight averaged over the depth of immersion of the Luna 16 drill γ = 1.2 g/cm^3. The specific weight of the mineral grains of the andesite-basaltic volcanic sand γ_y = 2.79 g/cm^3; the specific weight of the grains of crushed basalt γ_y = 2.98 g/cm^3. The specific weight of all three materials varies over wide limits as a function of compaction.

The specific weight in helium was determined by using a graduated beaker 11.3 mm in diameter, into which 1.9 g of the test surface material was poured. The volume it occupied was determined in the friable, heaped state, after compaction by rapping the beaker 50 times against a hard surface, and after additional compaction of the surface material with a plexiglas rod 8 mm in diameter, manually. The experimental results are in Table 3.

Mechanical characteristics of materials subjected to determination. The overall integrated characteristic of strength was taken as the specific resistance to penetration R (kg/cm^2); the angle of internal friction ϕ and the cohesion c (kg/cm^2) were taken as the parameters of resistance to shearing; the coefficient of relative compressibility a_o (cm^2/kg) was taken as the parameter characterizing deformability upon compression. The schemes of the experiments are shown in Fig. 1.

The specific resistance to penetration was determined by the depth of introduction into the surface material of a metal cone with a tip angle α = 30° when a given load P (kg) was applied to it. It was calculated by the formula:

$$R = k\frac{P}{\pi h^2 \operatorname{tg}^2 \frac{\alpha}{2}} \text{ kg/cm}^2 \qquad (1)$$

when $\alpha = 30^{\circ}$:

$$R = 4{,}44\, k_d^{\text{п}} \frac{P}{h^2} \text{ kg/cm}^2. \quad (2)$$

From the penetration results, strength can be computed at the same time, after P. A. Rebinder: /572

$$\tau_R = \frac{P}{h} \cdot \frac{\cos\frac{\alpha}{2}}{\pi \operatorname{tg}\frac{\alpha}{2}} k_d^{\text{п}} \text{ kg/cm}^2; \quad (3)$$

when $\alpha = 30^{\circ}$:

$$\tau_R = 1{,}08 \frac{P}{h^2} k_d^{\text{п}} \text{ kg/cm}^2. \quad (4)$$

A constant relationship exists between the specific resistance to penetration and strength, after P. A. Rebinder, and when $\alpha = 30^{\circ}$, this relationship is:

$$\tau_R \simeq 0{,}25R \text{ kg/cm}^2. \quad (5)$$

The angle of internal friction ϕ and the cohesion c (kg/cm^2) are determined from the Coulomb equation:

$$\tau_{\text{limit}} = \sigma \operatorname{tg}\varphi + c \text{ kg/cm}^2. \quad (6)$$

To calculate ϕ and c, we must conduct no less than two independent determinations of the limiting resistance to shearing τ_{limit} (kg/cm^2) for different values of the normal pressure σ (kg/cm^2).

In our experiments, the limiting resistance to shearing was determined on the rotational shearing instrument with a continuous rotational ribbed disk. During the course of the experiment, the limiting torque causing shearing along the horizontal plane beneath the ribbed disk was determined, and from the value of this moment the limiting resistance to shearing was calculated by the formula:

$$\tau_{\text{limit}} = 2 \frac{M_{\text{limit}}}{\pi r^3} \text{ kg/cm}^2. \quad (7)$$

The angle of internal friction and cohesion were determined by analytical plotting using a rectified plot of the limiting resistance to shearing as a function of the normal pressure on the sample:

$$\varphi = \operatorname{arctg}\left(\frac{\tau - c}{\sigma}\right). \quad (8)$$

TABLE 1. CHEMICAL COMPOSITION*

Material	Chemical constituents and their content, weight percent										
	SiO_2	TiO_2	Al_2O_3	Fe_2O_3	MgO	CaO	Na_2O	K_2O	MnO	Cr_2O_3	ZrO_2
Lunar surface material	41,70	3,39	15,32	16,80[2*]	8,70	12,20	0,37	0,10	0,21	0,31	0,015
Andesite-basaltic volcanic sand	60,35	1,01	15,91	5,56	3,67	5,40	—	—	0,10	—	—
Crushed basalt	49,50	—	17,00	14,50	6,50	9,40	—	—	0,70	—	—

*Composition of lunar surface material is presented based on data of A. P. Vinogradov [1]; the compositions of the other materials are based on the data of the MIIT.++

2* The entire iron content is expressed in terms of FeO.

TABLE 2. GRANULOMETRIC COMPOSITION*

Material	Fraction size, mm							
Andesite-basaltic volcanic sand	7–5 (1,72)	5–3 (3,68)	3–2 (2,56)	2–1 (3,51)	1–0,5 (5,99)	0,5–0,25(10,87)	0,25–0,10 (14,61)	0,10 (57,56)
Crushed basalt	10–5 (0,1)	—	5–2 (0,1)	2–1 (0,5)	1–0,5 (0,6)	0,5–0,25 (2,6)	0,25–0,10 (14,3)	0,10 (81,2)

*Data on the granulometric composition of the lunar surface material are presented in this collection in the paper [2].

Remark. The content (in percentage) is given in parentheses.

The coefficient of relative compressibility a_o (cm^2/kg) during the experiment were continually varied, so that the surface material under the effect of the normal pressure became compacted and its compressibility was reduced. Therefore the coefficient of relative compressibility was calculated separately for the different intervals of normal pressure by the formula:

++ MIIT [Moscow Institute of Railroad Transportation Engineers]

$$a_0 = k_d^{\text{п}} \frac{\Delta s_i}{H_i \Delta p_i} \text{ cm}^2/\text{kg}. \quad (9)$$

The following notation is adopted in the formulas presented above:

- α is the angle at the tip of the penetrometer cone;
- h is the depth of cone penetration into the surface material (cm);
- p is the load on the penetrometer cone (kg);
- M_{limit} is the limiting torque in rotational shearing (kg·cm);
- τ_{limit} is the limiting resistance to shearing (kg/cm^2);
- r is the radius of the ribbed disk (cm);
- σ_i is the normal pressure on the sample (kg/cm^2);
- Δp_i is the increment in the normal pressure over the experimental interval (kg/cm^2);
- H_i is the height of the sample at the beginning of the experimental interval (cm);
- ΔS_i is the reduction in the height of the sample over the experimental interval (cm); and
- $k_d^{\text{п}}$; $k_d^{\text{к}}$ are the coefficients allowing for the effect of the lateral walls on the cylinder on the penetration and compression values.

Use of the scheme of rotational shearing was adopted owing to the small amount of the lunar surface material allocated for the experiments in the TOR-1, with which it was not possible to use ordinary instruments of monoplane shearing or three-axis compression; Eq. (7) was adopted from the data of A. N. Zelenin et al. [3] and presupposes that the plot of the distribution of tangential stresses over the radius of the ribbed disk on attainment of the limiting resistance to shearing is triangular in shape.

Experimental conditions. The experiments were conducted in a TOR-1 vacuum chamber, described in [4]. The vacuum chamber makes it possible to conduct tests in an air atmosphere at normal pressure, in an atmosphere of sterilized, high-purity helium, and in a vacuum up to 10^{-5} torr. The sample temperature can be set at + 20° C (without heating) and up to + 140° C (with heating).

When the experiments were conducted in normal atmospheric conditions, the chamber was not hermeticized and was not evacuated. When the experiments were conducted in a helium atmosphere, preliminary evacuation of the chamber was conducted to a vacuum of $5 \cdot 10^{-5}$ torr, and then it was filled with helium. When the experi-

TABLE 3. SPECIFIC WEIGHT OF LUNAR SURFACE MATERIAL AND ITS ANALOGS

Condition of test material	Specific weight in different states, g/cm^3		
	lunar surface material	andesite-basaltic volcanic sand	crushed basalt
Friable, heaped	1.26	1.05	1.00
Compacted by rapping 50 times	1.90	1.41	1.58
Additionally compacted with a rod	1.90	1.46	1.73

ments were conducted in the vacuum, the chamber was evacuated to $(2-5)\cdot10^{-5}$ torr. In the experiments with heating, the sample was heated before the beginning of the evacuation to evaporate the moisture.

The lunar surface material was placed in a hermetic chamber where it was situated in the atmosphere of pure helium. The analogs of the lunar surface material was sent for testing in exposed form. Because of this, hygroscopic moisture in the amount of 1.5-3.0 percent by weight was present in the analogs. Upon evacuation of the TOR-1, this moisture was evaporated, and subsequent tests in the helium atmosphere and in vacuum were conducted with the dry material. Experience in working with the TOR-1 showed that in the presence of surface materials the evacuation must be conducted slowly, since a rapid pressure drop in the chamber leads to swelling of the surface materials under the effect of the expansion of air in the pores and vaporization through the evaporation of the hygroscopic moisture.

To test the samples, the TOR-1 was equipped with special measuring assemblies mounted on a common panel (see Figs. 2-5). The initial designs of the assemblies, developed in 1970 and described in /4/, were improved based on operating experience so that their operating reliability and precision of measurements were increased. Below are given the descriptions of the improved assemblies.

The sample of the surface material was placed in the central part of the plate within a cylindrical bowl 11.3 mm in diameter. The bowl was equipped with an electric heater. When the experiments were conducted for penetration and compression, the small bowl was immobile. When the experiments were conducted on rotational shearing, it was rotated about a vertical axis.

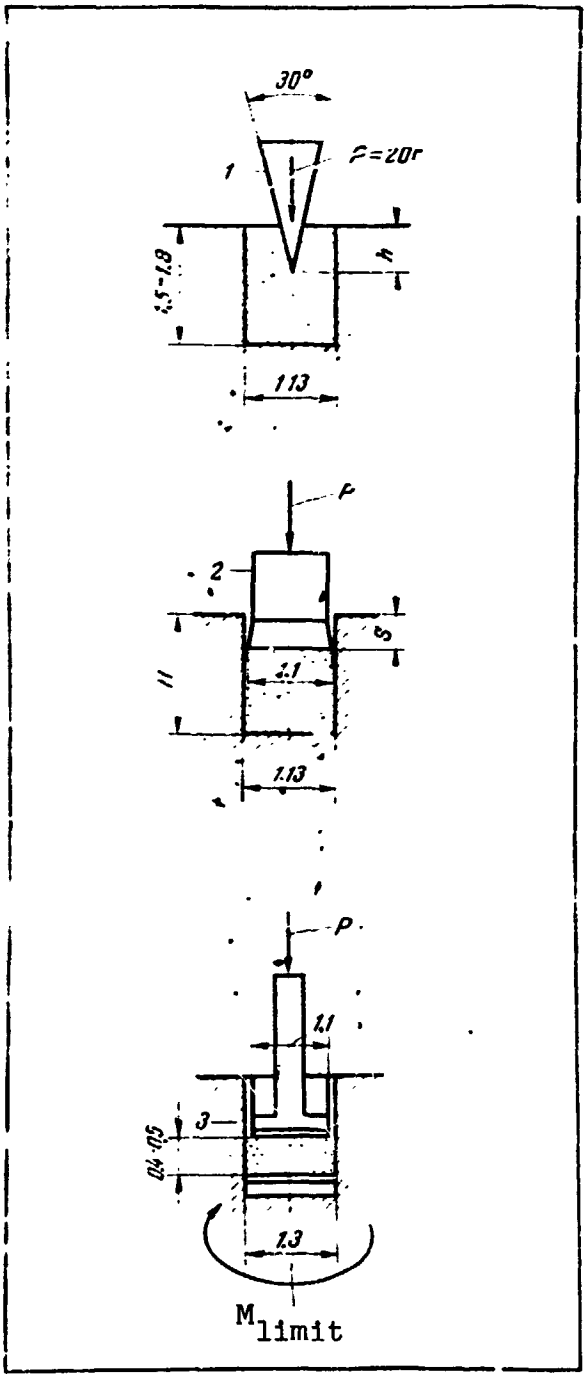

Fig. 1. Schemes for conducting experiments to determine the mechanical parameters of surface material. Above -- penetration; in the middle -- compression; below -- rotational shearing. 1. Cone; 2. Piston; 3. Ribbed disk

The individual measuring assemblies with working parts and devices for applying load and for measuring load and deformation were mounted on cantilevered beams that could be rotated in the vertical plane, bringing the working parts up against the surface of the surface material under study. The motion of the cantilevers beneath was limited by rigid stops, which ensured the exact placement of the working parts.

The vertical load was applied by means of a clamping beam, which also could be rotated in the vertical plane and, on being brought into contact with the head of the loading rod of a given assembly, lowered it.

Penetration assembly. /574 The working part consisted (Fig. 2) of a polished cone 1 with a tip angle $\alpha = 30^{\circ}$. The cone weighed 20 g. The introduction of the cone into the surface of the sample 2 placed in the small bowl 3 was carried out under its own weight. The cone was secured to a membrane 4, which freely lay on a circular support within the head of the assembly 5. A type MFKP strain gage was cemented to the membrane; the strain gage measured the force transmitted from the cone to the membrane. In the initial position the weight of the cone was transmitted to the membrane. During the course of the experiment, the clamping beam mounted on a separate rotating lever was shifted beneath the cone together with the measuring assembly up to the surface of the sample. The zero reading was recorded. With further slow movement, the cone

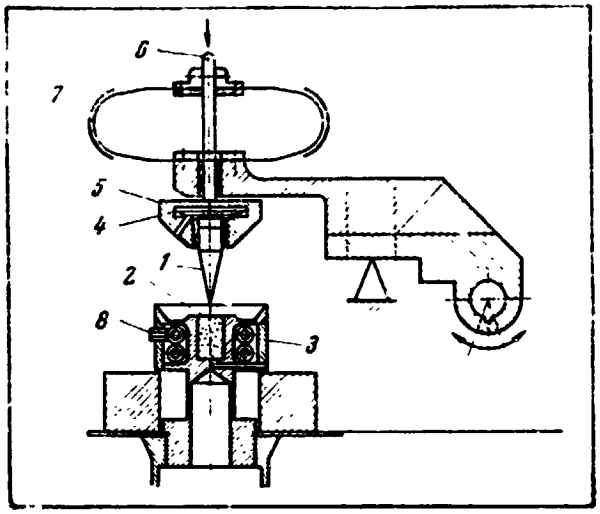

Fig. 2. Assembly for penetration experiments.

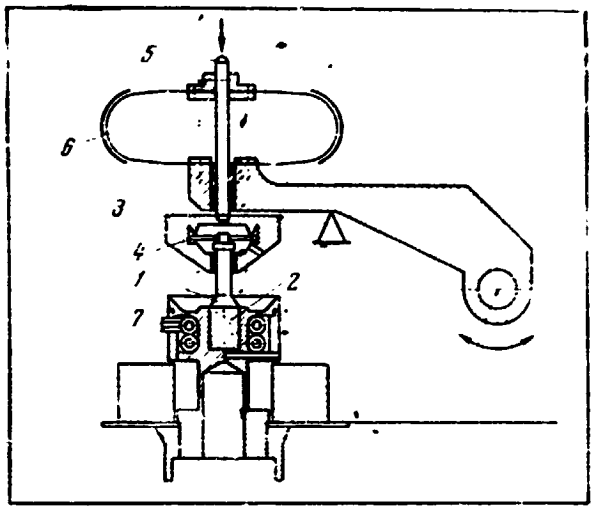

Fig. 3. Assembly for compression tests.

entered into contact with surface material. Gradually the entire weight was transmitted to the surface material, and the measuring membrane was completely ruptured, indicated by the readings of the transducer. The depth to which the cone was immersed was determined by the vertical displacement of rod 6 by means of elliptical spring 7 with type FKP strain gages cemented to it. The maximum depth of immersion was 1.8 cm. The sample in the small bowl could be heated with heater 8.

Compression assembly. The working part (Fig. 3) was a polished piston 1 with a flat base, 11 mm in diameter, applied to the surface of the sample 2. The piston was secured to the membrane 3 with a type MFKP strain gage cemented to it. The membrane was secured on a circular support within the head 4. The vertical displacement of the head was brought about by the action of the clamping beam on the top of the rod 5. Here the membrane was pressed against the piston and compelled it to move into the surface of the sample. The force of indentation was measured with the strain gage membrane, and the piston displacement was measured with elliptical spring 6 bearing type FKP strain gages. The sample could be heated with heater 7. The vertical pressure on the surface material could be varied from 0 to 1.5 kg/cm^2, and the depth of the piston insertion could be varied from 0 to 0.8 cm.

Rotational shearing assembly. The assembly (Fig. 4) was mounted on cantilever 1. Before testing, it was inclined to the working bowl of instrument 2 so that the working part -- ribbed disk 3 -- was brought into contact with the surface of sample 4. The vertical load on the working part was brought about with the

TABLE 4. COEFFICIENT OF RELATIVE COMPRESSIBILITY a_o (in cm^2/kg) IN HELIUM AT NORMAL PRESSURE AND TEMPERATURE +20° C*

Material	Range of normal pressure Δp_i, kg/cm^2			
	0-0.2	0.2-0.4	0.4-0.6	0.6-0.8
Lunar surface material	1.63	0.42	0.24	0.11
Andesite-basaltic volcanic sand	0.82	0.10	0.06	0.04
Crushed basalt	2.10	0.26	0.12	0.08

* The initial condition of the surface material was heaped, friable with the following values of the porosity coefficient: lunar surface material $\epsilon_o = 1.56$; andesite-basaltic sand $\epsilon_o = 1.59$; crushed basalt $\epsilon_o = 2.00$.

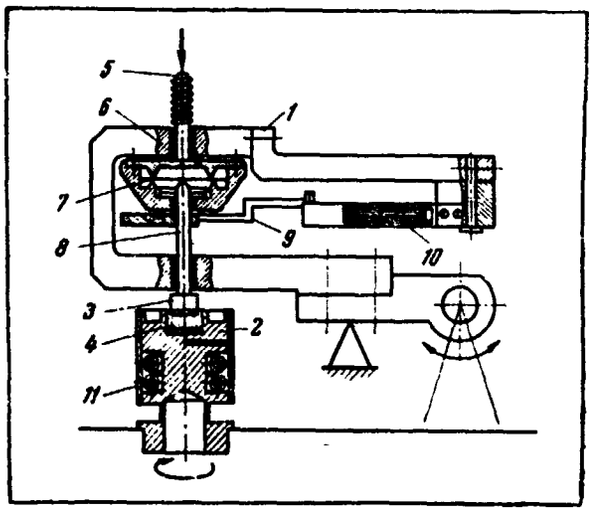

Fig. 4. Assembly for rotational shearing experiments.

clamped beam acting against the loading rod 5. The rod was shifted in the dried bushing 6 and transmitted its pressure via membrane 7 and the second rod 8 onto the ribbed disk.

After application of a specified vertical load, which was measured with the strain gage on membrane 7, the bowl containing the surface material samples was brought into rotational motion about the vertical axis and engaged with the ribbed disk and its rod. Secured to the rod was lever 9 with a support, touching the measuring strain gage beam 10. The FKP strain gages cemented to the beam measured the force of lever pressure. During the experiment, this force rose and, on reaching a maximum, remained constant or decreased. From the vertical force the limiting torque causing shearing of the sample beneath the ribbed disk was calculated. /575

The vertical load on the sample could be varied from 0 to 0.6 kg/cm^2, and the limiting torque -- from 0 to 0.150 kg·cm. The instrument bowl was equipped with heater 11.

The signals from the strain gage transducers for measuring the forces and deformations were fed to amplifier 8 ANCh-7M, and further, to PS-1 recorders. As results of each experiment, two plots of force and deformation as functions of time were obtained; they were interpreted with the aid of previously compiled calibration tables. The precision of the measurement averaged about 10 percent of the limiting values of the quantities.

In all the kinds of tests, the load was applied by successively increasing steps, where each step was maintained until there were no more deformations recorded on the recorder graph. On the average, the duration of the experiment for penetration was 0.5 min, for compression 10 min, and for rotational shearing 3 min. Considering the entire absence of the liquids in the pores of surface material and the impossibility of slowing down the deformations through processes of filtrational consolidation, this duration can be regarded as adequate in order to assume at each stage of the experiment that the deformations had been completed.

Since the lunar surface material was placed in the container in a helium atmosphere and was not brought into contact with the normal atmosphere, all its tests were conducted in helium. In order to find out the effect of vacuum and normal terrestrial atmosphere on mechanical properties, surface material-analogs were tested in all three regimes: in normal atmosphere, helium atmosphere, and in a vacuum of 10^{-5} torr at the temperatures + 20 and + (135-140)° C. The following were conducted: three penetration, two compression, and three experiments on rotational shearing. The above-presented data were obtained from the experiments in which no gross errors were detected.

Test results. Tables of the specific resistance to penetration for all the surface materials investigated were compiled from the penetration tests; then from these tables, a graph was plotted, shown in Fig. 6, indicating the dependence of R on the coefficient of surface material porosity ϵ.

From the compression tests, curves were plotted describing the dependence of the depth of piston immersion on the vertical pressure, shown in Fig. 7 and 8. From the interpretation of these curves, the values of the coefficients of relative compressibility for different pressure intervals, shown in Tables 4 and 5, were obtained. /576

From the tests for rotational shearing, plots were made of the dependence of the limiting resistance to shearing on the normal pressure, examples of which are shown in Fig. 9. Based on these graphs, values were obtained for the angles of internal friction and cohesion, shown in Tables 6 and 7.

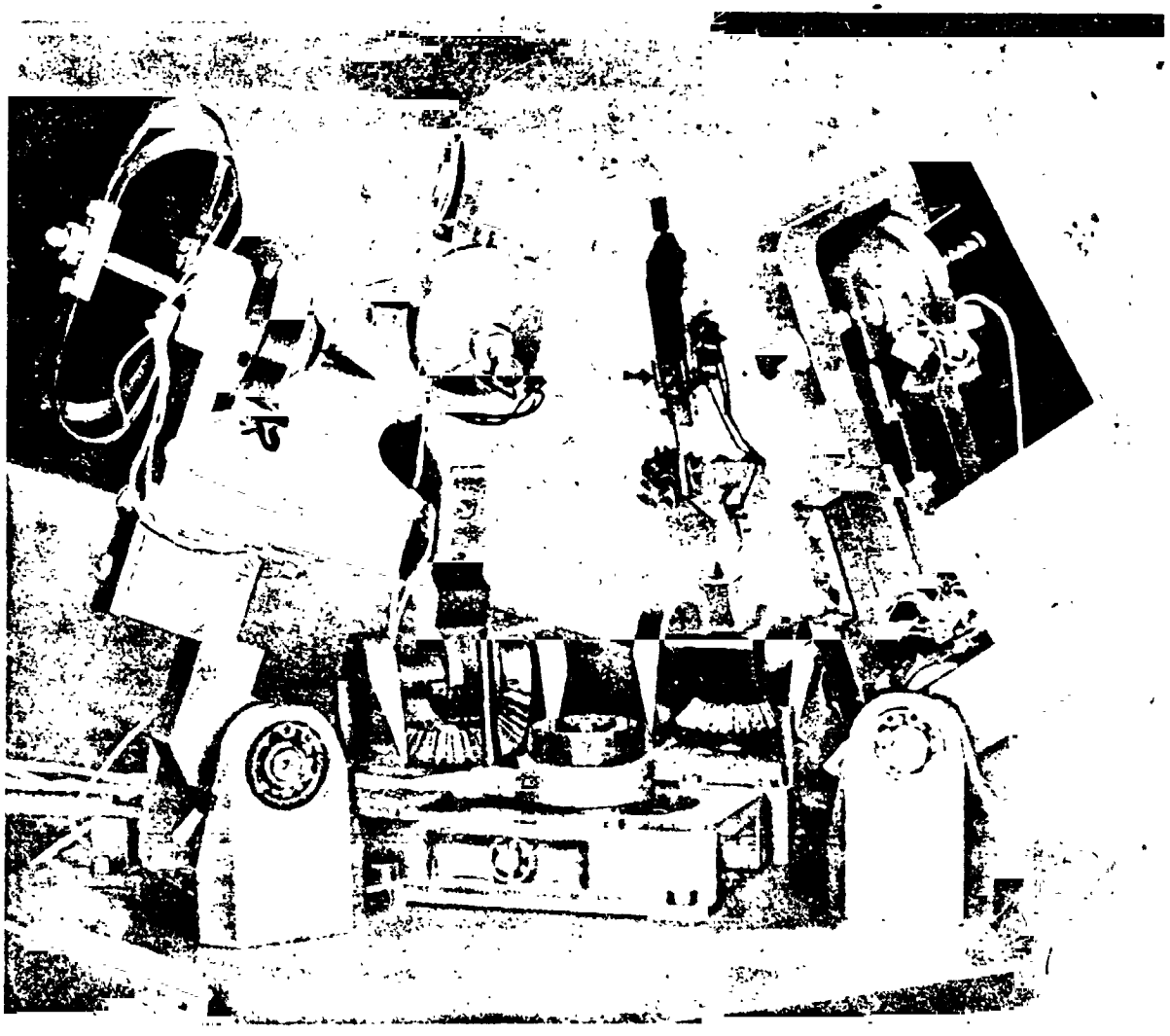

Fig. 5. Internal view of TOR-1 vacuum chamber housing test assemblies.

Penetration tests. The composite plot of the experimental results in helium at the temperatures + 20 and + 140° C and in the vacuum of 10^{-5} torr at + 140° C is in Fig. 6. From the graph it follows that the primary factor determining the specific resistance to penetration for all the materials investigated is their porosity coefficient. For the case of friable heaped surface materials, the specific resistance to penetration decreases to R = 0.012 kg/cm^2, while for surface materials compacted by rapping and area reduction with a stamp, it rose to 0.357-0.383 kg/cm^2. Compared with the effect of porosity, the effect of the

TABLE 5. COEFFICIENT OF RELATIVE COMPRESSIBILITY a_o (in cm^2/kg) IN DIFFERENT ATMOSPHERES AND IN VACUUM FOR SURFACE MATERIAL-ANALOGS*

Material and range of compression stresses, kg/cm^2	Test conditions		
	Helium + 20° C	Helium + 135° C	Vacuum, 10^{-5} torr, + 135° C
Crushed basalt			
0-0.1	2.22	2.55	2.84
0.1-0.2	0.286	0.22	0.47
0.2-1.0	0.064	0.071	0.08
Andesite-basaltic volcanic sand			
0.01	1.17	0.90	0.66
0.1-0.2	0.14	0.21	0.17
0.2-1.0	0.045	0.06	0.06

* The initial condition of the surface materials was friable, heaped with the following values of the porosity coefficient: basalt $\epsilon_o = 2.00$; andesite-basaltic sand $\epsilon_o = 1.39$.

TABLE 6. PARAMETERS OF THE RESISTANCE TO SHEARING IN HELIUM AT NORMAL PRESSURE AND TEMPERATURE + 20° C*

Material	Angle of internal friction, ϕ	Cohesion, c
Lunar surface material	29°30' (35°30')	0.030 (0.010)
Andesite-basaltic volcanic sand	26°00'	0.016
Crushed basalt	29°00'	0

* Before testing, the surface materials were compacted by rapping and by the repeated application of a vertical pressure $\sigma = 0.55$ kg/cm^2. Given in the table are the data for the averaged plots of the function $\tau_{limit} = F(\sigma)$. Given in the parentheses are the values of C and ϕ for the initial section of the plot of the lunar surface material.

medium and the temperature, within the limits tested, proved to be secondary. It can be noted that in the case of soils in the friable heaped state, the resistance to penetration in helium at + 140° C proved to be somewhat higher than at + 20° C, while in vacuum it

was nearly the same as in helium. For the case of compacted soils, the transition from + 20 to + 140° C in most cases led to some reduction in the resistance to penetration, and the same effect was brought about by the transition to vacuum. Overall, all the experimental results involving penetration must be regarded as preliminary, since they were too strongly affected by the conditions of heaping of the soils in the bowl of the instrument and their further processing.

Compression tests. First of all, compression curves were obtained for the lunar surface material and its analogs in a helium atmosphere at normal pressure and temperature + 20° C, shown in Fig. 7. From these curves, the values of a_o given in Table 4 were calculated.

Since no tests of the lunar surface material in vacuum could be made for a number of reasons, special experiments with the analogs in a helium atmosphere at + 20 and + 135° C were carried out, and in the vacuum of 10^{-5} torr at + 135° C to clarify the extent to which the properties of the surface material change in the transition from the helium atmosphere to vacuum. The results of these experiments are given in Fig. 8 and in Table 5.

Analysis of Table 4 shows that the lunar surface material in the friable heaped state has extremely high compressibility, which, however, upon the initial area reduction with a pressure of the order of 0.2 kg/cm^2 is reduced by several times, although even by the end of the experiment, for a compressive stress 0.6-0.8 kg/cm^2, still remains large, considerably exceeding the compressibility of the sandy surface materials common on Earth in the medium-compact and compact states that are customary for the latter. The same is also true of the surface material-analogs -- crushed basalt and volcanic andesite-basaltic sand, whose compressibility characteristics are close to the characteristics of lunar surface material and indicate high compressibility of these /577
materials in the friable heaped state. The test results indicate that in the conditions given above, these materials as analogs of the lunar surface material were successfully chosen and can serve as its substitutes in compressibility experiments.

Based on analysis of Table 5, it can be noted that in the case of both materials, in all test conditions for the same intervals of loading, the coefficients of compressibility have the same order of magnitude. In first importance is the initial area reduction, and the coefficient of relative compressibility takes on maximum values, while it then is sharply reduced, and in the last stage reaches the value 0.045-0.080 cm^2/kg. However, even these latter figures still considerably exceed the values $a_o \simeq 0.01$ cm^2/kg that are customary for mean-density terrestrial silty sands.

The effect of heating and vacuum on the properties of the samples shows up in different ways. In the case of crushed basalt, compressibility rises somewhat overall loading intervals, which probably can be associated with some unconsolidation of the samples on heating and evacuation. In the case of andesite-basaltic volcanic sand, at the first stage of loading compressibility becomes less, while in successive stages it increases somewhat. However, in both cases no abrupt change in the properties is noted, and in general it can be assumed that tests in helium atmosphere at normal pressure and temperature + 20° C yield approximately the same results as tests in the vacuum of 10^{-5} torr at + 135° C. The reason for this must be sought for, on the one hand, in the insufficiently high vacuum, and on the other hand, in the fact that within the sample of the finely dispersed surface material beneath the instrument piston, in all probability the vacuum is poorer than in the TOR-1 chamber overall. /578

Supplementing the tests described above, control experiments were made in which the surface material-analogs were compressed in the TOR-1 unit in an air atmosphere at + 20° C and 75 percent humidity. They showed that in most cases the compressibility of both analogs in air is appreciably higher than in helium and in vacuum, which is accounted for by the effect of the hygroscopic moisture. It was noted that both analogs, when dried to constant weight, intensively absorbed moisture from air and the hygroscopic moisture content in the different experiments varied from 1.5 to 3.0 percent.

It should be noted that carrying out compression in the miniaturized instrument must lead to understating of the compressibility coefficients owing to the friction of the surface material against the wall of the working cylinder. Preliminary data from the determination of the scaling factor indicate that in our case we can expect understating of the compressibility, where the scaling factor probably shows up differently at different stages of the experiment. Tables 4 and 5 give the values of a_o without allowing for the effect of the scaling factor.

Experiments on rotational shearing. The first tests were conducted to determine the properties of the lunar surface material and its analogs in the helium atmosphere at normal temperature and temperature + 20° C (see Fig. 9).

Analysis of Table 6 shows that on the average, the lunar surface material and its analogs have closely similar values of the resistance to shearing and that they are all characterized in the given test conditions by low cohesion from 0 to 0.016 kg/cm^2. Somewhat unexpected were the values of the angles of internal

TABLE 7. PARAMETERS OF RESISTANCE TO SHEARING IN DIFFERENT TEST CONDITIONS

Material	Test conditions					
	Air, 20° C		Vacuum, 10^{-5} torr, 20° C		Vacuum, 10^{-5} torr, 140° C	
	ϕ	c	ϕ	c	ϕ	c
Andesite-basaltic volcanic sand	27°30'	0	25°30'	0.004	23°40'	0.004
Crushed basalt	30°30'	0	26°50'	0.036	27°00'	0.004

friction, which averaged 26-30°. The data on lunar surface materials and the investigation of their terrestrial analogs earlier given in the literature generally fall in the area of 35-37° and even higher. Accordingly, additional experiments with analogs involving rotational shearing in an air atmosphere at + 20° C and in a vacuum of 10^{-5} torr at + 20 and + 140° C were carried out.

Table 6 gives the data for the averaged plots of the function τ_{limit}). As we can see from Table 7, the transition from the tests in the air atmosphere to the tests in vacuum led to the appearance of low cohesion and a reduction in the angle of internal friction. It should, however, be borne in mind that the graphs were plotted based on three points each and that their averaging by the inclined lines led to a distortion of the initial sections. In practice, the resistance to shearing under all three test regimes differed little. From these experiments, as can be seen /579 from the figures presented, low values of the angle of internal friction also resulted. The following factors can serve as the reasons for this:

1) the experiments were conducted with finely dispersed silty surface materials, while the earlier experiments involved coarser sandy varieties, which always have higher angles of friction;

2) the surface materials tested were compacted with a low pressure of 0.55 kg/cm^2 and had sufficiently high porosity, while it is known that with increase in porosity the angle of internal friction of granular surface materials becomes less; and

3) the miniature dimensions of the sample can lead to the appearance of a scaling factor that affects the experimental results.

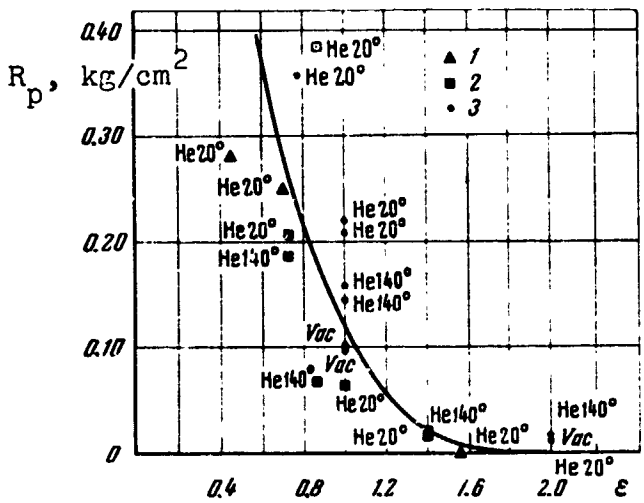

Fig. 6. Dependence of specific resistance to penetration R on the porosity coefficient of surface material ε and the experimental conditions
1. Lunar surface material
2. Andesite-basaltic volcanic sand
3. Crushed basalt. He 20° -- -- helium at normal pressure and temperature +20°; He 140° -- as above at +140°, Vac -- vacuum at +140° C.

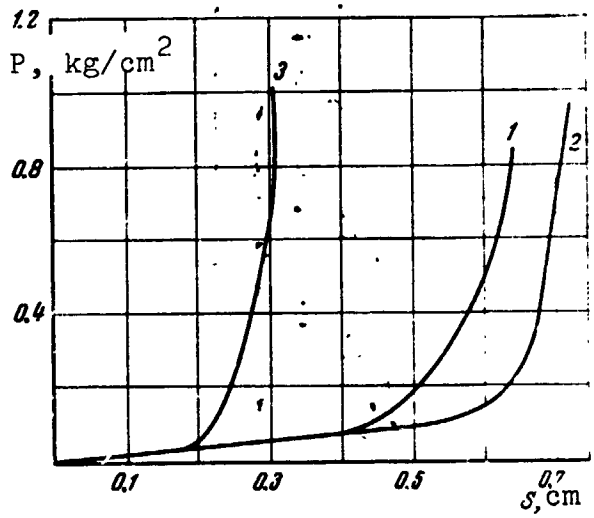

Fig. 7. Dependence of vertical compression of sample S on mean pressure beneath piston in compression testing P in helium atmosphere at normal pressure and temperature of 20° C.
1. Lunar surface material
2. Andesite-basaltic volcanic sand
3. Crushed basalt

Effect of scaling factor. With decrease in the dimensions of the test instruments and with increase in the ratio of the sample height to its diameter, the effect of the walls of the working cylinder in which the experiments are conducted on penetration, compression, and shearing becomes greater. The friction of the surface material against the walls leads to its more friable placement when freely heaped into the instrument; it causes additional resistance to compression in the compression test and can be reflected in the results of the rotational shearing experiment, since the movement of the peripheral grains of the sample material is restricted. In the penetration experiments, the walls interfere with the free expansion of the surface material laterally and increase the resistance of the surface material to the insertion of a cone.

Evidently, the use of instruments of these small dimensions for investigating the mechanical properties of surface material, such as were compelled in experiments involving the TOR-1, is

encountered for the first time in soil mechanics. Until now, the smallest diameter of a sample was assumed to be approximately 40 mm, which is 3.5 times greater than in the TOR-1. Accordingly, experimental investigations were conducted dealing with the scaling factor, which are still continuing. It was established for the penetration experiments that the ratio of the specific resistance to penetration when a 40 mm diameter bowl is used to the same value for an 11.3 mm diameter bowl is 0.33-0.45 for a cone with a 30° angle, weighing 20.5 g. Appropriate corrections were made into the results of the experiment and taken into account in plotting of the graph in Fig. 6.

As for the coefficient of relative compressibility, we can anticipate the opposite effect of sample scale, but the final values of the correction coefficients have not yet been established, and the data obtained without corrections are listed in Tables 4 and 5. The same is true of the rotational shearing experiments.

Conclusions. 1) The sample of Sea of Fertility lunar surface material that was investigated is characterized by a specific weight in the friable heaped state $\gamma_{friable} = 1.26$ g/cm^3 and in the compact state $\gamma_{compact} = 1.90$ g/cm^3, to which correspond the porosity coefficients, respectively, $\epsilon_{friable} = 1.46$ and $\epsilon_{compact} = 0.63$. Its terrestrial analogs -- andesite-basaltic volcanic sand and crushed basalt -- have lower values of specific weight in both the friable and the compacted states (see Table 3). /581

2. The specific resistance to penetration of lunar surface material is determined mainly by its density. In the friable heaped state, the surface material exerts virtually no resistance to the penetration of a cone, while in the compacted state R = 0.25-0.28 kg/cm^2. The surface material-analogs have similar values of specific resistance to penetration in identical test conditions.

3. The coefficient of relative compressibility of lunar surface material is very high at the first loading stage and in the interval of normal pressure 0-0.2 kg/cm^2 it is 1.63 cm^2/kg. Then the surface material becomes compacted and the coefficient of relative compressibility is reduced by severalfold. But even at a pressure of 1 kg/cm^2 it is 0.11 cm^2/kg, which is one order higher than the coefficient of compressibility for common sand in terrestrial conditions. The surface material-analogs have the same properties and closely simulate the lunar surface material with respect to compressibility at all loading stages.

4. The lunar surface material has an angle of internal friction of 35° at the first stage of the experiment, and 29° on the average for a cohesion of 0.01 and 0.03 kg/cm^2, respectively. The surface

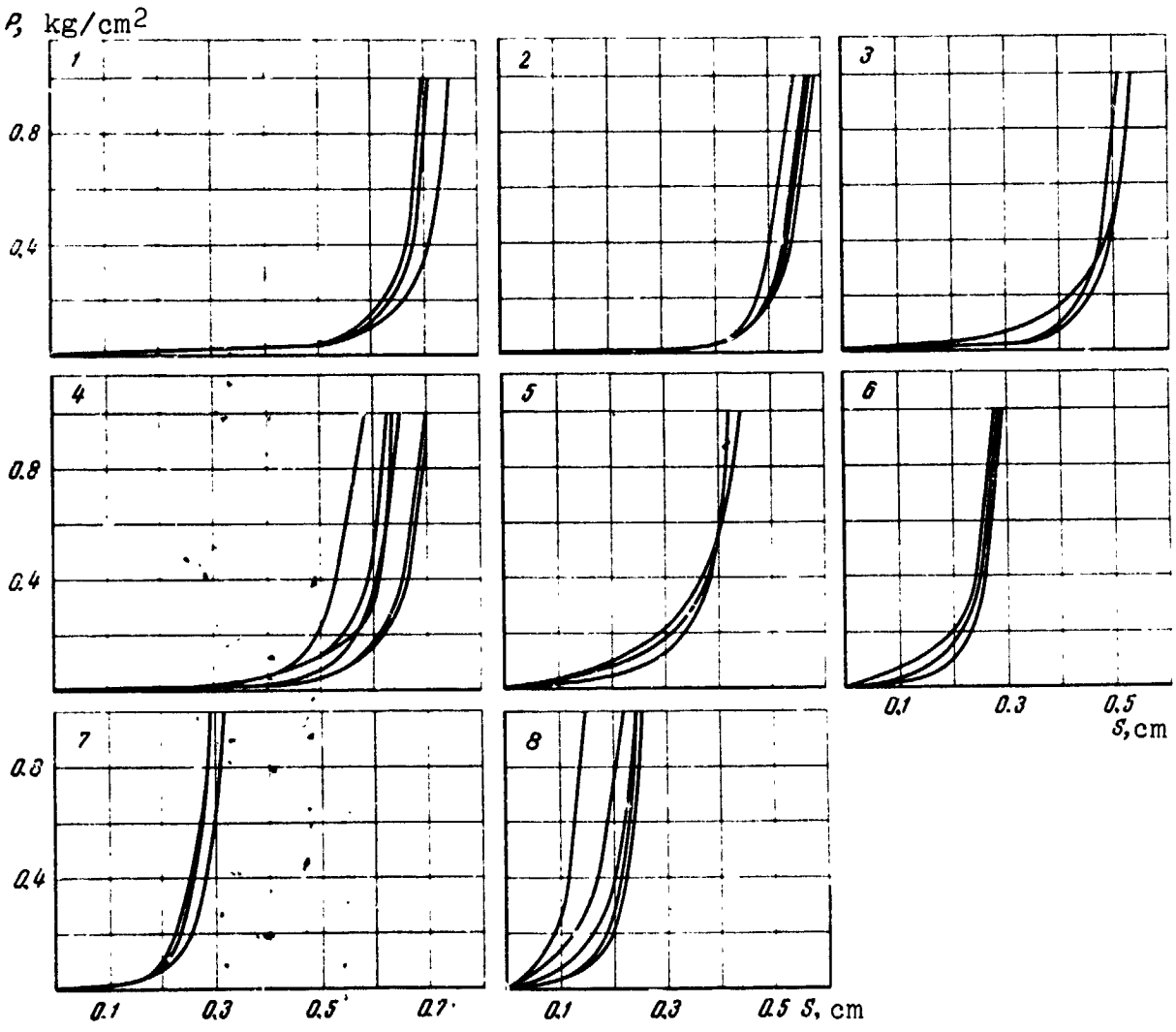

Fig. 8. Dependence of vertical compression of sample S on mean pressure beneath piston in compression testing P for different experimental conditions.

1. Crushed basalt in air at normal atmospheric pressure and temperature + 20° C;
2. As above in helium at atmospheric pressure and + 20° C;
3. As above in helium at atmospheric pressure and + 135° C;
4. As above in a vacuum of $2 \cdot 10^{-5}$ torr at + 135° C;
5. Andesite-basaltic volcanic sand in air at normal atmospheric pressure and temperature + 20° C;
6. As above in helium at atmospheric pressure and + 20° C;
7. As above in helium at atmospheric pressure and + 135° C;
8. As above in a vacuum of $2 \cdot 10^{-5}$ torr at + 135° C.

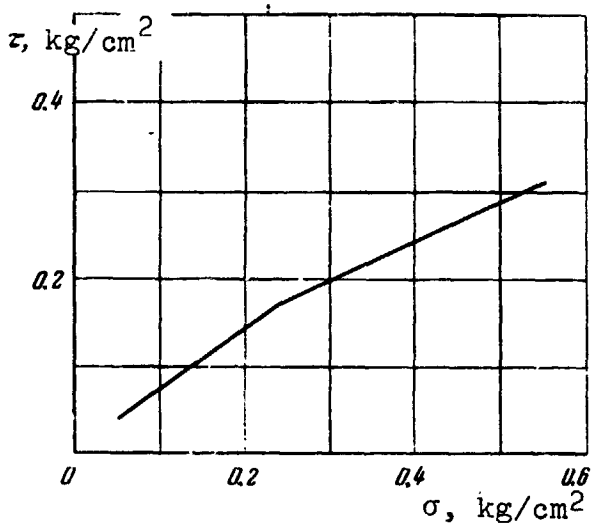

Fig. 9. Example of plot of the dependence of limiting resistance to shearing τ_{limit} on normal pressure σ for lunar surface material in helium atmosphere at + 20° C.

material-analogs have somewhat smaller values for both parameters. It should be noted that these data are somewhat smaller than those ordinarily published for lunar surface materials.

5. The miniature dimensions of the instrument dictated by the small volume of the surface material may have been reflected in the results of the determination of the mechanical parameters R, a_0, c, and ϕ. The effect of the scaling factor for penetration was found also in interpreting the experimental results; for compression and shearing, work on the determination of the correction factors for a_0, ϕ, and c is continuing.

6. Overall, the results of tests in helium at +20° C differ insubstantially from the test results for helium at +140° C and in a 10^{-5} torr vacuum at +140° C. In all probability, this is due to the impossibility of achieving a vacuum in the bulk of the surface material sample enclosed in a tight collar. It is necessary to continue experiments testing surface materials in vacuum by other techniques that would ensure total degassing of samples and the carrying out of these experiments in a higher vacuum.

7. At the present level of test apparatus, mass testing of lunar surface materials and their analogs is usefully conducted in a helium atmosphere at +20° C, ensuring identical conditions and elimination of random errors; also expedient are individual experiments aimed at finding the effect of high vacuum on the properties of lunar surface materials, carried out in accordance with paragraph 6.

REFERENCES

1. Vinogradov, A. P., "Preliminary Data on Lunar Surface Material Returned by Luna 16 Automatic Station," Geokhimiya (3), (1971).

2. Stakheyev, Yu. I., Vul'fson, Ye. K., Ivanov, A. V., and Florenskiy, K. P., "Granulometric Characteristics of Lunar Surface Material from the Sea of Fertility," present collection, p. 44.

3. Zelenin, A. N., Karasev, G. N., and Krasil'nikov, L. V., Laboratornyy praktikum po rezaniyu gruntov /Laboratory Handbook on Cutting Surface Materials/, "Vysshaya shkola" Press, 1969.

4. Drozhzhina, M. P., Dymov, V. V., Krylov, V. M., Markachev, V. V., Silin, A. A., and Shvarev, V. V., "TOR- Instrument for Investigating the Engineering-Physical Properties of Lunar Surface Material," Dokl. AN SSSR 199(5), (1971).

5. Druzhininskaya, V. A., Markachev, V. V., Serenov, A. V., Surkov, Yu. A., and Cherkasov, I. I., "Preliminary Results of Investigating the Mechanical Properties of Lunar Regolith," Dokl. AN SSSR 199(6), (1971).

All-Union Scientific Research Institute of Physical-Optical Measurements, Moscow

Moscow Institute of Transportation Engineers, Moscow

N75 11874

STUDY OF FRICTION PROPERTIES OF LUNAR SURFACE MATERIAL AND ITS ANALOGS

/582

Ye. A. Dukhovskoy, E. A. Motovilov,
A. A. Silin, M. I. Smorodinov, and V. V. Shvarev

Abstract

This study gives a description of instruments for determining the friction properties of the surficial layer of lunar surface material returned by the Luna 16 automatic lunar station, as well as the friction properties of its analogs: andesite-basaltic sand and basalts. The experimental method and results are presented.

The experiments were conducted in a helium atmosphere at normal barometric pressure, temperature + 20° C, as well as in conditions of vacuum $5 \cdot 10^{-6}$ mm Hg and at elevated temperatures (+ 150° C).

The values of the coefficients of friction for several nonmetallic and metallic materials were obtained when they were moved over the samples of lunar surface material and its analogs. The values of the friction characteristics for the lunar surface material are very close to the values for its analogs.

The ever increasing scope of studies of the Moon by spacecraft as well as the possibility of constructing long-term lunar stations on its surface confronts investigators and engineers with complex problems in developing new machines intended to operate in the specific conditions on the Moon.

Related to these new problems, the investigation of the physicomechanical properties of lunar surface materials and their terrestrial analogs is at the present time one of the fundamental engineering problems.

This work gives the results of a study of the friction properties of lunar surface material returned to Earth by the Luna 16 automatic lunar station, and for two of its terrestrial analogs -- andesite-basaltic sand sampled in the region of the Klyuchevskiy Volcano on Kamchatka, and basalt (in monolithic and crushed form from the Berestovetskiy pit in the Ukraine). Used as counterbodies were several samples of metallic and nonmetallic materials employed in space technology.

All the investigations were conducted with the TOR-1 universal instrument (Fig. 1 A, B, C), which is a complex of mechanisms with measuring devices intended for the investigation of engineering-physical properties of rocks in the monolithic and friable states, in inert gas and in vacuum in the temperature range + (20-150)° C. The TOR-1 instrument makes it possible to conduct studies based on existing standard methods, as well as by procedures specifically developed for small volumes of test rocks. The volume of the working chamber is 1 m^3.

This instrument consists of the following main components (see Fig. 1): located on the console plate (10), which is secured to the working flange (11), are eight mechanisms (1-7) with transducers and, in the center, a grip for securing the rock (8).

Each mechanism, by means of a vacuum bellows input (13), rod (12), and geared couple (7), is driven and permits interaction with the rock of the transducer that bears information about the property being investigated. To determine the friction and abrasive properties, as well as the regimes for the cutting of solid materials, the grip (9) can be driven in rotational motion by a motor with gear reducer (15) through a shaft that has a special vacuum seal (16) and helical geared couple (14). Built into the working flange is an illuminator (18) and lamps (19, 20, 21) for glow to provide for observation of the operation of the mechanisms.

The instrument evacuation system includes a VN IMG vacuum mechanical pump, producing a rarefaction of $3 \cdot 10^{-3}$ torr, and a VA-4-5 vacuum unit with maximum rarefaction $5 \cdot 10^{-7}$ torr.

Experiments to determine the coefficients of friction were carried out by the so-called digitate scheme, in the friction assembly of the TOR-1 instrument shown in Fig. 2. /583

Cylinders (1) of monolithic rock or cylindrical matrices of aluminum with a thin layer of deposited finely crushed rock were secured in the central part of the instrument using the grip mechanism and were driven into rotation. The counterbodies (2), fabricated in the form of cylindrical rods, were clamped to the sample with a small roller (4).

TABLE 1. COEFFICIENTS OF FRICTION OF LUNAR SURFACE MATERIAL AND ITS ANALOGS

Counterbody	Coefficient of friction: lunar surface material	crushed basalt	andesite-basaltic sand	Remark
Natural rubber	0.5	0.5	0.65	Wear is visible
Capron fabric, elastic	0.4	0.4	0.55	Wears out intensively
Phenylon	0.5	0.45	0.6	" " "
30RP natural rubber	0.55	0.5	0.6	Traces of wear are visible
Silicone rubber	0.55	0.5	0.6	No wear
Phenylon, kersey	0.40	0.35	0.40	Wears out intensively
Natural leather	0.40	0.5	0.45	Wear is visible
" "	0.35	0.4	0.4	" "
Magnesium alloy	0.3	0.2	0.3	Wears out intensively
Duralumin	0.45	0.25	0.4	Traces of wear are visible
Titanium alloy	0.35	0.3	0.3	No wear
Stainless steel	0.25	0.25	0.25	" "
Construction steel 3	0.30	0.25	0.3	" "
VK-8 hard alloy	0.30	0.40	0.3	" "

TABLE 2. COEFFICIENT OF FRICTION OF BASALT WITH DIFFERENT COUNTERBODIES

Counterbody	Coefficient of friction: Air		Vacuum	Helium	
	25° C	150° C	25° C	25° C	150° C
Natural rubber -- gloves	0,25	0,25	0,5	0,2	0,15
Elastic -- glove	0,25	0,25	0,4	0,2	0,3
Phenylone -- overalls	0,25	0,3	0,45	0,3	0,3
Natural rubber -- sole	0,4	0,25	0,5	—	—
Silicone rubber -- sole	0,35	0,3	0,5	0,4	0,3
Natural leather -- shoe upper	0,3	0,25	0,4	0,2	0,2
Natural leather -- sole	0,35	0,25	0,4	0,2	0,2
Magnesium alloy	0,25	0,15	0,2	0,2	0,15
Duralumin	0,35	0,3	0,3	0,35	0,2
Titanium alloy	0,35	0,35	0,35	0,25	0,3
Stainless steel	0,45	0,4	0,3	0,4	0,4
Construction steel 3	0,45	0,4	0,35	0,45	0,4
VK-8 hard alloy	0,5	0,5	0,4	0,55	0,4

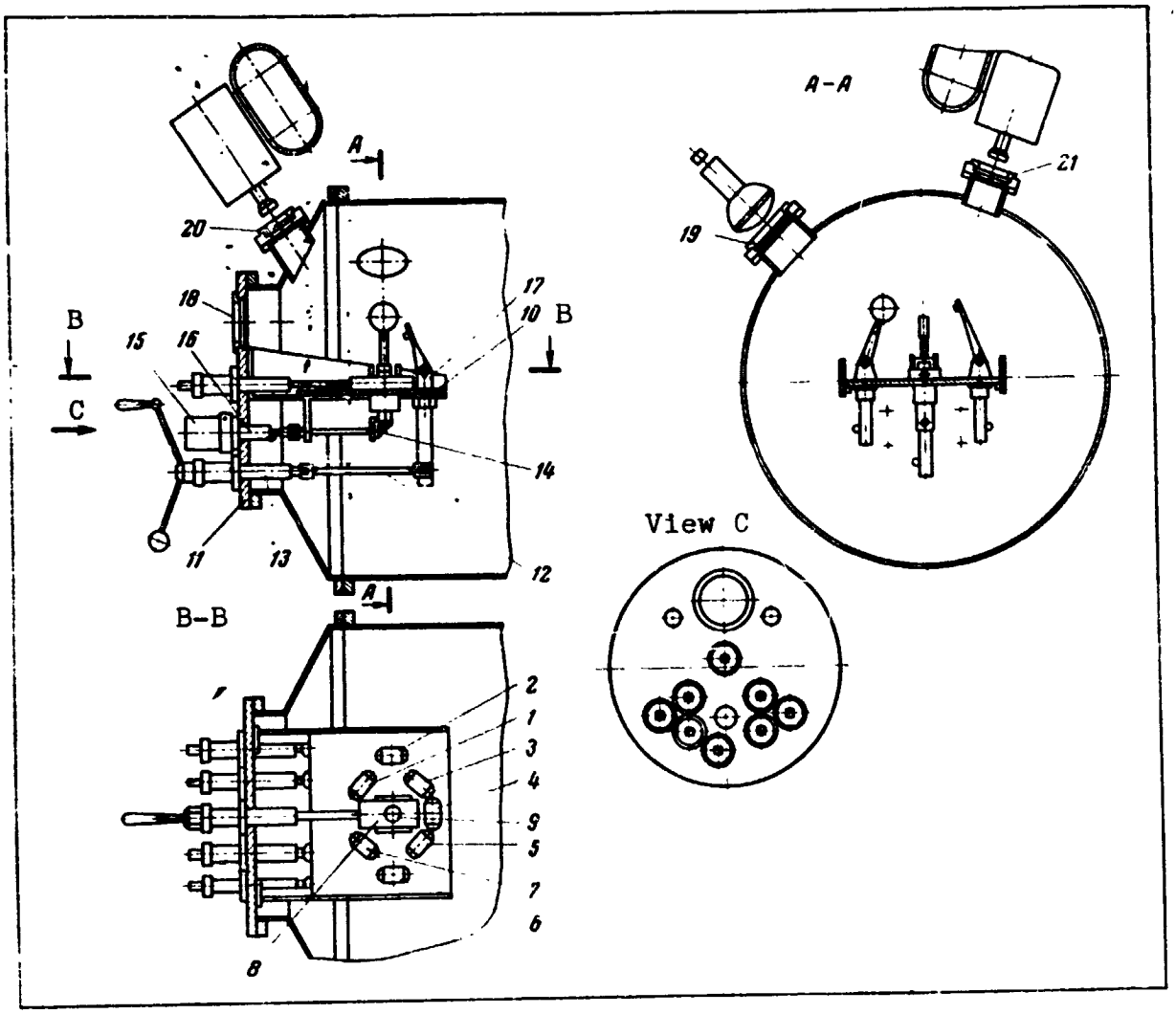

Fig. 1. Scheme of TOR-1 instrument.

The normal load was measured with a system of transducers (3). Tangential stresses arising in friction were recorded with transducers (5) secured to the roller (6). The friction assembly was placed on a rotating cantilever (7). The half-axles were powered and the unbalance of the transducers was amplified with the 8ANCh-7m amplifier. The counterbodies were made in the form of cylindrical rods, 8 mm in diameter, one side of which was dressed in the form of a truncated cone with an area 3 mm in diameter. /584
In the case of the nonmetallic samples, holders of similar shape were fabricated of duralumin, followed by cementing to the end surface 3 mm in diameter of the given test material (8). The samples were heated with a special 70-watt heater (9), capable

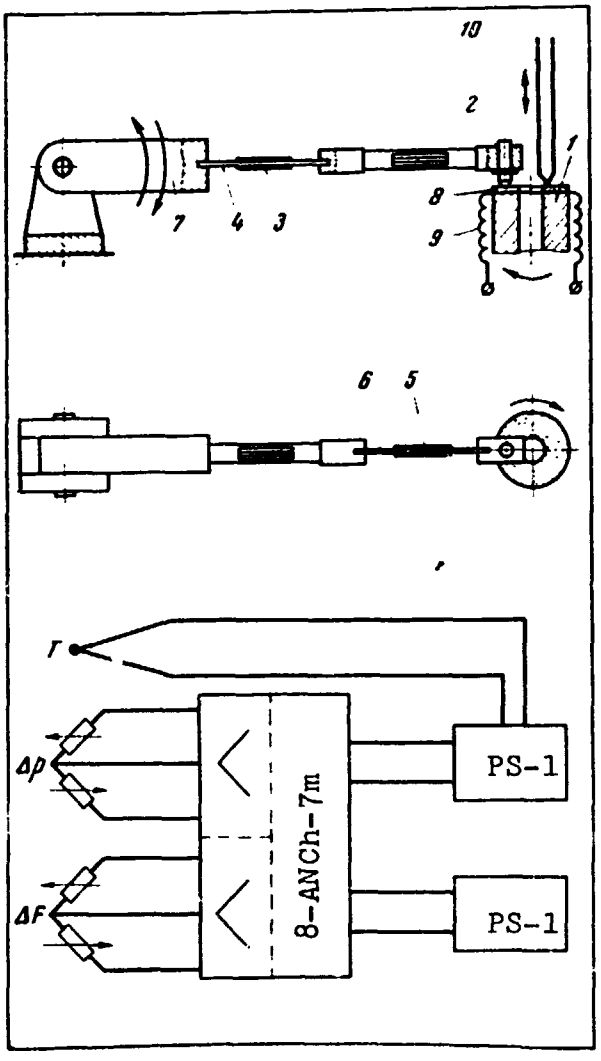

Fig. 2. Scheme of friction assembly

of raising the sample temperature to 200° C. The temperature was monitored with a chromel-copel thermocouple (10). A heater in the form of a linear heat source was placed on a special rotating cantilever.

Since one of the elements of the friction couple was driven, heat transfer by the contact method presented certain difficulties; accordingly, to simplify the design the method of radiation heating was adopted. The experiments were carried out at specific normal loads up to 2 kg/cm^2 with a constant friction rate 2 cm/sec. The normal and tangential forces were recorded simultaneously on two PS-1 electronic recorders. The sample heating temperature was recorded also on one of the PS-1 electronic recorders.

Owing to the small amount of the lunar surface material intended for these tests, a special technique of preparing the samples was developed. Essentially, this method consists in depositing the test material on one of the faces of a cylindrical aluminum matrix /585 on a layer of epoxy resin; in our case the test material was lunar surface material and two of its terrestrial analogs: andesite-basaltic sand and crushed basalt.

A comparison of the friction properties of the tested rocks in the monolithic and finely crushed states was made initially in the development of the method in normal atmospheric conditions on a special setup with reciprocating motion as the samples of magnesium and titanium alloys were brought into friction over the surface material analogs, basalt, foam concrete, and compact tuff. In these experiments these rocks were used both in the form of monolithic samples, as well as in the form of powder deposited on metallic plates. As shown by the results of measurements, the deviation in the coefficients of friction of the monolith with respect to the counterbody and of the powder deposited on the metallic plate with respect to the same counterbodies did not exceed 5-7 percent.

Further, this method was verified on the friction assembly of the TOR-1 instrument in a 10^{-5} torr vacuum. The friction characteristics of the aluminum and titanium alloys were investigated with respect to basalt in the friable and in the monolithic states. For the samples of aluminum and titanium alloys, the coefficients of friction were 0.36 and 0.40, and also 0.26 and 0.27, respectively. These data were obtained for a rubbing surface temperature of 25° C.

As part of the developed method, cylindrical duralumin samples 22 mm in diameter and 20 mm in height were fabricated. One of the end surfaces was coated with a thin layer of epoxy resin, on which was deposited through a sieve with a maximum opening of 0.2 mm a layer of the test material. About 70 mg of the material was used in making one sample. It should particularly be noted that the lunar surface material was deposited on the end surfaces of the cylinders in helium. Investigation of the friction properties of the tested materials was carried out in two stages. Initially, the friction properties of the lunar surface material and its two analogs were determined in an atmosphere of chemically pure helium at 20° C. The results of these investigations are in Table 1.

Analysis of the results of the first cycle of investigations showed that the lunar surface material in its friction properties is very close to terrestrial analogs, and of the two surface material analogs, basalt is closer to the lunar surface material.

This property of basalt led to a second cycle of investigations involving it being carried out dealing with the effect of vacuum and elevated temperatures on the friction properties of basalt.

The experimental method involved the following. The test friction couple was placed in the vacuum chamber. Initially, with the vacuum lock closed, the coefficient of friction was determined in normal atmospheric conditions at room temperature and at the elevated temperature. Next, air from the chamber was evacuated to a pressure of 10^{-5} torr, and in parallel with the evacuation the sample was heated. The temperature was monitored with a chromel-copel thermocouple, which by means of a special sliding device was pressed against the sample of the rock in the friction zone. After attainment of the maximum vacuum in /586
the required temperature, the thermocouple and the heater were moved away from the sample, the electric motor was turned on, driving the sample of rock, the counterbody was brought up, the steady thermal field of the rock sample and the counterbody was established, and the experiment was carried out. As was shown by experience, during the experimental period the temperature of the sample surface was reduced 7-12 percent, which did not show up appreciably in the measurements.

The results of the investigations to determine the friction characteristics obtained by this procedure are given in composite Table 2.

Analysis of the results in the second stage of the investigation suggests a number of conclusions.

1. In practice, for most of the friction couples a decrease in the coefficients of friction with increase in heating temperature was traced, both in atmospheric conditions as well as in vacuum.

2. For most friction couples, in the transition from atmospheric pressure to a vacuum of 10^{-5} torr, there was some reduction in the coefficients of friction. However, final conclusions on the effect of the degree of vacuum on the change of coefficients of friction can be made after experiments have been conducted in conditions of higher vacuum.

3. The effect of positive temperatures on a reduction in the coefficients of friction shows up more strongly in conditions of vacuum than in atmospheric conditions.

4. The transition from the air environment to the inert gas in the case of friction assemblies with metallic counterbodies led to some reduction in the coefficients of friction, while in the case of nonmetallic counterbodies there was a very appreciable rise in the coefficients of friction.

All-Union Scientific Research Institute of Optico-Physical Measurements, Moscow.

Scientific Research Institute of Foundations and Underground Structures, Moscow.

N75 11875

MICROBIOLOGICAL AND EXPERIMENTAL-HISTOLOGICAL INVESTIGATIONS OF LUNAR SAMPLES RETURNED BY THE LUNA 16 AUTOMATIC STATION

/587

D. R. Kaulen, T. I. Bulatova, A. Ya. Fridenshteyn, and Ye. B. Skvortsova

Abstract

Presented here are materials from a biological study of the properties of lunar surface material returned by the Luna 16 automatic station. No viable microorganisms were detected in the samples investigated. It was shown that the samples studied exhibit neither stimulant or inhibitory action on the growth of microorganisms, and also show no cytopathogenic action on tissue cultures. A suspension of lunar surface material particles is not toxic when parenterally administered to certain laboratory animals. The particles are subjected to intense phagocytosis by connective-tissue cells in vivo and in vitro.

In studies published earlier by American scientists /1, 2/ investigating samples of lunar surface material returned by Apollo 11 and Apollo 12, it was reported that there were no viable microorganisms in the lunar material, as well as no traces of microbes that had lived earlier. They also investigated the toxicity of the lunar surface material for animals, in tissue cultures, and pathogenecity with respect to certain terrestrial microorganisms. No biological activity of the lunar surface material with respect to these objects was found /1, 2/.

The investigation described in this article dealt with the biological properties of the lunar surface material returned by the Luna 16 automatic station. The lunar surface material was studied for its content of viable microorganisms (aerobic and anaerobic, fungi, and viruses); the effect of the lunar surface material on the growth of microorganisms and its interaction with somatic cells of mammals was studied.

To study the inoculability of lunar surface material by microorganisms, various nutrient media were used employed in microbiological work aimed at cultivating various anaerobes, aerobes, and fungi, as well as viruses. The following were used in the experiment: a meat medium with small pieces of raw meat under vaseline oil (Tarocci type medium), meat-peptone broth, casein-fungal medium, meat-peptone beveled medium, Saburo medium, and also tissue cultures.

In each of these media 25-50 mg of surface material was inoculated. Cultivation of the inoculations was carried out in four different temperature regimes: + 4, + 22, + 37, and + 56° C, and in both aerobic as well as in anaerobic conditions (in anaerostats, where the residual pressure was 15-20 mm Hg). These conditions of cultivation were provided to permit detection in the surface material of psichrophils (microorganisms growing at 0 and + 10° C), fungi, aerobes, and anaerobes growing at human body temperature (mesophils), and thermophils (growing at + 50 and + 60° C).

For enrichment and cultivation of the microorganisms that were possibly present, the surface material was inoculated initially on a tissue culture of fibroblasts of human fetus, and three days later a transfer inoculation was made to a Tarocci medium, meat-peptone broth, and Saburo medium. The repeated transinoculations were carried out from the initial inoculations of lunar surface material on the Tarocci medium to the same medium.

The inoculations that were incubated initially at + 56° C, after eight days' cultivation were transferred to other temperature conditions (+ 4° C), allowing for the change of temperatures on the Moon. A total of 52 inoculations were made.

During 30 days of observation, in none of the media inoculated with the surface material was the growth of microgrowth of microorganisms observed, either in the control or in the uninoculated media. There was no growth of microorganisms also after enrichment of the inoculation material (preliminary cultivation in a tissue culture and in a Tarocci medium).

In another series of experiments, the bacteriostatic, bacteri- /588
cidal, as well as the stimulant action of the lunar surface material on microbial growth were studied. For these investigations, strains E. coli No. 468 and staphylococcus No. 18 were used, which were cultivated in test tubes on meat-peptone broth and on solid nutrient medium in Petri dishes. Meat-peptone agar was used for the E. coli, and yellow-salt agar for the staphylococci.

In order to discover a bacteriostatic effect, the microorganisms were inoculated simultaneously with the introduction of the lunar

surface material. For these experiments, a 5 percent suspension of lunar surface material particles in physiological saline solution was prepared. The prepared suspension in the volume of 0.2 ml was introduced simultaneously with the inoculation of these strains into a liquid nutrient medium. The lunar surface material was not added to the control inoculations. To study the bacteriostatic effect, four holes 0.5 cm in diameter were made in the solid nutrient media in agar in the Petri dishes, and then the culture was inoculated in order to obtain a continuous crop. After the inoculation, the 5 percent solution of lunar surface material in the 0.2 ml volume of the physiological saline solution was introduced into the two holes. In two other holes only the physiological saline solution was added for the control. The inoculations were kept at 37° C for three days. In all the test tubes containing a liquid medium and in the solid media in the Petri dishes, the growth was uniform both in the presence as well as in the absence of the lunar surface material. Thus, neither a bacteriostatic or a bacteriostimulant effect was revealed (Fig. 1).

Similar investigations were conducted in order to discover any bactericidal effect of the lunar surface material. The experiments were carried out with the same strains in the same liquid and solid nutrient media. Initially, a diurnal growth of the strains used in the form of a continuous crop was produced on the solid nutrient media. Then in the agar four holes were made, and to two of these 0.2 ml each of the 5 percent suspension of lunar surface material particles was added. Only the physiological solution was added to the control holes.

A similar suspension of lunar surface material in the volume of 0.2 ml was also added to each of the test tubes with the diurnal growth of these microorganisms on broth. Only the physiological solution was added to the control test tubes containing a diurnal growth of microorganisms.

The test tubes and the Petri dishes, after the addition of the lunar surface material, were again placed in a thermostat at 37° C. The results were recorded every 24 hours. Over a period of three days no bactericidal or bacteriostimulant effect was revealed either in the liquid medium (Fig. 2) or in the solid nutrient medium in the Petri dishes.

Thus, these investigations made it possible to conclude that there is no bacteriostatic, bactericidal, or stimulant effect of lunar surface material particles on the bacterial growth.

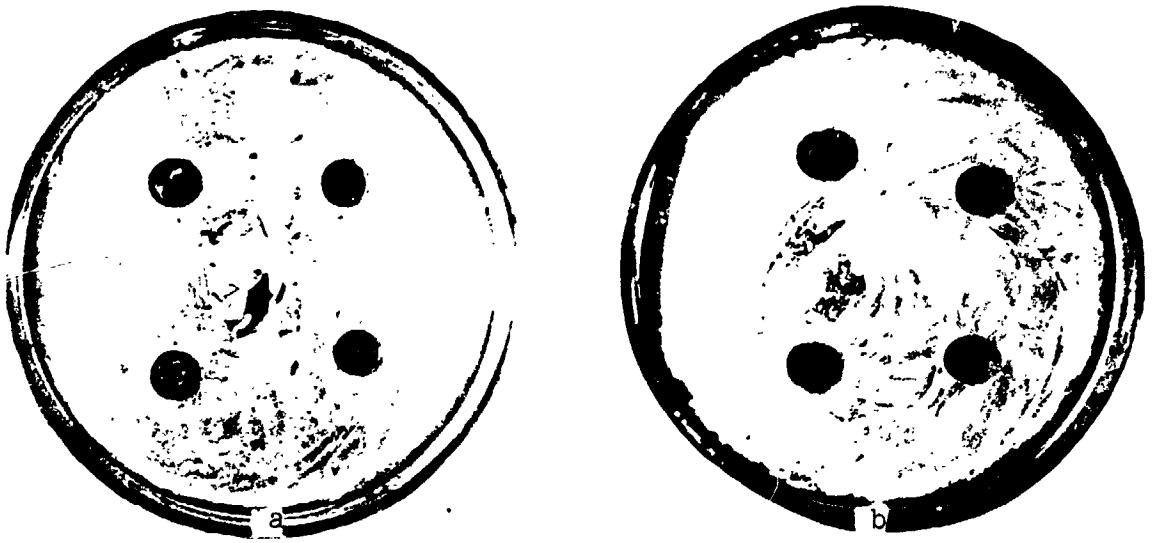

Fig. 1. Effect of particles of lunar surface material on bacterial growth in solid nutrient medium.
a. E. coli No. 468
b. Staphylococcus aureus No. 18
X = Holes containing lunar surface material

A parallel study was made of the interaction of lunar surface /589
materials particles with phagocytizing cells. Though the objects phagocytosis can be a broad class of compounds with diverse chemical composition and physical structure, it is by no means any compound that can be captured by cells. It is most essential that as a result of phagocytosis with a cell as well as with the phagocytized material, substantial changes can occur. In this respect, it was of interest to clarify whether the particles investigated were subjected to phagocytosis, how they acted on the cells absorbing them, and what was their fate within the cells. Since a special class of actively phagocytizing cells of the organism (cells of the RES /reticuloendothelial system/) play an essential role in the protective (and, in particular, in the immunological) processes, by regulating the interaction of the organism with its environment, it appeared to be of interest first of all to clarify the action of particles of lunar surface material on these cellular elements. For this purpose, particles in a volume of 0.5 ml of a 1 percent suspension were administered to the organism of mice and guinea pigs in four ways: a) intravenously to mice, b) intraperitoneally to mice, c) subcutaneously to guinea pigs, and d) intracutaneously to guinea pigs. In the second, third, and fourth cases, the response at the site of administration was determined; in all cases the response to particles in the cells of the RES present in the spleen, liver, kidneys, lungs, and lymph nodes were studied. The material was investigated in histological preparations in 3-7-14 days after

administration of the suspension. It was found that administration of the suspension had no effect in any case on the general condition of the animals. At the site of administration in the guinea pigs, the particles were subjected to intensive phagocytosis by macrophages and fibroblasts, and the particles also settled mainly in the substance of connective tissue. In this case, both the intracellularly as well as extracellularly localized particles caused neither in inflammatory or a proliferative reaction. They behaved as entirely indifferent inclusions even at high local concentration. The same is true also for particles administered intraperitoneally to mice and settling in abdominal walls. In intravenous and intraperitoneal administration, the particles could be found in the cytoplasm of the Kupffer cells of the liver (Fig. 3) and the reticular cells of the spleen (Fig. 4). In spite of the intense accumulation of phagocytized particles, they caused no changes in the cells absorbing them or in the surrounding tissue.

Fig. 2. Effect of particles of lunar surface material on bacterial growth in liquid nutrient medium.

1. Diurnal growth of bacteria with addition of lunar surface material
2. Sterile medium control
3. Diurnal growth of bacteria without the addition of lunar surface material

a. E. coli No. 468 b. Staphylococcus aureus No. 18

In another series of experiments, particles in the form of dense suspensions were administered in a culture medium of guinea pig marrow cultures and human fetal fibroblast cultures. The cells in the cultures disclosed effects of intensive phagocytosis. Particles of lunar surface material of different shape and size

were phagocytized at different intensities. Some of the particles remained adhering to the cellular surface, but did not penetrate /590
within the cytoplasm. Absorption of the particles did not damage the cells (Figs. 5 and 6). They continued to multiply, and the continuity of the cellular layer in the cultures was not disturbed. Nor were any signs of the disruption of the intracellular structures detected in the phagocytizing cells. An impression was given (it requires further refinement and verification precisely for these kinds of cultures) that the particles investigated have a stimulant action on the growth of cells in guinea pig marrow cultures.

Fig. 3. Phagocytosis of particles in Kupffer cells of mouse liver 14 days after intramuscular administration of lunar surface material.

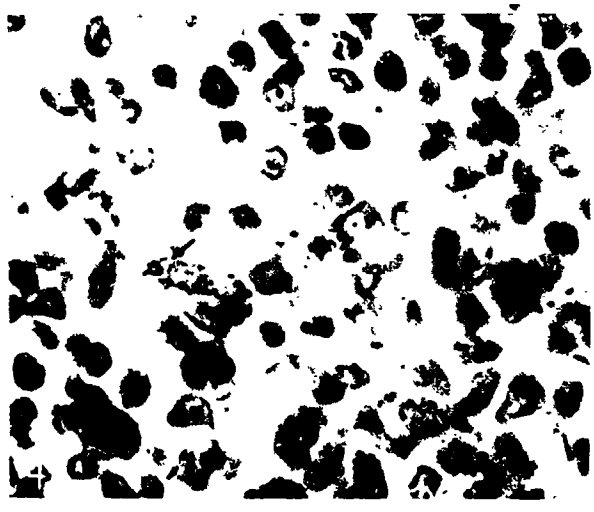

Fig. 4. Phagocytosis of particles by reticcular cells of mouse spleen 14 days after intramuscular administration of lunar surface material.

Overall, this investigation showed that the particles are in the category of objects subjected to intensive phagocytosis by connective cells in vivo and in vitro. They do not cause inflammatory reactions and, on being present within cells, have no toxic effect on them.

To study the effect of lunar surface material on the growth of human cells in a tissue culture, experiments were conducted with a 3-day culture of human fetal cells. In the first passage no essential changes of any kind were detected in the average number of cells in the ground substance.

Thus, the concentration of the human fetal cells in the /591
presence of the suspension of the lunar surface material was as follows (thousands per ml, arithmetic mean $\pm$ δ):

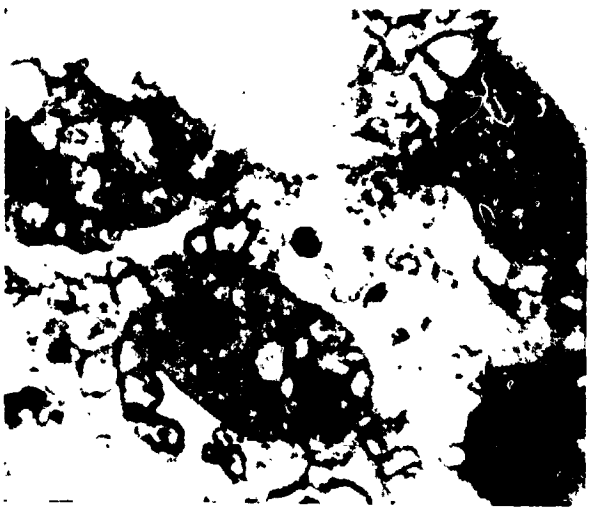

Fig. 5. Phagocytosis of particles of lunar surface material by reticular cells in culture of guinea pig marrow.

Fig. 6. Phagocytosis of particles of lunar surface material in cells of human fibroblast culture.

experiment	153.9 ± 30.8
control	153.3 ± 53.5

Comparison based on the t-criterion of the experimental and the control values confirmed that there is no significant difference between them.

Two "blind" passages (with preliminary adsorption) with culture fluid from the experimental and the control cultures were also carried out. As a result of counting the number of cells growing in the samples, no changes in the intensity of culture growth were found. These investigations revealed no distinctive cytopathic or proliferative changes in the culture of human fetal cells.

As a result of these investigations, the principal conclusion is that in the lunar surface material there are no microorganisms capable of growing on ordinary nutrient media used in microbiological practice, in different conditions of cultivation. Possibly, the investigations we conducted a single time are not sufficiently convincing to conclusively reject the possibility

of microorganisms being present on the Moon. However, two similar reports by United States scientists on this problem and our data, as a group characterizing the lunar surface material from three different regions of the lunar surface, indicate that there are no living microorganisms on the Moon.

It was established that particles of lunar surface material are subjected to intensive phagocytosis by connective-tissue cells in vivo and vitro and are not toxic to the cells. The impression was also given that here some stimulation of cell growth in vitro (in the cultures of guinea pig marrow) with a total absence of cytotoxicity occurred. The final conclusion as to the stimulant effect of particles of lunar surface material on cell growth in tissue culture can be made after additional investigations.

REFERENCES

1. "Preliminary Examination of Lunar Samples from Apollo 11," Science 165(3899), 1211-1227 (1969).

2. "Preliminary Examination of Lunar Samples from Apollo 12," Science 167(3923), 1325-1339 (1970).

Institute of Epidemiology and Microbiology imeni N. F. Gamaley, USSR Academy of Medical Sciences, Moscow.

N75 11876

INVESTIGATION OF BIOLOGICAL ACTIVITY OF FINE FRACTION OF LUNAR SURFACE MATERIAL RETURNED TO EARTH BY THE LUNA 16 AUTOMATIC STATION

V. V. Kustov, O. F. Ostapenko, and V. G. Petrukhin

By the time of the delivery to the Receiving Laboratory of the USSR Academy of Sciences of the Lunar Surface Material taken by the Luna 16 automatic station in the Sea of Fertility, investigations on the biological activity of the material returned to Earth by the crew of the Apollo 11 spacecraft from the Sea of Tranquillity and by the Apollo 12 crew from the Ocean of Storms had been completed.

These experiments showed the biological inertness of the lunar surface material returned by Apollo 11 for several kinds of protozoa, planaria, insects, oysters, shrimps, and fishes [1].

In addition, it was found that introducing the surface material into a nutrient medium caused the death of three types of bacterial cells during the first 10 hours. Upon the addition to the medium of the surface material returned by Apollo 12, these bacteria survived 67 days.

The differences in the action of the materials tested on the bacterial cells were attributed by the investigators to a special combination of minerals in each sample of the lunar rock [2]. Therefore it appeared useful to investigate the biological action of a sample of lunar surface material returned to Earth by the Luna 16 automatic station from a new region of the mare surface of the Moon, approximately 900 km east of the Apollo landing site [3].

A total of three series of experiments on male white mice each weighing 20-22 g were carried out.

In the series I of experiments, a study was made of the biological action of air previously passed through a weighed sample of lunar surface material at the rate of 0.5 liter/min. The experimental animals breathed this air for 4 hours a day for 4 days. The control group of mice was kept in a chamber through which previously clean air from the cylinder was drawn through at the same flow rate.

In the series II of experiments, a study was made of the biological action of compounds capable of migrating from the lunar material into water. For this purpose, 500 mg of the fine fraction of the lunar rock was poured into 10 ml of physiological saline solution. After 3-day standing, the suspension was centrifuged (at 8000 rpm); the supernatant liquid was filtered off and administered peritoneally in 0.2 ml doses to these experimental animals. The physiological saline solution served as the control.

In the experiments of series III, the biological action of the lunar material when it administered into the gastrointestinal tract was investigated. For this purpose, using a probe into the stomachs of the experimental mice was introduced a suspension of material prepared from distilled water (500 mg per 20 ml) at the rate of 0.25 ml/10 g bodyweight. Distilled water was administered to the control animals in the same amount, and to some of them -- a suspension of previously crushed river sand calcined at 250°.

To estimate the biological effect of the lunar surface material in all the experiments, the condition and behavior of the animals was observed; the intensity of their oxygen consumption was recorded by the N. I. Kalabukhov method [4]; the motor activity of the muscles, leucocyte and erythrocytes counts in the peripheral blood, and the activity of whole-blood chloinesterase were determined [5].

In 1 and 3 days after the completion of each series of experiments, some of the animals were sacrificed for subsequent pathomorphological and histochemical examination using the method of combination blocks [6]. The stomach, small intestine, lungs, liver, kidneys, adrenals, and pancreas were examined. Structural changes were found in the cells; the cellular content of glycogen, lipids, and ribonucleic acid was determined, along with the activity of succinate dehydrogenase, α-glycerophosphate dehydrogenase, glutamate dehydrogenase, monoaminoxidase, and alkaline phosphatase. /593

Experimental results were treated by application of Student's criterion to determine the reliability of the difference P at the probability level 0.05.

In the series I of experiments, it was found that a 4-day inspiration of air passed through a weighed amount of lunar surface material had no appreciable effect on the overall condition and the behavior of the experimental mice. This kind of exposure did not change the erythrocyte count in the peripheral blood and did not lead to marked shifts in the intensity or the oxygen consumption by the experimental animals and in their motor activity. The leucocyte content in the peripheral blood was practically the same as leucocyte count in the control group of mice. The activity of blood chloinesterase after the experiment on the experimental and control animals was practically identical (Table 1). After the pathomorphological and histochemical examinations, no distinct structural and metabolic disturbances in the cells of the internal organs of the experimental mice could be detected.

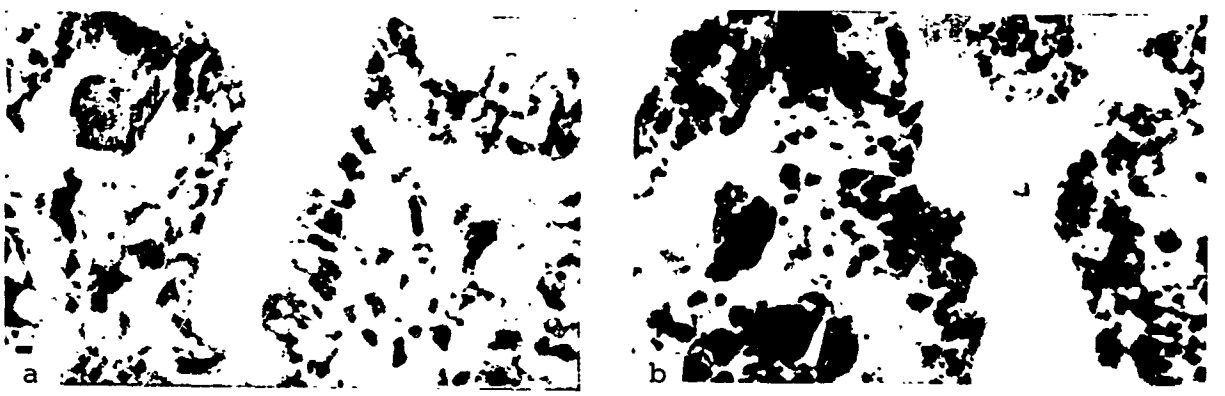

Fig. 1. Content of lipids in epithelial cells of the villa of the duodenum

a. in a control-group animal
b. 24 hours after the administration of lunar surface material into the stomach. The protoplasm of the epithelium and the lymph tracts of the villa are filled with fine and coarse droplets of lipids; cryostat, scarlet red, magnification 470.

The results of the series II of experiments, shown in Table 2, indicate that administration of the supernatant liquid to mice had no appreciable effect on the indicators studied.

In the pathomorphological and histochemical examinations, no detectable changes could be found either in the internal organs of the experimental mice.

The results of examining the animals of the series III of experiments are summarized in Table 3. From Table 3 it follows that administration of the suspension of lunar material to the stomach caused some reduction in the leucocyte count in the peripheral blood of the experimental mice ($P < 0.05$) and a reduction

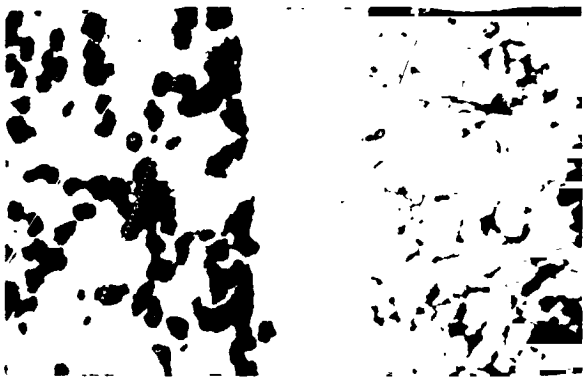

Fig. 2. Activity of alkaline phosphatase in kidney of control mouse (left); as about 24 hours after the introduction into the stomach of lunar surface material (right); method of combination blocks, Gomori reaction, magnification 160.

in the activity of blood cholinesterase compared with the control group of experimental animals, by nearly 28 percent ($P < 0.05$). For white mice receiving the suspension of the material, a moderate reduction in the intensity of the oxygen consumption was noted ($P < 0.05$). However, these shifts were also noted in the experimental animals after the administration of a suspension of river sand.

Pathomorphological examinations showed that administering the lunar material to previously well-nourished white mice caused, by the third hour of the experiment the accumulation of fine and coarse droplets of lipids in the protoplasm of the epithelial cells of the villi of the duodenum and the beginning section of the small intestine. In 24 hours after the aministration, nearly all epithelial cells of the villi were filled down to the bottom of the crypt with fat droplets. Aggregates of lipids stretched the lymph tracts of the villa (Fig. 1). The administration of lunar surface material and river sand to fasting animals does not lead to the accumulation of lipids in the intestinal epithelium. Therefore the above-listed shifts in previously well-nourished white mice evidently reflect only the process of the absorption of nutrient substances (fats, carbohydrates, and so on) in the small intestine and do not characterize the specific action of the lunar surface material on the organism of experimental animals. /595

TABLE 1. STATUS OF CERTAIN PHYSIOLOGICAL AND BIOCHEMICAL INDICATORS IN WHITE MICE BREATHING AIR PASSED THROUGH A LAYER OF LUNAR SURFACE MATERIAL /594

Group of animals	O_2 consump., ml/10 g/min			Extended activity, % of control			Activity of blood cholines (breakdown of acetylch. µg/min)			Leucocyte count, thousands/mm^3		
	before exper.	after exper.	P	before exp.	aft. exp	P	before exper.	after exper.	P	before exper.	after exper.	P
Experimental	1,27±0,051	1,34±0,038	0,05	95,5	85,9	—	—	332,5±19,7	—	13,61±1,02	9,00±0,81	0,05
Control	1,30±0,026	1,31±0,033	0,05	100	100	—	—	329,7±19,0	—	11,47±1,36	8,03±0,94	0,05
P	0,05	0,05	—	—				0,05		0,05	0,05	

TABLE 2. STATUS OF SEVERAL PHYSIOLOGICAL AND BIOCHEMICAL INDICATORS IN WHITE MICE AFTER PERITONEAL ADMINISTRATION OF SUPERNATANT LIQUID

Group of animals	O_2 consump., ml/10 g/min			Extended activity, % of control			Activity of blood cholines. (breakdown of acetylch. μg/min)			Leucocyte count, thousands/mm^3		
	before exper.	after exper.	P	before exper.	aft. exp.	P	before exp.	after exp.	P	before exp.	after exp.	P
Experimental	1,22±0,024	1,27±0,035	0,05	107,4	120	—	252,8±19,3	—		12,33±1,15	10,89±1,40	0,05
Control	1,28±0,058	1,33±0,041	0,05	100	100	—	260,6±13,6	—		9,60±1,23	12,18±1,44	0,05
P	0,05	0,05		—	—		0,05			0,05	0,05	

TABLE 3. STATUS OF SEVERAL PHYSIOLOGICAL AND BIOCHEMICAL INDICATORS IN WHITE MICE AFTER THE ADMINISTRATION OF A SUSPENSION OF LUNAR SURFACE MATERIAL INTO THE STOMACH

Group of animals	O_2 consump., ml/10 g/min			Extended activity, % of control			Activity of blood cholines. (breakdown of acetylch. μg/min)			Leucocyte count, thousands/mm^3		
	before exp.	after exp.	P	before exp.	aft. exp.	P	before exp.	after exp.	P	before exp.	after exp.	P
Experimental	1,33±0,044	1,16±0,028	0,05	98,7	119	—	263,2±10,8	—		12,41±1,1	7,91±0,61	0,05
Control	1,36±0,032	1,32±0,047	0,05	100	100	—	336,0±22,0	—		11,99±1,37	12,67±1,30	0,05
P	0,05	0,05		—	—		0,05			0,05	0,05	

Histochemical investigations revealed changes in the activity of certain enzymes in the cells of the intestine, liver, and kidneys. The activity of alkaline phosphatase, succinate dehydrogenase, and monoaminoxidase in the epithelial cells of the kidney was intensified. The activity of alkaline phosphatase was intensified in the cells of the convoluted tubules of the kidneys and in the loops of Henle, as well as in the cells of capillaries and veins (Fig. 2). The glycogen content in the liver cells was reduced; the activity of succinate dehydrogenase and alkaline phosphatase was increased; the activity of glutamate dehydrogenase was slightly reduced. Upon electron-microscopic examination, the hepatocytes disclosed swelling of the mitochondria and their cristae, dilation of the sarcoplasmatic reticulum, and an increase

in the count and size of the pinocytose vacuoles. Identical changes were found in the control animals after the administration of the river sand suspension; these changes, as in the case of the administration of the lunar surface material, can be associated with the mechanical irritation of the absorbing epithelium with the subsequent increase in the absorptivity by the intestinal walls of nutrient substances.

Thus, the experimental studies made it possible to conclude that the tested doses of the fine fraction of the lunar surface material returned to Earth by the Luna 16 automatic station from the Sea of Fertility is virtually innucuous for white mice.

REFERENCES

1. Aviat. Week and Space Technol. 92(12), 22 (1970).

2. Benschoter, C. A., Allison, T. C., Boyd, J. E. et al., Science 169(3944), 470 (1970).

3. Vinogradov, A. P.,"Preliminary Data on Lunar Surface Material Returned by Luna 16 Automatic Station," Geokhimiya (3), 261 (1971).

4. Kalabukhov, N. I., Metodika eksperimental'nykh issledovaniya po ekologii nazemnykh pozvonochnykh zhivotnykh [Methods of Experimental Investigation of the Ecology of Land Vertebrate Animals], "Nauka", 1951.

5. Golikov, S. N., Profilaktika i terapiya otravleniy fosfororganicheskimi insektitsidami [Prevention and Therapy of Intoxication With Organophosphorus Insecticides], "Meditsina", 1968.

6. Petrukhin, V. G., and Gaydamakin, N. A., Trudy Tselinogradsk. med. in-ta [Transactions of the Tselinograd Medical Institute] 3, 69 (1969).

N75 11877

EFFECT OF LUNAR SURFACE MATERIAL ON RADIATION DAMAGE IN MICE (INVESTIGATION OF BIOLOGICAL ACTION OF LUNAR SURFACE MATERIAL RETURNED TO EARTH BY LUNA 16 AUTOMATIC STATION)

/596

V. V. Antipov, B. I. Davydov, N. A. Gaydamakin, T. S. L'vova, V. G. Petrukhin, S. N. Komarova, and Ye. B. Skvortsova

Abstract

A study was made of the effect of a sample of the fine fraction of lunar surface material from the Sea of Fertility on the radiation reaction (damage) in mice caused by exposure to ionizing radiation. The material was administered to the organism in three ways -- aerogenically, through the esophagus, or peritoneally.

It was shown that administering the lunar surface material did not appreciably affect the death of the animals and the reaction of the peripheral blood caused by the action of radiation. In mice which prior to irradiation had been administered inhalationally or peritoneally the lunar surface material, a lag in the increment of bodyweight was observed. By the end of the eighth month of the investigation, in 20 animals neoplasms of different kinds and localizations were detected, and 16 of these animals in some form or other had been in contact with the lunar surface material.

Earlier we showed that such space flight factors as vibration, g-factor, altered gas composition, and others, can appreciably modify the response of the organism to irradiation /1-4/. Here the orientation and the extent of the modifying influence depend on the period of time after the integrated exposure at which the reaction was evaluated /4/. In our view, of no less theoretical interest and practical importance must be the investigation of the modifying action on the radiation response (damage) and space flight factors, for example, lunar surface material.

Owing to the successful study and mastery of the Moon by means of automatic devices, and also with man's participation, it appeared possible to make a detailed and varied investigation of lunar surface material. In several laboratories of the United States and the USSR, physicochemical analyses have been carried out and the biological activity of the surface material returned from different parts of the Moon has been studied.

Fig. 1. External view of tumor. Diagnosis: cancer of the mammary gland. 124th day after irradiation in combination with inhalation of constituents of lunar material.

When the biological experiments were carried out, directly contradictory results were obtained. Thus, in experiments with surface material returned on the Apollo 11 spacecraft from the Sea of Tranquillity, its biological inertness was shown for several species of protozoa, planaria, insects, oysters, shrimps, and fishes /5/. Soviet investigators conducting acute experiments with mice also concluded that the fraction of lunar material returned by the Luna 16 station from the Sea of Fertility was biologically inert /6/. /597

At the same time, there are data obtained by American scientists indicating the biological activity of the lunar surface material. Its addition to lunar soil accelerates the sprouting of seeds of cabbage, carrots, lettuce, and radishes, and stimulates plant development /7/. Thus, the above-mentioned material as well as other data enabled some investigators to suggest that the biological activity of the surface material is associated with the special combination of constituents in each sample of lunar rock /8/. The aim of this present study was to investigate the effect of a sample of lunar surface material returned by the Luna 16 station from the Sea of Fertility on the

irradiation response (damage) in mice caused by exposure to ionizing radiation. The constituents of the fine fraction of the lunar surface material were administered to the organism in three ways -- aerogenically, through the esophagus, or peritoneally.

Method. Three series of experiments (17 groups) were performed on 408 white, mixed-breed male mice aged three months, each weighing 20-22 g. In the first series nine groups were used. The experimental group was the one (No. 3) in which the mice were exposed to air that had passed at a flowrate of 0.5 liter/min through a weighed suspension of lunar surface material, followed by irradiation. The experimental animals breathed this air four hours a day for four days, and then 30 minutes after the last session they were irradiated with a 400 r dose (Co^{60} gamma rays, 28.3 r/min). The remaining six groups of the series were the control. The nature of the exposure in these groups is shown in Table 1. It should be noted that the conditions of airflow, irradiation, and the times between exposures in the control groups were naturally identical with the experimental group. Fifteen minutes before the irradiation, the animals in groups 7-9 were peritoneally administered a radiation protective agent -- 5-methoxytryptamine chlorhydrate (5 MOT) in a dose of 75 mg/kg bodyweight.

Four groups were in the second series. The animals of the experimental group (1 percent) were administered with a probe into the stomach a suspension of material prepared from distilled water (500 mg in 20 ml at the rate of 0.25 ml/10 g bodyweight). One hour after the administration, the mice were irradiated at the same dose as the first series animals. The remaining three groups were the control (Table 1).

The third series also consisted of four groups. The experimental-group mice (No. 14) were peritoneally administered supernatant liquid in the volume of 0.2 ml and in 30 minutes the animals were irradiated as in the preceding series, with a 400 r dose. The supernatant liquid was prepared as follows. Into 5 ml physiological saline solution was poured 500 mg of the fine fraction of the lunar rock. For three days the mixture was allowed to stand, then centrifuged at 8000 rpm and the supernatant liquid was allowed to stand. It can be assumed that during this time compounds capable of dissolving in water had migrated entirely into the solution. The rest of the series groups served as the control (see Table 1).

The following were selected as indicators with which the modifying action of lunar surface material was appraised: the number of succumbing animals, bodyweight dynamics, total leucocyte count, total erythrocyte count, leucocyte ratio, and so on.

TABLE 1. RESULTS OF EXPERIMENTS ON THE STUDY OF THE EFFECT OF LUNAR SURFACE MATERIAL THE RADIATION REACTION IN MICE

Series number	Group number	Characteristics of exposure	Number of animals	Number succumbing in 30 days	Number succumbing in 180 days	Number succumbing total	Number succumbing %	Number of tumors
	1	Biological control	20	—	1	1	5	—
	2	Irradiation with gamma-rays (400 r)	40	2	3	5	12,5	—
I	3	Inhalation of constituents of lunar surface material migrating in air, irradiation	40	2	5	7	17,5	4
	4	Inhalation of air + irradiation	20	—	2	2	10	—
	5	Inhalation of constituents of lunar surface material migrating in air	31	1	1	2	6,5	—
	6	Inhalation of air	20	—	1	1	5	—
	7	Inhalation of constituents of lunar surface material migrating in air, + 5 MOT + irradiation	20	—	2	2	10	—
	8	5 MOT + irradiation	20	1	2	3	15	—
	9	5 MOT	20	—	1	1	5	—
II	10	Intragastric administration of lunar surface material suspension + irradiation	38	—	3	3	7,9	2
	11	Intragastric administration of distilled water + irradiation	19	—	1	1	5,3	—
	12	Intragastric administration of lunar surface material suspension	20	1	—	1	5	—
	13	Intragastric administration of distilled water	20	—	1	1	5	—
III	14	Peritoneal administration of supernatant liquid containing lunar surface material + irradiation	20	4	3	7	35	1
	15	Peritoneal administration of physiological solution + irradiation	20	3	3	6	30	2
	16	Peritoneal administration of supernatant liquid containing lunar surface material	20	1	—	1	5	—
	17	Peritoneal administration of physiological solution	20	—	1	1	5	—

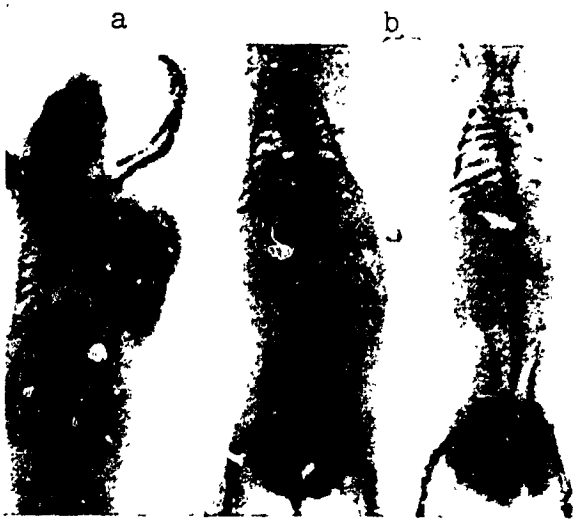

Fig. 2. Roentgenogram of two mice irradiated with a 400 r dose and subjected to preliminary fourfold inhalation of lunar surface material constituents migrating in the air of the intoxication chamber, four hours daily.
a. Cancer is on right side, unattached to the skeleton, see Fig. 3 for histological picture
b. Tumor in pelvic region, unattached to the skeleton, see Fig. 4 for histological picture

The experimental animals were under observation for 1.5 years in order to find the effect of the surface material on the remote sequelae of irradiation (leucoses, tumors, cataracts, shortening of longevity, and so on). /599

Clinical examination, weighing, and hematological examination were carried out and are continuing 1, 7, 30, and 60 days after irradiation and further, every two months.

Some of the animals succumbing during the observation period were autopsied and subjected to morphological and histochemical examination. Depending on the type of pathology found in the macroscopic investigation, the lungs, liver, spleen, thymus gland, ovaries, pieces of the intumescences, and the skin were taken and fixed in Carnua liquid or in 100 percent neutral formalin solution. Sections cast in formalin or frozen were stained with hematoxylin-eosin by the Van-Gizon method, with methyl green pyronine, and with scarlet red by the Shabadash method to reveal glycogen. /600

Results. The primary data on survival rate obtained six months after the beginning of the exposures are summarized in Table 1. From the table it is clear that by the 30-th day of observation, of the total number of animals -- 408 -- 15 mice succumbed. Thirteen of these had been subjected to irradiation (3.2 percent), and two mice died in the groups where there was no irradiation, but only lunar surface material was administered (0.5 percent).

By 180 days, the number of succumbing mice in all series rose to 45, and 36 of these had been irradiated (8.8 percent) and 9 had not (2.2 percent). Twenty-three mice of the total number of those dying had been in contact in some form with the lunar surface material. The greatest death rate (35 and 30 percent)

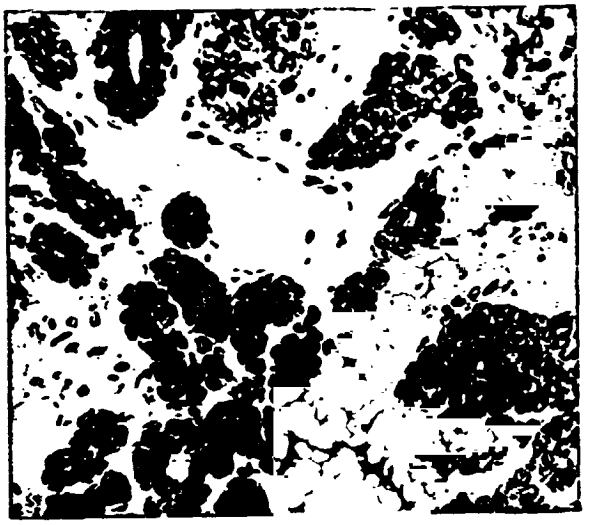

Fig. 3. Mammary gland cancer in mouse sacrificed 124 days after irradiation with a 400 r dose, with preliminary fourfold inhalation of lunar surface material constituents migrating in the air of the intoxication chamber, four hours daily. The cells form ferruginous complexes and infiltrate surrounding tissues; outlines of minosis can be seen (arrows). Hematoxylin-eosin. Power: 400, objective: 40.

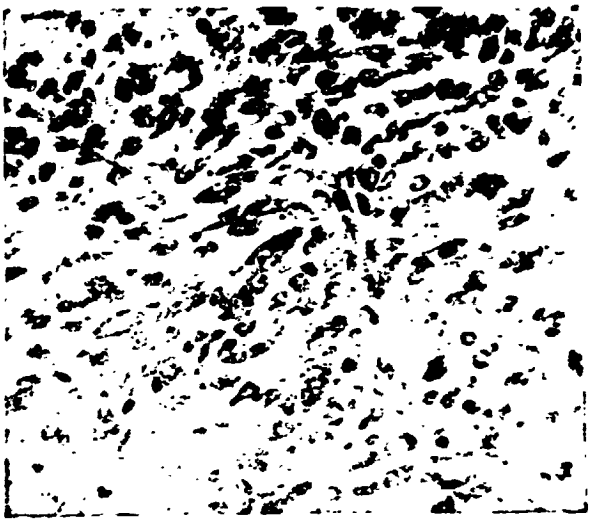

Fig. 4. Angiofibrosarcoma of soft tissues of pelvic region in mouse sacrificed 124 days after irradiation with a 400 r dose, with preliminary fourfold inhalation, four hours daily, of constituents of lunar surface material migrating in the air of the intoxication chamber. The cells are RNA-rich, with high mitotic activity. Methyl green pyronine. Power: 560, objective: 40.

was observed in groups 14 and 15, in which prior to irradiation the animals had been peritoneally administered the supernatant liquid from the surface material (group 14) or the physiological saline solution (group 15). It should be noted that in these groups the maximum death rate was observed also by the 30-th day. In the other experimental groups the percentage of mice dying did not differ appreciably from this indicator in the irradiation control.

Upon macroscopic and microscopic examination of the animals dying in the first two weeks after irradiation, regardless of whether additional exposures were involved, a typical pattern of radiation damage to tissues was recorded: hemorrhaging in lungs, reduction in size, and destruction of spleen and thymus gland, and sometimes edema of intestinal walls and moderate destruction of the intestine. In later periods -- 2-5 months after irradiation -- the causes of the death of mice included pneumonia and profound degenerative-dystrophic changes in tissues all the way to the formation in several organs (liver and spleen) of necrotic foci.

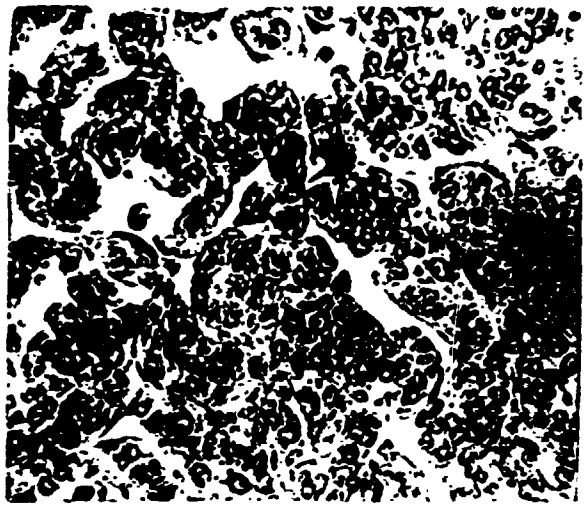

Fig. 5. Mammary gland cancer with infiltration into skeletal musculature; muscle fibers immured by cancer cells are in the state of profound dystrophic changes with nearly complete loss of longitudinal and transverse striation. The mouse was sacrificed 124 days after irradiation with preliminary peritoneal administration of physiological saline solution. Hematoxylin-eosin, objective: 40.

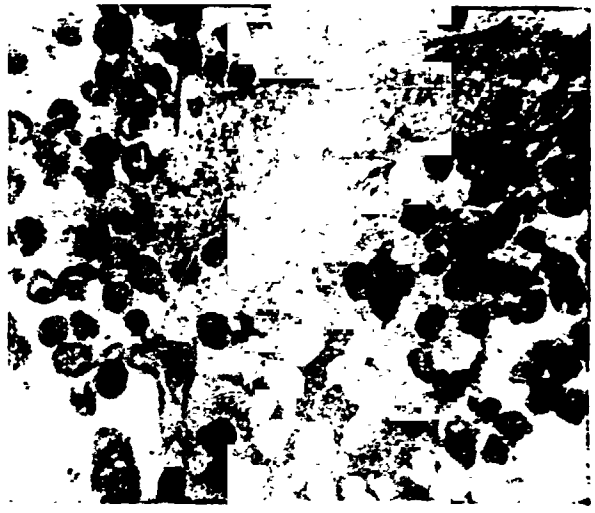

Fig. 6. Reticulosarcoma of thymus gland in mouse sacrificed 166 days after irradiation with preliminary peritoneal administration of physiological solution. Hematoxylin-eosin, objective: 40.

By the end of the third month after gamma irradiation, mice in several groups revealed neoplasms, of which the most common was mammary gland cancer. Some data from the investigation of the tumors are given in Table 2 and in Figs. 1-6.

As can be seen from Table 2, all nine mice in which neoplasms were detected had been gamma-irradiated, and seven animals had been in contact with the products of lunar surface material. In the two remaining animals that had tumors, whole-body radiation had been combined with peritoneal administration of a physiological saline solution.

Some data on the examination of peripheral blood in animals with tumors of different localization from the groups where lunar surface material had been used are given in Table 3. Upon examination of the table, one can note a reduced erythrocyte count in a mouse from group 14, and also neutrophilic leucocytosis, which was most pronounced for two animals from group 3.

Data from a study of the bodyweight dynamics obtained over six months of investigation are shown in Fig. 7-9. Their analysis

TABLE 2. DATA ON THE EXAMINATION OF TUMORS

Group number	Number of mice w/tumor	Days after irradiation	Diagnosis
3	4	124	Mammary gland cancer (2) Angiofibrosarcoma of pelvic soft tissues (1)
		192	Myxolipoma of pelvic tissues (1)
10	2	174	Mammary gland tumor Pulmonary reticulosarcoma
15	2	124	Mammary gland tumor Reticulosarcoma of thymus gland
14	1	132	Mammary gland cancer

reveals the following. A certain difference in weight between the groups began to appear only after the third month of observation. The largest increment in bodyweight was noted for animals that had been subjected only to a single irradiation (group 2). The lag in bodyweight increase was most pronounced in groups where irradiation had been combined with exposure to lunar surface materials through inhalation (group 3, Fig. 7) or peritoneally (group 14, Fig. 9). /601

Let us examine the results of hematological studies, summarized in Table 4 and shown in Fig. 10. From these it is clear that upon gamma-irradiation (group 4), a reduction in the total leucocyte count (down to 40 percent) and in the total lymphocyte count (down to 23.6 percent) occurs in the first-seventh days compared with the control (intact animals). The neutrophil count during these periods remained practically unchanged. At later periods of observation -- 30-th day and later -- these indicators in this group no longer substantially differed from the control.

Nearly as in group 2, these indicators changed in groups 3 and 4 (series I), that is, in the case when the animals prior to irradiation had been inhalationally administered the constituents of the lunar surface material or had inhaled air.

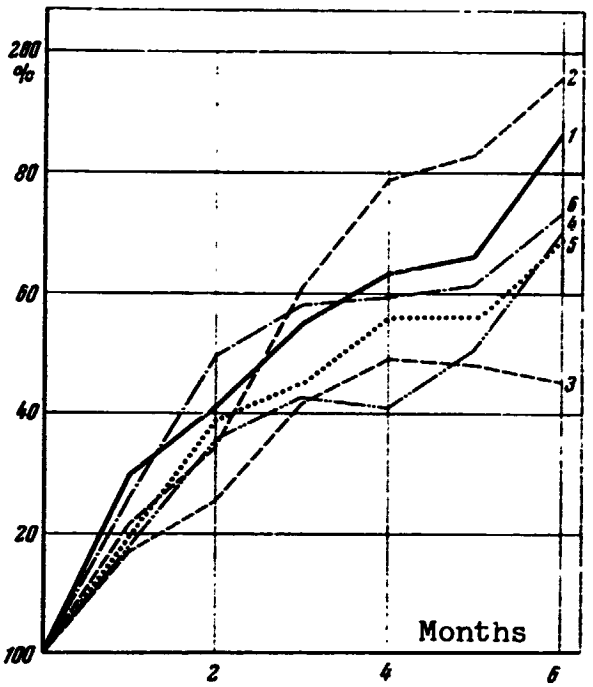

Fig. 7. Dynamics of bodyweight of mice -- intact (1), subjected to gamma-irradiation (2), upon inhaling constituents of lunar surface material (5), air (6), lunar surface material and irradiation (3), and air and irradiation (4)
1-6. Group numbers as in Table 1.

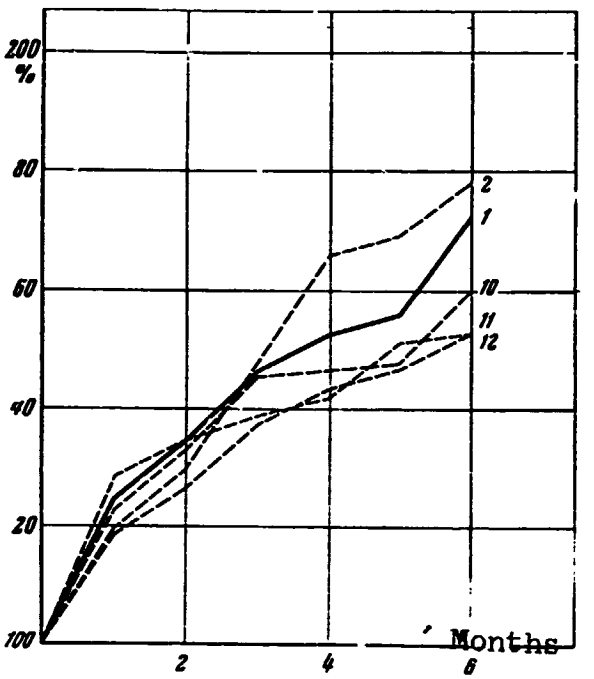

Fig. 8. Dynamics of bodyweight of mice -- intact (1), gamma-irradiated (2), intragastrically administered suspension of lunar surface material (12), lunar surface material and irradiation (10), and distilled water and irradiation (11)
1, 2, 10-12. Group numbers as in Table 1.

In groups 10 and 11 (series II), a suspension of lunar surface material or distilled water was administered to the mice orally prior to irradiation. In the animals of this group, just as in the case of a single irradiation, by the first-seventh day there was a drop in the total leucocyte count (most pronounced on the seventh day) and in the total lymphocyte count. The neutrophil count by the first day was appreciably increased (up to 216 percent), while on the seventn day it was somewhat reduced compared with the initial period.

In groups 14 and 15 (series III), prior to irradiation the supernatant liquid from the lunar surface material or physiological saline solution was administered peritoneally to the mice. In these animals, by the first-seventh day some differences were noted in the reaction of white blood cells to irradiation compared

TABLE 3. RESULTS OF EXAMINATION OF PERIPHERAL BLOOD

/602

Group number	Number of animals	Diagnosis	Days after irrad.	Erythrocytes, million	Leucocytes, thous.	Leucocyte ratio				
						Plat.	Neutr.	Eosin.	Mono.	Lymph.
3	2	Mammary gland cancer	120	6,1	12,9	1,9	4,8	1,0	0,8	4,5
	2	Mammary gland cancer	120	5,7	19,3	0,8	9,8	0,2	0,6	7,5
14	1	Mammary gland cancer	120	3,5	21,3	1,5	13,0	0,2	1,5	5,1

TABLE 4. COMPOSITE RESULTS OF HEMATOLOGICAL STUDIES

Group number	Period of exam., days	Erythrocytes, million	Leucocytes, thous.	Neutrophils thous.	Lymphocytes, thous.	Eosinphils, thous.
1	1	10,9	8,2	1,8	5,4	0,3
	7	10,2	11,0	3,6	5,1	1,2
	30	10,7	7,4	2,3	3,8	0,6
	60	9,6	7,7	2,1	5,0	0,36
	120	10,5	8,3	3,0	4,1	0,4
2	1	10,2	3,6	1,8	1,4	0,12
	7	10,3	4,4	2,6	1,2	0,04
	30	9,8	9,0	2,4	4,7	0,8
	60	9,9	9,4	2,3	5,5	0,2
	120	10,0	8,8	2,9	5,0	0,3
14	1	10,0	7,7	3,0	3,6	0,4
	7	10,3	7,6	4,7	1,8	0,015
	30	10,0	10,8	2,2	4,5	1,3
	60	9,7	9,3	2,0	5,3	0,7
	120	9,1	17,2	4,9	7,9	0,7
15	1	11,4	7,7	3,2	3,3	0,2
	7	8,8	4,7	2,5	1,5	0,13
	30	11,0	11,5	4,1	5,2	0,5
	60	9,5	9,5	2,7	5,7	0,3
	120	9,1	9,1	3,1	4,6	0,4
10	1	11,0	6,5	3,8	2,1	0,2
	7	10,4	3,8	2,3	0,9	0,05
	30	9,9	12,3	4,0	6,0	0,7
	60	9,6	9,1	2,2	5,7	0,5
	120	9,1	9,3	3,0	5,3	0,4
11	1	10,4	5,6	3,9	1,7	0,9
	7	10,0	5,3	3,1	1,4	0,03
	30	10,2	7,2	2,0	3,9	0,4
	60	10,2	10,0	2,2	5,7	0,6
	120	9,8	12,0	4,0	7,1	0,5
4	1	9,0	5,3	2,1	2,3	0,4
	7	8,8	3,1	1,5	1,3	0,01
	30	9,1	6,9	2,3	3,4	0,3
	60	10,2	14,3	6,2	6,0	1,0
	120	8,5	8,4	3,5	4,6	0,3
3	1	10,9	3,7	1,7	1,5	0,5
	7	9,4	3,9	2,4	1,3	0,02
	30	9,8	8,2	4,3	3,5	0,3
	60	10,3	13,8	5,1	6,7	0,4
	120	10,5	11,8	5,0	5,0	0,7

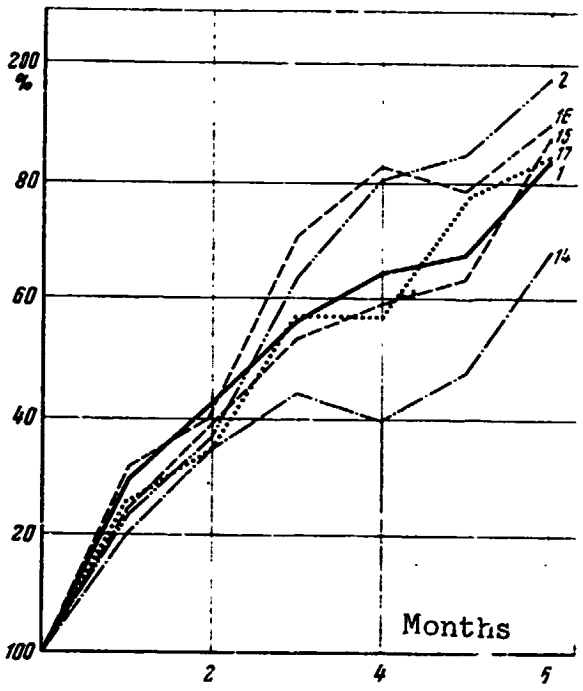

Fig. 9. Dynamics of bodyweight of mice -- intact (1), gamma-irradiated (2), peritoneally administered supernatant liquid (14), liquid and irradiation (15), physiological saline solution (17), and physiological saline solution and irradiation (16)
1, 2, 14-17. Group numbers as in Table 1.

with the reaction of group 2 mice. This, by the first day in these mice the total leucocyte ccunt remained practically unchanged, and it decreased by the seventh day to a lesser extent than in group 2. The lymphocyte count fell very slightly by the first day and the neutrophil count rose appreciably. In later periods of observation, as in series II, these indicators were somewhat higher compared with the initial background.

Upon investigation of the eosinophils, it was found that this indicator was significantly changed in the same period in all groups. By the seventh day after irradiation, a reduction in the eosinophil count was noted; in all remaining periods the fluctuations were within the limits of physiological scatter (see Table 4). In the cytological examination of peripheral blood cells, certain changes were found in the following groups. /603

In group 10 where the suspension of lunar surface material was administered to the mice orally, isolated degenerative-altered lymphocytes and monocytes were recorded. These changes were expressed in the plasmatization of the protoplasm and in the manifestation of vacuoles in the cell cytoplasm. In the animals of groups 14 and 15 (peritoneal administration of supernatant liquid or physiological saline solution) increased content of plasmatic cells was noted, as well as the appearance of degenerative-altered forms of monocytes and lymphocytes. The erythrocyte count in all the groups studied was practically unchanged, with the exception of individual animals with tumors, for which this indicator was considerably reduced (see Tables 3 and 4).

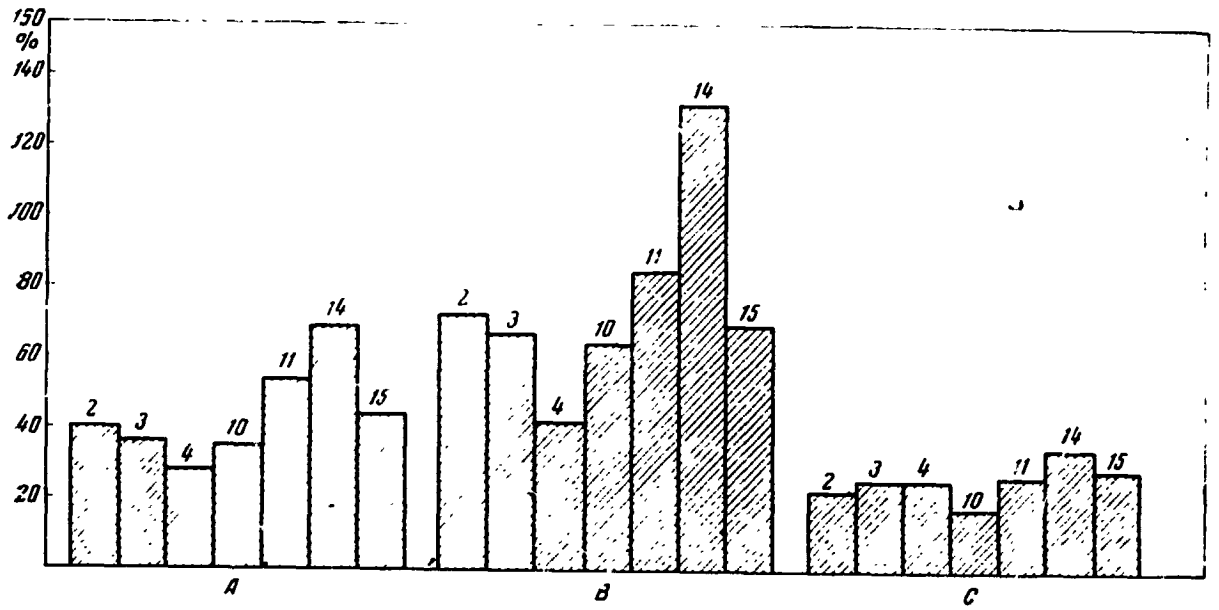

Fig. 10. Leucocytes (A), neutrophils (B), and lymphocytes (C) in mice gamma-irradiated (2), subjected to the combined effect of irradiation with inhalation of constituents of lunar surface material (3), air (4), orally administered a suspension of lunar surface material (10), distilled water (11), peritoneal administration of supernatant liquid (14), and physiological saline solution (15). Seventh day after irradiation 2-4, 10, 11, 14, and 15. Groups numbers in Table 1.

Conclusion. In analyzing these data, naturally an attempt must be made to answer the question that was raised at the beginning of the study, namely how the administration of lunar surface material could be reflected in the response of the organism to irradiation.

First of all let us examine the data on the survival rate and let us do this in a somewhat different aspect than was done in the presentation of the results. We divide the animals into two groups. In the first group we place the mice that had been subjected only to irradiation, and in the second group we place the mice that had been irradiated and in addition had been in contact with the lunar surface material. With this breakdown, 119 mice fall into group one and 118 mice into group two. The mortality 180 days after irradiation was 14.3 percent for the first group, and 16.1 percent for the second group, that is, practically the same. We also saw no appreciable difference in this indicator by comparing individually the experimental and control groups -- 3 and 4, 10 and 11, 14 and 15 (see Table 1). However, in all the three experimental groups the death rate of the animals was somewhat higher than in the control. The reasons for the relatively high death of animals in groups 14 and 15 compared with the other groups remain unclear.

Worthy of mention is the fact that in mice which prior to irradiation had been administered lunar surface material inhalationally or peritoneally, a lag in weight increment was observed. And in one of these groups (inhalational administration of lunar material), the largest number of tumors was detected. It is not of course precluded that this could have been a random coincidence.

As we have already indicated, beginning with the end of the third month after irradiation, neoplasms of different kinds and localization appeared in the mice of several groups. And they /604
all developed in animals that had been irradiated. However, where the irradiation was combined with the administration of lunar material, the tumors by the end of the sixth month of observation were encountered more often (5.9 percent) than for irradiation alone (1.7 percent). By the beginning of the eighth month, the pattern substantially changed. By this time there were now 20 animals with neoplasms that had been detected, where 16 of these in one form or the other had been in contact with lunar surface material.

Analysis of the hematological data shows that preliminary administration of the lunar surface material had no appreciable effect on the reaction of the peripheral blood to the radiation. The differences detected by the first to seventh day after irradiation, based on indicators such as total leucocyte count, and neutrophil count, in groups in which surface material had been orally or peritoneally administered, compared with the radiation control, are obviously associated with the irritation of the abdominal cavity or the gastrointestinal tract upon administration of the material. At the same time it could not but be noted that in mice which had been given the lunar surface material orally or peritoneally, cytological examination revealed degenerative-altered lymphocytes and monocytes. We did not detect the cells in the control groups.

In conclusion it must be emphasized that this report sums up the results only of a six-month observation and naturally from these results we cannot draw any final conclusions. At the same time it is obvious that the facts revealed are of definite interest and require revision and further verification in experiments on single-breed mice.

REFERENCES

1. Antipov, V. V., Davydov, B. I., Panchenkova, E. F., Saksonov, P. P., and Chernov, G. A., Kosmicheskiye issledovaniya 2(5), 797 (1964).

2. Konnova, N. I., Problemy kosmicheskoy biologii 14 (1971).

3. L'vova, T. S., Izv. AN SSSR, seriya biol. 3, 355 (1966).

4. Saksonov, P. P., Antipov, V. V., and Davydov, B. I., Problemy kosmicheskoy biologii 9, 133 (1968).

5. Benschoter, C. A., Allison, T. C., Boyd, J. E. et al., Science 169, 470 (1970).

6. Kustov, V. V., Ostapenko, O. F.,Petrukhin, V. G., Kosmicheskiye issledovaniya (1971) (in press).

7. Kustov, V. V., Ostapenko, O. F., and Petrukhin, V. G., Nauka i zhizn. 6, 51 (1971).

8. Kustov, V. V., Ostapenko, O. F., and Petrukhin, V. G., Aviat. Week and Space Technol. 92(12), 22 (1970).

REPRODUCIBILITY OF THE
ORIGINAL PAGE IS POOR